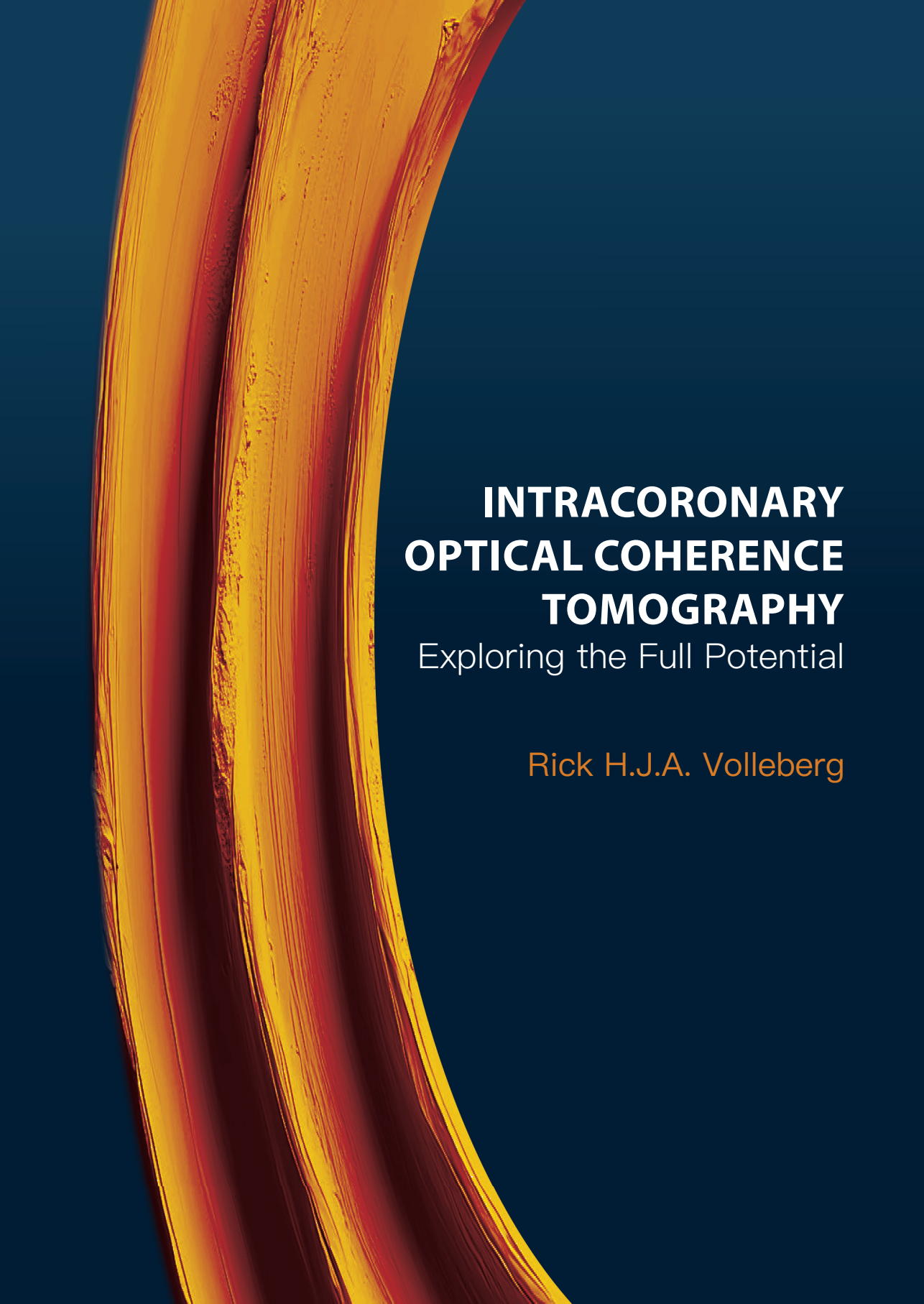

INTRACORONARY
OPTICAL COHERENCE
TOMOGRAPHY
Exploring the Full Potential
Rick H.J.A. Volleberg

Stellingen behorend bij het proefschrift

INTRACORONARY OPTICAL COHERENCE TOMOGRAPHY

Exploring the Full Potential

1. OCT is complementair aan angiografie en fysiologie tijdens evaluatie en behandeling van coronaire atherosclerose
   Dit proefschrift

2. Hoog-risico coronaire plaques zijn belangrijke markers voor een slechtere prognose op patiënt en laesie niveau
   Dit proefschrift

3. Non-culprit plaque rupturen zijn ondergewaardeerde tekenen van kwetsbaarheid door het gehele coronaire vaatsysteem
   Dit proefschrift

4. Hoewel de ontwikkeling van kunstmatige intelligentie in de interventiecardiologie veelbelovend is, moet er meer nadruk komen op transparantie en robuustheid
   Dit proefschrift

5. Automatische beoordeling van OCT middels kunstmatige intelligentie draagt bij aan betere risico stratificatie door in korte tijd meer en gedetailleerder informatie te verwerken dan wat manueel haalbaar is
   Dit proefschrift

6. Het gebruik van kunstmatige intelligentie bij OCT maakt IVUS en NIRS vrijwel overbodig
   Dit proefschrift

7. Ontwikkeling van klinisch waardevolle kunstmatige intelligentie vereist intensieve samenwerking tussen clinici en technici, en interesse in elkaars vakgebied
   Persoonlijke mening

8. Cultivate an ever-continuous power of observation
   John Singer Sargent

9. It's not enough that you believe what you see. You must also understand what you see
   Leonardo Da Vinci

10. Gót ver hiër vandán dan wette pas wat ge mist
    Pruuf Mar

Intracoronary Optical Coherence Tomography

Exploring the Full Potential

Rick Volleberg

ISBN: 978-94-6534-514-7
Cover and inside layout by: Bregje Jaspers | www.proefschriftOntwerp.nl
Printed by: Proefschriftmaken | www.proefschriftmaken.nl

Copyright © 2026, R.H.J.A. Volleberg
All rights reserved. No part of this thesis may be reproduced, stored in a retrieval system, or transmitted in any form or by any means without prior written permission by the author.

Intracoronary Optical Coherence Tomography

Exploring the Full Potential

Proefschrift ter verkrijging van de graad van doctor
aan de Radboud Universiteit Nijmegen
op gezag van de rector magnificus prof. dr. J.M. Sanders,
volgens besluit van het college voor promoties
in het openbaar te verdedigen op

vrijdag 9 oktober 2026
om 12.30 uur precies

door

Rick Henricus Johannes Antonius Volleberg
geboren op 15 juli 1996
te Venray

Promotoren:

Prof. dr. N. van Royen

Prof. dr. M. Prokop

Manuscriptcommissie:

Prof. dr. N.P. Riksen

Prof. dr. ir. C.L. de Korte

Dr. F.V.Y. Tjong (Amsterdam UMC)

CONTENT

Chapter 1	General introduction & Outline of the thesis	9
PART I	**PROCEDURAL GUIDANCE**	**23**
Chapter 2	Optical coherence tomography and coronary revascularization: from indication to procedural optimization *Trends in Cardiovascular Medicine 2023*	25
Chapter 3	Combining optical coherence tomography and fractional flow reserve for decision making in percutaneous coronary intervention: insights from the FUSION study *Journal of the Society for Cardiovascular Angiography & Interventions 2025*	55
Chapter 4	Dissection-like appearance of focal catheter-induced vasospasm in intracoronary optical coherence tomography *European Heart Journal 2024*	71
Chapter 5	Optical coherence tomography in motion: potential cause for artifacts *JACC Cardiovascular Interventions 2025*	79
PART II	**HIGH-RISK PLAQUE IDENTIFICATION**	**87**
Chapter 6	Fractional flow reserve-negative high-risk plaques and clinical outcomes after myocardial infarction *JAMA Cardiology 2023*	89
Chapter 7	High-risk plaques in non-culprit lesions and clinical outcome after NSTEMI vs. STEMI *European Heart Journal Cardiovascular Imaging 2025*	109
Chapter 8	Sex differences in plaque characteristics of fractional flow reserve-negative non-culprit lesions after myocardial infarction *Atherosclerosis 2024*	129
Chapter 9	Long-term clinical outcomes of high-risk plaques with negative fractional flow reserve: the PECTUS-obs study *EuroIntervention, online ahead of print*	147
Chapter 10	FFR-negative nonculprit high-risk plaques and clinical outcomes in high-risk populations: an individual patient-data pooled analysis from COMBINE (OCT-FFR) and PECTUS-obs *Circulation Cardiovascular Interventions 2025*	169

Chapter 11	Impact of clinical risk characteristics on the prognostic value of high-risk plaques *EuroIntervention 2025*	191
PART III	**ARTIFICIAL INTELLIGENCE-BASED IMAGE INTERPRETATION**	**213**
Chapter 12	Roadmap on the use of artificial intelligence for imaging of vulnerable atherosclerotic plaque in coronary arteries *Nature Reviews Cardiology 2024*	215
Chapter 13	Artificial intelligence for the analysis of intracoronary optical coherence tomography images: a systematic review *European Heart Journal Digital Health 2025*	247
Chapter 14	Comprehensive full-vessel segmentation and volumetric plaque quantification for intracoronary optical coherence tomography using deep learning *European Heart Journal Digital Health 2025*	277
Chapter 15	Real-world external validation of artificial intelligence-based full-vessel segmentation for intracoronary optical coherence tomography *Journal of the American Heart Association, in press*	305
Chapter 16	Deep learning-derived plaque burden for intracoronary optical coherence tomography: an intravascular ultrasound-based validation study *JACC Cardiovascular Interventions 2025*	329
Chapter 17	Artificial intelligence-based identification of thin-cap fibroatheromas and clinical outcomes: the PECTUS-AI study- *European Heart Journal 2025*	337
Chapter 18	General discussion	357
Chapter 19	Summary	373
	Nederlandse samenvatting	381
APPENDIX		**387**
	Research data management	389
	PhD portfolio	391
	Dankwoord	395
	Curriculum vitae	401
	List of publications	403



CHAPTER 1

General introduction
Outline of the thesis

GENERAL INTRODUCTION

Evolution of coronary imaging

Ever since the first selective coronary angiography was performed by dr. F. Mason Sones in 1958, angiography has remained the cornerstone of invasive coronary imaging. However, multiple limitations of this imaging modality need to be acknowledged. First, angiography results in a so-called luminogram, a two-dimensional representation of the lumen contour. Considering the three-dimensional nature of the lumen, at least two orthogonal views are required for proper evaluation of luminal dimensions and stenosis grades. Yet, even then, accurate estimation of stenosis severity remains challenging.[1] Second, foreshortening and overprojection further complicate coronary evaluation using angiography. Third, very limited information on the vascular wall and plaque morphology can be obtained using angiography as sole imaging modality. To better evaluate the hemodynamic and clinical significance of stenoses, hemodynamic indices, such as the fractional flow reserve, were introduced. Even though these hemodynamic indices improve guidance of percutaneous coronary revascularization as compared to angiography alone,[2] they provide limited information on plaque morphology and procedural success. Multiple intravascular imaging modalities were developed to overcome these limitations, among which are intravascular ultrasound (IVUS) and optical coherence tomography (OCT). OCT is a catheter-based imaging modality that employs near-infrared light for tomographic imaging of the coronary artery lumen and wall (Figure 1).

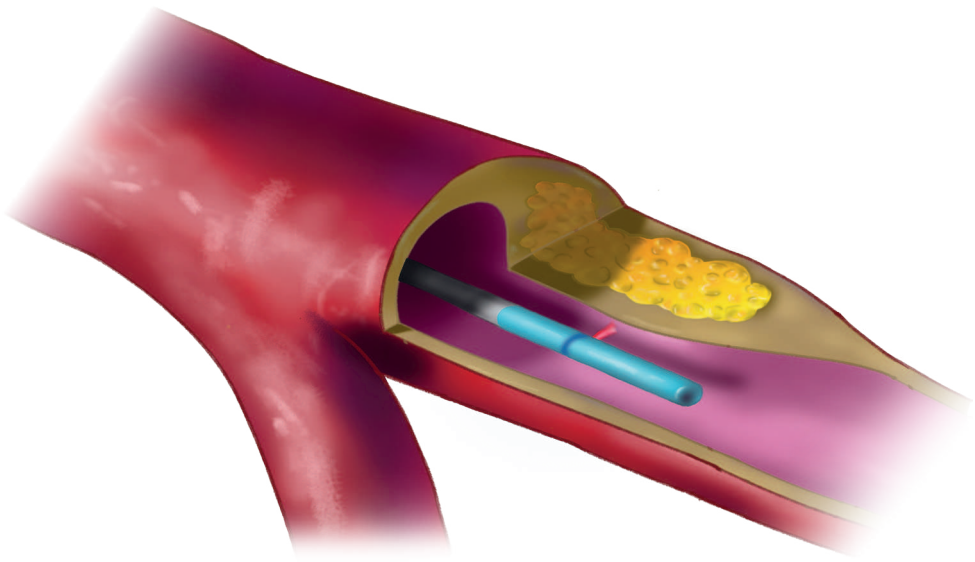


Figure 1. Schematic illustration of intracoronary optical coherence tomography.

OCT imaging of a 54-75 mm coronary segment can be performed in less than 3.0 seconds, resulting in a total of 375-540 cross-sectional images. First, the coronary lumen is cleared using continuous ionized contrast injection, or more experimentally with saline or low-molecular-weight dextran injection. During the subsequent automated pullback of the lens, light in the near-infrared spectrum (typical wavelength ~1.3 μm) is emitted from the catheter lens. After detection, the amount of backscattered or reflected light is translated into a function of delay time or depth within the vascular tissue using interferometry. The resulting information from each individual axial scanning line (A-line) acquired during helical movement of the lens and detector is translated to image data in polar coordinates (r,θ) (Figure 2A), wherein differences in refractive indices of individual tissue types determine image intensity. The corresponding Cartesian (x,y) transformed representation of the coronary is provided to the operator (Figure 2B). In these anatomical representative cross-sectional images, the center of the image represents the OCT catheter positioned in the coronary lumen. The guidewire, used to position the OCT catheter, is characterized by a conus-shaped artefact. In healthy arterial segments, the vessel wall exhibits a three-layered structure: from the inside towards the outside we encounter (1) the tunica intima represented by the first bright layer, (2) the tunica media as the first dark layer and (3) the tunica adventitia as the outer bright layer. A clinically important structure, the external elastic membrane (also referred to as the external elastic lamina) is defined as the border between the tunica media and the tunica adventitia (Figure 2C).

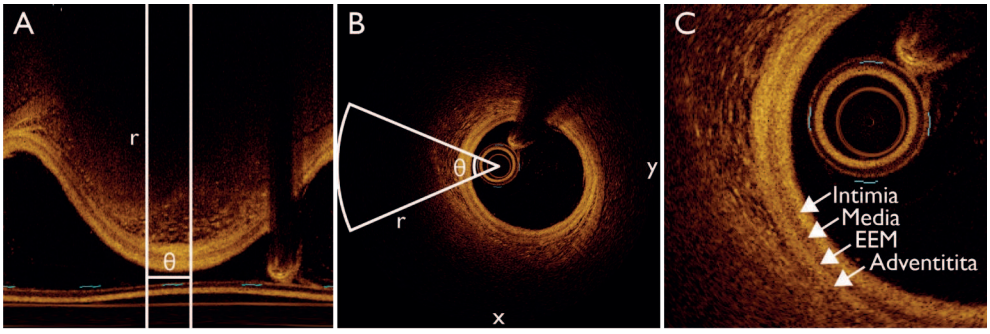


Figure 2. Polar and cartesian representation of intracoronary optical coherence tomography.
A) OCT image of an healthy vessel in polar (r,θ) coordinates. The horizontal axis represents individual A-lines obtained during rotational movement of the lens and the vertical axis represents the depth of each individual A-line. B) The corresponding Cartesian (x,y) transformation of the same image. C) Zoomed version of the same frame indicating the vessel layers.
EEM external elastic membrane.

The spatial resolution of OCT is superior to any other current coronary imaging modality, with an axial and lateral resolution of 10-15 μm and 20 μm, respectively. In comparison, the axial resolution of IVUS is approximately 100 μm. However, this superior resolution of OCT comes at a cost of limited penetration depth, ranging from 0.1 mm to 2.0 mm, dependent on the imaged tissue.

Besides very accurate evaluation of luminal and vessel dimensions, OCT additionally informs on plaque morphology and allows evaluation of implanted stents. Different type of plaques, including fibrotic plaques, calcified plaques, lipid plaques and layered plaques (Figure 3A-D), and microstructures such as microvessels, cholesterol crystals and macrophage accumulation can be distinguished using OCT. Additionally, OCT allows evaluation of implanted stents and acute procedural as well as long term stent-related complications (including stent underexpansion, malapposition, edge-dissections and in-stent restenosis, Figure 3E-H) with higher accuracy than angiography and IVUS.[3]

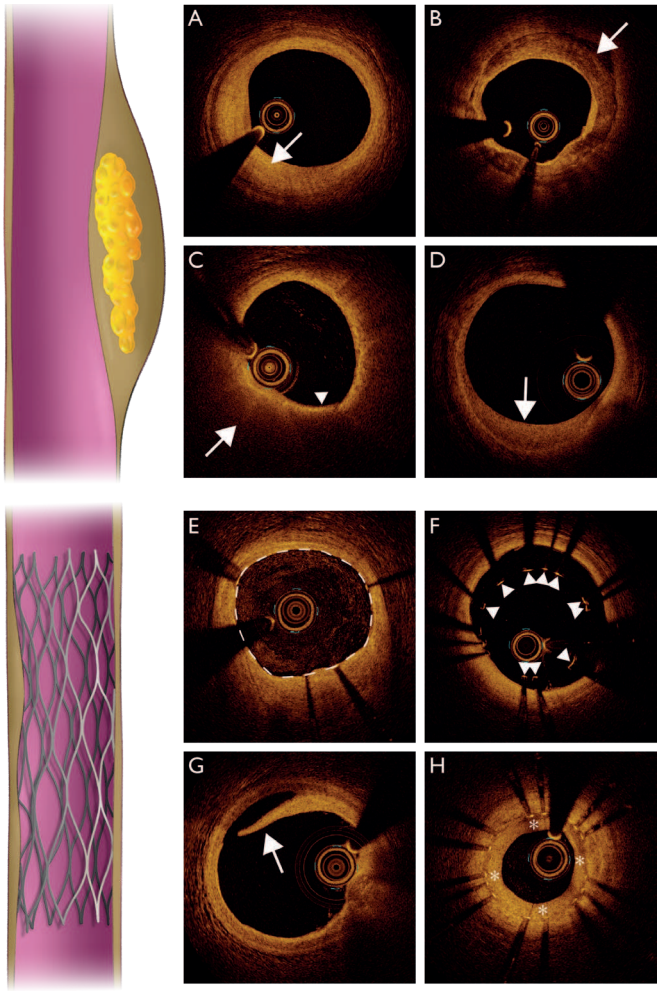


Figure 3. Examples of OCT images for the evaluation of plaque morphology and implanted stents.
A) Fibrous plaque (arrow) is characterized by homogeneous signal-rich thickening of the intimal layer. B) Calcified plaque (arrow) is defined as a signal-poor, sharply delineated area. C) Lipid plaque (arrow) is represented by a signal-

poor region, owing to complete light absorption by lipidic tissue, with diffuse borders that is separated from the coronary lumen by a signal-rich band (i.e. the fibrous cap), which is thin in the example (arrowhead). D) Layered plaque (arrow) is characterized by one or multiple layers of different densities with a clear demarcation from the surrounding tissue. E) Case of stent underexpansion in the distal half of the stent defined as a minimum stent area that is less than 80-90% of the corresponding distal or proximal reference lumen areas. The stent struts are characterized by areas of high intensity with an abluminal shadow artefact caused by the complete reflection of near-infrared light by the metal platform. The minimum stent area (dashed line) in this case measured 6.07 mm^2, whilst the distal reference lumen area measured 7.69 mm^2, resulting in a stent expansion of 79%. F) Stent malapposition (arrowheads) represented by stent struts not aligning with the lumen border. G) Edge dissection (arrow), that occur as acute iatrogenic laceration of the coronary vascular wall during stent implantation, is characterized by intimal or medial tears within 5mm of the stent edge. H) Circumferential in-stent restenosis (asterisks), which occurs over time, is characterized by neointima formation of neoatherosclerosis within the stent that causes reobstruction of the previously treated segment.

Guideline recommended applicability of intracoronary OCT

Contemporary guidelines endorse the use of intracoronary OCT for various indications, in particular for guidance of coronary revascularization, identification of the culprit coronary artery and evaluation of stent failure.[4-6]

Stent guidance and optimization

Accurate quantification of lumen and vessel sizes, as well as identification of stent landing zones that are free of atherosclerotic disease, allow for more precise decision making regarding stent sizes and stent placement. In particular, OCT guidance allows stent sizing to true vessel sizes,[7] thereby assuring larger minimum stent areas which is associated with better long term outcome.[8] Additionally, the stent edges can be positioned more accurately, avoiding residual disease at the stent edges and decreasing the risk of stent edge dissections and long-term stent failure.[8,9] Furthermore, OCT is useful for the identification of heavily calcified lesions that require lesion preparation to ensure optimal stent expansion.[10] After stent implantation, OCT allows optimization in case of suboptimal results.

In recent years, multiple large scale randomized controlled trials have demonstrated the benefit of intravascular imaging guidance – whether with IVUS or OCT – over angiography guidance, with significant reductions in (cardiac) mortality, stent thrombosis, target-vessel related myocardial infarction and target-lesion revascularization.[11,12] Meta-analyses of these trials demonstrated no apparent differences between IVUS or OCT.[11] Consequently, the recommendations for intravascular imaging-guided coronary revascularization have increased in prevailing guidelines in recent years. Whilst the 2018 ESC guidelines on myocardial revascularization provided a class IIa recommendation (level of evidence B) for intravascular imaging for stent optimization in selected patients,[4] the latest 2024 ESC guidelines on chronic coronary syndromes provide a class I recommendation (level of evidence A) for intravascular imaging guidance for percutaneous complex lesion revascularization.[6]

Culprit lesion identification

While the culprit lesion is often evident on angiography in patients with ST-segment elevation myocardial infarction, this is frequently not the case in patients with non-ST-segment elevation myocardial infarction. In fact, the wrong coronary artery is identified as culprit in almost 10% of the latter cases.[13,14] In such ambiguous cases, OCT may provide a benefit by the identification of plaque rupture, plaque erosion or spontaneous coronary artery dissections (Figure 4). One small pilot study provided preliminary evidence that OCT may help guide treatment strategies in patients with plaque erosion by omitting stent implantation.[15] Additionally, OCT is also endorsed in patients with myocardial infarction with non-obstructive coronary arteries to help identify potential culprit lesions that are not angiographically apparent. In the absence of a culprit lesion in these patients, alternative diagnoses should be considered.

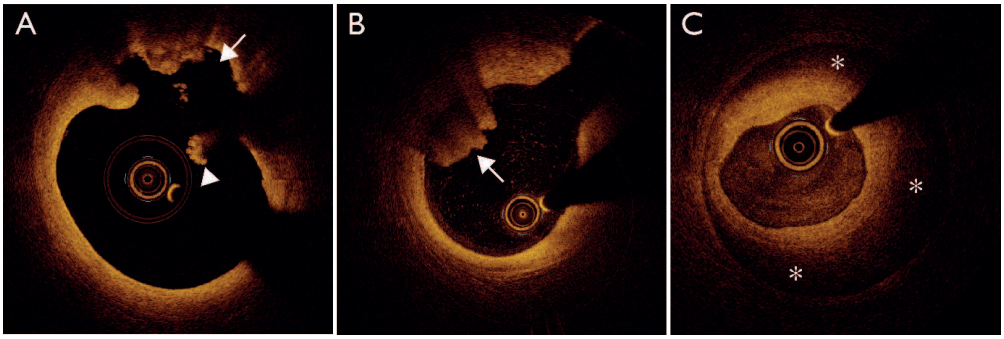


Figure 4. Culprit lesion identification.
A) Thrombotic plaque rupture which is characterized by a cavity in the atherosclerotic plaque (arrow) with overlying thrombus (arrowhead). B) A case of definite plaque erosion, defined as a thrombus (arrow) overlying an intact and visualized plaque, that is frequently fibrotic in nature. C) Spontaneous coronary artery dissection is represented as a crescent-shaped false lumen (asterisks) which can be filled with blood, flushing agent, or a combination of both.

Stent failure

Although coronary stents are designed to provide long term patency, stent failure may occur both at short-term and long-term follow-up. Several distinct types of stent failure can be distinguished, including stent thrombosis, neointimal hyperplasia and neoatherosclerosis. Stent thrombosis may occur acutely or during follow-up and is the most devastating manifestation of stent failure. In-stent thrombus formation may result in total occlusion of the stent and patients frequently present with acute myocardial infarction. In contrast, in-stent restenosis – whether neointimal hyperplasia or neoatherosclerosis – typically develops more gradually and is frequently diagnosed in patients who present with recurrent anginal complaints after percutaneous coronary intervention. In both scenarios, OCT is valuable to identify the underlying mechanism of stent failure. For example, stent thrombosis has been associated with uncovered and malapposed stent struts,[16] although conflicting evidence exists. In-stent restenosis is strongly associated with stent underexpansion and/or residual disease at the stent edges.[8] By identifying

the underlying mechanism responsible for stent failure, OCT can inform different treatment approaches such as further expansion of the previously implanted stent or additional stent implantation. However, it should be acknowledged that these approaches are primarily guided by mechanistic reasoning. Hence, the 2018 ESC guidelines on myocardial revascularization provide a class IIa recommendation with level of evidence C for the use of OCT to detect stent-related mechanical problems leading to restenosis.[4]

High-risk plaque identification

The high resolution imaging capabilities of OCT hold potential beyond current guideline recommendations, including *in vivo* evaluation of high-risk or vulnerable plaques. The rationale behind *in vivo* identification of high-risk plaques stems from (1) the post-mortem observation that ruptured coronary plaques are consistently characterized by large lipid pools or necrotic cores with a thin overlying fibrous cap, generally defined as <65 µm (Figure 3C), and (2) that many thrombotic events occur in non-stenotic lesions.[17] Consequently, focusing only on the stenotic phase of coronary lesions omits the majority of plaque progression. In the earliest phases, plaques demonstrate positive remodeling, the so-called Glagov effect.[18] It is only after plaque burden exceeds 40% that plaques demonstrate luminal encroachment.[18] The hypothesis is that early *in vivo* identification of high-risk plaques phenotypes, prior to their disruption, may help identify patients at increased risk for adverse cardiovascular events and may guide preventive treatment strategies in those patients to prevent future events.[19] This concept is particularly relevant in lesions that are currently considered safe to defer, which is generally the case for intermediate lesions (30-90% luminal obstruction) that do not have a significant hemodynamic effect. The latter can be evaluated non-invasively (e.g. with cardiac magnetic resonance imaging) or invasively using hyperemic and non-hyperemic flow indices such as the fractional flow reserve and instantaneous wave-free ratio, respectively.[2,20,21] For lesions evaluated during maximal hyperemia, a ≥20% translesional pressure gradient is considered significant, whereas for non-hyperemic indices pressure drop of ≥11% corresponds to a significant flow limitation. Although it is safe to defer revascularization of non-flow limiting lesions in the overall population with coronary artery disease,[22] its safety in specific subsets of patients has been questioned. Particularly, in patients presenting with acute myocardial infarction and additional non-flow limiting non-culprit coronary lesions (Figure 5), recurrent cardiovascular events occur more frequently than in patients with chronic coronary syndrome.[23] It has been postulated that an abundance of high-risk plaques in these deferred non-culprit lesions may be the driving force behind an increased incidence of future cardiovascular events. Importantly, such non-culprit coronary lesions are present in approximately 50% of patients with myocardial infarction, emphasizing the scale of this clinical problem.[24] Although prior studies have demonstrated the prognostic impact of high-risk plaques,[25-28] there is a paucity of data on this topic in confirmed absence of flow limitations.

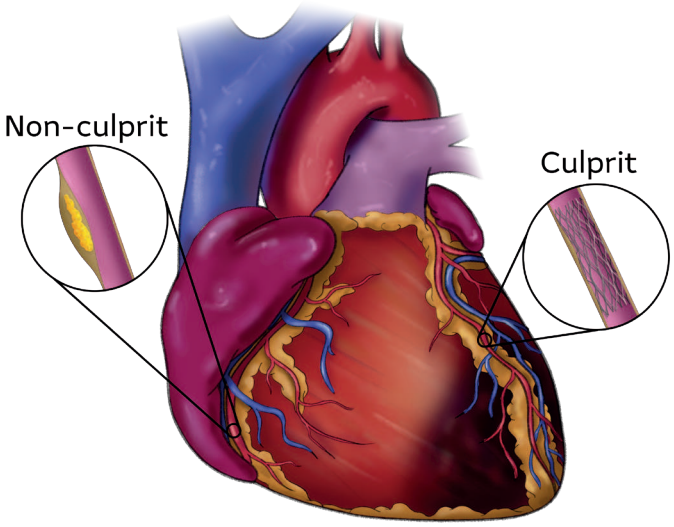


Figure 5. Culprit and non-culprit lesions in myocardial infarction.

Towards convenient, reliable clinical application

Despite aforementioned advantages of intracoronary OCT, the clinical adoption rate remains low. In the United States, intracoronary imaging – whether IVUS or OCT – is only applied in one in seven procedures.[29] A prolongation of the procedure due to time consuming manual interpretation and lack of training for use and interpretation of intracoronary OCT, are among the most frequently named reasons limiting widespread clinical adoption.[30] Additionally, the interobserver variability for OCT image interpretation is substantial, even among highly-experienced operators and core-laboratories.[31,32] Automated image analysis can help overcome these specific limitations and promote widespread clinical adoption by providing real-time, reliable and reproducible image assessment.

The inception of deep learning, a subdivision of artificial intelligence, has sparked an increased interest in and improved effectiveness of automated medical image analysis. Deep learning refers to multi-layered algorithms that are inspired by structure and function of the human neural network, and that are capable of learning directly from data. Commonly applied algorithms include artificial neural networks, convolutional neural networks (such as U-nets), and more recently generative models (including generative adversarial networks and diffusion models), transformer networks and foundation models. Deep learning has already been successfully applied to cardiovascular image analysis across various imaging modalities.[33] The unmatched spatial resolution of OCT makes it amenable for automated analysis by deep learning. The latest commercial software packages for OCT have integrated deep learning modules for a limited number of tasks, such as automated measurements of lumen and vessel

sizes, and automated identification of calcified plaques and stent struts.[34] However, most research efforts on the development of deep learning for OCT analysis have not made it to the clinic as of yet. Important considerations for clinical application of deep learning algorithms include robust model development and validation, mitigating the risk of bias. Although initial studies have demonstrated feasibility, they largely failed to address all these aspects.

OUTLINE OF THE THESIS

Considering the distinct advantages of OCT compared to angiography, new doors are opened through this invention to potentially improve patient outcome through various means. Theoretically, OCT could serve multiple additional purposes, but many of these potential applications currently lack a scientific base. Additionally, procedural duration may be increased substantially by more widespread application of OCT if not assisted by deep learning. Hence, the aims of this thesis were to investigate the value of OCT for procedural guidance, the value of OCT for high-risk plaque identification, and the possibilities of deep learning for automated OCT image interpretation. Therefore, in part I, we first focus on the value of OCT for guidance of percutaneous coronary revascularization. In part II, we assess the additional value of OCT on top of physiological lesion evaluation for prognostication of patients at increased risk for recurrent events through the identification of high-risk plaques. Last, in part III, we address the potential of automated OCT image interpretation by means of deep learning.

Part I – Procedural guidance

In **Chapter 2**, we provide an in-depth overview of the evidence supporting the current clinical application of intracoronary OCT and describe newly to be explored areas of research. Given the wide range of information obtained through OCT, we hypothesize that OCT may have the potential to serve as a future all-in-one tool to guide coronary revascularization, from guiding referral and deferral for revascularization to procedural optimization. In **Chapter 3**, we examine how the fractional flow reserve and OCT inform decision making, exploring the complementary nature of these modalities. In **Chapters 4** and **5**, we describe two artefacts that are frequently underappreciated but can have direct implications during percutaneous coronary revascularization if they are not recognized appropriately.

Part II – High-risk plaque identification

In **Chapter 6**, the primary results of the prospective, observational, natural-history PECTUS-obs study are reported. This study evaluated the association between OCT-identified high-risk plaques in non-flow limiting non-culprit lesions and cardiovascular events in patients with myocardial infarction. Differences in non-culprit plaque characteristics according to clinical presentation and sex are described in **Chapters 7** and **8**, respectively. The long-term outcome results of the PECTUS-obs study are presented in **Chapter 9**. In **Chapter 10**, we describe an individual patient data pooled analysis from the PECTUS-obs study and the similarly designed COMBINE (OCT-FFR) study that evaluated diabetic patients. This

pooled analysis provides a more robust assessment of the clinical impact of OCT-identified high-risk plaques in confirmed absence of flow limitations, including secondary hard clinical endpoints, targeted at populations at risk for recurrent cardiovascular events. In **Chapters 11**, we assess whether clinical risk factors can be used to identify patients that are likely to have high-risk plaques, to streamline the screening process. Additionally, we evaluate how the presence of high-risk plaques affect clinical outcome across various clinical risk profiles.

Part III – Artificial intelligence-based image interpretation

In **Chapter 12**, we provide a framework for the development of artificial intelligence methods for the automated identification of high-risk plaques across various imaging modalities, formulated based on a multidisciplinary consensus survey. In **Chapter 13**, we systematically review the current status of artificial intelligence-related research for intracoronary OCT, with regard to methodology, performance metrics and potential sources of bias. In **Chapter 14**, we describe the first preliminary results of a deep learning-based multiclass segmentation model for intracoronary OCT, including the first external validation against experienced readers as references standard. In **Chapter 15**, we provide a large scale real-world external validation study. We evaluate the performance of this algorithm for the evaluation of plaque burden in **Chapter 16**, and for prognostication through the identification of thin-cap fibroatheromas in **Chapter 17**.

Chapter 18 provides a general discussion on the findings of this thesis, which are summarized in **Chapter 19**.

REFERENCES

1. Zir LM, Miller SW, Dinsmore RE, Gilbert JP, Harthorne JW. Interobserver variability in coronary angiography. Circulation 1976;53:627-32.
2. Tonino PA, De Bruyne B, Pijls NH, Siebert U, Ikeno F, van' t Veer M et al. Fractional flow reserve versus angiography for guiding percutaneous coronary intervention. N Engl J Med 2009;360:213-24.
3. Prati F, Di Vito L, Biondi-Zoccai G, Occhipinti M, La Manna A, Tamburino C et al. Angiography alone versus angiography plus optical coherence tomography to guide decision-making during percutaneous coronary intervention: the Centro per la Lotta contro l'Infarto-Optimisation of Percutaneous Coronary Intervention (CLI-OPCI) study. EuroIntervention 2012;8:823-9.
4. Neumann FJ, Sousa-Uva M, Ahlsson A, Alfonso F, Banning AP, Benedetto U et al. 2018 ESC/EACTS Guidelines on myocardial revascularization. Eur Heart J 2019;40:87-165.
5. Byrne RA, Rossello X, Coughlan JJ, Barbato E, Berry C, Chieffo A et al. 2023 ESC Guidelines for the management of acute coronary syndromes. Eur Heart J 2023;44:3720-3826.
6. Vrints C, Andreotti F, Koskinas KC, Rossello X, Adamo M, Ainslie J et al. 2024 ESC Guidelines for the management of chronic coronary syndromes. Eur Heart J 2024;45:3415-3537.
7. Kubo T, Akasaka T, Shite J, Suzuki T, Uemura S, Yu B et al. OCT compared with IVUS in a coronary lesion assessment: the OPUS-CLASS study. JACC Cardiovasc Imaging 2013;6:1095-1104.
8. Landmesser U, Ali ZA, Maehara A, Matsumura M, Shlofmitz RA, Guagliumi G et al. Optical coherence tomography predictors of clinical outcomes after stent implantation: the ILUMIEN IV trial. Eur Heart J 2024;45:4630-4643.
9. Chamie D, Bezerra HG, Attizzani GF, Yamamoto H, Kanaya T, Stefano GT et al. Incidence, predictors, morphological characteristics, and clinical outcomes of stent edge dissections detected by optical coherence tomography. JACC Cardiovasc Interv 2013;6:800-13.
10. Fujino A, Mintz GS, Matsumura M, Lee T, Kim SY, Hoshino M et al. A new optical coherence tomography-based calcium scoring system to predict stent underexpansion. EuroIntervention 2018;13:e2182-e2189.
11. Stone GW, Christiansen EH, Ali ZA, Andreasen LN, Maehara A, Ahmad Y et al. Intravascular imaging-guided coronary drug-eluting stent implantation: an updated network meta-analysis. Lancet 2024;403:824-837.
12. Hong SJ, Lee SJ, Lee SH, Lee JY, Cho DK, Kim JW et al. Optical coherence tomography-guided versus angiography-guided percutaneous coronary intervention for patients with complex lesions (OCCUPI): an investigator-initiated, multicentre, randomised, open-label, superiority trial in South Korea. Lancet 2024;404:1029-1039.
13. Heitner JF, Senthilkumar A, Harrison JK, Klem I, Sketch MH, Jr., Ivanov A et al. Identifying the Infarct-Related Artery in Patients With Non-ST-Segment-Elevation Myocardial Infarction. Circ Cardiovasc Interv 2019;12:e007305.
14. Shanmuganathan M, Nikolaidou C, Burrage MK, Borlotti A, Kotronias R, Scarsini R et al. Cardiovascular Magnetic Resonance Before Invasive Coronary Angiography in Suspected Non-ST-Segment Elevation Myocardial Infarction. JACC Cardiovasc Imaging 2024;17:1044-1058.
15. Jia H, Dai J, He L, Xu Y, Shi Y, Zhao L et al. EROSION III: A Multicenter RCT of OCT-Guided Reperfusion in STEMI With Early Infarct Artery Patency. JACC Cardiovasc Interv 2022;15:846-856.
16. Adriaenssens T, Joner M, Godschalk TC, Malik N, Alfonso F, Xhepa E et al. Optical Coherence Tomography Findings in Patients With Coronary Stent Thrombosis: A Report of the PRESTIGE Consortium (Prevention of Late Stent Thrombosis by an Interdisciplinary Global European Effort). Circulation 2017;136:1007-1021.
17. Burke AP, Farb A, Malcom GT, Liang YH, Smialek J, Virmani R. Coronary risk factors and plaque morphology in men with coronary disease who died suddenly. N Engl J Med 1997;336:1276-82.
18. Glagov S, Weisenberg E, Zarins CK, Stankunavicius R, Kolettis GJ. Compensatory enlargement of human atherosclerotic coronary arteries. N Engl J Med 1987;316:1371-5.

19. Stone PH, Libby P, Boden WE. Fundamental Pathobiology of Coronary Atherosclerosis and Clinical Implications for Chronic Ischemic Heart Disease Management-The Plaque Hypothesis: A Narrative Review. JAMA Cardiol 2023;8:192-201.

20. Gotberg M, Christiansen EH, Gudmundsdottir IJ, Sandhall L, Danielewicz M, Jakobsen L et al. Instantaneous Wave-free Ratio versus Fractional Flow Reserve to Guide PCI. N Engl J Med 2017;376:1813-1823.

21. Davies JE, Sen S, Dehbi HM, Al-Lamee R, Petraco R, Nijjer SS et al. Use of the Instantaneous Wave-free Ratio or Fractional Flow Reserve in PCI. N Engl J Med 2017;376:1824-1834.

22. Escaned J, Ryan N, Mejia-Renteria H, Cook CM, Dehbi HM, Alegria-Barrero E et al. Safety of the Deferral of Coronary Revascularization on the Basis of Instantaneous Wave-Free Ratio and Fractional Flow Reserve Measurements in Stable Coronary Artery Disease and Acute Coronary Syndromes. JACC Cardiovasc Interv 2018;11:1437-1449.

23. Cerrato E, Mejia-Renteria H, Dehbi HM, Ahn JM, Cook C, Dupouy P et al. Revascularization Deferral of Nonculprit Stenoses on the Basis of Fractional Flow Reserve: 1-Year Outcomes of 8,579 Patients. JACC Cardiovasc Interv 2020;13:1894-1903.

24. Goldstein JA, Demetriou D, Grines CL, Pica M, Shoukfeh M, O'Neill WW. Multiple complex coronary plaques in patients with acute myocardial infarction. N Engl J Med 2000;343:915-22.

25. Stone GW, Maehara A, Lansky AJ, de Bruyne B, Cristea E, Mintz GS et al. A prospective natural-history study of coronary atherosclerosis. N Engl J Med 2011;364:226-35.

26. Waksman R, Di Mario C, Torguson R, Ali ZA, Singh V, Skinner WH et al. Identification of patients and plaques vulnerable to future coronary events with near-infrared spectroscopy intravascular ultrasound imaging: a prospective, cohort study. Lancet 2019;394:1629-1637.

27. Prati F, Romagnoli E, Gatto L, La Manna A, Burzotta F, Ozaki Y et al. Relationship between coronary plaque morphology of the left anterior descending artery and 12 months clinical outcome: the CLIMA study. Eur Heart J 2020;41:383-391.

28. Erlinge D, Maehara A, Ben-Yehuda O, Botker HE, Maeng M, Kjoller-Hansen L et al. Identification of vulnerable plaques and patients by intracoronary near-infrared spectroscopy and ultrasound (PROSPECT II): a prospective natural history study. Lancet 2021;397:985-995.

29. Fazel R, Yeh RW, Cohen DJ, Rao SV, Li S, Song Y et al. Intravascular imaging during percutaneous coronary intervention: temporal trends and clinical outcomes in the USA. Eur Heart J 2023;44:3845-3855.

30. Koskinas KC, Nakamura M, Raber L, Colleran R, Kadota K, Capodanno D et al. Current use of intracoronary imaging in interventional practice - Results of a European Association of Percutaneous Cardiovascular Interventions (EAPCI) and Japanese Association of Cardiovascular Interventions and Therapeutics (CVIT) Clinical Practice Survey. EuroIntervention 2018;14:e475-e484.

31. Kini AS, Vengrenyuk Y, Yoshimura T, Matsumura M, Pena J, Baber U et al. Fibrous Cap Thickness by Optical Coherence Tomography In Vivo. J Am Coll Cardiol 2017;69:644-657.

32. Gruslova AB, Singh S, Hoyt T, Vela D, Vengrenyuk Y, Buja LM et al. Accuracy of OCT Core Labs in Identifying Vulnerable Plaque. JACC Cardiovasc Imaging 2024;17:448-450.

33. Litjens G, Ciompi F, Wolterink JM, de Vos BD, Leiner T, Teuwen J et al. State-of-the-Art Deep Learning in Cardiovascular Image Analysis. JACC Cardiovasc Imaging 2019;12:1549-1565.

34. Cioffi GM, Pinilla-Echeverri N, Sheth T, Sibbald MG. Does artificial intelligence enhance physician interpretation of optical coherence tomography: insights from eye tracking. Front Cardiovasc Med 2023;10:1283338.

PART I

PROCEDURAL GUIDANCE



CHAPTER 2

Optical coherence tomography and coronary revascularization: from indication to procedural optimization

Rick Volleberg | Jan-Quinten Mol | Dirk van der Heijden | Martijn Meuwissen | Maarten van Leeuwen | Javier Escaned | Niels Holm | Tom Adriaenssens | Robert Jan van Geuns | Shengxian Tu | Filippo Crea | Gregg Stone | Niels van Royen

Trends in Cardiovascular Medicine
2023 Feb;33(2):92-106

ABSTRACT

Angiography alone is the most commonly used imaging modality for guidance of percutaneous coronary interventions. Angiography is limited, however, by several factors, including that it only portrays a low resolution, two-dimensional outline of the lumen and does not inform on plaque composition and functional stenosis severity. Optical coherence tomography (OCT) is an intracoronary imaging technique that has superior spatial resolution compared to all other imaging modalities. High-resolution imaging of the vascular wall enables precise measurement of vessel wall and luminal dimensions, more accurately informing about the anatomic severity of epicardial stenoses, and also provides input for computational models to assess functional severity. The very high-resolution images also permit plaque characterization that may be informative for prognostication. Moreover, periprocedural imaging provides valuable information to guide lesion preparation, stent implantation and to evaluate acute stent complications for which iterative treatment might reduce the occurrence of major adverse stent events. As such, OCT represent a potential future all-in-one tool that provides the data necessary to establish the indications, procedural planning and optimization, and final evaluation of percutaneous coronary revascularization.

INTRODUCTION

Percutaneous coronary intervention (PCI) is the cornerstone treatment in patients with acute coronary syndromes (ACS) and refractory chronic coronary syndromes (CCS). Several key decisions arise during the process of PCI, including whether or not to perform mechanical revascularization, the choice of procedural strategy and the need of iterative treatment after initial stent implantation for stent optimization. Historically, decision-making was based on non-invasive ischemia detection, followed by visual inspection of ischemia-causing lesions by angiography and subsequent selection of the stent size and length needed. The availability of pressure-based indices such as hyperemic Fractional Flow Reserve (FFR) and non-hyperemic measures (e.g. instantaneous wave-Free Ratio (iFR)) improved the decision-making process by enabling functional identification of specific ischemia-generating stenoses. Later, intravascular ultrasound (IVUS) allowed for more detailed device selection and optimization by providing intraluminal measurements. More recently, new intravascular imaging modalities have been developed that offer enhanced diagnostic alternatives. Among these is Optical Coherence Tomography (OCT), a near-infrared light-based imaging technique that has at least ten times greater spatial resolution and forty times greater speed of image acquisition than IVUS.[1] A rotating single optical fiber emits near-infrared light, which is either attenuated by surrounding tissue or backscattered and subsequently detected by an interferometer. Information concerning the amplitude and time between emission and detection, analogous to ultrasound, is used to generate consecutive axial frames (A-lines), which are presented as a two-dimensional cross-sectional image. During the rotational movement of the light source, the catheter is (automatically) pulled back to image a coronary segment of either 54 or 75 mm. Its high spatial resolution enables precise atherosclerotic plaque characterization and stent visualization.[2] Contemporary guidelines recommend that OCT should be considered to evaluate stent failure and in selected patients for stent optimization.[3] Yet the potential of OCT is not limited to these aspects, as indicated in consensus documents.[1,4] The integration of different features of OCT, including plaque characterization, automated estimation of the hemodynamic significance of lesions, and evaluation of procedural results potentially provide a future all-in-one tool for interventional cardiologists to further improve outcome of PCI.

OCT TO ASSESS THE INDICATIONS FOR REVASCULARIZATION

First-line treatment of patients with CCS is medical therapy, with the exception of those with left main stem disease and/or three vessel coronary artery disease and severe left ventricular dysfunction in whom myocardial revascularization will improve prognosis.[5,6] When CCS patients remain symptomatic or are intolerant to guideline-directed medical therapy (GDMT), contemporary guidelines support the use of non-invasive or invasive diagnostic testing for identification of ischemia-causing lesions and subsequent referral for revascularization.[7] Invasive functional lesion assessment by FFR or iFR has been studied extensively and is well-established.[8-10] While the use of OCT for referral or deferral of revascularization in

patients with CCS is not currently recommended in the guidelines, its use for this purpose based on its anatomic findings or novel physiologic transformation is under active development and testing.

OCT to derive anatomic and functional stenosis severity

OCT-derived cross-sectional images allow precise measurements of the minimal lumen area (MLA), the minimal lumen diameter (MLD) and calculation of the percentage area stenosis (%AS) (Figure 1A-D). Measurements of the MLA and MLD on OCT are generally larger than those obtained by quantitative coronary angiography (QCA) but smaller than those derived from IVUS.[11-13] However, the lumen area and diameter measured by OCT correspond to actual lumen dimensions in phantom models better than any other imaging modality.[12,13] OCT-derived MLA, MLD and %AS correlate with FFR significance, albeit with variable diagnostic accuracy (Table 1).[14-24] The weighted mean area under the curve demonstrates moderate agreement between MLA, MLD or %AS and FFR significance, with optimal cut-off values of 1.99 mm^2, 1.33 mm and 67.8%, respectively. Compared to IVUS-derived MLA, OCT-derived MLA had superior specificity and diagnostic accuracy for the detection of hemodynamically significant lesions with both FFR ≤0.75 and ≤0.80 in a meta-analysis including 6,919 patients.[25] These findings suggest that OCT-derived dimensions may be suitable to guide referral for revascularization. However, use of an anatomical measure is limited in that the cut-off values corresponding to ischemic significance may vary according to its location in the coronary tree and the amount of myocardium subtended.[26]

In the FORZA trial, 350 patients with intermediate coronary stenosis were randomized to OCT-guided versus FFR-guided revascularization. FFR ≤0.80 warranted revascularization in the FFR-arm whereas in the OCT arm, PCI was indicated when %AS was ≥75%, or 50-75% in combination with either a MLA <2.5 mm^2 or plaque rupture. OCT was also used for stent optimization. OCT-guided PCI resulted in a greater number of lesions treated. After 13 months of follow-up, the occurrence of major adverse cardiovascular events (MACE) (the composite of death, MI and target vessel revascularization [TVR]) or significant angina was lower after OCT-guided compared with FFR-guided revascularization (8.0% vs 14.8%, p=0.048). A trend towards fewer MACE alone (without significant angina) was also present (3.4% vs 9.0%, p=0.064).[27] Bias in this open-label trial could not be ruled out, especially as regards recurrent angina and the indication for follow-up revascularization procedures, and the extent to which OCT-guided stent optimization contributed to the outcomes is uncertain. Thus, while a larger randomized trial would be required for confirmation, the results of this trial are suggestive that OCT-guided PCI may serve the dual purpose of lesion selection and stent optimization as discussed further on.

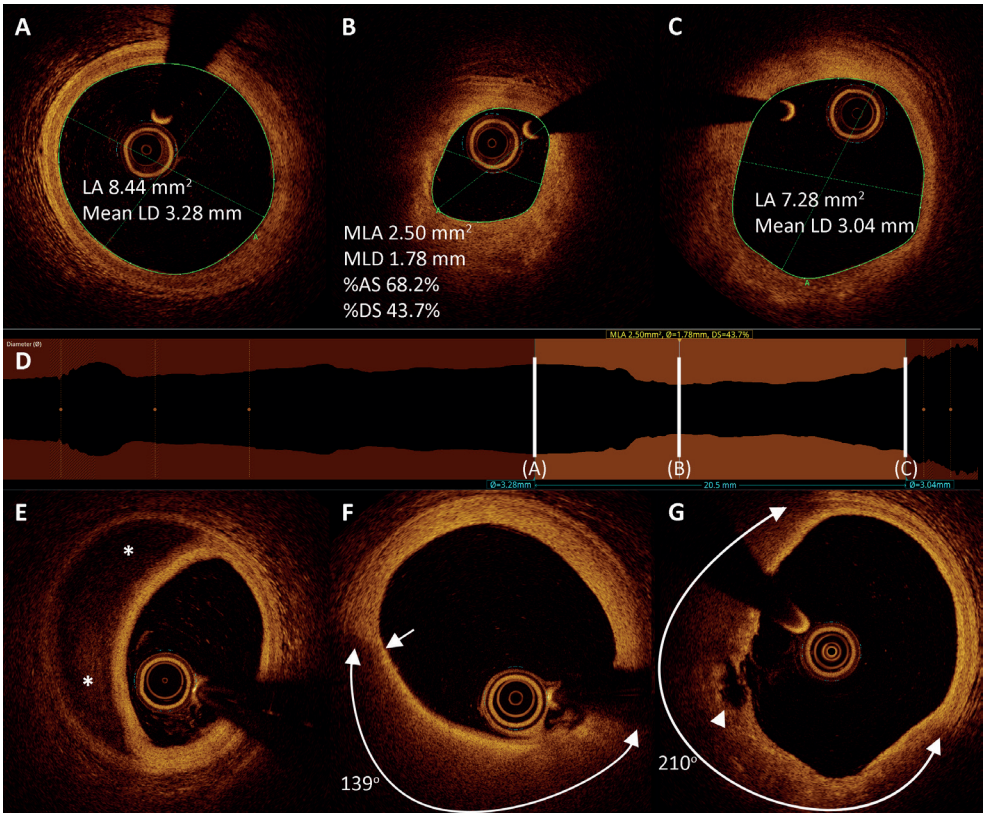


Figure 1. OCT for anatomical measurements and morphological diagnosis.

A-D) OCT acquired images and lumen outline of an atherosclerotic lesion enabling calculation of the degree of stenosis. A) Distal reference site cross-section image shows a healthy coronary segment in which the lumen contour is automatically traced. B) Cross-section at the site of the MLA; the %AS and %DS are calculated as one minus the ratio between the MLA or MLD and the mean of the proximal and distal reference lumen area or diameter, respectively, x100. C) Fibrous lesion at the proximal reference site. D) Longitudinal representation of the mean lumen diameter at each cross-section demonstrates the location of the MLA and the designated reference sites. E) Spontaneous coronary artery dissection with a crescent-shaped false lumen (*). F) Thin-cap fibroatheroma with a lipid arc extending 139 degrees and a fibrous cap thickness <65 µm (arrow). G) Thin-cap fibroatheroma with small plaque rupture (arrowhead).

%AS percentage area stenosis; %DS percentage diameter stenosis; LA lumen area; LD lumen diameter; MLA minimal lumen area; MLD minimal lumen diameter; OCT optical coherence tomography.

OCT-based computational assessment of functional stenosis severity

Several computed flow reserves, based upon OCT-derived dimensions, were developed, in which anatomical information is merged with mathematical fluid dynamic models to estimate the hemodynamic impact of a stenosis.[28-32] In general, a geometrical model needs to be created by delineating and reconstructing lumen contours of the entire OCT pullback. Subsequently, the hemodynamic boundary conditions need to be specified, usually by the estimation of hypothesized hyperemic flow rate. Finally, the fluid dynamics equation are solved on the geometrical model with the hemodynamic boundary conditions to obtain the pressure drop and FFR.[33] The so-called optical flow ratio (OFR), FFROCT, FFR-OCT and virtual flow reserve (VFR), in contrast to FFR, do not require establishment of hyperemia (Figure 2). The correlation of these computed reserves with FFR is stronger than that of single OCT-derived dimensions, with an overall diagnostic accuracy ranging from 86 to 93 percent,[29-32,34] and online mean analysis time of OFR is only 1 minute.[32] Diagnostic accuracy of VFR is currently being investigated in the FUSION trial (NCT04356027). Neither of these indices have been validated against non-invasive ischemia detection. How these indices compare to current pressure-based indices with respect to clinical outcomes in patients with CCS has yet to be determined in clinical trials. Moreover, computed indices are not yet available in current commercial systems and the required lumen area for advancement of the OCT catheter limits assessment of very tight stenoses. Another potential shortcoming of computed flow reserves is that collateral flow is not taken into account, and it is currently unknown to what extent collateral flow influences the accuracy of these indices.

Culprit lesion assessment in myocardial infarction

Conventional angiography is the gold standard for identification of the infarct-related coronary artery in acute myocardial infarction (MI). OCT may aid identification of the culprit lesion in cases with no obvious culprit or in cases with multiple potential culprit segments. Plaque rupture, plaque erosion and calcified nodules are the three major histopathologic substrates which initiate coronary thrombosis.[35] By OCT, plaque rupture (which may be multifocal) is characterized by the presence of a fibroatheroma with a disrupted overlying thin fibrous cap. Plaque erosion is considered definite in presence of intraluminal thrombus overlying a, frequently, fibrotic or fibrolipidic plaque in absence of plaque rupture, or probable in the case of luminal surface irregularity at the culprit lesion in absence of a thrombus or in the presence of a thrombus attenuating the underlying plaque, but without evidence of superficial lipid or calcification at the adjacent frames. It is important to consider that this differs from the histopathologic definition of endothelium denudation and laceration of the superficial intimal layers. However, there is currently no imaging modality that enables *in vivo* identification of a single-cell layer such as the endothelium. Calcified nodules are characterized by an irregular mass with high signal attenuation protruding into the lumen. Plaque rupture and calcified nodules typically result in more severe lumen obstruction than plaque erosion which may therefore be less evident on angiography.[36] Identification of the underlying cause of MI may have potential therapeutic consequences. Whereas plaque rupture and obstructive calcified nodules merit percutaneous revascularization, evidence from the randomized EROSION pilot trial has suggested that some cases of plaque erosion may be successfully managed conservatively with

antithrombotic therapy.[37] Awaiting confirmation in larger prospective trials, this alternative treatment strategy is not to be routinely advocated.

Table 1. Diagnostic performance of OCT-derived dimensions to predict fractional flow reserve significance.

Study	Patients	Lesions	Dimension	AUC	Optical cut-off	Accuracy (%)	Sensitivity (%)	Specificity (%)	PPV (%)	NPV (%)
Burzotta[21]	40	40	MLA, mm^2	0.83	2.5	85	64	93		
			%AS	0.87	70	83	45	97		
Gonzalo[14]	56	61	MLA, mm^2	0.74	1.95	72	82	63	66	80
			MLD, mm	0.73	1.34	73	82	67	68	81
			%AS	0.61	70	57	61	55	53	62
Lee[23]	330	365	MLA, mm^2	0.713	2.3	67.0	70.9	61.6	73.6	57.9
			%AS	0.687	65.0	62.6	67.3	55.6	69.8	52.6
Pawlowski[16]	48	71	MLA, mm^2	0.91	2.05	87	75	90	70.6	92.6
			MLD, mm	0.90	1.28	87	71	84	68.5	90.6
Pyxaras[18]	36	55	MLA, mm^2	0.78	2.88	72	73	71		
			MLD, mm	0.80	1.59	78	78	79		
Reith[17]	46	62	MLA, mm^2	0.813	1.59	77.4	75.8	79.3	80.6	74.2
			MLD, mm	0.816	1.31	80.6	87.9	72.4	78.4	84.0
			%AS	0.807	70.6	72.4	75.8	72.4	75.8	72.4
Reith[20]	100	142	MLA, mm^2	0.836	1.64		78.8	75.8	80.8	73.4
			MLD, mm	0.830	1.305		86.3	69.4	78.4	79.6
			%AS	0.794	71.1		77.5	69.4	76.5	70.5
Rivero[24]	41	41	MLA, mm^2	0.70	1.92	73	84	63	67	82
			MLD, mm	0.71	1.29	61	81	67	63	80
Shiono[15]	59	62	MLA, mm^2*	0.901	1.91	85.4	93.5	77.4	80.6	92.3
			MLD, mm*							
			%AS*	0.917	1.35	85.5	90.3	80.6	84.4	84.6
				0.940	70.0	90.3	96.8	83.9	85.7	96.3
Usui[22]	186	203	MLA, mm^2*	0.732	1.39	69.0	69.0	68.9	54.4	80.5
			MLA, mm^2							
				0.718	1.56	67.5	67.1	68.3	82.5	48.3
Zafar[19]	30	41	MLA, mm^2	0.80	1.62		70	97	89	91
			MLD, mm	0.76	1.23		70	87	64	90
Weighted mean	972	1,143	MLA, mm^2	0.77	1.99	72.1	73.8	70.9	76.8	67.0
	416	535	MLD, mm	0.82	1.33	78.7	81.9	74.9	73.8	81.8
	631	732	%AS	0.74	67.8	67.3	70.8	64.3	71.7	62.8

%AS percentage area stenosis; AUC area under the curve; MLA minimal lumen area; MLD minimal lumen diameter; PPV positive predictive value; NPV negative predictive value.

** Fractional flow reserve <0.75.*

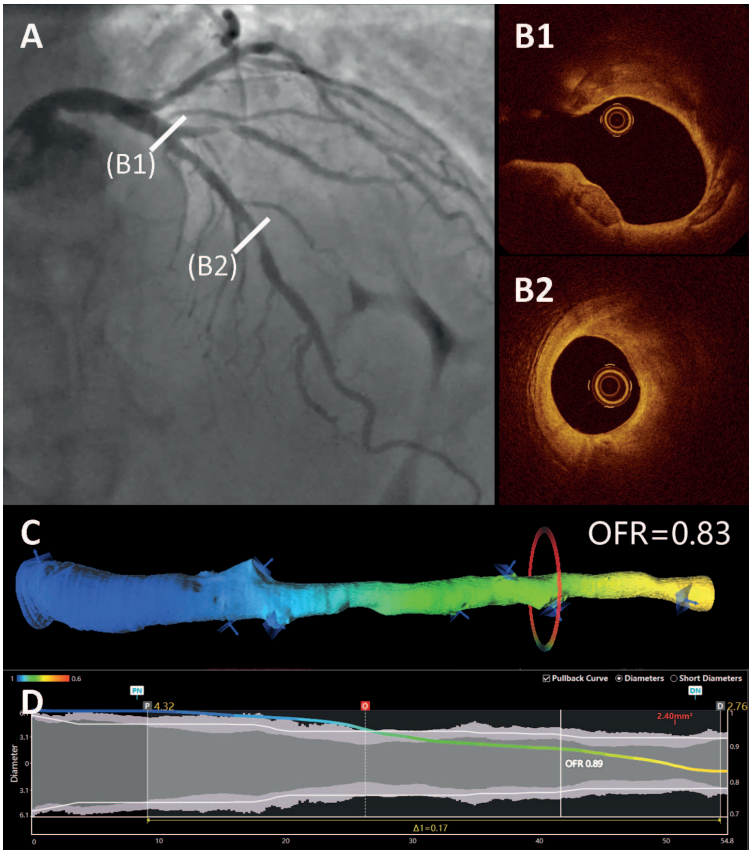


Figure 2. Illustrative case of the calculation of optical flow ratio.

A) Coronary angiogram demonstrating diffuse lesions in the left anterior descending artery. B) Optical coherence tomography-acquired cross-sections of the target left anterior descending artery. C) 3D-reconstruction of the imaged vessel with a superimposed color-coded representation of the computed OFR, which measures 0.83 at the distal end of the imaged coronary segment (right-hand side). D) Visualization of the mean diameter (gray outline) and the decline in OFR (colored line) over the length of the imaged coronary segment.

OFR optical flow ratio.

Spontaneous coronary artery dissection (SCAD) is another cause of MI that is being recognized with increasing frequency. Rupture of the intimal layer and intramural microvessel rupture have been offered as potential causes of SCAD. SCAD may present angiographically as a long spiral dissection, but in other cases may appear as a focal coronary dissection or haziness or may be although inapparent. Although guidewire passage and contrast injections are not recommended if angiography clearly shows SCAD, in less clear cases OCT can definitively diagnose SCAD. By OCT, SCAD appears as a crescent-shaped false lumen narrowing the true coronary lumen by external compression. Rupture of the intimal layer is further visualized as a flap-like structure with sometimes fenestrated passages to the true lumen, whereas microvessel rupture results in the occurrence of an intramural hematoma (Figure 1E).[38]

Non-culprit lesion assessment in myocardial infarction

Half of patients presenting with acute MI have angiographically evident residual coronary stenoses other than the infarct-related lesion.[39] In spite of favorable outcome after angiography-guided or FFR-guided complete revascularization compared to treatment of the culprit lesion only,[40-45] FFR-guided deferral of nonculprit lesions in patients with ACS is associated with higher rates of MACE than in CCS, mainly driven by recurrent MIs and target vessel revascularization.[46] FFR underestimation of lesion significance due to a temporary increase of microvascular resistance or a blunted response of the coronary vasculature to hyperemia-inducing agents in the acute MI setting may be responsible for this phenomenon. Conversely, iFR tends to overestimate hemodynamic significance of borderline lesions in ACS.[47] Perhaps more importantly, non-flow-limiting lesions with high-risk plaque characteristics (vulnerable plaques) are not detected by pressure-based indices. In patients with ACS, additional revascularization of nonculprit lesions aims at decreasing future acute coronary events, rather than relieve symptoms of stable angina. Therefore, OCT-guidance of PCI may be especially advantageous in patients with acute or recent MI since it not only informs on anatomic (and possibly functional) stenosis severity but also on high-risk plaque characteristics.

Vulnerable atherosclerotic plaques identified by optical coherence tomography

From histopathological studies, the plaque characteristics associated with an increased risk of plaque rupture include a large lipid-rich necrotic core, macrophage infiltration, and arguably most importantly a thin fibrous cap.[48] In the PROSPECT study, a lipid plaque burden ≥70%, a MLA ≤4.0 mm^2 and a fibroatheroma with a radiofrequency IVUS-defined fibrous cap thickness of <150 µm (the axial resolution of IVUS) were independently predictive of future MACE.[49] However, in post-mortem studies the mean cap thickness of ruptured plaques was 23±19 µm and 95% of ruptured plaques contained a cap <64 µm.[50] Based on these observations, a thin cap fibroatheroma (TCFA) has been defined as an atherosclerotic plaque containing a lipid-rich necrotic core with >90° arc with a thin overlying fibrous cap (<65 µm). High axial resolution is essential for *in vivo* measurement of a truly thin fibrous cap (Figure 1F-G) and only OCT affords sufficient capability.

In the prospective COMBINE (OCT-FFR) study, presence of a TCFA with median fibrous cap thickness of 60 µm was strongly associated with future target-lesion related MACE in 483 patients with diabetes mellitus and coronary lesions of intermediate stenosis: 13.3% of patients with TCFA experienced a target-lesion related MACE at 1.5-year follow-up compared with 3.1% of patients without TCFA (p<0.00001). As for the individual endpoints, the incidences of target-vessel MI, clinically-driven target lesion revascularization and hospitalization for unstable or progressive angina were significantly higher in patients with TCFA.[51] Similarly, Kubo et al. demonstrated that TCFAs with a fibrous cap thickness of <65 µm and a lipid arc of >180° in a non-culprit coronary artery markedly increased the risk of a future ACS at the lesion level (hazard ratio 19.14 [95%-CI 11.74-31.20]) in 1378 patients, mostly presenting with ACS. However, the prevalence of this combination was low.[52] Finally, in the CLIMA study, OCT was performed in untreated proximal left anterior descending artery (LAD) of 1003 patients, 53% of whom had ACS. A high-risk plaque, defined as the presence of MLA <3.5 mm^2, fibrous cap thickness <75 µm, a lipid

arc circumference of >180° and macrophages was associated with a greatly increased risk of cardiac death or target LAD segment MI (hazard ratio 7.54 [95%-CI 3.1-18.6]).[53] The currently ongoing PECTUS-obs study (NCT03857971) is assessing the relation between TCFA and future MACE in MI patients with FFR-negative non-culprit lesions.[54] Most of these studies comprise a population at high risk for future events and with a relative high prevalence of vulnerable plaques, both of which are critical for achieving substantial predictive value on the occurrence of future events. Yet, specificity of OCT-identified high-risk features remained low in all these studies. Moreover, certain histopathological features (i.e. foam cells, hemosiderin accumulation or microcalcifications at the luminal surface or an organized thrombus) as well as imaging artifacts (i.e. tangential signal drop-off) might mimic the OCT characteristics of TCFA, with consequent false-positive findings.[55,56] Also, higher cut-off values for the fibrous cap thickness for *in vivo* TCFA detection have been proposed to account for post-mortem fixation artifacts.[57] Ninety-five percent of ruptured plaques had a minimum cap thickness <80 µm when assessed *in-vivo* by OCT, whilst the most discriminating cut-off value was a fibrous cap thickness of 67 µm.[58] However, this study was performed with an occlusive balloon technique to obtain blood clearance, whereas in current practice, this is obtained by constant contrast infusion. Nevertheless, OCT-identified TCFA correlates to non-invasive high risk features, such as those identified on coronary computed tomographic angiography.[59,60]

OCT-guided treatment of vulnerable plaques

Considering the association between vulnerable plaques and the occurrence of MACE, preemptive or "preventive" stenting of vulnerable plaques may improve clinical outcomes. In the PROSPECT ABSORB trial, 182 patients with STEMI and NSTEMI with nonobstructive non-flow-limiting non-culprit lesions and plaque burden ≥65% as assessed by IVUS-near infrared spectroscopy (NIRS) were randomized to implantation of a bioresorbable vascular scaffold (BVS) and GDMT versus GDMT alone. Routine follow-up angiography at 25 months demonstrated that the MLA in the BVS-treated lesions was more than twice as large as that of GDMT alone-treated lesions. Although underpowered for clinical endpoints, the study demonstrated a trend towards fewer randomized lesion-related MACE in the BVS group when compared to the GDMT-alone group (4.3 vs 1.7%, p=0.12), mainly driven by progressive angina requiring revascularization.[61] Whether OCT might serve the same purpose is currently unknown considering the paucity of data regarding this subject. The PECTUS trial sought to investigate whether preemptive stenting of OCT-identified vulnerable plaques (i.e. ≥2 of the following characteristics: lipid arc >90°, fibrous cap thickness <65 µm, plaque rupture or thrombus formation) with Absorb BVS in addition to optimal medical therapy (OMT) results in reduced MACE compared to OMT only. This study was terminated prematurely due to retraction of Absorb from the market, at which timepoint 6.8% of patients were included, with no meaningful analyzable data.[62] The currently ongoing PREVENT trial (NCT02316886) is the largest upcoming study addressing this subject. This study will assess whether preventive stenting of vulnerable plaques plus OMT results in favorable clinical outcome compared to OMT only in 1600 patient with ACS or CCS. OCT, IVUS and NIRS are used to assess plaque vulnerability and results for each individual imaging modality will be assessed in sub-analyses.

The effect of intensified medical treatment on vulnerable plaques was studied in several OCT studies, demonstrating that the mean fibrous cap thickness increases and the lipid arc decreases after a period of intensified statin therapy.[63] Recently, the HUYGENS trial demonstrated a similar effect of PCSK9-inhibitors.[64] Therefore, presence of vulnerable plaques might be useful for guidance of intensified medical therapy. However, randomized trials on such strategy, powered for clinical outcomes, are currently lacking.

OCT GUIDANCE OF STENT IMPLANTATION

Initial PCI strategy and choice of stent size

Once the indication for revascularization is established, procedural strategy, including lesion preparation, stent sizing (length and diameter) and determining the stent deployment site can be optimized by OCT-guidance. First, OCT enables distinguishing superficial from deep calcification and assessment of calcification thickness. This information can be used to guide lesion preparation, including use of atherectomy, lithotripsy or cutting/scoring balloons. An OCT-based scoring system was developed to identify those lesions that would potentially benefit from lesion advanced preparation before stent implantation (i.e. lesions with a maximal calcium angle >180°, maximum calcium thickness >0.5 mm and a calcium length >5 mm).[65] Second, stent landing zones can be determined by identifying healthy or fibrous reference zones, avoiding lipidic plaques and TCFAs in particular.[66] Moreover, the appropriate stent diameter can be determined by measurements at the corresponding reference segments. In the prospective ILUMIEN I study, OCT guidance led to an alteration in treatment strategy in 55% of patients and 57% of lesions, including the adoption of a different stent length (25% decreased and 43% increased) and a different stent diameter (31% decreased and 8% increased).[67]

Compared to IVUS-guided treatment, OCT was found to result in the usage of smaller stent diameters both in the previously mentioned registry as well as the OPINION trial,[68,69] although other studies demonstrated no difference in the adopted stent diameters with OCT vs IVUS.[70,71] Use of stents with smaller diameters may lead to higher event rates considering that the achieved minimal stent area (MSA) is the strongest predictor of long-term outcomes.[72] There are several possible reasons for the differences in the stent size after OCT and IVUS. First, OCT-acquired measurements of luminal dimensions are smaller than for IVUS.[11-13] Second, criteria for stent sizing in IVUS are mainly based upon the measurement of the external elastic membrane (EEM), which defines the outer edge of the medial layer of the vascular wall. Although OCT visualizes the reference segment EEM in healthy reference segments and in many fibrous plaques, light attenuation by lipid inhibits EEM assessment in many plaques.[70] As a result, luminal measurements were often used for OCT guidance. To overcome this limitation, three new guidance strategies have been proposed, all resulting in the adoption of equally sized stents and the achievement of similar MSA. In the ILUMIEN III: OPTIMIZE PCI trial, stent sizing was primarily based on the EEM diameter of the reference sites (rounded down to the nearest 0.25 mm). Luminal measurements were only used when both proximal and distal EEM were not visible over an arc of at least 180° degrees. Importantly, sufficient visibility of the EEM

was common and did not differ between OCT and IVUS.[73] In the iSIGHT trial, a similar EEM-based algorithm was applied, with the addition that vessel tapering was also taken into account and the largest mean EEM of the reference sites was used.[74] The other proposed strategy from the MISTIC-1 trial includes the addition of 10% or 0.25 mm to the mean reference lumen diameter.[75] However, a subanalysis of the ILUMIEN III: OPTIMIZE PCI trial demonstrated that applying a correction factor to luminal measurements results in discordance in stent sizing in over half of patients and stent oversizing in 41% of cases.[76] In consequence, OCT-guided stent sizing should be based upon the EEM dimensions whilst luminal measurements should only be used on the occasion that the EEM visibility is insufficient.

Optimization after stent placement

Small MSA (often due to stent underexpansion, possibly with malapposition), edge dissections and residual untreated edge stenoses are the predominant characteristics of suboptimal stent implantation. OCT outperforms both angiography and IVUS for the detection of these findings (Figure 3). [11,12,66,71,73,77-79] Notably, a striking difference was demonstrated between the number of suboptimal stent characteristics identified by site operators and a dedicated core laboratory, stressing the necessity for automated detection algorithms.[67] Nonetheless, it is unclear to what degree minor features contributed to this discrepancy, and many features that are visible exclusively by OCT may be minor and often resolve without clinical sequelae.[66,80] On the other hand, OCT-identified major edge dissections and stent underexpansion in particular are more prevalent in patients with stent thrombosis.[81,82] Also, OCT-identified suboptimal stent deployment, and particularly a lower MSA, presence of distal edge dissections and reference lumen narrowing, was related to increased 1-year MACE in the CLI-OPCI II study (hazard ratio 3.53 [95%-CI 2.2-5.8]). In this study, proximal edge dissections were not found to be predictive of adverse outcome, nor was malapposition,[83] which is inconsistent with other studies reporting an association between malapposition and both early and late stent thrombosis.[82,84] Although the clinical impact of malapposition remains debated, presence of major malapposition justifies iterative treatment, especially when combined with other signs of suboptimal stent implantation.

Procedural outcome of routine OCT-guided PCI

QCA and OCT-derived lumen and stent measurements were comparable after OCT-guided and IVUS-guided stent sizing in the MISTIC-1 trial directly after intervention and 8 months thereafter, as was the percentage of patients with optimal stent implantation. However, in-segment MLA at follow-up was numerically larger in the OCT treated arm (4.33 vs. 3.71 mm^2, p=0.18).[75] In the randomized iSIGHT trial, OCT guidance was superior to angiography guidance and non-inferior to IVUS-guided stent sizing with respect to stent expansion. Although designed as a non-inferiority trial, a trend towards better stent expansion with OCT guidance compared to IVUS guidance was demonstrated. Accordingly, the percentage of patients with optimal stent expansion (≥90%) was higher in the OCT-arm compared to both other arms.[74]

OCT-guided stent optimization increases final MLA by approximately 10%,[79,85] decreases major malapposition by about 50% and decreases stent underexpansion and edge dissection from about 30%

and 10%, respectively, to 0%.[67] Three randomized trials have compared OCT to angiography alone for stent optimization. The %AS was lower and the total stent and lumen volume were larger after OCT-guided stent optimization with trends towards larger MLA at follow-up. The percentage of malapposed stent struts immediately after PCI and the percentage of uncovered struts at follow-up were lower in the OCT-guided group.[86-88]

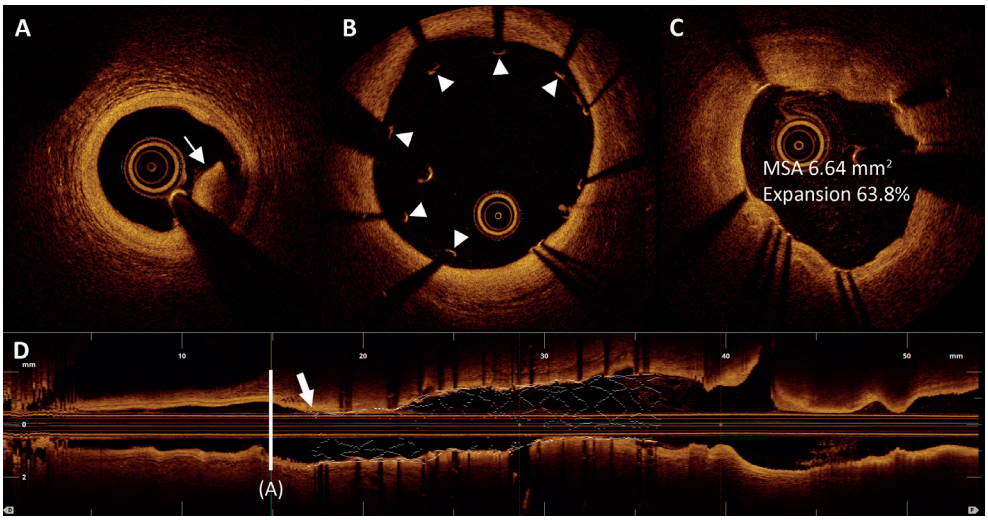


Figure 3. Characteristics of suboptimal stent implantation.

A) Optical coherence tomography-acquired cross sectional image with a major stent edge dissection (>200 µm) (arrow) within 5 mm of the stent edge (bold arrow in D, the longitudinal display of the vessel). B) Stent malapposition in another patient is visible as a clear separation of the stent struts and the luminal surface (>200 µm) (arrowheads). C) Cross sectional image of another patient showing stent underexpansion, defined as a MSA that is <90% of the mean proximal and distal reference lumen areas, which were 12.54 mm^2 and 8.26 mm^2 respectively in the represented case. *MSA minimal stent area.*

Some studies have incorporated the use of OCT for both stent guidance and stent optimization. In a small randomized trial, OCT-guided PCI was found to result in higher residual stenosis and smaller MSA as compared to IVUS-guided PCI.[70] However, a more recent propensity-matched study demonstrated that stent expansion was comparable between both groups, although absolute MSA, measured by the modality that guided the procedure, was larger in the IVUS-guided treatment group.[77] In the randomized ILUMIEN-III: OPTIMIZE PCI trial, final post-interventional MSA was similar following OCT-guided and IVUS-guided PCI, with both trending higher than angiography-guided PCI.[73] A retrospective observational study as well as the DETECT-OCT trial demonstrated larger luminal dimensions following OCT-guided PCI compared with angiography.[89,90] OCT-guidance was also found to result in higher post-procedural FFR values compared to angiography in the randomized DOCTORS trial (0.94±0.04 vs 0.92±0.05, p=0.005), which was accompanied by a smaller residual stenosis. Likewise, 82.5% of patients in the OCT-guided arm had FFR >0.90 compared to 64.2% in the other group.[79]

Synthesizing the available evidence to date, OCT-guided PCI seems to be non-inferior to IVUS-guided PCI with respect to acute post-procedural MSA and stent expansion but results in larger luminal dimensions than with angiography guidance. Furthermore, the findings suggest potential benefit of OCT guidance compared to angiography with respect to post-procedural blood flow. OCT guidance also results in the lowest rates of stent malapposition and untreated edge dissections, and the amount of uncovered stent struts at follow-up is lower after OCT-guided PCI (Table 2).

Table 2. Stent-related outcomes of routine OCT-guided stent placement.

			Outcome			
Study	**Patients**	**Endpoint**	**OCT**	**IVUS**	**Angiography**	**Main conclusion**
Acute						
DETECT-OCT[89]	894	MLD, mm* %DS*	2.84 ± 0.42 9.9 ± 7.1		2.75 ± 0.44† 10.9 ± 7.6	Fewer malapposed struts are seen postprocedural after OCT-guided PCI
DOCTORS[79]	240	MLD, mm* %DS* FFR	2.89 ± 0.40 7.0 ± 4.3 0.94 ± 0.04		2.90 ± 0.42 8.7 ± 6.3† 0.92 ± 0.05†	FFR is significantly higher after OCT-guided PCI
Khalifa[90]	390	MLD, mm* %DS* %AS*	2.55 ± 0.35 14 ± 4 15 ± 5		2.13 ± 0.50† 24 ± 10† 35 ± 17†	OCT-guided PCI results in favorable acute stent related outcome
Kim[87]	117	MLD,mm*	2.68 ± 0.52		2.78 ± 0.44	Similar post-procedural MLD is reached in both groups
OCTACS[86]	100	MSA, mm^2 MLA, mm^2 Malapposed struts, %	6.0 ± 1.6 6.0 ± 1.5 3.4 (0.3-7.6)		5.5 ± 2.0 5.6 ± 1.8 7.8 (2.3-19.4)†	Fewer malapposed struts are seen postprocedural after OCT-guided PCI
Habara[70]	70	Focal stent expansion, %‡ Diffuse stent expansion, %‡ MSA, mm^2	64.7 ± 13.7 84.2 ± 15.8 5.7 ± 2.1	80.3 ± 13.4† 98.8 ± 16.5† 6.9 ± 2.4†		Both focal and diffuse stent expansion is higher after IVUS-guided revascularization
ILUMIEN II[77]	572	Stent expansion, % MSA, mm^2 MLA, mm^2	72.8 (63.3-81.3) 5.0 (3.9-6.4) 5.0 (4.0-6.3)	70.6 (62.3-78.8) 5.5 (4.4-7.0)†‡ 5.5 (4.4-6.9)†‡		Post-procedural stent expansion is comparable after OCT- and IVUS-guided PCI
MISTIC-1[75]	109	MSA, mm^2 MLA, mm^2 Malapposed struts, %	6.24 (4.62-7.70) 4.57 (3.13-5.86) 3.5 (1.2-6.8)	6.50 (5.09-8.37) 4.21 (3.49-5.48) 3.4 (1.2-6.3)		The acute in-segment MLA is similar in both groups
OPINION[68]	829	In stent MLD, mm* In segment MLD, mm* In stent %DS* In segment %DS*	2.57 ± 0.43 2.25 ± 0.53 11 ± 6 22 ± 10	2.61 ± 0.46 2.27 ± 0.52 10 ± 6 22 ± 9		Acute procedural stent-related outcome is comparable

Table 2. Continued

iSIGHT[74]	151	Stent expansion, %	98.01 ± 16.14	91.69 ± 15.75	90.53 ± 14.84†	OCT-guidance is superior to angiography and non-inferior to IVUS with respect to stent expansion
		Stent expansion ≥90%, %	74.5	49.0†	50.9†	
		MSA, mm^2	7.18 ± 2.66	6.97 ± 2.09	7.26 ± 2.48	
		MLA, mm^2	6.93 ± 2.52	6.89 ± 2.01	7.24 ± 2.44	
		Malapposed struts, %	1.59 ± 2.14	3.07 ± 3.92†	4.14 ± 6.92†	
		Edge dissections, %	15.7	11.7	18.9	
ILUMIEN III: OPTIMIZE PCI[73,91]	450	Stent expansion, %	105.8 (97.8-119.8)	106.3 (96.7-116.6)	101.4 (91.9-110.2)†	MSA after OCT-directed stent guidance is non-inferior to IVUS- and not superior to angiography-guided stent implantation
		MSA, mm^2	5.79 (4.54-7.34)	5.89 (4.67-7.80)	5.49 (4.39-6.59)	
		Malapposition, %	41	39	59†	
		Edge dissections, %	28	40†	44†	
Follow-up						
DETECT-OCT[89]	894	MLD, mm*	2.77 ± 0.45		2.67 ± 0.46†	Fewer uncovered struts at 3 months are seen after OCT-guided PCI
		%DS*	10.9 ± 8.7		11.6 ± 8.2	
		Uncovered struts, %	7.5 (2.9-17.4)		9.9 (3.8-21.7)†	
		Malapposed struts, %	0.0 (0.0-2.4)		0.6 (0.0-5.1)†	
		MLD, mm*	2.77 ± 0.45		2.67 ± 0.46†	
Kala[88]	201	MLA, mm^2	6.67 ± 2.21		6.13 ± 2.25	Similar stent outcome was seen at 9 months follow-up
		MLD, mm	2.87 ± 0.50		2.75 ± 0.53	
		%AS	6.21 ± 23.44		17.84 ± 21.08†	
		Uncovered struts, %	12.78 ± 13.01		16.79 ± 15.80	
		Malapposed struts, %	0.82 ± 2.85		0.82 ± 1.43	
Kim[87]	117	MSA, mm^2	6.57 ± 1.96		6.61 ± 2.27	Fewer uncovered struts at 6 months are seen after OCT-guided PCI
		MLD, mm*	2.68 ± 0.52		2.78 ± 0.44	
		Uncovered struts, %	1.60 ± 1.84		4.51 ± 5.43†	
		Malapposed struts, %	0.19 ± 0.51		0.98 ± 2.53†	
OCTACS[86]	100	MSA, mm^2	6.2 ± 1.6		5.7 ± 1.9	Fewer uncovered struts at 6 months are seen after OCT-guided PCI
		MLA, mm^2	5.4 ±1.7		5.1 ± 2.2	
		Uncovered struts, %	4.3 (1.2-9.8)		9.0 (5.5-14.5)†	
		Malapposed struts, %	0.0 (0.0-0.8)		0.0 (0.0-14.8)	
OPINION*[68]	829	In stent MLD, mm*	2.39 ± 0.51		2.45 ± 0.51	Similar stent outcome was seen at 8 months follow-up
		In segment MLD, mm*	2.16 ± 0.56		2.17 ± 0.55	
		In stent %DS*	16 ± 11		15 ± 9	
		In segment %DS*	24 ± 13		24 ± 12	
MISTIC-1[75]	109	MSA, mm^2	6.06 (4.35-7.70)	6.28 (4.77-8.13)		At 8 months follow-up, the in-segment MLA is similar in both groups
		MLA, mm^2	4.33 (2.95-5.50)	3.71 (2.89-5.21)		
		Uncovered struts, %	0.0 (0.0-1.4)	0.0 (0.0-1.5)		
		Malapposed struts, %	0.0 (0.0-0.0)	0.0 (0.0-0.6)		

%AS percentage area stenosis; %DS percentage diameter stenosis; FFR fractional flow reserve; IVUS intravascular ultrasound; MLA minimal lumen area; MLD minimal lumen diameter; MSA minimal stent area; OCT optical coherence tomography; PCI percutaneous coronary intervention; RCT randomized controlled trial.

** Measured by quantitative coronary angiography.*

† Significant difference compared with OCT.

‡ Measured by IVUS.

Clinical outcome following routine OCT-guided PCI

The aforementioned MISTIC-1 trial, in which OCT was solely used for stent sizing, showed no differences in all-cause mortality, MI and revascularization after 3 years follow-up compared with IVUS-guided stent sizing.[75] Similarly, no differences in clinical endpoints were observed in the iSIGHT trial.[74] It should be noted though that both trials were clearly underpowered for clinical endpoints.

The first evidence of improved clinical outcome following OCT-guided stent optimization originated from a retrospective study in which OCT and angiography for stent optimization were examined in 670 patients. In this study, short term outcomes were similar, but after 12 months follow-up the risk of cardiac death or MI was significantly lower in the OCT-guided group. No differences in stent thrombosis or target lesion revascularization were demonstrated.[78] In a prospective registry comparing angiography, OCT-guided and IVUS-guided stenting, unadjusted and adjusted all-cause mortality rates were significantly higher after angiography-guided PCI after a median follow-up of 4.8 years. No difference in outcomes between OCT and IVUS guidance was found in an adjusted model. Of course, this registry is limited by the potential of bias considering its observational design.[69] No difference in clinical outcome was found in any of the three randomized trials comparing OCT to angiography; however these studies included only a limited number of patients in each trial.[86-88]

In the ILUMIEN III: OPTIMIZE PCI trial, no differences were seen in the acute procedural, 30-day[73] and 1 year MACE rates between OCT, IVUS and angiography guidance for both stent placement and optimization.[91] Also in the DOCTORS trial, no difference in MACE was demonstrated after 6 months between OCT and angiography. However, overall event rates in this trial were low with only 1 event (0.8%) in each group.[79] Notably, both studies were underpowered for clinical endpoints. In the sufficiently powered OPINION trial, 12-month target vessel failure (TVF) was demonstrated in 5.2% of patients after OCT-guided compared to 4.9% after IVUS-guided PCI (p=0.042 for non-inferiority).[68] Last, in a recent retrospective study, conducted by the same investigators, MACE rates were lower at 1-year follow-up in the OCT-guided PCI group compared to angiography.[90] These two studies were performed in Japan where intracoronary imaging is widely adopted. As a consequence, generalizability to other populations is difficult.

In summary, retrospective studies demonstrate that outcome following OCT-guided PCI may be favorable compared to an angiography-guided strategy, and OCT-guided PCI is non-inferior to IVUS-guided revascularization (Table 3). Numerous ongoing randomized trials will provide additional evidence. The outcomes of OCT-guided stent sizing using the ILUMIEN III EEM-based reference segment approach and stent optimization compared with angiography guidance is being tested in the ongoing 2500-patient ILUMIEN-IV: OPTIMAL PCI randomized trial (NCT03507777). Patients with high-risk clinical and/or high-risk angiographic characteristics are included. The primary endpoints are postprocedural MSA and TVF at 2-years follow-up. A similarly designed but smaller study (n=550), the COCOA trial (NCT03176810), is powered to assess MSA. Stent optimization based upon OCT findings in the angiography-guided treatment arm is allowed after assessment of the primary outcome,[92] enabling evaluation of OCT-guided stent implantation as regards clinical outcome. The OCTIVUS trial (NCT03394079) is assessing the non-inferiority of OCT guidance compared to IVUS in 2000 randomized patients. The primary endpoint is TVF at 1-year follow-up.[93]

Table 3. Clinical outcome of routine OCT-guided stent placement.

Study	Patients	Follow-up	Endpoint	Outcome			Main conclusion
				OCT	IVUS	Angiography	
CLI-OPCI[78]	670	12 months	MI, %	5.4		8.7	Lower 12-month risk of the composite of cardiac death or non-fatal MI was demonstrated after OCT-guided PCI
			TLR, %	3.3		3.3	
			Cardiac death, %	1.2		4.5*	
			Cardiac death or MI, %	6.6		13.0*	
			All-cause mortality, %	3.3		6.9*	
DOCTORS†[79]	240	6 months	MACE, %	2.5		1.6	Composite of death, MI and TVR is similar after six months of follow-up
			MI, %	0.8		0.8	
			TVR, %	1.6		0.8	
			All-cause mortality, %	0.8		0.0	
Kala†[88]	201	9 months	MACE, %	3		1	
			MI, %	1		0	
			TLR, %	2		1	
			All-cause mortality, %	0		0	
Khalifa[90]	390	1 year	MACE, %	5		12*	1-year MACE is lower after OCT-guided PCI
			MI, %	1		3	
			TLR, %	1		2	
			Cardiac death, %	3		6	
Kim†[87]	117	1 year	MACE, %	3.4		5.1	MACE at 1 -year follow-up is comparable
			TLR, %	3.4		3.4	
OCTACS†[86]	100	6 months	MACE, %	0		4	MACE at 6 months was rare in both groups
			Cardiac death, %	0		2	
MISTIC-1†[75]	109	1 year	MI,%	3.7	1.8		1-year clinical outcome is similar, as were outcome in the second and third year of follow-up
			TLR, %	1.9	5.5		
			Cardiac death, %	1.9	0.0		
			All-cause mortality, %	3.7	3.6		
OPINION[68]	829	12 months	TVF, %	5.2	4.9		TVF at 12 months is comparable
			MACE, %	2.9	3.5		
			MI, %	0.5	0.7		
			TVR, %	4.9	4.2		
			TLR, %	2.7	3.0		
ILUMIEN III: OPTIMIZE PCI†[73, 91]	450	30 days	MACE, %	3	1	1	30-day and 1-year MACE are comparable between all three groups
			MI, %	1	1	0	
			TLR, %	1	0	1	
		1 year	All-cause mortality, %	0	0	0	
			MACE, %	9.8	9.1	7.9	
			MI, %	2.6	2.2	2.3	
			TLR, %	1.3	2.9	1.4	
			All-cause mortality, %	0	0	0	
iSIGHT†[74]	151	2.5 years	MACE, %	7.8	4.0	6.1	Clinical outcome is similar after a median follow-up of 2.5 years
			TLR, %	1.9	0.0	0.0	
			Cardiac death, %	1.9	0.0	2.0	

Table 3. Continued

Jones	87,166	4.8 years	All-cause mortality, %	7.7	12.2*	15.7*	All-cause mortality is lower after OCT- than after IVUS- or angiography-guided PCI
			All-cause mortality propensity matched, %	9.60 8.96	 10.20	16.80	

FFR fractional flow reserve; IVUS intravascular ultrasound; MACE major adverse cardiovascular events; MI myocardial infarction; OCT optical coherence tomography; PCI percutaneous coronary intervention; RCT randomized controlled trial; TLR target lesion revascularization; TVF target vessel failure; TVR target vessel revascularization.

** Significant difference compared with OCT.*

† Underpowered to demonstrate clinical endpoints.

Last, previous studies demonstrated that IVUS-guided revascularization is especially advantageous in complex lesions, including long lesions, left main disease, chronic total occlusions (CTO) and bifurcation lesions.[94] Regarding the latter, three-dimensional OCT enables visualization of the implanted stent that can be used to optimize recrossing strategies.[95] Also, OCT guidance in PCI of left main disease was feasible in the pilot LEMON study[96] and non-inferior to IVUS guidance in a retrospective analysis.[97] Additional evaluation of OCT-guided PCI of complex lesions is currently under investigation. The OCTOBER trial is comparing an OCT-guided strategy to an angiography-guided strategy in 1200 patients with complex left main or non-left main bifurcation PCI with respect to 2-year MACE.[98] The OCCUPI trial randomizes 1604 patients to investigate whether OCT-guided PCI of complex lesions is superior to angiography-guidance as regards to 1-year MACE. In addition, the OCT-guided treatment arm will be subdivided into two treatment groups to compare full OCT-guidance to OCT-guided stent optimization only to investigate the additional value of OCT-guided stent implantation. The OPTIMUM trial is comparing three-dimensional OCT to angiography for guidance of bifurcation lesion revascularization in 106 patients. The primary endpoint consists of the percentage of malapposed struts directly after the procedure.[99]

LIMITATIONS OF OPTICAL COHERENCE TOMOGRAPHY

Technical limitations impair the imaging of aorta-ostial lesions and ectatic or tortuous coronary arteries by OCT. Also, OCT has not been studied for guidance of CTO revascularization. Therefore, IVUS may be the preferred modality for these coronary segments and lesions. Moreover, a survey of 1,105 physicians, mainly interventional cardiologists, demonstrated that cost, prolongation of the procedure, lack of training and the absence of established guiding criteria are the principle reasons that OCT is not routinely used.[100] Results from the FORZA trial demonstrate that costs are higher with OCT guidance than with FFR-guided PCI. However, a formal cost-effectiveness analysis comparing OCT to IVUS or angiography has not been performed.[27] Procedural time is indeed increased with approximately 15 minutes, including catheter preparation, setting up the system, image acquisition and image assessment,[67,73,79,85,86] which might be considered acceptable if other limitations were addressed. In this regard, Lee et al. and

Shlofmitz et al. have proposed two similar algorithmic approaches for use of OCT in real-time decision making.[101,102] Also, the MLD-MAX (Morphology, Length, Diameter – Medial dissection, Apposition, Xpansion) workflow is being used with increasing frequency. (Semi-)automated OCT interpretation might further enhance lesion interpretation and spur adoption. Most commercially available systems already contain an automated stent identification and lumen or EEM contour tool. Automated lesion morphology assessment by use of deep machine learning is currently being explored (Figure 4).[103,104]

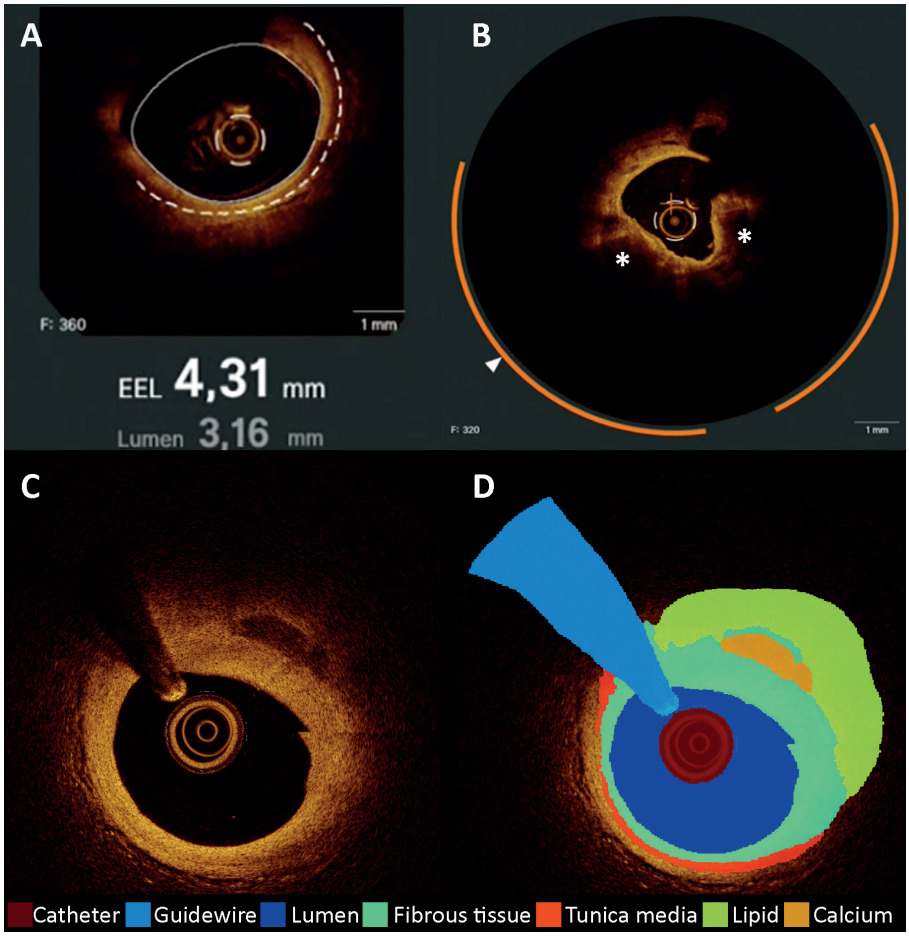


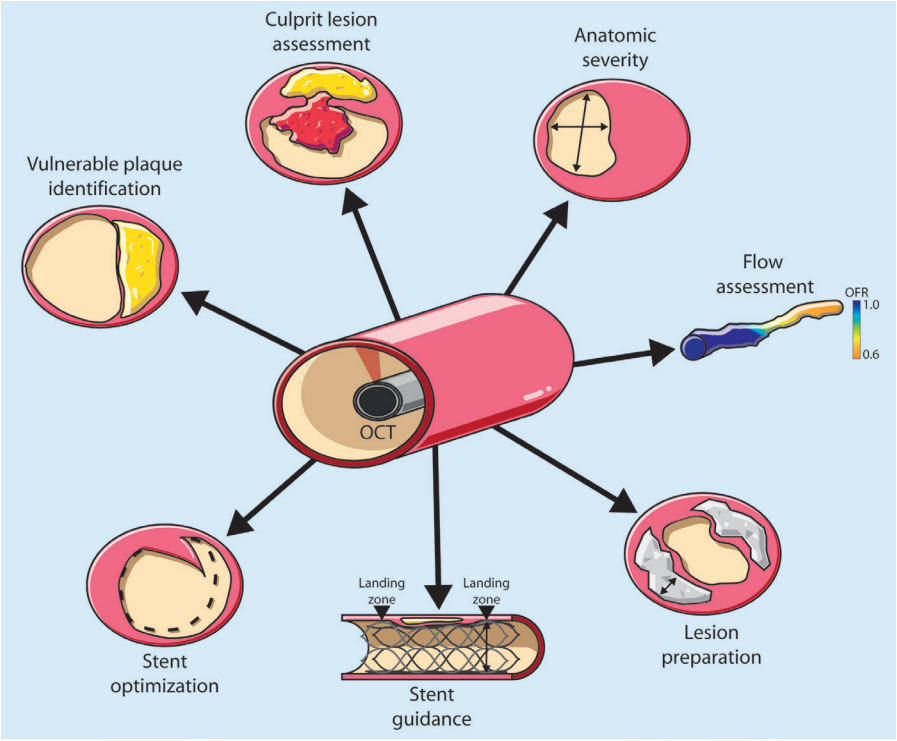
Figure 4. Automated assessment of OCT-acquired images.

A) Automated detection of the lumen contour (continuous line) and external elastic lamina (dashed line). B) Automated detection of the extent of calcifications (*) measured over a total arc of 204 degrees (orange angular lines). C) Cross-sectional reference image. D) The same image as in C following automated lesion characterization.
EEL external elastic lamina.

Another, although limited, concern raised in the aforementioned survey is the risk of complications.[100] First, blood clearance is generally obtained by continuous flushing with ionized contrast agents, with a significant increase in the amount of contrast used,[67,68,73,79] and may therefore be a concern for some physicians in patients with pre-existent kidney disease. Nevertheless, no increased incidence of contrast-induced nephropathy was reported in any of the larger controlled trials.[67,68,73,79] Moreover, other flushing agents, such as saline, have been tested and resulted in similar imaging quality.[105] Temporary side-effects include ventricular ectopic beats (3.3% of patients), transient vessel spasm (1.1%) and transient ST-segment elevation (0.3%).[106,107] Complications of OCT are rare with a combined incidence of 0-5.8%, among which life-threatening ventricular arrhythmias (0- 3.2%), and major coronary dissections (0-1%) are the most frequent.[68,70,73,75,78,106,108]

CONCLUSION

OCT provides information that can be used for lesion selection, procedural planning, stent optimization and assessment of acute procedural success in percutaneous revascularization (Central illustration). The collective findings from numerous observational studies and randomized trials to date support the adoption of OCT for stent guidance and optimization, enabling better stent expansion with fewer edge dissections, malapposition and untreated residual disease compared with angiography-guided PCI, and with higher diagnostic accuracy for the detection of major and minor acute stent complications compared with both IVUS and angiography. OCT also exceeds other imaging modalities for the identification of true TCFA, and evidence for the prognostic implications of these vulnerable plaques is robust. However, definitive data demonstrating improved clinical outcomes of OCT-guided PCI (let alone for preventive vulnerable plaque treatment) are lacking and are pending the results of ongoing and planned large-scale randomized trials. Finally, automated qualitative and quantitative image assessment and OCT-derived physiologic lesion assessment may further improve the ease of use and utility of intravascular OCT imaging and stimulate its routine adoption for daily clinical practice.



Central illustration. OCT as potential future all-in-one tool in percutaneous coronary revascularization.

Potential applications of OCT to guide decision-making processes during percutaneous revascularization procedures. These include identification and assessment of the culprit lesion and vulnerable plaques, assessment of anatomic and functional severity, lesion preparation, guidance of stent implantation and post-implantation stent optimization. *OFR optical flow ration; OCT optical coherence tomography.*

REFERENCES

1. Raber L, Mintz GS, Koskinas KC, Johnson TW, Holm NR, Onuma Y et al. Clinical use of intracoronary imaging. Part 1: guidance and optimization of coronary interventions. An expert consensus document of the European Association of Percutaneous Cardiovascular Interventions. Eur Heart J 2018;39:3281-3300.
2. Yabushita H, Bouma BE, Houser SL, Aretz HT, Jang IK, Schlendorf KH et al. Characterization of human atherosclerosis by optical coherence tomography. Circulation 2002;106:1640-5.
3. Neumann FJ, Sousa-Uva M, Ahlsson A, Alfonso F, Banning AP, Benedetto U et al. 2018 ESC/EACTS Guidelines on myocardial revascularization. Eur Heart J 2019;40:87-165.
4. Johnson TW, Raber L, di Mario C, Bourantas C, Jia H, Mattesini A et al. Clinical use of intracoronary imaging. Part 2: acute coronary syndromes, ambiguous coronary angiography findings, and guiding interventional decision-making: an expert consensus document of the European Association of Percutaneous Cardiovascular Interventions. Eur Heart J 2019;40:2566-2584.
5. Velazquez EJ, Lee KL, Jones RH, Al-Khalidi HR, Hill JA, Panza JA et al. Coronary-Artery Bypass Surgery in Patients with Ischemic Cardiomyopathy. N Engl J Med 2016;374:1511-20.
6. Yusuf S, Zucker D, Peduzzi P, Fisher LD, Takaro T, Kennedy JW et al. Effect of coronary artery bypass graft surgery on survival: overview of 10-year results from randomised trials by the Coronary Artery Bypass Graft Surgery Trialists Collaboration. Lancet 1994;344:563-70.
7. Knuuti J, Wijns W, Saraste A, Capodanno D, Barbato E, Funck-Brentano C et al. 2019 ESC Guidelines for the diagnosis and management of chronic coronary syndromes. Eur Heart J 2020;41:407-477.
8. Pijls NH, van Schaardenburgh P, Manoharan G, Boersma E, Bech JW, van't Veer M et al. Percutaneous coronary intervention of functionally nonsignificant stenosis: 5-year follow-up of the DEFER Study. J Am Coll Cardiol 2007;49:2105-11.
9. Gotberg M, Christiansen EH, Gudmundsdottir IJ, Sandhall L, Danielewicz M, Jakobsen L et al. Instantaneous Wave-free Ratio versus Fractional Flow Reserve to Guide PCI. N Engl J Med 2017;376:1813-1823.
10. Davies JE, Sen S, Dehbi HM, Al-Lamee R, Petraco R, Nijjer SS et al. Use of the Instantaneous Wave-free Ratio or Fractional Flow Reserve in PCI. N Engl J Med 2017;376:1824-1834.
11. Bezerra HG, Attizzani GF, Sirbu V, Musumeci G, Lortkipanidze N, Fujino Y et al. Optical coherence tomography versus intravascular ultrasound to evaluate coronary artery disease and percutaneous coronary intervention. JACC Cardiovasc Interv 2013;6:228-36.
12. Kubo T, Akasaka T, Shite J, Suzuki T, Uemura S, Yu B et al. OCT compared with IVUS in a coronary lesion assessment: the OPUS-CLASS study. JACC Cardiovasc Imaging 2013;6:1095-1104.
13. Kim IC, Nam CW, Cho YK, Park HS, Yoon HJ, Kim H et al. Discrepancy between frequency domain optical coherence tomography and intravascular ultrasound in human coronary arteries and in a phantom in vitro coronary model. Int J Cardiol 2016;221:860-6.
14. Gonzalo N, Escaned J, Alfonso F, Nolte C, Rodriguez V, Jimenez-Quevedo P et al. Morphometric assessment of coronary stenosis relevance with optical coherence tomography: a comparison with fractional flow reserve and intravascular ultrasound. J Am Coll Cardiol 2012;59:1080-9.
15. Shiono Y, Kitabata H, Kubo T, Masuno T, Ohta S, Ozaki Y et al. Optical coherence tomography-derived anatomical criteria for functionally significant coronary stenosis assessed by fractional flow reserve. Circ J 2012;76:2218-25.
16. Pawlowski T, Prati F, Kulawik T, Ficarra E, Bil J, Gil R. Optical coherence tomography criteria for defining functional severity of intermediate lesions: a comparative study with FFR. Int J Cardiovasc Imaging 2013;29:1685-91.

17. Reith S, Battermann S, Jaskolka A, Lehmacher W, Hoffmann R, Marx N, Burgmaier M. Relationship between optical coherence tomography derived intraluminal and intramural criteria and haemodynamic relevance as determined by fractional flow reserve in intermediate coronary stenoses of patients with type 2 diabetes. Heart 2013;99:700-7.

18. Pyxaras SA, Tu S, Barbato E, Barbati G, Di Serafino L, De Vroey F et al. Quantitative angiography and optical coherence tomography for the functional assessment of nonobstructive coronary stenoses: comparison with fractional flow reserve. Am Heart J 2013;166:1010-1018 e1.

19. Zafar H, Ullah I, Dinneen K, Matiullah S, Hanley A, Leahy MJ, Sharif F. Evaluation of hemodynamically severe coronary stenosis as determined by fractional flow reserve with frequency domain optical coherence tomography measured anatomical parameters. J Cardiol 2014;64:19-24.

20. Reith S, Battermann S, Hellmich M, Marx N, Burgmaier M. Correlation between optical coherence tomography-derived intraluminal parameters and fractional flow reserve measurements in intermediate grade coronary lesions: a comparison between diabetic and non-diabetic patients. Clin Res Cardiol 2015;104:59-70.

21. Burzotta F, Nerla R, Hill J, Paraggio L, Leone AM, Byrne J et al. Correlation between frequency-domain optical coherence tomography and fractional flow reserve in angiographically-intermediate coronary lesions. Int J Cardiol 2018;253:55-60.

22. Usui E, Yonetsu T, Kanaji Y, Hoshino M, Yamaguchi M, Hada M et al. Efficacy of Optical Coherence Tomography-derived Morphometric Assessment in Predicting the Physiological Significance of Coronary Stenosis: Head-to-Head Comparison with Intravascular Ultrasound. EuroIntervention 2018;13:e2210-e2218.

23. Lee JM, Choi KH, Koo BK, Zhang J, Han JK, Yang HM et al. Intravascular ultrasound or optical coherence tomography-defined anatomic severity and hemodynamic severity assessed by coronary physiologic indices. Rev Esp Cardiol (Engl Ed) 2020;73:812-821.

24. Rivero F, Antuna P, Garcia-Guimaraes M, Jimenez C, Cuesta J, Bastante T, Alfonso F. Correlation between fractional flow reserve and instantaneous wave-free ratio with morphometric assessment by optical coherence tomography in diabetic patients. Int J Cardiovasc Imaging 2020;36:1193-1201.

25. Ramasamy A, Chen Y, Zanchin T, Jones DA, Rathod K, Jin C et al. Optical coherence tomography enables more accurate detection of functionally significant intermediate non-left main coronary artery stenoses than intravascular ultrasound: A meta-analysis of 6919 patients and 7537 lesions. Int J Cardiol 2020;301:226-234.

26. Koo BK, Yang HM, Doh JH, Choe H, Lee SY, Yoon CH et al. Optimal intravascular ultrasound criteria and their accuracy for defining the functional significance of intermediate coronary stenoses of different locations. JACC Cardiovasc Interv 2011;4:803-11.

27. Burzotta F, Leone AM, Aurigemma C, Zambrano A, Zimbardo G, Arioti M et al. Fractional Flow Reserve or Optical Coherence Tomography to Guide Management of Angiographically Intermediate Coronary Stenosis: A Single-Center Trial. JACC Cardiovasc Interv 2020;13:49-58.

28. Lee KE, Lee SH, Shin ES, Shim EB. A vessel length-based method to compute coronary fractional flow reserve from optical coherence tomography images. Biomed Eng Online 2017;16:83.

29. Ha J, Kim JS, Lim J, Kim G, Lee S, Lee JS et al. Assessing Computational Fractional Flow Reserve From Optical Coherence Tomography in Patients With Intermediate Coronary Stenosis in the Left Anterior Descending Artery. Circ Cardiovasc Interv 2016;9.

30. Jang SJ, Ahn JM, Kim B, Gu JM, Sung HJ, Park SJ, Oh WY. Comparison of Accuracy of One-Use Methods for Calculating Fractional Flow Reserve by Intravascular Optical Coherence Tomography to That Determined by the Pressure-Wire Method. Am J Cardiol 2017;120:1920-1925.

31. Seike F, Uetani T, Nishimura K, Kawakami H, Higashi H, Aono J et al. Intracoronary Optical Coherence Tomography-Derived Virtual Fractional Flow Reserve for the Assessment of Coronary Artery Disease. Am J Cardiol 2017;120:1772-1779.

32. Yu W, Huang J, Jia D, Chen S, Raffel OC, Ding D et al. Diagnostic accuracy of intracoronary optical coherence tomography-derived fractional flow reserve for assessment of coronary stenosis severity. EuroIntervention 2019;15:189-197.

33. Tu S, Westra J, Adjedj J, Ding D, Liang F, Xu B et al. Fractional flow reserve in clinical practice: from wire-based invasive measurement to image-based computation. Eur Heart J 2020;41:3271-3279.

34. Huang J, Emori H, Ding D, Kubo T, Yu W, Huang P et al. Diagnostic performance of intracoronary optical coherence tomography-based versus angiography-based fractional flow reserve for the evaluation of coronary lesions. EuroIntervention 2020;16:568-576.

35. Virmani R, Kolodgie FD, Burke AP, Farb A, Schwartz SM. Lessons from sudden coronary death: a comprehensive morphological classification scheme for atherosclerotic lesions. Arterioscler Thromb Vasc Biol 2000;20:1262-75.

36. Jia H, Abtahian F, Aguirre AD, Lee S, Chia S, Lowe H et al. In vivo diagnosis of plaque erosion and calcified nodule in patients with acute coronary syndrome by intravascular optical coherence tomography. J Am Coll Cardiol 2013;62:1748-58.

37. Xing L, Yamamoto E, Sugiyama T, Jia H, Ma L, Hu S et al. EROSION Study (Effective Anti-Thrombotic Therapy Without Stenting: Intravascular Optical Coherence Tomography-Based Management in Plaque Erosion): A 1-Year Follow-Up Report. Circ Cardiovasc Interv 2017;10.

38. Jackson R, Al-Hussaini A, Joseph S, van Soest G, Wood A, Macaya F et al. Spontaneous Coronary Artery Dissection: Pathophysiological Insights From Optical Coherence Tomography. JACC Cardiovasc Imaging 2019;12:2475-2488.

39. Park DW, Clare RM, Schulte PJ, Pieper KS, Shaw LK, Califf RM et al. Extent, location, and clinical significance of non-infarct-related coronary artery disease among patients with ST-elevation myocardial infarction. JAMA 2014;312:2019-27.

40. Rathod KS, Koganti S, Jain AK, Astroulakis Z, Lim P, Rakhit R et al. Complete Versus Culprit-Only Lesion Intervention in Patients With Acute Coronary Syndromes. J Am Coll Cardiol 2018;72:1989-1999.

41. Wald DS, Morris JK, Wald NJ, Chase AJ, Edwards RJ, Hughes LO et al. Randomized trial of preventive angioplasty in myocardial infarction. N Engl J Med 2013;369:1115-23.

42. Gershlick AH, Khan JN, Kelly DJ, Greenwood JP, Sasikaran T, Curzen N et al. Randomized trial of complete versus lesion-only revascularization in patients undergoing primary percutaneous coronary intervention for STEMI and multivessel disease: the CvLPRIT trial. J Am Coll Cardiol 2015;65:963-72.

43. Mehta SR, Wood DA, Storey RF, Mehran R, Bainey KR, Nguyen H et al. Complete Revascularization with Multivessel PCI for Myocardial Infarction. N Engl J Med 2019;381:1411-1421.

44. Engstrom T, Kelbaek H, Helqvist S, Hofsten DE, Klovgaard L, Holmvang L et al. Complete revascularisation versus treatment of the culprit lesion only in patients with ST-segment elevation myocardial infarction and multivessel disease (DANAMI-3-PRIMULTI): an open-label, randomised controlled trial. Lancet 2015;386:665-71.

45. Smits PC, Abdel-Wahab M, Neumann FJ, Boxma-de Klerk BM, Lunde K, Schotborgh CE et al. Fractional Flow Reserve-Guided Multivessel Angioplasty in Myocardial Infarction. N Engl J Med 2017;376:1234-1244.

46. Liou KP, Ooi SM, Hoole SP, West NEJ. Fractional flow reserve in acute coronary syndrome: a meta-analysis and systematic review. Open Heart 2019;6:e000934.

47. van der Hoeven NW, Janssens GN, de Waard GA, Everaars H, Broyd CJ, Beijnink CWH et al. Temporal Changes in Coronary Hyperemic and Resting Hemodynamic Indices in Nonculprit Vessels of Patients With ST-Segment Elevation Myocardial Infarction. JAMA Cardiol 2019;4:736-744.

48. Virmani R, Burke AP, Farb A, Kolodgie FD. Pathology of the vulnerable plaque. J Am Coll Cardiol 2006;47:C13-8.

49. Stone GW, Maehara A, Lansky AJ, de Bruyne B, Cristea E, Mintz GS et al. A prospective natural-history study of coronary atherosclerosis. N Engl J Med 2011;364:226-35.

50. Burke AP, Farb A, Malcom GT, Liang YH, Smialek J, Virmani R. Coronary risk factors and plaque morphology in men with coronary disease who died suddenly. N Engl J Med 1997;336:1276-82.

51. Kedhi E, Berta B, Roleder T, Hermanides RS, Fabris E, AJJ IJ et al. Thin-cap fibroatheroma predicts clinical events in diabetic patients with normal fractional flow reserve: the COMBINE OCT-FFR trial. Eur Heart J 2021;42:4671-4679.

52. Kubo T, Ino Y, Mintz GS, Shiono Y, Shimamura K, Takahata M et al. Optical coherence tomography detection of vulnerable plaques at high risk of developing acute coronary syndrome. Eur Heart J Cardiovasc Imaging 2021.

53. Prati F, Romagnoli E, Gatto L, La Manna A, Burzotta F, Ozaki Y et al. Relationship between coronary plaque morphology of the left anterior descending artery and 12 months clinical outcome: the CLIMA study. Eur Heart J 2020;41:383-391.

54. Mol JQ, Belkacemi A, Volleberg RH, Meuwissen M, Protopopov AV, Laanmets P et al. Identification of anatomic risk factors for acute coronary events by optical coherence tomography in patients with myocardial infarction and residual nonflow limiting lesions: rationale and design of the PECTUS-obs study. BMJ Open 2021;11:e048994.

55. Fujii K, Hao H, Shibuya M, Imanaka T, Fukunaga M, Miki K et al. Accuracy of OCT, grayscale IVUS, and their combination for the diagnosis of coronary TCFA: an ex vivo validation study. JACC Cardiovasc Imaging 2015;8:451-460.

56. Phipps JE, Hoyt T, Vela D, Wang T, Michalek JE, Buja LM et al. Diagnosis of Thin-Capped Fibroatheromas in Intravascular Optical Coherence Tomography Images: Effects of Light Scattering. Circ Cardiovasc Interv 2016;9.

57. Tearney GJ, Regar E, Akasaka T, Adriaenssens T, Barlis P, Bezerra HG et al. Consensus standards for acquisition, measurement, and reporting of intravascular optical coherence tomography studies: a report from the International Working Group for Intravascular Optical Coherence Tomography Standardization and Validation. J Am Coll Cardiol 2012;59:1058-72.

58. Yonetsu T, Kakuta T, Lee T, Takahashi K, Kawaguchi N, Yamamoto G et al. In vivo critical fibrous cap thickness for rupture-prone coronary plaques assessed by optical coherence tomography. Eur Heart J 2011;32:1251-9.

59. Sato A, Hoshi T, Kakefuda Y, Hiraya D, Watabe H, Kawabe M et al. In vivo evaluation of fibrous cap thickness by optical coherence tomography for positive remodeling and low-attenuation plaques assessed by computed tomography angiography. Int J Cardiol 2015;182:419-25.

60. Nakazato R, Otake H, Konishi A, Iwasaki M, Koo BK, Fukuya H et al. Atherosclerotic plaque characterization by CT angiography for identification of high-risk coronary artery lesions: a comparison to optical coherence tomography. Eur Heart J Cardiovasc Imaging 2015;16:373-9.

61. Stone GW, Maehara A, Ali ZA, Held C, Matsumura M, Kjoller-Hansen L et al. Percutaneous Coronary Intervention for Vulnerable Coronary Atherosclerotic Plaque. J Am Coll Cardiol 2020;76:2289-2301.

62. Mol JQ, Bom MJ, Damman P, Knaapen P, van Royen N. Pre-Emptive OCT-Guided Angioplasty of Vulnerable Intermediate Coronary Lesions: Results from the Prematurely Halted PECTUS-Trial. J Interv Cardiol 2020;2020:8821525.

63. Ozaki Y, Garcia-Garcia HM, Beyene SS, Hideo-Kajita A, Kuku KO, Kolm P, Waksman R. Effect of Statin Therapy on Fibrous Cap Thickness in Coronary Plaque on Optical Coherence Tomography - Review and Meta-Analysis. Circ J 2019;83:1480-1488.

64. Nicholls SJ, Hucko T, Nissen SE, Prati F, Windecker S, Kataoka Y et al. Assessing the Impact of PCSK9 Inhibition on Coronary Plaque Phenotype with Optical Coherence Tomography: Primary results of the HUYGENS Study. Paper presented at: ESC Congress 2021; 2021 August 27-30; Digitally.

65. Fujino A, Mintz GS, Matsumura M, Lee T, Kim SY, Hoshino M et al. A new optical coherence tomography-based calcium scoring system to predict stent underexpansion. EuroIntervention 2018;13:e2182-e2189.

66. Chamie D, Bezerra HG, Attizzani GF, Yamamoto H, Kanaya T, Stefano GT et al. Incidence, predictors, morphological characteristics, and clinical outcomes of stent edge dissections detected by optical coherence tomography. JACC Cardiovasc Interv 2013;6:800-13.

67. Wijns W, Shite J, Jones MR, Lee SW, Price MJ, Fabbiocchi F et al. Optical coherence tomography imaging during percutaneous coronary intervention impacts physician decision-making: ILUMIEN I study. Eur Heart J 2015;36:3346-55.

68. Kubo T, Shinke T, Okamura T, Hibi K, Nakazawa G, Morino Y et al. Optical frequency domain imaging vs. intravascular ultrasound in percutaneous coronary intervention (OPINION trial): one-year angiographic and clinical results. Eur Heart J 2017;38:3139-3147.

69. Jones DA, Rathod KS, Koganti S, Hamshere S, Astroulakis Z, Lim P et al. Angiography Alone Versus Angiography Plus Optical Coherence Tomography to Guide Percutaneous Coronary Intervention: Outcomes From the Pan-London PCI Cohort. JACC Cardiovasc Interv 2018;11:1313-1321.

70. Habara M, Nasu K, Terashima M, Kaneda H, Yokota D, Ko E et al. Impact of frequency-domain optical coherence tomography guidance for optimal coronary stent implantation in comparison with intravascular ultrasound guidance. Circ Cardiovasc Interv 2012;5:193-201.

71. Kim IC, Yoon HJ, Shin ES, Kim MS, Park J, Cho YK et al. Usefulness of Frequency Domain Optical Coherence Tomography Compared with Intravascular Ultrasound as a Guidance for Percutaneous Coronary Intervention. J Interv Cardiol 2016;29:216-24.

72. Soeda T, Uemura S, Park SJ, Jang Y, Lee S, Cho JM et al. Incidence and Clinical Significance of Poststent Optical Coherence Tomography Findings: One-Year Follow-Up Study From a Multicenter Registry. Circulation 2015;132:1020-9.

73. Ali ZA, Maehara A, Genereux P, Shlofmitz RA, Fabbiocchi F, Nazif TM et al. Optical coherence tomography compared with intravascular ultrasound and with angiography to guide coronary stent implantation (ILUMIEN III: OPTIMIZE PCI): a randomised controlled trial. Lancet 2016;388:2618-2628.

74. Chamie D, Costa JR, Jr., Damiani LP, Siqueira D, Braga S, Costa R et al. Optical Coherence Tomography Versus Intravascular Ultrasound and Angiography to Guide Percutaneous Coronary Interventions: The iSIGHT Randomized Trial. Circ Cardiovasc Interv 2021;14:e009452.

75. Muramatsu T, Ozaki Y, Nanasato M, Ishikawa M, Nagasaka R, Ohota M et al. Comparison Between Optical Frequency Domain Imaging and Intravascular Ultrasound for Percutaneous Coronary Intervention Guidance in Biolimus A9-Eluting Stent Implantation: A Randomized MISTIC-1 Non-Inferiority Trial. Circ Cardiovasc Interv 2020;13:e009314.

76. Shlofmitz E, Jeremias A, Parviz Y, Karimi Galougahi K, Redfors B, Petrossian G et al. External elastic lamina vs. luminal diameter measurement for determining stent diameter by optical coherence tomography: an ILUMIEN III substudy. Eur Heart J Cardiovasc Imaging 2021;22:753-759.

77. Maehara A, Ben-Yehuda O, Ali Z, Wijns W, Bezerra HG, Shite J et al. Comparison of Stent Expansion Guided by Optical Coherence Tomography Versus Intravascular Ultrasound: The ILUMIEN II Study (Observational Study of Optical Coherence Tomography [OCT] in Patients Undergoing Fractional Flow Reserve [FFR] and Percutaneous Coronary Intervention). JACC Cardiovasc Interv 2015;8:1704-14.

78. Prati F, Di Vito L, Biondi-Zoccai G, Occhipinti M, La Manna A, Tamburino C et al. Angiography alone versus angiography plus optical coherence tomography to guide decision-making during percutaneous coronary intervention: the Centro per la Lotta contro l'Infarto-Optimisation of Percutaneous Coronary Intervention (CLI-OPCI) study. EuroIntervention 2012;8:823-9.

79. Meneveau N, Souteyrand G, Motreff P, Caussin C, Amabile N, Ohlmann P et al. Optical Coherence Tomography to Optimize Results of Percutaneous Coronary Intervention in Patients with Non-ST-Elevation Acute Coronary Syndrome: Results of the Multicenter, Randomized DOCTORS Study (Does Optical Coherence Tomography Optimize Results of Stenting). Circulation 2016;134:906-17.

80. Kume T, Okura H, Miyamoto Y, Yamada R, Saito K, Tamada T et al. Natural history of stent edge dissection, tissue protrusion and incomplete stent apposition detectable only on optical coherence tomography after stent implantation - preliminary observation. Circ J 2012;76:698-703.

81. Prati F, Kodama T, Romagnoli E, Gatto L, Di Vito L, Ramazzotti V et al. Suboptimal stent deployment is associated with subacute stent thrombosis: optical coherence tomography insights from a multicenter matched study. From the CLI Foundation investigators: the CLI-THRO study. Am Heart J 2015;169:249-56.

82. Adriaenssens T, Joner M, Godschalk TC, Malik N, Alfonso F, Xhepa E et al. Optical Coherence Tomography Findings in Patients With Coronary Stent Thrombosis: A Report of the PRESTIGE Consortium (Prevention of Late Stent Thrombosis by an Interdisciplinary Global European Effort). Circulation 2017;136:1007-1021.

83. Prati F, Romagnoli E, Burzotta F, Limbruno U, Gatto L, La Manna A et al. Clinical Impact of OCT Findings During PCI: The CLI-OPCI II Study. JACC Cardiovasc Imaging 2015;8:1297-305.

84. Guagliumi G, Sirbu V, Musumeci G, Gerber R, Biondi-Zoccai G, Ikejima H et al. Examination of the in vivo mechanisms of late drug-eluting stent thrombosis: findings from optical coherence tomography and intravascular ultrasound imaging. JACC Cardiovasc Interv 2012;5:12-20.

85. Viceconte N, Chan PH, Barrero EA, Ghilencea L, Lindsay A, Foin N, Di Mario C. Frequency domain optical coherence tomography for guidance of coronary stenting. Int J Cardiol 2013;166:722-8.

86. Antonsen L, Thayssen P, Maehara A, Hansen HS, Junker A, Veien KT et al. Optical Coherence Tomography Guided Percutaneous Coronary Intervention With Nobori Stent Implantation in Patients With Non-ST-Segment-Elevation Myocardial Infarction (OCTACS) Trial: Difference in Strut Coverage and Dynamic Malapposition Patterns at 6 Months. Circ Cardiovasc Interv 2015;8:e002446.

87. Kim JS, Shin DH, Kim BK, Ko YG, Choi D, Jang Y, Hong MK. Randomized comparison of stent strut coverage following angiography- or optical coherence tomography-guided percutaneous coronary intervention. Rev Esp Cardiol (Engl Ed) 2015;68:190-7.

88. Kala P, Cervinka P, Jakl M, Kanovsky J, Kupec A, Spacek R et al. OCT guidance during stent implantation in primary PCI: A randomized multicenter study with nine months of optical coherence tomography follow-up. Int J Cardiol 2018;250:98-103.

89. Lee SY, Kim JS, Yoon HJ, Hur SH, Lee SG, Kim JW et al. Early Strut Coverage in Patients Receiving Drug-Eluting Stents and its Implications for Dual Antiplatelet Therapy: A Randomized Trial. JACC Cardiovasc Imaging 2018;11:1810-1819.

90. Khalifa AKM, Kubo T, Shimamura K, Ino Y, Kishk YT, Hasan-Ali H et al. Impact of Optical Coherence Tomography Imaging on Decision-Making During Percutaneous Coronary Intervention in Patients Presented With Acute Coronary Syndromes. Circ J 2021;85:1781-1788.

91. Ali ZA, Karimi Galougahi K, Maehara A, Shlofmitz RA, Fabbiocchi F, Guagliumi G et al. Outcomes of optical coherence tomography compared with intravascular ultrasound and with angiography to guide coronary stent implantation: one-year results from the ILUMIEN III: OPTIMIZE PCI trial. EuroIntervention 2021;16:1085-1091.

92. Kubo T, Shinke T, Okamura T, Hibi K, Nakazawa G, Morino Y et al. Comparison between Optical COherence tomography guidance and Angiography guidance in percutaneous coronary intervention (COCOA): Study protocol for a randomized controlled trial. J Cardiol 2018;72:170-175.

93. Kang DY, Ahn JM, Park H, Lee PH, Kang SJ, Lee SW et al. Comparison of optical coherence tomography-guided versus intravascular ultrasound-guided percutaneous coronary intervention: Rationale and design of a randomized, controlled OCTIVUS trial. Am Heart J 2020;228:72-80.

94. Zhang YJ, Pang S, Chen XY, Bourantas CV, Pan DR, Dong SJ et al. Comparison of intravascular ultrasound guided versus angiography guided drug eluting stent implantation: a systematic review and meta-analysis. BMC Cardiovasc Disord 2015;15:153.

95. Nagoshi R, Okamura T, Murasato Y, Fujimura T, Yamawaki M, Ono S et al. Feasibility and usefulness of three-dimensional optical coherence tomography guidance for optimal side branch treatment in coronary bifurcation stenting. Int J Cardiol 2018;250:270-274.

96. Amabile N, Range G, Souteyrand G, Godin M, Boussaada MM, Meneveau N et al. Optical coherence tomography to guide percutaneous coronary intervention of the left main coronary artery: the LEMON study. EuroIntervention 2021;17:e124-e131.

97. Miura K, Tada T, Shimada T, Ohya M, Murai R, Kubo S et al. Three-dimensional optical coherence tomography versus intravascular ultrasound in percutaneous coronary intervention for the left main coronary artery. Heart Vessels 2021;36:630-637.

98. Holm NR, Andreasen LN, Walsh S, Kajander OA, Witt N, Eek C et al. Rational and design of the European randomized Optical Coherence Tomography Optimized Bifurcation Event Reduction Trial (OCTOBER). Am Heart J 2018;205:97-109.

99. Miyazaki Y, Muramatsu T, Asano T, Katagiri Y, Sotomi Y, Nakatani S et al. Online three-dimensional OFDI-guided versus angiography-guided PCI in bifurcation lesions: design and rationale of the randomised OPTIMUM trial. EuroIntervention 2021;16:1333-1341.

100. Koskinas KC, Nakamura M, Raber L, Colleran R, Kadota K, Capodanno D et al. Current use of intracoronary imaging in interventional practice - Results of a European Association of Percutaneous Cardiovascular Interventions (EAPCI) and Japanese Association of Cardiovascular Interventions and Therapeutics (CVIT) Clinical Practice Survey. EuroIntervention 2018;14:e475-e484.

101. Lee CH, Hur SH. Optimization of Percutaneous Coronary Intervention Using Optical Coherence Tomography. Korean Circ J 2019;49:771-793.

102. Shlofmitz E, Ali ZA, Maehara A, Mintz GS, Shlofmitz R, Jeremias A. Intravascular Imaging-Guided Percutaneous Coronary Intervention: A Universal Approach for Optimization of Stent Implantation. Circ Cardiovasc Interv 2020;13:e008686.

103. Min HS, Yoo JH, Kang SJ, Lee JG, Cho H, Lee PH et al. Detection of optical coherence tomography-defined thin-cap fibroatheroma in the coronary artery using deep learning. EuroIntervention 2020;16:404-412.

104. Chu M, Jia H, Gutierrez-Chico JL, Maehara A, Ali ZA, Zeng X et al. Artificial intelligence and optical coherence tomography for the automatic characterisation of human atherosclerotic plaques. EuroIntervention 2021;17:41-50.

105. Gore AK, Shlofmitz E, Karimi Galougahi K, Petrossian G, Jeremias A, Sosa FA et al. Prospective Comparison Between Saline and Radiocontrast for Intracoronary Imaging With Optical Coherence Tomography. JACC Cardiovasc Imaging 2020;13:2060-2062.

106. Imola F, Mallus MT, Ramazzotti V, Manzoli A, Pappalardo A, Di Giorgio A et al. Safety and feasibility of frequency domain optical coherence tomography to guide decision making in percutaneous coronary intervention. EuroIntervention 2010;6:575-81.

107. van der Sijde JN, Karanasos A, van Ditzhuijzen NS, Okamura T, van Geuns RJ, Valgimigli M et al. Safety of optical coherence tomography in daily practice: a comparison with intravascular ultrasound. Eur Heart J Cardiovasc Imaging 2017;18:467-474.

108. Leistner DM, Riedel M, Steinbeck L, Stahli BE, Frohlich GM, Lauten A et al. Real-time optical coherence tomography coregistration with angiography in percutaneous coronary intervention-impact on physician decision-making: The OPTICO-integration study. Catheter Cardiovasc Interv 2018;92:30-37.

SUPPLEMENTAL MATERIAL

Supplemental material related to this article can be found in the online version:
https://www.sciencedirect.com/science/article/pii/S1050173821001249



CHAPTER 3

Combining optical coherence tomography and fractional flow reserve for decision making in percutaneous coronary intervention: insights from the FUSION study

Rick Volleberg* | Doosup Shin* | Richard Shlofmitz | Aziz Maksoud | Bassem Chebab | Kanitha Phalakornkule | Jana Buccola | Nutte Tarn Teraphongphom | Ajay Gopinath | Ashley Netravali | Ziad Ali | Allen Jeremias

Journal of the Society for Cardiovascular Angiography & Interventions
2025 Oct 7;4(11):104001

* joined first authorship

ABSTRACT

Background Physiological indices and intracoronary imaging provide additional and complementary information to coronary angiography, which may enhance procedural decision making during percutaneous coronary intervention (PCI). This study aimed to evaluate the impact of fractional flow reserve (FFR) and optical coherence tomography (OCT) on revascularization decision making and PCI strategy compared with angiography guidance alone.

Methods In this secondary analysis from the prospective, observational FUSION (Validation of OCT-Based Functional Diagnosis of Coronary Stenosis) study, the impact of angiography, OCT, and FFR on procedural decision making was evaluated by comparing the intended treatment strategy after each step to the actual treatment strategy, which was left to the operator's discretion and was guided by the totality of diagnostic testing.

Results Among 224 patients (mean age, 67.4 ± 9.2 years; 30.8% women), 116 (51.8%) underwent coronary revascularization, while it was deferred in 108 (48.2%). Compared with the actual treatment strategy, the rate of intended revascularization was significantly higher when guided by angiography (62.5% vs 51.8%; P = .002) or OCT (66.5% vs 51.8%; P < .001), but similar when guided by FFR (53.6% vs 51.8%; P = .34). Among lesions undergoing PCI with available strategy information (n = 83), the intended stent size differed from the actual implanted stent size in 59.0% of cases based on angiography, compared with 12.1% of cases based on OCT findings (P < .001).

Conclusions FFR and OCT provide distinct yet complementary information that significantly impacts decision making during PCI. Specifically, FFR informs revascularization decision making, while OCT plays a crucial role in device sizing. Combining anatomical, morphological, and physiological variables in a single modality may enhance decision making and reduce resource utilization

INTRODUCTION

Invasive coronary angiography is the universal modality for guiding percutaneous coronary intervention (PCI) yet has significant limitations. First, angiographic assessment of lesion severity is often subjective, lacks reproducibility, and correlates poorly with downstream ischemia.[1,2] Second, its low-resolution and 2-dimensional lumenography limits accurate evaluation of vessel size and plaque morphology, which are critical for precise device selection.

Various interventional technologies can provide complementary information, overcoming these limitations. Physiological indices, such as fractional flow reserve (FFR), assess the physiological severity of lesions and allow identification of ischemia-causing stenoses. Intravascular imaging (IVI), such as optical coherence tomography (OCT), allows detailed anatomical and morphological lesion evaluation, enabling precise planning and optimization of PCI. Given their distinct yet complementary roles, coronary physiology and imaging play synergistic roles in guiding PCI. This study sought to evaluate their respective impacts on (1) revascularization decision making and (2) PCI strategy compared with angiography guidance alone.

MATERIAL AND METHODS

Study population

This study is a secondary analysis of the multicenter, prospective, observational FUSION study (Validation of OCT-Based Functional Diagnosis of Coronary Stenosis; ClinicalTrials.gov, NCT04356027), which evaluated the diagnostic performance of OCT-derived flow reserve (virtual flow reserve [VFR]) compared with pressure wire-derived FFR. The study design and primary results were reported previously.[3] Briefly, 312 patients undergoing invasive coronary angiography for stable, unstable, or silent angina, or non-ST segment elevation myocardial infarction with at least 1 intermediate native coronary artery stenosis (diameter stenosis of 40%-90% on visual estimation) underwent both pressure wire-based physiological evaluation and OCT imaging of all target lesions. Culprit lesions in non-ST segment elevation myocardial infarction and lesions requiring predilation were excluded. The study protocol was approved by the institutional review boards or ethics committee of each participating center and was performed in accordance with the Declaration of Helsinki. All patients provided written informed consent.

Study procedures

All patients underwent diagnostic coronary angiography according to local site protocols. Eligible patients subsequently underwent intracoronary OCT imaging and pressure wire-based physiological assessment. The OCT was performed using the Dragonfly OPTIS Imaging Catheter (Abbott Vascular) with a motorized pullback in survey mode, allowing evaluation of all target lesions within the proximal 75 mm of the target vessel. Physiological measurements were obtained using the PressureWire X (Abbott Vascular). After pressure equalization at the guiding catheter and administration of 200 µg of

intracoronary nitroglycerin, the pressure wire was advanced distal to the target lesion. The FFR was then measured following the induction of maximal hyperemia, achieved using either intravenous adenosine (140 µg/kg/min continuous infusion) or intracoronary adenosine (200 µg for the left coronary artery or 100 µg for the right coronary artery). A final drift check was performed after the pressure wire was pulled back to the coronary ostium. Repeat physiological assessment was performed in cases of significant drift (Figure 1).

Intended treatment strategy

This analysis evaluated the impact of angiography, OCT, and FFR on procedural decision making. Following each diagnostic modality, operators documented sequentially whether they intended to proceed with revascularization or defer treatment based on the findings. For cases in which revascularization was planned, the intended PCI strategy—including stent diameter and length—was also recorded after the initial angiographic assessment and after OCT analysis. These intended decisions regarding revascularization and PCI strategy were then compared with the actual treatment performed, which was left to the operator's discretion and was guided by the totality of diagnostic testing. A change in stent size between the intended and the actual stent implanted was defined as an absolute difference of ≥0.25 mm in diameter or ≥4.0 mm in length.

Statistical analyses

Categorical variables are reported as absolute value (percentage), while continuous variables are summarized as mean ± SD or median (IQR), when appropriate. Baseline clinical and procedural characteristics were analyzed using the independent samples Student *t* test, the χ^2 test, Fisher exact test, or Wilcoxon rank-sum test. Paired data on treatment plan and PCI strategy were evaluated using the McNemar test or the 1-sample paired *t* test. Revascularization decision making was evaluated in the complete cohort and for the 3 major coronary arteries separately. A 2-sided P value of <.05 was considered statistically significant. All statistical analyses were performed using SAS version 9.4 (SAS Institute) and R version 4.3.

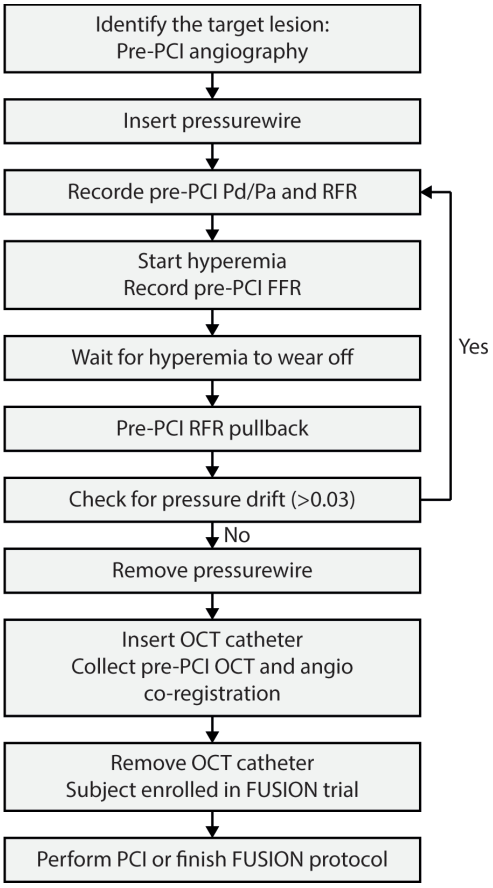


Figure 1. FUSION study protocol.

FFR fractional flow reserve; OCT optical coherence tomography; PCI percutaneous coronary intervention; RFR resting full-cycle ratio.

RESULTS

Study population

After the core laboratory review of the coronary angiogram, physiology assessment and OCT images, a total of 224 patients were included in the study. The mean age of the population was 67.4 ± 9.2 years, and 30.8% of patients were women (Table 1). Stable (48.2%) and unstable angina (37.1%) were the predominant indications for invasive coronary angiography. Revascularization was performed in 116 (51.8%) patients, while it was deferred in 108 (48.2%) patients. Compared with those who did not undergo revascularization, patients who underwent revascularization had lower rates of hypertension (75.9% vs 88.9%; P = .01) and a history of myocardial infarction (9.5% vs 19.4%; P = .03) or PCI in a nontarget vessel (15.5% vs 35.2%; P < .001).

Table 1. Baseline characteristics.

Characteristic	Revascularization N=116	No Revascularization N=108	P-value
Age, yr (mean ± SD)	67 ± 9.6	67.7 ± 8.8	.70
Female	30 (25.9)	39 (36.1)	.10
Hypertension	88 (75.9)	96 (88.9)	.01
Dyslipidemia	92 (79.3)	94 (87.0)	.12
Diabetes	47 (40.5)	34 (31.5)	.16
Renal insufficiency	10 (8.6)	9 (8.33)	.94
Current smoker	20 (17.2)	16 (14.8)	.62
Prior MI in non-target vessel	11 (9.5)	21 (19.4)	.03
Prior PCI in non-target vessel	18 (15.5)	38 (35.2)	<.001
Presentation			.02
Stable angina	60 (51.7)	48 (44.4%	.28
Unstable angina	35 (30.2)	48 (44.4)	.03
Silent ischemia	21 (18.1)	10 (9.3)	.06
NSTEMI	0 (0.0)	2 (1.9)	.14

Values are n (%) unless specified.

MI myocardial infarction; NSTEMI non-ST-segment elevation myocardial infarction; PCI percutaneous coronary intervention.

Target vessel and lesion characteristics

Vessel-level and lesion-level characteristics are summarized in Table 2. Among 226 target vessels, the majority were located in the left anterior descending artery (55.3%). The mean FFR was significantly lower in revascularized vessels compared with those in which revascularization was deferred (0.75 ± 0.10 vs 0.89 ± 0.07; P <.001). Across 228 target lesions, the mean maximal diameter stenosis was 65.7% ± 14.9%. The minimal lumen area was significantly smaller in revascularized lesions compared with deferred lesions (1.81 ± 1.48 vs 3.66 ± 2.88 mm^2; P = .02).

Table 2. Vessel-level and lesion-level characteristics.

Characteristic	Revascularization	No Revascularization	P-value
Vessel-Level	**n = 114**	**n = 112**	
Target vessel			<.001
Left anterior descending	75 (65.8%)	50 (44.6%)	.001
Left circumflex/ramus	26 (22.8%)	27 (24.1%)	.82
Right coronary artery	13 (11.4%)	35 (31.3%)	<.001
Fractional flow reserve	0.75 ± 0.10	0.89 ± 0.07	<.001
Lesion-Level	**n = 114**	**n = 114**	
Lesion length, mm	20.4 ± 8.9	18.3 ± 9.5	.01
Maximal diameter stenosis, %	73.9 ± 12.2	57.5 ± 12.6	<.001
Minimal lumen area, mm^2	1.81 ± 1.48	3.66 ± 2.88	.02

Values are n (%) or mean ± SD.

Treatment decision making based on different modalities

Compared with the actual treatment strategy, revascularization was more frequently intended based on angiographic (62.5% vs 51.8%; P =.002) and OCT (66.5% vs 51.8%; P <.001) findings (Figure 2). The intended revascularization rate based on physiological assessment was similar to the actual treatment performed (53.6% vs 51.8%; P = .34). Subgroup analyses per coronary artery demonstrated consistent results (Supplemental Figure S1).

Operator-determined PCI strategy based on angiography and OCT was available for 83 lesions. In paired comparisons with the actual length and diameter of the stent implanted, the intended stent length and diameter differed significantly more frequently when determined by angiography (59.0%) compared with OCT (12.1%; P < .001) (Figure 3). Specifically, stent length determined by angiography differed from the actual implanted stent length in 41.0% of cases, compared with 2.4% when determined by OCT (P < .001). Similarly, discrepancies in stent diameter occurred in 45.8% by angiography vs 10.8% by OCT (P < .001). Furthermore, the mean absolute differences between intended and actual stent length and diameter were significantly greater for angiography vs OCT guidance (stent length: 4.43 ± 6.2 vs 0.22 ± 0.86 mm, respectively; P < .001; stent diameter 0.18 ± 0.23 vs 0.03 ± 0.10 mm, respectively; P < .001).

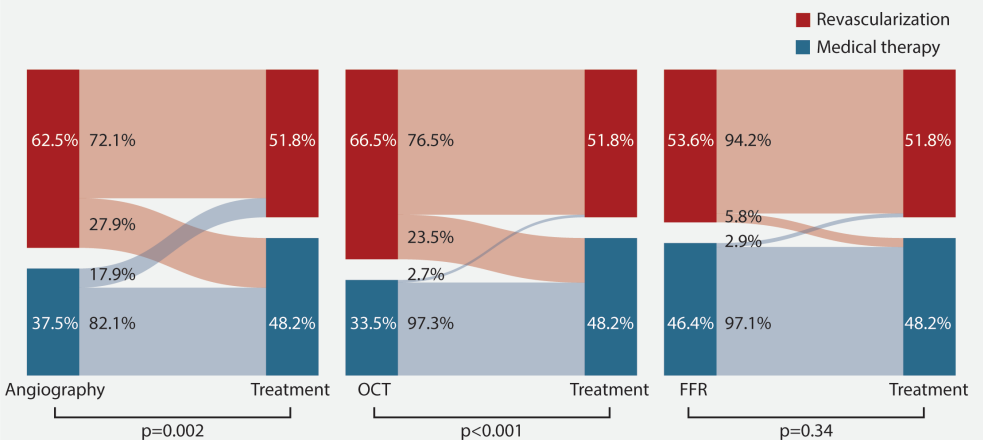


Figure 2. Intended and actual treatment strategies.

FFR fractional flow reserve; OCT optical coherence tomography.

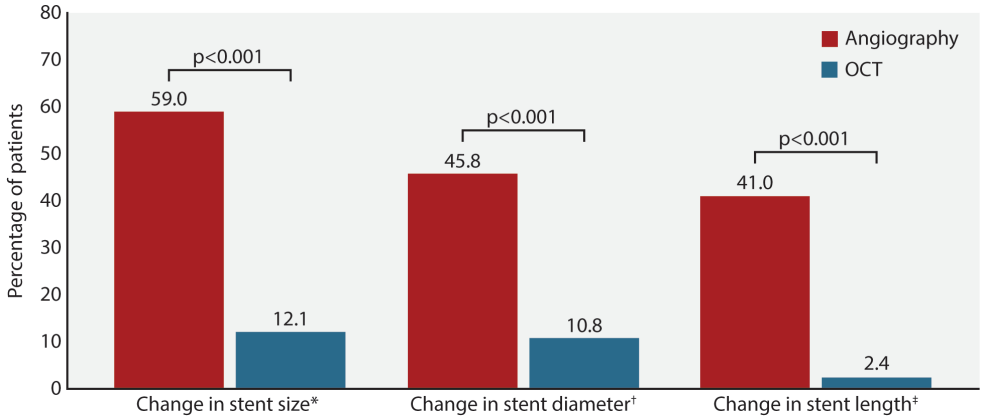


Figure 3. Changes in percutaneous coronary intervention strategy.

OCT optical coherence tomography.

** Defined as an absolute change in stent diameter of ≥0.25 mm and/or stent length of ≥4.0.*

† Defined as an absolute change of ≥0.25 mm.

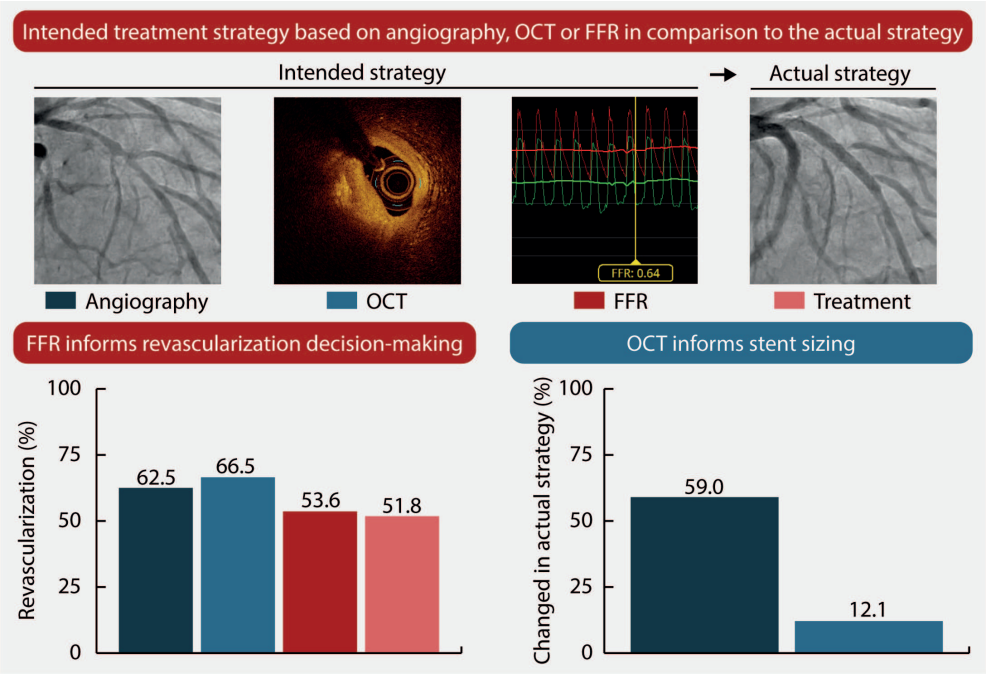
‡ Defined as an absolute change of ≥4.0 mm.

DISCUSSION

This study evaluated the individual impact of various diagnostic modalities in guiding revascularization decisions and PCI strategy. The main findings were as follows: (1) physiological assessment with FFR closely aligned with the final revascularization decisions, whereas angiography and OCT guidance led to significantly higher intended revascularization rates; and (2) OCT played a crucial role in determining

the PCI strategy, frequently prompting adjustments to stent length and diameter beyond angiography alone (Central Illustration).

As expected, this study indicates that the rate of intended revascularization based on angiography or IVI findings was substantially higher than that based on physiology, which ultimately had the greatest influence on the final treatment decision. These findings are consistent with prior randomized trials comparing FFR-guided vs IVI-guided revascularization strategies.[4-6] In the FORZA trial, revascularization was performed in 50.7% in the OCT-guided arm compared with only 29.3% in the FFR-guided group.[4,5] Similarly, in the FLAVOUR (Fractional FLow Reserve And IVUS for Clinical OUtcomes in Patients with InteRmediate Stenosis) trial, intravascular ultrasound guidance resulted in a significantly higher revascularization rate than FFR guidance (65.3% vs 44.4%, respectively).[6] Despite these differences in revascularization rates, both trials demonstrated no significant difference in clinical outcomes between IVI-guided and FFR-guided strategies, leading to substantial increases in resource utilization and cost among patients undergoing IVI-guided PCI.[4,7]



Central illustration. Impact of angiography, OCT, and FFR on periprocedural decision making.

Among patients in whom the intended percutaneous coronary intervention decision making was recorded based on angiographic findings, OCT findings, and FFR findings (upper panel), FFR-guided decision making closely resembled the actual treatment decision, while the intended revascularization rate was higher based on angiographic and OCT findings (left panel). In those undergoing revascularization, the intended stent size based on OCT differed in 12.1% of cases from the final stent size selected, compared with in 59.0% of cases based on angiography (right panel).

FFR fractional flow reserve; OCT optical coherence tomography.

As opposed to these trials, this study evaluated revascularization decisions for the same lesions using multiple modalities, demonstrating that IVI and physiology assessment fundamentally evaluate different procedural aspects and lead to changes in clinical decision making independent of each other. The safety and effectiveness of the FFR-based strategy—characterized by decreased utilization of stents and comparable clinical outcomes—further underscore the value of physiological assessment in guiding revascularization decisions in routine practice.

Not surprisingly, among patients undergoing PCI, the actual strategy on stent diameter and length, more closely aligned with OCT-based assessment rather than with those derived from angiography. Operators ultimately modified the initial angiography-based PCI strategy in approximately 60% of cases, with the final plan reflecting the OCT findings. Although we could not investigate the reasons why the actual stent dimensions differed from the OCT-based dimensions in 12.1% of cases, we hypothesized that this may be caused by operators also including angiographic and physiological findings into the final decision making, likely reflecting clinical judgment in routine practice. Our findings are consistent with early evidence from the ILUMIEN I (Observational Study of Optical Coherence Tomography in Patients Undergoing Fractional Flow Reserve and Percutaneous Coronary Intervention) study, where OCT-guided stent sizing influenced decision making in 57% of lesions compared with angiography.[8] Similarly, in the LightLab initiative, a dedicated pre-PCI OCT workflow altered lesion assessment and procedural planning in 80% of lesions.[9] Furthermore, randomized clinical trials have consistently demonstrated the benefits of IVI-guided PCI over angiography-guided PCI.[10] Collectively, these results underscore the value of OCT in PCI planning, contributing to enhanced procedural safety and efficacy.

Our results overall highlight the complementary roles of FFR and OCT—FFR informs revascularization decision making, while OCT guides PCI strategy. Despite their significant impact on precision PCI, time and resource constraints remain key challenges in routine practice because simultaneous use of pressure wires and imaging catheters is often impractical and cost prohibitive. Recently, it was demonstrated that OCT-based computational flow indices such as VFR allow conversion of anatomical information to physiological information with high accuracy.[3] As a result, anatomical, morphological, and functional information can be obtained with a single OCT pullback, potentially leveraging the strengths of both modalities (Figure 4). This integrated approach enables simultaneous lesion assessment and precise device selection, offering a more streamlined and effective strategy than using either modality alone. However, the clinical utility of VFR has yet to be fully validated in prospective studies.

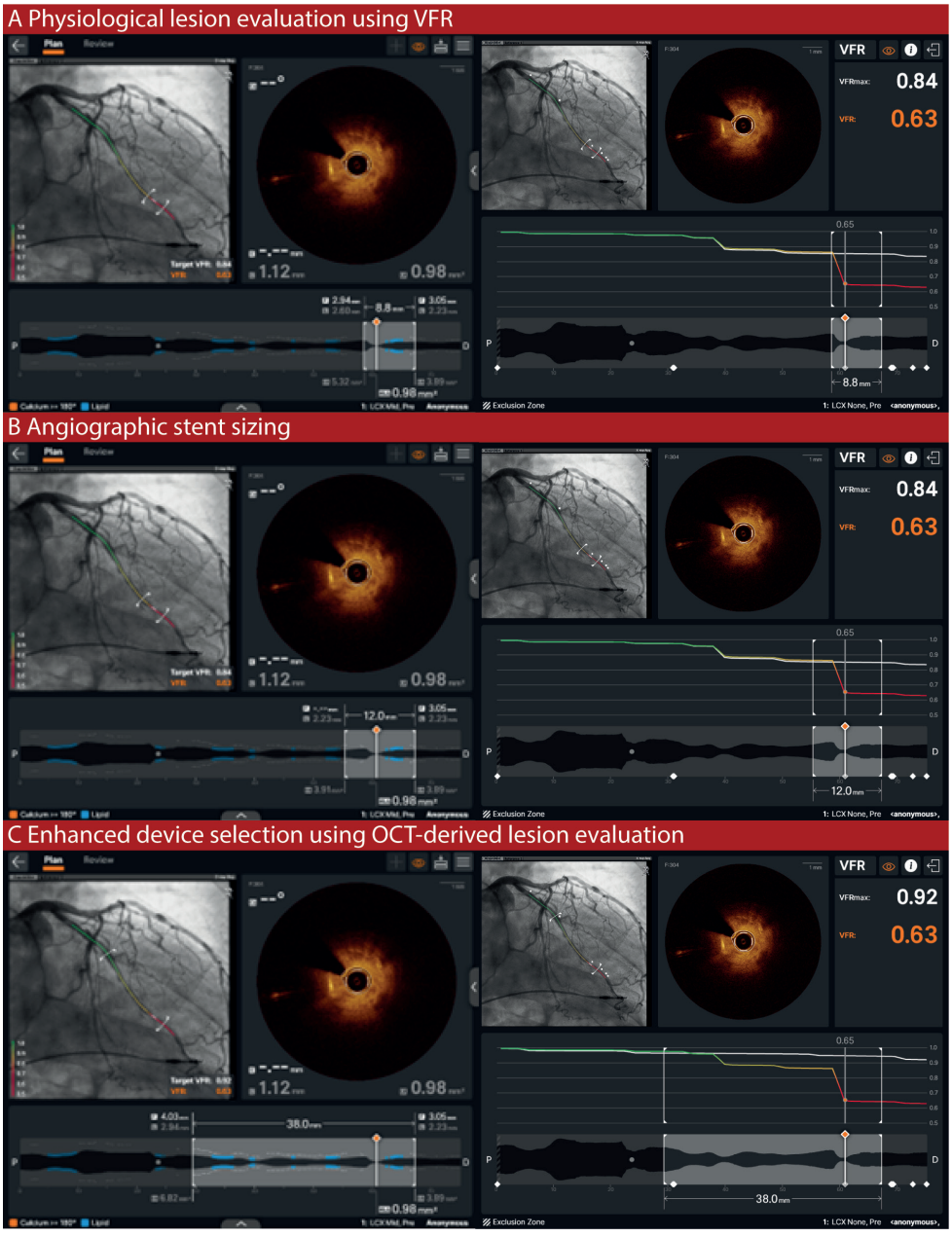


Figure 4. Combined anatomical, morphological, and physiological procedural planning using VFR.

A) The distal VFR was computed at 0.63, which is below the revascularization threshold of ≤0.80. Based on the VFR, the region of interest was identified in the distal LAD artery with a lesion length of 8.8mm. B) Following angiographic stent sizing, the intended stent length was 12.0 mm, which resulted in a maximum anticipated postprocedural VFR of 0.84. C) By combining the physiological information with the OCT imaging data, the stent length was extended to 38.0 mm, resulting in a maximum anticipated postprocedural VFR of 0.92.

LAD left anterior descending; OCT optical coherence tomography; VFR virtual flow reserve.

This study has several limitations. First, the intended PCI strategy based on each individual modality was only available in 72.8% of lesions that were subsequently revascularized. Second, the study predominantly included patients with silent, stable or unstable angina, potentially limiting generalizability to patients with myocardial infarction. Third, evaluations were restricted to the proximal 75-mm segment of each coronary artery, and it remains unclear whether the findings extend to more distal lesions with smaller vessel diameters. Fourth, the actual decisions regarding revascularization and the PCI strategy were left to the discretion of individual operators, and detailed rationales for these decisions were not systematically recorded. Finally, whether differences in revascularization decision making and PCI strategy impacts clinical outcome could not be evaluated in this study.

CONCLUSION

FFR and OCT provide complementary information for decision making on revascularization and PCI strategy. Combining anatomical, morphological, and physiological variables in a single modality may enhance decision making and reduce resource utilization.

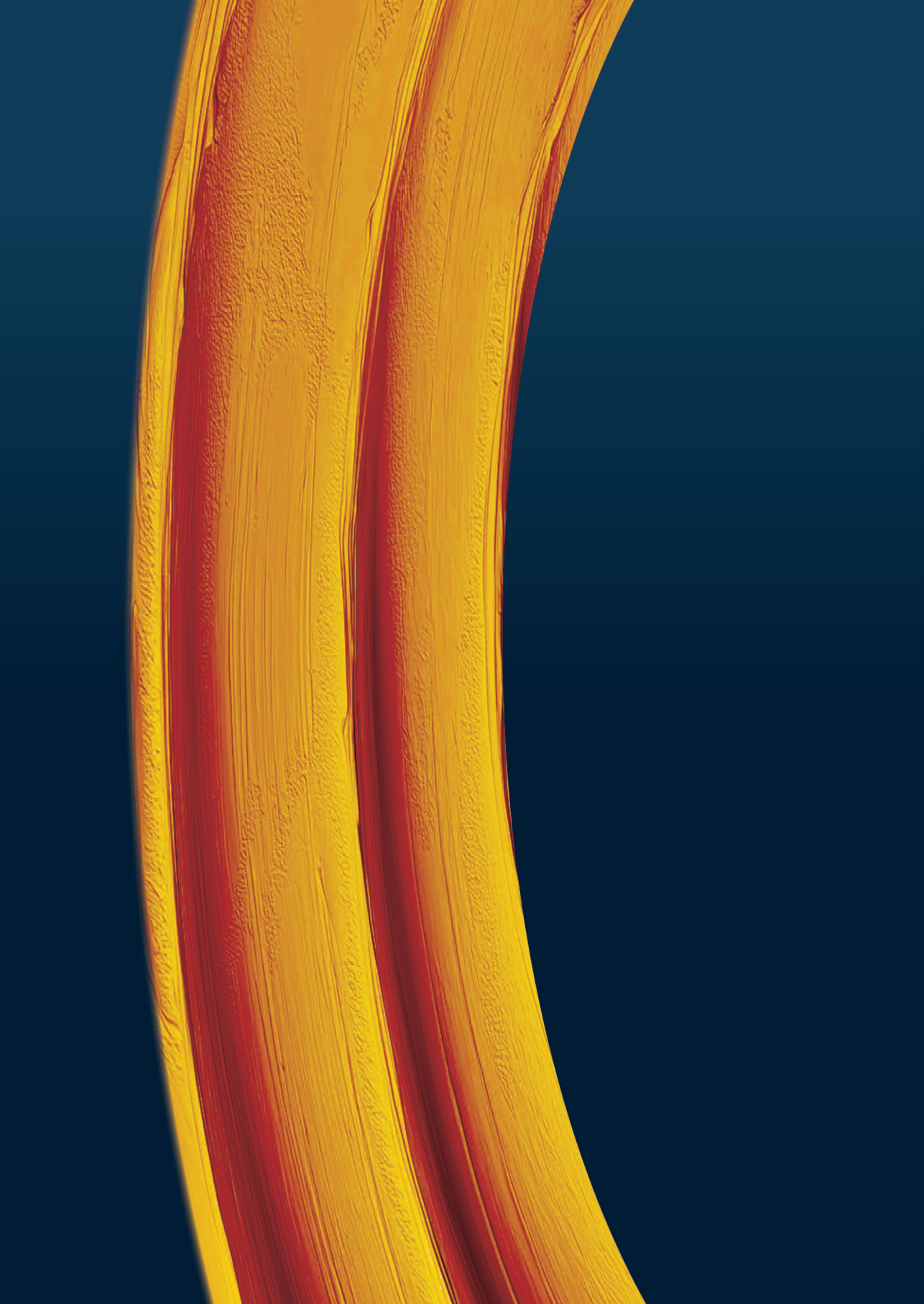
REFERENCES

1. Zir LM, Miller SW, Dinsmore RE, Gilbert JP, Harthorne JW. Interobserver variability in coronary angiography. Circulation 1976;53:627-32.
2. Tonino PA, Fearon WF, De Bruyne B, Oldroyd KG, Leesar MA, Ver Lee PN et al. Angiographic versus functional severity of coronary artery stenoses in the FAME study fractional flow reserve versus angiography in multivessel evaluation. J Am Coll Cardiol 2010;55:2816-21.
3. Jeremias A, Maehara A, Matsumura M, Shlofmitz RA, Maksoud A, Akasaka T et al. Optical Coherence Tomography-Based Functional Stenosis Assessment: FUSION-A Prospective Multicenter Trial. Circ Cardiovasc Interv 2024;17:e013702.
4. Burzotta F, Leone AM, Aurigemma C, Zambrano A, Zimbardo G, Arioti M et al. Fractional Flow Reserve or Optical Coherence Tomography to Guide Management of Angiographically Intermediate Coronary Stenosis: A Single-Center Trial. JACC Cardiovasc Interv 2020;13:49-58.
5. Burzotta F, Zito A, Aurigemma C, Romagnoli E, Bianchini F, Bianchini E et al. Fractional flow reserve or optical coherence tomography for angiographically intermediate coronary stenoses: 5-year outcomes in the FORZA trial. Eur Heart J 2024;45:2785-2788.
6. Koo BK, Hu X, Kang J, Zhang J, Jiang J, Hahn JY et al. Fractional Flow Reserve or Intravascular Ultrasonography to Guide PCI. N Engl J Med 2022;387:779-789.
7. Hwang D, Kim HL, Ko J, Choi H, Jeong H, Jang SA et al. Cost-effectiveness of Fractional Flow Reserve Versus Intravascular Ultrasound to Guide Percutaneous Coronary Intervention: Results From the FLAVOUR Study. Korean Circ J 2025;55:34-46.
8. Wijns W, Shite J, Jones MR, Lee SW, Price MJ, Fabbiocchi F et al. Optical coherence tomography imaging during percutaneous coronary intervention impacts physician decision-making: ILUMIEN I study. Eur Heart J 2015;36:3346-55.
9. Bergmark B, Dallan LAP, Pereira GTR, Kuder JF, Murphy SA, Buccola J et al. Decision-Making During Percutaneous Coronary Intervention Guided by Optical Coherence Tomography: Insights From the LightLab Initiative. Circ Cardiovasc Interv 2022;15:872-881.
10. Stone GW, Christiansen EH, Ali ZA, Andreasen LN, Maehara A, Ahmad Y et al. Intravascular imaging-guided coronary drug-eluting stent implantation: an updated network meta-analysis. Lancet 2024;403:824-837.

SUPPLEMENTAL MATERIAL

Supplemental material related to this article can be found in the online version:
https://www.jscai.org/article/S2772-9303(25)01447-4/fulltext





CHAPTER 4

Dissection-like appearance of focal catheter-induced vasospasm in intracoronary optical coherence tomography

Rick Volleberg | Peter Damman | Niels van Royen

European Heart Journal
2024 Aug 9;45(30):2793

Intracoronary optical coherence tomography (OCT) enables high-resolution cross-sectional imaging of the coronary lumen and vascular wall. Accurate interpretation of OCT images is pivotal in the decision-making process and, among others, requires an adequate understanding of potential image artefacts. While expert consensus documents and state-of-the-art reviews have previously outlined common artefacts such as non-uniform rotational distortion and seam artefacts,[1,2] we present here an additional artefact that was not described in the respective documents but is often observed and might have significant clinical implications.

Here, we present intracoronary OCT images of non-culprit lesions in five patients with an acute myocardial infarction. The images reveal a dissection-like appearance (Figure 1, left column). These features were predominantly located in non-diseased quadrants of the image and/or in non-diseased coronary segments (see Supplementary data online, Videos S1–S5). Angiographically, the OCT-detected image feature corresponded to a luminal indentation (Figure 1, middle columns). Repeat angiography after removal of the OCT imaging catheter and/or guidewire demonstrated complete resolution of the luminal indentation in all cases (Figure 1, right column).

While the exact mechanism underlying this image artefact remains to be elucidated, it may be related to OCT catheter-induced vasospasm, abrupt changes in luminal dimensions, and subsequent catheter position alterations. Notably, this artefact differs substantially from the 'intimal bump' OCT feature observed in more extensive vasospasm.[3,4]

In summary, the accurate recognition of this dissection-like appearing image artefact in intracoronary OCT is crucial for preventing false diagnoses of intimal dissections.

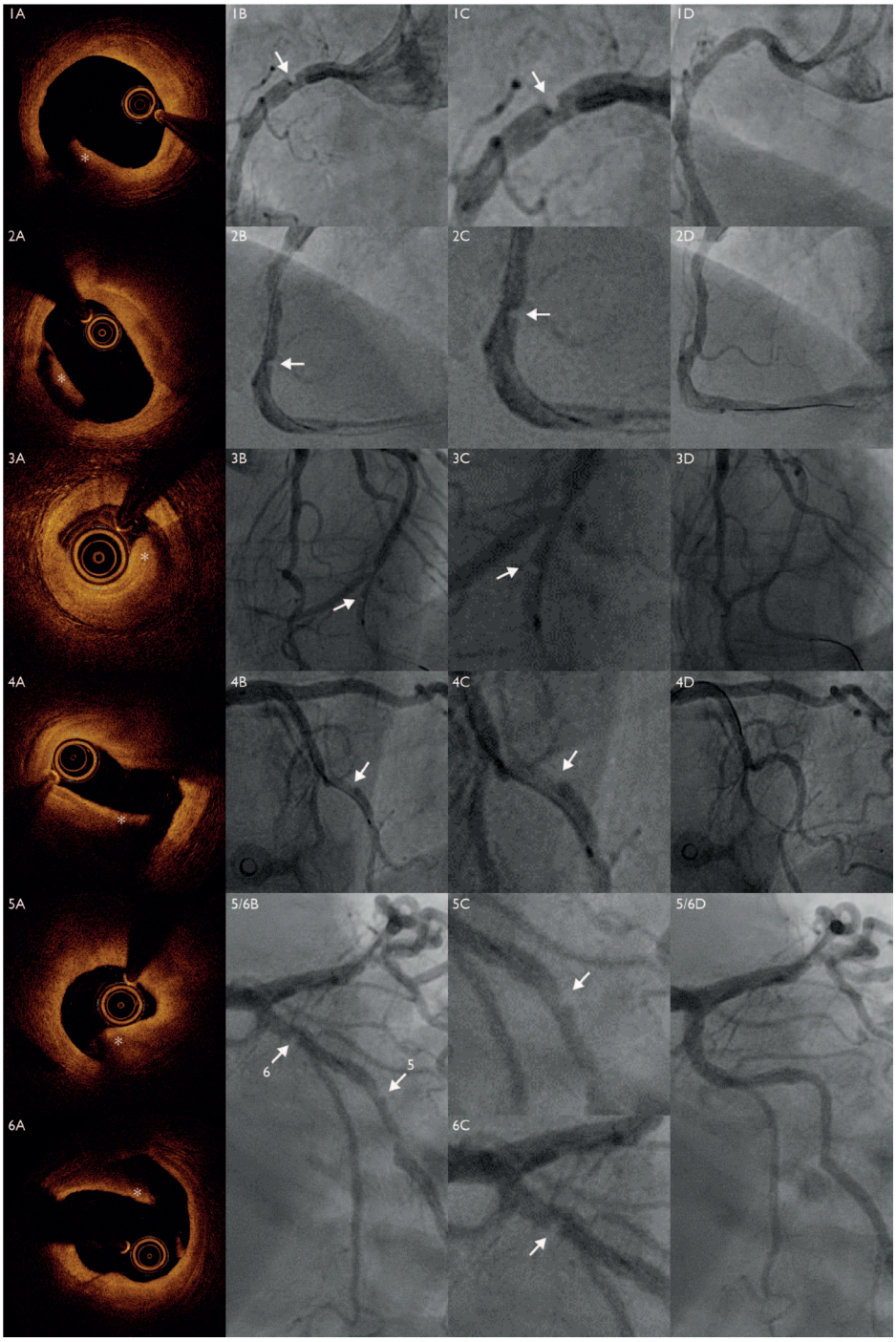


Figure 1. Dissection-like artefact.

REFERENCES

1. Araki M, Park SJ, Dauerman HL, Uemura S, Kim JS, Di Mario C et al. Optical coherence tomography in coronary atherosclerosis assessment and intervention. Nat Rev Cardiol 2022;19:684-703.
2. Ali ZA, Karimi Galougahi K, Mintz GS, Maehara A, Shlofmitz RA, Mattesini A. Intracoronary optical coherence tomography: state of the art and future directions. EuroIntervention 2021;17:e105-e123.
3. Tanaka A, Shimada K, Tearney GJ, Kitabata H, Taguchi H, Fukuda S et al. Conformational change in coronary artery structure assessed by optical coherence tomography in patients with vasospastic angina. J Am Coll Cardiol 2011;58:1608-13.
4. Reynolds HR, Maehara A, Kwong RY, Sedlak T, Saw J, Smilowitz NR et al. Coronary Optical Coherence Tomography and Cardiac Magnetic Resonance Imaging to Determine Underlying Causes of Myocardial Infarction With Nonobstructive Coronary Arteries in Women. Circulation 2021;143:624-640.

SUPPLEMENTAL MATERIAL

Supplemental material related to this article can be found in the online version:
https://academic.oup.com/eurheartj/article/45/30/2793/7658557





CHAPTER 5

Optical coherence tomography in motion: potential cause for artifacts

Rick Volleberg | Pierandrea Cancian | Niels van Royen

JACC Cardiovascular Interventions
2025 Mar 10;18(5):680-681

Cumulative evidence supports the use of intravascular imaging — whether through intravascular ultrasound or optical coherence tomography — for guidance of complex coronary lesion revascularization (Class 1, Level of Evidence: A).[1,2] However, for proper clinical implementation, understanding of image artifacts is essential, some of which have been outlined before.[3,4] Here we demonstrate an acquisition-related artifact that is of particular importance during preprocedural stent guidance and that might lead to an inadequate choice of stent length.

The artifact described here relates to unstable engagement of the guiding catheter, moving in and out of the coronary ostium (Video 1). The movement of the guiding catheter intermittently pushes the optical coherence tomographic imaging catheter back into the coronary artery. The pullback of the optical coherence tomographic lens, however, is continued as usual during this back-and-forth motion. This leads to repeat imaging of the same coronary segment 3 times (Figure 1, Video 2). In our case, the "distance" between the first and third times that the same frame was encountered measured 8 mm (79 frames at 18 mm/s). If this artifact remains unrecognized, stent length will be chosen inappropriately.

In summary, operators should be aware of the possibility of this acquisition artifact in case of unstable catheter engagement. Accurate recognition diminishes the chance of incorrect stent length measurements.

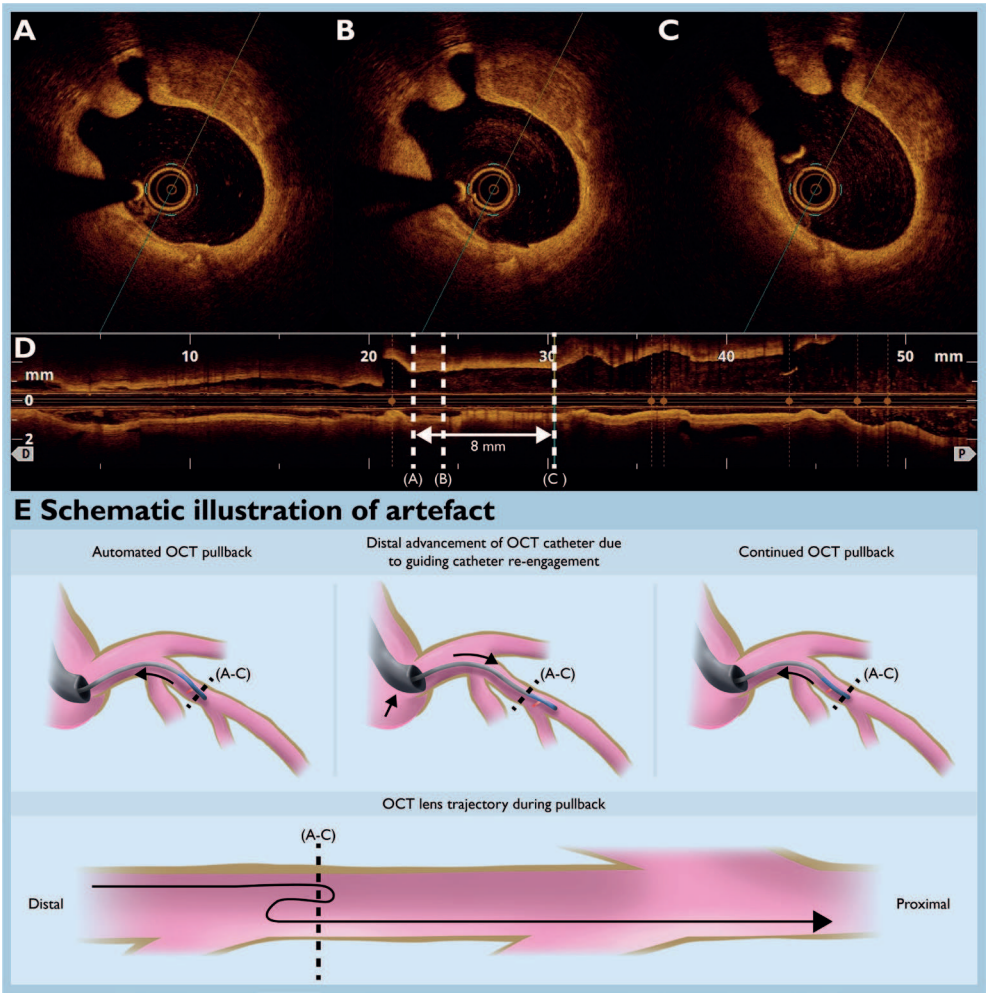


Figure 1. Accidental repeat imaging in intracoronary optical coherence tomography.

A-C) Cross-sectional optical coherence tomographic (OCT) images of a coronary segment that was repeatedly imaged, as can be recognized by the identical side branches and calcifications. D) Corresponding longitudinal representation with the locations of the 3 cross-sectional images at frames 226, 243 and 305 highlighted. E) Stepwise illustration of the mechanism underlying this acquisition artifact.

%AS percentage area

REFERENCES

1. Stone GW, Christiansen EH, Ali ZA, Andreasen LN, Maehara A, Ahmad Y et al. Intravascular imaging-guided coronary drug-eluting stent implantation: an updated network meta-analysis. Lancet 2024;403:824-837.
2. Vrints C, Andreotti F, Koskinas KC, Rossello X, Adamo M, Ainslie J et al. 2024 ESC Guidelines for the management of chronic coronary syndromes. Eur Heart J 2024;45:3415-3537.
3. Araki M, Park SJ, Dauerman HL, Uemura S, Kim JS, Di Mario C et al. Optical coherence tomography in coronary atherosclerosis assessment and intervention. Nat Rev Cardiol 2022;19:684-703.
4. Volleberg R, Damman P, van Royen N. Dissection-like appearance of focal catheter-induced vasospasm in intracoronary optical coherence tomography. Eur Heart J 2024;45:2793.

SUPPLEMENTAL MATERIAL

Supplemental material related to this article can be found in the online version:
https://www.jacc.org/doi/10.1016/j.jcin.2024.11.004



PART II

HIGH-RISK PLAQUE IDENTIFICATION



CHAPTER 6

Fractional flow reserve-negative high-risk plaques and clinical outcomes after myocardial infarction

Jan-Quinten Mol | Rick Volleberg | Anouar Belkacemi | Renicus Hermanides | Martijn Meuwissen | Alexey Protopopov | Peep Laanmets | Oleg Krestyaninov | Robert Dennert | Rohit Oemrawsingh | Jan-Peter van Kuijk | Karin Arkenbout | Dirk van der Heijden | Saman Rasoul | Erik Lipsic | Laura Rodwell | Cyril Camaro | Peter Damman | Tomasz Roleder | Elvin Kedhi | Maarten van Leeuwen | Robert-Jan van Geuns | Niels van Royen

JAMA Cardiology
2023 Nov 1;8(11):1013-1021

ABSTRACT

Importance Even after fractional flow reserve (FFR)-guided complete revascularization, patients with myocardial infarction (MI) have high rates of recurrent major adverse cardiovascular events (MACE). These recurrences may be caused by FFR-negative high-risk nonculprit lesions.

Objective To assess the association between optical coherence tomography (OCT)-identified high-risk plaques of FFR-negative nonculprit lesions and occurrence of MACE in patients with MI.

Design, setting and participants PECTUS-obs (Identification of Risk Factors for Acute Coronary Events by OCT After STEMI [ST-segment elevation MI] and NSTEMI [non-STEMI] in Patients With Residual Non–flow Limiting Lesions) is an international, multicenter, prospective, observational cohort study. In patients presenting with MI, OCT was performed on all FFR-negative (FFR > 0.80) nonculprit lesions. A high-risk plaque was defined containing at least 2 of the following prespecified criteria: (1) a lipid arc at least 90°, (2) a fibrous cap thickness less than 65 µm, and (3) either plaque rupture or thrombus presence. Patients were enrolled from December 14, 2018, to September 15, 2020. Data were analyzed from December 2, 2022, to June 28, 2023.

Main outcome and measure The primary end point of MACE, a composite of all-cause mortality, nonfatal MI, or unplanned revascularization, at 2-year follow-up was compared in patients with and without a high-risk plaque.

Results A total of 438 patients were enrolled, and OCT findings were analyzable in 420. Among included patients, mean (SD) age was 63 (10) years, 340 (81.0) were men, and STEMI and non-STEMI were equally represented (217 [51.7%] and 203 [48.3%]). A mean (SD) of 1.17 (0.42) nonculprit lesions per patient was imaged. Analysis of OCT images revealed at least 1 high-risk plaque in 143 patients (34.0%). The primary end point occurred in 22 patients (15.4%) with a high-risk plaque and 23 of 277 patients (8.3%) without a high-risk plaque (hazard ratio, 1.93 [95% CI, 1.08-3.47]; P = .02), primarily driven by more unplanned revascularizations in patients with a high-risk plaque (14 of 143 [9.8%] vs 12 of 277 [4.3%]; P = .02).

Conclusions and relevance Among patients with MI and FFR-negative nonculprit lesions, the presence of a high-risk plaque is associated with a worse clinical outcome, which is mainly driven by a higher number of unplanned revascularizations. In a population with a high recurrent event rate despite physiology-guided complete revascularization, these results call for research on additional pharmacological or focal treatment strategies in patients harboring high-risk plaques.

INTRODUCTION

Recurrent coronary events are frequently observed after myocardial infarction (MI), despite advances in primary treatment, complete revascularization, and secondary prevention.[1,2] The substrate for many of these recurrent events are atherosclerotic lesions at other sites in the coronary tree, anatomically unrelated to the lesion causing the initial MI.[3] The natural history of and potential treatment strategies for such nonculprit lesions are widely studied. A 2020 meta-analysis in patients with ST-segment elevation MI (STEMI)showed that preventive percutaneous coronary intervention (PCI) of nonculprit lesions with a significant stenosis results in fewer recurrent MIs and cardiovascular deaths, proving the benefit of additional treatment.[4] A large registry of patients with non-STEMI (NSTEMI) similarly showed a reduced death rate among patients who received complete revascularization.[5] Additional PCI of nonculprit lesions is guided either by angiography or by fractional flow reserve (FFR). However, FFR-guided revascularization in patients with MI yields less favorable outcomes compared with patients with stable coronary artery disease.[6,7] Also, the benefit of FFR over angiography is not well established in patients with MI, and rates of major adverse cardiac events (MACE) in patients with MI and FFR-deferred nonculprit lesions remain considerable.[8,9] This is probably related to the fact that FFR alone reveals plaque morphology to a limited extent.[10,11] Moreover, FFR might be false negative in the acute setting of MI.[12] Hence, additional diagnostic tools are needed to unmask high-risk nonculprit lesions in MI.

Pathological studies have identified the most important characteristics of lesions at high risk for plaque rupture and subsequent MI.[13] Ruptured plaques contain a large necrotic core and a thin (<65 µm) overlying fibrous cap. Intact lesions harboring these features, termed thin-cap fibroatheromas (TCFA), are thought to be potential precursors to plaque rupture. Vessels containing TCFA often show positive remodeling, resulting in nonobstructive lesions.[14] Plaque rupture can also occur without initially becoming clinically overt. However, these silent plaque ruptures are associated with rapid lesion progression and are linked to worse outcome.[15,16] Assessing the morphology of nonculprit lesions for TCFA or plaque rupture might therefore aid in identifying plaques at high risk of causing future MACE. Intravascular optical coherence tomography (OCT), a high-resolution invasive imaging modality, allows for identification of these anatomical lesion features *in vivo*. The present study is, to our knowledge, the first prospective study to assess the association between OCT-detected high-risk plaques in FFR-negative nonculprit lesions and MACE among patients with MI.

METHODS AND ANALYSIS

Study design

PECTUS-obs (Identification of Risk Factors for Acute Coronary Events by OCT After STEMI and NSTEMI in Patients With Residual Non–flow Limiting Lesions) is a prospective natural history cohort study that was conducted in 14 hospitals in 4 different countries (eMethods 1 in Supplement 1).[17] The goal of the study was to determine whether the presence of OCT-determined high-risk FFR-negative nonculprit

lesions in patients presenting with MI is associated with future adverse cardiovascular events. The study was approved by the medical ethics committee of the region Arnhem-Nijmegen and was conducted in accordance with the 1964 Declaration of Helsinki and its later amendments.[18] Every participant gave written informed consent; however, some patients entered the study after providing oral consent, and gave written consent thereafter. This study followed the Strengthening the Reporting of Observational Studies in Epidemiology (STROBE) reporting guideline. A detailed description of the rationale and design of PECTUS-obs has been published previously.[19]

Patients presenting with MI (STEMI or NSTEMI) who underwent coronary angiography were screened for eligibility after treatment of the culprit lesion. Patients were eligible for inclusion in the study if the coronary angiography revealed at least 1 nonculprit lesion of intermediate stenosis (30%-90%) in any of the coronary arteries that was not hemodynamically significant as determined by FFR measurement (FFR >0.80). Exclusion criteria were age younger than 18 years, pregnancy, hemodynamic instability, history of or indication for coronary artery bypass grafting, and a life expectancy of less than 3 years. Additional target lesion (ie, the FFR-negative nonculprit lesion imaged by OCT)-related exclusion criteria were in-stent restenosis and anatomy unsuitable for OCT catheter crossing or imaging. The FFR measurements and OCT imaging were performed either during the index procedure or during a staged procedure within 6 weeks. Severe stenoses and FFR-positive intermediate stenoses were treated according to contemporary guidelines. Enrolled patients underwent OCT imaging (54mm) of all eligible lesions under fluoroscopic guidance to attribute OCT findings to a specific vessel segment. Operators were not allowed to analyze the acquired images but were not completely blinded to allow for reimaging in case of insufficient image quality. After core laboratory analysis of OCT images, participants were divided into 2 groups. Patients with at least 1 OCT-determined high-risk plaque were regarded as at high risk, and patients without any high-risk plaques on OCT were considered at low risk, independently of the total amount of lesions assessed.

OCT imaging analysis

Analyses of OCT images were performed offline by a dedicated OCT core laboratory blinded to patient clinical characteristics and outcomes. The OCT analyses were performed on the targeted stenosis within the pullback. The process included a quality check to determine whether the imaging allowed for both qualitative and quantitative analysis of the targeted lesion. Images of insufficient quality were excluded from the analysis. Serial cross-sectional images of the vessel were scrutinized using CAAS IntraVascular software, version 2.0 (Pie Medical BV). Analyses were based on tissue characteristics as previously described in OCT expert consensus reports.[20,21] A detailed description of the analyses and a list of OCT definitions are provided in eMethods 2 in Supplement 1. A lesion was deemed high-risk if it contained at least 2 of the following 3 prespecified criteria: (1) a lipid arc of at least 90°, (2) a minimal fibrous cap thickness of less than 65 µm, and (3) either plaque rupture or thrombus presence (eFigure 1 in Supplement 1).

End points

The primary end point was the occurrence of MACE (composite of all-cause mortality, nonfatal MI, or unplanned revascularization) before the 2-year (±30 days) follow-up. Secondary end points are the individual components of the primary end point, cardiac mortality, target vessel failure and revascularization, and target lesion failure and revascularization. Target vessel failure and target lesion failure were defined as any nonfatal MI or unplanned revascularization attributed to the target vessel or lesion, respectively. End point definitions are provided in eMethods 3 in Supplement 1.

Follow-up and event adjudication

Structured follow-up was performed at 1 and 2 years (±30 days) after inclusion by telephone contact. Primary and secondary end points were verified using medical records from participating centers, primary care clinicians, and other medical centers. A clinical end point committee consisting of 2 independent, experienced interventional cardiologists blinded to the OCT data reviewed and adjudicated all (possible) events. When possible, any new MI or revascularization was allocated to a specific coronary vessel and lesion by comparison of baseline and event angiograms.

Statistical analysis

Data were analyzed from December 2, 2022, to June 28, 2023. A sample size of 394 participants was needed to provide more than 80% power with a 1-sided α of .025. This was based on an expected presence of high-risk plaques in 60% of targeted lesions, a total event rate of 10% to 25% in patients with MI with FFR-deferred nonculprit lesions after 2 years,[9,22] and an expected hazard ratio (HR) of 2.00 to 3.50 for OCT-defined high-risk plaques.[3] To compensate for an estimated 5% loss to follow-up and 5% inadequate OCT scans, the sample size was increased to a total of 438 participants.

Continuous variables are presented as mean (SD) if normally distributed or median (IQR) if not normally distributed. Categorical variables are presented as numbers (percentages). For the comparison of the baseline characteristics between the high-risk and non–high-risk groups, the independent unpaired t tests, Mann-Whitney tests, and χ^2 tests were performed when appropriate.

The analysis of the primary end point was performed comparing patients with and without a high-risk plaque. Patients were censored at their last known moment of follow-up or at 2 years (±30 days) after inclusion. Time-to-event data for the primary end point were presented descriptively using Kaplan-Meier curves, and a log-rank test was used to evaluate whether there was a difference between the groups. A univariate Cox proportional hazards regression model was performed to estimate the HR. Two additional multivariate Cox proportional hazards regression models were performed to account for potential confounders. The first model (model A) included the presence of a high-risk plaque and age, prior MI, type 1 or 2 diabetes, STEMI or NSTEMI at presentation, and estimated glomerular filtration rate as characteristics that were *a priori* determined to be associated with worse prognosis. The second model (model B) included the presence of a high-risk plaque and the baseline characteristics that showed a univariate association with the primary outcome ($P < .05$, corresponding to a 95% CI that does not cross 1) after checking for collinearity. Subdistribution HRs for the secondary end points were

estimated using the Fine-Gray model with noncardiac death and all-cause mortality as competing risk factors for cardiac death and all other secondary end points, respectively. Two-sided P < .05 was considered statistically significant. All analyses were performed using SPSS Statistics, version 24 (IBM Corp), and Stata, release 17 (StataCorp LLC). The trial protocol and full predefined statistical analysis plan are provided in Supplement 2.

RESULTS

Study flow

From December 14, 2018, to September 15, 2020, a total of 438 patients were enrolled in the study. The study flowchart is shown in Figure 1. In total, 420 patients had at least 1 OCT scan with sufficient quality and were included in the analysis. Imaging analysis resulted in 143 patients with (34.0%) and 277 patients without (66.0%) at least 1 high-risk plaque. Only 1 patient was lost to follow-up before the 2-year follow-up.

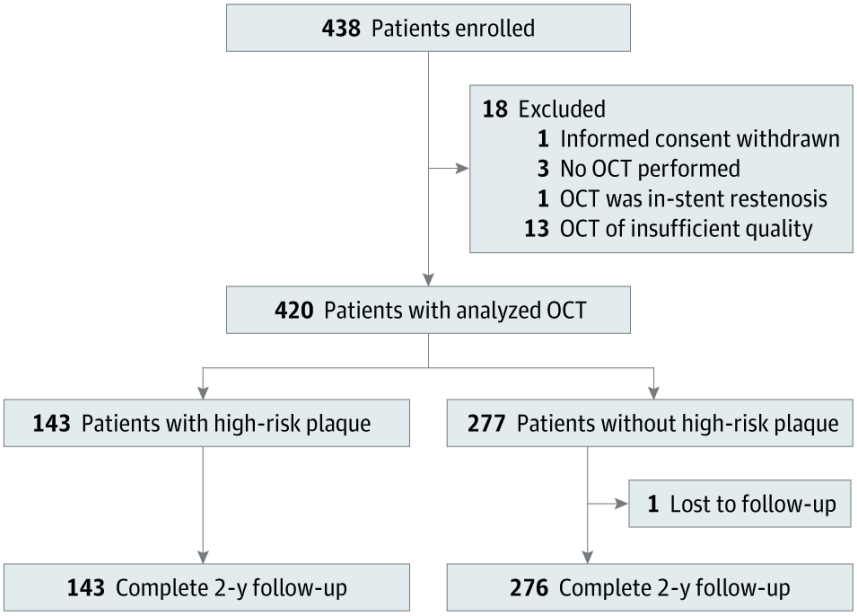


Figure 1. Study flowchart.
OCT optical coherence tomography.

Clinical and angiographical characteristics

Baseline clinical and procedural characteristics are shown in Table 1. The mean age of included patients was 63 (10) years; 340 (81.0%) were men and 80 (19.0%) were women. Data on race and ethnicity were not collected. A total of 217 patients (51.7%) presented with STEMI and 203 (48.3%) with NSTEMI. A mean (SD) of 1.17 (0.42) nonculprit lesions per patient was imaged. Hypertension was present in 222 patients (52.9%), and diabetes was present in 61 (14.5%). Furthermore, 63 patients (15.0%) had a history of MI prior to the index event. Patients with a high-risk plaque had higher low-density lipoprotein cholesterol levels at presentation (131.3 [46.3] vs 115.8 [46.3] mg/dL [to convert to mmol/L, multiply by 0.0259]; P = .03) and a less frequent history of PCI (14 [9.8%] vs 48 [17.3%]; P = .04). The culprit lesion was most often located in the left anterior descending artery (LAD) (167 [39.8%]). Targeted nonculprit lesions had a mean FFR of 0.89 (0.05) (eFigures 2 and 3 in Supplement 1) and were predominately located in the LAD (175 [41.7%]).

Lesion characteristics

Among the 420 patients included in the final analysis, 494 FFR-negative nonculprit lesions were imaged. The OCT-derived qualitative and quantitative measurements at the lesion level are shown in eTable 1 in Supplement 1. By definition, none of the lesions in non–high-risk patients contained a high-risk plaque. Among high-risk plaques, 154 (100%) had a lipid arc of at least 90°, 136 (88.3%) had a minimal cap thickness of less than 65 µm, 45 (29.2%) had a plaque rupture, and 34 (22.1%) had a thrombus present. Thin-cap fibroatheromas were found in 136 of 494 assessed lesions (27.5%). Macrophage accumulation was more frequently present in lesions with a high-risk plaque compared with those without a high-risk plaque (46 [29.9%] vs 68 [20.0%]; P = .02). Other plaque features often associated with plaque instability such as neovascularization and presence of a healed plaque phenotype were equally distributed between both groups. Non-high-risk plaques had a somewhat larger minimal lumen area and showed more extensive calcification.

Table 1. Baseline characteristics.

Characteristic[a]	Patient group		P value
	High-risk n=143	Non-high-risk n=277	
Age, mean (SD), years	62 (11)	64 (10)	.15
Sex			
Women	33 (23.1)	47 (17.0)	.13
Men	110 (76.9)	230 (83.0)	
BMI, mean (SD), kg/m^2	28.2 (4.7)	27.5 (4.5)	.18
Smoking status			
Current	44 (30.8)	79 (28.5)	.17
Previous	50 (35.0)	78 (28.2)	
Hypertension	72 (50.2)	150 (54.2)	.46
Type 1 or 2 diabetes	18 (12.6)	43 (15.5)	.42
Hypercholesterolemia	51 (35.7)	102 (36.8)	.86
Family history of premature atherosclerosis	43 (30.1)	85 (30.7)	.99
Previous MI	17 (11.9)	46 (16.6)	.20
Previous PCI	14 (9.8)	48 (17.3)	.04
Previous CVA	0 (0)	8 (2.9)	.06
History of carotid artery disease	3 (2.1)	10 (3.6)	.56
History of PAD	6 (4.2)	11 (4.0)	.91
STEMI presentation	78 (54.5)	139 (50.2)	.40
GRACE score, mean (SD)[b]	116 (34)	117 (32)	.57
Cholesterol level, mean (SD), mg/dl			
Total	200.8 (54.1)	193.1 (54.1)	.18
LDL	131.3 (46.3)	115.8 (46.3)	.03
Triglyceride level, mean (SD), mg/dL	159.3 (115.0)	185.8 (150.4)	.25
eGFR, mean (SD), mL/min/1.73m^2	79 (20)	80 (19)	.45
CRP, mean (SD), mg/dL	0.6 (1.4)	0.7 (2.5)	.60
Leukocyte count, mean (SD), cells/µL	9600 (3200)	9800 (3200)	.50
Lipid-lowering therapy at presentation	32 (22.4)	76 (27.4)	.26
Infarct-related artery			
LM	5 (3.5)	0 (0)	.004
LAD	63 (44.1)	104 (37.5)	.20
Cx	41 (28.7)	67 (24.2)	.32
RCA	45 (31.5)	112 (40.4)	.07
Nonculprit lesion assessment			
Immediate	54 (37.8)	102 (36.8)	.85
Staged	89 (62.2)	175 (63.2)	.85
Time to staged procedure, mean (SD), d	15 (15)	17 (15)	.18
Nonculprit lesion revascularization at baseline	28 (19.6)	59 (21.3)	.68
Without prior functional assessment	14 (9.8)	39 (14.1)	.21
Following positive FFR[c]	19 (13.3)	25 (9.0)	.18

Table 1. Continued

No. of FFR-negative nonculprit lesions			
Mean (SD)	1.29 (0.53)	1.12 (0.34)	<.001
1	107 (74.8)	245 (88.4)	<.001
2	31 (21.7)	31 (11.2)	.004
3	5 (3.5)	1 (0.4)	0.01
Nonculprit lesion distribution			
LM	1 (0.7)	3 (1.1)	>.99
LAD	59 (41.3)	116 (41.9)	.90
Cx	50 (35.0)	104 (37.5)	.60
RCA	52 (36.4)	70 (25.3)	.02
Targeted nonculprit lesion FFR, mean (SD)	0.88 (0.05)	0.89 (0.05)	.02

BMI body mass index (calculated as weight in kilograms divided by height in meters squared); CRP c-reactive protein; CVA cerebrovascular accident; Cx circumflex artery; eGFR estimated glomerular filtration rate; FFR fractional flow reserve; GRACE global registry of acute coronary events; LAD left anterior descending artery; LDL low-density lipoprotein; LM left main coronary artery; MI myocardial infarction; PAD peripheral artery disease; PCI percutaneous coronary intervention; RCA right coronary artery; SD standard deviation; STEMI ST-segment elevation myocardial infarction.

SI conversion factors: to convert cholesterol levels to mmol/L, multiply by 0.0259. To convert triglyceride levels to mmol/L, multiply by 0.0113. To convert CRP to mg/L, multiply by 10. To convert leukocyte count to $x10^9$/L, multiply by 0.001.

[a] *Unless otherwise indicated, data are expressed as No. (%) of patients.*

[b] *Scores range from 1 to 372, with higher scores indicating higher risk of mortality.*

[c] *A positive FFR indicates less than or equal to 0.80.*

Clinical outcomes

The primary and secondary end points in both groups are listed in Table 2. In the total population MACE occurred in 45 patients (10.7%) within 2 years after MI. The primary end point occurred in 22 patients in the high-risk group (15.4%) and 23 in the non-high-risk group (8.3%) (HR, 1.93 [95% CI, 1.08-3.47]; P = .02). The Kaplan-Meier curves for occurrence of the primary end point in both groups are shown in Figure 2A. Table 3 shows the multivariate Cox proportional hazards regression models. In the predefined model A, the presence of a high-risk plaque was the only factor associated with 2-year MACE (HR, 1.99 [95% CI, 1.10-3.61];P = .02). In model B, which included the variables that show a univariate association with the primary outcome (type of MI at presentation, estimated glomerular filtration rate, history of carotid artery disease, lipid-lowering therapy at discharge, and right coronary artery as infarct-related artery [eTable 2 in Supplement 1]), presence of a high-risk plaque was also independently associated with 2-year MACE (HR, 2.24 [95% CI, 1.21-4.13]; P = .01), next to history of carotid artery disease (HR, 3.80 [95% CI, 1.42-10.16]; P = .008), right coronary artery as the culprit artery (HR, 0.46 [95% CI, 0.22-0.97]; P = .04), and lipid-lowering therapy at discharge (HR, 0.20 [95% CI, 0.06-0.70]; P = .01). The primary end point was primarily driven by more unplanned revascularization in the high-risk plaque group (14 [9.8%] vs 12 [4.3%]; P = .02). The combined presence of either minimal lumen area less than 3.5mm^2 or

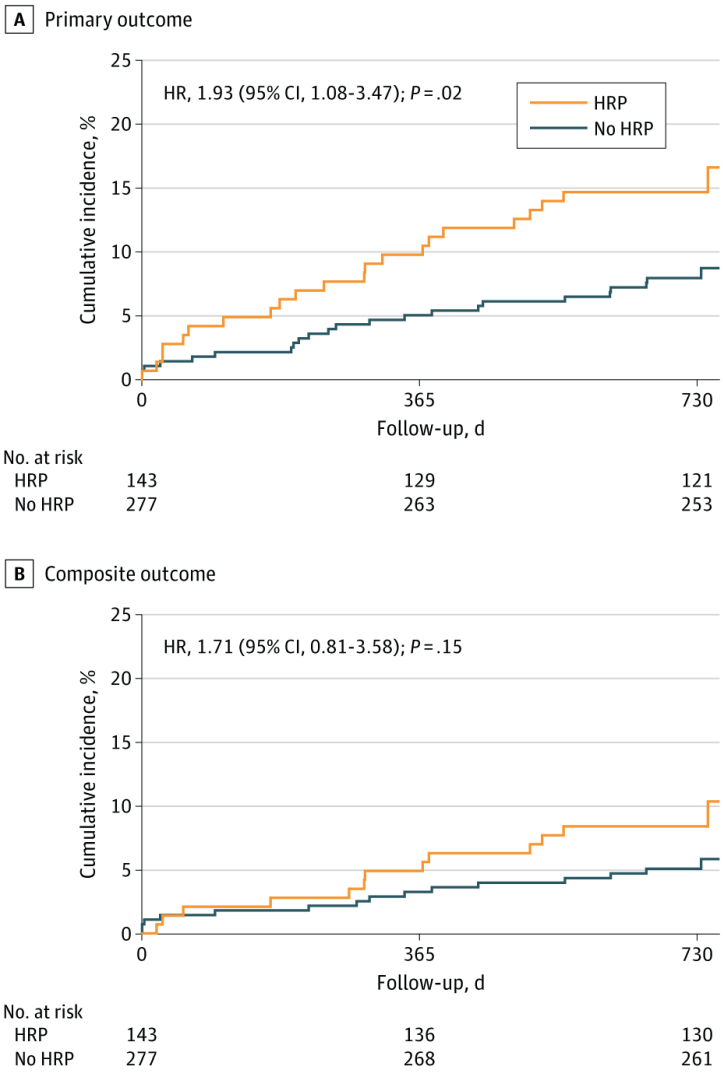


Figure 2. Primary and composite outcomes.

A) Kaplan-Meier curves for the primary outcome of major adverse cardiovascular events (including all-cause mortality, nonfatal myocardial infarction, or unplanned revascularization) at 2 year follow-up. B) Kaplan-Meier curves for the composite outcome of all-cause mortality or nonfatal myocardial infarction at 2-year follow-up. A hazard ratio greater than 1.00 indicates greater hazard in the high-risk plaque group.

CI confidence interval; HR hazard ratio; HRP high-risk plaque.

FFR less than 0.90 with a high-risk plaque did not increase the association with the primary end point compared with the presence of a high-risk plaque only (eFigure 4 in Supplement 1). All-cause mortality, cardiovascular death, nonfatal MI, and the composite of all-cause mortality and nonfatal MI (Figure 2B) occurred numerically more often in patients with a high-risk plaque but did not differ significantly between groups. Details on all unplanned revascularizations and nonfatal MIs are shown in eTables 3 and 4 in Supplement 1. The number of target vessel failures was 7 (4.9%) in the high-risk patient group and 4 (1.4%) in the non-high-risk patient group (P = .03), including 2 (1.4%) and 0 cases of target vessel MI, respectively. Target lesion failure occurred in 5 patients (3.5%) with a high-risk plaque and 3 (1.1%) without a high-risk plaque (P = .08). After exclusion of all stent-related events and all nonfatal MIs that were not attributable to a culprit segment, the combined primary end point occurred in 19 patients (13.3%) with a high-risk plaque compared with 18 (6.5%) without a high-risk plaque (P = .02) (eTable 5 in Supplement 1). Of note, guideline-directed medical treatment prescription was high and comparable between groups (eTable 6 in Supplement 1).

Table 2. Two year clinical outcome.

Outcome	Patient group		HR (95% CI)	P value
	High-risk n=143	Non-high-risk n=277		
Primary endpoint	22 (15.4)	23 (8.3)	1.93 (1.08-3.47)	.02
Death (any)	7 (4.9)	7 (2.5)	1.99 (0.70-5.68)	.19
Cardiac death	5 (3.5)	5 (1.8)	1.96 (0.57-6.74)[a]	.27
Nonfatal MI	6 (4.2)	8 (2.9)	1.44 (0.50-4.15)[b]	.48
Unplanned revascularization	14 (9.8)	12 (4.3)	2.33 (1.08-5.03)[b]	.02
Target vessel failure[c]	7 (4.9)	4 (1.4)	3.44 (1.01-11.72)[b]	.03
Target vessel revascularization[c]	7 (4.9)	4 (1.4)	3.44 (1.01-11.72)[b]	.03
Target lesion failure[c]	5 (3.5)	3 (1.1)	3.26 (0.78-13.63)[b]	.08
Target lesion revascularization[c]	5 (3.5)	3 (1.1)	3.26 (0.78-13.63)[b]	.08

CI confidence interval; HR hazard ratio; MI myocardial infarction.

[a] Estimated using the Fine-Gray model with noncardiac death as competing risk factor.

[b] Estimated using the Fine-Gray model with all-cause mortality as competing risk factor.

[c] Refers to the fractional flow reserve-negative nonculprit vessel or lesion imaged by optical coherence tomography.

DISCUSSION

Recurrent coronary events represent a major cause of morbidity and mortality in patients with MI. In the search for markers and underlying mechanisms for these recurrent events, the present cohort study shows for the first time in a prospective manner that in patients with MI, the presence of FFR-negative OCT-identified high-risk nonculprit lesions is associated with an increased risk of future MACE.

In a population of roughly equal numbers of patients with STEMI and NSTEMI, we observed recurrent MACE in 45 patients (10.7%) within 2 years after MI, even in the absence of FFR-positive nonculprit lesions. These events occurred more often in patients who had a high-risk plaque than in those who did not, with an HR of approximately 2. In the multivariate analyses, apart from the presence of carotid artery disease, the presence of a high-risk plaque resulted in the highest hazard ratio for future MACE. The increased MACE rate in patients with high-risk plaque was primarily driven by an increased rate of unplanned revascularization in this group. Also, the incidences of all secondary end points were numerically higher in the high-risk patient group. In our study, TCFA were found in 136 of 494 assessed lesions (27.5%). This is comparable to the prevalence of TCFA in nonobstructive nonculprit lesions in patients with STEMI in the COMPLETE (Complete vs Culprit-Only Revascularization to Treat Multi-Vessel Disease After Early PCI for STEMI) OCT substudy (23.2%)[23] or in FFR-negative lesions in patients with diabetes in the COMBINE (OCT-FFR) study (22.4%).[24]

Table 3. Multivariate Cox proportional hazards regression model for the primary endpoint.

Outcome	Patient group		HR (95% CI)	P value
	Patients with MACE n=45	Patients without MACE n=375		
Model A[a]				
Presence of high-risk plaque	22 (48.9)	121 (32.3)	1.99 (1.10-3.61)	.02
Age, mean (SD), y	64 (12)	63 (10)	0.99 (0.96-1.02)	.49
Prior MI	10 (22.2)	53 (14.1)	1.49 (0.71-3.13)	.29
Diabetes	10 (22.2)	51 (13.6)	1.35 (0.64-2.85)	.44
STEMI at presentation	16 (35.6)	201 (53.6)	0.55 (0.29-1.03)	.06
eGFR, mean (SD), mL/min/1.73m^2	74 (24)	80 (18)	0.99 (0.97-1.01)	.18
Model B[b]				
Presence of high-risk plaque	22 (48.9)	121 (32.3)	2.24 (1.21-4.13)	.01
History of carotid artery disease	5 (11.1)	8 (2.1)	3.80 (1.42-10.16)	.008
STEMI at presentation	16 (35.6)	201 (53.6)	0.59 (0.31-1.12)	.11
eGFR, mean (SD), mL/min/1.73m^2	74 (24)	80 (18)	0.99 (0.98-1.01)	.47
Lipid-lowering therapy at discharge	42 (93.3)	373 (99.5)	0.20 (0.06-0.70)	.01
RCA culprit	9 (20.0)	148 (39.5)	0.46 (0.22-0.97)	.04

CI confidence interval; eGFR estimated glomerular filtration rate; HR hazard ratio; MACE major adverse cardiovascular events; MI myocardial infarction; RCA right coronary artery; SD standard deviation; STEMI ST-segment elevation MI.

[a] Multivariate Cox proportional hazards regression model with the presence of a high-risk plaque and age, prior MI, diabetes, STEMI or non-STEMI at presentation and eGFR as a priori determined independent variables.

[b] Multivariate Cox proportional hazards regression model with the presence of a high-risk plaque and all baseline characteristics that showed a univariate relationship with the primary outcome (P < .05) after checking for collinearity.

These results highlight the additional value of intracoronary imaging in addition to physiological assessments of coronary lesions. Although an association is reported between FFR and certain plaque features,[10,11] FFR does not allow precise assessment of plaque morphology. Moreover, FFR measurements obtained during the index procedure in patients presenting with STEMI potentially underestimate lesion severity.[12] Nevertheless, FFR pullbacks could further help stratify patients at high risk of recurrent events by identifying lesions with a large translesional pressure gradient.[25,26]

PECTUS-obs adds to existing evidence that suggests a worse prognosis in patients with TCFA. In a large retrospective study by Kubo et al,[27] TCFA in nonculprit lesions of patients with acute coronary syndrome were associated with an increased risk of lesion level events (HR, 19.14 [95% CI, 11.74- 31.20]) within a median follow-up of 6 years. Moreover, in the prospective COMBINE (OCT-FFR) study,[24] the presence of FFR-negative TCFA lesions was associated with an increased risk of MACE (HR, 4.64 [95% CI, 1.99-10.89]) at 18 months in patients with diabetes. In addition to TCFA, the *a priori* definition of high-risk plaques in the present study included thrombus or plaque rupture in the presence of significant lipid accumulation. These features were found in 34 (22.1%) and 45 (29.2%) high-risk lesions, respectively, and therefore only constitute a small number of the high-risk plaques. Several other plaque characteristics have also been associated with plaque instability. Among them are healed plaques, neovascularization, protruding calcification, and the presence of macrophages. Indeed, in our study, macrophages were more often seen in high-risk plaques. In the CLIMA study,[28] among patients who had undergone OCT of the LAD the simultaneous presence of 4 plaque features (minimal lumen area <3.5 mm^2, minimal fibrous cap thickness <75 µm, a lipid arc >180°, and the presence of macrophages) resulted in an HR of 7.54 (95% CI, 3.1-18.6) for a composite end point of cardiac death or target segment MI after 1 year. However, this primary end point occurred only in 3.7% and the simultaneous presence of the prespecified OCT characteristics was found in only 3.6% of included patients in this study.[28]

In PECTUS-obs, only 5 patients (3.5%) in the high-risk plaque group had an event that was adjudicated to the target lesion and the yearly rate of target-vessel MI was only 0.7%. This is in line with the current view that atherosclerosis is a dynamic process in which plaques can develop and regress, and that lesions that rupture do not always result in clinical symptoms.[29] This could limit the effectiveness of focal treatment of high-risk lesions. Nonetheless, the presence of high-risk plaques was associated with MACE on a patient level. The worse prognosis seen in patients with a high-risk plaque might reflect a more advanced stage of atherosclerosis throughout the coronary tree. Considering that MI in itself is a marker of high-risk of future MACE, patients who also harbor high-risk plaques might especially benefit from aggressive lipid-lowering or anti-inflammatory therapy.[30,31] However, given the low rate of adverse events in contemporary PCI, focal stenting of high-risk plaques could also be proposed. The randomized PROSPECT (Providing Regional Observations to Study Predictors of Events in the Coronary Tree II) ABSORB substudy[32] demonstrated that preventive PCI was safe and resulted in enlarged luminal dimensions directly after bioresorbable vascular scaffold implantation and remained larger compared with optimal medical therapy only after a median follow-up of 4.2 years. These data, however, are only hypothesis generating, given the small sample size, and the positive predictive value of distinct high-risk

plaque features for lesion level events is low.[28] The effect of preventive PCI of high-risk plaques on clinical end points is currently under investigation in several large randomized trials.[33-36]

Limitations

This study has some limitations. We performed targeted imaging of FFR-negative nonculprit lesions instead of 3-vessel OCT. Therefore, we might have missed high-risk lesions. However, such targeted evaluation might be more feasible in clinical practice. We did not perform FFR pullbacks, which may further help identify high-risk patients. Operators were not blinded to OCT findings, which could potentially have led to altered decision-making. However, the OCT analyses were performed *post hoc* by an independent OCT core laboratory. Neither these analyses nor the group allocation was available to the operators or other clinicians involved. We did not perform OCT imaging of the culprit lesion. Therefore, a limited amount of nonculprit lesions with plaque rupture or thrombus could in fact be the culprit lesion, especially among patients with NSTEMI. Moreover, the assessment of the residual fibrous cap thickness in case of plaque rupture could be cumbersome. Women were underrepresented in the current cohort. Last, the prevalence of high-risk plaque and number of events in this study were lower than expected, and the study was not powered to assess differences in the individual components of the primary end point, of which only difference in unplanned revascularization was found to be statistically significant.

CONCLUSION

To our knowledge, PECTUS-obs is the first prospective cohort study to show that among patients with MI and FFR-negative nonculprit lesions, the presence of a high-risk plaque is associated with a worse clinical outcome, with higher number of unplanned revascularizations being a primary factor. In a population with a high rate of recurrent events, despite physiology-guided complete revascularization, these results call for research on the potential benefit of additional pharmacological or focal treatment strategies in patients harboring high-risk plaques.

REFERENCES

1. Peters SAE, Colantonio LD, Dai Y, Zhao H, Bittner V, Farkouh ME et al. Trends in Recurrent Coronary Heart Disease After Myocardial Infarction Among US Women and Men Between 2008 and 2017. Circulation 2021;143:650-660.
2. Jernberg T, Hasvold P, Henriksson M, Hjelm H, Thuresson M, Janzon M. Cardiovascular risk in post-myocardial infarction patients: nationwide real world data demonstrate the importance of a long-term perspective. Eur Heart J 2015;36:1163-70.
3. Stone GW, Maehara A, Lansky AJ, de Bruyne B, Cristea E, Mintz GS et al. A prospective natural-history study of coronary atherosclerosis. N Engl J Med 2011;364:226-35.
4. Bainey KR, Engstrom T, Smits PC, Gershlick AH, James SK, Storey RF et al. Complete vs Culprit-Lesion-Only Revascularization for ST-Segment Elevation Myocardial Infarction: A Systematic Review and Meta-analysis. JAMA Cardiol 2020;5:881-888.
5. Rathod KS, Koganti S, Jain AK, Astroulakis Z, Lim P, Rakhit R et al. Complete Versus Culprit-Only Lesion Intervention in Patients With Acute Coronary Syndromes. J Am Coll Cardiol 2018;72:1989-1999.
6. Liou KP, Ooi SM, Hoole SP, West NEJ. Fractional flow reserve in acute coronary syndrome: a meta-analysis and systematic review. Open Heart 2019;6:e000934.
7. Cerrato E, Mejia-Renteria H, Dehbi HM, Ahn JM, Cook C, Dupouy P et al. Revascularization Deferral of Nonculprit Stenoses on the Basis of Fractional Flow Reserve: 1-Year Outcomes of 8,579 Patients. JACC Cardiovasc Interv 2020;13:1894-1903.
8. Denormandie P, Simon T, Cayla G, Steg PG, Montalescot G, Durand-Zaleski I et al. Compared Outcomes of ST-Segment-Elevation Myocardial Infarction Patients With Multivessel Disease Treated With Primary Percutaneous Coronary Intervention and Preserved Fractional Flow Reserve of Nonculprit Lesions Treated Conservatively and of Those With Low Fractional Flow Reserve Managed Invasively: Insights From the FLOWER-MI Trial. Circ Cardiovasc Interv 2021;14:e011314.
9. Hakeem A, Edupuganti MM, Almomani A, Pothineni NV, Payne J, Abualsuod AM et al. Long-Term Prognosis of Deferred Acute Coronary Syndrome Lesions Based on Nonischemic Fractional Flow Reserve. J Am Coll Cardiol 2016;68:1181-1191.
10. Lee JM, Choi KH, Koo BK, Park J, Kim J, Hwang D et al. Prognostic Implications of Plaque Characteristics and Stenosis Severity in Patients With Coronary Artery Disease. J Am Coll Cardiol 2019;73:2413-2424.
11. Driessen RS, Stuijfzand WJ, Raijmakers PG, Danad I, Min JK, Leipsic JA et al. Effect of Plaque Burden and Morphology on Myocardial Blood Flow and Fractional Flow Reserve. J Am Coll Cardiol 2018;71:499-509.
12. van der Hoeven NW, Janssens GN, de Waard GA, Everaars H, Broyd CJ, Beijnink CWH et al. Temporal Changes in Coronary Hyperemic and Resting Hemodynamic Indices in Nonculprit Vessels of Patients With ST-Segment Elevation Myocardial Infarction. JAMA Cardiol 2019;4:736-744.
13. Burke AP, Farb A, Malcom GT, Liang YH, Smialek J, Virmani R. Coronary risk factors and plaque morphology in men with coronary disease who died suddenly. N Engl J Med 1997;336:1276-82.
14. Virmani R, Burke AP, Farb A, Kolodgie FD. Pathology of the vulnerable plaque. J Am Coll Cardiol 2006;47:C13-8.
15. Virmani R, Kolodgie FD, Burke AP, Farb A, Schwartz SM. Lessons from sudden coronary death: a comprehensive morphological classification scheme for atherosclerotic lesions. Arterioscler Thromb Vasc Biol 2000;20:1262-75.
16. Vergallo R, Uemura S, Soeda T, Minami Y, Cho JM, Ong DS et al. Prevalence and Predictors of Multiple Coronary Plaque Ruptures: In Vivo 3-Vessel Optical Coherence Tomography Imaging Study. Arterioscler Thromb Vasc Biol 2016;36:2229-2238.
17. Identification of risk factors for acute coronary events by OCT after STEMI and NSTEMI in patients with residual non–flow limiting lesions. ClinicalTrials.gov identifier: NCT03857971. Updated September 17, 2021. Accessed June 25, 2023. https://classic.clinicaltrials.gov/ct2/show/NCT03857971.

18. World Medical A. World Medical Association Declaration of Helsinki: ethical principles for medical research involving human subjects. JAMA 2013;310:2191-4.

19. Mol JQ, Belkacemi A, Volleberg RH, Meuwissen M, Protopopov AV, Laanmets P et al. Identification of anatomic risk factors for acute coronary events by optical coherence tomography in patients with myocardial infarction and residual nonflow limiting lesions: rationale and design of the PECTUS-obs study. BMJ Open 2021;11:e048994.

20. Tearney GJ, Regar E, Akasaka T, Adriaenssens T, Barlis P, Bezerra HG et al. Consensus standards for acquisition, measurement, and reporting of intravascular optical coherence tomography studies: a report from the International Working Group for Intravascular Optical Coherence Tomography Standardization and Validation. J Am Coll Cardiol 2012;59:1058-72.

21. Araki M, Park SJ, Dauerman HL, Uemura S, Kim JS, Di Mario C et al. Optical coherence tomography in coronary atherosclerosis assessment and intervention. Nat Rev Cardiol 2022;19:684-703.

22. Sels JW, Tonino PA, Siebert U, Fearon WF, Van't Veer M, De Bruyne B, Pijls NH. Fractional flow reserve in unstable angina and non-ST-segment elevation myocardial infarction experience from the FAME (Fractional flow reserve versus Angiography for Multivessel Evaluation) study. JACC Cardiovasc Interv 2011;4:1183-9.

23. Pinilla-Echeverri N, Mehta SR, Wang J, Lavi S, Schampaert E, Cantor WJ et al. Nonculprit Lesion Plaque Morphology in Patients With ST-Segment-Elevation Myocardial Infarction: Results From the COMPLETE Trial Optical Coherence Tomography Substudys. Circ Cardiovasc Interv 2020;13:e008768.

24. Kedhi E, Berta B, Roleder T, Hermanides RS, Fabris E, AJJ IJ et al. Thin-cap fibroatheroma predicts clinical events in diabetic patients with normal fractional flow reserve: the COMBINE OCT-FFR trial. Eur Heart J 2021;42:4671-4679.

25. Collet C, Sonck J, Vandeloo B, Mizukami T, Roosens B, Lochy S et al. Measurement of Hyperemic Pullback Pressure Gradients to Characterize Patterns of Coronary Atherosclerosis. J Am Coll Cardiol 2019;74:1772-1784.

26. Lee JM, Choi G, Koo BK, Hwang D, Park J, Zhang J et al. Identification of High-Risk Plaques Destined to Cause Acute Coronary Syndrome Using Coronary Computed Tomographic Angiography and Computational Fluid Dynamics. JACC Cardiovasc Imaging 2019;12:1032-1043.

27. Kubo T, Ino Y, Mintz GS, Shiono Y, Shimamura K, Takahata M et al. Optical coherence tomography detection of vulnerable plaques at high risk of developing acute coronary syndrome. Eur Heart J Cardiovasc Imaging 2021.

28. Prati F, Romagnoli E, Gatto L, La Manna A, Burzotta F, Ozaki Y et al. Relationship between coronary plaque morphology of the left anterior descending artery and 12 months clinical outcome: the CLIMA study. Eur Heart J 2020;41:383-391.

29. Libby P. The changing landscape of atherosclerosis. Nature 2021;592:524-533.

30. Raber L, Ueki Y, Otsuka T, Losdat S, Haner JD, Lonborg J et al. Effect of Alirocumab Added to High-Intensity Statin Therapy on Coronary Atherosclerosis in Patients With Acute Myocardial Infarction: The PACMAN-AMI Randomized Clinical Trial. JAMA 2022;327:1771-1781.

31. Montarello NJ, Singh K, Sinhal A, Wong DTL, Alcock R, Rajendran S et al. Assessing the Impact of Colchicine on Coronary Plaque Phenotype After Myocardial Infarction with Optical Coherence Tomography: Rationale and Design of the COCOMO-ACS Study. Cardiovasc Drugs Ther 2022;36:1175-1186.

32. Stone GW, Maehara A, Ali ZA, Held C, Matsumura M, Kjoller-Hansen L et al. Percutaneous Coronary Intervention for Vulnerable Coronary Atherosclerotic Plaque. J Am Coll Cardiol 2020;76:2289-2301.

33. Ahn JM, Kang DY, Lee PH, Ahn YK, Kim WJ, Nam CW et al. Preventive PCI or medical therapy alone for vulnerable atherosclerotic coronary plaque: Rationale and design of the randomized, controlled PREVENT trial. Am Heart J 2023;264:83-96.

34. Interventional strategy for non-culprit lesions with major vulnerability criteria at OCT in patients with ACS (INTERCLIMA). ClinicalTrials.gov identifier: NCT05027984. Updated August 31, 2021. Accessed March 7, 2024. https://clinicaltrials.gov/study/NCT05027984.

35. COMBINE-INTERVENE: combined ischemia and vulnerable plaque percutaneous intervention to reduce cardiovascular events. ClinicalTrials.gov identifier: NCT053330658. Updated April 18, 2022. Accesed March 7, 2025. https://clinicaltrials.gov/study/NCT05333068.

36. Treatment of functionally non-significant vulnerable plaques in patients with multicessel ST-elevation myocardial infarction the VULNERABLE trial (VULNERABLE). ClinicalTrials.gov identifier: NCT05599061. Updated March 4, 2024. Accessed Marc 7, 2024. https://clinicaltrials.gov/study/NCT05599061.

SUPPLEMENTAL MATERIAL

Supplemental material related to this article can be found in the online version:
https://jamanetwork.com/journals/jamacardiology/fullarticle/2809516





CHAPTER 7

High-risk plaques in non-culprit lesions and clinical outcome after NSTEMI vs. STEMI

Rick Volleberg* | Jan-Quinten Mol* | Anouar Belkacemi | Renicus Hermanides | Martijn Meuwissen | Alexey Protopopov | Peep Laanmets | Oleg Krestyaninov | Casper Laclé | Rohit Oemrawsingh | Jan-Peter van Kuijk | Karin Arkenbout | Dirk van der Heijden | Saman Rasoul | Erik Lipsic | Laura Rodwell | Cyril Camaro | Peter Damman | Tomasz Roleder | Elvin Kedhi | Maarten van Leeuwen | Robert-Jan van Geuns | Niels van Royen

European Heart Journal Cardiovascular Imaging
2025 Jan 31;26(2):197-206

* joined first authorship

ABSTRACT

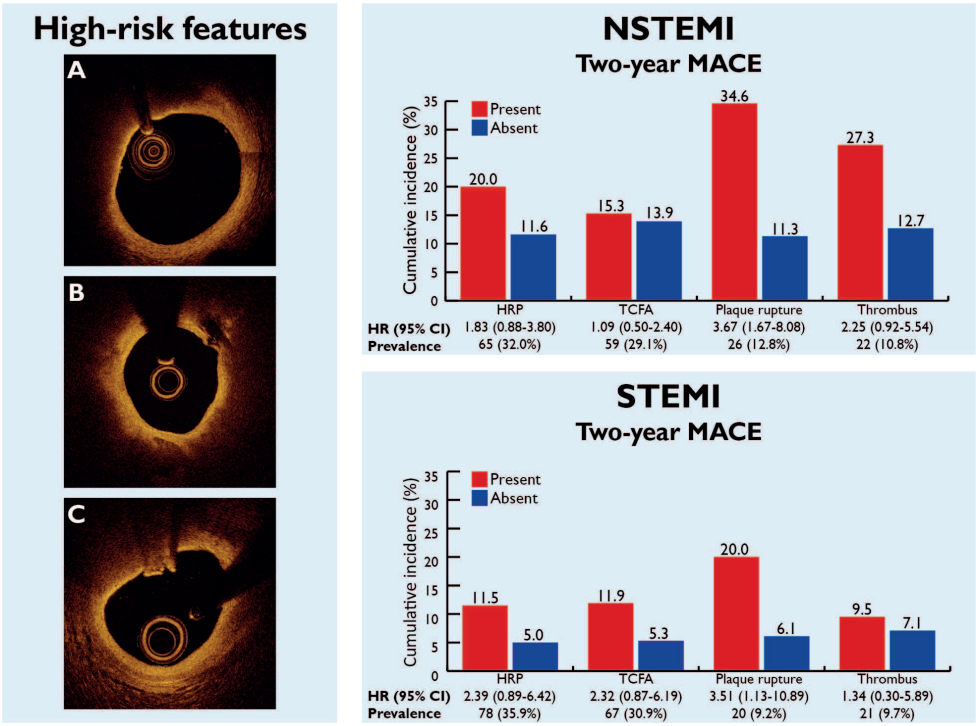
Aims Complete non-culprit (NC) revascularisation may help reduce recurrent events after non-ST-segment elevation myocardial infarction (NSTEMI), especially if NC lesions would harbour high-risk plaque (HRP) features similar to ST-segment elevation myocardial infarction (STEMI). This study aimed to assess differences in fractional flow reserve (FFR)-negative NC plaque morphology in patients presenting with NSTEMI vs. STEMI and assess the association of HRP morphology and clinical outcome.

Methods and results In the prospective PECTUS-obs study, 438 patients presenting with myocardial infarction (MI) underwent optical coherence tomography (OCT) of all FFR-negative intermediate NC lesions. The primary endpoint was the occurrence of major adverse cardiovascular events (MACE, composite of all-cause mortality, non-fatal MI or unplanned revascularisation) at 2-year follow-up. Four hundred and twenty patients had at least one analysable OCT, including 203 (48.3%) with NSTEMI and 217 (51.7%) with STEMI. The prevalence of HRPs, including thin-cap fibroatheromas, plaque rupture, and thrombus, was comparable between groups. MACE occurred in 29 (14.3%) NSTEMI patients and 16 (7.4%) STEMI patients ($P_{uni\text{-}variable} = 0.025$ and $P_{multi\text{-}variable} = 0.270$). Incidence of MACE was numerically higher among patients with HRP, irrespective of the clinical presentation at index ($P_{interaction} = 0.684$). Among HRP criteria, plaque rupture was associated with MACE in both NSTEMI ($P < 0.001$) and STEMI ($P = 0.020$)

Conclusions Presence of NC HRP is comparable between NSTEMI and STEMI and leads to numerically higher event rates in both. These results call for additional research on complete revascularisation in NSTEMI and treatment of HRP.

Trial registration number NCT03857971.

GRAPHICAL ABSTRACT



Graphical Abstract. The presence of at least one optical coherence tomography-identified high-risk plaque (pre-defined in the presence of at least two characteristics: (i) lipid arc ≥90° (A-C), (ii) minimum fibrous cap thickness <65 µm (A, C), and/or (iii) presence of either plaque rupture (B) or thrombus (C)) in a fractional flow reserve-negative intermediate non-culprit lesion leads to numerically higher incidences of major adverse cardiovascular events (composite endpoint of all-cause mortality, non-fatal myocardial infarction, or unplanned revascularisation) on a patient-level at 2-year follow-up after NSTEMI and STEMI (right panels). Among high-risk plaque features, plaque rupture was significantly associated with adverse outcome in both NSTEMI and STEMI.

CI confidence interval; HR hazard ratio; HRP high-risk plaque; MACE major adverse cardiovascular events; NSTEMI non-ST-segment elevation myocardial infarction; STEMI ST-segment elevation myocardial infarction; TCFA thin-cap fibroatheroma.

INTRODUCTION

ST-segment elevation myocardial infarction (STEMI) and non-ST-segment elevation myocardial infarction (NSTEMI) are often considered different clinical entities. Patients presenting with STEMI are on average younger and have less traditional risk factors.[1-3] Furthermore, *in vivo* studies with optical coherence tomography (OCT) and intravascular ultrasound (IVUS) demonstrated a higher prevalence of plaque rupture and high-risk plaque (HRP) features at the culprit site in patients with STEMI.[4-6] Yet, patients with NSTEMI exhibit more recurrent MI.[7-9] Hypotheses regarding this excess number of events include the wrong identification of the culprit coronary artery, thereby leaving the culprit lesion untreated,[10] and the presence of high-risk non-culprit (NC) lesions that are prone to rupture.[11,12] Approximately half of recurrent events after MI are indeed related to NC lesions, that are often non-flow-limiting.[12] Complete revascularisation of NC disease in patients with STEMI now has a class I (level of evidence A) recommendation.[13,14] NC revascularisation in STEMI reduces cardiac mortality or recurrent myocardial infarction (MI) and need for repeat revascularisation, which may partially be driven by sealing high-risk NC lesions.[15-17] Considering this hypothesis, and a diminished accuracy of the fractional flow reserve (FFR) in the acute setting of MI,[18,19] intracoronary imaging may provide adjunctive value on top of physiological evaluation of stenosis severity.

Evidence supporting complete revascularisation in NSTEMI is less robust.[20,21] However, complete revascularisation in NSTEMI could be a feasible option considering the excess in recurrent events, especially if NC lesions would harbour high-risk features similar to STEMI. Only limited evidence exists on differences in NC plaque morphology between NSTEMI and STEMI.[6,22] The aim of the present study is to assess differences in plaque characteristics of FFR-negative NC plaques in patients presenting with NSTEMI vs. STEMI and to assess the association of FFR-negative but high-risk NC plaques and clinical outcome in these patients.

METHODS

Study design

This is a pre-planned sub-group analysis of the multi-centre (see supplementary methods S1) PECTUS-obs (NCT03857971) study, a prospective, observational study that was designed to assess the association between OCT-identified HRP in FFR-negative NC lesions and major adverse cardiovascular events (MACE) in patients presenting with MI. The design and primary results of this study were published previously.[23,24] Briefly, 438 patients with NSTEMI or STEMI underwent OCT of all FFR-negative intermediate NC lesions (defined as visually estimated stenosis 30–90% with an FFR > 0.80) after treatment of the infarct-related artery. OCT acquisition was performed using the Dragonfly Optis catheter (Abbott Vascular, USA) under fluoroscopic guidance to ensure that OCT findings could be correlated to the coronary angiogram. Patients underwent structured clinical follow-up 1 and 2 years (± 30 days) after inclusion by means of telephone contact. The study was conducted in accordance with the 1964 Declaration of Helsinki and

was approved by the institutional review board and/or medical ethics committee of each participating centre. Written informed consent was obtained from all participants. For the present analysis, all patients with at least one analysable OCT pullback were included and were grouped according to the clinical syndrome at presentation (i.e. NSTEMI vs. STEMI).

OCT imaging analysis

OCT image analysis was performed offline using Caas IntraVascular (Pie Medical Imaging B.V., the Netherlands) by an independent OCT core laboratory (Real Solution Sp. Z o.o., Poland) blinded to patient characteristics and clinical outcome. Pullbacks with insufficient image quality for assessment of the target region were excluded. Quantitative and qualitative image analyses were performed in accordance with contemporary consensus documents.[25,26] Calcification was defined as a sharply delineated signal-poor or heterogeneous region. A lipid plaque was defined as a poorly delineated signal-poor region with a fast signal drop-off that is separated from the lumen by a signal-rich band, the fibrous cap. Thin cap fibroatheroma (TCFA) was defined according to the original pathological criteria[11] as a lipid plaque with a lipid arc ≥90° and a minimum fibrous cap thickness <65 µm. Plaque rupture was defined as a discontinuity of the fibrous cap with or without thrombus. Thrombus was defined as an intraluminal mass either homogeneous with low backscattering or highly backscattering with high attenuation. Healed plaques were defined as regions with one or more layers of different optical densities and a clear demarcation from underlying components. Macrophage accumulation was defined as signal-rich, distinct or confluent punctuate regions with a cast shadow behind. Cholesterol clefts were characterized by a thin, linear high-intensity region and neovascularisation as signal-poor voids that can be followed in multiple consecutive frames. A plaque was considered a HRP in the presence of at least two of the following three pre-specified criteria: (i) a lipid arc ≥90°, (ii) a minimum fibrous cap thickness <65 µm, and/or (iii) presence of either plaque rupture or thrombus.

Clinical endpoints

The primary clinical endpoint was defined as the occurrence of MACE, a composite endpoint of all-cause mortality, any non-fatal MI or unplanned revascularisation, at 2 year (± 30 days) follow-up. Secondary clinical endpoints include the individual components of the primary endpoint, cardiac death, target-vessel failure and revascularisation, and target-lesion failure and revascularisation. Endpoints definitions are provided in Supplementary methods S2. All potential clinical events were adjudicated by an independent event adjudication committee, of which the members were blinded to the results of the OCT analyses. Endpoints were adjudicated using medical records from participating centres, primary care clinicians, or other medical centres.

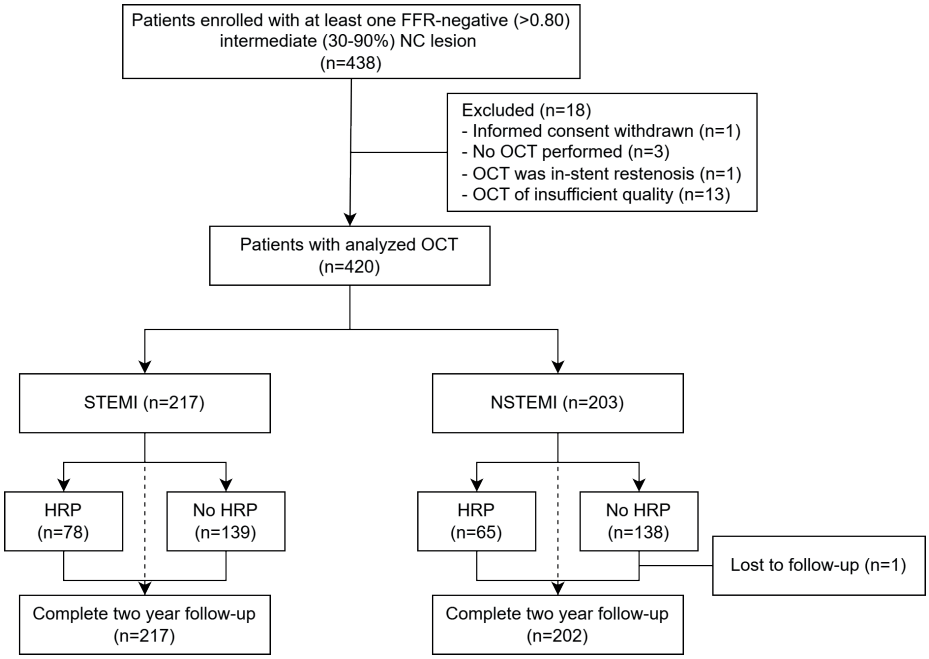


Figure 1. Study flowchart.

Flowchart of subjects included in the study.

FFR fractional flow reserve; HRP high-risk plaque; NSTEMI non-ST-segment elevation myocardial infarction; NC non-culprit, OCT optical coherence tomography, STEMI ST-segment elevation myocardial infarction.

Statistical analysis

Baseline demographics, procedural characteristics, OCT characteristics, and clinical outcome were compared between patients with NSTEMI and STEMI. Normally distributed continuous variables are expressed as means ± standard deviation (SD) and analysed using the Student's independent samples t-test, whereas non-normally distributed variables are expressed as medians with interquartile range and analysed using the Mann–Whitney U test. Categorical data are expressed as numbers and percentages and compared using the χ^2 test or Fisher's exact test, whenever appropriate. Lesion-level OCT characteristics were compared between groups using generalized estimating equations with an exchangeable correlation structure to account for potential within-patient clustering. The primary clinical endpoint was compared between groups using the log-rank test and is presented using cumulative incidence curves. Patients were censored at their last known moment of follow-up with a maximum of 2 years (+30 days) after inclusion. Uni-variable and multi-variable (correcting for all baseline clinical characteristics with a P-value <0.10 when compared between groups) Cox proportional hazards regression models were fitted to estimate the hazard ratio (HR) of NSTEMI at presentation for the primary clinical endpoint. HR for the secondary clinical endpoints were estimated using the Fine–Gray

model with non-cardiac death and all-cause mortality as competing risk factors for cardiac death and all other secondary clinical endpoints, respectively. Multi-variable analyses were only performed for the secondary endpoints that differed significantly between groups in uni-variable analysis. The association between HRP or its individual components and the primary clinical outcome were evaluated in the complete cohort using interaction terms and separately within the sub-groups using the log-rank test and uni-variable Cox proportional hazards regression model to estimate the HR. For these analyses, all patients with at least one HRP were considered high-risk and patients without any HRP were considered non-high-risk. Event rates for the secondary endpoints within the sub-groups according to the presence or absence of HRP were only provided descriptively. Statistical significance was considered at two-sided P-values <0.05. Data were analysed using IBM SPSS Statistics software version 27.0 (IBM Corp., USA) and Stata, release 17 (Stata-Corp LCC, USA).

Table 1. Baseline and procedural characteristics.

	NSTEMI n=203	STEMI n=217	P value
Age, years	65 ± 11	62 ± 10	0.004
BMI, kg/m^2	27.8 ± 5.0	27.7 ± 4.1	0.828
Female sex	44 (21.7%)	36 (16.6%)	0.185
Smoking status			0.221
Current	64 (32.0%)	59 (27.2%)	
Previous	65 (32.5%)	63 (29.0%)	
Hypertension	109 (53.7%)	113 (52.1%)	0.739
Diabetes	37 (18.2%)	24 (11.1%)	0.037
Hypercholesterolemia	84 (41.6%)	69 (31.8%)	0.038
Family history of premature atherosclerosis	77 (38.7%)	51 (23.5%)	<0.001
Previous MI	36 (17.7%)	27 (12.4%)	0.129
Previous PCI	39 (19.2%)	23 (10.6%)	0.013
Previous CVA	5 (2.5%)	3 (1.4%)	0.491
History of carotid artery disease	7 (3.4%)	6 (2.8%)	0.686
History of PAD	9 (4.4%)	8 (3.7%)	0.698
Total cholesterol, mmol/L	4.9 ± 1.3	5.1 ± 1.4	0.139
LDL-cholesterol, mmol/L	2.9 ± 1.2	3.2 ± 1.2	0.010
Triglycerides, mmol/L	2.1 ± 1.5	1.8 ± 1.4	0.037
eGFR, ml/min/1.73m^2	75.4 ± 18.8	83.9 ± 18.6	<0.001
CRP, mg/L	6.8 ± 16.9	7.0 ± 27.3	0.933
Leukocytes, x10^9/L	8.9 ± 2.8	10.5 ± 3.4	<0.001
Lipid lowering therapy at presentation	67 (33.0%)	41 (18.9%)	<0.001

Table 1. Continued

Infarct related artery			
LM	3 (1.5%)	2 (0.9%)	0.676
LAD	83 (40.9%)	84 (38.7%)	0.649
Cx	66 (32.5%)	42 (19.4%)	0.002
RCA	59 (29.1%)	98 (45.2%)	<0.001
Non-culprit lesion assessment			
Immediate	114 (56.2%)	42 (19.4%)	<0.001
Staged	89 (43.8%)	175 (80.6%)	<0.001
Time to staged procedure, days	16 ± 14	17 ± 16	0.598
Number of non-culprit lesions	1.19 ± 0.44	1.16 ± 0.39	0.450
Non-culprit lesion distribution			
LM	3 (1.5%)	1 (0.5%)	0.357
LAD	86 (42.4%)	89 (41.0%)	0.779
Cx	69 (34.0%)	85 (39.2%)	0.271
RCA	63 (31.0%)	59 (27.2%)	0.386
Targeted non-culprit FFR	0.89 ± 0.05	0.89 ± 0.05	0.256

BMI body mass index; CRP c-reactive protein; CVA cerebrovascular accident; Cx circumflex artery; eGFR estimated glomerular filtration rate; FFR fractional flow reserve; LAD left anterior descending artery; LDL low-density lipoprotein; LM left main coronary artery; MI myocardial infarction; NSTEMI non-ST-segment elevation myocardial infarction; PAD peripheral artery disease; PCI percutaneous coronary intervention; RCA right coronary artery; STEMI ST-segment elevation myocardial infarction.

RESULTS

Baseline and angiographic characteristics and clinical outcome

At least one OCT was analysable in 420 patients, of whom 203 (48.3%) presented with NSTEMI and 217 (51.7%) with STEMI (Figure 1). Baseline and angiographic characteristics are presented in Table 1. Patients with NSTEMI were on average older than patients with STEMI (mean age 65 ± 11 vs. 62 ± 10 years, P = 0.004). Patients with NSTEMI more frequently had a history of diabetes (18.2 vs. 11.1%, P = 0.037), hypercholesterolemia (41.6 vs. 31.8%, P = 0.038), and a family history for pre-mature atherosclerotic disease (38.7 vs. 23.5%, P < 0.001), resulting in an overall higher cardiovascular risk profile (see Supplementary data online, Figure S1). Moreover, NSTEMI patients more frequently had a history of PCI (19.2 vs. 10.6%, P = 0.013). Prescription of lipid lowering therapy at baseline was higher among patients with NSTEMI (33.0 vs. 18.9%, P < 0.001) and baseline LDL-cholesterol levels were lower (2.9 ± 1.2 vs. 3.2 ± 1.2 mmol/L, P = 0.010). Whilst the circumflex coronary artery was more frequently identified as the culprit artery in patients with NSTEMI (32.5 vs. 19.4%, P = 0.002), the right coronary artery was more frequently identified as culprit in patients with STEMI (29.1 vs. 45.2%, P < 0.001). No difference was observed in the number

of FFR-negative NC lesions (P = 0.450) or in the mean FFR measurement (P = 0.256). Guideline directed medical therapy prescription at discharge and during follow-up was comparable between groups (see Supplementary data online, Table S1).

Only one patient was lost to follow-up in between 1- and 2-years follow-up. Primary and secondary clinical endpoints are summarized in Table 2. At 2-year follow-up, the primary clinical endpoint of MACE had occurred in 29 (14.3%) patients with NSTEMI compared with 16 (7.4%) patients with STEMI (P = 0.025) (Figure 2). Specifically, non-fatal MI had occurred more often in patients with NSTEMI (6.4 vs. 0.5%, P = 0.011). After correcting for baseline differences between groups, statistical significance was maintained for non-fatal MI (P < 0.001) but not for MACE (P = 0.270).

Table 2. Two-year clinical outcome.

	NSTEMI n=203	STEMI n=217	Univariable HR (95% CI)	P value	Multivariable HR (95% CI)[a]	P value
Primary endpoint	29 (14.3%)	16 (7.4%)	1.99 (1.08-3.66)	0.025	1.51 (0.72-3.16)	0.270
Death (any)	8 (3.9%)	6 (2.8%)	1.40 (0.49-4.04)	0.531		
Cardiac Death	5 (2.5%)	5 (2.3%)	1.03 (0.30-3.50)[b]	0.960		
Non-fatal MI	13 (6.4%)	1 (0.5%)	13.87 (1.82-105.81)[c]	0.011	14.09 (1.62-122.48)	<0.001
Unplanned revascularization	16 (7.9%)	10 (4.6%)	1.70 (0.78-3.74)[c]	0.185		
Target vessel failure[d]	7 (3.4%)	4 (1.8%)	1.79 (0.53-6.06)[c]	0.347		
Target vessel revascularization[d]	7 (3.4%)	4 (1.8%)	1.79 (0.53-6.06)[c]	0.347		
Target lesion failure[d]	4 (2.0%)	4 (1.8%)	1.07 (0.27-4.27)[c]	0.925		
Target lesion revascularization[d]	4 (2.0%)	4 (1.8%)	1.07 (0.27-4.27)[c]	0.925		

CI confidence interval; HR hazard ratio; MI myocardial infarction; NSTEMI non-ST-segment elevation myocardial infarction; STEMI ST-segment elevation myocardial infarction.

[a] Multi-variable Cox proportional hazard regression models with NSTEMI at presentation, age, history of diabetes, history of hypercholesterolemia, family history for pre-mature atherosclerosis, history of percutaneous coronary intervention; baseline LDL-cholesterol levels, baseline triglyceride levels, baseline estimated glomerular filtration rate, baseline leukocyte levels, right coronary artery as culprit artery, and circumflex artery as culprit artery as independent variables.

[b] HR estimated using the Fine-Gray method with non-cardiac death as competing risk factor.

[c] HR estimated using the Fine-Gray method with all-cause mortality as competing risk factor.

[d] 'Target vessel/lesion' refers to the fractional flow reserve-negative NC vessel-lesion imaged by optical coherence tomography.

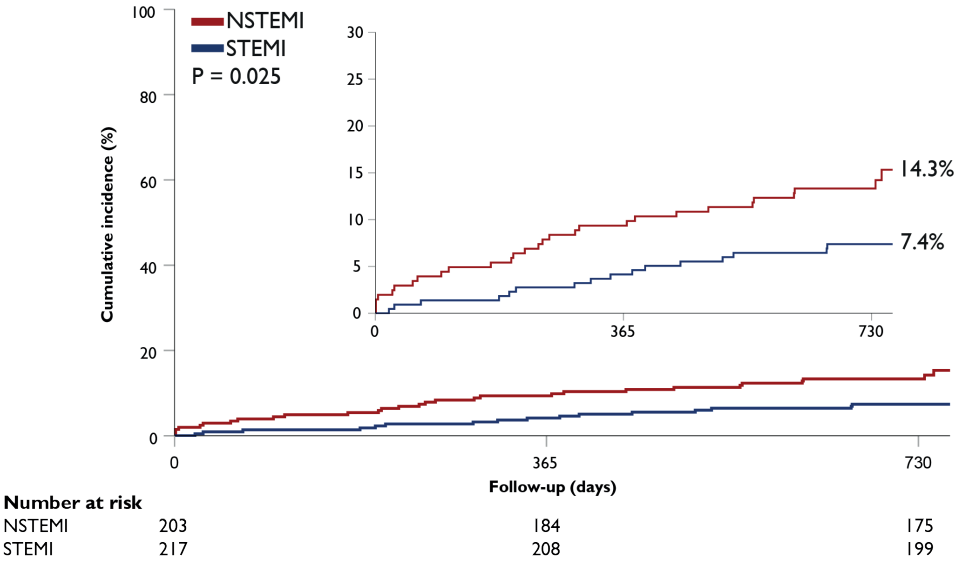


Figure 2. Two-year MACE.

Kaplan-Meier curve for the primary clinical outcome of MACE (composite endpoint of all-cause mortality, non-fatal MI, or unplanned revascularization) at 2 year follow-up.
NSTEMI non-ST-segment elevation myocardial infarction; STEMI ST-segment elevation myocardial infarction.

NC plaque characteristics

Luminal dimensions A total of 494 FFR-negative NC lesions were analysable, 242 in patients with NSTEMI and 252 in patients with STEMI. Lesion-level OCT characteristics are presented in Table 3. The mean minimum lumen area and diameter were significantly larger in patients with NSTEMI (2.84 ± 1.58 vs. 2.56 ± 1.48 mm^2, P = 0.048 and 1.55 ± 0.45 vs. 1.47 ± 0.44 mm, P = 0.045, respectively). Accordingly, the percentage area stenosis was smaller in these patients (60.5 ± 16.6% vs. 64.0 ± 15.4%, P = 0.016).

HRP features NC lesions in patients with NSTEMI less frequently had a lipid plaque (70.7 vs. 81.7%, P = 0.004) and lipid length was shorter (9.0 ± 6.7 vs. 10.6 ± 7.8 mm, P = 0.026). No difference was observed in the prevalence of HRP (29.3 vs. 32.9%, P = 0.412), but lesions in patients with NSTEMI less frequently had a lipid arc ≥90° (69.0 vs. 79.0%, P = 0.015). Plaque rupture was found in 27 (11.2%) lesions in patients with NSTEMI and in 21 (8.3%) lesions in patients with STEMI (P = 0.288). Thrombus was present in 22 (9.1%) and 21 (8.3%) lesions, respectively (P = 0.744). Macrophage accumulation was identified in 18.2% of lesions in NSTEMI compared with 27.8% in STEMI (P = 0.014).

Table 3. Lesion-level OCT characteristics according to clinical presentation.

	NSTEMI n=242	STEMI n=252	P value
Minimum lumen area, mm^2	2.84 ± 1.58	2.56 ± 1.48	0.048
Minimum lumen diameter, mm	1.55 ± 0.45	1.47 ± 0.44	0.045
Percentage area stenosis	60.5 ± 16.6	64.0 ± 15.4	0.016
Lesion length, mm	18.2 ± 8.6	19.2 ± 9.0	0.221
Calcification	162 (66.9%)	152 (60.3%)	0.128
Maximum calcification arc, °	151 ± 99	138 ± 86	0.215
Maximum calcification thickness, µm	860 ± 270	838 ± 244	0.455
Calcification length, mm	9.3 ± 8.1	8.6 ± 7.9	0.459
Protruding calcification	35 (14.5%)	24 (9.5%)	0.102
Lipid	171 (70.7%)	206 (81.7%)	0.004
Lipid length, mm	9.0 ± 6.7	10.6 ± 7.8	0.026
Maximum lipid arc, °	226 ± 83	224 ± 84	0.996
Lipid arc ≥90°	167 (69.0%)	199 (79.0%)	0.015
Minimum fibrous cap thickness, µm	106 ± 70	112 ± 68	0.444
Minimum cap thickness <65 µm	65 (26.9%)	71 (28.2%)	0.748
TCFA	65 (26.9%)	71 (28.2%)	0.748
Plaque rupture	27 (11.2%)	21 (8.3%)	0.288
Thrombus	22 (9.1%)	21 (8.3%)	0.744
Macrophage accumulation	44 (18.2%)	70 (27.8%)	0.014
Neovascularization	41 (16.9%)	37 (14.7%)	0.502
Healed plaque	48 (19.8%)	52 (20.6%)	0.781
Cholesterol clefts	21 (8.7%)	14 (5.6%)	0.187
High-risk plaque	71 (29.3%)	83 (32.9%)	0.412

NSTEMI non-ST-segment elevation myocardial infarction; STEMI ST-segment elevation myocardial infarction; TCFA thin cap fibroatheroma.

Association between clinical outcome and OCT characteristics

Sixty-five (32.0%) patients with NSTEMI and 78 (35.9%) patients with STEMI had at least one HRP. The incidence of MACE at 2-year follow-up was numerically higher in patients with at least one HRP compared with patients without a HRP, both in patients with NSTEMI (20.0 vs. 11.6%, P = 0.102, HR 1.83 [95% CI 0.88–3.80]) and with STEMI (11.5 vs. 5.0%, P = 0.075, HR 2.39 [95% CI 0.89–6.42]) ($P_{interaction}$ = 0.684) (Figure 3). All clinical endpoints according to the presence of HRPs within both groups are presented in Supplementary data online, Table S2. The association between the individual components of a HRP and MACE are presented in the Graphical Abstract. Among these, plaque rupture was significantly associated with MACE in patients with STEMI (P = 0.020, HR 3.51 [95% CI 1.13–10.89]) and NSTEMI (P < 0.001, HR 3.67 [95% CI 1.67–8.08]).

DISCUSSION

In this prospective contemporary cohort of patients with NSTEMI or STEMI, we found a higher incidence of MACE in NSTEMI patients. We also observed an equal prevalence of plaque features that could indicate 'left-behind' culprit lesions in NSTEMI and STEMI. There was no interaction between the clinical presentation and the association between presence of HRP and MACE. Among high-risk criteria, plaque rupture was significantly associated with MACE in both groups. These data call for additional research on NC revascularisation in NSTEMI patients similar to STEMI patients and on treatment of HRP.

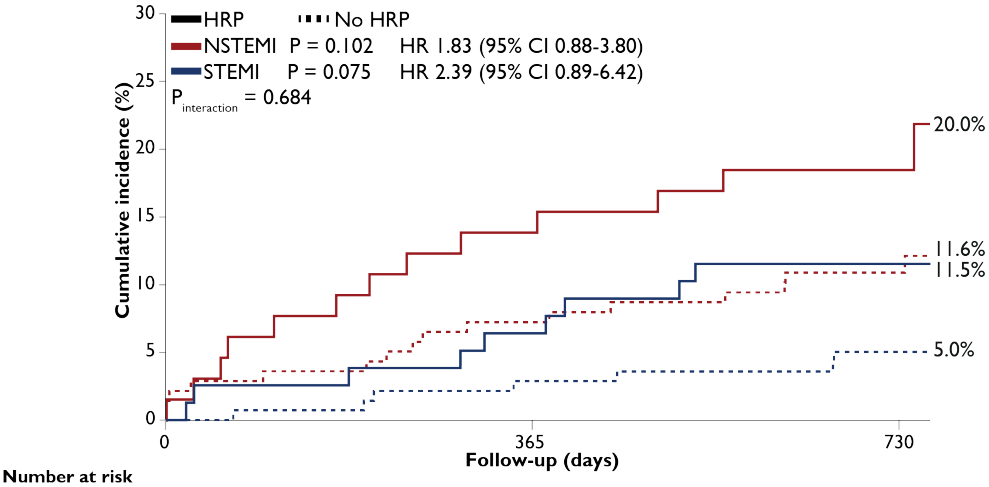


Figure 3. Two-year MACE and presence of HRP.

Kaplan-Meier curve for the primary clinical outcome of MACE (composite endpoint of all-cause mortality, non-fatal MI, or unplanned revascularization) at 2 year follow-up according to the presence of a HRP in NSTEMI and STEMI.
CI confidence interval; HR hazard ratio; HRP high-risk plaque; NSTEMI non-ST-segment elevation myocardial infarction; STEMI ST-segment elevation myocardial infarction.

HRP features of NC lesions

A limited number of studies have assessed differences in NC plaque characteristics between NSTEMI and STEMI. In a sub-study of the PROSPECT study, including 668 patients (457 NSTEMI and 211 STEMI) who underwent 3-vessel greyscale and virtual histology-IVUS, no differences in NC plaque characteristics were identified on a patient-level, including an equal presence of TCFA.[22] Fang et al. performed three-vessel OCT and found that the percentage area stenosis and prevalence of plaque rupture, calcification and neovascularisation were higher in NC plaques of patients with STEMI. The prevalence of TCFA and calcified plaques were 17.2% and 37.3%, respectively.[6] In contrast, we observed a prevalence of 27.5%

and 63.6%, respectively. This disparity may be related to the type of lesions included (i.e. three-vessel imaging versus targeted NC lesion imaging). The median minimum lumen area in the cohort of Fang et al. was 4.5 mm^2 (IQR 4.2–4.8) for NSTEMI and 4.2 mm^2 (IQR 4.0–4.4) for STEMI,[6] whereas we found a mean minimum lumen area of 2.84 ± 1.58 mm^2 and 2.56 ± 1.48 mm^2, respectively. Indeed, relative prevalence of TCFA and calcification increases with the degree of stenosis.[27,28]

Clinical outcome

Despite an equal presence of HRPs in the present cohort, we observed a higher incidence of MACE, and non-fatal MI in particular, in patients with NSTEMI, which was partially attributable to more traditional risk factors in these patients. This observed higher incidence of events during follow-up in patients with NSTEMI is in accordance with large-scale registry data in which this effect was also partly attributable to more cardiovascular comorbidities among these patients.[8,9] Such comorbidities have been associated with rapid lesion progression and future MI.[29,30]

Association between clinical outcome and OCT characteristics

In the primary analysis of the PECTUS-obs study, we demonstrated a significant association between OCT-identified HRP and 2-year MACE after MI.[24] These observations suggest incremental value of intracoronary imaging on top of physiological lesion assessment, also considering a diminished accuracy of the FFR in the acute setting of MI due to a temporary increased microvascular resistance,[18] and higher recurrent event rates among STEMI patients after FFR-guided deferral of NC revascularisation compared with those patients undergoing revascularisation with a positive FFR.[19] Although the present analysis was not powered to demonstrate statistically significant associations within sub-groups, we report no significant interaction between the primary outcome and the clinical syndrome at presentation. Presence of a HRP led to numerically higher incidence of MACE both in NSTEMI and STEMI compared with absence of HRP, irrespective of the more adverse clinical profile of patients with NSTEMI. STEMI patients without a HRP were at low risk for subsequent events (2-year incidence of MACE 5.0%). On the contrary, especially patients with NSTEMI and HRP were at very high risk for recurrent events with a 2-year incidence of MACE of 20.0%. Likewise, in a multi-national registry, encompassing 1474 patients (5.1% NSTEMI and 7.1% STEMI), patients with lipid rich plaques and NC related MACE during follow-up were more likely to have presented with NSTEMI at baseline.[31] These results challenge the hypothesis of reduced impact of HRP in NSTEMI and support ongoing research on complete revascularisation of NC plaques in these patients as well as studies on intensified medical treatment or focal treatment for HRP after MI.[32-35] Recently, the PREVENT trial demonstrated for the first time a potential benefit with regards to the latter, but included a very small proportion of patient with MI and OCT-identified HRPs drove revascularisation in a minority of cases.[36] Future studies assessing the clinical value of preventive treatment of HRP, ideally in more high-risk populations, are warranted for more definitive conclusions. It should however be acknowledged that recurrent events also occur in absence of HRP in the imaged segments. In this study, a strategy of targeted imaging of intermediate NC lesions was adopted rather than three-vessel imaging. We therefore cannot rule out that HRP phenotypes were present in other

segments without intermediate obstruction. Additionally, other plaque phenotypes other than the predefined PECTUS-obs criteria may be related to adverse outcome, calling for a retrospective evaluation of lesions progressing to cause events. Finally, OCT imaging was performed at a single point in time, which precluded assessment of plaque evolution over time.

Interestingly, plaque rupture was associated with recurrent events both in NSTEMI and STEMI. (Sub) clinical plaque rupture is a sign of pancoronary vulnerability and can lead to acute manifestations when resulting in acute thrombotic occlusion or to rapid lesion progression after subclinical healing.[37-39] Plaque rupture could therefore be a potential target for pre-emptive treatment both in NSTEMI and STEMI. However, considering that presence of plaque rupture and/or thrombus were only included in the pre-defined high-risk criteria of PECTUS-obs and not in earlier natural history studies, confirmation of the prognostic impact in additional studies is warranted. Nevertheless, the FORZA trial demonstrated that indication for revascularisation based on OCT-criteria, among which was plaque rupture, appeared to be a safe alternative to FFR-guided revascularisation.[40,41] However, this population consisted predominantly of patients with chronic coronary syndrome and was not powered to demonstrate differences in clinical outcome. Additional evidence may arise from the ongoing COMBINE-INTERVENE and INTERCLIMA trials, in which plaque rupture and thrombus are incorporated in the HRP criteria, respectively.[42,43]

Potential culprit lesion misidentification

The culprit lesion is generally easily identifiable in STEMI. In contrast, no culprit lesion can be identified by coronary angiography in one-third of NSTEMI patients, 60% of whom have evidence of focal MI on cardiac magnetic resonance. Furthermore, among the two-third of patients in whom a lesion is designated as culprit based on the coronary angiogram, cardiac magnetic resonance identifies another artery as culprit in one in seven cases.[10] The strong association between plaque rupture and future MACE in NSTEMI (2 year incidence of MACE 34.6%) and the observed trend towards higher MACE in the presence of thrombus could indicate that some of the NC lesions imaged may have in fact been the culprit lesion. However, in accordance with the findings of the PROSPECT study,[22] we report equal proportions of NC lesions with presence of plaque rupture or thrombus in NSTEMI and STEMI, contradicting the potential of missed culprit lesions. It is however unknown how true culprit lesions are distributed among FFR-positive and FFR-negative lesions. Irrespectively, pursuing complete angiographic NC revascularisation would imply treatment of all potential culprit lesions.

The present study has some limitations. First, OCT was performed of FFR-negative intermediate NC lesions only rather than three-vessel OCT. The results therefore only apply to FFR-negative lesions and it remains uncertain whether the imaged lesions were indeed all NC lesions, especially in NSTEMI. Furthermore, the latest ESC guidelines on acute coronary syndrome advocates complete angiography-guided revascularisation rather than FFR-guided revascularisation of NC lesions.[14] Although the present study is not in line with this recommendation, no recommendations on guidance of NC revascularisation were made in the prevailing guidelines during the conduct of the study. Additionally, although medical prescription rates were largely comparable between groups, only few patients were on PCSK9-inhibitors and effectiveness of prescribed lipid lowering therapy could not be assessed in absence of cholesterol

levels during follow-up. Last, the study was not powered to demonstrate differences in secondary endpoints in the complete cohort or in clinical outcome within the sub-groups and results on the association between HRP components and clinical outcome should therefore be considered hypothesis generating and require confirmation in larger studies.

CONCLUSION

FFR-negative NC lesions in patients with NSTEMI have a lower degree of stenosis and less frequently harbour lipid plaques compared with patients with STEMI, but prevalence of HRP is comparable. NC HRP leads to numerically higher event rates in both clinical scenarios. These results call for additional research on complete revascularisation in NSTEMI as well as on treatment of HRP after MI.

REFERENCES

1. Chan MY, Sun JL, Newby LK, Shaw LK, Lin M, Peterson ED et al. Long-term mortality of patients undergoing cardiac catheterization for ST-elevation and non-ST-elevation myocardial infarction. Circulation 2009;119:3110-7.
2. Biswas S, Andrianopoulos N, Papapostolou S, Noaman S, Duffy SJ, Lefkovits J et al. Does the subtype of acute coronary syndrome treated by percutaneous coronary intervention predict long-term clinical outcomes? Eur Heart J Qual Care Clin Outcomes 2018;4:318-327.
3. van Leeuwen MA, Daemen J, van Mieghem NM, de Boer SP, Boersma E, van Geuns RJ et al. Comparison of long-term outcomes in STEMI and NSTE-ACS after coronary stent placement: an analysis in a real world BMS and DES population. Int J Cardiol 2013;167:2082-7.
4. Iannaccone M, Quadri G, Taha S, D'Ascenzo F, Montefusco A, Omede P et al. Prevalence and predictors of culprit plaque rupture at OCT in patients with coronary artery disease: a meta-analysis. Eur Heart J Cardiovasc Imaging 2016;17:1128-37.
5. Dong L, Mintz GS, Witzenbichler B, Metzger DC, Rinaldi MJ, Duffy PL et al. Comparison of plaque characteristics in narrowings with ST-elevation myocardial infarction (STEMI), non-STEMI/unstable angina pectoris and stable coronary artery disease (from the ADAPT-DES IVUS Substudy). Am J Cardiol 2015;115:860-6.
6. Fang C, Yin Y, Jiang S, Zhang S, Wang J, Wang Y et al. Increased Vulnerability and Distinct Layered Phenotype at Culprit and Nonculprit Lesions in STEMI Versus NSTEMI. JACC Cardiovasc Imaging 2022;15:672-681.
7. Fox KA, Carruthers KF, Dunbar DR, Graham C, Manning JR, De Raedt H et al. Underestimated and under-recognized: the late consequences of acute coronary syndrome (GRACE UK-Belgian Study). Eur Heart J 2010;31:2755-64.
8. Park HW, Yoon CH, Kang SH, Choi DJ, Kim HS, Cho MC et al. Early- and late-term clinical outcome and their predictors in patients with ST-segment elevation myocardial infarction and non-ST-segment elevation myocardial infarction. Int J Cardiol 2013;169:254-61.
9. Fokkema ML, James SK, Albertsson P, Aasa M, Akerblom A, Calais F et al. Outcome after percutaneous coronary intervention for different indications: long-term results from the Swedish Coronary Angiography and Angioplasty Registry (SCAAR). EuroIntervention 2016;12:303-11.
10. Heitner JF, Senthilkumar A, Harrison JK, Klem I, Sketch MH, Jr., Ivanov A et al. Identifying the Infarct-Related Artery in Patients With Non-ST-Segment-Elevation Myocardial Infarction. Circ Cardiovasc Interv 2019;12:e007305.
11. Burke AP, Farb A, Malcom GT, Liang YH, Smialek J, Virmani R. Coronary risk factors and plaque morphology in men with coronary disease who died suddenly. N Engl J Med 1997;336:1276-82.
12. Stone GW, Maehara A, Lansky AJ, de Bruyne B, Cristea E, Mintz GS et al. A prospective natural-history study of coronary atherosclerosis. N Engl J Med 2011;364:226-35.
13. Writing Committee M, Lawton JS, Tamis-Holland JE, Bangalore S, Bates ER, Beckie TM et al. 2021 ACC/AHA/SCAI Guideline for Coronary Artery Revascularization: Executive Summary: A Report of the American College of Cardiology/American Heart Association Joint Committee on Clinical Practice Guidelines. J Am Coll Cardiol 2022;79:197-215.
14. Byrne RA, Rossello X, Coughlan JJ, Barbato E, Berry C, Chieffo A et al. 2023 ESC Guidelines for the management of acute coronary syndromes. Eur Heart J 2023;44:3720-3826.
15. Mehta SR, Wood DA, Storey RF, Mehran R, Bainey KR, Nguyen H et al. Complete Revascularization with Multivessel PCI for Myocardial Infarction. N Engl J Med 2019;381:1411-1421.
16. Engstrom T, Kelbaek H, Helqvist S, Hofsten DE, Klovgaard L, Holmvang L et al. Complete revascularisation versus treatment of the culprit lesion only in patients with ST-segment elevation myocardial infarction and multivessel disease (DANAMI-3-PRIMULTI): an open-label, randomised controlled trial. Lancet 2015;386:665-71.

17. Smits PC, Abdel-Wahab M, Neumann FJ, Boxma-de Klerk BM, Lunde K, Schotborgh CE et al. Fractional Flow Reserve-Guided Multivessel Angioplasty in Myocardial Infarction. N Engl J Med 2017;376:1234-1244.

18. van der Hoeven NW, Janssens GN, de Waard GA, Everaars H, Broyd CJ, Beijnink CWH et al. Temporal Changes in Coronary Hyperemic and Resting Hemodynamic Indices in Nonculprit Vessels of Patients With ST-Segment Elevation Myocardial Infarction. JAMA Cardiol 2019;4:736-744.

19. Denormandie P, Simon T, Cayla G, Steg PG, Montalescot G, Durand-Zaleski I et al. Compared Outcomes of ST-Segment-Elevation Myocardial Infarction Patients With Multivessel Disease Treated With Primary Percutaneous Coronary Intervention and Preserved Fractional Flow Reserve of Nonculprit Lesions Treated Conservatively and of Those With Low Fractional Flow Reserve Managed Invasively: Insights From the FLOWER-MI Trial. Circ Cardiovasc Interv 2021;14:e011314.

20. Rathod KS, Koganti S, Jain AK, Astroulakis Z, Lim P, Rakhit R et al. Complete Versus Culprit-Only Lesion Intervention in Patients With Acute Coronary Syndromes. J Am Coll Cardiol 2018;72:1989-1999.

21. Biscaglia S, Guiducci V, Escaned J, Moreno R, Lanzilotti V, Santarelli A et al. Complete or Culprit-Only PCI in Older Patients with Myocardial Infarction. N Engl J Med 2023.

22. Brener SJ, Weisz G, Maehara A, Mehran R, McPherson J, Farhat N et al. Does clinical presentation affect outcome among patients with acute coronary syndromes undergoing percutaneous coronary intervention? Insights from the Providing Regional Observations to Study Predictors of Events in the Coronary Tree study. Am Heart J 2012;164:561-7.

23. Mol JQ, Belkacemi A, Volleberg RH, Meuwissen M, Protopopov AV, Laanmets P et al. Identification of anatomic risk factors for acute coronary events by optical coherence tomography in patients with myocardial infarction and residual nonflow limiting lesions: rationale and design of the PECTUS-obs study. BMJ Open 2021;11:e048994.

24. Mol JQ, Volleberg R, Belkacemi A, Hermanides RS, Meuwissen M, Protopopov AV et al. Fractional Flow Reserve-Negative High-Risk Plaques and Clinical Outcomes After Myocardial Infarction. JAMA Cardiol 2023;8:1013-1021.

25. Araki M, Park SJ, Dauerman HL, Uemura S, Kim JS, Di Mario C et al. Optical coherence tomography in coronary atherosclerosis assessment and intervention. Nat Rev Cardiol 2022;19:684-703.

26. Tearney GJ, Regar E, Akasaka T, Adriaenssens T, Barlis P, Bezerra HG et al. Consensus standards for acquisition, measurement, and reporting of intravascular optical coherence tomography studies: a report from the International Working Group for Intravascular Optical Coherence Tomography Standardization and Validation. J Am Coll Cardiol 2012;59:1058-72.

27. Pinilla-Echeverri N, Mehta SR, Wang J, Lavi S, Schampaert E, Cantor WJ et al. Nonculprit Lesion Plaque Morphology in Patients With ST-Segment-Elevation Myocardial Infarction: Results From the COMPLETE Trial Optical Coherence Tomography Substudys. Circ Cardiovasc Interv 2020;13:e008768.

28. Tian J, Dauerman H, Toma C, Samady H, Itoh T, Kuramitsu S et al. Prevalence and characteristics of TCFA and degree of coronary artery stenosis: an OCT, IVUS, and angiographic study. J Am Coll Cardiol 2014;64:672-80.

29. Mohammad MA, Stone GW, Koul S, Olivecrona GK, Bergman S, Persson J et al. On the Natural History of Coronary Artery Disease: A Longitudinal Nationwide Serial Angiography Study. J Am Heart Assoc 2022;11:e026396.

30. Plakht Y, Gilutz H, Shiyovich A. When More Means Less: The Prognosis of Recurrent Acute Myocardial Infarctions. J Clin Med 2021;10.

31. Xing L, Higuma T, Wang Z, Aguirre AD, Mizuno K, Takano M et al. Clinical Significance of Lipid-Rich Plaque Detected by Optical Coherence Tomography: A 4-Year Follow-Up Study. J Am Coll Cardiol 2017;69:2502-2513.

32. Raber L, Ueki Y, Otsuka T, Losdat S, Haner JD, Lonborg J et al. Effect of Alirocumab Added to High-Intensity Statin Therapy on Coronary Atherosclerosis in Patients With Acute Myocardial Infarction: The PACMAN-AMI Randomized Clinical Trial. JAMA 2022;327:1771-1781.

33. Pustjens TFS, Streukens B, Vainer J, Gho B, Ruiters AW, Stein M et al. Design and rationale of ischaemia-driven complete revascularisation versus usual care in patients with non-ST-elevation myocardial infarction and multivessel coronary disease: the South Limburg Myocardial Infarction (SLIM) trial. Neth Heart J 2020;28:75-80.

34. Montarello NJ, Singh K, Sinhal A, Wong DTL, Alcock R, Rajendran S et al. Assessing the Impact of Colchicine on Coronary Plaque Phenotype After Myocardial Infarction with Optical Coherence Tomography: Rationale and Design of the COCOMO-ACS Study. Cardiovasc Drugs Ther 2022;36:1175-1186.

35. Complete revascularization versus culprit only PCI in NSTEMI (Complete-NSTEMI). ClinicalTrials.gov identifier: NCT05786131. Updated July 6, 2023. Accessed August 21, 2023. https://classic.clinicaltrials.gov/ct2/show/NCT05786131.

36. Park SJ, Ahn JM, Kang DY, Yun SC, Ahn YK, Kim WJ et al. Preventive percutaneous coronary intervention versus optimal medical therapy alone for the treatment of vulnerable atherosclerotic coronary plaques (PREVENT): a multicentre, open-label, randomised controlled trial. Lancet 2024;403:1753-1765.

37. Aguirre AD, Arbab-Zadeh A, Soeda T, Fuster V, Jang IK. Optical Coherence Tomography of Plaque Vulnerability and Rupture: JACC Focus Seminar Part 1/3. J Am Coll Cardiol 2021;78:1257-1265.

38. Vergallo R, Crea F. Atherosclerotic Plaque Healing. N Engl J Med 2020;383:846-857.

39. Vergallo R, Uemura S, Soeda T, Minami Y, Cho JM, Ong DS et al. Prevalence and Predictors of Multiple Coronary Plaque Ruptures: In Vivo 3-Vessel Optical Coherence Tomography Imaging Study. Arterioscler Thromb Vasc Biol 2016;36:2229-2238.

40. Burzotta F, Leone AM, Aurigemma C, Zambrano A, Zimbardo G, Arioti M et al. Fractional Flow Reserve or Optical Coherence Tomography to Guide Management of Angiographically Intermediate Coronary Stenosis: A Single-Center Trial. JACC Cardiovasc Interv 2020;13:49-58.

41. Burzotta F, Zito A, Aurigemma C, Romagnoli E, Bianchini F, Bianchini E et al. Fractional flow reserve or optical coherence tomography for angiographically intermediate coronary stenoses: 5-year outcomes in the FORZA trial. Eur Heart J 2024;45:2785-2788.

42. COMBINE-INTERVENE: combined ischemia and vulnerable plaque percutaneous intervention to reduce cardiovascular events. ClinicalTrials.gov identifier: NCT053330658. Updated April 18, 2022. Accesed March 7, 2025. https://clinicaltrials.gov/study/NCT05333068.

43. Interventional strategy for non-culprit lesions with major vulnerability criteria at OCT in patients with ACS (INTERCLIMA). ClinicalTrials.gov identifier: NCT05027984. Updated August 31, 2021. Accessed March 7, 2024. https://clinicaltrials.gov/study/NCT05027984.

SUPPLEMENTAL MATERIAL

Supplemental material related to this article can be found in the online version:
https://academic.oup.com/ehjcimaging/article/26/2/197/7886852





CHAPTER 8

Sex differences in plaque characteristics of fractional flow reserve-negative non-culprit lesions after myocardial infarction

Rick Volleberg | Jan-Quinten Mol | Anouar Belkacemi | Renicus Hermanides | Martijn Meuwissen | Alexey Protopopov | Peep Laanmets | Oleg Krestyaninov | Robert Dennert | Rohit Oemrawsingh | Jan-Peter van Kuijk | Karin Arkenbout | Dirk van der Heijden | Saman Rasoul | Erik Lipsic | Laura Rodwell | Cyril Camaro | Peter Damman | Tomasz Roleder | Elvin Kedhi | Maarten van Leeuwen | Robert-Jan van Geuns | Niels van Royen

Atherosclerosis
2024 Oct:397:118568

ABSTRACT

Background and aims Recurrent events after myocardial infarction (MI) are common and often originate from native non-culprit (NC) lesions that are non-flow limiting. These lesions consequently pose as targets to improve long-term outcome. It is however largely unknown whether these lesions differ between sexes. The aim of this study was to assess such potential differences.

Methods From the PECTUS-obs study, we assessed sex-related differences in plaque characteristics of fractional flow reserve (FFR)-negative intermediate NC lesions in 420 MI-patients.

Results Among included patients, 80 (19.1%) were female and 340 (80.9%) male. Women were older and more frequently had hypertension and diabetes. In total, 494 NC lesions were analyzed. After adjustment for clinical characteristics and accounting for within-patients clustering, lesion length was longer in female patients (20.8 ± 10.0 vs 18.3 ± 8.5 mm, p=0.048) and minimum lumen area (2.30 ± 1.42 vs 2.78 ± 1.54 mm^2, p<0.001) and minimum lumen diameter (1.39 ± 0.45 vs 1.54 ± 0.44 mm, p<0.001) were smaller. The minimum fibrous cap thickness was smaller among females (96 ± 53 vs 112 ± 72 µm, p=0.025), with more lesions harboring a thin cap fibroatheroma (39.3% vs 24.9%, p<0.001). Major adverse cardiovascular events at two years occurred in 6.3% of female patients and 11.8% of male patients (p=0.15).

Conclusions FFR-negative NC lesions after MI harbored more high-risk plaque features in female patients. Although this did not translate into an excess of recurrent events in female patients in this modestly sized cohort, it remains to be investigated whether this difference affects clinical outcome.

INTRODUCTION

Recurrent events after two years occur in up to 15-20% of patients presenting with myocardial infarction (MI), approximately half of which originate from native non-culprit (NC) lesions.[1] As such, these lesions pose as potential targets to improve patient outcome. Complete NC revascularization, either guided by coronary angiography or fractional flow reserve (FFR), has been shown to improve clinical outcome compared to culprit-lesion revascularization only.[2] Nevertheless, recurrent event rates in FFR-guided deferred NC lesions following MI remain markedly higher compared to FFR-guided deferral in chronic coronary syndrome.[3,4] Importantly, FFR targets evaluation of hemodynamic significance and provides only limited information on plaque morphology.

Intracoronary optical coherence tomography (OCT) allows *in vivo* assessment of plaque morphology and composition, allowing identification of plaque features that are associated with plaque instability such as thin cap fibroatheromas (TCFA).[5] Indeed, the COMBINE (OCT-FFR) study and PECTUS-obs studies demonstrated the incremental value of OCT in NC lesions to identify patients at increased risk for recurrent events despite a negative FFR.[6,7] Yet, evidence on sex-related differences in such NC lesions after MI is scarce.[8-11]

Although coronary artery disease impacts both sexes, existing evidence indicates sex-related differences in the clinical presentation and pathophysiology. Women on average present with coronary complications a decade later[12,13] and symptomatology is often less typical.[14] Histopathological studies demonstrated that plaque erosion predominantly causes MI in women, whilst plaque rupture is the leading cause of MI in men.[15,16] However, plaque rupture becomes increasingly important with increasing age in female patients.[17] We hypothesized that differences in plaque composition between men and women are not limited to culprit plaques only but are also present in NC plaques. However, previous studies demonstrated conflicting results.[18] For example, female patients had a higher lesion-level lipid burden in the Lipid Rich Plaque study,[8] whereas no differences in high-risk plaques were observed in the PROSPECT study.[9] We therefore compared sex-related differences in FFR-negative NC plaque characteristics as assessed by OCT in this exploratory subgroup analysis of the PECTUS-obs study.

PATIENTS AND METHODS

Study design

PECTUS-obs (NCT03857971) is a multicenter, prospective, observational study designed to assess the association between OCT-identified high-risk plaques in FFR-negative NC lesions and future adverse cardiovascular events in patients presenting with MI. The design, including in- and exclusion criteria, and primary outcome of this study were described before.[7,19] In brief, 438 patients with ST-segment-elevation myocardial infarction (STEMI) or non-ST-segment-elevation myocardial infarction (NSTEMI) underwent OCT of all FFR-negative intermediate NC lesion (defined as an angiographically assessed stenosis grade of 30-90% with a FFR > 0.80) after primary percutaneous coronary intervention (PCI) of the

culprit artery. OCT acquisition was performed using the Dragonfly Optis catheter (Abbott Vascular, USA) under fluoroscopic guidance to ensure OCT findings could be correlated to the coronary angiogram. Structured clinical follow-up was obtained one and two years (± 30 days) after inclusion by means of telephone contact. The study was conducted in accordance with the 1964 Declaration of Helsinki and was approved by the institutional review boards and/or medical ethics committee of each participating center. All patients provided written informed consent. For the present prespecified subgroup analysis, all patients with at least one analyzable OCT were divided in two groups according to their sex assigned at birth.

OCT imaging analysis

OCT images were analyzed offline by an independent OCT core laboratory (Real Solution Sp. Z o.o., Wroclaw, Poland) blinded to clinical outcome using Caas IntraVascular (Pie Medical Imaging B.V., Maastricht, the Netherlands). Pullbacks with insufficient image quality at the target region for both qualitative and quantitative analysis were excluded. Analyses were performed in accordance with contemporary consensus documents.[5,20] Quantitative analyses included lesion length, minimum lumen area (MLA), minimum lumen diameter (MLD), proximal and distal reference area, proximal and distal reference diameter and percentage area stenosis (%AS, calculated using interpolation of reference lumen areas). Calcification was defined as signal-poor or heterogenous regions with a sharply delineated border. Protruding calcification was defined as a lesion meeting the definition of a calcification with the calcified region protruding into the lumen. Lipid plaques were defined as signal-poor regions with poorly delineated borders with a fast signal drop-off that is separated from the lumen by an overlying signal-rich band, the fibrous cap. TCFA was defined as a lipid plaque with a lipid arc extending over ≥90° and with a minimum fibrous cap thickness <65 µm. Plaque rupture was defined as a discontinuity of the fibrous cap and thrombus as an intraluminal mass either homogeneous with low backscattering or highly backscattering with high attenuation. Healed plaques were defined as regions with one or more layers of different optical densities and a clear demarcation from underlying components. Macrophage accumulation was characterized as signal-rich, distinct or confluent punctate regions that exceed the intensity of background speckle noise and that has a cast shadow behind and cholesterol clefts as thin, linear regions with high intensity. Neovascularization was characterized as signal-poor voids that can be followed in multiple consecutive frames. A lesion was deemed as a high-risk plaque in the presence of ≥2 of the following prespecified criteria: 1) a lipid arc ≥90°, 2) a minimum fibrous cap thickness <65 µm, and/or 3) presence of either plaque rupture or thrombus.

Clinical outcome

The primary clinical endpoint was the occurrence of major adverse cardiovascular events (MACE), a composite endpoint of all-cause mortality, non-fatal MI and unplanned revascularization, at two year (±30 days) follow-up. All potential clinical events were adjudicated by an independent event adjudication committee, of which the members were blinded to the OCT analyses.

Statistical analysis

Baseline demographics, procedural characteristics, OCT characteristics and clinical outcome were compared between male and female patients. Continuous variables were expressed as means ± standard deviation (SD) and analyzed using the Student's independent samples t-test when Gaussian distribution was confirmed. Non-Gaussian distributed variables were expressed as medians with interquartile ranges (IQR) and analyzed with the Mann-Whitney U test. Categorical data was expressed as numbers and percentages and compared with the Chi squared tests or Fisher's exact test, whenever appropriate. Comparison of lesion-level OCT characteristics between groups was performed using generalized estimating equations with an exchangeable correlation structure to account for potential within-subject correlation due to multiple plaques analyzed per patient. Multivariable linear and logistic regression models were used to assess the impact of sex on OCT-derived plaque components after correcting for all baseline characteristics with a p-value <0.10 when compared between groups. Additional univariate and multivariable regression analyses were performed to assess the predictive value of clinical and angiographic characteristics for the presence of a high-risk plaque. Clinical outcome was compared between sexes using the log-rank test and is presented using Kaplan-Meier curves. Statistical significance was considered at p-values < 0.05. Data was analyzed using IBM SPSS Statistics software version 29.0 (IBM Corp., Armon, NY, USA).

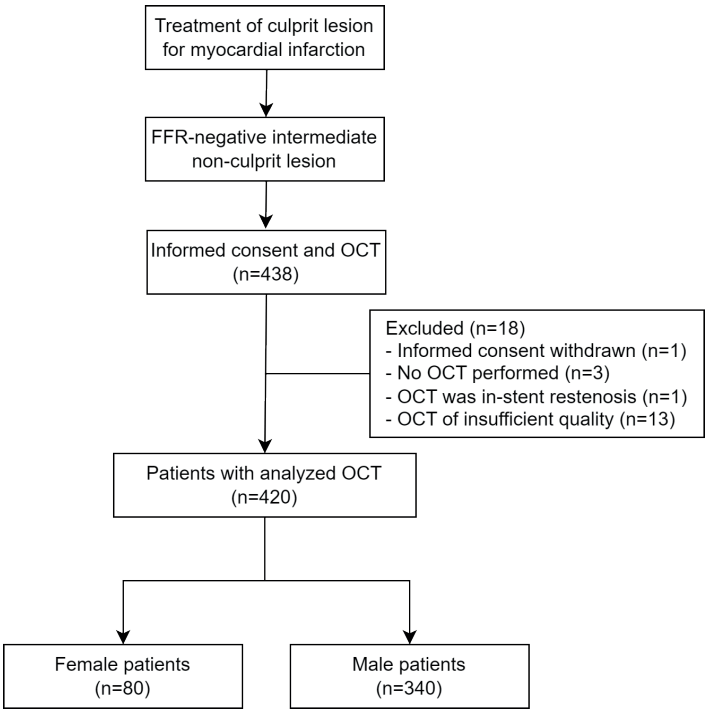


Figure 1. Study flowchart.

FFR fractional flow reserve; OCT optical coherence tomography.

RESULTS

Baseline demographics and angiographic characteristics

Among 420 patients with at least one analyzable NC lesion, 80 were female (19.1%) and 340 (80.9%) were male (Figure 1). Baseline demographics and angiographic characteristics are presented in Table 1. Women were older (mean age 68 ± 9 vs 62 ± 10 years, p<0.001) and had a higher prevalence of hypertension (63.7% vs 50.3%, p=0.030) and diabetes (26.3% vs 11.8%, p<0.001). Renal function was significantly lower in female patients (mean eGFR 75 ± 17 vs 81 ± 19 ml/min/1.73m^2, p=0.010), whereas baseline triglyceride levels were higher among male patients (1.6 ± 0.8 vs 2.0 ± 1.6 mmol/l, p=0.010). There was no difference in the clinical presentation between women and men (STEMI 45.0% vs 53.2% and NSTEMI 55.0% vs 46.8%, p=0.19). Culprit and NC plaque distribution was comparable in both groups. The mean FFR of targeted NC lesions was 0.89 ± 0.05 and did not differ between sexes (p=0.19).

Table 1. Baseline characteristics according to sex.

	Female n=80	**Male n=340**	***p***
Age, y	68 ± 9	62 ± 10	<0.001
BMI, kg/m^2	27.9 ± 5.8	27.7 ± 4.2	0.78
Smoking status			
Current	23 (28.7%)	100 (29.7%)	0.07
Previous	17 (21.3%)	111 (32.9%	
Hypertension	51 (63.7%)	171 (50.3%)	0.030
Diabetes	21 (26.3%)	40 (11.8%)	<0.001
Hypercholesterolemia	32 (40.5%)	121 (35.6%)	0.41
Family history of premature atherosclerosis	25 (31.6%)	103 (30.6%)	0.85
Previous MI	16 (20.0%)	47 (13.8%)	0.16
Previous PCI	14 (17.5%)	48 (14.1%)	0.44
Previous CVA	2 (2.5%)	6 (1.8%)	0.65
History of carotid artery disease	0 (0%)	13 (3.8%)	0.14
History of PAD	4 (5.0%)	13 (3.8%)	0.54
STEMI at presentation	36 (45.0%)	181 (53.2%)	0.19
GRACE score	119 ± 29	116 ± 33	0.46
Total cholesterol, mmol/L	5.0 ± 1.4	5.0 ± 1.4	0.98
LDL-cholesterol, mmol/L	3.0 ± 1.4	3.0 ± 1.2	0.74
Triglycerides, mmol/L	1.6 ± 0.8	2.0 ± 1.6	0.010
eGFR, ml/min/1.73m^2	75 ± 17	81 ± 19	0.010
CRP, mg/L	7.6 ± 18.7	6.7 ± 22.7	0.80
Leukocytes x10^9/L	10.1 ± 3.3	9.7 ± 3.2	0.31

Table 1. Continued

Lipid-lowering therapy at presentation	26 (32.5%)	82 (24.1%)	0.12
Infarct-related artery			
LM	4 (1.2%)	1 (1.3%)	1.00
LAD	33 (41.3%)	134 (39.4%)	0.76
Cx	18 (22.5%)	90 (26.5%)	0.47
RCA	31 (38.8%)	126 (37.1%)	0.78
Number of non-culprit lesions	1.11 ± 0.39	1.19 ± 0.42	0.11
Nonculprit lesion distribution			
LM	1 (1.3%)	3 (0.9%)	0.57
LAD	31 (38.8%)	144 (42.4%)	0.56
Cx	27 (33.8%)	127 (37.4%)	0.55
RCA	26 (32.5%)	96 (28.2%)	0.45
Targeted nonculprit lesion FFR	0.88 ± 0.05	0.89 ± 0.05	0.19

BMI body mass index; CRP c-reactive protein; CVA cerebrovascular accident; Cx circumflex artery; eGFR estimated glomerular filtration rate; FFR fractional flow reserve; LAD left anterior descending artery; LDL low-density lipoprotein; LM left main coronary artery; MI myocardial infarction; PAD peripheral artery disease; PCI percutaneous coronary intervention; RCA right coronary artery; STEMI ST-segment elevation myocardial infarction, y years.

Optical coherence tomography characteristics

A total of 494 NC lesions were assessed using OCT, 89 (18.0%) in women and 405 (82.0%) in men (Figure 2). OCT characteristics on a lesion level are summarized in Table 2. After correction for potentially contributing baseline characteristics, mean lesion length was longer in female patients (20.8 ± 10.0 vs 18.3 ± 8.5 mm, p=0.048) and mean MLA (2.30 ± 1.42 vs 2.78± 1.54 mm^2, p<0.001) and MLD (1.39 ± 0.45 vs 1.54 ± 0.44 mm, p<0.001) were significantly smaller. However, no difference was observed in %AS between groups (63.0 ± 15.9 vs 62.1 ± 16.1%, p=0.69). There was no difference in the presence and extent of calcified plaques in men and women. The number of lipid plaques was similar in both groups (77.5% vs 76.0%, p=0.79). Although the mean lipid length (11.9 ± 9.9 vs 9.4 ± 6.6 mm, p=0.045) was greater in female patients in univariate analysis, statistical significance was not maintained in multivariable analysis (p=0.05). NC lesions in female patients more frequently classified as a high-risk plaque (39.3% vs 29.4%, p=0.009). In particular, the mean minimum fibrous cap thickness was smaller among female patients (96 ± 53 vs 112 ± 72 mm, p=0.025), with more lesions classifying as a TCFA (39.3% vs 24.9%, p<0.001) and thrombus was more frequently present in women (13.5% vs 7.7%, p<0.008). No difference was observed in the mean maximum lipid arc between groups (244 ± 89 vs 221 ± 81°, p=0.16) or prevalence of microstructures often associated with plaque vulnerability such as macrophage accumulation (p=0.64) and neovascularization (p=0.52). Female sex was independently associated with the presence of a high-risk plaque in multivariable analysis (p=0.048) correcting for all characteristics with a potential association (p<0.10 in univariate analysis, Supplementary Table 1).

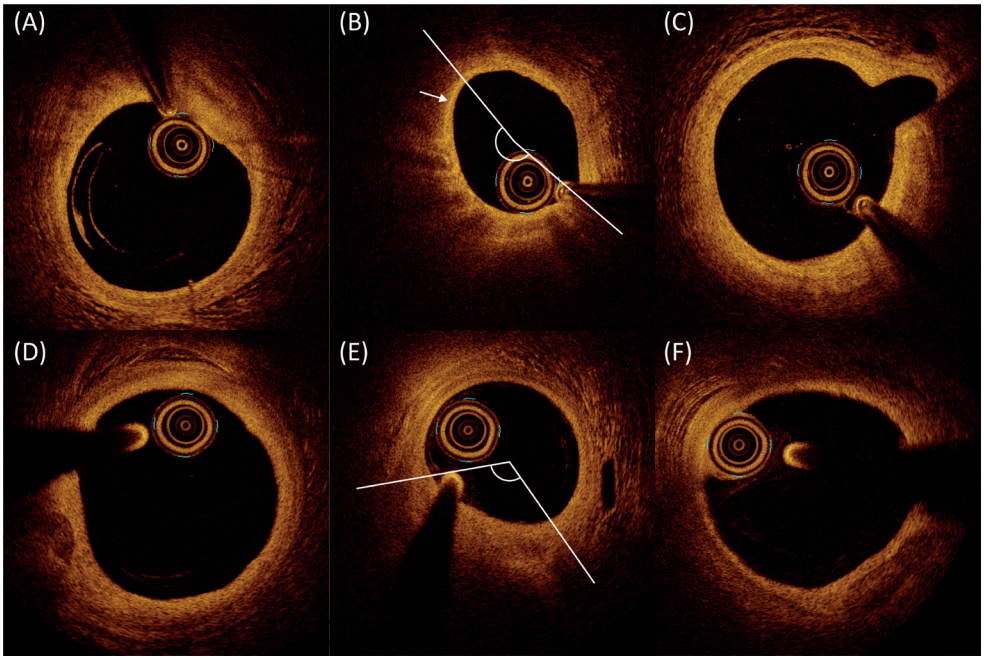


Figure 2. Case examples of non-culprit plaques in female and male patients.
Case examples of a non-culprit plaque in the proximal left circumflex in a female (A-C) and male (D-F) patient. A-C) In the female patient, the minimum lumen area measured 2.72 mm^2 (B) and the proximal (A) and distal (C) reference areas measured 5.31 mm^2 and 5.59 mm^2, respectively, resulting in a 50.3% area stenosis. At the site of the minimum lumen area (B), a lipid plaque with a thin fibrous cap (arrow) was observed. D-F) In the male patient, the minimum lumen area measured 3.24 mm^2 (E) and the proximal (D) and distal (F) reference areas measured 6.55 mm^2 and 6.51 mm^2, respectively, resulting in a 49.8% area stenosis. At the site of the minimum lumen area (E), a lipid plaque with a thick fibrous cap was observed.

Table 2. Lesion-level OCT characteristics according to sex.

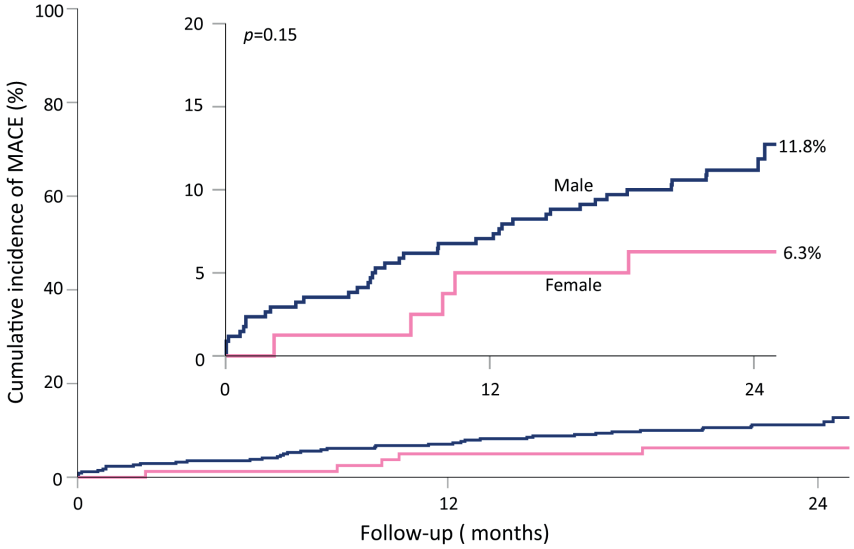
	Univariate			Multivariable[a]		
	Female n=89	**Male n=405**	***p***	**B**	**SE**	***p***
Minimum lumen area, mm^2	2.30 ± 1.42	2.78 ± 1.54	0.005	-0.626	0.170	<0.001
Minimum lumen diameter, mm	1.39 ± 0.45	1.54 ± 0.44	0.005	-0.192	0.055	<0.001
Percentage area stenosis	63.0 ± 15.9	62.1 ± 16.1	0.69			
Proximal reference						
Lumen area, mm^2	7.33 ± 2.98	8.56 ± 3.80	0.001	-1.439	0.434	<0.001
Mean lumen diameter, mm	3.00 ± 0.60	3.23 ± 0.69	0.003	-0.258	0.084	0.002
Distal reference						
Lumen area, mm^2	5.62 ± 2.59	6.98 ± 3.63	<0.001	-1.796	0.350	<0.001
Mean lumen diameter, mm	2.61 ± 0.58	2.90 ± 0.72	<0.001	-0.371	0.076	<0.001
Lesion length, mm	20.8 ± 10.0	18.3 ± 8.5	0.032	2.710	1.371	0.048
Calcification	61 (68.5%)	253 (62.5%)	0.28			
Calcification length, mm	10.0 ± 8.9	8.7 ± 7.8	0.27			
Maximum calcification arc, °	151 ± 100	143 ± 91	0.54			
Maximum calcification thickness, µm	835 ± 244	853 ± 261	0.78			
Protruding calcification	15 (16.9%)	44 (10.9%)	0.11			
Lipid	69 (77.5%)	308 (76.0%)	0.79			
Lipid length, mm	11.9 ± 9.9	9.4 ± 6.6	0.045	2.636	1.346	0.05
Maximum lipid arc, °	244 ± 89	221 ± 81	0.06	20.097	14.254	0.16
Minimum fibrous cap thickness, µm	96 ± 53	112 ± 72	0.045	-20.347	9.053	0.025
TCFA	35 (39.3%)	101 (24.9%)	0.007	0.994	0.294	<0.001
Plaque rupture	8 (9.0%)	40 (9.9%)	0.89			
Thrombus	12 (13.5%)	31 (7.7%)	0.09	1.089	0.411	0.008
Macrophage accumulation	22 (24.7%)	92 (22.7%)	0.64			
Neovascularization	12 (13.5%)	66 (16.3%)	0.52			
Healed plaque	20 (22.5%)	80 (19.8%)	0.57			
Cholesterol clefts	5 (5.6%)	30 (7.4%)	0.54			
High-risk plaque	35 (39.3%)	119 (29.4%)	0.07	0.788	0.300	0.009

TCFA thin cap fibroatheroma.

[a] Multivariable linear and binary logistic regression models with female sex, age, hypertension, diabetes, smoking status, baseline triglycerides level and estimated glomerular filtration rate as independent covariables.

Clinical outcome

After two-years of follow-up, MACE occurred in 6.3% of female patients compared to 11.8% of male patients (p=0.15) (Figure 3).



Number at risk			
Female	80	76	74
Male	340	316	302

Figure 3. Kaplan-Meier curves of two year MACE according to sex.
MACE major adverse cardiovascular events.

DISCUSSION

In this prospective and unselected cohort of MI patients with FFR-negative NC lesions, women were underrepresented, were older and had more cardiovascular risk factors compared to men. After correction for age and other risk factors, absolute luminal dimensions of FFR-negative NC lesions were smaller and mean lesion length was longer in women. Although the number of lipid plaques was equally distributed, lipid plaques in females had less favorable plaque characteristics including smaller minimum fibrous cap thicknesses. Consequently, NC lesions in women more frequently contain a high-risk plaque including TCFA after adjustment for clinical characteristics. However, this did not lead to a higher incidence of clinical events among female patients (Figure 4).

Quantitative lesion characteristics

Previous histopathological as well as *in vivo* imaging studies demonstrated that female patients harbor less extensive atherosclerosis in the coronary circulation as compared to male patients,[9,21] with an 8-10 year delay in plaque formation in females.[22] Interestingly, mean NC lesion length in women was larger

in the present study. We postulate that this can be explained by the fact that we performed targeted NC lesion imaging rather than three-vessel OCT, whilst the other studies assessed total atherosclerotic burden in female versus male patients.[9,21] Additionally, female patients in the present study were older. Consistent with previous studies,[8,9] we found smaller MLA and MLD in female patients compared to males, which can probably be attributed to a difference in body composition between sexes considering that reference lumen dimensions were also smaller in female patients and that %AS was comparable. Indeed, a substudy of the Lipid Rich Plaque study demonstrated no difference in the MLA corrected for body surface area.[8] Correspondingly, the mean external elastic membrane area was smaller in female patients in the sex-substudy of the PROSPECT study.[9]

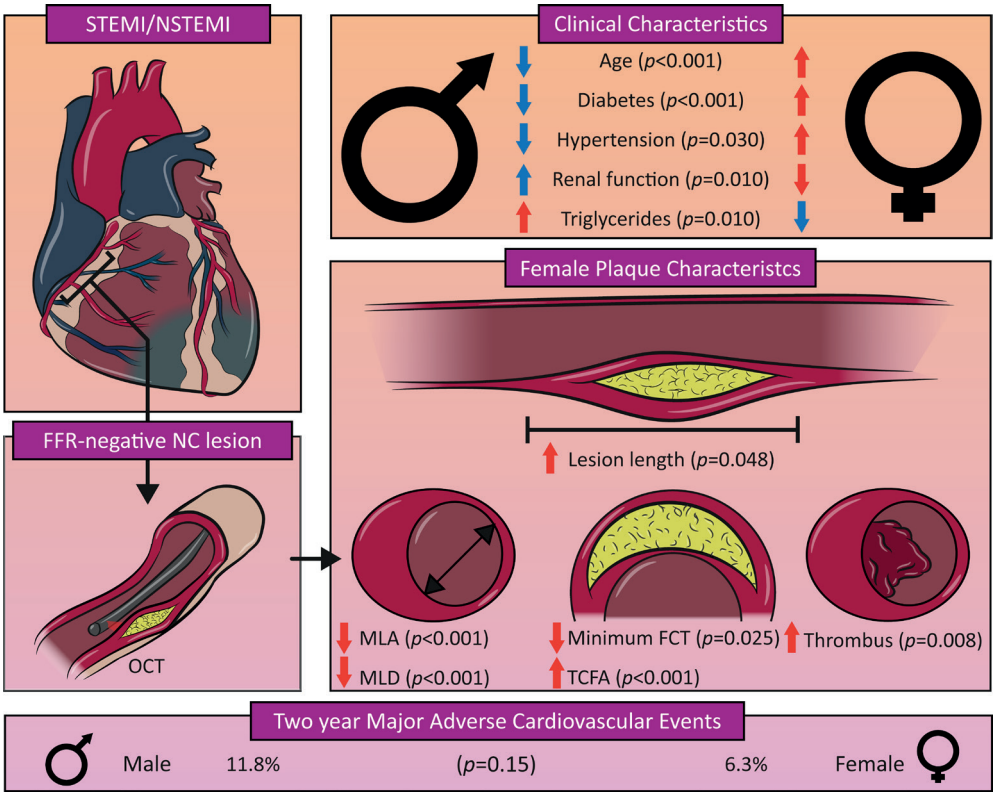


Figure 4. Central illustration.

FCT fibrous cap thickness; FFR fractional flow reserve; MLA minimum lumen area; MLD minimum lumen diameter; NC non-culprit; NSTEMI non-ST-segment elevation myocardial infarction; OCT optical coherence tomography; STEMI ST-segment elevation myocardial infarction; TCFA thin-cap fibroatheroma.

Plaque composition

Multiple studies assessed differences in plaque morphology between sexes in various clinical scenarios with conflicting observations.[18] Only a limited number of studies addressed this topic in the context of NC lesions after MI. Kataoka et al. retrospectively analyzed 675 NC plaques in coronary arteries undergoing revascularization in 435 patients using OCT, which was performed at operator's discretion. They found a significantly higher prevalence of calcified plaques in male compared to female patients (24% vs 10%, p=0.01) within a subset of 222 NC plaques in 115 patients presenting with acute coronary syndrome.[10] In contrast, we report an overall higher prevalence of calcification but without sex-related differences. This discrepancy may be explained by the difference in study design. In particular, we studied hemodynamically insignificant lesions spatially unrelated to the culprit lesion, whereas Kataoka and colleagues studied NC plaques in vessels requiring PCI. Moreover, the prevalence of traditional risk factors for coronary artery disease was much lower in our cohort. Notwithstanding an equal prevalence of lipid plaques in the present analysis, we found a larger mean lipid length in women compared to men, a difference that was at least partially attributable to the observed differences in clinical profile between female and male patients.

Plaque vulnerability

Intracoronary OCT allows identification of plaque phenotypes that are considered to be prone to plaque rupture. Among these high-risk features is TCFA, a fibroatheroma characterized by a large lipid pool or necrotic core with a thin overlying fibrous cap.[23] In the PECTUS-obs study, we demonstrated that presence of a high-risk plaque in FFR-negative NC lesions was associated with an almost twofold increased risk of future events,[7] similar to the observations of COMBINE (OCT-FFR) in diabetic patients.[6] Correspondingly, TCFA in addition to a large plaque burden and a MLA ≤4.0 mm^2 was associated with a more than threefold increased risk of future events in the PROSPECT study.[1]

We now report a higher prevalence of TCFA and high-risk plaques in NC lesions of female patients also after correction for baseline characteristics. Although this might seem alarming in view of the high-risk plaque hypothesis, we did not observe a higher event rate among female patients during two years follow-up. Similarly, a recent analysis by Kataoka and colleagues demonstrated that female patients harbor more modifiable NC lesions (i.e. more condensed lipid plaques) as assessed by IVUS-near infrared spectroscopy, but alike our results that did not lead to higher event rates among female patients.[11] Consequently, we hypothesize that other clinical[24] and plaque features may need to be identified for prognostication in female patients, or perhaps a combination of both. This may ultimately lead to better patient-tailored treatment strategies to reduce recurrent events following MI.

Conversely, no difference in the prevalence of TCFA was found in a sex substudy of the PROSPECT study, nor in a combined analyses of the ATHEROREMO-IVUS and IBIS-4 studies.[9,25] Eight out of eleven NC lesions causing a recurrent event in female patients harbored a TCFA in the PROSPECT substudy and TCFA was the strongest predictor of future NC-lesion related events during follow-up in these patients.[9] Additionally, no difference was observed in prevalence of high-risk plaques in a substudy of one CCTA registry,[26] while high-risk plaques were slightly more common among male patients in another.[22]

However, these studies assessed plaque morphology using virtual histology intravascular ultrasound (VH-IVUS) or CCTA which have insufficient spatial resolution for TCFA identification. Indeed, only a third of TCFA identified by VH-IVUS correspond to TCFA on OCT,[27] and OCT-identified TCFA is only found in 40% of lesions meeting two high-risk plaque criteria on CCTA.[28] Furthermore, patients with prior MI were excluded in the CCTA registries.[22,26] In contrast to the previous analyses,[9,22,25,26] the mean age of female patients in the present cohort was >65 years old. Culprit lesions in female patients contain more TCFA with increasing age.[17,29] Likewise, in another sex-related substudy from PROSPECT, NC lesions in female patients over the age of 65 years old had a higher percentage of necrotic core, whilst such difference was not present in patients below 65 years of age.[30] Age-related effects may therefore have contributed to the disparity in results, and these findings therefore require confirmation in future studies.

Limitations

This study should be interpreted with a number of limitations in mind. First, we performed targeted NC lesions OCT rather than three vessel OCT, therefore this study only implies to lesions with a visually estimated stenosis grade of 30-90% that are hemodynamically insignificant. Moreover, only patients presenting with MI were included. However the impact of identification of high-risk plaques seems limited following FFR-guided deferral in patients with CCS without a very-high risk profile (e.g. diabetes). Although multivariable analyses were performed to correct for baseline differences between sexes, we cannot rule out that these baseline differences have a more profound effect on differences in plaque characteristics. Importantly, the PECTUS-obs study was not designed or powered to demonstrate differences in clinical endpoints between sexes. The limited number of female patients and a modest period of follow-up resulted in a low absolute number of cardiovascular events in the subgroups. Consequently, the absence of a difference in clinical outcome may result from a lack of power to demonstrate such differences. Additionally, these limitations precluded assessment of the clinical impact of HRP within the subgroups and assessment of NC lesion-related events. Therefore, the results of this study remain hypothesis-generating and require confirmation.

CONCLUSION

In conclusion, FFR-negative NC lesions in female patients presenting with MI harbor more high-risk plaque features compared to male patients, independently of the more adverse clinical profile of female patients. Although this did not translate into an excess of recurrent events among female patients in the present cohort, the true effect of this difference on clinical outcome remains to be investigated.

REFERENCES

1. Stone GW, Maehara A, Lansky AJ, de Bruyne B, Cristea E, Mintz GS et al. A prospective natural-history study of coronary atherosclerosis. N Engl J Med 2011;364:226-35.
2. Bainey KR, Engstrom T, Smits PC, Gershlick AH, James SK, Storey RF et al. Complete vs Culprit-Lesion-Only Revascularization for ST-Segment Elevation Myocardial Infarction: A Systematic Review and Meta-analysis. JAMA Cardiol 2020;5:881-888.
3. Liou KP, Ooi SM, Hoole SP, West NEJ. Fractional flow reserve in acute coronary syndrome: a meta-analysis and systematic review. Open Heart 2019;6:e000934.
4. Cerrato E, Mejia-Renteria H, Dehbi HM, Ahn JM, Cook C, Dupouy P et al. Revascularization Deferral of Nonculprit Stenoses on the Basis of Fractional Flow Reserve: 1-Year Outcomes of 8,579 Patients. JACC Cardiovasc Interv 2020;13:1894-1903.
5. Araki M, Park SJ, Dauerman HL, Uemura S, Kim JS, Di Mario C et al. Optical coherence tomography in coronary atherosclerosis assessment and intervention. Nat Rev Cardiol 2022;19:684-703.
6. Kedhi E, Berta B, Roleder T, Hermanides RS, Fabris E, AJJ IJ et al. Thin-cap fibroatheroma predicts clinical events in diabetic patients with normal fractional flow reserve: the COMBINE OCT-FFR trial. Eur Heart J 2021;42:4671-4679.
7. Mol JQ, Volleberg R, Belkacemi A, Hermanides RS, Meuwissen M, Protopopov AV et al. Fractional Flow Reserve-Negative High-Risk Plaques and Clinical Outcomes After Myocardial Infarction. JAMA Cardiol 2023;8:1013-1021.
8. Mensink FB, Ten Cate TJF, Damen SAJ, Roes K, Di Mario C, Singh V et al. Near-infrared spectroscopy predicts events in men and women: Results from the Lipid Rich Plaque study. Int J Cardiol Heart Vasc 2022;39:100985.
9. Lansky AJ, Ng VG, Maehara A, Weisz G, Lerman A, Mintz GS et al. Gender and the extent of coronary atherosclerosis, plaque composition, and clinical outcomes in acute coronary syndromes. JACC Cardiovasc Imaging 2012;5:S62-72.
10. Kataoka Y, Puri R, Hammadah M, Duggal B, Uno K, Kapadia SR et al. Sex Differences in Nonculprit Coronary Plaque Microstructures on Frequency-Domain Optical Coherence Tomography in Acute Coronary Syndromes and Stable Coronary Artery Disease. Circ Cardiovasc Imaging 2016;9.
11. Kataoka Y, Nicholls SJ, Puri R, Kitahara S, Kiyoshige E, Nishimura K et al. Sex Differences in the Density of Lipidic Plaque Materials: Insights From the REASSURE-NIRS MultiCenter Registry. Circ Cardiovasc Imaging 2023;16:e015107.
12. Lerner DJ, Kannel WB. Patterns of coronary heart disease morbidity and mortality in the sexes: a 26-year follow-up of the Framingham population. Am Heart J 1986;111:383-90.
13. Anand SS, Islam S, Rosengren A, Franzosi MG, Steyn K, Yusufali AH et al. Risk factors for myocardial infarction in women and men: insights from the INTERHEART study. Eur Heart J 2008;29:932-40.
14. Goldberg RJ, O'Donnell C, Yarzebski J, Bigelow C, Savageau J, Gore JM. Sex differences in symptom presentation associated with acute myocardial infarction: a population-based perspective. Am Heart J 1998;136:189-95.
15. Farb A, Burke AP, Tang AL, Liang TY, Mannan P, Smialek J, Virmani R. Coronary plaque erosion without rupture into a lipid core. A frequent cause of coronary thrombosis in sudden coronary death. Circulation 1996;93:1354-63.
16. Kramer MC, Rittersma SZ, de Winter RJ, Ladich ER, Fowler DR, Liang YH et al. Relationship of thrombus healing to underlying plaque morphology in sudden coronary death. J Am Coll Cardiol 2010;55:122-32.
17. Seegers LM, Araki M, Nakajima A, Yonetsu T, Minami Y, Ako J et al. Sex Differences in Culprit Plaque Characteristics Among Different Age Groups in Patients With Acute Coronary Syndromes. Circ Cardiovasc Interv 2022;15:e011612.

18. Gurgoglione FL, Solinas E, Pfleiderer B, Vezzani A, Niccoli G. Coronary atherosclerotic plaque phenotype and physiopathologic mechanisms: Is there an influence of sex? Insights from intracoronary imaging. Atherosclerosis 2023;384:117273.

19. Mol JQ, Belkacemi A, Volleberg RH, Meuwissen M, Protopopov AV, Laanmets P et al. Identification of anatomic risk factors for acute coronary events by optical coherence tomography in patients with myocardial infarction and residual nonflow limiting lesions: rationale and design of the PECTUS-obs study. BMJ Open 2021;11:e048994.

20. Tearney GJ, Regar E, Akasaka T, Adriaenssens T, Barlis P, Bezerra HG et al. Consensus standards for acquisition, measurement, and reporting of intravascular optical coherence tomography studies: a report from the International Working Group for Intravascular Optical Coherence Tomography Standardization and Validation. J Am Coll Cardiol 2012;59:1058-72.

21. Roger VL, Weston SA, Killian JM, Pfeifer EA, Belau PG, Kottke TE et al. Time trends in the prevalence of atherosclerosis: a population-based autopsy study. Am J Med 2001;110:267-73.

22. Lee SE, Sung JM, Andreini D, Al-Mallah MH, Budoff MJ, Cademartiri F et al. Sex Differences in Compositional Plaque Volume Progression in Patients With Coronary Artery Disease. JACC Cardiovasc Imaging 2020;13:2386-2396.

23. Burke AP, Farb A, Malcom GT, Liang YH, Smialek J, Virmani R. Coronary risk factors and plaque morphology in men with coronary disease who died suddenly. N Engl J Med 1997;336:1276-82.

24. Rajendran A, Minhas AS, Kazzi B, Varma B, Choi E, Thakkar A, Michos ED. Sex-specific differences in cardiovascular risk factors and implications for cardiovascular disease prevention in women. Atherosclerosis 2023;384:117269.

25. Ten Haaf ME, Rijndertse M, Cheng JM, de Boer SP, Garcia-Garcia HM, van Geuns RM et al. Sex differences in plaque characteristics by intravascular imaging in patients with coronary artery disease. EuroIntervention 2017;13:320-328.

26. Conte E, Dwivedi A, Mushtaq S, Pontone G, Lin FY, Hollenberg EJ et al. Age- and sex-related features of atherosclerosis from coronary computed tomography angiography in patients prior to acute coronary syndrome: results from the ICONIC study. Eur Heart J Cardiovasc Imaging 2021;22:24-33.

27. Ueki Y, Yamaji K, Losdat S, Karagiannis A, Taniwaki M, Roffi M et al. Discordance in the diagnostic assessment of vulnerable plaques between radiofrequency intravascular ultrasound versus optical coherence tomography among patients with acute myocardial infarction: insights from the IBIS-4 study. Int J Cardiovasc Imaging 2021;37:2839-2847.

28. Kinoshita D, Suzuki K, Usui E, Hada M, Yuki H, Niida T et al. High-Risk Plaques on Coronary Computed Tomography Angiography: Correlation With Optical Coherence Tomography. JACC Cardiovasc Imaging 2024;17:382-391.

29. Sato T, Minami Y, Asakura K, Katamine M, Kato A, Katsura A et al. Age- and Gender-Related Differences in Coronary Lesion Plaque Composition on Optical Coherence Tomography. Circ J 2020;84:463-470.

30. Ruiz-Garcia J, Lerman A, Weisz G, Maehara A, Mintz GS, Fahy M et al. Age- and gender-related changes in plaque composition in patients with acute coronary syndrome: the PROSPECT study. EuroIntervention 2012;8:929-38.

SUPPLEMENTAL MATERIAL

Supplemental material related to this article can be found in the online version:
https://www.atherosclerosis-journal.com/article/S0021-9150(24)01140-7/fulltext





CHAPTER 9

Long-term clinical outcomes of high-risk plaques with negative fractional flow reserve: the PECTUS-obs study

Rick Volleberg | Jan-Quinten Mol | Geert Versteeg | Joske van der Zande | Anouar Belkacemi | Renicus Hermanides | Martijn Meuwissen | Alexey Protopopov | Peep Laanmets | Oleg Krestyaninov | Casper Laclé | Rohit Oemrawsingh | Jan-Peter van Kuijk | Karin Arkenbout | Dirk van der Heijden | Saman Rasoul | Erik Lipsic | Laura Rodwell | Cyril Camaro | Peter Damman | Tomasz Roleder | Elvin Kedhi | Maarten van Leeuwen | Robert-Jan van Geuns | Niels van Royen

EuroIntervention
Online ahead of print

ABSTRACT

Background High-risk plaques (HRP) in non-flow limiting, deferred non-culprit lesions have been associated with adverse short-term cardiovascular outcomes after myocardial infarction (MI). However, the long-term prognostic implications remain largely unknown.

Aims This study sought to evaluate the long-term association between HRP and clinical outcome after MI.

Methods In the prospective, observational PECTUS-obs study, 438 patients with recent MI underwent optical coherence tomography (OCT) of all fractional flow reserve-negative non-culprit lesions. Patients were grouped according to the presence or absence of at least one OCT-identified HRP. The current study evaluates the final long-term outcome. The primary endpoint was defined as major adverse cardiovascular events (MACE), a composite of cardiac death, non-fatal MI or unplanned revascularization, excluding all periprocedural, indeterminate and all stent failure-related events.

Results After a median follow-up of 1,828 days (interquartile range [IQR] 1,821-1,842 days), the presence of at least one HRP was associated with MACE (hazard ratio [HR] 1.87, 95% confidence interval [CI]: 1.11-3.14; p=0.017). Among the individual endpoint components, non-fatal MI (HR 4.07, 95% CI: 1.23-13.52; p=0.013) and unplanned revascularization (HR 1.97, 95% CI: 1.07-3.64; p=0.027) occurred more frequently in patients with at least one HRP. In an exploratory landmark analysis, the risk associated with presence of HRP was observed only during the first 2 years of follow-up. The lesion-level incidence of target lesion failure did not differ significantly between groups (HR 1.65, 95% CI: 0.91-2.96; p=0.097).

Conclusions Non-flow limiting, high-risk non-culprit plaques are associated with adverse patient-level clinical outcomes during long-term follow-up after MI, potentially with a more pronounced short-term risk.

INTRODUCTION

After myocardial infarction, complete revascularization of non-culprit lesions is endorsed by guidelines to reduce the risk of recurrent cardiovascular events.[1-3] Indeed, approximately half of recurrent events are related to the destabilization or progression of non-culprit lesions. However, despite fractional flow reserve (FFR)-guided complete revascularization, recurrent cardiovascular events among patients with myocardial infarction remain common.[4] Various prospective, observational studies, using a variety of imaging modalities, have demonstrated that high-risk plaques (HRP) in deferred non-culprit lesions may be important drivers of recurrent events.[5-7] Such lesions are typically characterised by a large lipidic plaque burden, separated from the lumen by a thin overlying fibrous cap. We previously demonstrated in the prospective, observational PECTUS-obs study that presence of an optical coherence tomography (OCT)-identified HRP was associated with an increased risk of recurrent patient-level cardiovascular events at 2 years after myocardial infarction.[7] The long-term prognostic impact of OCT-identified HRP in non-flow limiting, deferred lesions after myocardial infarction remains unknown.

This study sought to evaluate the association between OCT-identified HRP and long-term clinical outcomes at the final 5 year follow-up in PECTUS-obs.

METHODS

Study design

PECTUS-obs (ClinicalTrials.gov: NCT03857971) was a prospective, observational, natural history study on the association between OCT-identified HRP in FFR-negative non-culprit lesions (i.e., target lesions) and major adverse cardiovascular events (MACE) after myocardial infarction. The study was conducted in 14 hospitals in 4 countries and is reported in accordance with the STROBE reporting guidelines (https://www.strobe-statement.org/). The rationale, design and the primary results at 2-year follow-up were published previously.[7,8] In brief, patients presenting with ST-segment elevation myocardial infarction (STEMI) or non-STEMI (NSTEMI) and undergoing invasive coronary angiography were screened for eligibility after treatment of the culprit lesion. All patients with at least one intermediate non-culprit lesion (visually estimated stenosis 30-90%) that was FFR-negative (FFR >0.80) were eligible for inclusion. The exclusion criteria were age <18 years, pregnancy, hemodynamic instability, previous or current indication for coronary artery bypass grafting, and a life expectancy of <3 years. The two target lesion-related (i.e., related to the FFR-negative non-culprit lesion to be imaged with OCT) exclusion criteria were anatomy unsuitable for OCT catheter crossing and the presence of in-stent restenosis. Physiological and imaging evaluation of all eligible target lesions was performed during the index procedure or during a staged procedure within 6 weeks after myocardial infarction. The FFR was obtained according to local site protocol. Severe stenoses (visually estimated stenosis >90%) and FFR-positive intermediate stenoses were treated according to contemporary guidelines. OCT acquisition was performed using the Dragonfly OPTIS imaging catheter (Abbott) while cine recording the pullback to ensure that OCT findings could

be correlated to the coronary angiogram based on anatomical landmarks (i.e., side branches and ostia). Operators were not allowed to evaluate plaque morphology on the OCT images, but they were not blinded to the images to allow for repeat imaging in case of insufficient image quality. The OCT images were not available to other inpatient- or outpatient-treating physicians, nor to patients.

The study was conducted in accordance with the 1964 Declaration of Helsinki and was approved by the institutional review board and/or medical ethics committee of each participating centre. Written informed consent was obtained from all participants.

Core laboratory-based OCT imaging analysis

Manual OCT image analysis was performed by an independent OCT core laboratory (Real Solution Sp. Z o.o., Poland) using CAAS IntraVascular 2.0 (Pie Medical Imaging BV). The core laboratory personnel were blinded to patient characteristics and clinical outcomes. After excluding pullbacks with insufficient quality for quantitative and qualitative analyses of the target lesion, serial cross-sectional images of all target lesions were analysed according to previously described criteria.[7] According to the original, prespecified PECTUS-obs criteria, a lesion was considered a HRP in the presence of at least 2 out of 3 criteria: (1) a lipid arc ≥90°, (2) a minimum fibrous cap thickness <65 µm, and (3) the presence of either plaque rupture or thrombus. Patients, operators, and treating physicians were blinded to OCT image analysis results.

Endpoints

For the current analysis, the primary patient-level endpoint was defined as MACE (which was defined in this study as a composite of cardiac mortality, non-fatal myocardial infarction, or unplanned revascularisation) before 5-year follow-up (±30 days), excluding all cases of non-fatal myocardial infarction that were periprocedural or that could not be attributed to a specific coronary segment (indeterminate events) and all stent failure-related events. As part of the latter criterium, all events originating from the original culprit lesion were excluded from endpoint analyses. Secondary patient-level endpoints were the individual components of the primary endpoint. Individual endpoint definitions are reported in Supplementary Appendix 1.

The secondary lesion-level endpoints were defined as target lesion failure (TLF; which was defined in this study as a composite of cardiac death, target vessel-related myocardial infarction, or target lesion-related unplanned revascularisation), excluding stent failure-related events, the individual components of TLF, and the composite of target vessel-related myocardial infarction or target lesion-related unplanned revascularisation.

The exclusion of periprocedural, intermediate, and stent failure-related events and the inclusion of an exploratory lesion-level evaluation represent amendments in endpoints as compared with those evaluated at 2-year follow-up. The endpoint amendments were approved by the overseeing ethical committee prior to database closure and data analysis.

Follow-up and clinical event adjudication

Structured follow-up was performed at 1, 2, and 5 years (±30 days) after inclusion by means of telephone contact. All (possible) events were monitored by a clinical event adjudication committee with two independent, experienced interventional cardiologists who were blinded to the OCT image analyses. The (possible) events were verified using medical records obtained from participating centres, general practitioners, or other medical centres. All revascularisations and myocardial infarctions occurring during follow-up were allocated to a specific coronary segment and lesion by comparison of baseline and follow-up coronary angiograms, if performed. Specifically for target lesion revascularisation, events were adjudicated on a lesion level and not a segment level; the latter was evaluated using the SYNTAX coding system. Myocardial infarction events were considered indeterminate if coronary angiography was not performed or if the coronary angiogram did not reveal a new culprit lesion.

Statistical analysis

Categorical variables are presented as number (percentage) and were compared using the chi-square test or Fisher's exact test, as appropriate. Continuous variables are presented as mean±standard deviation and were analysed using the Student's independent samples t-test when normally distributed. Non-normally distributed variables are expressed as median (interquartile range) and were analysed using the Mann-Whitney U test.

For the analysis of all clinical endpoints, patients were censored at their last known moment of follow-up with a maximum of 5 years (+30 days) after inclusion. The hazard ratios associated with the presence of an HRP and individual HRP features were evaluated using univariable and multivariable Cox proportional hazard regression models. Two multivariable models were constructed. In model A, age, prior myocardial infarction, type 1 or 2 diabetes, STEMI or NSTEMI at presentation, and estimated glomerular filtration rate were included as *a priori* selected correcting variables. In model B, all baseline characteristics that demonstrated a univariable association with the primary outcome were included, after checking for collinearity (defined as r >0.80). For lesion-level endpoints, robust standard errors were estimated to account for withinpatient clustering in case of multiple target lesions. Exploratory landmark analyses were conducted to evaluate outcomes during the initial 2 years and the final 3 years of follow-up. Missing data were not imputed. Statistical significance was considered at a two-sided p-value <0.05. All statistical analyses were performed using SPSS Statistics, version 27.0 (IBM) and R, version 4.4.1 (R Foundation for Statistical Computing).

RESULTS

Study flow

The study flowchart is presented in Figure 1. A total of 438 patients were enrolled in PECTUS-obs between December 2018 and September 2020. Among 420 patients who had at least one core laboratory-analysed OCT, 143 (34.0%) had at least one HRP in an evaluable target lesion, while 277 (66.0%) patients did not have an HRP.

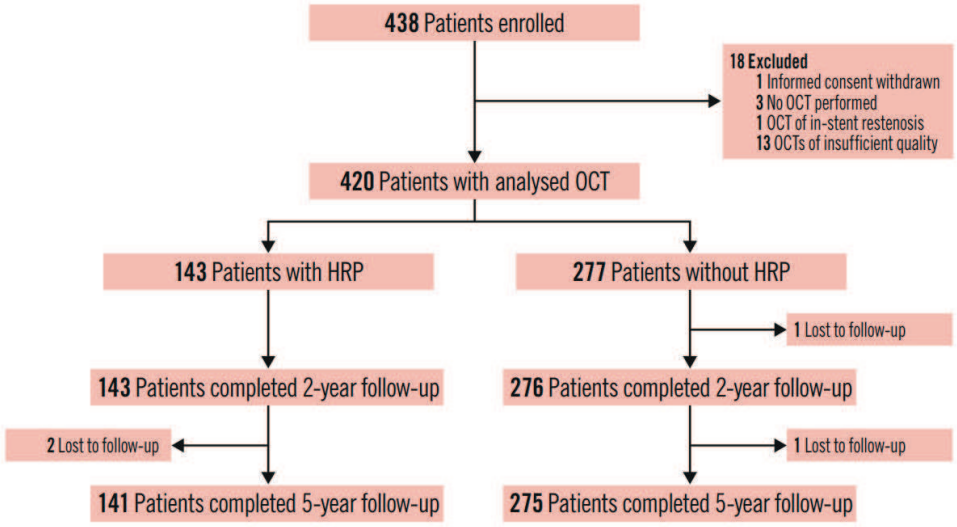


Figure 1. Study flowchart.
HRP high-risk plaque; OCT optical coherence tomography.

Clinical, procedural and angiographic characteristics

Baseline clinical, procedural and angiographic characteristics are presented in Table 1. The mean age of included patients was 63±10 years, and 80 patients (19.0%) were female. The proportions of patients that had presented with STEMI and NSTEMI were 51.7% and 48.3%, respectively. The mean total cholesterol level was 4.97±1.36 mmol/L, with 108 patients (25.7%) using lipid-lowering therapy. Patients with at least one HRP less frequently had a history of percutaneous coronary revascularisation (9.8% vs 17.3%; p=0.039) and had higher low-density lipoprotein levels (3.28±1.20 mmol/L vs 2.90±1.18 mmol/L; p=0.006).

Medical therapy prescription during follow-up is presented in Supplementary Table 1. Lipid-lowering therapy was prescribed in 415 patients (98.8%) at discharge and in 384 (92.8%), 375 (91.9%) and 336 patients (89.6%) at 1-, 2-, and 5-year follow-up, respectively, without between-group differences.

Table 1. Baseline characteristics.

Characteristic	n	High-risk plaque (n=143)	No high-risk plaque (n=277)	P-value
Age, years		62±11	64±10	0.148
Female sex		33 (23.1)	47 (17.0)	0.131
BMI, kg/m^2	414	28.2±4.7	27.6±4.5	0.181
Smoking status	417			0.170
Current smoker		44 (31.0)	79 (28.7)	
Former smoker		50 (35.2)	78 (28.4)	
Hypertension		72 (50.3)	150 (54.2)	0.460
Type 1 or 2 diabetes		18 (12.6)	43 (15.5)	0.418
Hypercholesterolemia	419	51 (35.9)	102 (36.8)	0.855
Family history of premature atherosclerosis	416	43 (30.7)	85 (30.8)	0.986
Previous MI		17 (11.9)	46 (16.6)	0.199
Previous PCI		14 (9.8)	48 (17.3)	0.039
Previous CVA		0 (0)	8 (2.9)	0.055
History of carotid artery disease		3 (2.1)	10 (3.6)	0.556
History of PAD		6 (4.2)	11 (4.0)	0.912
Baseline lipid-lowering therapy		32 (22.4)	76 (27.4)	0.261
Index presentation				0.396
STEMI		78 (54.5)	139 (50.2)	
NSTEMI		65 (45.5)	138 (49.8)	
GRACE score	416	116±34	117±32	0.578
Cholesterol level, mmol/L				
Total	354	5.15±1.35	4.88±1.37	0.083
LDL	334	3.28±1.20	2.90±1.18	0.006
HDL	338	1.15 (0.99-1.40)	1.10 (0.92-1.35)	0.130
Triglyceride level, mmol/L	350	1.52 (1.02-2.10)	1.63 (1.10-2.41)	0.391
eGFR, mL/min/1.73m^2	416	79±20	80±19	0.450
CRP, mg/L	330	3.0 (1.0-5.0)	2.4 (1.0-5.0)	0.500
Leukocyte count, x10^9/L	414	9.58±3.18	9.81±3.23	0.495
Infarct-related artery				
LM		5 (3.5)	0 (0)	0.004
LAD		63 (44.1)	104 (37.5)	0.196
LCx		41 (28.7)	67 (24.2)	0.319
RCA		45 (31.5)	112 (40.4)	0.072

Table 1. Continued

Target lesion evaluation timing			0.850
Immediate	54 (37.8)	102 (36.8)	
Staged	89 (62.2)	175 (63.2)	
Number of target lesions	1.29±0.53	1.12±0.34	<0.001

Values are n (%), mean±standard deviation, or median (interquartile range).

BMI body mass index; CRP C-reactive protein; CVA cerebrovascular accident; eGFR estimated glomerular filtration rate; GRACE Global Registry of Acute Coronary Events; HDL high-density lipoprotein; LAD left anterior descending artery; LCx left circumflex artery; LDL low-density lipoprotein; LM left main stem; MI myocardial infarction; NSTEMI non-ST-segment elevation myocardial infarction; PAD peripheral artery disease; PCI percutaneous coronary intervention; RCA right coronary artery; STEMI ST-segment elevation myocardial infarction.

Lesion-level characteristics

Lesion-level characteristics are summarised in Table 2. Compared with lesions without a HRP, high-risk lesions were more frequently located in the right coronary artery (33.8% vs 24.7%; p=0.037) and had a slightly lower mean FFR (0.88±0.05 vs 0.90±0.05; p=0.005). Based on core laboratory OCT analyses, high-risk lesions were longer and had a higher degree of percentage area stenosis. While high-risk lesions were more lipid rich and had more macrophage accumulation, lesions that were not high risk had a greater calcification burden.

Table 2. Lesion-level characteristics.

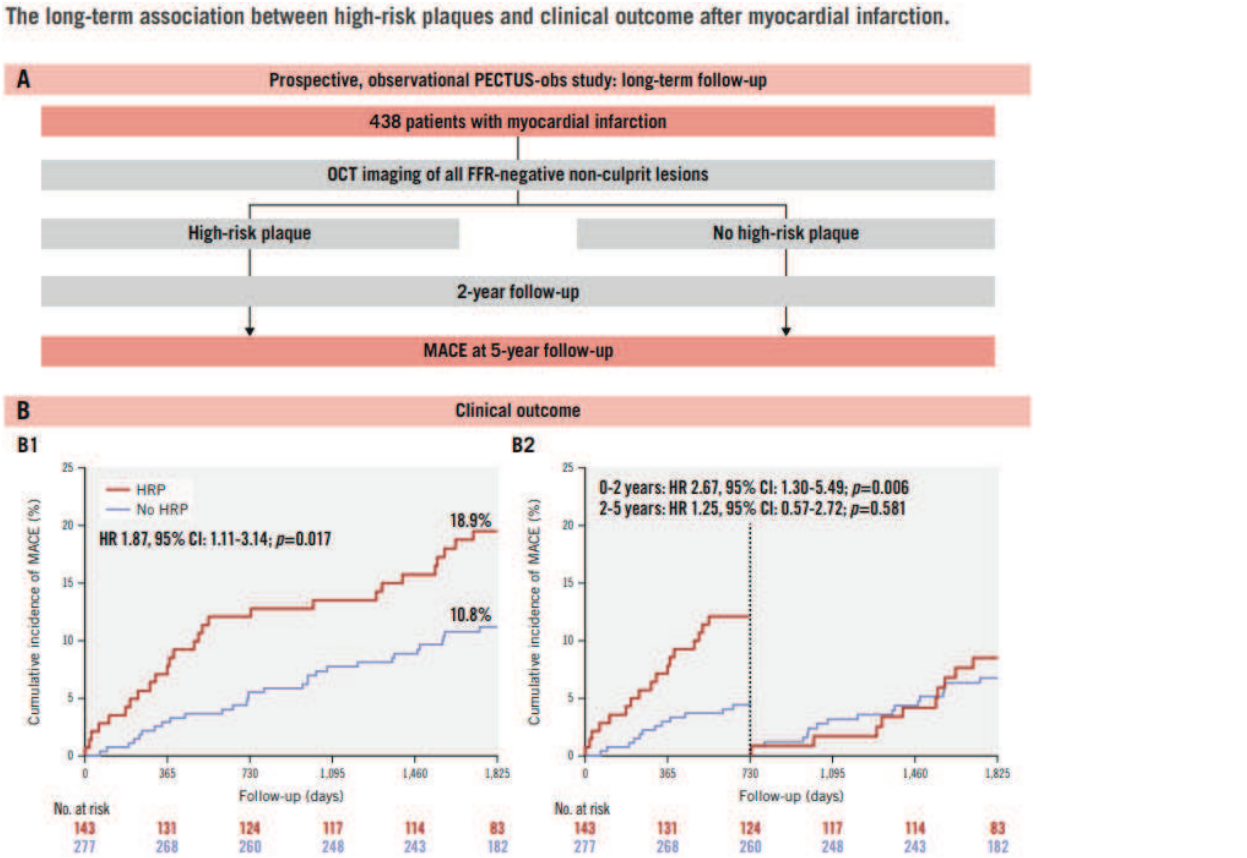
Characteristic	High-risk plaque (n=154)	Non-high-risk plaque (n=340)	P-value
Target lesion distribution			
LM	0 (0)	4 (1.2)	0.315
LAD	58 (37.7)	129 (37.9)	0.953
LCx	44 (28.6)	123 (36.2)	0.098
RCA	52 (33.8)	84 (24.7)	0.037
Fractional flow reserve	0.88±0.05	0.90±0.05	0.005
Core-laboratory-based OCT analyses			
Lesion length, mm	20.6±9.2	17.9±8.5	0.002
Minimum lumen diameter, mm	1.46±0.39	1.53±0.47	0.071
Minimum lumen area, mm^2	2.27 (1.60-3.21)	2.43 (1.62-3.43)	0.220
Percentage area stenosis, %	68.4 (58.6-75.2)	64.3 (52.1-72.8)	0.013
Lipid plaque	154 (100)	223 (65.6)	<0.001
Lipid length, mm	10.3 (7.0-15.7)	6.7 (3.6-11.3)	<0.001
Maximum lipid arc, °	254 (169-308)	200 (144-271)	<0.001
Minimum fibrous cap thickness, µm	59 (54-63)	120 (93-170)	<0.001
Calcific plaque	103 (66.9)	211 (62.1)	0.302
Calcium length, mm	4.6 (2.2-9.0)	7.5 (2.9-14.6)	0.005
Maximum calcium arc, °	102 (68-178)	116 (78-214)	0.129
Maximum calcium thickness, µm	802±250	873±259	0.021
Protruding calcification	13 (8.4)	46 (13.5)	0.106
Plaque rupture	45 (29.2)	3 (0.9)	<0.001
Thrombus	34 (22.1)	9 (2.6)	<0.001
Microvessel	21 (13.6)	57 (16.8)	0.377
Cholesterol cleft	12 (7.8)	23 (6.8)	0.680
Macrophage accumulation	46 (29.9)	68 (20.0)	0.016
Layered plaque	30 (19.5)	70 (20.6)	0.777

Values are n (%), mean±standard deviation, or median (interquartile range).
LAD left anterior descending artery; LCx left circumflex artery; LM left main stem; OCT optical coherence tomography; RCA right coronary artery.

Clinical outcomes

Follow-up was complete in 416 (99.0%) patients. One patients was lost to follow-up before 2 years, and 3 patients were lost to follow-up between 2 and 5 years.

During a median follow-up of 1,828 days (interquartile range 1,821-1,842 days), the primary endpoint of MACE had occurred in 27 patients (18.9%) with at least one HRP and 30 patients (10.8%) without an HRP (HR 1.87, 95% CI: 1.11-3.14; p=0.017) (Central illustration, Table 3). Among the individual components of the primary endpoint, the incidences of non-fatal myocardial infarction (5.6% vs 1.4%, HR 4.07, 95% CI: 1.23-13.52; p=0.013) and unplanned revascularisation (14.0% vs 7.6%, HR 1.97, 95% CI: 1.07-3.64; p=0.027) were higher in patients with at least one HRP (Table 3, Supplementary Figure 1). An overview of all revascularisation events is given in Supplementary Table 2. In multivariable analysis, HRPs were independently associated with MACE (model A: HR 1.89, 95% CI: 1.12-3.19; p=0.018; model B: HR 2.39, 95% CI: 1.36-4.18; p=0.002) (Supplementary Table 3). In an exploratory landmark analysis, the hazard ratio associated with the presence of at least one HRP was 2.67 (95% CI: 1.30-5.49; p=0.006) during the first 2 years of follow-up and 1.25 (95% CI: 0.57-2.72; p=0.581) during the final 3 years of follow-up (Central illustration). Three patients (2.1%) with at least one HRP and 12 patients (4.3%) without a HRP only had periprocedural, non-attributable, or stent failure-related events that were excluded from these analyses (p=0.242).



Central Illustration. A) Study overview. B) Time-to-event curves for the composite patient-level clinical outcome of MACE during the complete duration of follow-up (B1) and in the exploratory landmark analysis (B2).

CI confidence interval; FFR fractional flow reserve; HR hazard ratio; HRP high-risk plaque; MACE major adverse cardiovascular events; OCT optical coherence tomography.

Table 3. Clinical outcome.

	High-risk plaque	No high-risk plaque	HR (95% CI)	P-value
Patient-level outcome	**n = 143**	**n = 277**		
MACE	27 (18.9)	30 (10.8)	1.87 (1.11-3.14)	0.017
Cardiac death	8 (5.6)	9 (3.2)	1.76 (0.68-4.57)	0.238
Non-fatal MI	8 (5.6)	4 (1.4)	4.07 (1.23-13.52)	0.013
Unplanned revascularization	20 (14.0)	21 (7.6)	1.97(1.07-3.64)	0.027
All-cause death	16 (11.2)	28 (10.1)	1.14 (0.62-2.10)	0.682
Lesion-level outcome	**n = 154**	**n = 340**		
TLF	18 (11.7)	25 (7.4)	1.65 (0.91-2.96)	0.097
Cardiac death	8 (5.2)	11 (3.2)	1.64 (0.67-4.01)	0.282
TVMI	5 (3.2)	4 (1.2)	2.87 (0.90-9.13)	0.074
TLR	9 (5.8)	13 (3.8)	1.57(0.67-3.67)	0.300
TVMI or TLR	11 (7.1)	14 (4.1)	1.79(0.84-3.82)	0.152

Values are n (%) or hazard ratio (95% CI).

CI confidence interval; HR hazard ratio; MACE major adverse cardiovascular events; MI; myocardial infarction; TLF target lesion failure; TLR target lesion revascularization; TVMI target vessel myocardial infarction.

Lesion-level TLF had occurred in 18 lesions (11.7%) meeting the HRP criteria and 25 lesions (7.4%) that were classified as non-HRP (HR 1.65, 95% CI: 0.91-2.96; p=0.097) (Figure 2). The individual lesion-level components and the composite of target vessel myocardial infarction or target lesion unplanned revascularisation are reported in Table 3, Supplementary Figure 2, and Supplementary Figure 3. In an exploratory landmark analysis, the hazard ratio was 2.04 (95% CI: 0.87-4.79; p=0.104) in the first 2 years of follow-up and 1.38 (95% CI: 0.62-3.10; p=0.432) during the final 3 years of follow-up (Figure 2).

Among different HRP features, plaque rupture was associated with both patient-level MACE (HR 3.20, 95% CI: 1.75-5.85; p<0.001) and lesion-level TLF (HR 3.18, 95% CI: 1.57-6.45; p=0.001) (Table 4).

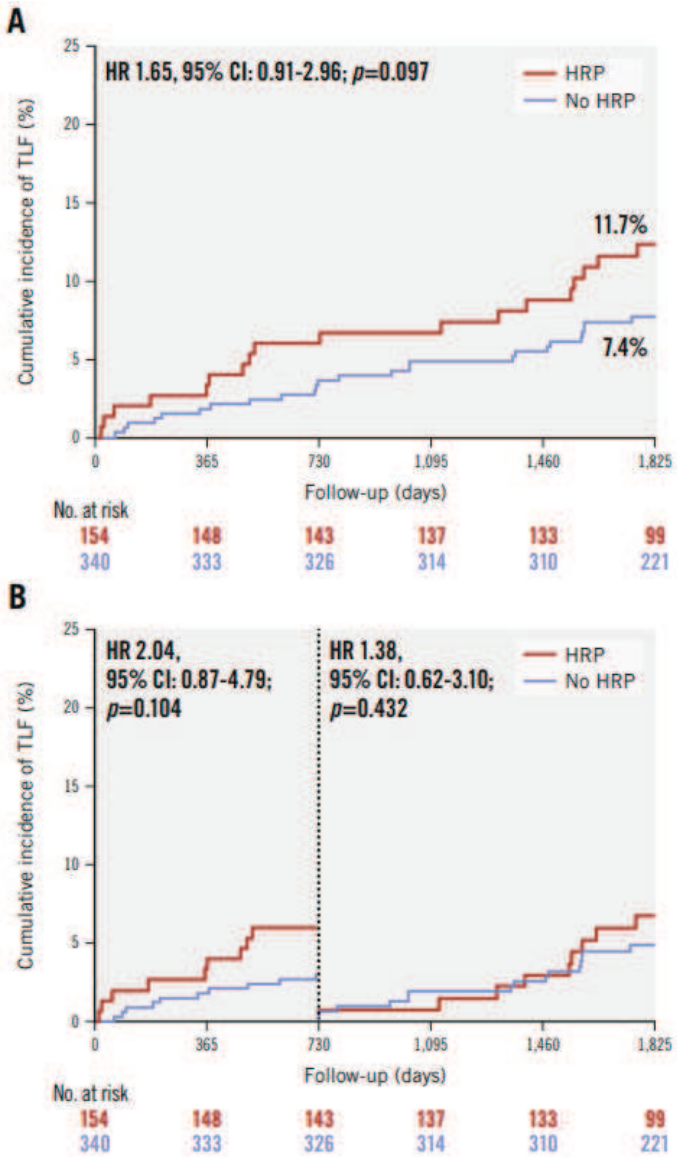


Figure 2. Lesion-level target lesion failure.

Time-to-event curves for the composite lesion-level clinical outcome of TLF during the complete duration of follow-up (A) and in the exploratory landmark analysis (B).

CI confidence interval; HR hazard ratio; HRP high-risk plaque; TLF target lesion failure.

Table 4. Distinct plaque vulnerability features and clinical outcome.

OCT Characteristic	Patient-level prevalence	MACE: univariable HR (95% CI)	P-value	Lesion-level prevalence	TLF: univariable HR (95% CI)	P-value
HRP	143 (34.0)	1.87 (1.11-3.14)	0.017	154 (31.2)	1.65 (0.91-2.96)	0.097
TCFA	126 (30.0)	1.63 (0.96-2.77)	0.068	136 (27.5)	1.59 (0.87-2.89)	0.132
Plaque rupture	46 (11.0)	3.20 (1.75-5.85)	<0.001	48 (9.7)	3.18 (1.57-6.45)	0.001
Thrombus	43 (10.2)	1.31 (0.59-2.88)	0.508	43 (8.7)	1.11 (0.39-3.13)	0.841
Microvessel	75 (17.9)	1.61 (0.89-2.90)	0.112	78 (15.8)	1.80 (0.94-3.43)	0.077
Cholesterol cleft	35 (8.3)	0.61 (0.19-1.94)	0.395	35 (7.1)	0.65 (0.16-2.58)	0.540
Macrophage accumulation	108 (25.7)	1.46 (0.84-2.54)	0.173	114 (23.1)	1.44 (0.75-2.75)	0.274
Layered plaque	94 (22.4)	1.15 (0.63-2.10)	0.655	100 (20.2)	1.20 (0.56-2.58)	0.643

Values are n (%) or hazard ratio (95% CI).

CI confidence interval; HR hazard ratio; HRP high-risk plaque; MACE major adverse cardiovascular events; TCFA thin-cap fibroatheroma; TLF target lesion failure.

DISCUSSION

This study evaluated the association between OCT-identified HRP in non-flow limiting, deferred, non-culprit lesions and long-term adverse clinical outcomes after myocardial infarction. In PECTUS-obs we demonstrated that patients with HRP were at a twofold increased risk of MACE during the first 2 years after myocardial infarction.[7] In the present long-term follow-up analysis, with 5-year follow-up complete in 99.0% of patients, the prognostic implications of HRP were sustained at 5 year follow-up, driven by an increased risk of unplanned revascularization and spontaneous, non-fatal myocardial infarction. The risk associated with HRP appeared to be most pronounced in the first years of follow-up. Additionally, among different individual HRP features, non-culprit plaque rupture demonstrated the strongest association with adverse clinical outcomes.

Non-culprit lesions are important targets to improve prognosis after myocardial infarction, considering that approximately half of recurrent events originate from such lesions.[5,6] Complete non-culprit revascularisation guided by angiography or physiology improves hard clinical endpoints.[3] However, previous studies have questioned the validity of functional lesion evaluation to provide optimal risk stratification after myocardial infarction.[4,9-11] Indeed, physiological lesion evaluation informs predominantly on the ischaemia-generating potential of an evaluated lesion but provides limited information on its morphology. In this study, we provide long-term evidence on the prognostic implications of high-risk non-culprit lesions in the confirmed absence of ischaemia against a background of guideline-endorsed medical treatment: patients with at least one HRP were at an almost twofold increased risk for MACE throughout 5-year follow-up. Compared with earlier prospective studies on HRP imaging after myocardial infarction,[5,6] the current study uniquely confirmed the absence of significant flow limitations and reports the longest and most complete follow-up to date. Overall, this study supports guideline recommendations on complete revascularisation and intensive medical management after myocardial infarction.[1,2] It also supports the potential of further intensification of medical treatment in higher-risk patients.

Our findings correspond to those from COMBINE (OCT-FFR), comprising 390 diabetic patients (15.9% with myocardial infarction), which demonstrated an association between non-flow-limiting thin-cap fibroatheroma and an increased risk of adverse outcome after a mean follow-up of 3.5 years.[12] Similarly, HRP in the proximal left anterior descending artery were associated with cardiac death or target segment-related myocardial infarction in the CLIMA extended follow-up study (39.7% with myocardial infarction) at a median follow-up of 1,825 days (interquartile range 1,137-1,825 days).[13] However, haemodynamic stenosis severity was not systematically evaluated in the latter study. The totality of evidence highlights the complementary value of intracoronary OCT and physiology for prognostication.

Intriguingly, in an exploratory landmark analysis, the risk associated with the presence of at least one HRP was only observed in the first 2 years of follow-up. This observation may indicate that OCT-identified HRP predominantly have prognostic implications in the shorter term. Atherosclerosis has indeed been shown to be a dynamic process. Consequently, it is reasonable to assume that HRP may stabilise over time if they have not ruptured during their unstable phase. Conversely, non-HRP may transform into high-risk

counterparts. Hypothetically, the longevity of the prognostic implications of HRP may differ between those identified with varying imaging modalities. With OCT, most focus is paid to a thin fibrous cap, which can be dynamic in nature and can be rapidly modified with intensive medical therapy. Conversely, plaque burden, which is the main focus with intravascular ultrasound, is less likely to fluctuate or regress following the initiation of medical therapy.[14,15]

Although we do not report a significant association between HRP and lesion-level adverse outcome, point estimates provide a potential indication towards a comparable risk for lesion-level events. In a previous individual patient-data pooled analysis from PECTUS-obs and COMBINE (OCT-FFR) comprising 810 patients, non-flow-limiting deferred lesions meeting the HRP criteria were indeed also significantly associated with lesion-level adverse outcome.[16]

Among individual HRP features, plaque rupture carried the strongest prognostic implications, similar to that reported in the referenced individual patient-data pooled analysis.[16] Especially among myocardial infarction patients, multiple plaque ruptures are common.[17] We hypothesise that systemic factors such as enhanced inflammation diffusely induce fibrous cap thinning through enhanced matrix degradation, predisposing the whole coronary vasculature to rupture. These patients may remain susceptible to future plaque disruption causing clinically overt acute spontaneous events or stepwise lesion progression after asymptomatic disruption and healing.[18] Future studies exploring systemic markers in patients with multiple plaque ruptures and possibilities to reduce systemic rupture proneness are warranted. Also, at a lesion level, we observed that plaque rupture may indicate increased risk. Interestingly, a recent OCT study indicated that the increased risk of lesion-level recurrent events in previously disrupted plaques may be related to areas of intact thin-cap fibroatheroma.[19] If confirmed in future studies, this could support targeting non-culprit plaque rupture for preventive revascularisation, especially in the copresence of non-ruptured thin-cap fibroatheroma segments.

Limitations

The PECTUS-obs study was not powered to evaluate individual components of the primary endpoint or lesion-level endpoints. These analyses therefore merit careful interpretation. Second, operators were not blinded to the OCT images. Regardless, OCT image analyses were performed by an independent core laboratory, with the results masked to patients, operators, and treating physicians. Additionally, event adjudication was performed blinded. Third, the use of specific biomarkers for adjudicating events were not standardised and differed per centre, and revascularisation events included both clinically driven and non-clinically driven events. Fourth, we adopted the targeted imaging of non-culprit lesions, and only those segments were analysed, which may have resulted in an underestimation of the number of patients with HRP.[20] Fifth, plaque burden was not estimated using OCT, given the limited penetration depth, particularly in lipidic tissue. Sixth, baseline lipoprotein(a) levels were not systematically collected. Finally, proprotein convertase subtilisin/kexin type 9 were prescribed in a limited number of patients, and the effectiveness of lipid-lowering therapy was not systematically monitored via cholesterol levels during follow-up.

CONCLUSION

Non-flow-limiting but high-risk non-culprit plaques are associated with adverse clinical outcomes during long-term follow-up after myocardial infarction. The risk associated with OCT-identified HRP appears to be most pronounced during the first years after identification.

REFERENCES

1. Byrne RA, Rossello X, Coughlan JJ, Barbato E, Berry C, Chieffo A et al. 2023 ESC Guidelines for the management of acute coronary syndromes. Eur Heart J 2023;44:3720-3826.
2. Rao SV, O'Donoghue ML, Ruel M, Rab T, Tamis-Holland JE, Alexander JH et al. 2025 ACC/AHA/ACEP/NAEMSP/SCAI Guideline for the Management of Patients With Acute Coronary Syndromes: A Report of the American College of Cardiology/American Heart Association Joint Committee on Clinical Practice Guidelines. Circulation 2025;151:e771-e862.
3. Mehta SR, Tiong DTW, Böhm F, Ramasundarahettige C, Biscaglia S, Campo G et al. Complete versus culprit lesion-only revascularisation for acute myocardial infarction (Complete Revascularisation Trialists' Collaboration): an individual patient data meta-analysis of randomised trials. Lancet 2025.
4. Cerrato E, Mejia-Renteria H, Dehbi HM, Ahn JM, Cook C, Dupouy P et al. Revascularization Deferral of Nonculprit Stenoses on the Basis of Fractional Flow Reserve: 1-Year Outcomes of 8,579 Patients. JACC Cardiovasc Interv 2020;13:1894-1903.
5. Stone GW, Maehara A, Lansky AJ, de Bruyne B, Cristea E, Mintz GS et al. A prospective natural-history study of coronary atherosclerosis. N Engl J Med 2011;364:226-35.
6. Erlinge D, Maehara A, Ben-Yehuda O, Botker HE, Maeng M, Kjoller-Hansen L et al. Identification of vulnerable plaques and patients by intracoronary near-infrared spectroscopy and ultrasound (PROSPECT II): a prospective natural history study. Lancet 2021;397:985-995.
7. Mol JQ, Volleberg R, Belkacemi A, Hermanides RS, Meuwissen M, Protopopov AV et al. Fractional Flow Reserve-Negative High-Risk Plaques and Clinical Outcomes After Myocardial Infarction. JAMA Cardiol 2023;8:1013-1021.
8. Mol JQ, Belkacemi A, Volleberg RH, Meuwissen M, Protopopov AV, Laanmets P et al. Identification of anatomic risk factors for acute coronary events by optical coherence tomography in patients with myocardial infarction and residual nonflow limiting lesions: rationale and design of the PECTUS-obs study. BMJ Open 2021;11:e048994.
9. van der Hoeven NW, Janssens GN, de Waard GA, Everaars H, Broyd CJ, Beijnink CWH et al. Temporal Changes in Coronary Hyperemic and Resting Hemodynamic Indices in Nonculprit Vessels of Patients With ST-Segment Elevation Myocardial Infarction. JAMA Cardiol 2019;4:736-744.
10. Puymirat E, Cayla G, Simon T, Steg PG, Montalescot G, Durand-Zaleski I et al. Multivessel PCI Guided by FFR or Angiography for Myocardial Infarction. N Engl J Med 2021;385:297-308.
11. Denormandie P, Simon T, Cayla G, Steg PG, Montalescot G, Durand-Zaleski I et al. Compared Outcomes of ST-Segment-Elevation Myocardial Infarction Patients With Multivessel Disease Treated With Primary Percutaneous Coronary Intervention and Preserved Fractional Flow Reserve of Nonculprit Lesions Treated Conservatively and of Those With Low Fractional Flow Reserve Managed Invasively: Insights From the FLOWER-MI Trial. Circ Cardiovasc Interv 2021;14:e011314.
12. Fabris E, Berta B, Hommels T, Roleder T, Hermanides RS, Rivero F et al. Long-term outcomes of patients with normal fractional flow reserve and thin-cap fibroatheroma. EuroIntervention 2023;18:e1099-e1107.
13. Biccirè FG, Fabbiocchi F, Gatto L, La Manna A, Ozaki Y, Romagnoli E et al. Long-Term Prognostic Impact of OCT-Derived High-Risk Plaque Features: Extended Follow-Up of the CLIMA Study. JACC Cardiovasc Interv 2025;18:1361-1372.
14. Fujimoto D, Fuster V, Jang IK. The sequence of changes in intravascular imaging findings during lipid-lowering therapy and its implication. Nat Cardiovasc Res 2025;4:661-676.
15. Jukema RA, Maaniitty T, Nurmohamed NS, Raijmakers PG, Hoek R, Driessen RS et al. The time-varying prognostic value of stenosis and plaque burden in coronary artery disease. Eur Heart J Cardiovasc Imaging 2026;27:696-703.

16. Volleberg R, Rroku A, Mol JQ, Hermanides RS, van Leeuwen M, Berta B et al. FFR-Negative Nonculprit High-Risk Plaques and Clinical Outcomes in High-Risk Populations: An Individual Patient-Data Pooled Analysis From COMBINE (OCT-FFR) and PECTUS-obs. Circ Cardiovasc Interv 2025;18:e014667.
17. Vergallo R, Uemura S, Soeda T, Minami Y, Cho JM, Ong DS et al. Prevalence and Predictors of Multiple Coronary Plaque Ruptures: In Vivo 3-Vessel Optical Coherence Tomography Imaging Study. Arterioscler Thromb Vasc Biol 2016;36:2229-2238.
18. Vergallo R, Crea F. Atherosclerotic Plaque Healing. N Engl J Med 2020;383:846-857.
19. Zhao J, Zhao R, Chen Y, Cui L, Ma X, Chen J et al. Long-term clinical outcomes of non-culprit plaque rupture in STEMI. EuroIntervention 2026;22:e32-e43.
20. Volleberg R, Luttikholt TJ, van der Waerden RGA, Cancian P, van der Zande JL, Gu X et al. Artificial intelligence-based identification of thin-cap fibroatheromas and clinical outcomes: the PECTUS-AI study. Eur Heart J 2025;46:5032-5041.

SUPPLEMENTAL MATERIAL

Supplemental material related to this article can be found in the online version: https://eurointervention.pcronline.com/article/long-term-clinical-outcomes-of-high-risk-plaques-with-negative-fractional-flow-reserve-the-pectus-obs-study





CHAPTER 10

FFR-negative nonculprit high-risk plaques and clinical outcomes in high-risk populations: an individual patient-data pooled analysis from COMBINE (OCT-FFR) and PECTUS-obs

Rick Volleberg | Andi Rroku | Jan-Quinten Mol | Renicus Hermanides | Maarten van Leeuwen | Balázs Berta | Martijn Meuwissen | Fernando Alfonso | Wojciech Wojakowski | Anouar Belkacemi | Tomasz Roleder | Elvin Kedhi* | Niels van Royen*

Circulation Cardiovascular Interventions
2025 Feb;18(2):e014667

* joined senior authorship

ABSTRACT

Background Despite fractional flow reserve (FFR)–guided deferral of revascularization, recurrent events in patients with diabetes or after myocardial infarction remain common. This study aimed to assess the association between FFR-negative but high-risk nonculprit lesions and clinical outcomes.

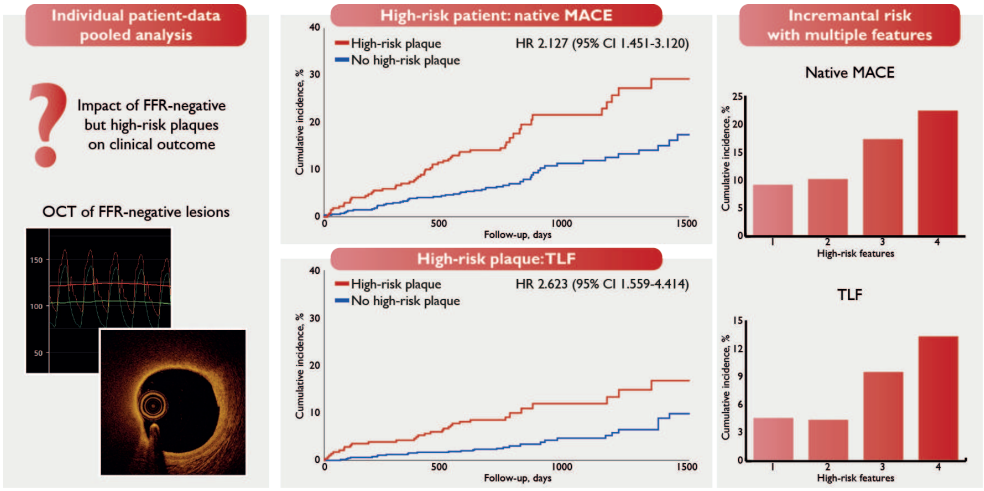
Methods This is a patient-level pooled analysis of the prospective natural-history COMBINE (OCT-FFR) study (Optical Coherence Tomography Morphologic and Fractional Flow Reserve Assessment in Diabetes Mellitus Patients) and PECTUS-obs study (Identification of Risk Factors for Acute Coronary Events by OCT After STEMI and NSTEMI Patients With Residual Non- Flow Limiting Lesions). Optical coherence tomography was performed on all FFR-negative (FFR >0.80) native nonculprit lesions. Patients or lesions with a high-risk plaque were compared with those without a high-risk plaque. A high-risk plaque was defined in the presence of at least 2 prespecified criteria: (1) lipid arc ≥90°, (2) minimum fibrous cap thickness <65 μm, and (3) presence of either plaque rupture or thrombus. The primary end points were native major adverse cardiovascular events (composite of all-cause mortality, nonfatal myocardial infarction, or unplanned revascularization excluding stent-failure-related events and nonattributable events) and target lesion failure (composite of cardiac death, target vessel myocardial infarction, or target lesion revascularization).

Results Among 810 patients, 450 (55.6%) had a history of diabetes and 482 (59.5%) presented with myocardial infarction. At least 1 high-risk plaque was identified in 271 (33.5%) patients and 287 (30.6%) lesions. Over a median follow-up of 761 (interquartile range, 731–1175) days, the presence of a high-risk plaque was associated with patient-level native major adverse cardiovascular events (hazard ratio, 2.127 [95% CI, 1.451–3.120]; P<0.001) and lesion-level target lesion failure (hazard ratio, 2.623 [95% CI, 1.559–4.414]; P<0.001). The risk of adverse outcomes increased with the copresence of multiple high-risk features.

Conclusions FFR-negative but high-risk nonculprit lesions are associated with adverse patient- and lesion-level clinical outcomes. These findings emphasize the additional value of intracoronary imaging in patients with FFR-negative nonculprit lesions.

Trial registration numbers NCT02989740 and NCT03857971.

GRAPHICAL ABSTRACT



Graphical Abstract. Optical coherence tomography-identified high-risk plaques in fractional-flow reserve negative deferred non-culprit lesions in patients with diabetes and/or after myocardial infarction are associated with the primary endpoints of patient-level native major adverse cardiovascular events and lesion-level target lesion failure.
CI confidence interval; OCT optical coherence tomography; FFR fractional flow reserve; HR hazard ratio; MACE major adverse cardiovascular events; TLF target lesion failure.

INTRODUCTION

Fractional flow reserve (FFR) is well established to evaluate ischemia and guide revascularization indications in the overall population with chronic coronary syndrome.[1,2] However, its effectiveness in specific populations and acute coronary syndrome has been questioned. Among patients with diabetes, FFR-guided deferral results in an up to 2-fold increased risk of adverse cardiovascular events including cardiac death compared with deferral in patients without diabetes.[3,4] Likewise, the incidence of major adverse cardiovascular events (MACE) after FFR-guided deferral in acute coronary syndrome exceeds the incidence in chronic coronary syndrome.[5] Moreover, the FLOWER-MI trial (Flow Evaluation to Guide Revascularization in Multi-Vessel ST-Elevation Myocardial Infarction) failed to demonstrate the superiority of an FFR-guided revascularization approach compared with an angiography-guided treatment strategy in patients with ST-segment elevation myocardial infarction (MI) and multivessel disease.[6]

It has been postulated that the observed residual risk despite the absence of hemodynamically significant flow limitations may be related to the presence of atherosclerotic plaques that are prone to rupture, so-called vulnerable or high-risk plaques. Among these are thin-cap fibroatheromas (TCFA) that are characterized by a large lipid pool with an intact but thin overlying fibrous cap (originally defined as <65 µm). This high-risk plaque hypothesis,[7] which stresses the importance of also addressing nonobstructive lesions, was initiated by histopathologic studies in which it was demonstrated that almost all ruptured coronary plaques had a thin fibrous cap infiltrated by macrophages[8] and that coronary lesions often display positive remodeling before compromising the coronary lumen.[9] It has been postulated that high-risk plaques also implicate a more general vulnerability throughout the coronary tree.[7]

Recent advances in imaging technologies allow *in vivo* assessment of high-risk plaques, and multiple natural-history studies have demonstrated an association between such plaques and adverse clinical outcomes.[10-16] To date, only 2 prospective studies assessed this association in the confirmed absence of flow limitation. The COMBINE (OCT-FFR) study (Optical Coherence Tomography Morphologic and Fractional Flow Reserve Assessment in Diabetes Mellitus Patients) demonstrated a 5-fold increased risk of adverse clinical outcomes in patients with diabetes in the presence of an optical coherence tomography (OCT)-identified high-risk deferred lesion.[15] Similarly, high-risk nonculprit plaques were associated with a 2-fold increased risk of adverse clinical outcomes in patients with MI in the PECTUS-obs study (Identification of Risk Factors for Acute Coronary Events by OCT After STEMI and NSTEMI Patients With Residual Non-Flow Limiting Lesions).[16] However, these studies were modestly sized, which precluded assessment of individual clinical end points and lesion-level analyses. The aim of the present individual patient-level data pooled analysis of these 2 studies was to further assess the additional value of identifying high-risk plaques in FFR-negative deferred lesions.

METHODS

Study design

This is an individual patient-data pooled analysis of the prospective, investigator-initiated, international COMBINE (OCT-FFR) (NCT02989740) and PECTUS-obs (NCT03857971) natural-history studies. The study is reported in accordance with the STROBE reporting guidelines (Strengthening of the Reporting of Observational Studies in Epidemiology). The rationale, design, and primary results of both studies were published previously.[15-18] In brief, both studies aimed to assess the association between OCT-identified high-risk plaques in FFR-negative, native coronary segments, and clinical outcomes. COMBINE (OCT-FFR) prospectively enrolled 550 patients with diabetes undergoing clinically indicated coronary angiography for chronic or acute coronary syndrome, among which 423 had at least 1 deferred FFR-negative intermediate (visually estimated 40%-80% stenosis) nonculprit lesion. Only these 423 patients were included in the present analysis. In PECTUS-obs, 438 patients presenting with an acute MI with at least 1 deferred FFR-negative intermediate (visually estimated 30%-90% stenosis) nonculprit lesion were prospectively included. Inclusion and exclusion criteria are listed in the Supplemental Methods. Included patients underwent OCT of all native, deferred, FFR-negative (FFR >0.80) intermediate nonculprit lesions, which are referred to as the target lesions. The FFR was evaluated using pressure wires during predominantly adenosine-induced maximal hyperemia according to the local site protocol. Structured clinical follow-up was obtained according to the respective study protocols. Both studies were conducted in accordance with the 1964 Declaration of Helsinki and were approved by the institutional review boards and medical ethics committees of each participating center. All patients provided written informed consent. The present analysis comprises all patients with at least 1 analyzable OCT pullback. The data that support the findings of this study are available from the corresponding authors upon reasonable request.

OCT imaging analysis

All OCT images for both studies were analyzed by the same independent OCT core laboratory, of which the members were blinded to patient outcomes. Image analysis was performed using CAAS IntraVascular 2.0 (Pie Medical Imaging B.V., the Netherlands). The target lesion was identified on OCT using manual coregistration with the angiogram based on anatomic landmarks (eg, side branches). Pullbacks with image artifacts interfering with the assessment of the target lesion were excluded at the discretion of the core laboratory. Quantitative and qualitative image analyses were performed in accordance with the latest consensus document on OCT image analysis.[19] For the current analysis, the PECTUS-obs criteria of a high-risk plaque were adopted to define groups and were defined as the presence of at least 2 of the following 3 prespecified criteria: (1) a lipid arc ≥90° , (2) a minimum fibrous cap thickness <65 µm, and (3) presence of either plaque rupture or thrombus. TCFA was defined in the presence of a lipid arc ≥90° and a minimum fibrous cap thickness <65 µm (Figure 1). OCT image analysis results were blinded to patients, operators, and treating physicians.

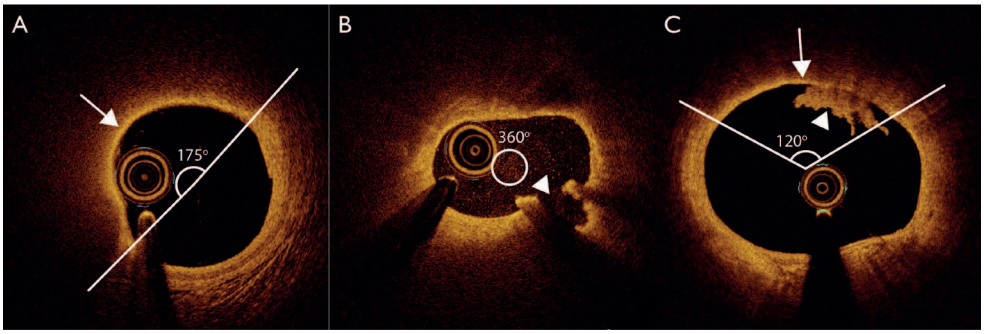


Figure 1. Examples of high-risk plaques.

Optical coherence tomography images meeting the criteria for a high-risk plaques based on (A) minimum fibrous cap thickness <65 µm (arrow) and lipid arc ≥90°, (B) lipid arc ≥90° and plaque rupture (arrowhead), and (C) minimum fibrous cap thickness <65 µm (arrow), lipid arc ≥90° and thrombus (arrowhead).

Clinical endpoints

The primary clinical end points of the present analysis were native MACE and target lesion failure (TLF). Native MACE was defined as the composite of all-cause mortality, nonfatal MI that was attributable and not related to stent failure, or unplanned revascularization not related to stent failure. TLF was defined as the composite of cardiac death, target vessel MI, or target lesion revascularization. Target vessel MI and target lesion revascularization were only considered if clearly attributable to the target vessel and lesion, respectively. Native MACE was evaluated at a patient level, and TLF was evaluated at a lesion level. Secondary end points include the individual components of the primary end points and attributable TLF (aTLF), defined as TLF excluding cases of cardiac death not clearly attributable to the target lesion. End point definitions of the respective studies are listed in the Supplemental Methods. Two blinded independent clinical end point committees consisting of at least 2 experienced interventional cardiologists adjudicated all potential clinical events for the respective studies. Events were adjudicated using medical records and by comparing baseline and follow-up angiograms.

Statistical analysis

Categorical data are presented as numbers (percentages) and were compared using the χ^2 test or the Fisher exact test, whenever appropriate. Continuous variables are expressed as mean ± SD if normally distributed or as median (interquartile range) if not normally distributed and were evaluated using the Student independent samples t test or the Mann-Whitney U test, respectively. Time-to-first events for the primary end points are presented using cumulative incidence curves and were evaluated using the log-rank test. Patients were censored at their last known moment of follow-up. Univariable and multivariable Cox proportional hazards regression models were performed to estimate the hazard ratio (HR) between high-risk plaque characteristics and the patient-level primary or secondary clinical end points. For the lesion-level clinical end points, robust standard errors were estimated to account for within patient clustering when patients had multiple target lesions. Baseline variables that were associated

with either of the primary end points in univariable analysis were entered into the multivariable models after checking for collinearity. Subgroup analyses were evaluated with the use of interaction terms. For the secondary end points, multivariable models were performed only for those end points with P<0.05 in univariable analysis. The association between the number of high-risk plaque features and clinical outcome was evaluated using the P value for trend and regression models with no high-risk plaque feature as a reference standard. Missing data were not imputed. Data were analyzed using IBM SPSS Statistics software, version 27.0 (IBM Corp), and RStudio, version 2023.09.1 (PBC).

RESULTS

Study flow

Patients were enrolled from March 2015 to December 2018 in COMBINE (OCT-FFR) and from December 2018 to September 2020 in PECTUS-obs. In total, 810 patients had at least 1 analyzable OCT and were enrolled in the present analysis, including 390 patients from COMBINE (OCT-FFR) and 420 patients from PECTUS-obs. The study flowchart is shown in Figure 2. A serious adverse event during OCT image acquisition occurred in 3 cases (Table S1). OCT image analysis revealed a high-risk plaque in 271 (33.5%) patients.

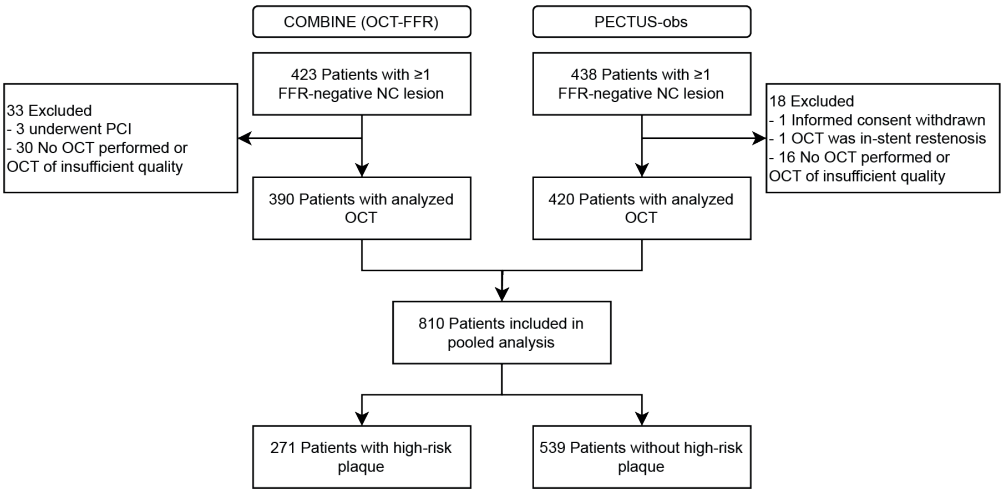


Figure 2. Study flowchart.

FFR fractional flow reserve; NC nonculprit; OCT optical coherence tomography; PCI percutaneous coronary intervention

Baseline characteristics

Baseline clinical and angiographic characteristics are presented in Table 1. The mean age of included patients was 65±10 years, and 585 (72.2%) patients were male; 511 (63.1%) and 450 (55.6%) patients had a history of hypertension and diabetes, respectively. MI during the index hospitalization was diagnosed in 482 (59.5%) patients, including 230 (28.4%) with ST-segment elevation MI and 252 (31.1%) with non-ST-segment elevation MI. The mean number of target lesions per patient was 1.18±0.43, and the mean FFR was 0.89±0.05. Patients with a high-risk plaque less frequently were on statin therapy before inclusion (44.6% versus 54.0%; P=0.012), had higher levels of low-density lipoprotein-cholesterol (3.02±1.21 versus 2.71±1.19 mmol/L; P=0.004), more frequently had a target nonculprit lesion located in the right coronary artery (41.2% versus 25.4%; P<0.001) and less frequently in the left anterior descending artery (42.1% versus 51.0%; P=0.016). Patients with a high-risk plaque more frequently underwent percutaneous coronary intervention of nontarget lesions at baseline (72.3% versus 64.2%; P=0.020). No difference in clinical risk profile (eg, history of diabetes and hypertension) was observed (Figure S1). Medical therapy during follow-up is described in Table S2.

Lesion-level OCT characteristics

A total of 939 FFR-negative nonculprit lesions were analyzable, including 287 (30.6%) lesions with a high-risk plaque. Lesion-level quantitative and qualitative OCT analyses are shown in Table 2. Lesions harboring a high-risk plaque were longer (23.4±10.7 versus 19.8±9.9 mm; P<0.001) and had a smaller minimal lumen area (2.58±1.23 versus 2.84±1.54 mm^2; P=0.007) and higher percentage area stenosis (65.0±12.7 versus 60.9±15.0%; P<0.001). Macrophage accumulation and cholesterol clefts were more prevalent in high-risk plaques (P<0.001 for both), whereas non-high-risk plaques had more extensive calcification and more protruding calcifications.

Table 1. Baseline characteristics.

Variables	N=810	High-risk plaque (n=271)	No high-risk plaque (n=539)	P value
Age, y		65 ± 11	66 ± 10	0.353
Male sex		194 (71.6)	391 (72.5)	0.775
BMI, kg/m^2	780	28.9 ± 4.9	28.6 ± 4.8	0.374
Smoking status				
Current		70 (27.2)	128 (25.2)	
Previous	764	83 (32.3)	132 (26.0)	0.076
Never		104 (40.5)	247 (48.7)	
Diabetes		146 (53.9)	304 (56.4)	0.495
Hypertension	808	165 (61.1)	346 (64.3)	0.373
Hypercholesterolemia	808	126 (46.8)	259 (48.1)	0.745
Family history of premature CVD	796	96 (36.4)	172 (32.3)	0.257

Previous MI		65 (24.0)	126 (23.4)	0.847
Previous PCI		69 (25.5)	137 (25.4)	0.989
Previous CVA		15 (5.5)	25 (4.6)	0.578
MI at presentation		162 (59.8)	320 (59.4)	0.911
STEMI		83 (51.2)	147 (45.9)	0.271
NSTEMI		79 (48.8)	173 (54.1)	
MINOCA		6 (3.7)	16 (5.0)	0.519
ST-elevation		1 (16.7)	2 (12.5)	1.000
Non-ST-elevation		5 (83.3)	14 (87.5)	
Statin at presentation		121 (44.6)	291 (54.0)	0.012
Laboratory assessment				
Creatinine, µmol/L	743	88.2 ± 25.2	87.0 ± 25.1	0.531
C-reactive protein, mg/L	483	3.00 (1.10-6.00)	2.90 (1.00-5.60)	0.387
Total cholesterol, mmol/L	629	4.78 ± 1.28	4.60 ± 1.31	0.110
LDL-cholesterol, mmol/L	502	3.02 ± 1.21	2.71 ± 1.19	0.004
HDL-cholesterol, mmol/L	506	1.10 (0.94-1.38)	1.10 (0.92-1.35)	0.549
Triglycerides, mmol/L	521	1.63 (1.14-2.20)	1.67 (1.12-2.46)	0.754
Glycated hemoglobin, %	183	7.46 ± 1.05	7.56 ± 1.36	0.631
PCI of non-target lesion(s)		196 (72.3)	346 (64.2)	0.020
No. of target lesions		1.28 ± 0.51	1.13 ± 0.37	<0.001
Target lesion distribution				
LM		2 (0.7)	10 (1.9)	0.355
LAD		114 (42.1)	275 (51.0)	0.016
LCx		94 (34.7)	194 (36.0)	0.714
RCA		112 (41.3)	137 (25.4)	<0.001
Target lesion FFR		0.88 ± 0.05	0.89 ± 0.05	0.073

BMI body mass index; CVA cerebrovascular accident; CVD cardiovascular disease; FFR fractional flow reserve; HDL high-density lipoprotein; LAD left anterior descending artery; LCx left circumflex artery; LDL low-density lipoprotein; LM left main coronary artery; MI myocardial infarction; MINOCA myocardial infarction with nonobstructive coronary arteries; NSTEMI non-ST-segment elevation myocardial infarction; PCI percutaneous coronary intervention; RCA right coronary artery; STEMI ST-segment elevation myocardial infarction.

Table 2. Lesion-level OCT characteristics.

Variables	N=939	High-risk plaque n=287	Non-high-risk plaque n=652	P value
MLA, mm^2		2.58 ± 1.23	2.84 ± 1.54	0.007
MLD, mm		1.47 ± 0.37	1.55 ± 0.44	0.007
Percentage area stenosis	937	65.0 ± 12.7	60.9 ± 15.0	<0.001
Lesion length, mm		23.4 ± 10.7	19.8 ± 9.9	<0.001
Calcification		221 (77.0)	476 (73.0)	0.197
Maximal calcification arc, °		142 ± 91	163 ± 98	0.007
Protruding calcification		61 (21.3)	191 (29.3)	0.010
Lipid		287 (100)	395 (60.6)	<0.001
Maximal lipid arc, °		238 ± 76	194 ± 78	<0.001
Lipid arc ≥90°		287 (100)	370 (56.7)	<0.001
Minimum FCT, µm		70 ± 39	159 ± 87	<0.001
Minimum FCT <65µm		239 (83.3)	0 (0)	<0.001
Plaque rupture		88 (30.7)	7 (1.1)	<0.001
In absence of minimum FCT <65µm		23 (8.0)	7 (1.1)	<0.001
Thrombus	938	102 (35.5)	41 (6.3)	<0.001
In absence of minimum FCT <65µm		35 (12.2)	41 (6.2)	0.002
Macrophage accumulation	938	132 (46.2)	211 (32.4)	<0.001
Microvessel		133 (46.3)	265 (40.6)	0.104
Cholesterol clefts	935	107 (37.4)	152 (23.4)	<0.001
Layered plaque	937	65 (22.5)	124 (19.1)	0.209

FCT fibrous cap thickness, MLA minimum lumen area; MLD minimum lumen diameter; OCT optical coherence tomography.

High-risk plaques and clinical outcome

The mean time of follow-up was 952±375 days (median, 761 days; interquartile range, 731–1175 days). The primary and secondary end points are presented in Table 3. The primary end point of native MACE occurred in 52 (19.2%) patients with and 53 (9.8%) patients without a high-risk plaque (HR, 2.127 [95% CI, 1.451– 3.120]; P<0.001; Figure 3A). The incidence of TLF was 10.8% among high-risk lesions compared with 4.4% in non-high-risk lesions (HR, 2.623 [95% CI, 1.559– 4.414]; P<0.001; Figure 3B). Results were consistent in subgroup analyses (Figure S2). The difference in native MACE was mainly driven by a higher incidence of nonfatal MI (4.8% versus 1.7%; P=0.008) and unplanned revascularization (14.4% versus 5.6%; P<0.001). The difference in TLF was mainly driven by target vessel-related MI (2.8% versus 0.3%; P=0.004) and target lesion revascularization (7.0% versus 2.1%; P<0.001). None of the cardiac deaths were clearly attributable to the target lesion. High-risk lesions had an HR for aTLF of 3.803 (95% CI, 1.946–7.434; P<0.001; Figure 3C). In multivariable analysis, correcting for baseline characteristics associated with the primary end points (Tables S3 and S4), statistical significance remained for all end points tested (Table 3).

Table 3. Clinical outcome.

Variables	High-risk plaque	Non-high-risk plaque	Univariable HR (95% CI)	P value	Multivariable HR (95% CI)*	P value
Patient-level	n=271	n=539				
Native MACE	52 (19.2)	53 (9.8)	2.127 (1.451-3.120)	<0.001	2.034 (1.380-2.998)	<0.001
All-cause mortality	15 (5.5)	21 (3.9)	1.471 (0.758-2.853)	0.251		
Non-fatal MI	13 (4.8)	9 (1.7)	2.975 (1.272-6.961)	0.008	3.104 (1.311-7.353)	0.010
Unplanned revascularization	39 (14.4)	30 (5.6)	2.793 (1.735-4.497)	<0.001	2.749 (1.697-4.453)	<0.001
Lesion-level	n=287	n=652				
TLF	31 (10.8)	29 (4.4)	2.623 (1.559-4.414)	<0.001	2.413 (1.429-4.074)	<0.001
Cardiac death	10 (3.5)	15 (2.3)	1.557 (0.679-3.570)	0.296		
Target-vessel MI	8 (2.8)	2 (0.3)	9.419 (2.013-44.070)	0.004	8.436 (1.832-38.850)	0.006
Target-lesion revascularization	20 (7.0)	14 (2.1)	3.454 (1.744-6.841)	<0.001	3.161 (1.603-6.233)	<0.001
aTLF	22 (7.7)	14 (2.1)	3.803 (1.946-7.434)	<0.001	3.502 (1.795-6.833)	<0.001

aTLF attributable target lesion failure; CI confidence interval; HR hazard ratio; MACE major adverse cardiovascular event; MI myocardial infarction; TLF target lesion failure.

** Multivariable Cox proportional hazard regression models (patient level) or robust standard errors (lesion level) with the following independent and dependent variables: presence of a high-risk plaque, history of diabetes, history of percutaneous coronary intervention; presentation with MI, statin therapy at discharge, oral anticoagulation therapy at discharge, target lesion in the left anterior descending artery and target lesion in the left circumflex artery as independent variables with native MACE or its components as dependent variables. Presence of high-risk plaque, oral anticoagulation therapy at discharge, and lesion-level fractional flow reserve as independent variables with (a)TLF or its components as dependent variables.*

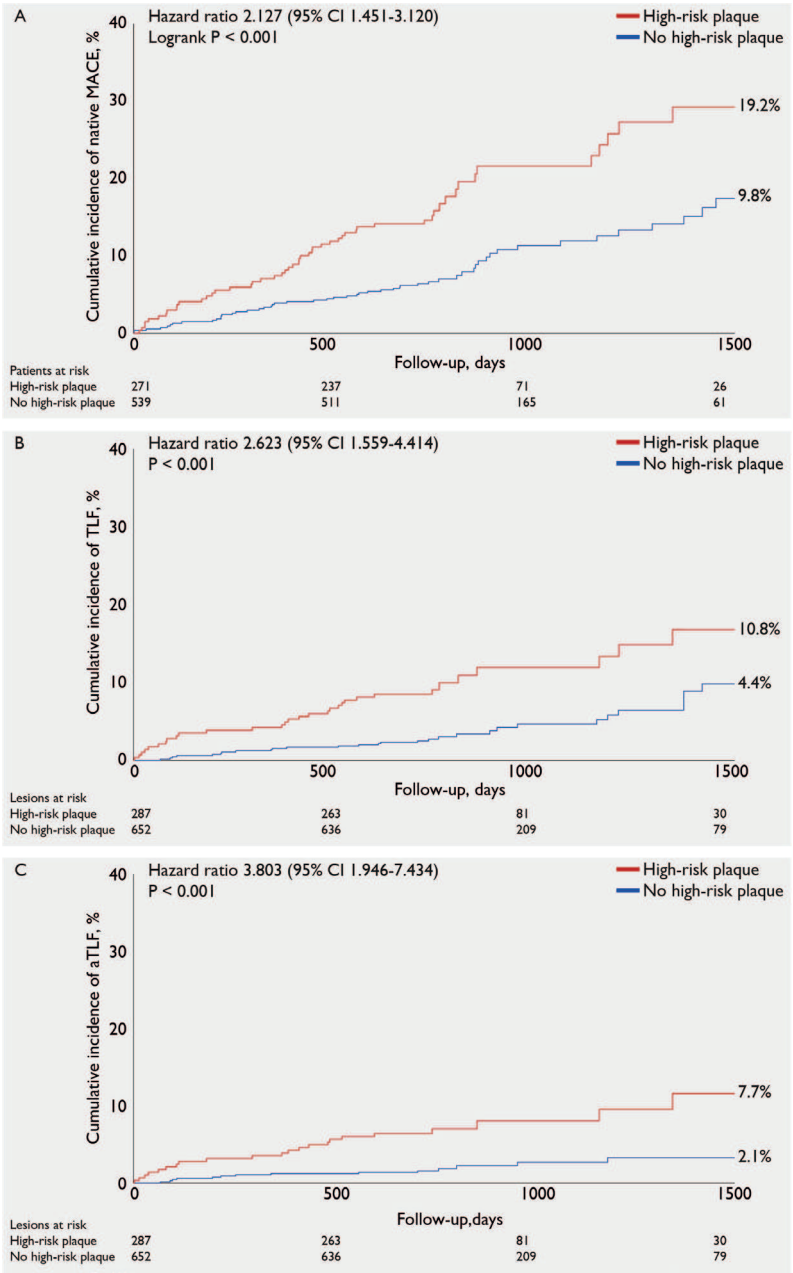


Figure 3. Cumulative incidences of the composite end points.

Cumulative incidence curves for the cumulate endpoints of native major adverse cardiovascular event (A), target lesion failure (B) and attributable TLF (C) truncated at 1500 days.

aTLF attributable target lesion failure; CI confidence interval; MACE major adverse cardiovascular events; TLF target lesion failure.

Two hundred twenty-four (27.7%) patients had a minimum fibrous cap thickness <65 µm, 592 (73.1%) had a maximum lipid arc ≥90°, 93 (11.5%) had plaque rupture, and 142 (17.5%) had thrombus presence. On a lesion level, the prevalence of these features was 25.5%, 70.0%, 20.1%, and 10.4%, respectively. Associations between the individual high-risk plaque criteria and the composite end points are presented in Figures 4 and 5 and Figure S3. The risk of native MACE, TLF, and aTLF increased when more high-risk plaque features coexisted (P_{trend}<0.001 for all endpoints; Figures 4 and 5 and Figure S3).

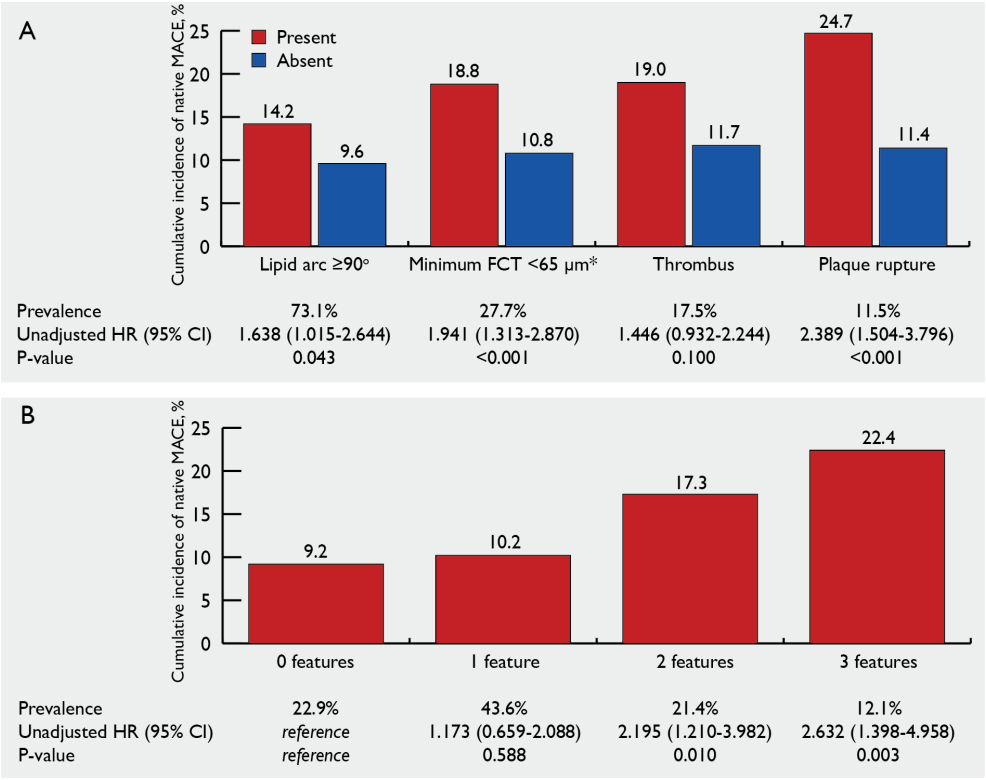


Figure 4. High-risk plaque components and major adverse cardiovascular events.

A) Association between individual high-risk plaque features and native MACE. B) Association between the number of high-risk plaque features and native MACE, in which the presence of plaque rupture and thrombus is considered 1 high-risk plaque feature.

CI confidence interval; FCT fibrous cap thickness; HR hazard ratio; MACE major adverse cardiovascular event.

** Considering that all lesions with a minimum FCT <65 µm had a lipid arc ≥90°, all these lesions are qualified as a thin-cap fibroatheroma.*

TCFA was present in 224 (27.7%) patients (Table S5). Patients or lesions with a TCFA had a higher incidence of native MACE (HR, 1.941 [95% CI, 1.313–2.870]; P<0.001) and TLF (HR, 2.306 [95% CI, 1.375–3.869]; P=0.002), respectively (Figure S4). The presence of TCFA was associated with a higher incidence of nonfatal MI (HR, 3.264 [95% CI, 1.410–7.559]; P=0.003), unplanned revascularization (HR, 2.615 [95% CI, 1.630– 4.197]; P<0.001), target vessel-related MI (HR, 7.028 [95% CI, 1.836–26.910]; P=0.004), and target lesion revascularization (HR, 3.138 [95% CI, 1.597–6.167]; P<0.001), also after correcting for potential confounders (Table S6).

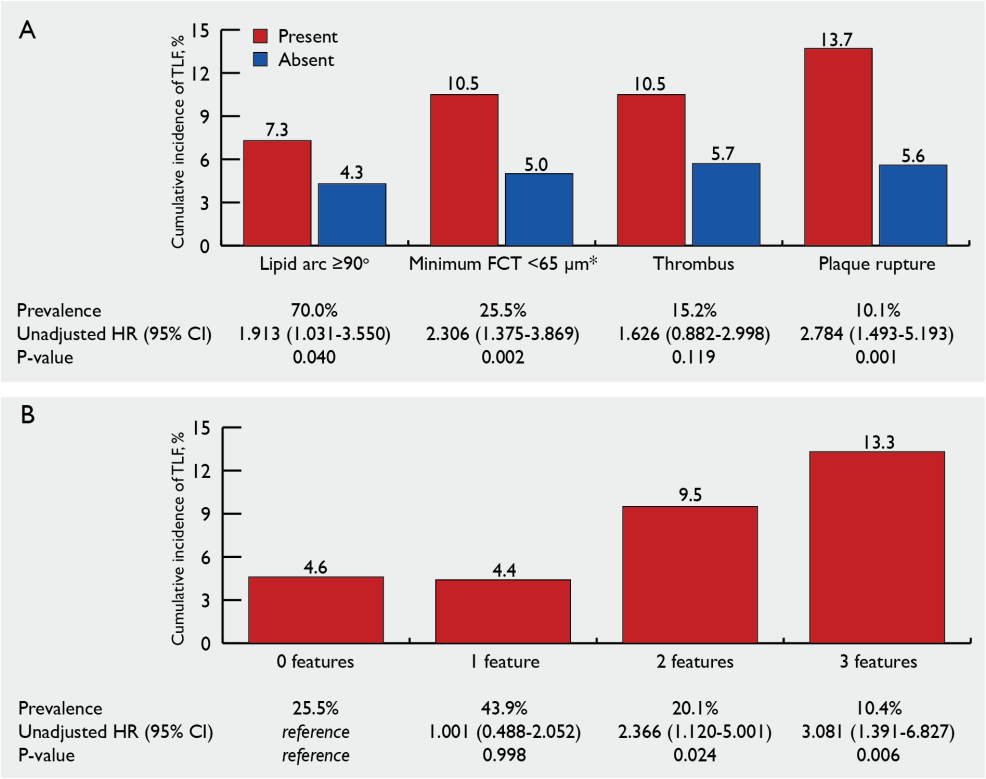


Figure 5. High-risk plaque components and target lesion failure.

A) Association between individual high-risk plaque features and TLF. B) Association between the number of high-risk plaque features and TLF, in which the presence of plaque rupture and thrombus is considered 1 high-risk plaque feature.

CI confidence interval; FCT fibrous cap thickness; HR hazard ratio; TLF target lesion failure.

** Considering that all lesions with a minimum FCT <65 µm had a lipid arc ≥90°, all these lesions are qualified as a thin-cap fibroatheroma.*

DISCUSSION

This pooled analysis from the COMBINE (OCT-FFR) and PECTUS-obs studies, comprising all available prospective data on the association between FFR-negative but high-risk nonculprit plaques and clinical outcome, illustrates the value of intracoronary imaging complementary to physiology for identification of patients at risk of adverse clinical outcome. The presence of a high-risk plaque was associated with an approximately 2-fold increased risk of patient-level native MACE and lesion-level TLF, and over 3-fold increased risk of lesion-level aTLF, both in univariable and multivariable analyses. This increased risk was driven by any and target vessel-related nonfatal MI and by any and target lesion-related unplanned revascularization. The coexistence of multiple high-risk plaque features resulted in an incremental risk of both native MACE and (a)TLF. Similar results were observed using TCFA as a marker of plaque vulnerability. These results support the high-risk patient and plaque hypotheses and ongoing studies on the treatment of high-risk plaques.

High-risk plaques and clinical outcome

Multiple prospective natural-history studies provided evidence on the association between high-risk plaques and patient- or lesion-level clinical outcomes, among which are the PROSPECT study (Providing Regional Observations to Study Predictors of Events in the Coronary Tree) using 3-vessel intravascular ultrasound,[10] PROSPECT-II (Providing Regional Observations to Study Predictors of Events in the Coronary Tree II) and LRP (Lipid-Rich Plaque) studies using near-infrared spectroscopy,[11,12] and the CLIMA study (Relationship Between OCT Coronary Plaque Morphology and Clinical Outcome) using OCT of the left anterior descending artery in patients with MI.[13] In PROSPECT and PROSPECT-II, including solely patients with acute coronary syndromes, the risk of patient- and lesion-level events was increased up to over 2-fold and 11-fold, respectively.[10,11] However, both studies included quantitative measures of luminal obstruction in the high-risk plaque criteria and therefore not only focus on plaque morphology but also on lesion severity. Nevertheless, the plaque morphology-related criteria were also significantly associated with adverse outcomes in both studies.[10,11] Intriguingly, the mean diameter stenosis of nonculprit lesions causing recurrent events in PROSPECT was only 32±21%, fueling the high-risk plaque hypothesis.[10] In the LRP study (≈17% MI and 37% diabetes), high-risk plaques were associated with a 2-fold increased risk in patient-level events and a 4-fold increased risk in lesion-level events at a 2-year follow-up.[12] More recently, Jiang et al[14] retrospectively studied 883 patients (3757 lesions) with acute MI in whom 3-vessel OCT was performed and found that the presence of TCFA and a minimum lumen area <3.5 mm^2 were independently associated with both patient- and lesion-level adverse cardiac events.

Importantly, however, functional assessment was not routinely performed in any of these studies. Therefore, we can only make estimations about the flow-limiting status of included lesions. In PROSPECT, only 6% of lesions had a diameter stenosis of at least 50%,[10] and only 0.15% of included lesions had an intravascular ultrasound-derived FFR ≤0.80.[20] The latter finding should, however, be treated with caution considering the lack of external validation and the modest correlation between intracoronary imaging-derived FFR and pressure wire-derived FFR.[21] Similarly, in the study by Jiang et al,[14] the mean percentage

diameter stenosis assessed by quantitative coronary angiography (42.5±10.2%) and the OCT-derived percentage area stenosis (47.4±17.8%) were also limited. Nonetheless, the present analysis is unique in that the absence of flow limitation is confirmed in all included lesions and, therefore, truly emphasizes the additional value of intracoronary imaging complementary to physiological assessment in populations in which FFR-guided deferral is less safe.[4,5] Furthermore, the adopted approach of targeted imaging of FFR-negative nonculprit lesion imaging is more feasible in clinical care than 3-vessel intracoronary imaging.

High-risk plaque definition

In the present analysis, the PECTUS-obs predefined criterion of a high-risk plaque that includes, but is not limited to, TCFA was adopted and was effective in identifying patients at risk of recurrent events. Multiple criteria have been used throughout the years to define high-risk plaques. A recent meta-analysis of 30 observational studies, including 4 studies using OCT, demonstrated that TCFA was the high-risk feature with the highest HR for patient-level events (3-fold increased risk) and second highest HR for lesion-level events (6-fold increased risk), with a positive predictive value of 24% (95% CI, 2%–46%) and 9% (95% CI, 3%–15%), respectively.[22] We now report a positive predictive value for TCFA of 18.8% for native MACE and 10.5% for TLF (negative predictive values 89.2% and 95.0%, respectively) using a cutoff value of <65 and ≥90° for minimum fibrous cap thickness and lipid arc, respectively.

The presence of nonculprit plaque rupture as a marker of plaque vulnerability hitherto received little attention in natural-history studies. We observed an HR of over 2 for native MACE and TLF in the presence of nonculprit plaque rupture, which calls for attention in future studies. Earlier findings support the concept of nonculprit plaque rupture as an indicator of vulnerability. First, plaque disruption requires an internal milieu predisposing the plaque to destabilization, which could be a combination of mechanical but also biochemical factors, the latter of which could affect the whole coronary tree. Indeed, culprit plaque rupture has been associated with signs of panvulnerability, including more nonculprit TCFA and plaque rupture.[23] Furthermore, multiple nonculprit plaque ruptures are more common among patients with acute coronary syndrome compared with patients with chronic coronary syndrome.[24] Second, subclinical nonculprit plaque rupture in the presence of a well-functioning healing capacity[25] contributes to rapid, stepwise lesion progression[26] and can consequently induce ischemia requiring revascularization.[27]

Importantly, we observed the highest HR and positive predictive value in lesions harboring all 3 features, which is in line with the referenced meta-analysis illustrating an incremental risk with multiple coexistent high-risk features.[22] The optimal tradeoff between the desired positive predictive value and the number of high-risk plaque features included in the definition, which is inversely related to the proportion of patients meeting the respective high-risk definition, remains to be determined. This is a critical consideration when defining treatment strategies targeting high-risk plaques, especially considering a large number of high-risk plaques not proceeding to cause future events. This is of particular importance for focal treatment strategies.

Limitations

This study has some limitations. First, the study only applies to intermediate FFR-negative nonculprit lesions. Second, inherent to the inclusion criteria, the high-risk clinical profile (ie, diabetes or MI) of the present cohort may impede extrapolating our results to the general population undergoing percutaneous coronary intervention. Specifically, the HR for adverse events may be lower in the overall population. Third, female patients were underrepresented in both cohorts. Fourth, the end point definitions differed slightly between studies. Fifth, target vessel MI was evaluated rather than target lesion MI. However, identifying the exact culprit lesion can be challenging with a large thrombus load. Sixth, analyses were limited to OCT features analyzed by the core laboratory. Therefore, other variables of potential interest (eg, type of calcified nodule or volumetric fibrous cap evaluations) could not be evaluated. Finally, the positive predictive value remains relatively low, potentially limiting the effectiveness of preventive treatment. Whether the addition of other nonanatomic factors (eg, inflammatory and thrombogenic milieu) would increment the predictive value of the diagnosis of high-risk plaques in selected high-risk patients remains unsettled and warrants further investigation.

CONCLUSION

In conclusion, the presence of an OCT-identified high-risk plaque in an FFR-negative nonculprit lesion is associated with patient-level native MACE and lesion-level TLF in patients with diabetes or after MI. Co-occurrence of multiple high-risk plaque features results in an incremental risk of adverse outcomes. These findings emphasize the additional value of intracoronary imaging in the absence of flow limitation and support the high-risk patient and plaque hypotheses, as well as ongoing studies on systemic or focal treatment of high-risk plaques.

REFERENCES

1. Tonino PA, De Bruyne B, Pijls NH, Siebert U, Ikeno F, van' t Veer M et al. Fractional flow reserve versus angiography for guiding percutaneous coronary intervention. N Engl J Med 2009;360:213-24.
2. De Bruyne B, Pijls NH, Kalesan B, Barbato E, Tonino PA, Piroth Z et al. Fractional flow reserve-guided PCI versus medical therapy in stable coronary disease. N Engl J Med 2012;367:991-1001.
3. Kennedy MW, Hermanides RS, Kaplan E, Hemradj V, Fabris E, Koopmans PC et al. Fractional Flow Reserve-Guided Deferred Versus Complete Revascularization in Patients With Diabetes Mellitus. Am J Cardiol 2016;118:1293-1299.
4. Ekmejian A, Sritharan H, Selvakumar D, Venkateshka V, Allahwala U, Ward M et al. Outcomes of deferred revascularisation following negative fractional flow reserve in diabetic and non-diabetic patients: a meta-analysis. Cardiovasc Diabetol 2023;22:22.
5. Cerrato E, Mejia-Renteria H, Dehbi HM, Ahn JM, Cook C, Dupouy P et al. Revascularization Deferral of Nonculprit Stenoses on the Basis of Fractional Flow Reserve: 1-Year Outcomes of 8,579 Patients. JACC Cardiovasc Interv 2020;13:1894-1903.
6. Puymirat E, Cayla G, Simon T, Steg PG, Montalescot G, Durand-Zaleski I et al. Multivessel PCI Guided by FFR or Angiography for Myocardial Infarction. N Engl J Med 2021;385:297-308.
7. Stone PH, Libby P, Boden WE. Fundamental Pathobiology of Coronary Atherosclerosis and Clinical Implications for Chronic Ischemic Heart Disease Management-The Plaque Hypothesis: A Narrative Review. JAMA Cardiol 2023;8:192-201.
8. Burke AP, Farb A, Malcom GT, Liang YH, Smialek J, Virmani R. Coronary risk factors and plaque morphology in men with coronary disease who died suddenly. N Engl J Med 1997;336:1276-82.
9. Glagov S, Weisenberg E, Zarins CK, Stankunavicius R, Kolettis GJ. Compensatory enlargement of human atherosclerotic coronary arteries. N Engl J Med 1987;316:1371-5.
10. Stone GW, Maehara A, Lansky AJ, de Bruyne B, Cristea E, Mintz GS et al. A prospective natural-history study of coronary atherosclerosis. N Engl J Med 2011;364:226-35.
11. Erlinge D, Maehara A, Ben-Yehuda O, Botker HE, Maeng M, Kjoller-Hansen L et al. Identification of vulnerable plaques and patients by intracoronary near-infrared spectroscopy and ultrasound (PROSPECT II): a prospective natural history study. Lancet 2021;397:985-995.
12. Waksman R, Di Mario C, Torguson R, Ali ZA, Singh V, Skinner WH et al. Identification of patients and plaques vulnerable to future coronary events with near-infrared spectroscopy intravascular ultrasound imaging: a prospective, cohort study. Lancet 2019;394:1629-1637.
13. Prati F, Romagnoli E, Gatto L, La Manna A, Burzotta F, Ozaki Y et al. Relationship between coronary plaque morphology of the left anterior descending artery and 12 months clinical outcome: the CLIMA study. Eur Heart J 2020;41:383-391.
14. Jiang S, Fang C, Xu X, Xing L, Sun S, Peng C et al. Identification of High-Risk Coronary Lesions by 3-Vessel Optical Coherence Tomography. J Am Coll Cardiol 2023;81:1217-1230.
15. Kedhi E, Berta B, Roleder T, Hermanides RS, Fabris E, AJJ IJ et al. Thin-cap fibroatheroma predicts clinical events in diabetic patients with normal fractional flow reserve: the COMBINE OCT-FFR trial. Eur Heart J 2021;42:4671-4679.
16. Mol JQ, Volleberg R, Belkacemi A, Hermanides RS, Meuwissen M, Protopopov AV et al. Fractional Flow Reserve-Negative High-Risk Plaques and Clinical Outcomes After Myocardial Infarction. JAMA Cardiol 2023;8:1013-1021.
17. Kennedy MW, Fabris E, Ijsselmuiden AJ, Nef H, Reith S, Escaned J et al. Combined optical coherence tomography morphologic and fractional flow reserve hemodynamic assessment of non- culprit lesions to better predict

adverse event outcomes in diabetes mellitus patients: COMBINE (OCT-FFR) prospective study. Rationale and design. Cardiovasc Diabetol 2016;15:144.

18. Mol JQ, Belkacemi A, Volleberg RH, Meuwissen M, Protopopov AV, Laanmets P et al. Identification of anatomic risk factors for acute coronary events by optical coherence tomography in patients with myocardial infarction and residual nonflow limiting lesions: rationale and design of the PECTUS-obs study. BMJ Open 2021;11:e048994.
19. Araki M, Park SJ, Dauerman HL, Uemura S, Kim JS, Di Mario C et al. Optical coherence tomography in coronary atherosclerosis assessment and intervention. Nat Rev Cardiol 2022;19:684-703.
20. Seike F, Mintz GS, Matsumura M, Ali ZA, Liu M, Jeremias A et al. Impact of Intravascular Ultrasound-Derived Lesion-Specific Virtual Fractional Flow Reserve Predicts 3-Year Outcomes of Untreated Nonculprit Lesions: The PROSPECT Study. Circ Cardiovasc Interv 2022;15:851-860.
21. Ziedses des Plantes AC, Scoccia A, Gijsen F, van Soest G, Daemen J. Intravascular Imaging-Derived Physiology-Basic Principles and Clinical Application. Interv Cardiol Clin 2023;12:83-94.
22. Gallone G, Bellettini M, Gatti M, Tore D, Bruno F, Scudeler L et al. Coronary Plaque Characteristics Associated With Major Adverse Cardiovascular Events in Atherosclerotic Patients and Lesions: A Systematic Review and Meta-Analysis. JACC Cardiovasc Imaging 2023;16:1584-1604.
23. Vergallo R, Ren X, Yonetsu T, Kato K, Uemura S, Yu B et al. Pancoronary plaque vulnerability in patients with acute coronary syndrome and ruptured culprit plaque: a 3-vessel optical coherence tomography study. Am Heart J 2014;167:59-67.
24. Vergallo R, Uemura S, Soeda T, Minami Y, Cho JM, Ong DS et al. Prevalence and Predictors of Multiple Coronary Plaque Ruptures: In Vivo 3-Vessel Optical Coherence Tomography Imaging Study. Arterioscler Thromb Vasc Biol 2016;36:2229-2238.
25. Vergallo R, Crea F. Atherosclerotic Plaque Healing. N Engl J Med 2020;383:846-857.
26. Araki M, Yonetsu T, Kurihara O, Nakajima A, Lee H, Soeda T et al. Predictors of Rapid Plaque Progression: An Optical Coherence Tomography Study. JACC Cardiovasc Imaging 2021;14:1628-1638.
27. Kurihara O, Russo M, Kim HO, Araki M, Shinohara H, Lee H et al. Clinical significance of healed plaque detected by optical coherence tomography: a 2-year follow-up study. J Thromb Thrombolysis 2020;50:895-902.
28. Bohula EA, Bonaca MP, Braunwald E, Aylward PE, Corbalan R, De Ferrari GM et al. Atherothrombotic Risk Stratification and the Efficacy and Safety of Vorapaxar in Patients With Stable Ischemic Heart Disease and Previous Myocardial Infarction. Circulation 2016;134:304-13.
29. Inker LA, Eneanya ND, Coresh J, Tighiouart H, Wang D, Sang Y et al. New Creatinine- and Cystatin C-Based Equations to Estimate GFR without Race. N Engl J Med 2021;385:1737-1749.

SUPPLEMENTAL MATERIAL

Supplemental material related to this article can be found in the online version: https://www.ahajournals.org/doi/10.1161/CIRCINTERVENTIONS.124.014667[28,29]





CHAPTER 11

Impact of clinical risk characteristics on the prognostic value of high-risk plaques

Rick Volleberg | Andi Rroku | Jan-Quinten Mol | Renicus Hermanides | Maarten van Leeuwen | Balázs Berta | Martijn Meuwissen | Fernando Alfonso | Wojciech Wojakowski | Anouar Belkacemi | Giuseppe de Luca | Laura Rodwell | Tomasz Roleder | Elvin Kedhi | Niels van Royen

EuroIntervention
2025 Oct 6;21(19):e1147-1158

ABSTRACT

Background High-risk coronary plaques (HRPs) are associated with adverse cardiovascular outcomes. However, the clinical practicality of HRP identification is challenged by their modest prevalence and low positive predictive value.

Aims We aimed to evaluate the association between clinical risk factors and HRPs, as well as the clinical impact of HRPs across different clinical risk profiles.

Methods This is a pooled analysis of individual patient data from the prospective observational COMBINE (OCT-FFR) and PECTUS-obs studies. A modified version of the Thrombolysis in Myocardial Infarction Risk Score for Secondary Prevention (TRS-2P) was used for risk stratification. The composite endpoint of major adverse cardiovascular events (MACE) was evaluated on a patient level, and target lesion failure (TLF), also a composite endpoint, was evaluated on a lesion level.

Results Among 810 patients, 311, 265, and 234 were at low (TRS-2P 0-1), intermediate (TRS-2P 2), and high risk (TRS-2P ≥3), respectively. The modified TRS-2P had no discriminative value for the identification of patients with an HRP (area under the receiver operating characteristic curve 0.51, 95% confidence interval [CI]: 0.47-0.56). A consistent trend towards worse clinical outcome in the presence of an HRP was observed across different clinical risk profiles ($p_{interaction}$=0.539 for MACE and 0.337 for TLF). For TLF, the highest event rate per 100 lesion-years was observed in high-risk patients with HRPs (6.28, 95% CI: 3.52-10.36; 13.6% absolute risk at 2 years).

Conclusions and relevance HRPs are associated with a negative clinical outcome, without apparent differences between clinical risk profiles. This highlights the independent value of optical coherence tomography for prognostication beyond clinical risk factors. The high event rates in high-risk patients with HRPs necessitate the search for additional therapeutic strategies to mitigate this risk.

INTRODUCTION

Histopathological and *in vivo* imaging studies have significantly advanced our understanding of coronary lesions that are at increased risk of causing future cardiovascular events.[1,2] These high-risk plaques (HRPs) are typically characterised by a large lipid burden with a thin overlying fibrous cap, of which the thin-cap fibroatheroma is considered the prototype. In recent years, numerous studies have demonstrated the prognostic impact of *in vivo*-identified HRPs in deferred lesions on patient- and lesion-level clinical outcomes.[2-4] However, the clinical applicability of *in vivo* identification is challenged by various factors, especially when pursuing preventive focal treatment of HRPs.[5]

First, the positive predictive value for future events remains limited, especially for lesion-level events.[2] For example, the COMBINE (OCT-FFR) and PECTUS-obs studies assessed the clinical impact of HRPs in non-flow-limiting lesions in patients with diabetes and myocardial infarction, respectively.[3,4] In an individual patient data pooled analysis from these studies, HRPs were significantly associated with patient- and lesion-level adverse outcomes in patients at risk for recurrent events. However, the positive predictive value ranged between 9.2% and 22.4% for patient-level events and between 2.1% to 13.3% for lesion-level events, depending on the number of HRP criteria included.[6] Second, HRPs are only found in up to one-third of patients.[2-4] Therefore, a multitude of patients need to be screened to identify those at increased risk of adverse cardiovascular outcomes. Upfront identification of patients who are likely to have HRPs could streamline the screening process, and screening patients in whom HRPs are likely to have a profound effect on clinical outcomes may provide more benefits, thereby reducing resource utilisation.

We hypothesised that traditional clinical risk factors could help identify patients that are more likely to have HRPs. Second, we postulated that HRPs would have the most profound effect on clinical outcomes among patients at high clinical risk. Therefore, this study aimed to assess the association between clinical risk factors and the presence of HRPs, as well as the impact of HRPs on clinical outcomes across different clinical risk profiles.

METHODS

Study design

This analysis is performed on an individual patient-level data pooled analysis of the prospective, natural history COMBINE (OCT-FFR) study (ClinicalTrials.gov: NCT02989740) and the PECTUS-obs study (NCT03857971). Both studies aimed to assess the association between optical coherence tomography (OCT)-identified HRPs in fractional flow reserve (FFR)-negative deferred native lesions and clinical outcomes in patients with diabetes or after myocardial infarction, respectively. The design and primary results of both studies were published previously.[3,4,7,8] In brief, OCT was performed on all native, FFR-negative (FFR >0.80), deferred, intermediate lesions, which we refer to as target lesions. Patients subsequently underwent structured clinical follow-up according to the respective study protocols.

The inclusion and exclusion criteria of the respective studies are listed in Supplementary Appendix 1. The details on pooling the individual patient data and the primary combined analysis were published previously.[6] In total, 810 patients had at least one analysable OCT and were included in the pooled analysis, including 390 patients from COMBINE (OCT-FFR) and 420 from PECTUS-obs. Both studies were conducted in accordance with the 1964 Declaration of Helsinki and were approved by the institutional review boards and/or medical ethics committees of each participating centre. All patients provided written informed consent.

Clinical risk stratification

The Thrombolysis in Myocardial Infarction Risk Score for Secondary Prevention (TRS-2P) was used to classify patients by their risk of cardiovascular disease.[9] The original score assigns one point to each variable included: congestive heart failure, hypertension, age ≥75 years, diabetes mellitus, prior stroke, prior coronary artery bypass grafting, other vascular disease (peripheral), renal dysfunction (defined as an estimated glomerular filtration rate <60 mL/min/1.73 m^2), and current smoking status. For the present analysis, the score was modified to account for missing baseline variables (i.e., data on "congestive heart failure" and "other vascular disease [peripheral]" were unavailable). Consequently, the modified score ranged from 0 to 7, with higher values indicating higher risk. The glomerular filtration rate was estimated using the 2021 Chronic Kidney Disease Epidemiology Collaboration (CKD-EPI) creatinine formula.[10] Missing values required for calculation of the modified TRS-2P were imputed using the most prevalent value or the mean across the population for categorical and continuous variables, respectively. Specifically, hypertension was considered absent in 2 patients, and 12 patients were considered non-smokers. Creatinine was imputed as 1.00 mg/dL in 67 patients. Data on all seven TRS-2P criteria were available for 733 patients. Patients were categorised according to the original cutoff values into low (0 or 1 indicator), intermediate (2 indicators), or high risk (≥3 indicators).

OCT image analysis

OCT image analysis was performed in accordance with the latest consensus document.[11] OCT analyses were performed by the same independent OCT core laboratory using CAAS Intravascular 2.0 (Pie Medical Imaging). Members of the core laboratory were blinded to clinical outcomes. To identify the target lesion on OCT, manual coregistration with the angiogram was performed based on anatomical landmarks (e.g., side branches). Pullbacks with insufficient image quality for qualitative and quantitative analyses of the target lesion were excluded at the discretion of the core laboratory. The predefined HRP criteria from PECTUS-obs were adopted in accordance with the primary combined analysis of COMBINE (OCT-FFR) and PECTUS-obs.[6] An HRP was defined by the presence of at least 2 of the 3 following criteria: (1) a lipid arc ≥90° , (2) a minimum fibrous cap thickness <65 µm, and (3) the presence of either plaque rupture or thrombus. Patients, operators, and treating physicians were blinded to the OCT image analysis results.

Clinical endpoints

Two composite endpoints were evaluated in the present analysis. Major adverse cardiovascular events (MACE) was defined as the composite of all-cause mortality, non-fatal myocardial infarction that was attributable to a specific coronary segment and that was not related to stent failure, or unplanned revascularisation not related to stent failure. Target lesion failure (TLF) was defined as the composite of cardiac death, target vessel myocardial infarction or target lesion revascularisation, for which target vessel myocardial infarction and target lesion revascularisation were only considered if clearly attributable to the target vessel or lesion, respectively. The definitions of the individual endpoints are summarised in Supplementary Appendix 2. All potential events were adjudicated by two blinded, independent clinical endpoint committees, using medical records and by comparing baseline and follow-up angiograms. Each committee consisted of at least two experienced interventional cardiologists.

Statistical analysis

Categorical variables are presented as absolute frequencies (percentages), while continuous variables are presented as mean ± standard deviation or median (interquartile range [IQR]), as appropriate. The association between clinical risk factors and the presence of an HRP at the patient level was evaluated using binary logistic regression. All variables with a p-value <0.10 in univariable analyses were simultaneously included in the multivariable model. In cases of high collinearity (defined as r >0.80), the variable with the highest level of significance was included. Analyses were performed using the study of origin as a fixed parameter to account for differences in inclusion and exclusion criteria from COMBINE (OCT-FFR) and PECTUS-obs that may have influenced the TRS-2P score (e.g., diabetes mellitus).

For comparative analyses of the three risk profile groups, the chi-squared test or Fisher's exact test was used for the analyses of categorical data. Bonferroni correction was applied during subsequent evaluation of differences between two risk groups. Normally distributed continuous data were analysed using one-way analysis of variance (ANOVA) with Tukey's *post hoc* test or one-way ANOVA with Welch's statistic and Games-Howell *post hoc* tests. Non-normally distributed data were analysed using the Kruskal-Wallis test. The discriminatory value of the modified TRS-2P for the identification of HRPs was evaluated using the area under the receiver operating characteristic curve (AUC).

For the analyses of the composite clinical endpoints, patients were censored at their last moment of follow-up. For MACE, the hazard ratio (HR) associated with the presence of at least one HRP was evaluated using Cox proportional hazards models. For TLF, robust standard errors were estimated to account for within-patient clustering, given patients could have had multiple lesions. Differences in the prognostic impact of HRPs across different clinical risk profiles were evaluated using interaction terms. The study of origin was included as a fixed parameter in both patient- and lesion-level analyses.

Data were imputed only for variables included in the modified TRS-2P score. Sensitivity analyses were performed including only patients in whom information on all seven TRS-2P criteria was available without imputation. A 2-sided p-value <0.05 was considered statistically significant. Data were analysed using SPSS Statistics software, version 27.0 (IBM), and R version 4.4.1 (R Foundation for Statistical Computing).

RESULTS

Study flow

Patient enrolment took place from March 2015 to December 2018 in COMBINE (OCT-FFR) and from December 2018 to September 2020 in PECTUS-obs (Figure 1). The study is reported in accordance with the STrengthening the Reporting of OBservational studies in Epidemiology (STROBE) guidelines (www.strobe-statement.org).

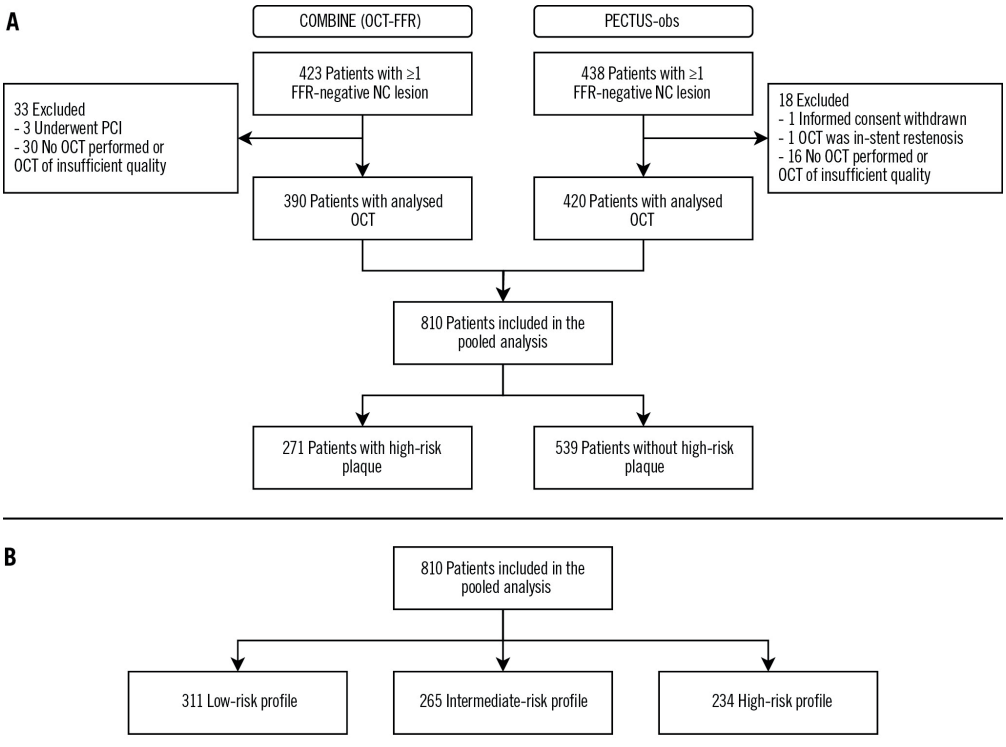


Figure 1. Study flowchart.

Study flowchart for the presence of a high-risk plaque (A) and for the classification of patients into clinical risk profiles (B).

FFR fractional flow reserve; NC non-culprit; OCT optical coherence tomography; PCI percutaneous coronary intervention.

Association between baseline characteristics and high-risk plaques

At least one HRP was identified in 271 patients, while 539 patients had solely non-HRPs (Figure 1A). Univariable analyses exploring the relationship for each clinical characteristic separately identified 3 clinical characteristics (age ≥75, statin use at baseline, and baseline low-density lipoprotein cholesterol levels) and 5 procedural characteristics (percutaneous coronary intervention at index, number of target lesions, target lesion in the left anterior descending artery or right coronary artery, and target lesion FFR) as potential predictors for the presence of an HRP (Table 1). In multivariable analysis, percutaneous coronary intervention at the index procedure (p=0.003), number of target lesions (p=0.001), and a target lesion in the right coronary artery (p=0.005) were independently associated with the presence of at least one HRP. Statin therapy at baseline (p=0.036) and target lesion FFR (p=0.007) were also significantly associated with HRP in a sensitivity analysis following imputation of low-density lipoprotein cholesterol levels, which was performed to account for missing laboratory values (Supplementary Table 1). Results were overall consistent when analysing only those 733 patients in whom information on all seven TRS-2P criteria was available (Supplementary Table 2).

Table 1. Association between baseline variables and high-risk plaques.

Variables	N=810	High-risk plaque n=271	No high-risk plaque n=539	Univariable[a]		Multivariable	
				OR (95% CI)	P-value	OR (95% CI)	P-value
Age, years		65 ± 11	66 ± 10	0.59 (0.23-1.48)[b]	0.258[b]		
≥75 years		63 (23.2)	98 (18.2)	1.38 (0.96-1.98)	0.078	1.41 (0.86-2.32)	0.175
Male sex		194 (71.6)	391 (72.5)	0.94 (0.67-1.31)	0.712		
BMI, kg/m^2	780	28.9 ± 4.9	28.6 ± 4.8	1.02 (0.99-1.05)	0.324		
Current smoker		70 (25.8)	128 (23.7)	1.11 (0.79-1.56)	0.541		
Diabetes		146 (53.9)	304 (56.4)	0.81 (0.45-1.45)	0.480		
Hypertension		166 (61.3)	347 (64.4)	0.88 (0.65-1.20)	0.420		
Hypercholesterolemia	808	126 (46.8)	259 (48.1)	0.96 (0.71-1.30)	0.806		
Family history of premature CVD	796	96 (36.4)	172 (32.3)	1.20 (0.88-1.64)	0.248		
Previous MI		65 (24.0)	126 (23.4)	1.05 (0.74-1.49)	0.782		
Previous PCI		69 (25.5)	137 (25.4)	1.02 (0.72-1.44)	0.911		
Previous CABG		6 (2.2)	6 (1.1)	2.10 (0.66-6.64)	0.207		
Previous CVA		15 (5.5)	25 (4.6)	1.23 (0.63-2.40)	0.537		
MI at presentation		162 (59.8)	320 (59.4)	0.89 (0.49-1.60)	0.691		
STEMI		83 (51.2)	147 (45.9)	Reference			
NSTEMI		79 (48.8)	173 (54.1)	0.82 (0.56-1.21)	0.312		
Statin at presentation		121 (44.6)	291 (54.0)	0.61 (0.43-0.87)	0.006	0.81 (0.50-1.30)	0.379
Laboratory assessment							
eGFR, mL/min/1.73 m^2		80.5 ± 19.8	81.1 ± 19.1	1.00 (0.99-1.01)	0.603		
eGFR <60 mL/min/1.73 m^2		46 (17.0)	84 (15.6)	1.12 (0.75-1.67)	0.572		
C-reactive protein, mg/L	483	3.00 (1.10-6.00)	2.90 (1.00-5.60)	1.00 (0.99-1.01)	0.667		
Total cholesterol, mmol/L	629	4.78 ± 1.28	4.60 ± 1.31	1.11 (0.98-1.27)	0.105		
LDL-cholesterol, mmol/L	502	3.02 ± 1.21	2.71 ± 1.19	1.27 (1.08-1.49)	0.003	1.18 (0.99-1.40)	0.070
HDL-cholesterol, mmol/L	506	1.10 (0.94-1.38)	1.10 (0.92-1.35)	1.20 (0.85-1.69)	0.292		

Triglycerides, mmol/L	521	1.63 (1.14-2.20)	1.67 (1.12-2.46)	1.00 (0.88-1.13)	0.991		
Glycated hemoglobin, %	183	7.46 ± 1.05	7.56 ± 1.36	0.94 (0.73-1.21)	0.630		
PCI at index[c]		196 (72.3)	346 (64.2)	1.78 (1.18-2.68)	0.006	2.57 (1.37-4.79)	0.003
Number of target lesions		1.28 ± 0.51	1.13 ± 0.37	2.15 (1.54-3.00)	<0.001	2.14 (1.35-3.38)	0.001
Target lesion distribution							
LM		2 (0.7)	10 (1.9)	0.39 (0.09-1.81)	0.231		
LAD		114 (42.1)	275 (51.0)	0.69 (0.52-0.93)	0.015	0.85 (0.54-1.35)	0.491
LCx		94 (34.7)	194 (36.0)	0.94 (0.69-1.28)	0.688		
RCA		112 (41.3)	137 (25.4)	2.07 (1.51-2.82)	<0.001	1.94 (1.22-3.08)	0.005
Target lesion FFR		0.88 ± 0.05	0.89 ± 0.05	0.97 (0.94-1.00)[d]	0.069	0.97 (0.93-1.01)[d]	0.175

Data are given as mean±standard deviation, n (%) or median (IQR), unless otherwise indicated. BMI body mass index; CABG coronary artery bypass grafting; CI confidence interval; CVA cerebrovascular accident; CVD cardiovascular disease; eGFR estimated glomerular filtration rate; FFR fractional flow reserve; HDL high-density lipoprotein; LAD left anterior descending artery; LCx left circumflex artery; LDL low-density lipoprotein; LM left main coronary artery; MI myocardial infarction; NSTEMI non-ST-segment elevation myocardial infarction; OR odds ratio; PCI percutaneous coronary intervention; RCA right coronary artery; STEMI ST-segment elevation myocardial infarction.

[a] Adjusted for the original study of inclusion.

[b] Logarithmic transformation was applied to ensure linearity.

[c] The index procedure refers to the invasive coronary angiography before inclusion in the study. In patients with myocardial infarction, this refers to the initial invasive coronary angiography, irrespective of whether patients were included during this procedure or during a staged procedure.

[d] Per 0.01 increase.

TRS-2P and high-risk plaques

According to the modified TRS-2P, 311 patients were classified as low risk, 265 as intermediate risk, and 234 as high risk (Figure 1B). Baseline characteristics according to clinical risk profile are presented in Table 2. Patients at low risk presented significantly more often with a myocardial infarction (p<0.001) and more frequently underwent percutaneous coronary intervention of non-target lesions at baseline (p<0.001). No differences were observed in the number or distribution of target lesions. Prescription rates of secondary prevention medication at discharge and during follow-up were higher among patients with a low clinical risk profile (Table 3).

Among patients with a low-, intermediate-, and high-risk profile, the patient-level prevalence of at least one HRP was 32.8%, 32.1%, and 35.9%, respectively (p=0.633). The modified TRS-2P had no discriminative value for the identification of HRPs (AUC 0.51, 95% confidence interval [CI]: 0.47-0.56; p=0.584) (Central illustration). Among the 733 with information available for all seven TRS-2P criteria, the AUC was 0.51 (95% CI: 0.46-0.55; p=0.751).

Table 2. Baseline characteristics according to clinical risk profile.

Variables	N=810	Low risk n=311	Intermediate risk n=265	High risk n=234	P-value
Age, years		62 ± 9	65 ± 10	71 ± 10	<0.001[a,b,c]
≥75 years		13 (4.2)	37 (14.0)	111 (47.4)	<0.001[a,b,c]
Male sex		54 (17.4)	80 (30.2)	91 (38.9)	<0.001[a,b]
BMI, kg/m^2	780	27.4 ± 4.2	29.5 ± 5.2	29.5 ± 4.7	<0.001[a,b]
Current smoker		52 (16.7)	68 (25.7)	78 (33.3)	<0.001[a,b]
Diabetes		46 (14.8)	187 (70.6)	217 (92.7)	<0.001[a,b,c]
Hypertension		90 (28.9)	207 (78.1)	216 (92.3)	<0.001[a,b,c]
Hypercholesterolemia	808	90 (28.9)	143 (54.2)	152 (65.2)	<0.001[a,b,c]
Family history of premature CVD	796	100 (32.3)	94 (36.2)	74 (32.7)	0.582
Previous MI		40 (12.9)	69 (26.0)	82 (35.0)	<0.001[a,b]
Previous PCI		41 (13.2)	78 (29.4)	41 (13.2)	<0.001[a,b]
Previous CABG		0 (0.0)	2 (0.8)	10 (4.3)	<0.001[b,c]
Previous CVA		1 (0.3)	4 (1.5)	35 (15.0)	<0.001[b,c]
MI at presentation		277 (89.1)	120 (45.3)	85 (36.3)	<0.001[a,b]
STEMI		154 (55.6)	53 (44.2)	23 (27.1)	<0.001[b,c]
NSTEMI		123 (44.4)	67 (55.8)	62 (72.9)	
Statin at presentation		80 (25.7)	157 (59.2)	175 (74.8)	<0.001[a,b,c]
Laboratory assessment					
eGFR, mL/min/1.73 m^2		89.1 ± 13.6	82.4 ± 17.1	68.3 ± 21.7	<0.001[a,b,c]
eGFR <60 ml/min/1.73 m^2		2 (0.6)	25 (9.4)	103 (44.0)	<0.001[a,b,c]
C-reactive protein, mg/L	483	2.30 (1.00-4.50)	3.00 (1.30-5.90)	4.80 (1.43-8.00)	<0.001[b,c]
Total cholesterol, mmol/L	629	5.00 ± 1.31	4.59 ± 1.34	4.26 ± 1.11	<0.001[a,b,c]

Table 2. Continued

LDL-cholesterol, mmol/L	502	3.08 ± 1.17	2.72 ± 1.19	2.46 ± 1.17	<0.001[a,b]
HDL-cholesterol, mmol/L	506	1.14 (1.00-1.40)	1.10 (0.90-1.36)	1.05 (0.90-1.30)	0.008[b]
Triglycerides, mmol/L	521	1.52 (1.01-2.10)	1.70 (1.22-2.56)	1.90 (1.25-2.79)	0.002[a,b]
Glycated hemoglobin, %	183	7.62 ± 1.60	7.56 ± 1.15	7.48 ± 1.27	0.865
PCI at index[d]		275 (88.4)	157 (59.2)	110 (47.0)	<0.[001a,b,c]
Number of target lesions		1.17 ± 0.42	1.18 ± 0.40	1.20 ± 0.47	0.774
Target lesion distribution					
LM		1 (0.3)	5 (1.9)	6 (2.6)	0.080
LAD		154 (49.5)	130 (49.1)	105 (44.9)	0.516
LCx		120 (38.6)	92 (34.7)	76 (32.5)	0.318
RCA		106 (34.1)	72 (27.2)	71 (30.3)	0.198
Target lesion FFR		0.89 ± 0.05	0.88 ± 0.05	0.89 ± 0.05	0.007[a]

Data are given as mean±standard deviation, n (%) or median (IQR), unless otherwise indicated. BMI body mass index; CABG coronary artery bypass grafting; CI confidence interval; CVA cerebrovascular accident; CVD cardiovascular disease; eGFR estimated glomerular filtration rate; FFR fractional flow reserve; HDL high-density lipoprotein; LAD left anterior descending artery; LCx left circumflex artery; LDL low-density lipoprotein; LM left main coronary artery; MI myocardial infarction; NSTEMI non-ST-segment elevation myocardial infarction; OR odds ratio; PCI percutaneous coronary intervention; RCA right coronary artery; STEMI ST-segment elevation myocardial infarction.

[a] Significant difference between low risk and intermediate risk.

[b] Significant difference between low risk and high risk.

[c] Significant difference between intermediate risk and high risk.

[d] The index procedure refers to the invasive coronary angiography before inclusion in the study. In patients with myocardial infarction, this refers to the initial invasive coronary angiography, irrespective of whether patients were included during this procedure or during a staged procedure.

Table 3. Medical therapy during follow-up.

Variables	Low risk n=311	Intermediate risk n=265	High risk n=234	P-value
Medication at discharge (n=810)				
Statin	301 (96.8)	233 (87.9)	201 (85.9)	<0.001[a,b]
Acetylsalicylic acid	297 (95.5)	238 (89.8)	212 (90.6)	0.022[a]
P2Y12-inhibitor	286 (92.0)	183 (69.1)	142 (60.7)	<0.001[a,b]
Dual antiplatelet therapy	280 (90.0)	173 (65.3)	138 (59.0)	<0.001[a,b]
Anticoagulation	26 (8.4)	34 (12.8)	45 (19.2)	<0.001[b]
Betablocker	265 (85.2)	213 (80.4)	187 (79.9)	0.188
ACE-inhibitor	241 (77.5)	163 (61.5)	134 (57.3)	<0.001[a,b]
Last-known medication after discharge (n=777)				
Statin	254 (83.8)	199 (78.0)	164 (74.9)	0.036[b]
Acetylsalicylic acid	267 (88.1)	190 (74.5)	139 (63.5)	<0.001[a,b,c]
P2Y12-inhibitor	33 (10.9)	28 (11.0)	36 (16.4)	0.113
Dual antiplatelet therapy	25 (8.3)	16 (6.3)	18 (8.2)	0.625
Anticoagulation	25 (8.3)	49 (19.2)	46 (21.0)	<0.001[a,b]
Betablocker	174 (57.4)	173 (67.8)	149 (68.0)	0.012[a,b]
ACE-inhibitor	210 (69.3)	140 (54.9)	112 (51.1)	<0.001[a,b]

Data are given as n (%). ACE angiotensin-converting enzyme.

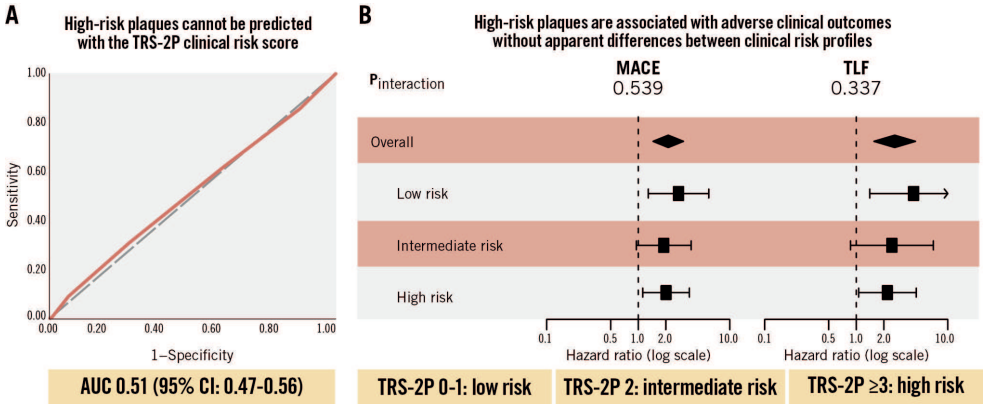
[a] Significant difference between low risk and intermediate risk.

[b] Significant difference between low risk and high risk.

[c] Significant difference between intermediate risk and high risk.

High-risk plaques and clinical outcomes across different risk profiles

The median time of follow-up was 761 (IQR 731-1,175) days. Per 100 person-years, patient-level MACE rates were 4.19 (95% CI: 2.76-6.09), 4.69 (95% CI: 3.23-6.59), and 6.98 (95% CI: 5.09-9.34) in patients with a low-, intermediate-, and high-risk clinical profile, respectively ($p_{\text{low vs intermediate}}$=0.486 and $p_{\text{low vs high}}$=0.033). At the lesion level, TLF rates per 100 lesion-years were 1.85 (95% CI: 1.01-3.10), 1.77 (95% CI: 0.99-2.91), and 3.95 (95% CI: 2.69-5.61), respectively ($p_{\text{low vs intermediate}}$=0.981 and $p_{\text{low vs high}}$=0.059). Event rates at 2-year follow-up are reported in Figure 2, given that follow-up was complete for almost all patients at this timepoint. Over the complete available follow-up, HRPs were associated with increased risks of MACE (HR 2.13, 95% CI: 1.45-3.12) and TLF (HR 2.63, 95% CI: 1.56-4.44). No interaction was observed for the association between HRPs and adverse clinical outcomes across the clinical risk profiles ($p_{\text{interaction}}$=0.539 for MACE; $p_{\text{interaction}}$=0.337 for TLF) (Central illustration, Figure 3). The event rates at 2-year follow-up in the subgroups according to the presence of HRPs are reported in Figure 2.



Central illustration. The association between clinical risk factors and the presence and prognostic implications of high-risk plaques.

A) AUC curve of the discriminatory value of the number of TRS-2P criteria for the prediction of at least one high-risk plaque. B) Forest plot of the risk associated with the presence of at least one high-risk plaque according to clinical risk profile.

AUC area under the receiver operating characteristic curve; CI confidence interval; MACE major adverse cardiovascular events; TLF target lesion failure; TRS-2P thrombolysis in myocardial infarction risk score for secondary prevention.

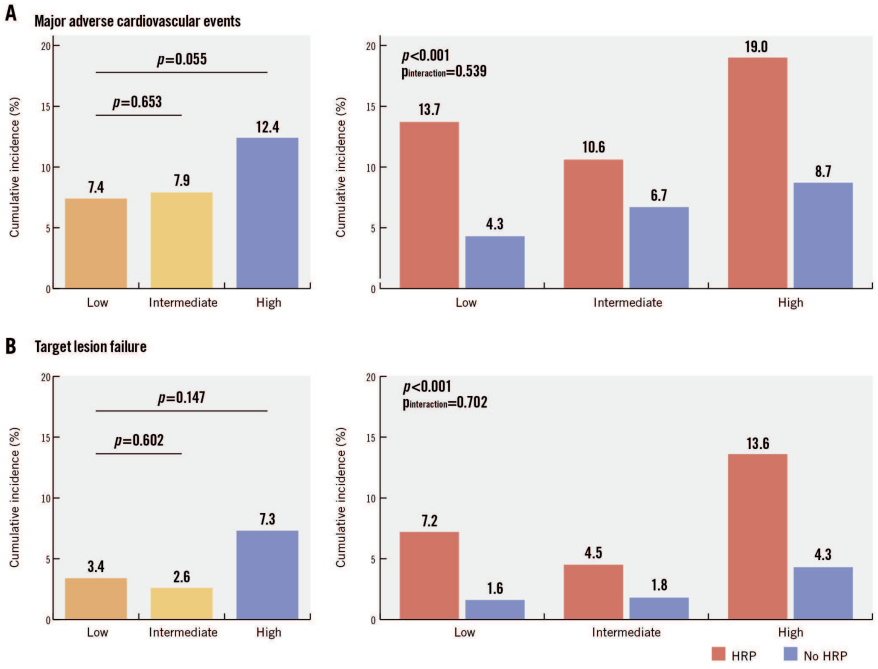


Figure 2. Cumulative incidences of the composite endpoints at two-year follow-up across different risk subgroups.

Cumulative incidences of the composite endpoints of patient-level major adverse cardiovascular events (A) and lesion-level target lesion failure (B) at two-year follow-up.

HRP high-risk plaque.

Various sensitivity analyses showed consistent results, including the following: evaluation of the proportion of patients in whom information on all seven TRS-2P criteria was available (Supplementary Figure 1), analyses correcting for differences in medical therapy at discharge (Supplementary Figure 2), analyses for the composite of target vessel myocardial infarction and target lesion revascularisation – performed to account for the fact that none of the cardiac deaths were clearly attributable to a target lesion-related event (Supplementary Figure 3) – and analyses using different risk scores (Supplementary Figure 4, Supplementary Figure 5).

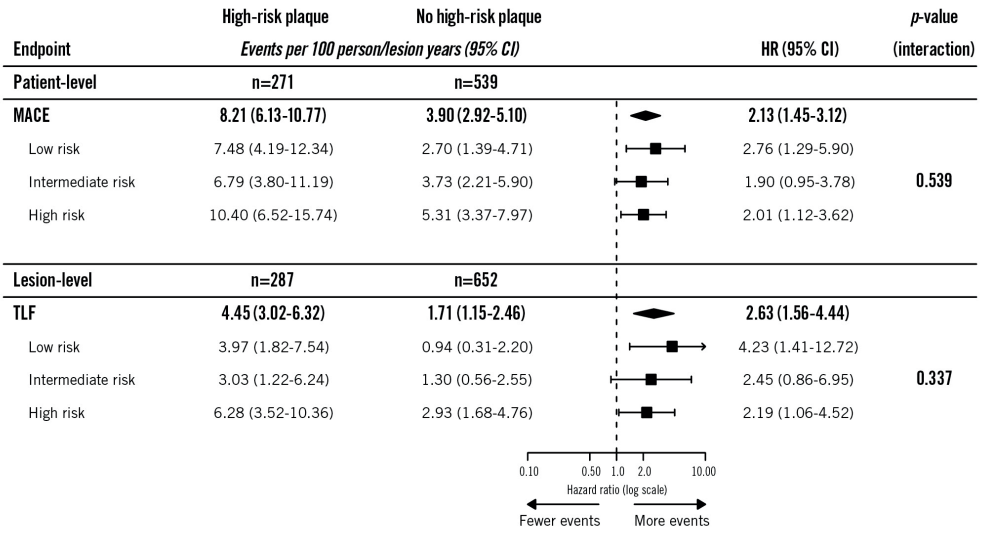


Figure 3. Clinical impact of high-risk plaques across clinical risk profiles.
Associations between high-risk plaques and the composite clinical endpoints across clinical risk profiles.
CI confidence interval; HR hazard ratio; MACE major adverse cardiovascular events; TLF target lesion failure.

DISCUSSION

The present analysis sought to evaluate the association between clinical risk factors and high-risk coronary plaques in non-flow-limiting deferred lesions among patients at risk for recurrent events, as well as the prognostic impact of HRPs across clinical risk profiles. The main findings were that traditional clinical risk factors had minimal, if any, association with the presence of HRPs. Particularly, the TRS-2P had no discriminative value for the identification of patients harbouring HRPs. Furthermore, the adverse prognostic implication of HRPs on both patient- and lesion-level cardiovascular outcomes appears to be consistent across patients with different clinical risk profiles, highlighting the independent value of OCT for prognostication beyond clinical risk factors. Nevertheless, by combining clinical risk factors and HRP identification using OCT, we were able to identify patients at the greatest risk for adverse patient-level and lesion-level events, which resulted in the highest positive predictive value. The high lesion-level

event rate in high-risk patients with an HRP emphasises the need for additional therapeutic strategies to mitigate this risk.

A priori prediction of high-risk plaques

Numerous studies with various imaging modalities have demonstrated a significant association between HRP phenotypes and adverse outcomes.[2-4] These findings have led to multiple randomised trials aimed at evaluating the efficacy and safety of preventive treatment of HRPs. The PREVENT trial recently provided the first evidence that preventive treatment of HRPs may indeed improve patient outcomes.[5] However, the absolute clinical benefit was modest and was largely driven by unplanned revascularisation and rehospitalisation for unstable or progressive angina. Furthermore, the PREVENT trial highlighted the impracticality of large-scale screening for HRPs, as over half of the screened patients had no HRPs. This observation underscores the need for alternative strategies to *a priori* identify patients that are likely to harbour HRPs, for instance by assessing their clinical risk profile.

In the present study, none of the traditional clinical risk factors were independently associated with the presence of at least one non-flow-limiting, HRP. Similarly, in a retrospective OCT study, diabetes and metabolic syndrome were not significantly associated with plaque vulnerability.[12] Consistent with our findings, poor discriminative value of clinical risk factors for the identification of HRPs was also observed in a secondary analysis from the prospective observational PROSPECT study, in which three-vessel intravascular ultrasound was used for the identification of HRPs. Although the Framingham risk score was significantly associated with the presence of at least one HRP in that study, the AUC of only 0.55 indicated very limited discriminative power.[13] Likewise, the TRS-2P had no discriminative value (AUC 0.51) in that regard in the present analysis. These results emphasise the complexity in the development and progression of coronary atherosclerosis that extends beyond traditional risk factors[14] and illustrate that risk factors are insufficient to improve patient selection for targeted screening. Other potential strategies that could be explored to increase the likelihood of finding an HRP include a stepwise approach with non-invasive imaging as a gatekeeper,[15] evaluation of circulating inflammatory markers or lipid spectrum analyses, or the incorporation of haemodynamic measures.[16] In regard to the former, coronary computed tomography angiography is increasingly adopted as a first-line diagnostic in patients with suspected coronary artery disease. Although recent evidence demonstrates a significant relationship between computed tomography-identified and OCT-identified HRPs, the correlation was modest.[15] Whether newer-generation photon-counting detector computed tomography has superior discriminative value is unknown.

Nevertheless, a number of procedural variables related to more extensive (multivessel) coronary artery disease were associated with the presence of an HRP, including percutaneous coronary intervention during the index procedure and a larger number of FFR-negative target lesions. Additionally, HRPs were more likely in the presence of a target lesion in the right coronary artery. This observation is potentially related to the fact that HRPs are found throughout the right coronary artery, while they have a more clustered distribution in the proximal segments of the left anterior descending and left circumflex arteries.[17]

Clinical impact of high-risk plaques across risk profiles

In the present analysis, the prognostic impact of HRPs was independent of the baseline clinical risk profile. These results indicate that intensive medical therapy for plaque stabilisation and prevention of patient-level events may be beneficial across the clinical risk spectrum. A consistent hazard among lower-risk patients is in line with earlier evidence demonstrating that plaque progression and new development of HRP phenotypes is not limited to high-risk patients.[18] In fact, the presence of HRPs is associated with increased plaque progression and statin non-response, independently of clinical risk factors.[19]

Nevertheless, while patients with a low-risk clinical profile and without an HRP were at the lowest risk for TLF (0.94 events per 100 lesion-years), patients with a high-risk clinical profile and an HRP were at the highest risk (6.28 events per 100 lesion-years). These findings translate into higher positive predictive values among high-risk patients and, thus, a lower number of patients required to be screened and preventively treated focally to prevent one event. Assuming an 88% relative risk reduction following pre-emptive treatment of HRPs,[5] the number needed to treat to prevent one TLF event per 100 lesion-years would be 18.1 in high-risk patients, compared to 28.7 in lower-risk patients. Regarding the 2-year follow-up data, the number needed to stent in patients with a high-risk clinical profile in combination with an HRP would only be 8.4. Given the relatively low number needed to treat, restricting preventive focal treatment to these very high-risk patients could be considered. However, the benefit of pre-emptive treatment remains to be established from ongoing, dedicated clinical trials. The ultimate clinical value of such a strategy will be dependent on the absolute magnitude of the effect achieved, which may, in turn, be dependent on the characteristics of the studied population, and the balance between risk and benefit.

If the clinical risk score without OCT were used to indicate pre-emptive treatment, the number needed to treat among high-risk patients would be 50.4 per 100 lesion-years, assuming neither benefit nor harm of pre-emptive treatment among patients without an HRP. As such, this study highlights the independent value of intracoronary OCT for prognostication in the studied population of patients with myocardial infarction and/or diabetes.

Limitations

This study should be interpreted in view of its limitations. The analyses described were not prespecified in either of the included studies, and the results therefore remain exploratory. Therefore, no definitive or causal conclusions can be drawn from this study. Second, the TRS-2P was originally designed as a clinical risk score for secondary prevention after myocardial infarction. However, 40% of patients in the present population had not presented with myocardial infarction. Nevertheless, the TRS-2P had comparable prognostic implications in patients with chronic coronary syndrome and unstable angina in a long-term validation study.[20] Furthermore, we used a modified version of the TRS-2P to account for missing variables and imputed values for three indicators. However, considering that the TRS-2P has a graded association with adverse clinical outcomes, we hypothesise that leaving out those two indicators has not profoundly impacted our results. Nevertheless, bias related to these adaptations and data imputation cannot be completely ruled out, and the findings therefore remain hypothesis-generating. The absence of other

variables precluded the evaluation of other risk scores, including those specifically designed for patients with chronic coronary syndrome. Third, the duration of follow-up was shorter than the 10-year follow-up period for which the TRS-2P was validated and differed between studies. Finally, the results only apply to patients with diabetes or myocardial infarction. The absolute risk difference in a lower-risk population may be negligible. Additionally, these inclusion criteria may have influenced the analyses. In particular, all patients from COMBINE (OCT-FFR) already had one indicator (i.e., diabetes), and they were therefore less likely to be classified as low risk. However, this is in line with the general population, as patients with diabetes frequently exhibit multiple other risk factors. For instance, in a real-world evaluation of the TRS-2P, less than 5% of diabetic patients had no other indicator.[20] Importantly, correction for this potential confounding factor was applied by incorporating the study of origin as a fixed parameter in the analyses.

CONCLUSIONS

The modified TRS-2P has no discriminative value for the identification of patients with HRPs in non-flow-limiting deferred lesions. Furthermore, HRPs in such lesions are associated with adverse patient- and lesion-level clinical outcomes, without apparent differences between clinical risk profiles. This highlights the independent value of OCT for prognostication beyond traditional risk factors in patients at risk for recurrent events. Nevertheless, combining clinical risk scores with HRP detection allows identification of patients at greatest risk for adverse outcomes.

REFERENCES

1. Burke AP, Farb A, Malcom GT, Liang YH, Smialek J, Virmani R. Coronary risk factors and plaque morphology in men with coronary disease who died suddenly. N Engl J Med 1997;336:1276-82.
2. Gallone G, Bellettini M, Gatti M, Tore D, Bruno F, Scudeler L et al. Coronary Plaque Characteristics Associated With Major Adverse Cardiovascular Events in Atherosclerotic Patients and Lesions: A Systematic Review and Meta-Analysis. JACC Cardiovasc Imaging 2023;16:1584-1604.
3. Kedhi E, Berta B, Roleder T, Hermanides RS, Fabris E, AJJ IJ et al. Thin-cap fibroatheroma predicts clinical events in diabetic patients with normal fractional flow reserve: the COMBINE OCT-FFR trial. Eur Heart J 2021;42:4671-4679.
4. Mol JQ, Volleberg R, Belkacemi A, Hermanides RS, Meuwissen M, Protopopov AV et al. Fractional Flow Reserve-Negative High-Risk Plaques and Clinical Outcomes After Myocardial Infarction. JAMA Cardiol 2023;8:1013-1021.
5. Park SJ, Ahn JM, Kang DY, Yun SC, Ahn YK, Kim WJ et al. Preventive percutaneous coronary intervention versus optimal medical therapy alone for the treatment of vulnerable atherosclerotic coronary plaques (PREVENT): a multicentre, open-label, randomised controlled trial. Lancet 2024;403:1753-1765.
6. Volleberg R, Rroku A, Mol JQ, Hermanides RS, van Leeuwen M, Berta B et al. FFR-Negative Nonculprit High-Risk Plaques and Clinical Outcomes in High-Risk Populations: An Individual Patient-Data Pooled Analysis From COMBINE (OCT-FFR) and PECTUS-obs. Circ Cardiovasc Interv 2025;18:e014667.
7. Kennedy MW, Fabris E, Ijsselmuiden AJ, Nef H, Reith S, Escaned J et al. Combined optical coherence tomography morphologic and fractional flow reserve hemodynamic assessment of non- culprit lesions to better predict adverse event outcomes in diabetes mellitus patients: COMBINE (OCT-FFR) prospective study. Rationale and design. Cardiovasc Diabetol 2016;15:144.
8. Mol JQ, Belkacemi A, Volleberg RH, Meuwissen M, Protopopov AV, Laanmets P et al. Identification of anatomic risk factors for acute coronary events by optical coherence tomography in patients with myocardial infarction and residual nonflow limiting lesions: rationale and design of the PECTUS-obs study. BMJ Open 2021;11:e048994.
9. Bohula EA, Bonaca MP, Braunwald E, Aylward PE, Corbalan R, De Ferrari GM et al. Atherothrombotic Risk Stratification and the Efficacy and Safety of Vorapaxar in Patients With Stable Ischemic Heart Disease and Previous Myocardial Infarction. Circulation 2016;134:304-13.
10. Inker LA, Eneanya ND, Coresh J, Tighiouart H, Wang D, Sang Y et al. New Creatinine- and Cystatin C-Based Equations to Estimate GFR without Race. N Engl J Med 2021;385:1737-1749.
11. Araki M, Park SJ, Dauerman HL, Uemura S, Kim JS, Di Mario C et al. Optical coherence tomography in coronary atherosclerosis assessment and intervention. Nat Rev Cardiol 2022;19:684-703.
12. Yonetsu T, Kato K, Uemura S, Kim BK, Jang Y, Kang SJ et al. Features of coronary plaque in patients with metabolic syndrome and diabetes mellitus assessed by 3-vessel optical coherence tomography. Circ Cardiovasc Imaging 2013;6:665-73.
13. Bourantas CV, Garcia-Garcia HM, Farooq V, Maehara A, Xu K, Genereux P et al. Clinical and angiographic characteristics of patients likely to have vulnerable plaques: analysis from the PROSPECT study. JACC Cardiovasc Imaging 2013;6:1263-72.
14. Libby P. The changing landscape of atherosclerosis. Nature 2021;592:524-533.
15. Kinoshita D, Suzuki K, Usui E, Hada M, Yuki H, Niida T et al. High-Risk Plaques on Coronary Computed Tomography Angiography: Correlation With Optical Coherence Tomography. JACC Cardiovasc Imaging 2024;17:382-391.
16. Sakai K, Mizukami T, Leipsic J, Belmonte M, Sonck J, Norgaard BL et al. Coronary Atherosclerosis Phenotypes in Focal and Diffuse Disease. JACC Cardiovasc Imaging 2023;16:1452-1464.

17. Araki M, Soeda T, Kim HO, Thondapu V, Russo M, Kurihara O et al. Spatial Distribution of Vulnerable Plaques: Comprehensive In Vivo Coronary Plaque Mapping. JACC Cardiovasc Imaging 2020;13:1989-1999.

18. Han D, Berman DS, Miller RJH, Andreini D, Budoff MJ, Cademartiri F et al. Association of Cardiovascular Disease Risk Factor Burden With Progression of Coronary Atherosclerosis Assessed by Serial Coronary Computed Tomographic Angiography. JAMA Netw Open 2020;3:e2011444.

19. van Rosendael SE, van den Hoogen IJ, Lin FY, Andreini D, Al-Mallah MH, Budoff MJ et al. Clinical and Coronary Plaque Predictors of Atherosclerotic Nonresponse to Statin Therapy. JACC Cardiovasc Imaging 2023;16:495-504.

20. Zafrir B, Adawi S, Khalaily M, Jaffe R, Eitan A, Barnett-Griness O et al. Long-Term Risk Stratification of Patients Undergoing Coronary Angiography According to the Thrombolysis in Myocardial Infarction Risk Score for Secondary Prevention. J Am Heart Assoc 2019;8:e012433.

SUPPLEMENTAL MATERIAL

Supplemental material related to this article can be found in the online version: https://eurointervention.pcronline.com/article/impact-of-clinical-risk-characteristics-on-the-prognostic-value-of-high-risk-plaques



PART III

ARTIFICIAL INTELLIGENCE-BASED IMAGE INTERPRETATION



CHAPTER 12

Roadmap on the use of artificial intelligence for imaging of vulnerable atherosclerotic plaque in coronary arteries

Bernhard Föllmer* | Michelle Williams* | Damini Dey | Armin Arbab-Zadeh | Pál Maurovich-Horvat | Rick Volleberg | Daniel Rueckert | Julia Schnabel | David Newby | Marc Dweck | Giulio Guagliumi | Volkmar Falk | Aldo Vázquez Mézquita | Federico Biavati | Ivana Išgum† | Marc Dewey†

Nature Reviews Cardiology
2024 Jan;21(1):51-64

** joined first authorship*
† joined senior authorship

ABSTRACT

Artificial intelligence (AI) is likely to revolutionize the way medical images are analysed and has the potential to improve the identification and analysis of vulnerable or high-risk atherosclerotic plaques in coronary arteries, leading to advances in the treatment of coronary artery disease. However, coronary plaque analysis is challenging owing to cardiac and respiratory motion, as well as the small size of cardiovascular structures. Moreover, the analysis of coronary imaging data is time-consuming, can be performed only by clinicians with dedicated cardiovascular imaging training, and is subject to considerable interreader and intrareader variability. AI has the potential to improve the assessment of images of vulnerable plaque in coronary arteries, but requires robust development, testing and validation. Combining human expertise with AI might facilitate the reliable and valid interpretation of images obtained using CT, MRI, PET, intravascular ultrasonography and optical coherence tomography. In this Roadmap, we review existing evidence on the application of AI to the imaging of vulnerable plaque in coronary arteries and provide consensus recommendations developed by an interdisciplinary group of experts on AI and non-invasive and invasive coronary imaging. We also outline future requirements of AI technology to address bias, uncertainty, explainability and generalizability, which are all essential for the acceptance of AI and its clinical utility in handling the anticipated growing volume of coronary imaging procedures.

INTRODUCTION

Initially perceived with scepticism, artificial intelligence (AI; Fig. 1) is now a part of our everyday lives. A case in point is AI-based, automated speech and facial recognition, which was believed not to be possible in the 1960s, but is now available on many smartphones.[1] In the past decade, AI-based methods have been increasingly used in cardiovascular medicine, especially in cardiovascular imaging.[2-5] The majority of these AI methods have been developed for the diagnosis, risk stratification and prognostic assessment of patients with coronary artery disease, heart failure or rhythm disorders.[6] The evidence on the prognostic implications of a vulnerable atherosclerotic plaque in coronary arteries, which is considered to precede acute coronary events through plaque rupture and subsequent thrombosis,[7] has become more robust in the past 10 years.[8-10] Accurate non-invasive or invasive imaging approaches that can identify patients at high risk of adverse events might help to guide focal strategies or intensified medical treatment. However, visual and especially quantitative coronary plaque detection and characterization are time-consuming, require a high level of expertise, and have substantial intraobserver and interobserver variability.[11,12]

Among non-invasive imaging modalities, coronary CT angiography (CCTA) is the best for visualizing coronary arteries and atherosclerotic plaques.[13] AI technologies have also been implemented in the analysis of images derived from invasive intravascular ultrasonography (IVUS) or optical coherence tomography (OCT).[13] Research that initially focused on (semi-)automated lumen detection for stenosis grading[14] has now moved on to the promising field of automated plaque characterization.[15,16]

In this Roadmap, we review the existing evidence on and provide interdisciplinary consensus recommendations for the application of AI to the imaging of atherosclerotic plaque in coronary arteries, focusing on the most advanced imaging modalities in this field (CCTA, IVUS and OCT[13]). In addition, we discuss the current and future approaches to addressing bias, explainability, uncertainty and generalizability of AI-guided imaging of coronary plaque. Consensus was reached using a Delphi methodology similar to that used to reach a consensus on myocardial ischaemia imaging at the first Quantitative Cardiovascular Imaging (QCI) meeting.[17] Detailed clinical consensus recommendations on the preferred use of each imaging technique for coronary plaque and stenosis imaging in specific patient populations are provided in a Consensus Statement derived from the second QCI meeting.[13]

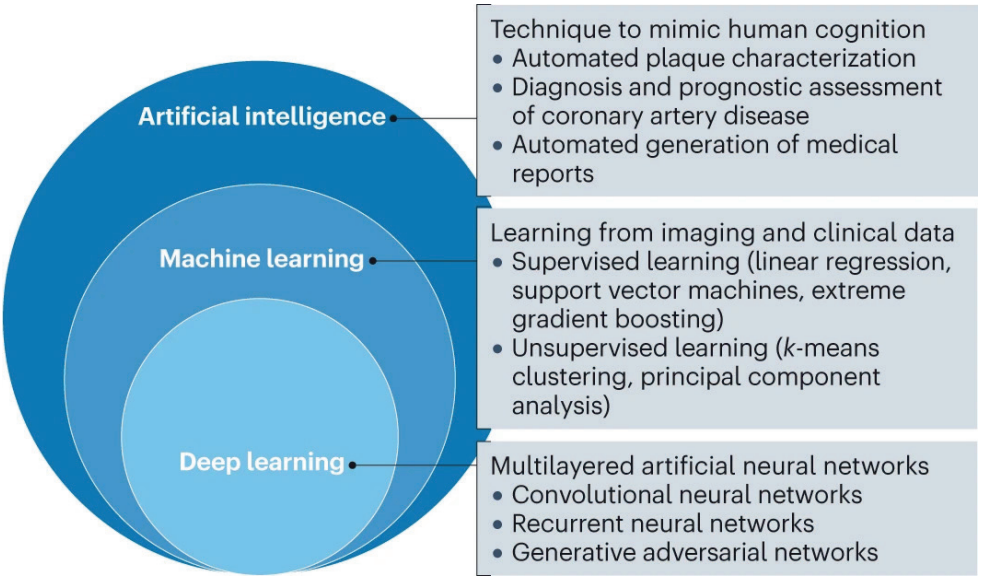


Figure 1. Basics of artificial intelligence, machine learning and deep learning.

Artificial intelligence in medicine mimics the intelligence of a human in performing various medical tasks. Machine learning is a subfield of artificial intelligence with a focus on how computers learn from examples. Deep learning is a specific form of machine learning involving an algorithm that learns directly from data.[48]

METHODOLOGY FOR CONSENSUS RECOMMENDATIONS

The application of AI to cardiovascular imaging has received increasing interest over the past 10 years.[18] However, many technical and clinical aspects of its application to the imaging of vulnerable plaques in coronary arteries require additional attention to ensure reliability and to improve the prognostic and diagnostic value of different cardiovascular imaging modalities before widespread clinical use. During the second QCI meeting on coronary artery stenosis and atherosclerosis imaging in September 2022, a questionnaire regarding the clinical appropriateness of different imaging modalities was conducted using a three-round Delphi method. This Roadmap describes the findings that have emerged using this multidisciplinary approach and encompasses the views of clinicians (cardiologists, radiologists and a cardiac surgeon), biomedical engineers and computer scientists using a similar method to that used for the first QCI meeting.[17] The questionnaire included eight questions on AI for coronary imaging, and no consensus was noted after the third and final round of questions (Supplementary Table 1), which led to a second Delphi process with two additional rounds needed to reach a consensus.[19,20] The questions were sent to 14 scientists and physicians directly involved in the research and development of AI tools for cardiovascular imaging. A total of 15 questions (Supplementary Table 2) were answered using a Likert scale from 1 to 9, categorical replies or free text. The reasoning for each answer was provided

as text. Before beginning the second round, the overall results from the first round were sent to the participants. The questions answered using a Likert scale were presented as a median and interquartile range, the categorical replies were presented as percentages, and the relevant or conflicting replies in the text were highlighted. The final results of the Delphi voting are summarized in Table 1, with a level of consensus between experts indicated as no consensus, partial consensus or consensus. The level of consensus for answers in the form of the Likert scale or ordinal scale was defined using previously proposed parameters (<0.6 indicated no consensus, 0.6–0.8 indicated partial consensus and ≥0.8 indicated consensus).[21] For answers on ordinal scales and related to multiple modalities, the measure of agreement was averaged across all modalities. For answers on a nominal scale, consensus was measured using normalized entropy with the same thresholds.

Table 1. Consensus recommendations on AI applied to imaging of vulnerable plaques in coronary arteries.

Question	Level of consensus[a]	Consensus recommendations
Current state of AI for analysis of plaques in coronary arteries		
Q1: reference standard for plaque imaging	Consensus	Histology would be preferable but clinically impractical; IVUS and OCT are superior to CT with regard to resolution but availability is limited; OCT is more precise than IVUS and can detect high-risk plaque features associated with plaque progression
Q2a: importance of multiple observers	Partial consensus	Multiple observers are essential to compensate for interobserver variability, provide generalizability and help with uncertainty estimation
Q2b: required level of expertise for annotation of plaques	Partial consensus	The number of analysed scans and years of experience should both be considered; the number of expected analysed scans varied from 100 to >1,000; the number of years of experience ranged from 24 weeks to 5 years; and certifications of cardiovascular CT experience (such as SCCT level III) might be sufficient
Q3: availability of AI tools for automated plaque analysis in academic research	Partial consensus	AI tools exist for all modalities, with more tools available for CT; however, access to research tools is limited
Q4: availability of FDA-approved or CE-approved AI tools for automated plaque analysis in clinical practice	No consensus	Large discrepancies in the definition of AI tools led to discordance between experts; the technologies used (such as simple thresholding or deep learning) are mostly hidden from the user, making it difficult to define AI tools
Current challenges with AI in automated plaque analysis and prognosis		
Q5: quality level of current automated vessel wall and lumen segmentation for coronary plaque analysis	Consensus	No standardization on how to quantify plaque burden is available at present; most of the available tools are challenged by the presence of artefacts and severe calcifications; CT is limited in the case of heavy calcification; data interpretation is subjective with a paucity of quantification, and segmentations are sparse and noisy; and OCT is more advanced than IVUS in AI segmentation, especially in the case of insufficient image quality (such as blood artefacts)
Q6: susceptibility of AI tools for plaque analysis to image artefacts	Partial consensus	Current AI tools are highly susceptible to image artefacts and most AI tools do not account for them

Table 1. Continued

Q7: technology suited for classification of coronary plaques into stable and vulnerable plaques	Partial consensus	A combination of radiomics and deep learning provides incremental utility compared with either method alone; deep learning might be superior to radiomics, but requires more data, which are not currently available
Trustworthy AI		
Q8: mandatory visual confirmation of automated segmentation of plaques	Consensus	Visual confirmation is required until full confidence is achieved; physicians need to be able to modify or correct coronary segmentations
Q9: requirement for randomized controlled trials	No consensus	Randomized controlled trials are required to verify clinical effectiveness and test advantages over standard care, whereas retrospective studies are sufficient if AI tools only facilitate simple human tasks (such as image segmentation)
Q10: confidence measure to explain uncertainty	Partial consensus	Well-calibrated and reliable quantitative measures are required (such as with 95% confidence interval); visual methods (such as heatmaps) are required to ensure clarity in interpretation; and low confidence should alert physicians that further testing might be required
Q11: bias mitigation	Partial consensus	AI tools should be developed and tested on large and diverse populations to ensure their generalizability; the limitations of AI tools with respect to non-representative populations should be clearly demonstrated; biases should be evaluated and quantified; and bias in datasets should be mitigated by adding or upweighting minority samples when possible
Outlook and future directions		
Q12: reading time of an imaging test in clinical practice	Consensus	Images are quickly screened in clinical practice (5–10 min) without measuring plaque features, whereas detailed plaque analysis can take >1 h; reading time highly depends on the complexity of the case
Q13: AI-supported time savings	Consensus	Quantitative plaque assessment is not performed regularly in current clinical practice; AI tools could provide full quantification without changing reading time; and higher accuracy and reproducibility are important advantages in addition to time savings
Q14: on-site or cloud-based plaque analysis	Consensus	Issues of data protection and data privacy preservation must be addressed before cloud-based solutions can be used; OCT and IVUS require immediate assessment (real-time systems) to guide decision-making
Q15: automated generation of structured medical reports	Consensus	Structured reports should provide treatment recommendations together with explanations and should include a breakdown of findings (plaque burden and subtypes) and quantitative measurements with a summary; the ability to add user-defined free text is also required

AI artificial intelligence; IVUS intravascular ultrasonography; OCT optical coherence tomography; SCCT Society of Cardiovascular Computed Tomography.

[a] The level of consensus between experts is graded as no consensus, partial consensus or consensus.

The full questionnaire with individual responses is shown in Supplementary Table 2.

THE CONCEPT OF VULNERABLE PLAQUE IMAGING

In most patients, acute coronary syndrome is triggered by the rupture or erosion of coronary atherosclerotic plaques.[22] These plaques have specific features, such as a large necrotic core and a thin fibrous cap, known as a thin-cap fibroatheroma (TCFA). The identification of these features, which can be visualized using imaging modalities, led to the concept of the vulnerable plaque that is prone to rupture (Fig. 2). Many clinical studies using invasive and non-invasive techniques have found an association between vulnerable plaques and adverse outcomes in patients.[13,23] However, findings from both pathology and clinical imaging studies have also consistently shown that the rupture of these vulnerable plaques often occurs without clinical syndromes, representing an integral part of plaque progression.[24] Furthermore, although stenting of lesions with vulnerable plaque features is safe,[25] there is currently a paucity of data supporting focal treatment of vulnerable plaques. Therefore, the concept of the vulnerable plaque remains controversial.[13,23] The clinical implications of quantitative non-invasive and invasive imaging of vulnerable plaques in coronary arteries have also been described in a consensus statement derived from findings from the second QCI meeting on clinical quantitative coronary artery stenosis and coronary atherosclerosis imaging.[13] Further characterization of coronary atherosclerosis using AI might result in the identification of additional features associated with rapid plaque progression and increased risk of adverse events.

Imaging modalities

Coronary atherosclerotic plaque can be assessed by a range of invasive and non-invasive imaging modalities.[13] CT and MRI facilitate non-invasive structural imaging of coronary plaque, whereas X-ray coronary angiography, IVUS, OCT and near-infrared spectroscopy (NIRS) are invasive imaging techniques that can be used to assess coronary artery morphology. Although OCT and IVUS are superior to CT in terms of resolution, these invasive modalities are not widely available.[13] Beyond anatomical imaging, coronary plaque biology can be assessed non-invasively through the use of appropriately targeted radiotracers. Only PET, which again is not widely available, allows the assessment of coronary atherosclerotic plaque biology via radiotracer uptake.[26]

Non-invasive plaque imaging. CCTA is a non-invasive imaging modality that facilitates the identification of qualitative high-risk plaque features, such as the napkin-ring sign, and the quantification of total plaque burden using CCTA[27] correlates well with assessment by IVUS.[28,29] Moreover, the CCTA-derived measure of plaque attenuation can be used to determine plaque composition, including total, calcified, non-calcified or low attenuation plaque (Fig. 2). Low attenuation plaque is of particular interest because it correlates with the lipid-rich necrotic core of atheromatous plaques and has been associated with adverse outcomes.[8] Importantly, CT quantification of coronary atherosclerotic burden can be used to predict the risk of fatal or non-fatal myocardial infarction in patients with stable or unstable coronary artery disease.[8,27,30,31] Of note, however, CCTA is associated with exposure to a modest level of radiation, and image quality can be compromised by cardiac motion or coronary calcification.

Invasive plaque imaging. Coronary X-ray angiography is the most frequently used invasive modality for imaging the coronary arteries because it allows excellent visualization of the coronary lumen, but not of coronary plaque. Therefore, invasive assessment of coronary plaque requires intravascular imaging techniques such as IVUS, OCT and NIRS.[9,32] Specifically, plaque imaging using IVUS or OCT is instrumental for studying vulnerable plaque features,[33] and has been used to guide percutaneous coronary interventions[33,34] and to monitor vascular tissue response.[35,36] OCT is currently the only imaging modality with sufficient spatial resolution to identify the thin cap (<0.065 mm) that defines true TCFA. Of note, these invasive techniques cannot be used to assess severe stenotic disease, small-caliber vessels or deeper plaque structures. Of note, intracoronary imaging is expensive, can cause serious complications because of its invasive nature and is, therefore, impractical for population-wide application.

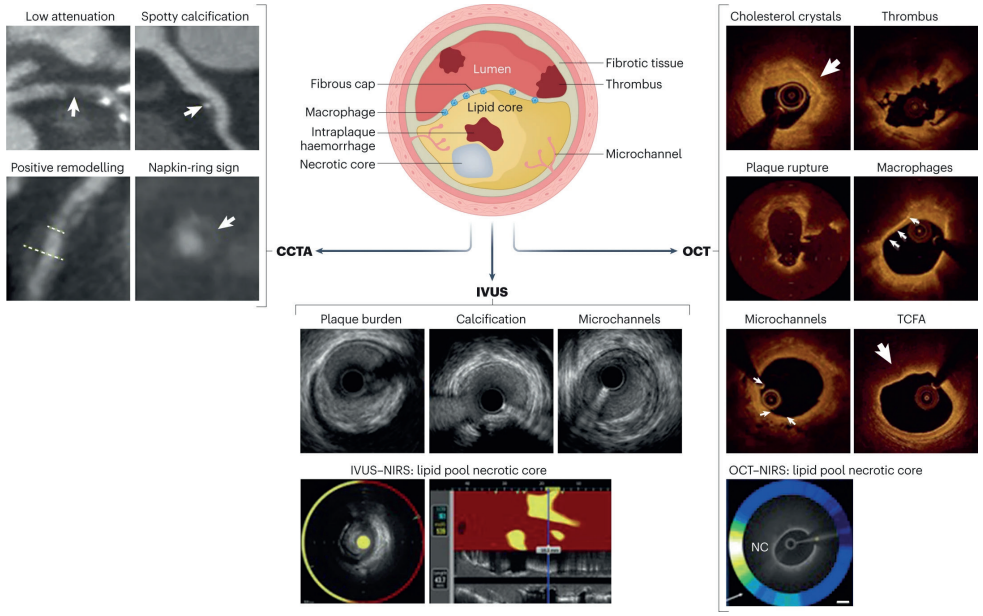


Figure 2. The concept of vulnerable plaques and high-risk plaque features in CCTA, IVUS and OCT images.

The figure provides an overview of vulnerable plaque components (lipid core, necrotic core and thin fibrous cap) and associated high-risk plaque features in coronary CT angiography (CCTA; the arrows point to low attenuation, spotty calcification and napkin-ring sign, whereas the dashed lines indicate positive remodeling), intravascular ultrasonography (IVUS; plaque burden, calcification and microchannels) and optical coherence tomography (OCT; the large arrow points to cholesterol crystals and thin-cap fibroatheroma (TCFA), whereas the small arrows indicate macrophages and microchannels.

CCTA coronary computed tomography angiography; IVUS intravascular ultrasound; NC necrotic core; NIRS near-infrared spectroscopy; OCT optical coherence tomography.

Prognostic value of identifying vulnerable plaques

The prognostic importance of coronary plaque assessment has been established using various non-invasive and invasive imaging modalities. TCFA, identified using IVUS or OCT, has been associated with worse outcomes in several prospective studies.[9,37-39] Vulnerable plaques that can be visually identified on CCTA have been linked to an increased risk of subsequent adverse cardiac events in registry studies[40] and in randomized controlled trials (RCTs).[8,31,41] In the PROMISE trial,[31] vulnerable plaques were present in 15% of patients presenting with suspected coronary artery disease and were associated with an almost twofold increase in major adverse cardiovascular events, after adjusting for cardiovascular risk factors. However, this study did not adjust for the overall disease burden. In addition, findings from studies that quantitatively assessed vulnerable plaques suggest that increased plaque volume and imaging markers of TCFA are associated with a higher risk of subsequent adverse cardiac events. In the PROSPECT study,[9] a plaque burden of ≥70% and a minimal lumen area of ≤4.0 mm^2, as measured on IVUS, were independently associated with disease progression and recurrent chest pain at follow-up in patients presenting with acute coronary syndrome. In the SCOT-HEART trial,[27] a low attenuation plaque burden on CCTA was a strong predictor of myocardial infarction, over and above the cardiovascular risk score, calcium score and presence of stenosis. Patients with a low attenuation plaque burden of >4% were nearly five times more likely to have a subsequent myocardial infarction event than patients who had a low attenuation plaque burden of ≤4%. Conversely, preliminary results from the ISCHEMIA trial[42] did not find low attenuation plaque to be predictive of death or myocardial infarction when adjusted for total plaque burden. Importantly, the positive predictive value of vulnerable plaque features is low, and it is not possible at present to predict which patients will have plaque progression that would ultimately cause major adverse cardiovascular events. Larger studies and the incorporation of AI technology will hopefully improve the assessment of vulnerable plaque in the future.[43,44] Aside from traditional high-risk plaque features, AI technology can support the automatic identification of additional high-risk plaque features that are not visible to the human eye to improve diagnosis and prognosis.

AI FOR VULNERABLE PLAQUE ASSESSMENT

AI is a branch of computer science that aims to mimic human cognition in performing tasks such as object or pattern recognition and has been applied to the field of medical imaging.[45] Machine learning, a subfield of AI, enables computer algorithms to automatically learn and improve from experience using supervised or unsupervised learning. Deep learning is a specific form of machine learning that uses multilayered artificial neural networks to make predictions directly from input (Fig. 1). Unlike traditional machine learning techniques, deep learning has emerged in the field of cardiovascular imaging only in the past 7 years,[46] but has already accelerated research on the assessment of vulnerable plaques and on prerequisite tasks such as lumen and plaque segmentation.[46,47] The most commonly used deep learning networks for image analysis are convolutional neural networks (CNNs). CNNs contain many layers, including one or more convolutional layers that create a feature map summarizing the

presence of detected features in the input. The most common implementation of CNNs allows image segmentation or image classification. Although the success of deep learning depends on the availability of large datasets, standard models, such as U-Net and convolutional Long Short-Term Memory networks, as well as specialized networks have been applied to vulnerable plaque segmentation.[47] In addition, radiomics is a technique involving the extraction of a large number of quantitative features (such as shape, texture and grey-level statistics) that are often not visible to the human eye to describe texture and spatial complexity. Machine learning methods are used to perform precision phenotyping and can build predictive models on the basis of radiomic patterns. Radiomics can be used to identify high-risk plaque features, characterize plaque vulnerability[48,49] and find associations that are predictive of an increased risk of major adverse cardiovascular events.[50]

AI technology allows the quantitative assessment of coronary plaque and the identification of adverse plaque characteristics in the coronary arteries. Automatically quantified biomarkers (Fig. 3) can improve diagnosis and facilitate patient-specific cardiovascular risk stratification.[27,51] Relevant studies that have assessed the prognostic value of vulnerable plaque and their level of automation using AI are listed in Supplementary Table 3.

Non-invasive assessment

CCTA is a first-line non-invasive test for assessing patients with suspected coronary artery disease.[52] Visual or semi-automatic analysis of CCTA focuses on grading stenosis severity and assessing basic plaque features. AI-based methods can automate not only these time-consuming and cumbersome quantification tasks, but also the characterization of coronary artery plaque and stenosis grading[46] (Fig. 3).

Automated coronary artery calcium scoring. Automated quantification of coronary artery calcification in non-contrast CT[53] and low-dose chest CT[54] shows excellent agreement with non-automated human quantification in terms of risk stratification. Automated quantification of coronary artery calcification identified on CCTA has good accuracy compared with non-automated quantification of the traditional Agatston scores derived from non-contrast CT.[55,56]

Centerline extraction. Methods that detect both calcified and non-calcified plaque and stenosis usually require the generation of a coronary artery centreline to facilitate analysis of the artery and its immediate vicinity.[46] Therefore, a number of automatic or semi-automatic methods have been developed for coronary artery tree extraction, plaque segmentation and stenosis grading using conventional machine learning or deep learning techniques.[46,48,57]

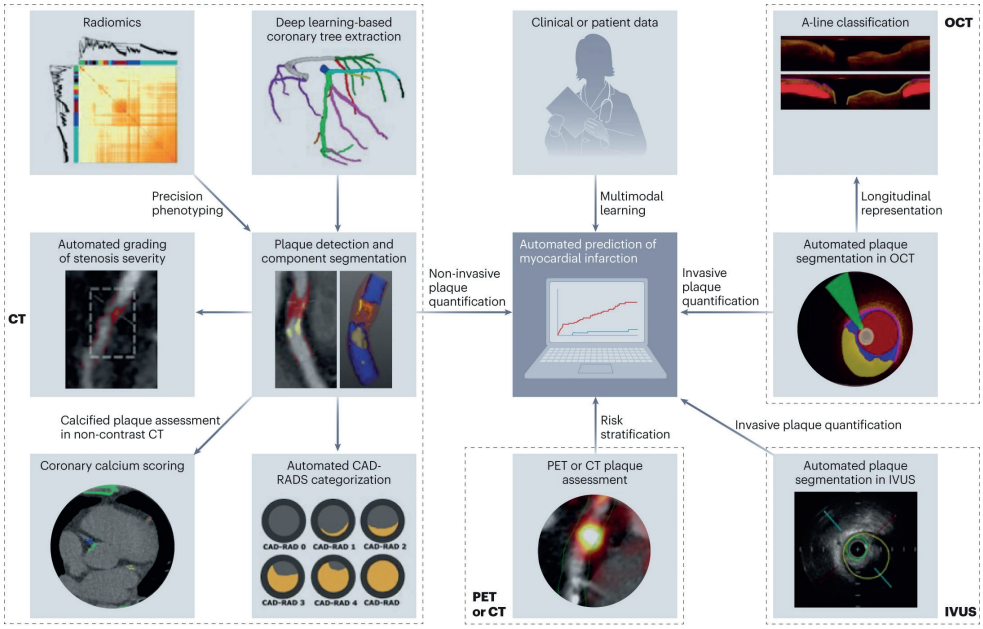


Figure 3. The interaction between tasks supported by AI tools for the assessment of vulnerable plaques in coronary arteries.

The figure summarizes the tools for the assessment of vulnerable plaques supported by artificial intelligence (AI) in CT, intravascular ultrasonography (IVUS) and optical coherence tomography (OCT). AI-supported tasks include segmentation (coronary tree extraction, calcium soring and plaque segmentation), feature extraction (radiomics, PET or CT plaque assessment and stenosis grading, classification tasks (Coronary Artery Disease Reporting and Data System (CAD-RADS) categorization(120) and multimodal learning), risk stratification and prediction of major adverse cardiovascular events.

CT computed tomography; IVUS intravascular ultrasound; OCT optical coherence tomography; PET positron emission tomography.

Identification of vulnerable plaque characteristics. Aside from quantifying plaque burden, AI-based methods have also been used to identify vulnerable plaque characteristics, such as positive remodeling, low attenuation plaque, spotty calcification and the napkin-ring sign.[48,58]

Radiomics can extract a large number of quantitative features, most of which are invisible to the human eye, from medical images (Fig. 3). These features capture the complex spatial relationships between voxels by describing textural patterns or geometric properties within a given imaging region of interest, such as a segmented coronary plaque. CCTA-based radiomics have been used to improve the identification of the napkin-ring sign[58] and other vulnerable plaque characteristics.[59] In this context, machine learning techniques have resulted in the identification of imaging biomarkers associated with culprit lesions in acute coronary syndrome.[60]

Multimodal plaque assessment. In cardiovascular imaging, AI algorithms can be used both to quantify new imaging biomarkers and to integrate data from many different sources for comprehensive, patient-tailored risk prediction (Fig. 3). For example, in a machine learning analysis of findings from a multicentre prospective registry, the combination of patient, clinical and plaque characteristics using an iterative LogitBoost algorithm was found to predict 5-year all-cause mortality more accurately than using existing clinical or CCTA metrics alone.[53] Another study combined qualitative and quantitative plaque features in XGBoost models to identify precursors of culprit lesions in patients with acute coronary syndrome; this boosted ensemble algorithm outperformed the use of traditional metrics of diameter stenosis, CCTA-related high-risk plaque features and lesion-level characteristics in the detection of culprit lesions.[61] Furthermore, several studies have used machine learning to combine plaque characteristics, including size, geometry and density, to identify myocardial ischaemia.[62-65] Investigators in a multicentre trial involving 254 patients combined clinical data with quantitative and qualitative plaque characteristics using a LogitBoost algorithm to detect lesion-specific ischaemia that was defined by invasive fractional flow reserve.[66] This approach predicted the presence of lesion-specific ischaemia (area under the receiver operating characteristic curve (AUC) 0.84) more accurately than parameters such as quantitative stenosis (AUC 0.76), total plaque volume (AUC 0.74) and pre-test likelihood of coronary artery disease (AUC 0.63), highlighting the usefulness of analysing detailed plaque characteristics.

AI has been used to improve cardiovascular risk prediction by integrating complex clinical data with multimodality coronary plaque data.[67] One study showed that machine learning by extreme gradient boosting using clinical data, quantitative CCTA plaque analysis and measures of coronary plaque activity from ^{18}F-sodium fluoride (^{18}F-NaF) PET could predict adverse clinical outcomes in patients with established coronary artery disease.[68] The investigators demonstrated that the AI model that best predicted myocardial infarction (AUC 0.85) combined clinical data with both quantitative measures of anatomical coronary plaque from CCTA and coronary disease activity from ^{18}F-NaF PET.[68]

Investigators in an international multicentre study involving 921 patients undergoing CCTA developed and validated a deep learning system for CCTA-derived measures of plaque volume and stenosis severity.[47] The deep learning convolutional network was trained to segment plaques in all patients and then validated in a test set involving >200 patients, including 50 patients undergoing coronary IVUS within 1 month of CCTA. The deep learning system completed plaque analysis in less time than expert readers (5.7 s versus 25.7 min), with good or excellent agreement between the two sets of measurements.[47] There was also excellent agreement between the deep learning-derived measurements and the expert-derived measurements with regard to IVUS for total plaque volume and minimal luminal area, as well as in the assignment of patients to categories of stenosis severity.[69] The investigators further validated the capacity of deep learning-based plaque quantification to predict cardiovascular outcomes in another external cohort of 1,611 patients from the SCOT-HEART trial.[47] A deep learning-based total plaque volume of ≥238 mm^3 was associated with a fivefold higher risk of myocardial infarction, adding prognostic value to the presence of obstructive stenosis and the clinical risk score.

Invasive assessment

Manual expert quantification of plaque burden and vulnerable plaque characteristics (Fig. 2), such as measuring lipid arcs and minimal fibrous cap thickness in images derived from OCT and IVUS, is very time-consuming and requires real-time decision-making (Table 1). The use of AI technology can improve the efficiency and accuracy of these processes.

Automatic segmentation in OCT. To date, automation of the quantification and characterization of atherosclerotic plaque is mostly restricted to automatic segmentation. Deep learning approaches allow accurate and very fast segmentation in a matter of milliseconds.[15] These technologies relieve human experts of repetitive tasks and allow real-time analysis, which is crucial in intravascular imaging. Moreover, experts have an opportunity to understand what segmentation the AI model has performed, which improves trust and user acceptance (Table 1).

A-line-based classification. For A-line-based classification,[70-72] the cross-sectional view is rearranged longitudinally and plaques are subsequently classified circumferentially on each A-line. These algorithms use the natural direction of light emitted by the OCT catheter and are independent of the indeterminable external elastic membrane resulting from complete light attenuation in lipid plaques (Fig. 2). This technique also allows fibrous cap detection and quantification after manual adjustment in 5.5% of frames.[73]

Pixel-based deep learning. Conversely, pixel-based deep learning algorithms allow the segmentation of individual plaque components on cross-sectional views and can incorporate 3D spatial information, which is fundamental for intravascular image analysis. Investigators have developed a U-shaped neural network that automatically segments a single OCT frame in 0.07 ± 0.01 s with a mean Dice similarity coefficient of 0.764, which had lower accuracy for high-risk plaque components (such as macrophage accumulation) than for plaque segmentation.[15] In this study, the overall diagnostic accuracy for region segmentation and characterization of the external validation cohort was 86.6%.[15] A pixel-based approach using CNNs developed by another group of investigators resulted in sensitivities and specificities of >85% for the identification of lipid and calcified plaques.[74] Classification can also be performed in a binary per-frame fashion (for example, for TCFA identification).[75,76] In a study that assessed the utility of a DenseNet model to classify frames with OCT-derived TCFA, the deep learning algorithm accurately detected an OCT-derived TCFA with high reproducibility in their internal validation set of almost 10,000 frames (AUC 0.96).[75] However, the percentage of false-positive classifications was 6% at the frame level and 31% at the vessel level. The time required to analyse a pullback was only 2.1 ± 0.3 s compared with 289 ± 270 s for manual assessment. Interestingly, the results of histology-based training in addition to OCT-based training were found to be superior to OCT-based training only.[77]

Automated segmentation in IVUS. Image-based approaches in IVUS are limited by low spatial resolution. Consequently, most algorithms use binary per-frame or circumferential plaque segmentation.[16,78] Deep

learning-based plaque analysis with feature extraction has led to promising results for the identification of TCFA (AUC 0.84–0.91), with OCT as the gold standard.[78] Furthermore, in another study, the Dice similarity coefficients for the identification of calcified plaque and attenuation were 0.79 and 0.74 at the angle-level, respectively, after degree-wise learning.[16]

Availability of AI tools

Although numerous AI methods for the assessment of coronary artery plaques have been developed and used in research, they are not widely available for clinical use (Table 2). Published scientific papers often do not provided access to the source code, data or trained models in public repositories, which prevents reproducibility analysis. The QCI expert group reached a partial consensus on the current state of the availability of AI tools for plaque assessment in academic research. However, the underlying technologies in a commercial product might not be accessible to the user, leading to the discordance about their availability in clinical practice. Furthermore, most applications have not overcome the technical and regulatory challenges of full automation, and require human intervention.[79,80]

To identify relevant research tools and the CE-certified and FDA-certified products for coronary plaque assessment, we analysed AI-enabled and machine learning-enabled medical device databases[81-86] (Table 2). Automated calcium scoring analysis in electrocardiogram (ECG)-synchronized or non-ECG-synchronized CT has been established in numerous cardiovascular imaging software products. Several products focus on plaque assessment in CCTA and numerous research tools that have been evaluated in clinical studies[44,87] are gradually being implemented in clinical practice. Most of the available software packages contain tools for the automatic segmentation of tissue types and anatomical structures, such as the vessel wall and the lumen. However, depending on image quality and the presence of anatomical variants, manual correction, such as centreline correction or vessel wall adjustment and lumen or plaque segmentation, is often still required for quality assurance, calling into question the time savings and cost efficiency of AI-based tools.

Similarly, commercially available CE-certified and FDA-certified products for plaque analysis in intravascular modalities are emerging. The latest OCT software packages incorporate lumen, stent, external elastic membrane and calcium detection, and some even include AI-based plaque assessment.[15] However, AI-based plaque assessment is currently available for research purposes.

Challenges with AI tools in clinical practice

AI is an emerging technology in cardiovascular imaging, and the future benefits of AI in vulnerable plaque imaging are difficult to predict.[80] Importantly, high expectations should not obscure the challenges that still have to be overcome before AI becomes a standard tool in clinical practice. A major challenge for the development of clinical AI tools is the availability of large, diverse, anonymized and annotated datasets with available outcome data for testing, training and validation. The collection, curation and annotation of large sets of images required for AI development are very time-consuming (Table 1). The quality of the annotations is also an important concern, and the expertise required for annotation will depend on the task in question. In addition, AI tools must be tested on external validation datasets with clinical

outcomes to ensure their generalizability to wider populations. Poor image quality can also cause difficulties for AI development and use. Many AI tools are trained on curated and annotated datasets with high image quality and, therefore, under-perform in real-world clinical practice. In addition, image artefacts and variation in image acquisition might preclude the use of AI tools or result in inaccurate or unreliable output (Table 1). Standardization of image acquisition would aid AI development, including consistent naming, conformity in the reconstruction of algorithms and structured reporting.

For clinical use, an AI-based tool must provide results in a way that clinicians will understand and trust. Machine learning models might generate a probability of a result, but this outcome is not usually communicated by the AI tools. Methods to improve interpretability — so-called explainable AI — include dedicated models, *post hoc* assessments, feature importance and graphical visualization. Code, data and model sharing can also help other researchers to reproduce research results and to facilitate clinical uptake, but might be challenging in terms of data privacy and research use of data. Large-scale prospective RCTs of the clinical utility of cardiovascular imaging AI tools have not been conducted.[88] For the assessment of certain tasks, such as segmentation, such trials might not be required. However, for many tasks that can affect subsequent patient management, it is imperative that AI tools meet the same clinical standards as other medical treatments, and that both efficacy and cost-effectiveness are assessed. A 2022 systematic review found only 41 RCTs of medical AI tools, with none adhering to standardized reporting guidelines, and the overall risk of bias was high in seven of these trials.[89] The selection of appropriate metrics to assess the capabilities of AI tools is essential, as is the use of standardized reporting guidelines for AI research. Given that AI tools must be integrated into the usual clinical workflow, an important research task is to investigate how to facilitate human–AI interactions in clinical practice.

Table 2. Relevant AI tools for plaque imaging in research and clinical practice.

Modality	Device or software	Manufacturer	Approval pathway	Approval number	AI support	Intended use	Refs.
CT	vascuCAP	Elucid Bioimaging	FDA 510(k) 2017; CE mark October 2017	K1830212	Full 3D segmentations of lumen, wall and each tissue type on CCTA	Not intended to provide a diagnosis, but intended to assist trained physicians with patients who have been identified as hiving atherosclerosis	(103-105)
	cvi42 Auto Imaging Software Application	Circle Cardiovascular Imaging	FDA 510(k) July 2022; CE mark February 2019	K213998	Calcium scoring and centreline placement in coronary vessels	To assist physicians in performing calcium scoring and in semi-automatic placement of the centreline in coronary vessels	(82, 106)
	Syngo.CT CaScoring (SOMARIS/8 VB50)	Siemens Medical Solutions USA	FDA 510(k) May 2020; CE mark May 2019	K201034	Automated coronary calcium scoring on ECG-gated non-contrast CT	To support the physician in evaluating and documenting calcified lesions in coronary arteries	(82, 107)
	iNtuition-Structural Heart Module	TeraRecon	FDA 510(k) July 2019	K191585	Automatic centreline extraction and automated coronary calcium scoring	To assist in the assessment of calcium in the coronary arteries for calcium scoring	(108)
	AI-Rad Companion (Cardiovascular)	Siemens Medical Solutions USA	FDA 510(k) September 2019; CE mark August 2019	K183268	Deep learning-based automated coronary calcium scoring on non-gated CT	To support radiologists in the quantification of total calcium volume in the coronary arteries	(82, 109)
	AVIEW	Coreline Soft	FDA 510(k) September 2020	K200714	Automatic deep learning-based calcium scoring; segments and provides overlay of four main arteries and myocardium	To support the segmentation of coronary arteries and quantification of coronary artery calcium scores	(110, 111)
	Cleerly Labs v2.0	Cleerly	FDA 510(k) October 2020	K202280	Deep learning tool to identify high-quality images, segment and label coronary arteries, and segment lumen and vessel walls on CCTA	Not to replace a qualified medical practitioner, but to provide a more robust semi-automatic segmentation software	(112, 113)

	Cardiac Solution (HealthCCSng)	Nanox.AI (Zebra Medical Vision)	FDA 510(k) September 2021	K210085	AI algorithm for coronary calcium scoring from non-cardiac gated, non-contrast CT	Not intended to be used alone, but intended to provide radiologists with an estimated coronary artery calcium detection category (low, medium or high)	(114, 115)
	HeartFlow Analysis	HeartFlow	FDA 510(k) October 2022	K213857	Automatic machine learning-based detection and characterization of coronary artery plaques	Intended to support risk assessment for coronary artery disease	(116, 117)
	Autoplaque	Cedars-Sinai Medical Center	FDA 510(k) May 2023	K212758	Automatic deep learning-based vessel, plaque and lumen segmentation	Intended to be used as an interactive tool for viewing and analysing cardiac CT data for determining the presence and extent of coronary plaques	(87)
OCT	Ultreon 1.0	Abbott	FDA 510(k); CE mark April 2021	K210458	Automatic detection of lumen, stent, external elastic membrane and calcium	The physician might use the acquired parameters along with other information to determine if therapeutic intervention is indicated	(118, 119)

AI artificial intelligence; CCTA coronary computed tomography; CT computed tomography; OCT optical coherence tomography.

Trustworthy AI

Although there is a huge potential for AI to improve clinical coronary plaque imaging, the lack of trustworthy AI approaches remains a serious concern. According to the EU's ethics guidelines,[90] trustworthy AI must be lawful, ethical and robust from both a technical and a social perspective (Box 1). In the context of clinical AI solutions, these tools should support decision-making rather than make autonomous decisions, be robust and safe, and provide transparent and unbiased recommendations. In fulfilling these criteria, AI solutions could maximize the benefit for clinicians and patients alike while minimizing the risk to patients.

During clinical deployment, the robustness and safety of AI solutions should be determined in terms of accuracy, reliability and reproducibility. The trustworthiness of AI solutions depends not only on technical aspects, but also on human factors that affect their performance in real-world settings. This requirement necessitates comprehensive and transparent evaluation of AI solutions in accordance with established reporting guidelines. For example, diagnostic accuracy before clinical deployment should be evaluated using the STARD-AI guidelines,[91] whereas the DECIDE-AI guidelines[92] contain recommendations for evaluating the diagnostic accuracy of the tool in the early phases of clinical deployment. Finally, the CONSORT-AI guidelines[93] for the evaluation of AI solutions should be used in the context of RCTs. The question of when RCTs are needed to verify clinical effectiveness and to test advantages over standard care and when retrospective studies are sufficient for the evaluation of simple human tasks (such as segmentation tasks) is controversial among experts (Table 1). In the context of clinical deployment, AI solutions should increase the confidence in the recommendations in a suitable manner, ideally in a quantitative fashion, so that clinicians can easily interpret their output (Table 1).

Box 1. Requirements for trustworthy AI.

Requirements for trustworthy AI

The following characteristics are required for an artificial intelligence (AI) tool to be trustworthy when applied to the imaging of vulnerable plaques in coronary arteries.

Robust AI

- Technical and clinical robustness (image noise and artefacts, anatomic abnormalities, and evidence from randomized controlled trials)
- Reliability
- Safety
- Real-time decision-making (guided by optical coherence tomography or intravascular ultrasonography)
- Generalizability (patient population and scanner type)
- Technical developments (photon counting CT and reconstruction algorithm)
- Confidence communication of AI (95% CI, heatmap)

Ethical and fair AI

- Safety (recommendation of interventions, such as percutaneous coronary intervention or coronary artery bypass graft surgery)
- Privacy and security (anonymization of patient data)
- Transparency (accessibility of data to the patient)
- Fairness and inclusivity
- Unbiased AI models (for example, no bias against age, sex or ethnicity)
- Explanation and interpretation of automated diagnosis and prognosis for physicians and patients

Lawful AI

- Certification of devices and software (CE-approved or FDA-approved)
- General data protection regulation
- Medical device regulation

Explainability, interpretability and generalizability

AI explainability and interpretability are often used interchangeably, but differ slightly in meaning. AI explainability refers to inspecting the AI model interior to confirm its output, whereas AI interpretability more formally puts cause and effect into relation, so that the model output can always be linked back to the model input. These standards are included in the EU ethics guidelines for trustworthy AI[90] and in the WHO guidance on ethics and governance of AI for health,[94] as part of a move to ensure transparency and fairness in AI development and deployment (Fig. 4). In the context of atherosclerotic plaque imaging, editable contours for segmentation models or visualization of output probability distributions might be used to provide information on decision-making.

AI models for plaque analysis require careful creation and curation of training datasets to ensure their generalizability. Changes in input data quality could have undesired effects on predictions, such as when models are trained on quality-controlled research data and then applied to clinical data acquired across a variety of clinical situations or with a different imaging technique, or when AI software for atherosclerotic plaque analysis trained on datasets acquired with energy-integrated detectors might fail when applied to photon-counting CT datasets. Solutions for dealing with these domain shifts include:

transfer learning, in which the model is retrained on a small subset of the new data; data augmentation, by simulating the new domain properties; use of training data from a large variety of domains; and a combination of these techniques.[95] Finally, differences in plaque annotations by different radiologists with varying levels of experience and expertise can also lead to differences in model performance. In these cases, model output uncertainty should be reported to inform a clinician to revisit their own findings, or to include annotation uncertainty in the model training for more robust output. The QCI experts of this Roadmap reached a consensus that multiple observers in training datasets are required to compensate for interobserver variability and provide generalizability and can support the uncertainty estimation process.

Fairness and bias mitigation in plaque imaging

Data-driven AI solutions are susceptible to biases that can amplify health-care disparities,[96-98] which is an important area of concern. In the context of imaging of vulnerable plaques in coronary arteries, bias can arise from systematic errors such as disproportionate over-representation or under-representation of certain patient subgroups, over-representation of patients at high risk of disease, or applying AI solutions to subgroups who were not included in the initial training (for example, using an AI model in patients with stable chest pain when it was trained in patients with acute chest pain). Unequal representation in training datasets can particularly affect ethnic and other minority groups, in which AI solutions might perform poorly if these groups were not included in the training datasets.[99]

Two main sources of bias exist: first, in the data used to train AI algorithms and, second, in the implementation and deployment of these AI algorithms.[100] Representation biases can be addressed during the collection or preprocessing of training data via reweighting or resampling of minority groups in the training data or via data augmentation.[100,101] Ideally, clinical data used to train AI algorithms should be based on data from large-scale clinical trials with a pragmatic trial design and minimal exclusion criteria to ensure high external validity.

In addition, features used in training can be adjusted not to correlate with sensitive attributes or to use adversarial learning approaches to de-bias AI solutions. When an AI solution has been developed, it is possible to reduce any biases in its performance by using techniques such as calibrated equalized odds (Table 1).

CONCLUSIONS

Coronary plaque burden and type are important prognostic markers and can guide patient management. A variety of non-invasive and invasive imaging modalities can be used to assess plaque and identify vulnerable plaques. The revolution and the hype surrounding AI have inspired clinicians and scientists to develop tools to automate the assessment of vulnerable plaques. AI has the potential to transform plaque assessment by improving speed and accuracy, but before fully automated AI tools can be integrated into clinical practice, numerous technical challenges must be addressed (Fig. 4), including

reproducibility, robustness, generalizability and reliability, and AI tools must be evaluated using large and diverse datasets. AI tools in research have achieved near-human performance in various plaque assessment tasks, but have mainly been validated in small, preselected and biased study populations. Evidence from RCTs of the clinical utility and cost-effectiveness of approved commercial software solutions is still lacking. Concepts for developing and evaluating trustworthy AI systems that are safe, transparent, fair, interpretable and explainable are still limited and need to be adapted for vulnerable plaque assessment.

This Roadmap for the adoption of AI tools applied to the imaging of vulnerable plaque in coronary arteries includes the development of novel AI tools for the identification of vulnerable plaques in coronary arteries while addressing the many challenges of AI that have been described. Optimizing the integration of AI tools into the clinical workflow will provide coronary plaque metrics together with other clinical and imaging markers of coronary artery disease, including physiology, flow and pericoronary structures. If this Roadmap is adopted, the use of AI systems in close collaboration with physicians[102] to facilitate the imaging of vulnerable plaque in coronary arteries has the potential to revolutionize the diagnosis, prognostic assessment and management of patients with coronary artery disease.

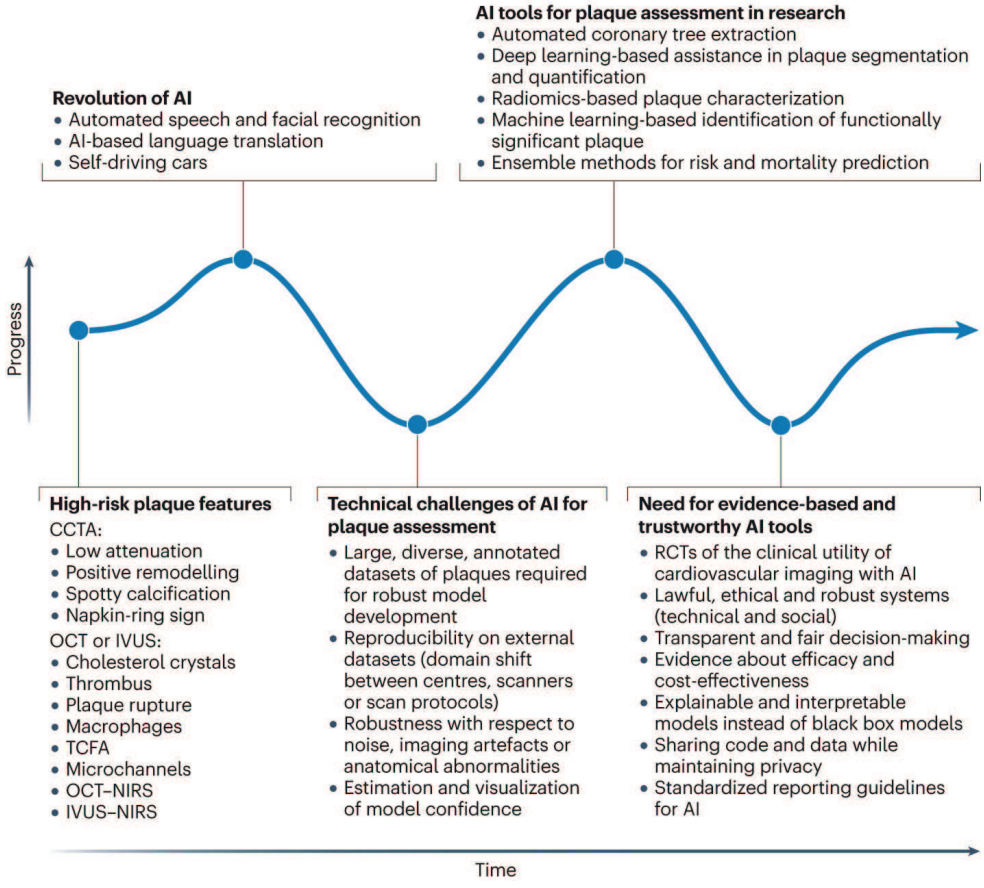


Figure 4. Roadmap for AI in the imaging of vulnerable plaques.

The figure shows the advances and regressions that have occurred during the integration of artificial intelligence (AI)-based tools into clinical practice, starting from clinical evidence for high-risk plaque features through the revolution of AI, technical challenges for AI for plaque assessment, available AI tools for plaque assessment in research, and the need for evidence-based and trustworthy AI tools.

AI artificial intelligence; CCTA coronary computed tomography angiography; IVUS intravascular ultrasonography; NIRS near-infrared spectroscopy; OCT optical coherence tomography; RCT randomized controlled trial; TCFA thin-cap fibroatheroma.

REFERENCES

1. Roberts, J. Thinking machines: the search for artificial intelligence. Science History Institute https://www.sciencehistory.org/distillations/thinking-machines-the-search-for-artificial-intelligence (2016).
2. Quer G, Arnaout R, Henne M, Arnaout R. Machine Learning and the Future of Cardiovascular Care: JACC State-of-the-Art Review. J Am Coll Cardiol 2021;77:300-313.
3. Al'Aref SJ, Anchouche K, Singh G, Slomka PJ, Kolli KK, Kumar A et al. Clinical applications of machine learning in cardiovascular disease and its relevance to cardiac imaging. Eur Heart J 2019;40:1975-1986.
4. Shameer K, Johnson KW, Glicksberg BS, Dudley JT, Sengupta PP. Machine learning in cardiovascular medicine: are we there yet? Heart 2018;104:1156-1164.
5. Litjens G, Ciompi F, Wolterink JM, de Vos BD, Leiner T, Teuwen J, Isgum I. State-of-the-Art Deep Learning in Cardiovascular Image Analysis. JACC Cardiovasc Imaging 2019;12:1549-1565.
6. Friedrich S, Gross S, Konig IR, Engelhardt S, Bahls M, Heinz J et al. Applications of artificial intelligence/machine learning approaches in cardiovascular medicine: a systematic review with recommendations. Eur Heart J Digit Health 2021;2:424-436.
7. Muller JE, Tofler GH, Stone PH. Circadian variation and triggers of onset of acute cardiovascular disease. Circulation 1989;79:733-43.
8. Williams MC, Moss AJ, Dweck M, Adamson PD, Alam S, Hunter A et al. Coronary Artery Plaque Characteristics Associated With Adverse Outcomes in the SCOT-HEART Study. J Am Coll Cardiol 2019;73:291-301.
9. Stone GW, Maehara A, Lansky AJ, de Bruyne B, Cristea E, Mintz GS et al. A prospective natural-history study of coronary atherosclerosis. N Engl J Med 2011;364:226-35.
10. Kedhi E, Berta B, Roleder T, Hermanides RS, Fabris E, AJJ IJ et al. Thin-cap fibroatheroma predicts clinical events in diabetic patients with normal fractional flow reserve: the COMBINE OCT-FFR trial. Eur Heart J 2021;42:4671-4679.
11. Jonas RA, Weerakoon S, Fisher R, Griffin WF, Kumar V, Rahban H et al. Interobserver variability among expert readers quantifying plaque volume and plaque characteristics on coronary CT angiography: a CLARIFY trial sub-study. Clin Imaging 2022;91:19-25.
12. Gruslova A, Vengrenyuk Y, Buja LM, Litovsky S, Maehara A, Kini A et al. TCT-312 International OCT Core Labs Can Identify Stable but Not Unstable Coronary Plaque. J Am Coll Cardiol 2022;80:B125.
13. Mezquita AJV, Biavati F, Falk V, Alkadhi H, Hajhosseiny R, Maurovich-Horvat P et al. Clinical quantitative coronary artery stenosis and coronary atherosclerosis imaging: a Consensus Statement from the Quantitative Cardiovascular Imaging Study Group. Nat Rev Cardiol 2023;20:696-714.
14. Sihan K, Botha C, Post F, de Winter S, Gonzalo N, Regar E et al. Fully automatic three-dimensional quantitative analysis of intracoronary optical coherence tomography: method and Validation. Catheter Cardiovasc Interv 2009;74:1058-65.
15. Chu M, Jia H, Gutierrez-Chico JL, Maehara A, Ali ZA, Zeng X et al. Artificial intelligence and optical coherence tomography for the automatic characterisation of human atherosclerotic plaques. EuroIntervention 2021;17:41-50.
16. Cho H, Kang SJ, Min HS, Lee JG, Kim WJ, Kang SH et al. Intravascular ultrasound-based deep learning for plaque characterization in coronary artery disease. Atherosclerosis 2021;324:69-75.
17. Dewey M, Siebes M, Kachelriess M, Kofoed KF, Maurovich-Horvat P, Nikolaou K et al. Clinical quantitative cardiac imaging for the assessment of myocardial ischaemia. Nat Rev Cardiol 2020;17:427-450.
18. Sermesant M, Delingette H, Cochet H, Jais P, Ayache N. Applications of artificial intelligence in cardiovascular imaging. Nat Rev Cardiol 2021;18:600-609.

19. de Villiers MR, de Villiers PJ, Kent AP. The Delphi technique in health sciences education research. Med Teach 2005;27:639-43.

20. Nasa P, Jain R, Juneja D. Delphi methodology in healthcare research: How to decide its appropriateness. World J Methodol 2021;11:116-129.

21. Tastle WJ, Wierman MJ. An information theoretic measure for the evaluation of ordinal scale data. Behav Res Methods 2006;38:487-94.

22. Finn AV, Nakano M, Narula J, Kolodgie FD, Virmani R. Concept of vulnerable/unstable plaque. Arterioscler Thromb Vasc Biol 2010;30:1282-92.

23. Gaba P, Gersh BJ, Muller J, Narula J, Stone GW. Evolving concepts of the vulnerable atherosclerotic plaque and the vulnerable patient: implications for patient care and future research. Nat Rev Cardiol 2023;20:181-196.

24. Arbab-Zadeh A, Fuster V. The myth of the "vulnerable plaque": transitioning from a focus on individual lesions to atherosclerotic disease burden for coronary artery disease risk assessment. J Am Coll Cardiol 2015;65:846-855.

25. Yamamoto MH, Maehara A, Stone GW, Kini AS, Brilakis ES, Rizik DG et al. 2-Year Outcomes After Stenting of Lipid-Rich and Nonrich Coronary Plaques. J Am Coll Cardiol 2020;75:1371-1382.

26. Joshi NV, Vesey AT, Williams MC, Shah AS, Calvert PA, Craighead FH et al. 18F-fluoride positron emission tomography for identification of ruptured and high-risk coronary atherosclerotic plaques: a prospective clinical trial. Lancet 2014;383:705-13.

27. Williams MC, Kwiecinski J, Doris M, McElhinney P, D'Souza MS, Cadet S et al. Low-Attenuation Noncalcified Plaque on Coronary Computed Tomography Angiography Predicts Myocardial Infarction: Results From the Multicenter SCOT-HEART Trial (Scottish Computed Tomography of the HEART). Circulation 2020;141:1452-1462.

28. Matsumoto H, Watanabe S, Kyo E, Tsuji T, Ando Y, Otaki Y et al. Standardized volumetric plaque quantification and characterization from coronary CT angiography: a head-to-head comparison with invasive intravascular ultrasound. Eur Radiol 2019;29:6129-6139.

29. Conte E, Mushtaq S, Pontone G, Li Piani L, Ravagnani P, Galli S et al. Plaque quantification by coronary computed tomography angiography using intravascular ultrasound as a reference standard: a comparison between standard and last generation computed tomography scanners. Eur Heart J Cardiovasc Imaging 2020;21:191-201.

30. Meah MN, Tzolos E, Wang KL, Bularga A, Dweck MR, Curzen N et al. Plaque Burden and 1-Year Outcomes in Acute Chest Pain: Results From the Multicenter RAPID-CTCA Trial. JACC Cardiovasc Imaging 2022;15:1916-1925.

31. Ferencik M, Mayrhofer T, Bittner DO, Emami H, Puchner SB, Lu MT et al. Use of High-Risk Coronary Atherosclerotic Plaque Detection for Risk Stratification of Patients With Stable Chest Pain: A Secondary Analysis of the PROMISE Randomized Clinical Trial. JAMA Cardiol 2018;3:144-152.

32. Aguirre AD, Arbab-Zadeh A, Soeda T, Fuster V, Jang IK. Optical Coherence Tomography of Plaque Vulnerability and Rupture: JACC Focus Seminar Part 1/3. J Am Coll Cardiol 2021;78:1257-1265.

33. Mintz GS, Guagliumi G. Intravascular imaging in coronary artery disease. Lancet 2017;390:793-809.

34. Maehara A, Matsumura M, Ali ZA, Mintz GS, Stone GW. IVUS-Guided Versus OCT-Guided Coronary Stent Implantation: A Critical Appraisal. JACC Cardiovasc Imaging 2017;10:1487-1503.

35. Raber L, Koskinas KC, Yamaji K, Taniwaki M, Roffi M, Holmvang L et al. Changes in Coronary Plaque Composition in Patients With Acute Myocardial Infarction Treated With High-Intensity Statin Therapy (IBIS-4): A Serial Optical Coherence Tomography Study. JACC Cardiovasc Imaging 2019;12:1518-1528.

36. Guagliumi G, Shimamura K, Sirbu V, Garbo R, Boccuzzi G, Vassileva A et al. Temporal course of vascular healing and neoatherosclerosis after implantation of durable- or biodegradable-polymer drug-eluting stents. Eur Heart J 2018;39:2448-2456.

37. Cheng JM, Garcia-Garcia HM, de Boer SP, Kardys I, Heo JH, Akkerhuis KM et al. In vivo detection of high-risk coronary plaques by radiofrequency intravascular ultrasound and cardiovascular outcome: results of the ATHEROREMO-IVUS study. Eur Heart J 2014;35:639-47.

38. Calvert PA, Obaid DR, O'Sullivan M, Shapiro LM, McNab D, Densem CG et al. Association between IVUS findings and adverse outcomes in patients with coronary artery disease: the VIVA (VH-IVUS in Vulnerable Atherosclerosis) Study. JACC Cardiovasc Imaging 2011;4:894-901.

39. Prati F, Romagnoli E, Gatto L, La Manna A, Burzotta F, Ozaki Y et al. Relationship between coronary plaque morphology of the left anterior descending artery and 12 months clinical outcome: the CLIMA study. Eur Heart J 2020;41:383-391.

40. Motoyama S, Ito H, Sarai M, Kondo T, Kawai H, Nagahara Y et al. Plaque Characterization by Coronary Computed Tomography Angiography and the Likelihood of Acute Coronary Events in Mid-Term Follow-Up. J Am Coll Cardiol 2015;66:337-46.

41. Ferencik M, Mayrhofer T, Puchner SB, Lu MT, Maurovich-Horvat P, Liu T et al. Computed tomography-based high-risk coronary plaque score to predict acute coronary syndrome among patients with acute chest pain--Results from the ROMICAT II trial. J Cardiovasc Comput Tomogr 2015;9:538-45.

42. Min JK, Reynolds H, Anthopolos R, Crabtree T, Mancini J, Leipsic J et al. Whole-Heart Quantification and Characterization of Coronary Atherosclerotic Burden and Risk of Major Adverse Cardiovascular Events: The Ischemia Trial. Circulation 2021;144:E575-E576.

43. Arbab-Zadeh A, Fuster V. From Detecting the Vulnerable Plaque to Managing the Vulnerable Patient: JACC State-of-the-Art Review. J Am Coll Cardiol 2019;74:1582-1593.

44. Williams MC, Earls JP, Hecht H. Quantitative assessment of atherosclerotic plaque, recent progress and current limitations. J Cardiovasc Comput Tomogr 2022;16:124-137.

45. Hosny A, Parmar C, Quackenbush J, Schwartz LH, Aerts H. Artificial intelligence in radiology. Nat Rev Cancer 2018;18:500-510.

46. Hampe N, Wolterink JM, van Velzen SGM, Leiner T, Isgum I. Machine Learning for Assessment of Coronary Artery Disease in Cardiac CT: A Survey. Front Cardiovasc Med 2019;6:172.

47. Lin A, Manral N, McElhinney P, Killekar A, Matsumoto H, Kwiecinski J et al. Deep learning-enabled coronary CT angiography for plaque and stenosis quantification and cardiac risk prediction: an international multicentre study. Lancet Digit Health 2022;4:e256-e265.

48. Lin A, Kolossvary M, Motwani M, Isgum I, Maurovich-Horvat P, Slomka PJ, Dey D. Artificial Intelligence in Cardiovascular Imaging for Risk Stratification in Coronary Artery Disease. Radiol Cardiothorac Imaging 2021;3:e200512.

49. Hampe N, van Velzen SGM, Planken RN, Henriques JPS, Collet C, Aben JP et al. Deep learning-based detection of functionally significant stenosis in coronary CT angiography. Front Cardiovasc Med 2022;9:964355.

50. Chen Q, Pan T, Wang YN, Schoepf UJ, Bidwell SL, Qiao H et al. A Coronary CT Angiography Radiomics Model to Identify Vulnerable Plaque and Predict Cardiovascular Events. Radiology 2023;307:e221693.

51. Chang HJ, Lin FY, Lee SE, Andreini D, Bax J, Cademartiri F et al. Coronary Atherosclerotic Precursors of Acute Coronary Syndromes. J Am Coll Cardiol 2018;71:2511-2522.

52. Group DT, Maurovich-Horvat P, Bosserdt M, Kofoed KF, Rieckmann N, Benedek T et al. CT or Invasive Coronary Angiography in Stable Chest Pain. N Engl J Med 2022;386:1591-1602.

53. Motwani M, Dey D, Berman DS, Germano G, Achenbach S, Al-Mallah MH et al. Machine learning for prediction of all-cause mortality in patients with suspected coronary artery disease: a 5-year multicentre prospective registry analysis. Eur Heart J 2017;38:500-507.

54. van Velzen SGM, Lessmann N, Velthuis BK, Bank IEM, van den Bongard D, Leiner T et al. Deep Learning for Automatic Calcium Scoring in CT: Validation Using Multiple Cardiac CT and Chest CT Protocols. Radiology 2020;295:66-79.

55. Wolterink JM, Leiner T, de Vos BD, van Hamersvelt RW, Viergever MA, Isgum I. Automatic coronary artery calcium scoring in cardiac CT angiography using paired convolutional neural networks. Med Image Anal 2016;34:123-136.

56. Follmer B, Biavati F, Wald C, Stober S, Ma J, Dewey M, Samek W. Active multitask learning with uncertainty-weighted loss for coronary calcium scoring. Med Phys 2022;49:7262-7277.

57. Jia D, Zhuang X. Learning-based algorithms for vessel tracking: A review. Comput Med Imaging Graph 2021;89:101840.

58. Kolossvary M, Karady J, Szilveszter B, Kitslaar P, Hoffmann U, Merkely B, Maurovich-Horvat P. Radiomic Features Are Superior to Conventional Quantitative Computed Tomographic Metrics to Identify Coronary Plaques With Napkin-Ring Sign. Circ Cardiovasc Imaging 2017;10:e006843.

59. Murgia A, Balestrieri A, Crivelli P, Suri JS, Conti M, Cademartiri F, Saba L. Cardiac computed tomography radiomics: an emerging tool for the non-invasive assessment of coronary atherosclerosis. Cardiovasc Diagn Ther 2020;10:2005-2017.

60. Lin A, Kolossvary M, Cadet S, McElhinney P, Goeller M, Han D et al. Radiomics-Based Precision Phenotyping Identifies Unstable Coronary Plaques From Computed Tomography Angiography. JACC Cardiovasc Imaging 2022;15:859-871.

61. Al'Aref SJ, Singh G, Choi JW, Xu Z, Maliakal G, van Rosendael AR et al. A Boosted Ensemble Algorithm for Determination of Plaque Stability in High-Risk Patients on Coronary CTA. JACC Cardiovasc Imaging 2020;13:2162-2173.

62. Diaz-Zamudio M, Dey D, Schuhbaeck A, Nakazato R, Gransar H, Slomka PJ et al. Automated Quantitative Plaque Burden from Coronary CT Angiography Noninvasively Predicts Hemodynamic Significance by using Fractional Flow Reserve in Intermediate Coronary Lesions. Radiology 2015;276:408-15.

63. Yang S, Koo BK, Hoshino M, Lee JM, Murai T, Park J et al. CT Angiographic and Plaque Predictors of Functionally Significant Coronary Disease and Outcome Using Machine Learning. JACC Cardiovasc Imaging 2021;14:629-641.

64. von Knebel Doeberitz PL, De Cecco CN, Schoepf UJ, Duguay TM, Albrecht MH, van Assen M et al. Coronary CT angiography-derived plaque quantification with artificial intelligence CT fractional flow reserve for the identification of lesion-specific ischemia. Eur Radiol 2019;29:2378-2387.

65. Coenen A, Kim YH, Kruk M, Tesche C, De Geer J, Kurata A et al. Diagnostic Accuracy of a Machine-Learning Approach to Coronary Computed Tomographic Angiography-Based Fractional Flow Reserve: Result From the MACHINE Consortium. Circ Cardiovasc Imaging 2018;11:e007217.

66. Dey D, Gaur S, Ovrehus KA, Slomka PJ, Betancur J, Goeller M et al. Integrated prediction of lesion-specific ischaemia from quantitative coronary CT angiography using machine learning: a multicentre study. Eur Radiol 2018;28:2655-2664.

67. Dey D, Slomka PJ, Leeson P, Comaniciu D, Shrestha S, Sengupta PP, Marwick TH. Artificial Intelligence in Cardiovascular Imaging: JACC State-of-the-Art Review. J Am Coll Cardiol 2019;73:1317-1335.

68. Kwiecinski J, Tzolos E, Meah MN, Cadet S, Adamson PD, Grodecki K et al. Machine Learning with (18)F-Sodium Fluoride PET and Quantitative Plaque Analysis on CT Angiography for the Future Risk of Myocardial Infarction. J Nucl Med 2022;63:158-165.

69. Canan A, Ranganath P, Goerne H, Abbara S, Landeras L, Rajiah P. CAD-RADS: Pushing the Limits. Radiographics 2020;40:629-652.

70. Lee J, Prabhu D, Kolluru C, Gharaibeh Y, Zimin VN, Dallan LAP et al. Fully automated plaque characterization in intravascular OCT images using hybrid convolutional and lumen morphology features. Sci Rep 2020;10:2596.

71. Lee J, Kolluru C, Gharaibeh Y, Prabhu D, Zimin VN, Bezerra H, Wilson D. Automatic A-line coronary plaque classification using combined deep learning and textural features in intravascular OCT images. Proc SPIE Int Soc Opt Eng 2020;11315.

72. Cheimariotis GA, Riga M, Haris K, Toutouzas K, Katsaggelos AK, Maglaveras N. Automatic Classification of A-Lines in Intravascular OCT Images Using Deep Learning and Estimation of Attenuation Coefficients. Applied Sciences-Basel 2021;11:7412.

73. Lee J, Pereira GTR, Gharaibeh Y, Kolluru C, Zimin VN, Dallan LAP et al. Automated analysis of fibrous cap in intravascular optical coherence tomography images of coronary arteries. Sci Rep 2022;12:21454.

74. Lee J, Prabhu D, Kolluru C, Gharaibeh Y, Zimin VN, Bezerra HG, Wilson DL. Automated plaque characterization using deep learning on coronary intravascular optical coherence tomographic images. Biomed Opt Express 2019;10:6497-6515.

75. Min HS, Yoo JH, Kang SJ, Lee JG, Cho H, Lee PH et al. Detection of optical coherence tomography-defined thin-cap fibroatheroma in the coronary artery using deep learning. EuroIntervention 2020;16:404-412.

76. Niioka H, Kume T, Kubo T, Soeda T, Watanabe M, Yamada R et al. Automated diagnosis of optical coherence tomography imaging on plaque vulnerability and its relation to clinical outcomes in coronary artery disease. Sci Rep 2022;12:14067.

77. Holmberg O, Lenz T, Koch V, Alyagoob A, Utsch L, Rank A et al. Histopathology-Based Deep-Learning Predicts Atherosclerotic Lesions in Intravascular Imaging. Front Cardiovasc Med 2021;8:779807.

78. Jun TJ, Kang SJ, Lee JG, Kweon J, Na W, Kang D et al. Automated detection of vulnerable plaque in intravascular ultrasound images. Med Biol Eng Comput 2019;57:863-876.

79. Nicol ED. Machine Learning Assessment of CAD: A Giant Leap or a Small Step for Coronary CTA? JACC Cardiovasc Imaging 2023;16:206-208.

80. Nicol ED, Weir-McCall JR, Shaw LJ, Williamson E. Great debates in cardiac computed tomography: OPINION: "Artificial intelligence and the future of cardiovascular CT - Managing expectation and challenging hype". J Cardiovasc Comput Tomogr 2023;17:11-17.

81. US Food and Drug Administration. Artificial intelligence and machine learning (AI/ML)-enabled medical devices. FDA https://www.fda.gov/medical/devices/software-medical-device-samd/artificial-intelligence-and-machine-learning-aiml-enabled-medical-devices (2022).

82. Muehlematter UJ, Daniore P, Vokinger KN. Approval of artificial intelligence and machine learning-based medical devices in the USA and Europe (2015-20): a comparative analysis. Lancet Digit Health 2021;3:e195-e203.

83. Wu E, Wu K, Daneshjou R, Ouyang D, Ho DE, Zou J. How medical AI devices are evaluated: limitations and recommendations from an analysis of FDA approvals. Nat Med 2021;27:582-584.

84. The Medical Futurist. FDA-approved A.I.-based algorithms. TMF https://medicalfuturist.com/fda-approved-ai-based-algorithms/ (2023).

85. ACR Data Science Institute. Radiology SaMD dashboard. AI Central https://aicentral.acrdsi.org/ (2023).

86. Radboud University Medical Center. Products. AI for Radiology https://grand-challenge.org/aiforradiology/ (2023).

87. US Food and Drug Administration. Autoplaque: 510(k) premarket notification. FDA https://www.accessdata.fda.gov/scripts/cdrh/cfdocs/cfpmn/pmn.cfm?ID=K212758 (2023).

88. Zhou Q, Chen ZH, Cao YH, Peng S. Clinical impact and quality of randomized controlled trials involving interventions evaluating artificial intelligence prediction tools: a systematic review. NPJ Digit Med 2021;4:154.

89. Plana D, Shung DL, Grimshaw AA, Saraf A, Sung JJY, Kann BH. Randomized Clinical Trials of Machine Learning Interventions in Health Care: A Systematic Review. JAMA Netw Open 2022;5:e2233946.

90. European Commission. Ethics Guidelines for trustworthy AI. European Commission https://digital-strategy.ec.europa.eu/en/library/ethics-guidelines-trustworthy-ai (2019).

91. Sounderajah V, Ashrafian H, Golub RM, Shetty S, De Fauw J, Hooft L et al. Developing a reporting guideline for artificial intelligence-centred diagnostic test accuracy studies: the STARD-AI protocol. BMJ Open 2021;11:e047709.

92. Vasey B, Nagendran M, Campbell B, Clifton DA, Collins GS, Denaxas S et al. Reporting guideline for the early-stage clinical evaluation of decision support systems driven by artificial intelligence: DECIDE-AI. Nat Med 2022;28:924-933.

93. Liu X, Cruz Rivera S, Moher D, Calvert MJ, Denniston AK, Spirit AI, Group C-AW. Reporting guidelines for clinical trial reports for interventions involving artificial intelligence: the CONSORT-AI extension. Nat Med 2020;26:1364-1374.

94. World Health Organization. Ethics and Governance of Artificial Intelligene for Health: WHO Guidance., 2021.

95. Statistical atlases and computational models of the heart. Multi-disease, multi-view, and multi-center right ventricular segmentation in cardiac MRI challenge. In: Puyol Antón E, Pop M, Martín-Isla C, et al., editors., 2022.

96. Adamson AS, Smith A. Machine Learning and Health Care Disparities in Dermatology. JAMA Dermatol 2018;154:1247-1248.

97. Obermeyer Z, Powers B, Vogeli C, Mullainathan S. Dissecting racial bias in an algorithm used to manage the health of populations. Science 2019;366:447-453.

98. Seyyed-Kalantari L, Zhang H, McDermott MBA, Chen IY, Ghassemi M. Underdiagnosis bias of artificial intelligence algorithms applied to chest radiographs in under-served patient populations. Nat Med 2021;27:2176-2182.

99. Bavli I, Jones DS. Race Correction and the X-Ray Machine - The Controversy over Increased Radiation Doses for Black Americans in 1968. N Engl J Med 2022;387:947-952.

100. Bernhardt M, Jones C, Glocker B. Potential sources of dataset bias complicate investigation of underdiagnosis by machine learning algorithms. Nat Med 2022;28:1157-1158.

101. Suresh H, Guttag J. A framework for understanding sources of harm throughout the machine learning life cycle. ACM Digital Library https://dl.acm.org/doi/pdf/10.1145/3465416.3483305 (2021).

102. Dewey M, Wilkens U. The Bionic Radiologist: avoiding blurry pictures and providing greater insights. NPJ Digit Med 2019;2:65.

103. US Food and Drug Administration. vascuCAP: 510(k) premarket notification. FDA https://www.accessdata.fda.gov/cdrh_docs/pdf18/K183012.pdf (2018).

104. Buckler AJ, Karlof E, Lengquist M, Gasser TC, Maegdefessel L, Perisic Matic L, Hedin U. Virtual Transcriptomics: Noninvasive Phenotyping of Atherosclerosis by Decoding Plaque Biology From Computed Tomography Angiography Imaging. Arterioscler Thromb Vasc Biol 2021;41:1738-1750.

105. Endovascular Today. CRISP consortium study evaluates Elucid Bio's vascuCAP AI software to predict stroke. Endovascular Today https://evtoday.com/news/crisp-consortium-study-evaluates-elucid-bios-vascucap-ai-software-to-predict-stroke (2020).

106. US Food and Drug Administration. cvi42: 510(k) premarket notification. FDA https://www.accessdata.fda.gov/cdrh_docs/pdf14/K141480.pdf (2014).

107. US Food and Drug Administration. Syngo.CT CaScoring: 510(k) premarket notification. FDA https://www.accessdata.fda.gov/cdrh_docs/pdf20/K201034.pdf (2020).

108. US Food and Drug Administration. iNtuition-Structural Heart Module: 510(k) premarket notification. FDA https://www.accessdata.fda.gov/cdrh_docs/pdf19/K191585.pdf (2019).

109. US Food and Drug Administration. AI-Rad Companion (Cardiovascular): 510(k) premarket notification. FDA https://www.accessdata.fda.gov/cdrh_docs/pdf18/K183268.pdf (2019).

110. US Food and Drug Administration. AVIEW: 510(k) premarket notification. FDA https://www.accessdata.fda.gov/cdrh_docs/pdf20/K200714.pdf (2020).

111. Radboud University Medical Center. AVIEW CAC: Coreline Soft. AI for Radiology https://grand-challenge.org/aiforradiology/product/coreline-soft-aview-cac/ (2022).

112. US Food and Drug Administration. Cleerly Labs v2.0: 510(k) premarket notification. FDA https://www.accessdata.fda.gov/cdrh_docs/pdf20/K202280.pdf (2020).

113. US Food and Drug Administration. Cleerly Labs: 510(k) premarket notification. FDA https://www.accessdata.fda.gov/cdrh_docs/pdf19/K190868.pdf (2019).

114. US Food and Drug Administration. HealthCCSng: 510(k) premarket notification. FDA https://www.accessdata.fda.gov/cdrh_docs/pdf21/K210085.pdf (2021).

115. Business Wire. Nanox announces issuance of American Medical Association New Category III CPT® code for its coronary artery calcium population health solution. businesswire https://www.businesswire.com/news/home/20220111005789/en/Nanox-Announces-Issuance-of-American-Medical-Association-New-Category-III%CPT%C2%AE-Code-for-Its-Coronary-Artery-Calcium-Population-Health-Solution (2022).

116. US Food and Drug Administration. HeartFlow Analysis: 510(k) premarket notification. FDA https://www.accessdata.fda.gov/cdrh_docs/pdf21/K213857.pdf (2022).

117. Radboud University Medical Center. HeartFlow FFRCT Analysis: HeartFlow. AI for Radiology https://grand-challenge.org/aiforradiology/product/heartflow-frct-analysis/ (2022).

118. US Food and Drug Administration. OPTIS™ Mobile Next Imaging System, OPTIS™ Integrated Next Imaging System with Ultreon™ Software 1.0: 510(k) premarket notification. FDA https://www.accessdata.fda.gov/cdrh_docs/pdf21/K210458.pdf (2021).

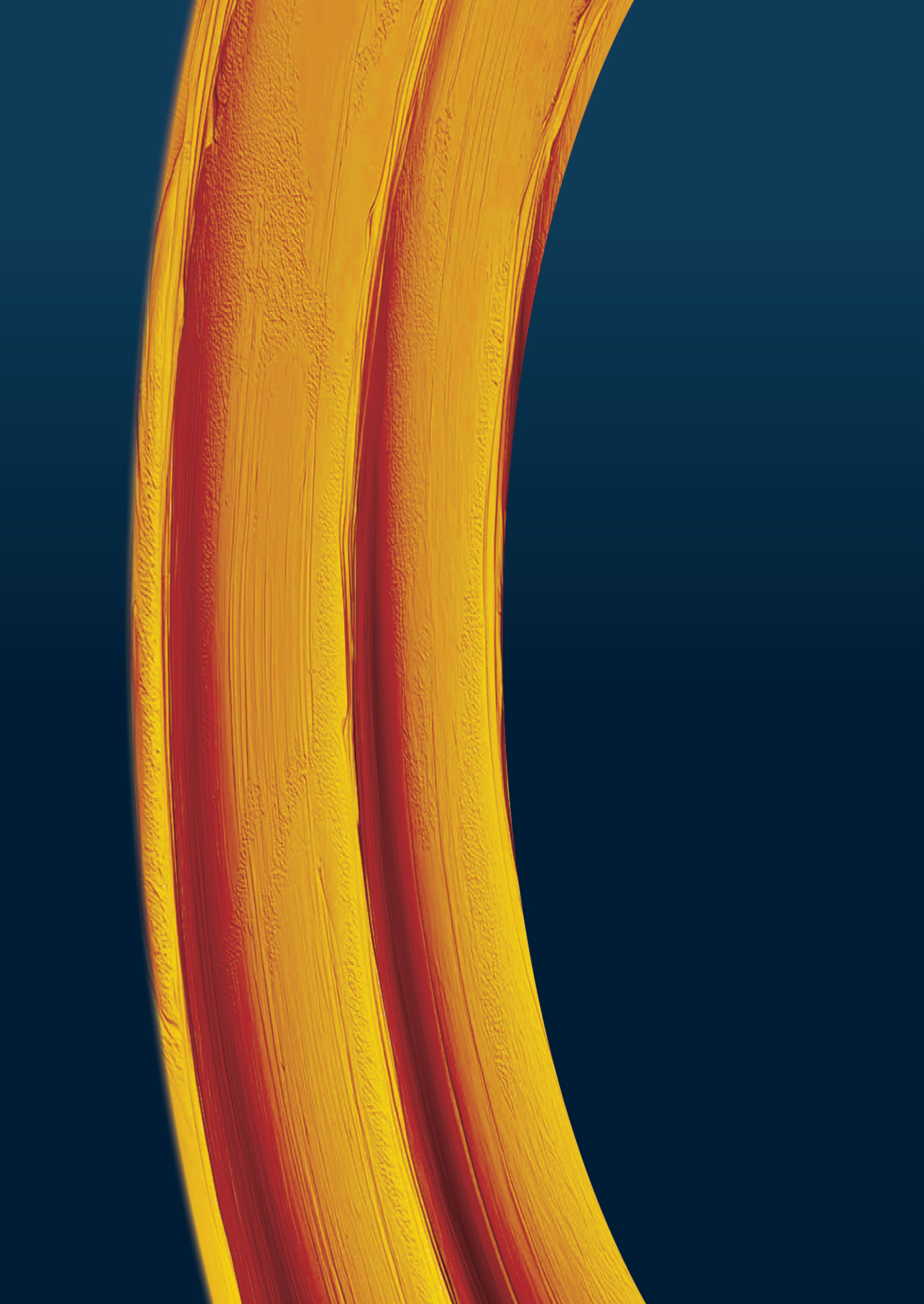
119. Abbott. Abbott receives FDA clearance for its imaging technology using artificial intelligence for vessels in the heart. Abbott https://abbott.mediaroom.com/2021-08-03-Abbott-Receives-FDA-Clearance-for-its-Imaging-Technology-Using-Artificial-Intelligence-for-Vessels-in-the-Heart (2021).

120. Cury RC, Leipsic J, Abbara S, Achenbach S, Berman D, Bittencourt M et al. CAD-RADS 2.0 - 2022 Coronary Artery Disease-Reporting and Data System: An Expert Consensus Document of the Society of Cardiovascular Computed Tomography (SCCT), the American College of Cardiology (ACC), the American College of Radiology (ACR), and the North America Society of Cardiovascular Imaging (NASCI). J Cardiovasc Comput Tomogr 2022;16:536-557.

SUPPLEMENTAL MATERIAL

Supplemental material related to this article can be found in the online version:
https://www.nature.com/articles/s41569-023-00900-3





CHAPTER 13

Artificial intelligence for the analysis of intracoronary optical coherence tomography images: a systematic review

Ruben van der Waerden* | Rick Volleberg* | Thijs Luttikholt | Pierandrea Cancian | Joske van der Zande | Gregg Stone | Niels Holm | Elvin Kedhi | Javier Escaned | Dario Pellegrini | Giulio Guagliumi | Shamir Mehta | Natalia Pinilla-Echeverri | Raúl Moreno | Lorenz Räber | Tomasz Roleder | Bram van Ginneken | Clara Sánchez | Ivana Išgum | Niels van Royen | Jos Thannhauser

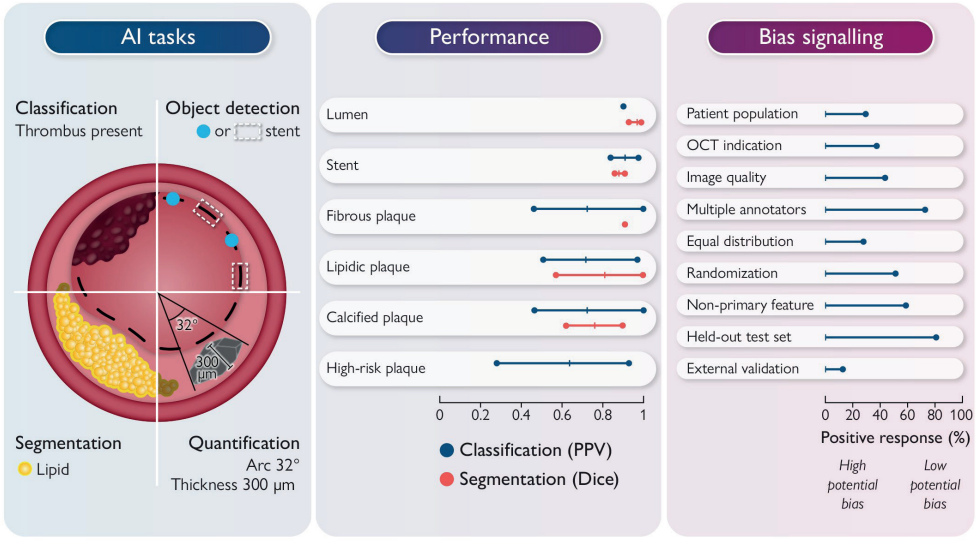
European Heart Journal Digital Health
2025 Jan 28;6(2):270-284

** joined first authorship*

ABSTRACT

Intracoronary optical coherence tomography (OCT) is a valuable tool for, among others, periprocedural guidance of percutaneous coronary revascularization and the assessment of stent failure. However, manual OCT image interpretation is challenging and time-consuming, which limits widespread clinical adoption. Automated analysis of OCT frames using artificial intelligence (AI) offers a potential solution. For example, AI can be employed for automated OCT image interpretation, plaque quantification, and clinical event prediction. Many AI models for these purposes have been proposed in recent years. However, these models have not been systematically evaluated in terms of model characteristics, performances, and bias. We performed a systematic review of AI models developed for OCT analysis to evaluate the trends and performances, including a systematic evaluation of potential sources of bias in model development and evaluation.

GRAPHICAL ABSTRACT



Graphical Abstract.

Systematic review on artificial intelligence (AI) tasks in intracoronary optical coherence tomography (OCT): performance and bias signalling. Left panel: Typical tasks for AI for the automated assessment of intracoronary OCT images include classification, object detection, and segmentation. Classification can be performed framewise or on individual A-lines and is typically used in a binary fashion (i.e. presence or absence of the feature of interest) or with multiple classes (e.g. lipidic plaque, calcified plaque, fibrous plaque, etc.). Object detection refers to the task of localizing a feature of interest, and is typically performed with bounding boxes (dashed lines) or a centroid (blue dot). Semantic segmentation refers to pixel-wise labelling of the feature(s) of interest. Quantification is frequently performed using post-processing steps after semantic segmentation or A-line classification and includes for example measurements of plaque components. Middle panel: Among all identified models, the overall performances (reported as medians with minimum and maximum values) for lumen and stent assessment were excellent, while plaque analysis showed varied results. Right panel: The bias signalling questionnaire, containing several questions related to data management, model development, and validation, revealed potential caveats in model training and evaluation that should be addressed in future studies.

INTRODUCTION

The high resolution of intracoronary optical coherence tomography (OCT) enables detailed *in vivo* assessment of coronary morphology, pathology, and implanted stents.[1] Despite its promise, prevailing guidelines consider the use of OCT only for selective indications.[2,3] Nevertheless, increasing evidence underscores the value of OCT, particularly for periprocedural guidance of percutaneous coronary intervention (PCI)[4-6] but also for identification of lesions at risk for future events.[7-10] Consequently, an increase in clinical use can be foreseen in the near future,[11] which might result in a shift in end-users from highly trained experts to low-volume operators as well. However, on-site interpretation of the voluminous data available from a single OCT pullback demands a high level of expertise and is time consuming, but is nonetheless pivotal for transforming OCT into an actionable application with clinical value.[12] To overcome these challenges, automated analysis of OCT frames has been proposed, either through mathematical models or artificial intelligence (AI).

The adoption of AI for medical image analysis has increased substantially in recent years and has proven successful for numerous applications.[13-15] Artificial intelligence refers to advanced computational systems designed to mimic 'human intelligence' and includes both machine learning as well as more sophisticated deep learning methods. Machine learning focuses on specific tasks, enabling computers to learn from data. Deep learning involves advanced neural networks applicable for complex pattern recognition. Typical applications of AI in medical image analysis include tasks such as classification, object detection, segmentation, and regression, which can be used for the quantification of coronary morphology and/or stents (Graphical Abstract). Specifically for OCT, these tasks can be clinically useful for applications such as segmentation of the lumen (e.g. for stent sizing), detection of stent struts (e.g. for assessing malapposition), classification of plaque morphology (e.g. for identifying thin-cap fibroatheroma), and regression analysis of OCT-derived fractional flow reserve (FFR). Moreover, AI models could be investigated for the prediction of clinical or procedural outcomes. AI models targeted for clinical use require trustworthy development and validation, in order to avoid potential bias, to ensure generalizability, and to achieve robust performance.[16,17] We, therefore, performed a systematic review to provide a comprehensive overview of existing AI models employed in OCT analysis. We analysed trends in this application area, focusing on different tasks and performances of currently proposed methods. Moreover, we aimed to assess potential sources of bias across reported AI models, and highlighted the next steps required for clinical adoption of such models.

METHODS

General Information

This systematic review was prospectively registered in PROSPERO (CRD42023441903) and the manuscript is reported in accordance with the Preferred Reporting Items for Systematic Reviews and Meta-Analyses (PRISMA) statement.[18] Table 1 provides definitions of commonly used terms.

Table 1. Definitions.

Term	Definition
A-line	Individual axial scan line.
Artificial intelligence	Advanced computer systems designed to mimic human intelligence.
Cartesian co-ordinates	Cross-sectional representation of an OCT image.
Datasets	
Training set	Subset of data used to train an AI model, providing examples for the algorithm to learn patterns and features from.
Validation set	Separate subset of data used to fine-tune and optimize the parameters of the model during the training process.
Held-out test set	Independent set of data, derived from the internal data source, not seen by the algorithm during training or validation, used to assess the performance and generalization ability of the trained model.
External test set	Independent set of data, derived from a different data source, not seen by the algorithm during training or validation, used to assess the performance and generalization ability of the trained model.
Deep learning	Part of machine learning that involves advanced neural networks applicable for complex pattern recognition.
Dice score	Performance metric used for segmentation tasks, calculated as two times the area of overlap divided by the total area of the class of interest in the prediction and reference standard.
Machine learning	AI subset enabling systems to learn from data.
Polar co-ordinates	Representation of an OCT image with the angle (Θ) and radius (r).
Quantification	The precise measurement and assessment of characteristics such as plaque angle measurement, mostly using post-processing.
Tasks	
Classification	AI task that aims to categorize input features into output classes, which can be dichotomous (e.g. present vs. absent) or multiclass (e.g. lipid vs. calcified vs. fibrous).
Object detection	AI task that aims to localize the feature of interest using for example bouding boxes or centroids.
Regression	AI task that aims to predict a continuous variable.
Segmentation	AI task that aims to pixel-wise label the input image.

AI artificial intelligence; OCT optical coherence tomography.

Search strategy and selection criteria

A systematic electronic literature search was performed on Embase, Pubmed, Scopus, and Web of Science for papers that use AI for intracoronary OCT. The final search was performed on 31 December 2023. Search terms included; 'Artificial Intelligence', 'Optical Coherence Tomography', and 'Coronary Vessels' or synonyms. The exact search queries can be found in Supplementary material online, Table S1. We included articles which (i) used intracoronary OCT, (ii) employed AI models based on machine learning or deep learning, and (iii) focused on human coronary arteries, either *in vivo* or *ex vivo*. The main exclusion criteria were (i) sole use of non-AI models, e.g. mathematical models, (ii) conference abstracts or proceedings, (iii) non-English articles, (iv) articles unavailable for full-text analysis, and (v) articles not reporting exact performance metrics and/or outcome measures.

After the removal of duplicates, titles and abstracts were screened for potential inclusion. Full-text articles were subsequently evaluated for the finale eligibility.

Study evaluation and data extraction

We systematically abstracted data on study characteristics, AI model characteristics (e.g. machine learning, deep learning, etc.), AI-specific tasks (e.g. classification, segmentation, etc.), outcome measures, and performance metrics. Performance metrics of interest included accuracy, sensitivity, specificity, positive predictive value (PPV), negative predictive value (NPV), F1 score, Dice and Jaccard scores. The best-performing algorithm was included when multiple algorithms were tested for the same task within a single study. Screening and data extraction were performed independently by two investigators (R.W. and R.V.). Cases of discrepancy were resolved through discussion with a third investigator (J.T.). The full study evaluation form can be found in Supplementary material online, File S1.

Bias signalling assessment

Contemporary bias assessment tools employed for systematic reviews on diagnostic accuracy studies (e.g. QUADAS-2),[19] are considered less suitable to identify AI-specific biases.[20] Important sources of bias in AI studies include data collection, data preparation, model training, and model evaluation.[21,22] To the best of our knowledge, only one AI-specific bias assessment tool is published, that primarily involves a subjective evaluation of articles.[23] Therefore, we evaluated each article using nine objective bias signalling questions, each one linked to a specific source of bias within AI (Table 2).[21,22] All questions were answered with yes (+), no (–), or unknown (?). Questions were independently evaluated by two investigators (R.W. and R.V.), and discrepancies were resolved through discussion with a third investigator (J.T.).

Table 2. Bias signalling questions.

Category	Keyword	Question
Data collection		
1. Population bias	Patient population	Is a description available of the patient population?
2. Population bias	OCT indication	Is a description available of the indication for OCT and/or the type of lesions?
3. Representation bias	Image quality	Is information available on the management of image quality/ artefacts?
Data preparation		
4. Annotator bias	Multiple annotators	Does the annotation procedure include multiple annotators?
Model training		
5. Sampling bias	Equal distribution	Is/are the primary feature(s) of interest equally distributed between the training and test set?[a]
6. Sampling bias	Randomization	Are the training and test set randomized/split on either a patient or pullback level (i.e. are frames of the same pullback not present in both training and test set)?
7. Training data bias	Non-primary feature	Do the training and test set include samples without the primary feature(s) of interest?
Model evaluation		
8. Evaluation bias	Held-out test set	Is a held-out test set used for model evaluation?
9. Population bias	External validation	Is the held-out test set obtained from an external cohort?

OCT optical coherence tomography.

[a] *Defined as a relative difference ≤20%.*

RESULTS

Study selection

A total of 9513 articles were identified, of which 4855 remained after removal of duplicates (Figure 1). Subsequently, 4473 articles were excluded based on title and abstract screening. Among the 382 remaining articles, 291 were excluded based on full-text evaluation. Finally, 91 articles were included for analysis.

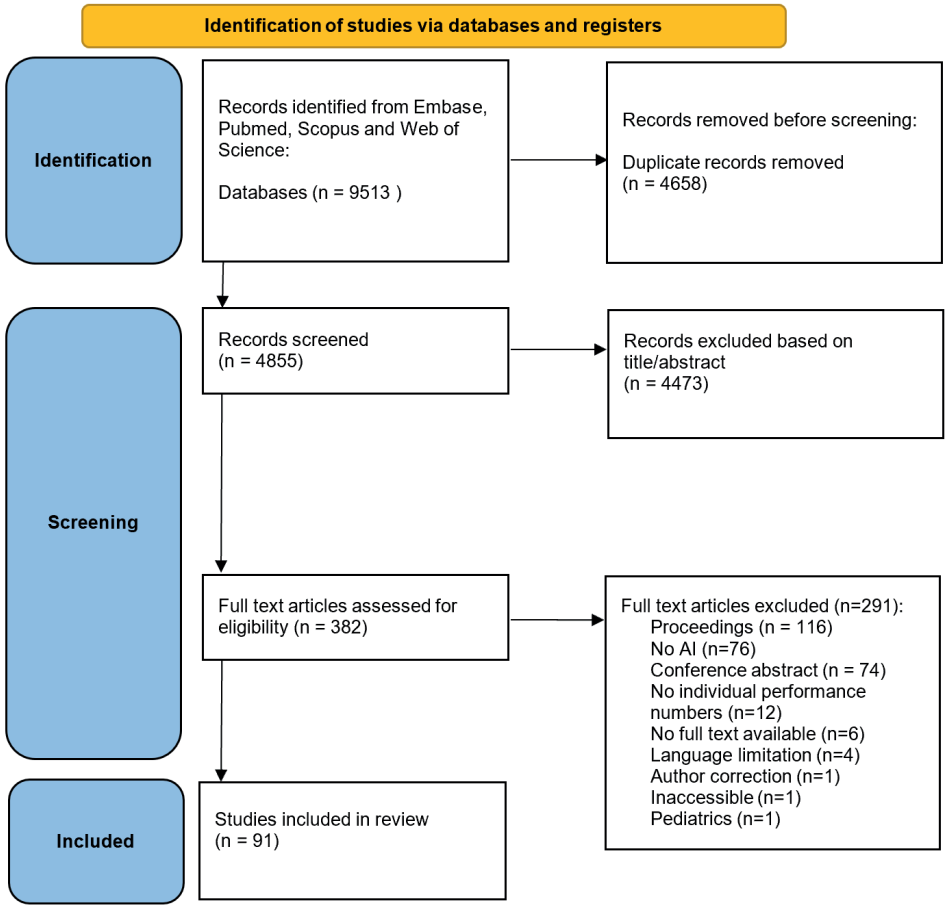


Figure 1. Flowchart of study selection.

AI artificial intelligence.

Study characteristics

The clinical scenario in which OCT was performed was specified in 19 (21%) articles, including six (32%) that solely included patients presenting with acute coronary syndrome (ACS), and four (21%) with chronic coronary syndrome, whilst nine (47%) included patients with either. The number of patients included among the articles ranged from 1 to 1791 [median 41 (interquartile range, IQR 15–67)]. Sex was reported in 21 (23%) articles with the proportion of female patients ranging from 15% to 100% [median 25% (IQR 22–31)]. Studies were predominantly conducted *in vivo* [86 articles, (95%)] and histology served as the reference standard in four (4%) articles. Individual study and patient characteristics are reported in Supplementary material online, Tables S2 and S3.

Model characteristics and tasks

A total of 97 models were described. Model characteristics are provided in Supplementary material online, Table S4. A notable shift in different AI methods was observed over time, with sole development of machine learning methods between 2012 and 2015, followed by an increasing adoption of deep learning methods (Figure 2). Thirty-six (37%) models analysed OCT frames in polar co-ordinates, 34 (35%) used Cartesian co-ordinates, and three (3%) used a combination of both (Figure 3A). Additionally, 80 models (82%) used a 2D analysis approach (i.e. single frame input). Among the 97 models, 100 distinct tasks were identified, predominantly segmentation [48 tasks, (48%)] and classification [42 tasks, (42%)]. Other AI tasks included object detection [7 tasks, (7%)] and regression [3 tasks, (3%)] (Figure 4A–C). Most tasks focused on the assessment of atherosclerotic plaques, the coronary lumen, and stent struts (Figure 4D). Additionally, 19 models (20%) performed a subsequent quantitative evaluation of the primary feature of interest. The algorithm code was shared with the publication in two articles (2%), while data and code are available upon request for 27 (30%) and one (1%) articles, respectively.

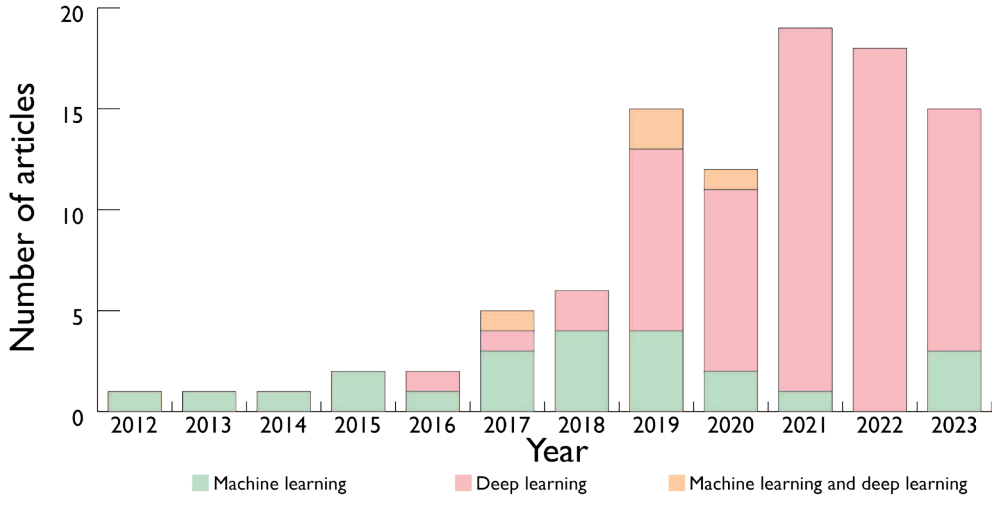


Figure 2. Annual publications on machine learning and deep learning.

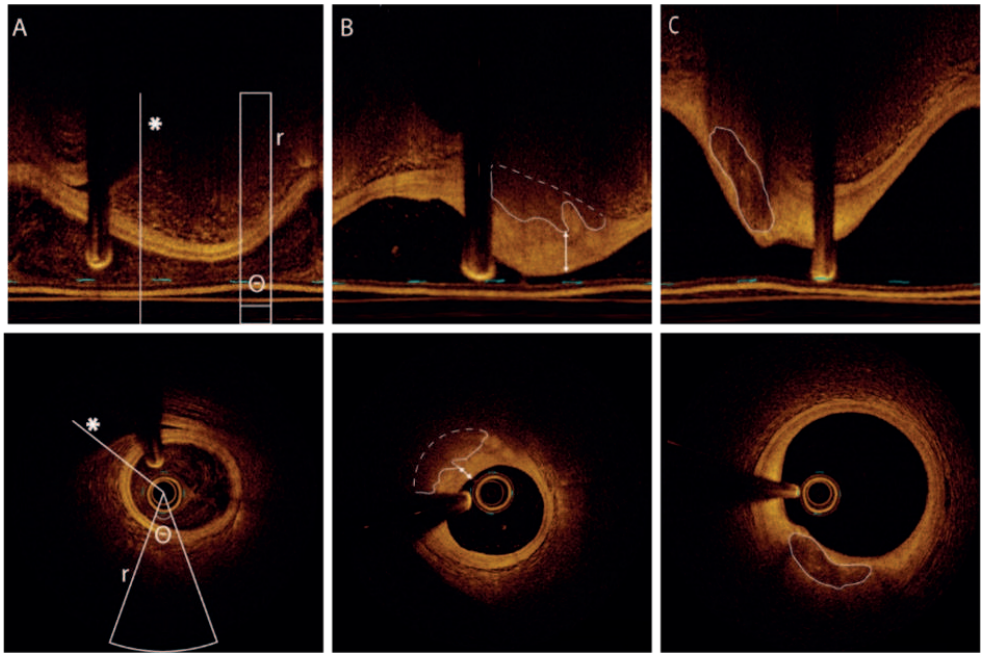


Figure 3. Examples of intracoronary optical coherence tomography images in polar and Cartesian views.
The top row presents three optical coherence tomography frames in polar view, while the reconstructed Cartesian view is displayed in the bottom row. (A) Polar and Cartesian view of the same frame illustrating the y-axis aligning with radius (r) and the x-axis corresponding to the angle (*Θ*). Corresponding A-lines are denoted by an asterisk. (B) Example of an optical coherence tomography frame with a lipidic plaque with a thick fibrous cap (arrows). The inner boundary of the lipidic plaque is outlined with a continuous line, while the estimated outer boundary is represented by a dashed line. (C) Example of an optical coherence tomography frame with a calcified plaque (white outline).

Model performances

Overall and individual model performances are reported in Table 3 and Supplementary material online, Tables S5–S24, respectively. Results are presented as median (minimum–maximum values). The median Dice score across all studies for segmentation of the lumen was 0.972 (0.933–0.988). The mean difference between the AI-based lumen area and the reference standard was <0.50 mm^2 in seven of the eight (87.5%) studies reporting on the quantification of the lumen (see Supplementary material online, Table S25). Segmentation of the media was reported in two studies with one study reporting a Dice score of 0.9108 and the other a pixel-level accuracy of 87%.

Lipidic plaque classification resulted in a median accuracy of 90.6% (75.4–99.2%) with a median sensitivity of 85.6% (67–100%) and PPV of 71.5% (50.6–97.1%). For calcified plaque classification, the median accuracy was 92.8% (73.4–100%), the median sensitivity was 84% (37.6–100%), and the median PPV was 72.5% (46.1–100%), whilst the median accuracy, sensitivity and PPV for classification of fibrous plaques were 94% (81.6–96%), 94% (55–94%), and 65.8% (reported in one article), respectively.

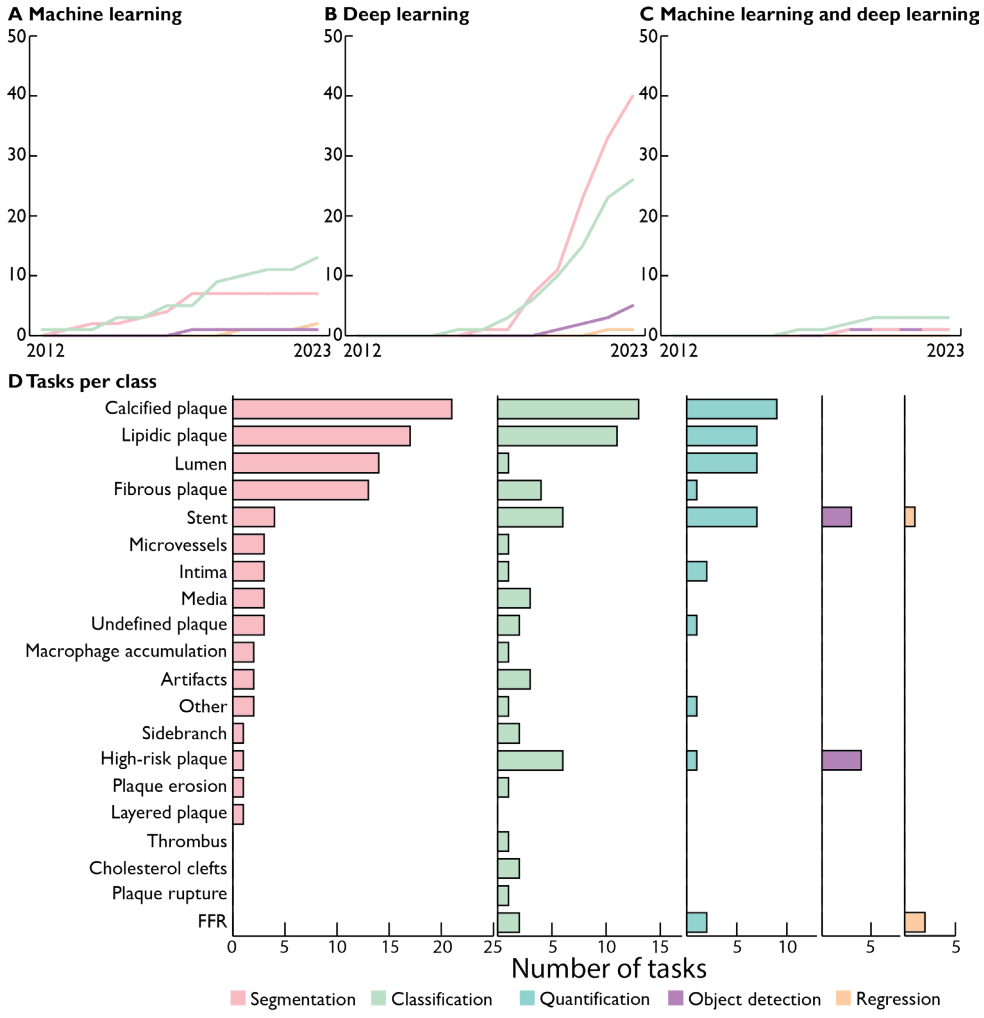


Figure 4. Distributions of tasks per class.

Cumulative number of identified tasks for segmentation, classification, object detection, and regression over time (A–C) and per class (D). Quantification is not an artificial intelligence task but refers to transforming the model output into numerical variables to quantify for example plaque volume or fractional flow reserve.

FFR Fractional flow reserve.

Table 3. Overview of model performances.

Class/Task	Acc (%)	Sens (%)	Spec (%)	PPV (%)	NPV (%)	F1 (%)	AUC-ROC	Dice	Jaccard
Lumen									
Classification	98.2	95.9	98.5	90.0	99.4	-	0.96	-	-
Segmentation	98.1 (98.0-98.2)	94.5 (90.6-99.0)	98.8 (93.0-99.7)	96.9	-	97.2 (95.4-99.0)	-	0.97 (0.93-0.99)	0.92 (0.88-0.97)
Intima									
Classification	92.0	90.0	94.0	-	-	-	-	-	-
Segmentation	90.0	96.0 (93.0-98.9)	86.0	98.9	-	99.0	-	0.95 (0.91-0.99)	-
Media									
Classification	92.0	94.0	90.0	-	-	-	-	-	-
Segmentation	87.0	91.0	82.0	-	-	99.0	-	0.91	-
Side branch									
Classification	95.7 (93.4-97.9)	98.3 (98.1-98.5)	79.2 (60.1-98.4)	96.1 (94.7-97.5)	-	98.0 (96.3-99.7)	0.97 (0.94-1.00)	-	-
Segmentation	-	89.0	-	81.5	-	-	-	0.85	-
Lipid plaque									
Classification	90.6 (75.4-99.2)	85.6 (67.0-100)	91.1 (78.1-99.0)	71.5 (50.6-97.1)	91.9 (85.0-95.9)	81.2 (57.9-98.5)	0.90 (0.82-0.98)	-	-
Segmentation	88.0 (74.1-96.4)	81.0 (71.0-99.0)	91.9 (82.9-96.0)	81.2 (68.0-91.8)	95.0 (94.3-95.7)	80.1 (62.0-92.7)	0.86 (0.85-0.86)	0.81 (0.57-1.00)	0.69 (0.45-0.99)
High-risk plaque									
Classification	93.2 (90.0-96.7)	92.2 (88.6-94.1)	90.9 (84.2-93.2)	63.3 (28.0-92.9)	99.0 (99.0-99.0)	92.9 (92.2-93.7)	0.96 (0.91-1.00)	-	-
Detection	71.6	93.7 (88.0-95.0)	-	94.2 (83.3-88.8)	-	-	0.87	-	-
Segmentation	93.3	91.4	94.3	-	-	-	-	-	-
Calcified plaque									
Classification	92.8 (73.4-100)	84.0 (37.6-100)	95.3 (85.4-100)	72.5 (46.1-100)	97.0 (80.4-99.4)	88.3 (41.4-100)	0.97 (0.93-1.00)	-	-
Segmentation	91.1 (72.1-99.0)	87.4 (67.8-92.9)	92.0 (76.4-99.0)	83.0 (65.9-95.7)	89.0 (80.6-93.1)	78.1 (66.8-93.6)	0.90 (0.89-0.91)	0.76 (0.62-0.90)	0.59 (0.34-0.83)
Fibrous plaque									
Classification	94.0 (81.6-96.0)	94.0 (55.0-94.0)	96.0 (90.5-99.0)	65.8	85.8	59.9	-	-	-
Segmentation	93.0 (81.9-100)	88.6 (74.0-95.0)	94.0 (85.0-98.6)	86.3 (73.0-96.0)	95.0 (85.0-98.6)	88.7 (83.0-94.4)	0.85	0.91	0.58 (0.34-0.81)

Plaque rupture									
Classification	-	81.7 (74.3-83.3)	93.8 (84.9-96.4)	70.6 (44.6-96.0)	89.2 (67.5-99.0)	-	0.94 (0.90-0.98)	-	-
Plaque erosion									
Classification	-	84.9 (80.0-92.7)	84.5 (73.4-88.5)	69.7 (56.7-80.2)	94.8 (86.1-98.7)	-	0.92 (0.90-0.94)	-	-
Layered plaque									
Classification	76.8 (76.0-77.6)	77.1 (76.5-77.7)	76.8 (76.0-77.6)	-	-	-	0.85 (0.85-0.86)	-	-
Segmentation	-	67.0	96.0	53.0	96.0	-	0.86	-	0.36
Undefined plaque									
Classification	81.7 (74.7-9`.7)	87.7 (53.8-90.0)	84.0 (61.5-92.4)	52.9	84.5	72.4 (53.4-91.3)	-	-	-
Segmentation	93.0 (90.2-96.0)	90.0 (76.3-97.0)	95.0 (93.5-95.0)	74.0	94.3	84.0 (75.1-96.0	-	-	-
Thrombus									
Classification	98.0	97.0	99.0	-	-	-	-	-	-
Macrophages									
Classification	92.0	89.0	97.0	-	-	-	-	-	-
Segmentation	48.1	56.8	42.9	-	-	-	-	0.49	-
Cholesterol clefts									
Segmentation	94.7	50.8	-	54.3	-	-	-	0.53	-
Microvessels									
Classification	92.5 (90.0-95.0)	85.0 (80.0-90.0)	98.5 (97.0-100)	-	-	-	-	-	-
Segmentation	-	64.4 (60.4-85.5)	99.8	59.8	-	-	-	0.60 (0.55-0.73)	-
Stents									
Classification	89.7 (82.8-96.5)	93.9 (87.4-95.8)	90.0	90.1 (84.0-97.5)	-	-	0.97	-	-
Detection	-	95.4 (91.5-96.0)	87.9	98.7 (97.9-99.5)	-	93.3 (90.0-96.6)	-	-	-
Segmentation	-	92.0 (90.0-96.6)	92.2 (90.4-94.0)	92.9 (92.0-94.3)	-	92.3 (91.0-93.6)	-	0.88 (0.86-0.91)	0.84
Regression	84.0	87.0	82.0	-	-	-	0.85	-	-

Table 3. Continued

Fractional flow reserve									
Classification	83.2 (77.5-91.7)	89.6 (72.9-98.3)	70.6 (61.5-81.5)	85.7 (77.8-92.1)	77.4 (77.2-88.9)	-	0.76	-	-
Regression	85.4 (75.5-95.2)	87.1 (74.1-100)	85.0 (77.1-92.9)	83.0 (78.4-87.5)	85.3 (72.5-100)	-	0.90 (0.82-0.98)	-	-
Artefacts									
Classification	88.6 (81.2-95.8)	94.8 (90.6-99.0)	93.4 (87.1-99.6)	65.2 (34.7-95.1)	99.6 (99.2-99.9)	98.4	0.98 (0.96-1.00)	-	-
Segmentation	99.3	94.6 (92.0-97.1)	99.9	93.3 (87.0-99.6)	99.3	98.4	-	0.89	-

Overall model performances according to the different classes and tasks. Results are reported as median (minimum-maximum), or as a single value in case of a single article presenting the specific performance metric.

Acc accuracy; AUC-ROC area under the receiver operating characteristic curve; NPV negative predictive value; PPV positive predictive value; Sens sensitivity; Spec specificity.

The median Dice scores for segmentation of lipid and calcified plaques were 0.814 (0.565–0.995) and 0.756 (0.618–0.897), respectively. Quantification of calcified (e.g. calcium arc) or lipidic plaques [e.g. minimum fibrous cap thickness (FCT) or lipid arc] was performed in nine and seven articles, respectively (see Supplementary material online, Table S25). The median accuracy for the classification of high-risk plaques was 93.2% (90–96.7%) with a sensitivity of 92.2% (88.6–94.1%) and PPV of 63.3% (28.0–92.9%). Using detection methods for high-risk plaque assessment, the median sensitivity and PPV were 93.7% (88.0–95.0%) and 84.2% (83.3–88.8%), respectively. Only four and three studies compared the model prediction for lipid and calcified plaque to histology, respectively (see Supplementary material online, Tables S9 and S11).

Classification of plaque rupture and plaque erosion were reported in only one and two studies, respectively (see Supplementary material online, Tables S13 and S14). The median reported sensitivities for plaque rupture and plaque erosion were 81.7% (74.3–83.3%) and 84.9% (80–92.7%), respectively.

The median sensitivity and PPV for the classification of stent struts, mostly performed and evaluated on a strut level, were 93.9% (87.4– 95.8%) and 90.1% (84–97.5%), respectively. The median correlation of the predicted stent area and malapposition distance with the reference standard was 0.962 (0.918–0.990) and 0.99 (0.98–1.00), respectively (see Supplementary material online, Table S25).

Two papers reported on a model for the classification of lesions with a pressure wire-derived FFR of ≤0.80 vs. >0.80 (see Supplementary material online, Table S22). The median accuracy was 83.2% (77.5–91.7%), the median sensitivity was 89.6% (72.9–98.3%), and the median PPV was 85.7% (77.8–92.1%). Two papers described a regression model for the prediction of the OCT-derived FFR value and reported a median accuracy of 85.4% (75.5–95.2%) and a median area under the receiver operating characteristic curve of 0.90 (0.82–0.98) to identify lesions with a pressure wire-derived FFR ≤0.80 vs. >0.80.

Histological validation

Among four studies with histology-based validation of the AI methods, one performed A-line-based classification of lipidic plaques (A-line sensitivity 83.6% and specificity 91.1%). In the three studies on semantic segmentation of lipidic, fibrous, calcified, and/or layered plaques, reported pixel-wise accuracies were 87.7%, 97.4%, 97.6%, and unreported. Median Jaccard indices were 0.57 (0.45–0.68), 0.34, 0.43 (0.34–0.51), and 0.36, respectively.

Prognosis

Associations between AI-detected plaque features and either stent-related, plaque-related, or clinical outcomes were reported in one, two, and three studies, respectively (see Supplementary material online, Table S26). As for the latter, high-risk plaques as defined in the respective studies were associated with an increased risk of study-defined clinical events in all three studies, with a median hazard ratio of 2.56 (1.87–19.13) on a patient level and 12.12 (10.72–13.53) on a lesion level.

Bias signalling questions

The bias signalling questions were evaluated in 88 articles (Figure 5, Supplementary material online, Table S27), excluding three articles that did not report a new model. The patient population characteristics and indication for OCT were described in 26 (30%) and 33 (38%) articles, respectively, with 39 (44%) articles reported on their approach to manage suboptimal frame quality. Sixty-nine (81%) articles evaluated their model on a held-out test set, while 10 (12%) articles used an external test set.

Inference time and software packages

Inference times were reported for 15 models. For classification tasks, the median inference times were 0.385 s (0.003–16) at the frame level, and 60 s (0.025–605) at the pullback level. For segmentation tasks, the median inference times were 0.1725 s (0.0044–30) at the frame level and 37.7 s (0.366–120) at the pullback level.

A total of five software packages were identified in the included studies. Of these, one focused on calcified plaque segmentation, one on stent analysis, and three on plaque and stent assessment.

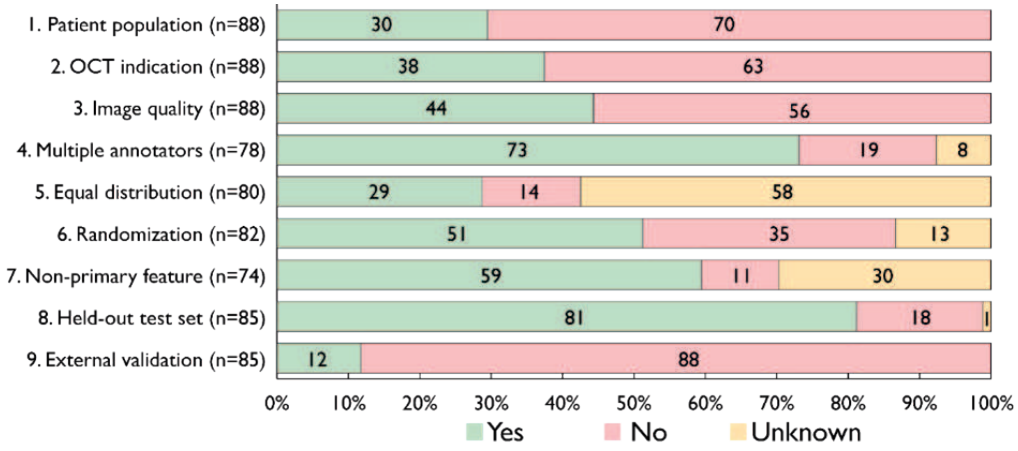


Figure 5. Results of bias signalling questions.
OCT optical coherence tomography.

DISCUSSION

This systematic review provides a comprehensive overview of current AI models for the analysis of intracoronary OCT frames, highlighting the growing interest and increasing use of AI for intracoronary OCT analysis in recent years. Most reported models have targeted assessment of coronary lumen, plaques, and stents, with some also allowing quantification of these structures. The described models demonstrate the feasibility of AI for automated analysis of the extensive data generated by a single OCT pullback for several tasks, including segmentation, classification, and object detection. Specifically, excellent overall performances were reported for lumen and stent evaluation, while more varied performances were reported for plaque analysis.

Despite these efforts, only a limited number of software packages were identified, and none of the proposed models was clinically evaluated in a randomized controlled trial. Additionally, this overview highlights potential bias-related caveats in model training and evaluation that should be prioritized in future studies. In particular, data presentation among articles was diverse, and important information was frequently unavailable. These considerations are essential for ensuring the robustness of AI solutions for intracoronary OCT and to chart a pathway for their clinical adoption.

Evolution of artificial intelligence models for optical coherence tomography analysis

Since the 1990s, AI models have increasingly been applied for medical image analysis, with the first AI model for intracoronary OCT appearing in 2012, which targeted stent strut classification using machine learning.[24] Recently, there has been a notable shift towards more sophisticated deep learning approaches. This transition has aligned with a revolution of AI-related tasks, shifting from relatively simple classification tasks to more intricate studies involving pixel-wise semantic segmentation of OCT frames, and detection of high-risk plaques. It should be acknowledged that while mathematical models have also been proposed,[25,26] these fall outside the scope of the present review.

Periprocedural guidance of revascularization

Multiple randomized trials have compared intravascular imaging to angiography for guidance of coronary revascularization. The totality of evidence indicates significant clinical benefit with intravascular imaging guidance particularly for complex coronary lesions.[4-6] Notably, real-world OCT-guidance has been shown to result in altered decision-making in over 80% of lesions undergoing PCI, highlighting that real-time accurate OCT interpretation is pivotal.[27] The findings of this systematic review suggest that AI can serve as a valuable tool in various stages of this process.

First, OCT is employed to determine stent sizes, which requires accurate quantification of lumen and vessel dimensions. We identified fourteen AI algorithms for lumen segmentation which demonstrated excellent performance. Mean differences between predicted and reference lumen areas were generally <0.50 mm^2. Although vessel-based sizing is preferred over lumen-based stent sizing, only two studies reported media segmentation. In coronary OCT, assessing vessel sizes can be challenging in the presence

of lipidic or thick calcified plaques, due to the light-attenuating nature of these tissues. Chu et al.[28] extrapolated the visible parts of the internal elastic lamina to approximate the vessel area in their nine-class segmentation model based on 11673 frames with and without plaque (Figure 6A) and achieved a Dice score of 0.989 for vessel area segmentation. This model was also externally validated, showing a good correlation (ICC 0.81) with co-registered intravascular ultrasound-derived plaque burden.[29]

Second, OCT is recommended post-PCI to detect signs of suboptimal stent implantation, such as underexpansion, malapposition, and edge dissections. Overall, identified AI models targeting stent classification, detection, or segmentation showed excellent performance. For example, Yang et al.[30] introduced a deep learning-based segmentation model to identify multiple stent layers (Figure 6B). The model performed well in identifying stent struts with both thin and thick tissue coverage (PPV 93.2 ± 0.9% and 85.6 ± 1.9% on a strut level, respectively), without excluding any frames. Overall, correlations between manual and automated stent area assessment were high (>0.90) in all studies. Additionally, the highest absolute mean difference between prediction and the reference standard was 0.36 mm^2 for stent area and the mean differences for malapposition distance was <20 μm in both studies reporting this measure,[31,32] suggesting that current models accurately enable detection of suboptimal stent placement. However, none of the algorithms addressed other clinically significant features such as tissue protrusion, edge dissections, or residual disease.

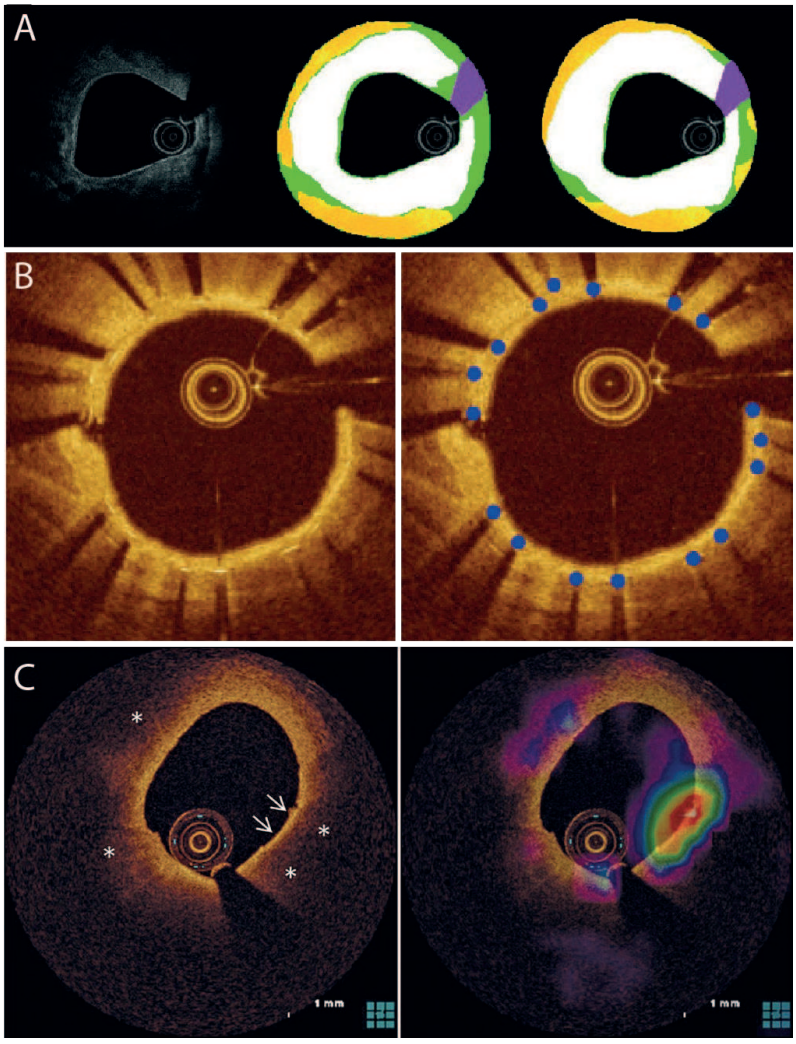


Figure 6. Examples of artificial intelligence algorithms for different tasks.
A) Multiclass semantic segmentation model proposed by Chu et al. The raw optical coherence tomography image is presented in the left image, the reference standard in the middle image, and the model prediction in the right image. White represents calcium, green represents intima/fibrous, yellow represents lipid, and purple represents guidewire artefact. Used with permission of EuroIntervention, from Artificial intelligence and optical coherence tomography for the automatic characterization of human atherosclerotic plaques, Chu, 17, 1, 2021; permission conveyed through Copyright Clearance Center, Inc.[28] B) Detection model for the localization of metal stent struts using centroids proposed by Yang et al. Adapted with permission from Yang et al.[30] © Optica Publishing Group. C) Framewise classification for the presence vs. absence of thin-cap fibroatheroma proposed by Min et al. The right panel represents the gradient-weighted class activation mapping (Grad-CAM) with red colours indicating the high attended regions to predict thin-cap fibroatheroma. Used with permission of EuroIntervention, from Detection of optical coherence tomography defined thin-cap fibroatheroma in the coronary artery using deep learning, Min, 16, 5, 2020; permission conveyed through Copyright Clearance Center, Inc.[33]

Lesion preparation

Achieving optimal stent expansion is pivotal for long-term stent durability, but challenging in case of extensive calcification. Fujino et al.[34] previously proposed an OCT-based risk score to identify lesions requiring specialized preparation to achieve sufficient stent expansion (i.e. calcified lesions with the combined presence of a calcium arc >180°, thickness >500 µm, and length >5 mm). While studies showed lower performances in evaluating calcified plaque compared with lumen and stent assessment, efforts to quantify calcification continue. Lee et al.[35] performed multiple studies and achieved reasonable mean differences in calcium arc (13.2 ± 16.8°) and length (10.8 ± 20.1 mm) compared with core lab analysis, and excellent reproducibility in a cadaveric *ex vivo* dataset.[36]

Incorporating volumetric measures, such as total calcification volume, or differentiating types of calcification, could theoretically improve predictions.[37] However, on-site evaluation of calcification volume is infeasible without computer assistance. Among 21 studies addressing calcified plaque segmentation, only three studies compared predicted calcium area or volume to a reference standard, all with high agreement. Notably, only one study employed AI to predict acute stent expansion from pre-interventional OCT frames and achieved a good correlation (0.94) between the predicted and actual minimum lumen area after PCI. The model had a sensitivity of 87% and a PPV of 84% for the prediction of proper stent expansion (defined as >80%).[38] Intriguingly, this model outperformed the calcium score proposed by Fujino et al.[34] However, the latter showed poor discrimination on the testing dataset (AUC 0.521), underscoring the need for external validation of both this score and the AI model.

Lipidic and high-risk plaque assessment

Compared with calcified plaques, manually detecting lipidic plaques on OCT frames is more challenging and exhibits substantial interobserver variability,[39] and an even larger variability compared to histology.[40] We identified several classification and segmentation models for automated lipid assessment. While these models show reasonable performance for framewise identification of lipidic plaques, moderate pixel-wise performances were observed, likely due to difficulties in predicting the abluminal lipid border caused by its light-attenuating nature. For instance, the Dice score for lipidic plaques in the study by Chu et al.[28] for stable coronary lesions was 0.772 (Figure 6A). It is important to note that most models were evaluated against expert image analysis, with only a few studies using histology as a reference standard, calling for more extensive validation against histology.

Quantification of lipidic plaques can be particularly relevant for the identification of high-risk plaques, which are lipidic plaques prone to rupture and are characterized by a thin fibrous cap (variably defined as ≤55–75 µm), large lipid arc (variably defined as ≥90–180˚), small lumen area (variably defined as ≤3.0–4.0 mm^2), and in some studies the presence of macrophages.[1] Numerous prospective observational studies have demonstrated that high-risk plaques provide important prognostic information,[7-10] and preventive treatment of such plaques is under active investigation. Intensive lipid lowering or anti-inflammatory therapy can indeed help stabilize high-risk plaques[41] and preventive focal treatment has been proposed to seal high-risk plaques.[42] Both strategies require accurate identification of high-risk plaques, that should also be readily available when pursuing focal treatment. We identified six studies targeting high-

risk plaque classification, with a median accuracy and sensitivity >90%. In contrast, only modest PPV has been reported. For example, the study by Min et al.[33] (Figure 6C) achieved a high framewise classification accuracy for thin-cap fibroatheroma of 90%, but a PPV of only 51% in the held-out test set and 28% in a small external test set. Furthermore, the relatively high false positive rate at the vessel level of 31% would be unacceptable in clinical practice, if used to guide preventive focal treatment of high-risk plaques. Besides classification, preliminary attempts on high-risk plaque localization using detection models exhibit promising results.[43-46] However, these studies used relatively small datasets (up to 2500 frames), emphasizing the need for validation in larger studies, and none compared the performance to histology. Whether AI-assisted high-risk plaque identification can contribute to prognostication remains largely unclear. To date, three studies showed an association between AI-identified high-risk plaques and adverse clinical outcomes, with a PPV ranging between 5.2–14.0%, which seems slightly lower than manual core lab analyses.[7] For example, Biccirè et al.[47] found a substantially lower PPV for AI compared with the original core lab analysis (5.2% vs. 19.4%) on the CLIMA dataset.[10] As such, there is insufficient evidence to support AI-driven high-risk plaque detection in its current state, highlighting the need for further research.

Culprit lesion identification

In addition to analysing plaque composition, OCT could help identify the culprit lesion when it is ambiguous, such as in myocardial infarction without obstructive coronary artery disease, as well as elucidate mechanisms like plaque rupture, erosion, coronary dissection, and vasospasm, which may not always be visible on coronary angiograms. However, AI training for these models faces challenges due to the rarity of such structures, including thrombus, intimal ruptures, or dissections. In a study by Park et al.,[48] a transformer model demonstrated high performances for diagnosing plaque erosion, achieving a frame-level AUC of 0.94 and a lesion-level AUC of 0.91 in the external test set. Notably, the model was validated in a reader study to experienced and inexperienced physicians, outperforming the latter group in identifying plaque erosion. Further research is needed to establish the specific benefits of AI in identifying culprit lesions

Optical coherence tomography-derived fractional flow reserve estimation

The integration of computational flow indices could further enhance the utility of OCT, omitting the concurrent need for a pressure wire. Preliminary attempts were performed to employ AI to predict pressure wire-derived FFR from OCT images in small datasets, resulting in a sensitivity and PPV of 72.9–100% and 77.8-92.1%, respectively. These performances, which seem below those obtained using computational fluid dynamics models,[49,50] suggest a limited applicability of currently proposed AI models for OCT-derived FFR for determining the haemodynamic significance of coronary lesions.

Potential sources of bias

The potential of introducing systematic bias is a critical consideration throughout the process of development and evaluation of AI models. The bias signalling questions revealed a lack of reporting

with regard to numerous aspects. Therefore, we advocate for the adherence to AI-specific reporting guidelines.[51] Additionally, data leakage could not be ruled out in 49% of the articles in which the data were not randomized on a patient or pullback level, posing a risk of a substantial overestimation of model performance. In this context, validating models on external datasets is crucial before clinical adoption, a step only under taken in 12% of the reviewed articles. Importantly, a positive answer to any of the signalling questions does not automatically rule out bias. For instance, in the majority of articles detailing the management of suboptimal frame quality, frames with significant artefacts were manually excluded, potentially limiting the generalizability of such algorithms to routine clinical OCT pullbacks. A potential solution is adopting a parallel classification model to identify frames with suboptimal quality, as proposed by Park et al.[48]

Future perspectives

Overall, the identified algorithms demonstrate the feasibility of AI-aided interpretation of intracoronary OCT frames. However, multiple barriers need to be addressed to ensure clinical adoption. First, future efforts should account for potential sources of bias to ensure trustworthiness and generalizability. Furthermore, evaluating model performances and assessing clinical significance requires comparison with both inter- and intra-observer variability among expert physicians. The importance of histology-based OCT studies is underscored by these variabilities and strengthened by our findings, which show that pixel-wise metrics, as well as PPV, appeared lower in histology-based evaluation when compared with studies relying solely on manual OCT image interpretation. Consequently, incorporating histology as a reference standard could further improve the accuracy of AI-based OCT analysis, which has thus far only been implemented in four studies. Second, inference times ranged from seconds to minutes for both classification and segmentation tasks. Balancing model performance with fast real-time decision-making poses a challenge for clinical implementation. Third, the integration of user-friendly software packages would enhance the daily use of autonomous AI models. Despite reviewing nearly 100 articles, only five software packages were identified.[28,32,52-54] Among these, only one CE-certified software package (Ultreon) is currently available that allows automated assessment of the lumen, media, stents, and calcium. [54] Integration of this software package in a standardized workflow (MLD-MAX)[55] has been shown to streamline image interpretation and a modest yet significant reduction in analysis time compared with the former, non-AI-aided, software package.[54] Overall, unlocking the full potential of AI algorithms for intracoronary OCT will require improved infrastructure, extensive validation, regulatory frameworks, and sustainable business models—a stepwise process that has been outlined in recent work.[16,56]

Furthermore, large multicentre evaluations are generally lacking, and none of the models have been tested in a randomized clinical trial. This is particularly important for validating AI-guided treatment strategies of high-risk plaques or guidance of revascularization based on AI-derived flow indices, but could also be valuable for AI-aided periprocedural stent guidance. In the observational LightLab initiative, the AI-assisted MLD-MAX workflow for periprocedural guidance improved acute stent-related outcomes compared with variable workflows, with reduced resource usage and without prolonging

procedural duration.[57] This real-world impact of this AI-assisted workflow will be further evaluated in the prospective observational ILUMIEN-V AERO study, in which an all-comer population of 2000 patients will be included.[58] Last, enhancing code and data availability could improve the interpretation of model performances, although availability is frequently restricted by ethical, legal, and/or financial considerations.

CONCLUSIONS

In this systematic review focusing on the use of AI for the analysis of intracoronary OCT images, we observed a notable transition from traditional machine learning models to the development of deep learning-based methods. These advanced models primarily concentrated on tasks related to the analysis of the intracoronary lumen, atherosclerotic plaques and their composition, and the assessment of stents. While evaluation results for the coronary lumen and stent struts were excellent, AI-based assessment of atherosclerotic plaques remains challenging. Despite these advancements, important considerations related to potential bias are present and must be addressed in future research, to ensure the overall trustworthiness of developed AI models and to pave the way towards their clinical adoption.

REFERENCES

1. Araki M, Park SJ, Dauerman HL, Uemura S, Kim JS, Di Mario C et al. Optical coherence tomography in coronary atherosclerosis assessment and intervention. Nat Rev Cardiol 2022;19:684-703.
2. Neumann FJ, Sousa-Uva M, Ahlsson A, Alfonso F, Banning AP, Benedetto U et al. 2018 ESC/EACTS Guidelines on myocardial revascularization. Eur Heart J 2019;40:87-165.
3. Byrne RA, Rossello X, Coughlan JJ, Barbato E, Berry C, Chieffo A et al. 2023 ESC Guidelines for the management of acute coronary syndromes. Eur Heart J 2023;44:3720-3826.
4. Holm NR, Andreasen LN, Neghabat O, Laanmets P, Kumsars I, Bennett J et al. OCT or Angiography Guidance for PCI in Complex Bifurcation Lesions. N Engl J Med 2023;389:1477-1487.
5. Stone GW, Christiansen EH, Ali ZA, Andreasen LN, Maehara A, Ahmad Y et al. Intravascular imaging-guided coronary drug-eluting stent implantation: an updated network meta-analysis. Lancet 2024;403:824-837.
6. Hong SJ, Lee SJ, Lee SH, Lee JY, Cho DK, Kim JW et al. Optical coherence tomography-guided versus angiography-guided percutaneous coronary intervention for patients with complex lesions (OCCUPI): an investigator-initiated, multicentre, randomised, open-label, superiority trial in South Korea. Lancet 2024;404:1029-1039.
7. Gallone G, Bellettini M, Gatti M, Tore D, Bruno F, Scudeler L et al. Coronary Plaque Characteristics Associated With Major Adverse Cardiovascular Events in Atherosclerotic Patients and Lesions: A Systematic Review and Meta-Analysis. JACC Cardiovasc Imaging 2023;16:1584-1604.
8. Kedhi E, Berta B, Roleder T, Hermanides RS, Fabris E, AJJ IJ et al. Thin-cap fibroatheroma predicts clinical events in diabetic patients with normal fractional flow reserve: the COMBINE OCT-FFR trial. Eur Heart J 2021;42:4671-4679.
9. Mol JQ, Volleberg R, Belkacemi A, Hermanides RS, Meuwissen M, Protopopov AV et al. Fractional Flow Reserve-Negative High-Risk Plaques and Clinical Outcomes After Myocardial Infarction. JAMA Cardiol 2023;8:1013-1021.
10. Prati F, Romagnoli E, Gatto L, La Manna A, Burzotta F, Ozaki Y et al. Relationship between coronary plaque morphology of the left anterior descending artery and 12 months clinical outcome: the CLIMA study. Eur Heart J 2020;41:383-391.
11. Fazel R, Yeh RW, Cohen DJ, Rao SV, Li S, Song Y et al. Intravascular imaging during percutaneous coronary intervention: temporal trends and clinical outcomes in the USA. Eur Heart J 2023;44:3845-3855.
12. Koskinas KC, Nakamura M, Raber L, Colleran R, Kadota K, Capodanno D et al. Current use of intracoronary imaging in interventional practice - Results of a European Association of Percutaneous Cardiovascular Interventions (EAPCI) and Japanese Association of Cardiovascular Interventions and Therapeutics (CVIT) Clinical Practice Survey. EuroIntervention 2018;14:e475-e484.
13. Quer G, Arnaout R, Henne M, Arnaout R. Machine Learning and the Future of Cardiovascular Care: JACC State-of-the-Art Review. J Am Coll Cardiol 2021;77:300-313.
14. Litjens G, Ciompi F, Wolterink JM, de Vos BD, Leiner T, Teuwen J et al. State-of-the-Art Deep Learning in Cardiovascular Image Analysis. JACC Cardiovasc Imaging 2019;12:1549-1565.
15. Liu X, Faes L, Kale AU, Wagner SK, Fu DJ, Bruynseels A et al. A comparison of deep learning performance against health-care professionals in detecting diseases from medical imaging: a systematic review and meta-analysis. Lancet Digit Health 2019;1:e271-e297.
16. Follmer B, Williams MC, Dey D, Arbab-Zadeh A, Maurovich-Horvat P, Volleberg R et al. Roadmap on the use of artificial intelligence for imaging of vulnerable atherosclerotic plaque in coronary arteries. Nat Rev Cardiol 2024;21:51-64.
17. Ethical guidelines for thrustworthy AI. Accessed August 31, 2023. https://digital-strategy.ec.europa.eu/en/library/ethics-guidelines-trustworthy-ai.

18. Page MJ, McKenzie JE, Bossuyt PM, Boutron I, Hoffmann TC, Mulrow CD et al. The PRISMA 2020 statement: an updated guideline for reporting systematic reviews. Bmj 2021;372:n71.
19. Whiting PF, Rutjes AW, Westwood ME, Mallett S, Deeks JJ, Reitsma JB et al. QUADAS-2: a revised tool for the quality assessment of diagnostic accuracy studies. Ann Intern Med 2011;155:529-36.
20. Sounderajah V, Ashrafian H, Rose S, Shah NH, Ghassemi M, Golub R et al. A quality assessment tool for artificial intelligence-centered diagnostic test accuracy studies: QUADAS-AI. Nat Med 2021;27:1663-1665.
21. Drukker K, Chen W, Gichoya J, Gruszauskas N, Kalpathy-Cramer J, Koyejo S et al. Toward fairness in artificial intelligence for medical image analysis: identification and mitigation of potential biases in the roadmap from data collection to model deployment. J Med Imaging (Bellingham) 2023;10:061104.
22. Mehrabi N, Morstatter F, Saxena N, Lerman K, Galstyan A. A Survey on Bias and Fairness in Machine Learning. ACM Comput Surv 2021;54:Article 115.
23. Al-Zaiti SS, Alghwiri AA, Hu X, Clermont G, Peace A, Macfarlane P et al. A clinician's guide to understanding and critically appraising machine learning studies: a checklist for Ruling Out Bias Using Standard Tools in Machine Learning (ROBUST-ML). Eur Heart J Digit Health 2022;3:125-140.
24. Lu H, Gargesha M, Wang Z, Chamie D, Attizzani GF, Kanaya T et al. Automatic stent detection in intravascular OCT images using bagged decision trees. Biomed Opt Express 2012;3:2809-24.
25. Wang Z, Chamie D, Bezerra HG, Yamamoto H, Kanovsky J, Wilson DL et al. Volumetric quantification of fibrous caps using intravascular optical coherence tomography. Biomed Opt Express 2012;3:1413-26.
26. Zahnd G, Karanasos A, van Soest G, Regar E, Niessen W, Gijsen F et al. Quantification of fibrous cap thickness in intracoronary optical coherence tomography with a contour segmentation method based on dynamic programming. Int J Comput Assist Radiol Surg 2015;10:1383-94.
27. Bergmark B, Dallan LAP, Pereira GTR, Kuder JF, Murphy SA, Buccola J et al. Decision-Making During Percutaneous Coronary Intervention Guided by Optical Coherence Tomography: Insights From the LightLab Initiative. Circ Cardiovasc Interv 2022;15:872-881.
28. Chu M, Jia H, Gutierrez-Chico JL, Maehara A, Ali ZA, Zeng X et al. Artificial intelligence and optical coherence tomography for the automatic characterisation of human atherosclerotic plaques. EuroIntervention 2021;17:41-50.
29. Huang J, Tu S, Masuda S, Ninomiya K, Dijkstra J, Chu M et al. Plaque burden estimated from optical coherence tomography with deep learning: In vivo validation using co-registered intravascular ultrasound. Catheter Cardiovasc Interv 2023;101:287-296.
30. Yang G, Mehanna E, Li C, Zhu H, He C, Lu F et al. Stent detection with very thick tissue coverage in intravascular OCT. Biomed Opt Express 2021;12:7500-7516.
31. Lu H, Lee J, Ray S, Tanaka K, Bezerra HG, Rollins AM et al. Automated stent coverage analysis in intravascular OCT (IVOCT) image volumes using a support vector machine and mesh growing. Biomed Opt Express 2019;10:2809-2828.
32. Wu P, Gutiérrez-Chico JL, Tauzin H, Yang W, Li Y, Yu W et al. Automatic stent reconstruction in optical coherence tomography based on a deep convolutional model. Biomed Opt Express 2020;11:3374-3394.
33. Min HS, Yoo JH, Kang SJ, Lee JG, Cho H, Lee PH et al. Detection of optical coherence tomography-defined thin-cap fibroatheroma in the coronary artery using deep learning. EuroIntervention 2020;16:404-412.
34. Fujino A, Mintz GS, Matsumura M, Lee T, Kim SY, Hoshino M et al. A new optical coherence tomography-based calcium scoring system to predict stent underexpansion. EuroIntervention 2018;13:e2182-e2189.
35. Lee J, Prabhu D, Kolluru C, Gharaibeh Y, Zimin VN, Dallan LAP et al. Fully automated plaque characterization in intravascular OCT images using hybrid convolutional and lumen morphology features. Sci Rep 2020;10:2596.
36. Lee J, Gharaibeh Y, Kolluru C, Zimin VN, Dallan LAP, Kim JN et al. Segmentation of Coronary Calcified Plaque in Intravascular OCT Images Using a Two-Step Deep Learning Approach. IEEE Access 2020;8:225581-225593.

37. Shin D, Karimi Galougahi K, Spratt JC, Maehara A, Collet C, Barbato E et al. Calcified Nodule in Percutaneous Coronary Intervention: Therapeutic Challenges. JACC Cardiovasc Interv 2024;17:1187-1199.

38. Gharaibeh Y, Lee J, Zimin VN, Kolluru C, Dallan LAP, Pereira GTR et al. Prediction of stent under-expansion in calcified coronary arteries using machine learning on intravascular optical coherence tomography images. Sci Rep 2023;13:18110.

39. Kini AS, Vengrenyuk Y, Yoshimura T, Matsumura M, Pena J, Baber U et al. Fibrous Cap Thickness by Optical Coherence Tomography In Vivo. J Am Coll Cardiol 2017;69:644-657.

40. Gruslova AB, Singh S, Hoyt T, Vela D, Vengrenyuk Y, Buja LM et al. Accuracy of OCT Core Labs in Identifying Vulnerable Plaque. JACC Cardiovasc Imaging 2024;17:448-450.

41. Raber L, Ueki Y, Otsuka T, Losdat S, Haner JD, Lonborg J et al. Effect of Alirocumab Added to High-Intensity Statin Therapy on Coronary Atherosclerosis in Patients With Acute Myocardial Infarction: The PACMAN-AMI Randomized Clinical Trial. JAMA 2022;327:1771-1781.

42. Park SJ, Ahn JM, Kang DY, Yun SC, Ahn YK, Kim WJ et al. Preventive percutaneous coronary intervention versus optimal medical therapy alone for the treatment of vulnerable atherosclerotic coronary plaques (PREVENT): a multicentre, open-label, randomised controlled trial. Lancet 2024;403:1753-1765.

43. Shi P, Xin J, Zheng N. A-line-based thin-cap fibroatheroma detection with multi-view IVOCT images using multi-task learning and contrastive learning. J Opt Soc Am A Opt Image Sci Vis 2022;39:2298-2306.

44. Liu R, Zhang Y, Zheng Y, Liu Y, Zhao Y, Yi L. Automated Detection of Vulnerable Plaque for Intravascular Optical Coherence Tomography Images. Cardiovasc Eng Technol 2019;10:590-603.

45. Sun CY, Hong XJ, Shi S, Shen ZY, Zhang HD, Zhou LX. Cascade Faster R-CNN Detection for Vulnerable Plaques in OCT Images. IEEE Access 2021;9:24697-24704.

46. Shi P, Xin J, Wu J, Deng Y, Cai Z, Du S et al. Detection of thin-cap fibroatheroma in IVOCT images based on weakly supervised learning and domain knowledge. J Biophotonics 2023;16:e202200343.

47. Biccirè FG, Budassi S, Ozaki Y, Boi A, Romagnoli E, Di Pietro R et al. Optical coherence tomography-derived lipid core burden index and clinical outcomes: results from the CLIMA registry. Eur Heart J Cardiovasc Imaging 2023;24:437-445.

48. Park S, Araki M, Nakajima A, Lee H, Fuster V, Ye JC et al. Enhanced Diagnosis of Plaque Erosion by Deep Learning in Patients With Acute Coronary Syndromes. JACC Cardiovasc Interv 2022;15:2020-2031.

49. Yu W, Huang J, Jia D, Chen S, Raffel OC, Ding D et al. Diagnostic accuracy of intracoronary optical coherence tomography-derived fractional flow reserve for assessment of coronary stenosis severity. EuroIntervention 2019;15:189-197.

50. Hu F, Ding D, Westra J, Li Y, Yu W, Wang Z et al. Diagnostic accuracy of optical flow ratio: an individual patient-data meta-analysis. EuroIntervention 2023;19:e145-e154.

51. Mongan J, Moy L, Kahn CE, Jr. Checklist for Artificial Intelligence in Medical Imaging (CLAIM): A Guide for Authors and Reviewers. Radiol Artif Intell 2020;2:e200029.

52. Oikawa R, Doi A, Ishida M, Chakraborty B. Automatic detection and visualization system for coronary artery calcification using optical frequency domain imaging. Artificial Life and Robotics 2023;28:460-470.

53. Lee J, Kim JN, Gharaibeh Y, Zimin VN, Dallan LAP, Pereira GTR et al. OCTOPUS - Optical coherence tomography plaque and stent analysis software. Heliyon 2023;9:e13396.

54. Cioffi GM, Pinilla-Echeverri N, Sheth T, Sibbald MG. Does artificial intelligence enhance physician interpretation of optical coherence tomography: insights from eye tracking. Front Cardiovasc Med 2023;10:1283338.

55. Shlofmitz E, Croce K, Bezerra H, Sheth T, Chehab B, West NEJ et al. The MLD MAX OCT algorithm: An imaging-based workflow for percutaneous coronary intervention. Catheter Cardiovasc Interv 2022;100 Suppl 1:S7-s13.

56. Jain SS, Elias P, Poterucha T, Randazzo M, Lopez Jimenez F, Khera R et al. Artificial Intelligence in Cardiovascular Care-Part 2: Applications: JACC Review Topic of the Week. J Am Coll Cardiol 2024;83:2487-2496.

57. Khuddus MA, Darki A, Padaliya BB, West NEJ, Rapoza RJ, Buccola J et al. Improving efficiency and operator proficiency during percutaneous coronary interventions utilizing a standardized optical coherence tomography workflow. Catheter Cardiovasc Interv 2022;100 Suppl 1:S14-s24.

58. ILUMIEN-V—AERO: All-comEr Registry of OCT (AERO). ClinicalTrials.gov identifier: NCT05324683. Updated May 11, 2023. https://classic.clinicaltrials.gov/show/NCT05324683. (Accessed 06 February 2024).

SUPPLEMENTAL MATERIAL

Supplemental material related to this article can be found in the online version:
https://academic.oup.com/ehjdh/article/6/2/270/7985683





CHAPTER 14

Comprehensive full-vessel segmentation and volumetric plaque quantification for intracoronary optical coherence tomography using deep learning

Rick Volleberg | Ruben van der Waerden | Thijs Luttikholt | Joske van der Zande | Pierandrea Cancian | Xiaojin Gu | Jan-Quinten Mol | Silvan Quax | Mathias Prokop | Clara Sánchez | Bram van Ginneken | Ivana Išgum | Jos Thannhauser | Simone Saitta | Kensuke Nishimiya | Tomasz Roleder | Niels van Royen

European Heart Journal Digital Health
2025 Mar 15;6(3):404-416

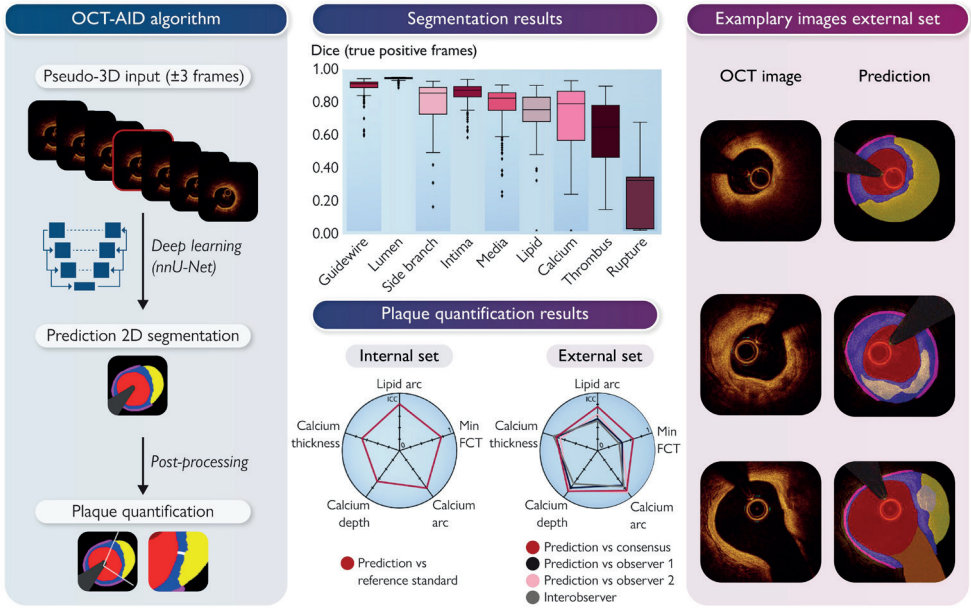
ABSTRACT

Aims Intracoronary optical coherence tomography (OCT) provides detailed information on coronary lesions, but interpretation of OCT images is time-consuming and subject to interobserver variability. The aim of this study was to develop and validate a deep learning-based multiclass semantic segmentation algorithm for OCT (OCT-AID).

Methods and results A reference standard was obtained through manual multiclass annotation (guidewire artefact, lumen, side branch, intima, media, lipid plaque, calcified plaque, thrombus, plaque rupture, and background) of OCT images from a representative subset of pullbacks from the PECTUS-obs study. Pullbacks were randomly divided into a training and internal test set. An additional independent dataset was used for external testing. In total, 2808 frames were used for training and 218 for internal testing. The external test set comprised 392 frames. On the internal test set, the mean Dice score across nine classes was 0.659 overall and 0.757 on the true-positive frames, ranging from 0.281 to 0.989 per class. Substantial to almost perfect agreement was achieved for frame-wise identification of both lipid (κ=0.817, 95% CI 0.743–0.891) and calcified plaques (κ=0.795, 95% CI 0.703–0.887). For plaque quantification (e.g. lipid arc, calcium thickness), intraclass correlations of 0.664–0.884 were achieved. In the external test set, κ-values for lipid and calcified plaques were 0.720 (95% CI 0.640– 0.800) and 0.851 (95% CI 0.794–0.908), respectively.

Conclusions The developed multiclass semantic segmentation method for intracoronary OCT images demonstrated promising capabilities for various classes, while having included difficult frames, such as those containing artefacts or destabilized plaques. This algorithm is an important step towards comprehensive and standardized OCT image interpretation.

GRAPHICAL ABSTRACT



Graphical Abstract.

FCT fibrous cap thickness; ICC intraclass correlation coefficient; nnU-Net no-new-Net; OCT optical coherence tomography.

INTRODUCTION

Intracoronary optical coherence tomography (OCT) has distinct advantages compared with conventional coronary angiography, among which are its exceptionally high spatial resolution and the ability to visualize vessel wall morphology. Routine use of intracoronary imaging to optimize percutaneous coronary revascularization improves clinical outcome,[1] and is now supported with a class I recommendation for guidance of complex lesion revascularization.[2] Additionally, OCT can be a valuable tool to identify culprit lesions as well as high-risk plaques, lipidic plaques at increased risk of causing future cardiovascular events.[3,4] Nevertheless, the clinical adoption of intracoronary imaging remains low.[5] Limiting factors include unfamiliarity with OCT images, a prolonged procedure duration due to time-consuming image interpretation, and substantial interobserver variability.[6-8]

Automated OCT image interpretation through the application of deep learning (DL) can help overcome these limitations, and the high-resolution images obtained using OCT are particularly amenable to automated analyses. Indeed, commercially available tools already allow automated identification of lumen and vessel contours, calcified plaques, and stent struts, while algorithms for lumen and vessel contours are only now becoming available for intravascular ultrasound. Several other algorithms for OCT targeting these and other structures have been proposed over the past decades. In a recent systematic review from our group, we identified 91 articles on this topic. While the overall performance for the evaluation of the lumen and stent struts was very high, performance metrics for the identification and quantification of plaque types were generally lower. Furthermore, proposed algorithms predominantly focus on classification (e.g. classifying frames as plaque-containing or non-plaque-containing) or segmentation of a limited number of classes, and are not developed for complete OCT image interpretation. Importantly, external validation was only performed in 1 out of 8 studies.[9] We therefore developed and validated a fully automatic, multiclass, DL-based algorithm for semantic segmentation of intracoronary OCT images to enable standardized image interpretation and reduce interobserver variability.

METHODS

Study population and datasets

This study is reported in accordance with the CLAIM reporting guidelines (see Supplementary material online, Method S1). The internal dataset comprised a random subset of patients from the multinational, prospective PECTUS-obs study.[4,10] In PECTUS-obs, 438 patients underwent OCT of all intermediate, non-flow limiting, non-culprit lesions after treatment of the infarct-related artery for ST-segment elevation or non-ST-segment elevation myocardial infarction between December 2018 and September 2020. Inclusion and exclusion criteria are provided in Supplementary material online, Method S2. The study was conducted in accordance with the Declaration of Helsinki and its later amendments and was

approved by the local medical-ethics committee or institutional review board of all participating centres. All patients provided informed consent prior to inclusion. The internal dataset was used for model development, including training and internal testing (Figure 1). Details on data splits are presented in Supplementary material online, Method S3.

An independent external cohort of patients originating from a Core Lab registry (Real Solution Sp. Z o.o., Poland) was used for external testing. All patients underwent clinically indicated OCT, and inclusion was not limited to non-flow limiting lesions.

Data acquisition and handling

All pullbacks were acquired using the Dragonfly Optis imaging catheter (Abbott Vascular, USA), predominantly with a pullback speed of 18 mm/s (54 mm) and 540 frames per pullback. OCT pullbacks were exported as DICOM files. Pullbacks were not used if an independent OCT core laboratory deemed the pullback of insufficient quality for further analysis. Additionally, frames without intima visibility due to significant artefacts (e.g. substantial blood artefacts) and frames with stent struts were excluded. Frames with destabilized plaques (i.e. thrombus or plaque rupture) or with artefacts that did not interfere with the interpretation were not excluded.

Reference standard

The reference standard for model training and internal testing was defined by trained personnel with 1–4 years of experience in OCT image interpretation in accordance with contemporary guidelines.[3] Supervision was provided by an interventional cardiologist with >10 years of experience with OCT. Pixel-wise annotation using ITK-SNAP 4.0[11] was performed on every 40th frame of the pullback and on frames in-between in case typical plaque examples or examples with rare features (e.g. plaque rupture) were present. A total of ten labels were used for pixel-wise annotation: guidewire artefact, lumen, side branch, intima, media, lipid plaque, calcified plaque, thrombus, plaque rupture, and background. The abluminal border of lipid plaques was estimated visually based on the visible parts of the tunica media. Weekly meetings were held to discuss challenging frames and reach consensus where needed.

Model architecture, training, and post-processing

We propose OCT-AID, which is based on the no-new-Net (nnU-Net),[12] for multiclass semantic segmentation, which refers to the task of pixel-wise labelling the images. The nnU-Net is a state-of-the art, flexible framework for medical image segmentation, automatically adjusting its configuration to suit the given task and dataset. During training, the nnU-Net learns to assign each pixel in the input image to one of the predefined classes, effectively delineating different structures or regions within the image. To incorporate spatial information available within a pullback and to mimic expert visual analysis, the DL model was fed with seven consecutive cross-sectional frames stacked along the channel dimension (pseudo-3D). Preliminary results demonstrated better prediction results using seven frames as input compared with one, three, or five frames. The output was a 2D semantic segmentation of the central frame. During model testing, segmentation predictions were post-processed using connected

component analysis to remove small, isolated predictions for all classes but plaque rupture and thrombus. Model architecture, training parameters and post-processing are detailed in Supplementary material online, Methods S3 and S4. The algorithm pipeline is presented in Figure 1.

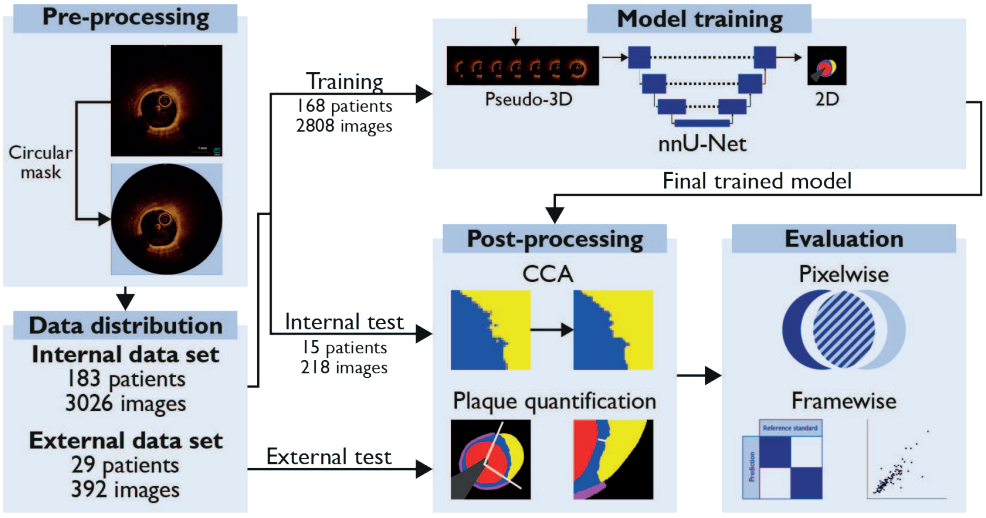


Figure 1. Study flow and OCT-AID pipeline.

Study and algorithm flow for model training and evaluation.

CCA connected component analysis; nnU-Net no-new-Net.

Plaque quantification

Lipid and calcified plaques were quantified from the segmentation output (Figure 2). Arcs were calculated by evaluating the presence of each plaque type along ray casts as assessed from the centroid of the lumen. For plaques visible on both sides of the guidewire artefact, the arc was measured continuously across the guidewire artefact. The minimum fibrous cap thickness (FCT) and calcium depth were calculated as the minimum difference between lumen and lipid or calcium, respectively. The fibrous cap area was calculated as the total area labelled as intima within the lipid arc, and the fibrous cap ratio was defined as the fibrous cap area divided by the lipid arc. The calcium thickness was calculated as the maximum difference between the adluminal and abluminal border of a calcified plaque measured from the centroid of the lumen. A lipid-rich plaque was defined as a lipid plaque with an arc ≥90°.

Internal testing

Pixel-wise segmentation performance was evaluated using the Dice similarity coefficient on the held-out internal test set. In addition, the DL model segmentation predictions were evaluated on a frame basis for their ability to identify each class in a binary fashion (i.e. absence or presence) and for plaque quantification compared with manual measurements. Cumulative lipid arcs, calcium arcs and fibrous cap

areas were used when multiple non-overlapping areas of the same plaque type were present in a single frame. To further evaluate the correspondence in arc locations, a lipid and calcium arc correspondence score was calculated. This metric was defined as two times the correspondence in the lipid/calcium arcs (°) of the reference standard and prediction divided by the sum of the lipid/calcium arcs (°) of the reference standard and the prediction (Figure 2D).

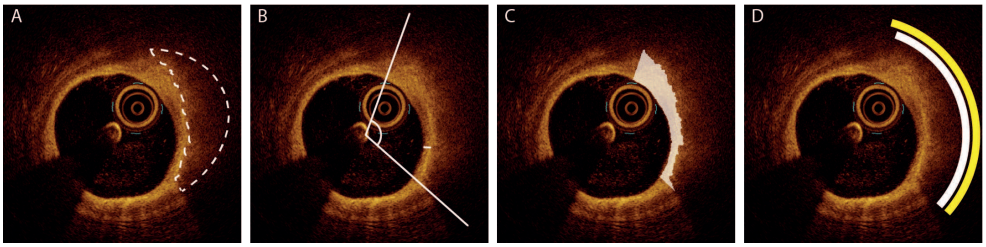


Figure 2. Lipid plaque quantification.

Example of a lipid plaque delineated with white dashed line (A) and corresponding quantification measures, including the lipid arc and minimum fibrous cap thickness (B), fibrous cap area (C), and lipid arc correspondence score (D). In this particular example, the reference standard lipid arc was 112° (white arc) and the predicted lipid arc was 118° (yellow arc) with a correspondence of 112°, resulting in a correspondence score of 0.974.

External testing

For external testing, OCT-AID was similarly evaluated compared with manual assessment of two independent interventional cardiologists (KN and TR) with large experience in OCT studies from different institutes. The independent assessors were blinded to the model predictions. Performance was evaluated on all frames in which both observers confirmed the presence or absence of the class evaluated. For continuous variables, the mean of the two independent assessors was used as reference. The Dice scores, arc correspondence scores, fibrous cap area and fibrous cap ratio were not evaluated in the external test set as this requires pixel-wise labelling. Performance of the algorithm was also evaluated on the complete external test set with direct comparison to one of the observers while the other observer served as reference, to allow a complete evaluation of the model performance on the complete dataset. Interobserver variability was evaluated by comparing the individual interpretations of the observers.

Statistical analysis

Categorical baseline variables are expressed as numbers (percentages) and continuous variables are presented as means ± standard deviation. The χ^2 tests and independent Student's t-tests were used to evaluate categorical and continuous variables, respectively. Missing data were not imputed. Interobserver variability was assessed using Cohen's kappa[13] for frame-wise identification of each class, and intraclass correlation coefficient (ICC) for absolute agreement in a two-way random model[14] for

evaluation of quantification measures. Likewise, agreement between reference standard and predicted frame-wise class identification was evaluated using conventional performance metrics and Cohen's kappa. Dice similarity coefficients for semantic segmentation are reported on all true-positive, false-positive, or false-negative frames as well as on true-positive frames only. Quantification measures were evaluated on true-positive frames only and measurements were presented in scatterplots and evaluated using ICC for absolute agreement in a two-way random model. Bias was assessed using Bland–Altman plots. 95%-Confidence intervals (CI) were calculated for all metrics. A two-sided P-value <0.05 was considered statistically significant. Statistical analyses were performed using SPSS Statistics version 27 (IBM Corp., USA) and RStudio version 2023.09.1 (PBC, USA).

RESULTS

Study population

Among 438 patients included in PECTUS-obs, 183 were included in the present study with a total of 207 pullbacks and 3026 frames. These 183 patients were randomly included from the complete dataset of patients with at least one analysable OCT. One hundred sixty-eight patients (192 pullbacks and 2808 frames) were randomly assigned to the training set and 15 patients (15 pullbacks, 218 frames) to the internal test set (Figure 1). Baseline characteristics were well balanced between sets (Table 1). The frame-wise prevalence of each class is presented in Supplementary material online, Table S1.

Table 1. Patient-level baseline characteristics of included sets

Variable	Overall n=183	Training n=168	Test n=15	P value
Age, years	64 ± 10	64 ± 10	67 ± 10	0.354
Female sex	32 (17.5%)	29 (17.3%)	3 (20.0%)	0.729
Hypertension	87 (47.5%)	80 (47,6%)	7 (46.7%)	0,.944
Diabetes	33 (18.0%)	29 (17.3%)	4 (26.7%)	0.480
Previous myocardial infarction	29 (15.8%)	27 (16.1%)	2 (13.3%)	1.000
Clinical scenario at presentation				
STEMI	74 (40.4%)	70 (41.7%)	4 (26.7%)	0.257
NSTEMI	109 (59.6%)	98 (58.3%)	11 (73.3%)	0.257

NSTEMI non-ST-segment elevation myocardial infarction; STEMI ST-segment elevation myocardial infarction.

Semantic segmentation

Figure 3 provides examples of the performance of OCT-AID for multiclass semantic segmentation. On the internal test set, the mean per class Dice score was 0.659 overall (Figure 4A). The mean Dice score for the lumen, intima, and media were 0.989 ± 0.010, 0.894 ± 0.064, and 0.786 ± 0.199, respectively. The mean Dice scores for lipid and calcified plaques were 0.636 ± 0.311 and 0.526 ± 0.391, respectively. The

mean Dice scores obtained in the internal test set were comparable to the respective validation folds (see Supplementary material online, Method S2). Among true-positive frames only, the mean per class Dice score was 0.757. Dice scores for lipid plaques, calcified plaques, side branch, thrombus, and plaque rupture were 0.763 ± 0.135, 0.716 ± 0.264, 0.792 ± 0.211, 0.628 ± 0.226, and 0.281 ± 0.289, respectively (Figure 4B).

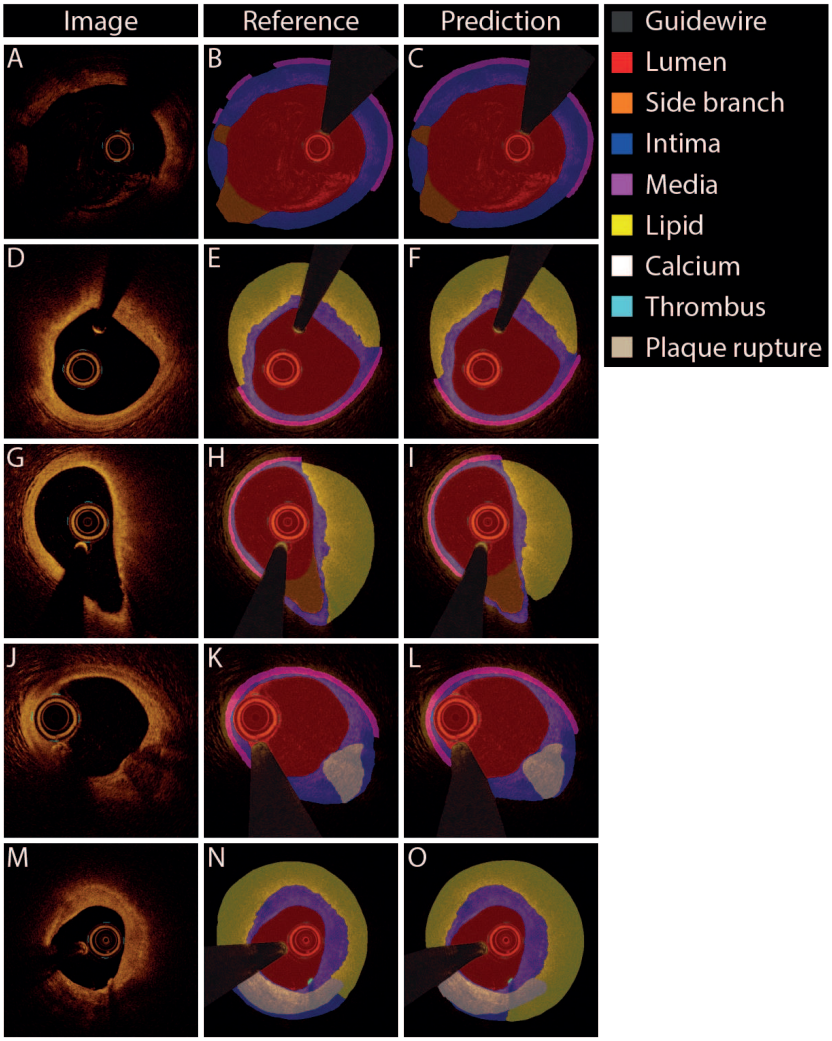


Figure 3. Multiclass semantic segmentation examples.

Examples of the cross-sectional optical coherence tomography image (left column) reference standard (middle column) and predictions by OCT-AID (right column) in the held-out test set. A–C) Frame affected by blood artefacts. D–F) Lipid plaque. G–I) Lipid plaque with a side branch. J–L) Calcified plaque. M–O) Combined lipid and calcified plaque and a small thrombus.

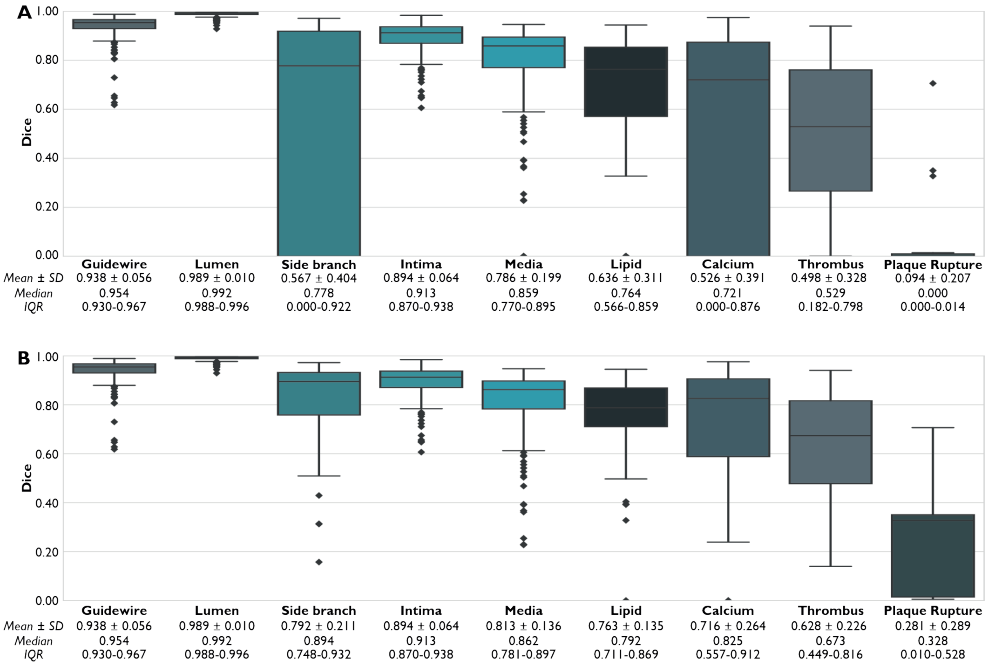


Figure 4. Per-frame dice scores.

Boxplots for the per-frame Dice score per class across all true-positive, false-positive, and false-negative frames (A) and across true-positive frames only (B). A score of 1 indicates perfect overlap and a score of 0 represent no overlap. False-positive and false-negative frames are awarded a score of 0.

IQR inter-quartile range; SD standard deviation.

Frame-wise identification

In the internal test set, substantial to almost perfect agreement was achieved for frame-wise identification of lipid plaques (κ=0.817, 95% CI 0.743–0.891), lipid-rich plaque (κ=0.843, 95% CI 0.769–0.917), calcified plaques (κ=0.795, 95% CI 0.703–0.887), side branches (κ=0.736, 95% CI 0.624–0.848) and for thrombus (κ=0.871, 95% CI 0.759– 0.983), and fair to substantial for plaque rupture (κ=0.480, 95% CI 0.210–0.750). Performance metrics and confusion matrices for each class are presented in Table 2 and Supplementary material online, Tables S2–S7.

Lipid and calcified plaque quantification

In the internal test set, moderate to good reliability was achieved for the lipid arc measurements (ICC 0.814, 95% CI 0.714–0.877) with a mean difference of 16.3 ± 45.9° (see Supplementary material online, Figure S1A and B). The mean lipid arc correspondence score was 0.902 ± 0.120. For the minimum FCT, reliability was moderate to good (ICC 0.766, 95% CI 0.671–0.836). The mean difference was 6.8 ± 75.4 µm (see Supplementary material online, Figure S1C and D). The algorithm achieved moderate to good reliability for the fibrous cap area (ICC 0.768, 95% CI 0.559–0.867) and good to excellent reliability for the fibrous cap ratio (ICC 0.884, 95% CI 0.774–0.934) with a mean difference of 0.24 ± 0.42 mm^2 and 0.0009 ± 0.0017 $mm^2/°$, respectively (see Supplementary material online, Figure S1E-H).

Calcified plaque quantification and bias is reported in Table 2 and Supplementary material online, Figure S2. The ICC for calcium arc, calcium depth, and calcium thickness were 0.808 (95% CI 0.444–0.917), 0.664 (95% CI 0.455–0.801), and 0.690 (95% CI 0.502–0.815), respectively. The mean calcium arc correspondence score was 0.829 ± 0.193.

Table 2. Frame-wise performance metrics for identification and quantification.

Class	Prevalence	TP frames	Accuracy (%)	Sensitivity (%)	Specificity (%)	PPV (%)	NPV (%)	Kappa/ICC[a]
Lipid plaque	102 (46.8%)	100 (98.0%)	90.8 (86.2-94.3)	98.0 (93.1-99.8)	84.5 (76.6-90.5)	84.7 (77.0-90.7)	98.0 (93.0-99.8)	0.817 (0.743-0.891)
Arc	-	-	-	-	-	-	-	0.814 (0.714-0.877)
Minimum FCT	-	-	-	-	-	-	-	0.766 (0.671-0.836)
FC area	-	-	-	-	-	-	-	0.768 (0.559-0.867)
FC ratio	-	-	-	-	-	-	-	0.884 (0.774-0.934)
LRP[b]	76 (34.9%)	73 (96.1%)	92.7 (88.4-95.7)	96.1 (88.9-99.2)	90.8 (84.9-95.0)	84.9 (75.5-91.7)	97.7 (93.5-99.5)	0.843 (0.769-0.917)
Calcified plaque	53 (24.3%)	47 (88.7%)	92.2 (87.8-95.4)	88.7 (77.0-95.7)	93.3 (88.4-96.6)	81.0 (68.6-90.1)	96.3 (92.0-98.6)	0.795 (0.703-0.887)
Arc	-	-	-	-	-	-	-	0.808 (0.444-0.917)
Depth	-	-	-	-	-	-	-	0.664 (0.455-0.801)
Thickness	-	-	-	-	-	-	-	0.690 (0.502-0.815)
Side branch	46 (21.1%)	36 (78.3%)	91.3 (86.7-94.7)	78.3 (63.6-89.1)	94.8 (90.3-97.6)	80.0 (65.4-90.4)	94.2 (89.6-97.2)	0.736 (0.624-0.848)
Thrombus	21 (9.6%)	19 (90.5%)	97.7 (94.7-99.3)	90.5 (69.6-98.8)	98.5 (95.6-99.7)	86.4 (65.1-97.1)	99.0 (96.4-99.9)	0.871 (0.759-0.983)
Plaque rupture	6 (2.8%)	5 (83.3%)	95.4 (91.7-97.8)	83.3 (35.9-99.6)	95.8 (92.1-98.0)	35.7 (12.8-64.9)	99.5 (97.3-100)	0.480 (0.210-0.750)

Metrics are reported as value (95% confidence interval).

FC fibrous cap; FCT fibrous cap thickness; ICC intraclass correlation coefficient; LRP lipid-rich plaque; NPV negative predictive value; PPV positive predictive value; TP true-positive.

[a] *Kappa is calculated for categorical variables (lipid plaque, calcified plaque, side branch, thrombus, and plaque rupture) and ICC is calculated for continuous variables (lipid arc, minimum FCT, FC area, FC ratio calcium arc, calcium depth, and calcium thickness).*

[b] *defined as a lipid plaque with an arc ≥90°.*

Table 3. External test set: interobserver variability and model performance across consensus frames.

Class	Interobserver	External testing in consensus frames								
	Kappa/ICC[a]	Frames with consensus[b]	Prevalence	TP frames	Accuracy (%)	Sensitivity (%)	Specificity (%)	PPV (%)	NPV (%)	Kappa/ICC[a]
Lipid plaque	0.535 (0.451-0.619)	306 (78.1%)	104 (34.0%)	93 (89.4%)	86.9 (82.6-90.5)	89.4 (81.9-94.6)	85.6 (80.0-90.2)	76.2 (67.7-83.5)	94.0 (89.6-97.0)	0.720 (0.640-0.800)
Arc	0.516 (0.359-0.644)	-	-	-	-	-	-	-	-	0.761 (0.614-0.849)
Minimum FCT	0.392 (0.126-0.586)	-	-	-	-	-	-	-	-	0.649 (0.513-0.753)
LRP[c]	0.757 (0.665-0.849)	304 (77.6%)	64 (21.1%)	50 (78.1%)	92.1 (88.5-94.9)	78.1 (66.0-87.5)	95.8 (92.5-98.0)	83.3 (71.5-91.7)	94.3 (90.6-96.8)	0.757 (0.665-0.849)
Calcified plaque	0.905 (0.860-0.950)	376 (95.9%)	115 (30.6%)	105 (91.3%)	93.6 (90.7-95.9)	91.3 (84.6-95.8)	94.6 (91.2-97.0)	88.2 (81.0-93.4)	96.1 (93.0-98.1)	0.851 (0.794-0.908)
Arc	0.772 (0.566-0.869)	-	-	-	-	-	-	-	-	0.857 (0.623-0.931)
Depth	0.708 (0.569-0.802)	-	-	-	-	-	-	-	-	0.870 (0.815-0.910)
Thickness	0.803 (0.715-0.864)	-	-	-	-	-	-	-	-	0.756 (0.658-0.828)
Side branch	0.945 (0.906-0.984)	385 (98.2%)	77 (20.0%)	65 (84.4%)	94.0 (91.2-96.2)	84.4 (74.4-91.7)	96.4 (93.7-98.2)	85.5 (75.6-92.5)	96.1 (93.3-98.0)	0.812 (0.738-0.886)
Thrombus	0.560 (0.303-0.817)	383 (97.7%)	6 (1.6%)	4 (66.7%)	98.2 (96.3-99.3)	66.7 (22.3-95.7)	98.7 (96.9-99.6)	44.4 (13.7-78.8)	99.5 (98.1-99.9)	0.524 (0.214-0.834)
Plaque rupture	0.498 (-0.102-1.000)	390 (99.5%)	1 (0.3%)	0 (0%)	97.4 (95.3-98.8)	0.0 (0.0-97.5)	97.7 (95.7-98.9)	0.0 (0.0-33.6)	99.7 (98.5-100)	-0.005 (-0.013-0.003)

Metrics are reported as value (95% confidence interval).

FCT fibrous cap thickness; ICC intraclass correlation coefficient; LRP lipid-rich plaque; NPV negative predictive value; PPV positive predictive value; TP true-positive.

[a] *Kappa is calculated for categorical variables (lipid plaque, calcified plaque, side branch, thrombus, and plaque rupture) and ICC is calculated for continuous variables (lipid arc, minimum FCT, FC area, FC ratio calcium arc, calcium depth, and calcium thickness).*

[b] *refers to frames on which the independent observers agreed on the presence or absence of the evaluated class.*

[c] *defined as a lipid plaque with an arc ≥90°*

External evaluation

The external test set comprised 29 patients (29 pullbacks, 392 frames). Table 3 provides an overview of the interobserver variability and the performance of OCT-AID compared with consensus in external testing. Supplementary material online, Videos S1 and S2 provide examples of the model interpretation including a challenging case with artefacts.

The proposed algorithm had substantial agreement for frame-wise lipid plaque identification (κ=0.720, 95% CI 0.640–0.800) and substantial to almost perfect for lipid-rich plaques (κ=0.757, 95% CI 0.665–0.849). The ICCs for lipid arc (ICC 0.761, 95% CI 0.614–0.849) and minimum FCT (ICC 0.649, 95% CI 0.513–0.753) indicated moderate to good reliability (Figure 5). For calcified plaques, substantial to almost perfect agreement for frame-wise identification was achieved (κ=0.851, 95% CI 0.794–0.908). The ICCs for calcium arc, depth, and thickness indicate moderate to excellent (ICC 0.857, 95% CI 0.623–0.931), good to excellent (ICC 0.870, 95% CI 0.815–0.910), and moderate to good reliability (ICC 0.756, 95% CI 0.658–0.828), respectively (Figure 5). Bland–Altman plots are presented in Supplementary material online, Figure S3. Mean differences for the lipid arc, minimum FCT, calcium arc, calcium depth, and calcium thickness were −17.3 ± 40.3°, 18.8 ± 89.0 µm, −20.4 ± 29.3°, −3.8 ± 49.2 µm, and −38.9 ± 183.2 µm, respectively. Kappa values for side branch, thrombus, and plaque rupture were 0.812 (95% CI 0.738–0.886), 0.524 (95% CI 0.214–0.834), and −0.005 (95% CI −0.013–0.003), respectively. Evaluation metrics compared with one of the individual independent assessors as reference standard are presented in Tables 4 and 5.

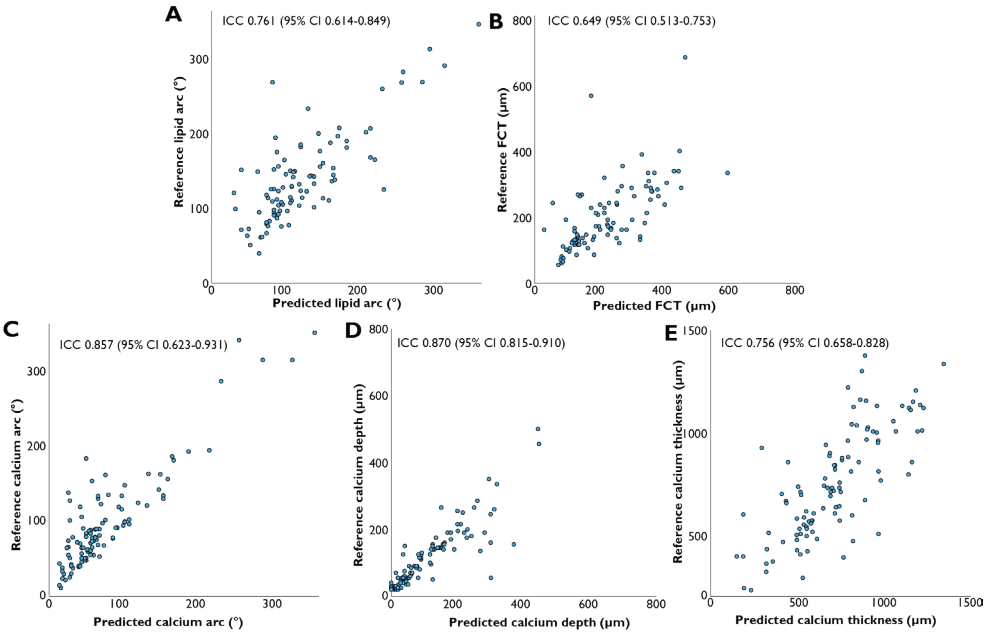


Figure 5. Correlation in plaque quantification in the external test set.

Scatterplots for lipid arc (A), minimum fibrous cap thickness (B), calcium arc (C), calcium depth (D), and calcium thickness (E).

CI confidence interval; FCT fibrous cap thickness; ICC intraclass correlation coefficient..

Table 4. External test set: first observer as reference standard.

Class	Prevalence	TP frames	Accuracy (%)	Sensitivity (%)	Specificity (%)	PPV (%)	NPV (%)	Kappa/ICC[a]
Second observer vs. first observer								
Lipid plaque	132 (33.7%)	104 (78.8%)	78.1 (73.6-82.1)	78.8 (70.8-85.4)	77.7 (72.1-82.6)	64.2 (56.3-71.6)	87.8 (82.9-91.8)	0.535 (0.451-0.619)
Arc	-	-	-	-	-	-	-	0.516 (0.359-0.644)
Minimum FCT	-	-	-	-	-	-	-	0.392 (0.126-0.586)
LRP[b]	91 (23.2%)	64 (70.3%)	77.6 (73.1-81.6)	70.3 (59.8-79.5)	79.7 (74.7-84.1)	51.2 (42.1-60.2)	89.9 (85.6-93.2)	0.443 (0.347-0.539)
Calcified plaque	127 (32.4%)	115 (90.6%)	95.9 (93.5-97.6)	90.6 (84.1-95.0)	98.5 (96.2-99.6)	96.6 (91.6-99.1)	95.6 (92.4-97.7)	0.905 (0.860-0.950)
Arc	-	-	-	-	-	-	-	0.772 (0.566-0.869)
Depth	-	-	-	-	-	-	-	0.708 (0.569-0.802)
Thickness	-	-	-	-	-	-	-	0.803 (0.715-0.864)
Side branch	83 (21.2%)	77 (92.8%)	98.2 (96.4-99.3)	92.8 (84.9-97.3)	99.7 (98.2-100)	98.7 (93.1-100)	98.1 (95.9-99.3)	0.945 (0.906-0.984)
Thrombus	9 (2.3%)	6 (66.7%)	97.7 (95.7-98.9)	66.7 (29.9-92.5)	98.4 (96.6-99.4)	50.0 (21.1-78.9)	99.2 (97.7-99.8)	0.560 (0.303-0.817)
Plaque rupture	1 (0.3%)	1 (100%)	99.5 (98.2-99.9)	100 (2.5-100)	99.5 (98.2-99.9)	33.3 (0.8-90.6)	100 (99.1-100)	0.498 (-0.102-1.000)
Model prediction vs. first observer								
Lipid plaque	132 (33.7%)	100 (75.8%)	71.9 (67.2-76.3)	75.8 (67.5-82.8)	70.0 (64.0-75.5)	56.2 (48.6-63.6)	85.0 (79.6-89.5)	0.421 (0.333-0.509)
Arc	-	-	-	-	-	-	-	0.552 (0.389-0.679)
Minimum FCT	-	-	-	-	-	-	-	0.447 (0.200-0.624)
LRP[b]	91 (23.2%)	57 (62.6%)	80.4 (76.1-84.2)	62.6 (51.9-72.6)	85.7 (81.2-89.5)	57.0 (46.7-66.9)	88.4 (84.1-91.8)	0.467 (0.365-0.569)

Calcified plaque	127 (32.4%)	107 (84.3%)	90.8 (87.5-93.5)	84.3 (76.7-90.1)	94.0 (90.4-96.5)	87.0 (79.7-92.4)	92.6 (88.8-95.4)	0.789 (0.724-0.854)
Arc	-	-	-	-	-	-	-	0.742 (0.358-0.875)
Depth	-	-	-	-	-	-	-	0.797 (0.715-0.857)
Thickness	-	-	-	-	-	-	-	0.753 (0.627-0.835)
Side branch	83 (21.2%)	69 (83.1%)	93.6 (90.7-95.8)	83.1 (73.3-90.5)	96.4 (93.7-98.2)	86.3 (76.7-92.9)	95.5 (92.6-97.5)	0.806 (0.733-0.879)
Thrombus	9 (2.3%)	4 (44.4%)	97.4 (95.4-98.8)	44.4 (13.7-78.8)	98.7 (97.0-99.6)	44.4 (13.7-78.8)	98.7 (97.0-99.6)	0.431 (0.141-0.721)
Plaque rupture	1 (0.3%)	0 (0%)	97.2 (95.0-98.6)	0.0 (0.0-97.5)	97.4 (95.3-98.8)	0.0 (0.0-30.8)	99.7 (98.6-100)	-0.005 (-0.013-0.003)

Metrics are reported as value (95% confidence interval).

FC fibrous cap; FCT fibrous cap thickness; ICC intraclass correlation coefficient; LRP lipid-rich plaque; NPV negative predictive value; PPV positive predictive value; TP true-positive.

[a] *Kappa is calculated for categorical variables (lipid plaque, calcified plaque, side branch, thrombus, and plaque rupture) and ICC is calculated for continuous variables (lipid arc, minimum FCT, FC area, FC ratio calcium arc, calcium depth, and calcium thickness).*

[b] *defined as a lipid plaque with an arc ≥90°.*

Table 5. External test set: second observer as reference standard.

Class	Prevalence	TP frames	Accuracy (%)	Sensitivity (%)	Specificity (%)	PPV (%)	NPV (%)	Kappa/ICC[a]
First observer vs. second observer								
Lipid plaque	162 (41.3%)	104 (64.2%)	78.1 (73.6-82.1)	64.2 (56.3-71.6)	87.8 (82.9-91.8)	78.8 (70.8-85.4)	77.7 (72.1-82.6)	0.535 (0.451-0.619)
Arc	-	-	-	-	-	-	-	0.516 (0.359-0.644)
Minimum FCT	-	-	-	-	-	-	-	0.392 (0.126-0.586)
LRP[b]	125 (31.9%)	64 (51.2%)	77.6 (73.1-81.6)	51.2 (42.1-60.2)	89.9 (85.6-93.2)	70.3 (59.8-79.5)	79.7 (74.7-84.1)	0.443 (0.347-0.539)
Calcified plaque	119 (30.4%)	115 (96.6%)	95.9 (93.5-97.6)	96.6 (91.6-99.1)	95.6 (92.4-97.7)	90.6 (84.1-95.0)	98.5 (96.2-99.6)	0.905 (0.860-0.950)
Arc	-	-	-	-	-	-	-	0.772 (0.566-0.869)
Depth	-	-	-	-	-	-	-	0.708 (0.569-0.802)
Thickness	-	-	-	-	-	-	-	0.803 (0.715-0.864)
Side branch	78 (19.9%)	77 (98.7%)	98.2 (96.4-99.3)	98.7 (93.1-100)	98.1 (95.9-99.3)	92.8 (84.9-97.3)	99.7 (98.2-100)	0.945 (0.906-0.984)
Thrombus	12 (3.1%)	6 (50.0%)	97.7 (95.7-98.9)	50.0 (21.1-78.9)	99.2 (97.7-99.8)	66.7 (29.9-92.5)	98.4 (96.6-99.4)	0.560 (0.303-0.817)
Plaque rupture	3 (0.8%)	1 (33.3%)	99.5 (98.2-99.9)	33.3 (0.8-90.6)	100.0 (99.1-100)	100.0 (2.5-100)	99.5 (98.2-99.9)	0.498 (-0.102-1.000)
Model prediction vs. second observer								
Lipid plaque	162 (41.3%)	142 (87.7%)	85.7 (81.9-89.0)	87.7 (81.6-92.3)	84.3 (79.0-88.8)	79.8 (73.1-85.4)	90.7 (85.9-94.2)	0.710 (0.639-0.781)
Arc	-	-	-	-	-	-	-	0.630 (0.466-0.742)
Minimum FCT	-	-	-	-	-	-	-	0.449 (0.309-0.571)
LRP[b]	125 (31.9)	83 (66.4%)	84.9 (81.0-88.3)	66.4 (57.4-74.6)	93.6 (90.0-96.2)	83.0 (74.2-89.8)	85.6 (81.1-89.4)	0.634 (0.550-0.718)

Calcified plaque	119 (30.4%)	107 (89.9%)	92.9 (89.8-95.2)	89.9 (83.0-94.7)	94.1 (90.7-96.6)	87.0 (79.7-92.4)	95.5 (92.3-97.7)	0.833 (0.774-0.892)
Arc	-	-	-	-	-	-	-	0.895 (0.840-0.930)
Depth	-	-	-	-	-	-	-	0.851 (0.784-0.898)
Thickness	-	-	-	-	-	-	-	0.682 (0.566-0.772)
Side branch	78 (19.9%)	65 (83.3%)	92.9 (89.8-95.2)	83.3 (73.2-90.8)	95.2 (92.2-97.3)	81.2 (71.0-89.1)	95.8 (93.0-97.8)	0.778 (0.700-0.856)
Thrombus	12 (3.1%)	4 (33.3%)	96.7 (94.4-98.2)	33.3 (9.9-65.1)	98.7 (97.0-99.6)	44.4 (13.7-78.8)	97.9 (95.9-99.1)	0.364 (0.095-0.633)
Plaque rupture	3 (0.8%)	1 (33.3%)	97.2 (95.0-98.6)	33.3 (0.8-90.6)	97.7 (95.7-98.9)	10.0 (0.3-44.5)	99.5 (98.1-99.9)	0.144 (-0.123-0.411)

Metrics are reported as value (95% confidence interval).

FC fibrous cap; FCT fibrous cap thickness; ICC intraclass correlation coefficient; LRP lipid-rich plaque; NPV negative predictive value; PPV positive predictive value; TP true-positive.

[a] *Kappa is calculated for categorical variables (lipid plaque, calcified plaque, side branch, thrombus, and plaque rupture) and ICC is calculated for continuous variables (lipid arc, minimum FCT, FC area, FC ratio calcium arc, calcium depth, and calcium thickness).*

[b] *defined as a lipid plaque with an arc ≥90°.*

Algorithm misidentification

Exemplary images of disagreement between the reference standard and the prediction by OCT-AID are presented in Figure 6. Among false-positive predictions of lipid, 38.9% (7/18) in the internal test set and 27.6% (8/29) in the external test set were predictions of lipid behind large calcifications. False-positive lipid diagnoses were also found in presence of attenuating artefacts (22.2% in the internal test set and 13.8% in the external test set). Regarding the low positive predictive value for plaque rupture, the majority of false-positive predictions were found in frames exhibiting thrombus without plaque rupture.

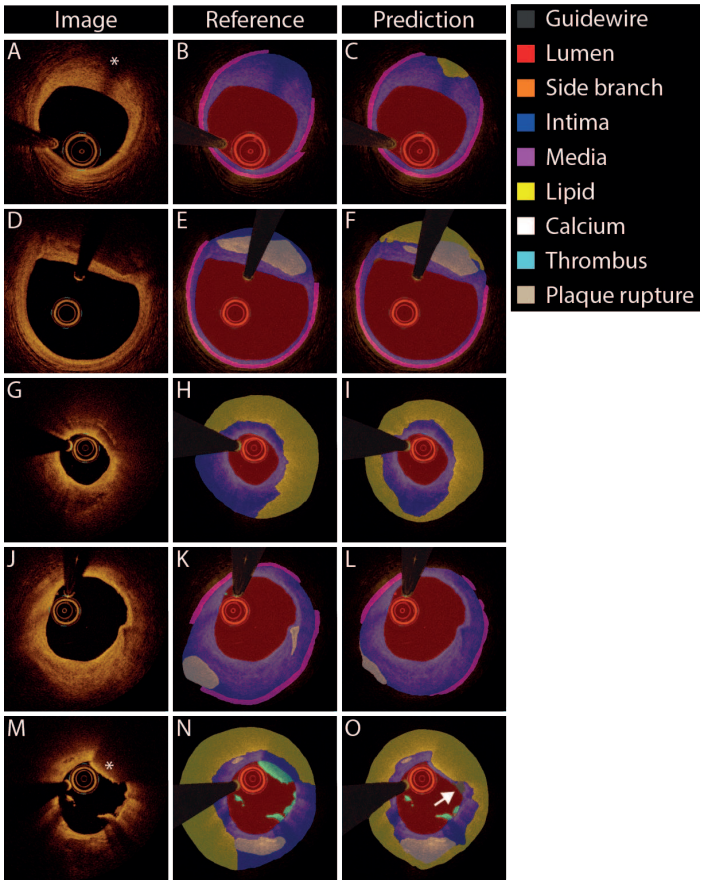


Figure 6. Algorithm misidentification.

Examples of the cross-sectional optical coherence tomography image (left column), reference standard (middle column) and prediction by OCT-AID (right column) in the held-out test set. False positive predictions of lipid due to artefacts (A-C, asterisk in A) or at the abluminal side of a large calcified plaque (D–F). Overestimation of the lipid arc in presence of a large layered plaque/intraplaque hemorrhage (G–I). False negative prediction of a small calcification, resulting in a substantial underestimation of the calcium depth (J–L). False prediction of plaque rupture (arrow in O) and false negative prediction of thrombus at 2 O' clock (asterisk in M) (M–O).

Inference time

Inference was run on a NVIDIA GeForce RTX 3080 with 64 gigabytes of memory. Mean analysis time was 0.84 ± 0.03 s/frame, including 0.05 ± 0.02 s/frame for pre-processing, 0.73 ± 0.03 s/frame for inference, and 0.07 ± 0.01 s/frame for post-processing.

DISCUSSION

The proposed OCT-AID algorithm for multiclass semantic segmentation of intracoronary OCT images achieved promising performance for semantic segmentation and frame-wise identification of several plaque-related and non-plaque-related features. Besides conventional plaque quantification, for which the reliability was overall moderate to excellent, OCT-AID allows further volumetric plaque quantification. Importantly, these results were obtained while including difficult frames, such as those containing artefacts (Figure 3A–C; Supplementary material online, Video S2) or destabilized plaques (Figure 5M–O), which is in contrast to earlier works. With future improvements addressing its current challenges, including optimization of the algorithm for combined or destabilized plaques, and optimization of inference times, OCT-AID has the potential to allow accurate, standardized OCT image interpretation and reduce interobserver variability.

Evolution of artificial intelligence models for optical coherence tomography analysis

Time-consuming image analysis of intracoronary OCT images and substantial intraobserver and interobserver variability remain a clinical challenge.[6-8] As a result, real-time evaluation during a clinical procedure is limited to scanning of pullbacks, and *post hoc* core lab analyses are generally limited to single frame evaluations at set intervals. To overcome these challenges, several AI-based approaches have been investigated previously. However, these were predominantly classification algorithms or segmentation models with a limited number of classes.[9]

Conversely, OCT-AID was trained for comprehensive image interpretation. The average Dice score of our approach was 0.659 across nine classes, including an excellent performance for semantic segmentation of the lumen, intima and media. For lipid and calcified plaques, Dice scores among true-positive frames were 0.763 ± 0.135 and 0.716 ± 0.264. However, expressing the model performance for semantic segmentation of lipid and thick calcified plaques in terms of Dice score may be inadequate, owing to the limited penetration depth of OCT. Indeed, the arc correspondence scores of 0.902 ± 0.120 and 0.829 ± 0.193 for lipid and calcified plaques confirm the ability of our algorithm to correctly localize these plaques. These results were obtained within <1 s/frame using hardware feasible for daily clinical care, which is considerably faster compared with manual labelling, which can take up to 30 min/frame but slightly slower than the median in a recent systematic review.[9] However, our algorithm provides multiclass segmentation, while the referenced median value also comprises algorithms for single class

segmentation. Nevertheless, higher-end hardware and model adaptions may further reduce inference times to wards real-time full-vessel segmentation.

Only a limited number of other multiclass segmentation models have been proposed previously. Shibutani et al. developed a DL algorithm for multiclass (fibrocalcific plaque, pathological intimal thickening, lipid plaque, layered plaque, and background) semantic segmentation using 1103 OCT frames, co-registered with histopathology, as reference standard. In the held-out test set, the Jaccard index for lipid, calcified, and layered plaques were 0.45, 0.51, and 0.36, respectively.[15] Chu et al. used a U-net for multiclass (fibrous plaque, lipid plaque, calcified plaque, cholesterol crystals, macrophages, microvessels, guidewire artefact, side branches, and internal elastic lamina) semantic segmentation and achieved a mean per class Dice score of 0.764. The Dice score for lipid and calcified plaques were 0.772 and 0.848 in internal testing and accuracy for region-wise identification of these plaques were 90.5% and 88.5% in external testing.[16] Comparing those results to the present findings is however challenging for several reasons. First and foremost, it is generally unclear whether Dice scores in previous efforts were published on true-positive frames only or whether false-positive and false-negative frames were also included. Hence, we report our metrics in both scenarios to allow future comparison of our results to other algorithms. Second, challenging frames exhibiting plaque rupture, thrombus, dissections, and intramural hematoma were excluded by Chu et al. Third, expert analysts were asked to classify pre-delineated regions for external testing in the study by Chu et al., which may have biased their decision-making, compared with evaluation of a non-delineated frame as was performed in the present study.

The performance in the external test set appeared lower for some classes compared with the internal test set. We hypothesize that the difference in study population between the two sets had the most profound effect on this disparity. In particular, the internal test set comprised images of non-obstructive lesions performed for research purposes, while the external dataset contained OCT images from daily clinical care, which are more likely to be obstructive as OCT is predominantly performed for stent guidance and optimization. Therefore, future data enrichment for obstructive and potentially culprit lesions is warranted. Additionally, large scale external testing studies, including a web-based reader study, are needed and being planned to confirm the findings of the present study.

Lipid plaque identification and quantfication

Identification and quantification of lipid plaques is particularly challenging for humans, as highlighted by the substantial interobserver variability for these tasks in the present study and in literature.[7] For automated identification of lipid plaques, the performances of our proposed methodology were at least on par with manual interobserver agreement by two expert readers. However, difficulties remain in specific situations, including presence of combined lipid and calcified (Figure 6D–F), layered (Figure 6G–I), or destabilized plaques (Figure 6M–O). Particularly, we observed that a substantial proportion of false-positive predictions were related to lipid predictions behind large calcifications. From a clinical point of view, identification of such deep lipid plaques may have limited value, which may have led to a lower identification rate by the independent assessors. In contrast, semantic segmentation requires labelling of each pixel which may have led to the models' overprediction of lipid in these deep-lying low

intensity areas. However, judging by experience from newest generation OCT catheters with superior penetration depth, the algorithm may also be correct.[17] Future histology-based evaluation studies of AI-algorithms may provide additional insights.

OCT-AID also allows quantification of lipid plaques including the fibrous cap. So far, identification of high-risk plaques predominantly relies on manual single-point measures of the FCT, which may only provide a part of the puzzle as it omits volumetric and spatial information.[18] The earliest approaches for automated quantification of the fibrous cap were based on mathematical models related to changes in light intensity.[19-21] DL has been tested to this regard more recently. An algorithm proposed by Lee et al. significantly underestimated the minimum FCT (0.121 ± 0.024 vs. 0.151 ± 0.035 mm).[22] In another hybrid approach, using both DL and dynamic programming, the mean difference in the minimum FCT between two users was of 4.2 ± 14.6 µm after manual modification of the FCT in 5.5 ± 0.9% of frames.[23] However, these values only reflect the interuser reproducibility, and a comparison between the algorithm-derived FCT with manual measurement is lacking. In a recent study specifically targeting segmentation of the fibrous cap, the R^2 for mean FCT was 0.909 in a held-out test set comprising 1362 images from 74 pullbacks.[24] However, the FCT was evaluated on A-lines which can result in an overestimation in cases with eccentric OCT catheter placement, and the minimum FCT was not evaluated.

Our approach demonstrates promising results for quantification of the fibrous cap, including area-based measures with moderate to excellent reliability for the fibrous cap ratio. These area-based measures can be transformed in volumetric measures that provide theoretical benefits compared with single-point measurement, so far not tested in studies. Indeed, an association between such volumetrics measures and clinical outcome is yet to be established and our area-based measures require external validation.

Calcified plaque identification

OCT-AID achieved particularly high performance for the identification and quantification of calcified plaques. However, a small number of outliers negatively impacted the correlation coefficients (Figure 6J–L; Supplementary material online, Figure S2C-D). Additionally, Bland-Altman analysis revealed a slight underestimation of the model compared with the reference standard for calcium arc and thickness.

The proposed algorithm may allow differentiating distinct calcification types based on their depth, arcs and volumes. Additionally, elaborate calcified plaque quantification can become helpful for downstream tasks such as the prediction of acute procedural success. To that regard, Gharaibeh et al. recently demonstrated that a machine learning algorithm with multiple lumen and calcification-related features, including calcification area and volume, outperformed the conventional calcium score for the prediction of stent expansion.[25] These results indicate that additional predictive value can be obtained by incorporating more elaborate calcification-related variables. However, these cannot be obtained manually on-site, emphasizing the need for automated analyses.

Thrombus and plaque rupture identification

In the present study, the model performance for the identification of thrombus and especially plaque rupture was substantially lower than for other classes. However, the low prevalence of these classes

precluded a thorough evaluation. Nevertheless, we observed that OCT-AID had the tendency to predict presence of plaque rupture whenever there was thrombus predicted (Figure 6M–O), which requires further attention. However, our rationale to include these classes was to provide contextual information and to increase the generalizability of our algorithm by, in contrast to previous attempts, not excluding such frames. Separate dedicated algorithms targeting identification of such features will likely be more efficient and could subsequently be combined with a multiclass model.

LIMITATIONS

This study has some limitations. First, only non-flow limiting non-culprit lesions were used for training and internal testing. However, the external test set comprised a diverse dataset of patients undergoing clinically indicated OCT. Second, the outer border of the lipid pool was estimated based on the visible parts of the media and it has not been correlated to intracoronary ultrasound. This inherent limitation of intracoronary OCT limits the evaluation of plaque burden. Third, although images with artefacts were included in the training and test sets, those with severe artefacts limiting accurate manual segmentation were excluded. Increasing the number of frames with moderate artefacts may enhance the generalizability. Fourth, the performance of OCT-AID for the segmentation and identification of plaque rupture and to a smaller degree thrombus was suboptimal and requires further attention and enrichment of the dataset for these classes. Last, computational constraints precluded incorporation of a large number of frames in the pseudo-3D approach or a full 3D approach.

CONCLUSIONS

Our proposed OCT-AID algorithm for multiclass semantic segmentation of intracoronary OCT images demonstrated promising capabilities for the identification and quantification of various non-plaque-related and plaque-related features. Importantly, these results were obtained while including difficult frames, such as those containing artefacts or de stabilized plaques, which is in contrast to earlier works. This algorithm has the potential to allow comprehensive and standardized OCT image interpretation.

REFERENCES

1. Stone GW, Christiansen EH, Ali ZA, Andreasen LN, Maehara A, Ahmad Y et al. Intravascular imaging-guided coronary drug-eluting stent implantation: an updated network meta-analysis. Lancet 2024;403:824-837.
2. Vrints C, Andreotti F, Koskinas KC, Rossello X, Adamo M, Ainslie J et al. 2024 ESC Guidelines for the management of chronic coronary syndromes. Eur Heart J 2024;45:3415-3537.
3. Araki M, Park SJ, Dauerman HL, Uemura S, Kim JS, Di Mario C et al. Optical coherence tomography in coronary atherosclerosis assessment and intervention. Nat Rev Cardiol 2022;19:684-703.
4. Mol JQ, Volleberg R, Belkacemi A, Hermanides RS, Meuwissen M, Protopopov AV et al. Fractional Flow Reserve-Negative High-Risk Plaques and Clinical Outcomes After Myocardial Infarction. JAMA Cardiol 2023;8:1013-1021.
5. Fazel R, Yeh RW, Cohen DJ, Rao SV, Li S, Song Y et al. Intravascular imaging during percutaneous coronary intervention: temporal trends and clinical outcomes in the USA. Eur Heart J 2023;44:3845-3855.
6. Koskinas KC, Nakamura M, Raber L, Colleran R, Kadota K, Capodanno D et al. Current use of intracoronary imaging in interventional practice - Results of a European Association of Percutaneous Cardiovascular Interventions (EAPCI) and Japanese Association of Cardiovascular Interventions and Therapeutics (CVIT) Clinical Practice Survey. EuroIntervention 2018;14:e475-e484.
7. Kini AS, Vengrenyuk Y, Yoshimura T, Matsumura M, Pena J, Baber U et al. Fibrous Cap Thickness by Optical Coherence Tomography In Vivo. J Am Coll Cardiol 2017;69:644-657.
8. Gruslova AB, Singh S, Hoyt T, Vela D, Vengrenyuk Y, Buja LM et al. Accuracy of OCT Core Labs in Identifying Vulnerable Plaque. JACC Cardiovasc Imaging 2024;17:448-450.
9. van der Waerden RGA, Volleberg R, Luttikholt TJ, Cancian P, van der Zande JL, Stone GW et al. Artificial intelligence for the analysis of intracoronary optical coherence tomography images: a systematic review. Eur Heart J Digit Health 2025;6:270-284.
10. Mol JQ, Belkacemi A, Volleberg RH, Meuwissen M, Protopopov AV, Laanmets P et al. Identification of anatomic risk factors for acute coronary events by optical coherence tomography in patients with myocardial infarction and residual nonflow limiting lesions: rationale and design of the PECTUS-obs study. BMJ Open 2021;11:e048994.
11. Yushkevich PA, Yang G, Gerig G. ITK-SNAP: An interactive tool for semi-automatic segmentation of multi-modality biomedical images. Annu Int Conf IEEE Eng Med Biol Soc 2016;2016:3342-3345.
12. Isensee F, Jaeger PF, Kohl SAA, Petersen J, Maier-Hein KH. nnU-Net: a self-configuring method for deep learning-based biomedical image segmentation. Nat Methods 2021;18:203-211.
13. McHugh ML. Interrater reliability: the kappa statistic. Biochem Med (Zagreb) 2012;22:276-82.
14. Koo TK, Li MY. A Guideline of Selecting and Reporting Intraclass Correlation Coefficients for Reliability Research. J Chiropr Med 2016;15:155-63.
15. Shibutani H, Fujii K, Ueda D, Kawakami R, Imanaka T, Kawai K et al. Automated classification of coronary atherosclerotic plaque in optical frequency domain imaging based on deep learning. Atherosclerosis 2021;328:100-105.
16. Chu M, Jia H, Gutierrez-Chico JL, Maehara A, Ali ZA, Zeng X et al. Artificial intelligence and optical coherence tomography for the automatic characterisation of human atherosclerotic plaques. EuroIntervention 2021;17:41-50.
17. Ali ZA, Dager A, Zuniga M, Fonseca J, Arana C, Chamie D et al. First-in-Human Experience With a Novel Multimodality DeepOCT-NIRS Intracoronary Imaging System. J Soc Cardiovasc Angiogr Interv 2024;3:101344.
18. Sun J, Singh P, Shami A, Kluza E, Pan M, Djordjevic D et al. Spatial Transcriptional Mapping Reveals Site-Specific Pathways Underlying Human Atherosclerotic Plaque Rupture. J Am Coll Cardiol 2023;81:2213-2227.

19. Zahnd G, Karanasos A, van Soest G, Regar E, Niessen W, Gijsen F et al. Quantification of fibrous cap thickness in intracoronary optical coherence tomography with a contour segmentation method based on dynamic programming. Int J Comput Assist Radiol Surg 2015;10:1383-94.

20. Wang Z, Chamie D, Bezerra HG, Yamamoto H, Kanovsky J, Wilson DL et al. Volumetric quantification of fibrous caps using intravascular optical coherence tomography. Biomed Opt Express 2012;3:1413-26.

21. Radu MD, Yamaji K, Garcia-Garcia HM, Zaugg S, Taniwaki M, Koskinas KC et al. Variability in the measurement of minimum fibrous cap thickness and reproducibility of fibroatheroma classification by optical coherence tomography using manual versus semi-automatic assessment. EuroIntervention 2016;12:e987-e997.

22. Lee J, Prabhu D, Kolluru C, Gharaibeh Y, Zimin VN, Bezerra HG et al. Automated plaque characterization using deep learning on coronary intravascular optical coherence tomographic images. Biomed Opt Express 2019;10:6497-6515.

23. Lee J, Pereira GTR, Gharaibeh Y, Kolluru C, Zimin VN, Dallan LAP et al. Automated analysis of fibrous cap in intravascular optical coherence tomography images of coronary arteries. Sci Rep 2022;12:21454.

24. Lee J, Kim JN, Dallan LAP, Zimin VN, Hoori A, Hassani NS et al. Deep learning segmentation of fibrous cap in intravascular optical coherence tomography images. Sci Rep 2024;14:4393.

25. Gharaibeh Y, Lee J, Zimin VN, Kolluru C, Dallan LAP, Pereira GTR et al. Prediction of stent under-expansion in calcified coronary arteries using machine learning on intravascular optical coherence tomography images. Sci Rep 2023;13:18110.

SUPPLEMENTAL MATERIAL

Supplemental material related to this article can be found in the online version:
https://academic.oup.com/ehjdh/article/6/3/404/8078941





CHAPTER 15

Real-world external validation of artificial intelligence-based full-vessel segmentation for intracoronary optical coherence tomography

Rick Volleberg | Doosup Shin | Ruben van der Waerden | Craig Porter | Susan Thomas | Fernando Sosa | Simone Saitta | Aysun Cetinyurek-Yavuz | Joske van der Zande | Thijs Luttikholt | Pierandrea Cancian | Xiaojin Gu | Leah Heil | Jos Thannhauser | Clara Sánchez | Bram van Ginneken | Ivana Išgum | Allen Jeremias | Evan Shlofmitz | Richard Shlofmitz | Ziad Ali* | Niels van Royen*

Journal of the American Heart Association
In press

** joined senior authorship*

ABSTRACT

Background Artificial intelligence (AI) allows automated evaluation of intracoronary optical coherence tomography (OCT) images. However, algorithms are mostly developed and validated on well-curated datasets, which may not represent real-world data.

Objectives We sought to externally validate a previously developed algorithm performing full-vessel segmentation for OCT in an unselected consecutive real-world dataset.

Methods This was a retrospective, single-center, external validation study comprising 100 consecutive patients undergoing clinically indicated OCT. A previously developed algorithm (OCT-AID) was used for automated pixelwise labeling of OCT images, distinguishing among lumen, guidewire artefact, intima, media, lipid plaque, calcium plaque, side branch, plaque rupture, thrombus, microvessel and background. The AI-based predictions were compared on a frame level to the reference standard obtained through manual OCT image analysis by expert readers.

Results Among 2560 analyzable frames, the agreement between the automated OCT image analysis and the reference standard was excellent for calcified plaque identification (κ=0.88, 95% confidence interval [CI] 0.84-0.92) and quantification (intraclass correlation coefficient [ICC] values ranged between 0.79 and 0.93), with a performance close to interobserver variability. For lipid plaque identification and quantification, the model performance was reasonable (κ=0.68, 95% CI 0.64-0.72; ICC for lipid arc 0.79, 95% CI 0.76-0.81; ICC for minimum fibrous cap thickness 0.59, 95% CI 0.55-0.63) and largely superior to interobserver variability. The algorithm performance for low-prevalence features (e.g. plaque rupture) was limited.

Conclusions AI-based fully automated evaluation of OCT images is feasible with performances consistent with interobserver variability in a real-world dataset of consecutive patients, supporting generalizability of the proposed methodology.

INTRODUCTION

Recently updated guidelines have strengthened their endorsement of intracoronary optical coherence tomography (OCT) for guiding coronary revascularization.[1,2] Furthermore, the prognostic value of OCT is supported by a growing body of evidence.[3] Accurate and comprehensive evaluation of OCT image features is paramount to guide real-time decision making. However, the time-demanding nature of OCT image interpretation and lack of operator familiarity may limit widespread clinical adoption.[4] Subjectiveness in image interpretation and consequent interobserver variability impede leveraging the details available within OCT pullbacks.[5,6]

Artificial intelligence (AI)-based automated OCT image analysis has been shown to have the potential to overcome these limitations.[7] However, previous studies on proposed algorithms were frequently at substantial risk of bias, particularly due to the lack of robust external validation.[7] For the small number of algorithms that underwent external validation, the external validation datasets were modestly sized and frequently comprised a selective cohort of patients and frames, precluding a thorough evaluation of the generalizability of the respective models.

We recently developed and validated OCT-AID, a deep learning-based algorithm for comprehensive full-vessel segmentation for intracoronary OCT. In the first internal and external validation study, this algorithm demonstrated high accuracy for atherosclerotic plaque identification and quantification.[8] However, for such an algorithm to be clinically valuable, it requires generalizability with high performance in diverse and real-world datasets, which so far has not been demonstrated. This study aimed to externally validate the performance of OCT-AID in relation to the interobserver variability in a consecutive, real-world cohort of patients undergoing OCT, that was not used for training or internal testing of OCT-AID.

METHODS

Study design and study population

The study was performed in accordance with the Declaration of Helsinki. Written informed consent was waived by the institutional Review Board at St. Francis Hospital & Heart Center due to minimal risk. The data underlying this article are available from the corresponding author upon reasonable request. The code and annotated data underlying this manuscript cannot be made publicly available due to funding source restrictions.

One hundred consecutive patients undergoing clinically indicated intracoronary OCT at St. Francis Hospital & Heart Center (Roslyn, NY, USA) with at least one analyzable baseline OCT pullback were retrospectively evaluated. Baseline OCT pullbacks were considered ineligible if obtained after balloon angioplasty for an uncrossable lesion, from a bypass graft, if the targeted lesion was in-stent restenosis, or if image quality at the target lesion was insufficient.

OCT imaging acquisition and data handling

All OCT pullbacks were acquired using the Dragonfly Optis or Dragonfly Opstar imaging catheter (Abbott Vascular, USA) according to a standard protocol with a 75 mm pullback length (image acquisition speed 36 mm/s) after manual contrast injection. Data were exported in DICOM format in Cartesian coordinates with a field of view set to 7 mm or 9 mm, a size of 704x704 pixels per frame, and spatial resolution of 9.9x9.9 µm or 12.8x12.8 µm per pixel, respectively. All data were pseudonymized prior to analysis.

Manual OCT image interpretation

OCT pullbacks were analyzed by five investigators with 5-17 years of experience in OCT image interpretation in accordance with contemporary consensus.[9] Each pullback was read independently by two readers, blinded to each other's interpretations and to the automated analysis results. OCT image analyses were performed at 2 mm intervals (every 10 frames), excluding frames with severe artefacts, visible stent struts, ectatic vessel segments, or those obtained within the guiding (extension) catheter. Readers were allowed to scroll through the pullbacks. In case of multiple baseline OCT pullbacks covering the same segment, the overlapping segment was analyzed from a single pullback.

Included images were analyzed for the presence or absence of lipid plaque, calcified plaque, side branch, plaque rupture, thrombus, and microvessel. Lipid plaques were subsequently quantified by minimum fibrous cap thickness (FCT) and lipid arc. If multiple non-overlapping lipid arcs were present within a single frame, the arcs were summed. Furthermore, arcs were measured continuously across the guidewire artefact when the same plaque type was present on both sides. Thin-cap fibroatheroma (TCFA) was defined as a lipid plaque with a minimum FCT <65 µm and a lipid arc ≥90°, and a lipid rich plaque as a lipid plaque with a lipid arc ≥90°. For calcified plaques, minimum calcium depth (minimum distance from the lumen border to the most proximal calcium border), maximum calcium thickness (maximum distance between the adluminal and abluminal calcium border), and calcium arc (sum of all calcium arcs) were obtained for each frame.

Discrepant cases between the two readings were evaluated by a third investigator to obtain the final reference standard. For arc measurements, a discrepancy was defined as an absolute difference between the two readings of >30°. For depth or thickness measurements, a discrepancy was defined as a combined relative difference of >10% compared with the mean value of the two readings and an absolute difference >60 µm between the two values. For plaque quantification measures not classified as discrepant, the mean of the two readings was used as the final reference standard.

Automated OCT image analysis

OCT-AID was used for automated image analysis of the complete OCT pullback. Details on the initial development and evaluation were published previously.[8] This study utilizes the latest iteration based on the nnU-Net version 2.[10] This algorithm was trained to segment lumen, guidewire artefact, intima, media, lipid plaque, calcium plaque, side branch, plaque rupture, thrombus, microvessel and background. The model was trained on 4300 frames using stratified five-fold cross-validation, ensuring that data from the same patient did not appear in both training and validation sets. An independent set of 218 frames from

different patients was used for internal testing. Data from the internal test set were not used during model training or hyperparameter tuning. Details on the algorithm are summarized in Supplemental Method 1. In brief, the algorithm operates on a pseudo-3D input (±3 OCT images in Cartesian coordinates) to incorporate longitudinal spatial context, and provides a 2D semantic segmentation of the central frame. To remove small isolated pixel areas of predicted lumen, guidewire artefact, intima, media, lipid plaque, calcium plaque, side branch, and background, algorithm predictions were post-processed using connected component analysis as detailed elsewhere.[8] Post-processing was not applied to plaque rupture, thrombus and microvessel, considering that pixel areas of these classes can be naturally small. The minimum FCT, lipid arc, minimum calcium depth, maximum calcium thickness and calcium arc were obtained from the segmentation predictions as detailed elsewhere.[8] The obtained measurements were used to identify the presence of TCFA and lipid-rich plaque. The AI-based predictions were compared on a frame level to the final reference standard, in which a frame was considered AI-positive for a specific class if at least one pixel belonging to that class was present in the final prediction after post-processing.

Statistical analysis

Categorical variables are expressed in absolute numbers (percentages) while continuous variables are summarized as mean ± standard deviation or as median (interquartile range), as appropriate. Missing data were not imputed. Interobserver variability between the two expert readings and the agreement between the automated OCT image analysis and the final reference standard were evaluated using conventional performance metrics and unweighted Cohen's kappa for frame-wise binary identification of the evaluated classes (presence vs. absence). Plaque quantification variables were evaluated using the intraclass correlation coefficient (ICC) for absolute agreement in a one-way random model. Bias and limits of agreement were evaluated using Bland-Altman analysis. Ninety-five percent confidence intervals were calculated for all performance metrics. Differences between individual kappa or ICC values were evaluated using bootstrapping with 1000 resamples. No formal sample size calculation was performed. Statistical significance was achieved when a two-sided p-values was less than 0.05. No multiplicity correction was performed. Statistical analyses were performed using IBM SPSS Statistics software version 29.0 (IBM Corp., USA) and R version 4.4.1 (R Foundation for Statistical Computing, Austria).

RESULTS

Study population

Between January 1st 2022 and February 16th 2022, 146 consecutive patients underwent clinically indicated OCT, of whom 100 patients with eligible baseline OCT pullbacks were included in the final analysis (Figure 1). The mean age of included patients was 66 ± 11 years, and 76 (76.0%) were male (Table 1). The majority of patients underwent invasive coronary angiography for chronic coronary syndrome or

silent ischemia (54.0%) or unstable angina (40.0%). At least one imaged lesion was revascularized after baseline OCT in 79.0% of patients.

Out of 4218 frames from 111 pullbacks in 100 patients, 2560 (60.7%) frames were included in the final analysis, after excluding 1043 (24.7%) frames of the guiding (or extension) catheter, 108 (2.6%) frames with stent struts, 92 (2.2%) frames from overlapping segments, 27 (0.6%) frames of ectatic vessel segments, and 388 (9.2%) frames with insufficient image quality, of which 318 (82.0%) were located at the proximal or distal end of the pullback (Figure 1).

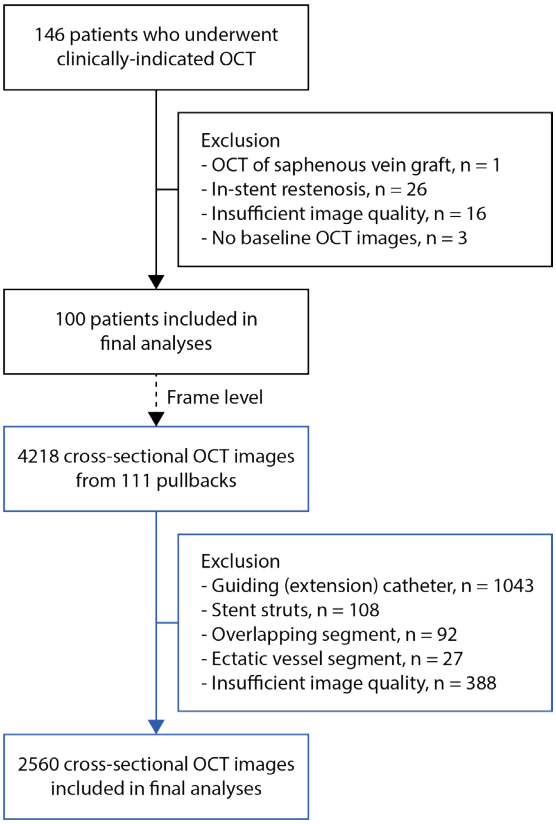


Figure 1. Study flowchart.

OCT optical coherence tomography.

Table 1. Baseline characteristics.

Characteristic	Total Population N=100
Age, years	66 ± 11
Male sex	76 (76.0)
BMI, kg/m^2	29.0 ± 6.0
Hypertension	75 (75.0)
Diabetes mellitus	35 (35.0)
Hyperlipidemia	77 (77.0)
Current smoking status	9 (9.0)
Previous myocardial infarction	17 (17.0)
Previous percutaneous coronary intervention or CABG	35 (35.0)
Indication for invasive coronary angiography	
CCS/silent ischemia	54 (54.0)
Unstable angina	40 (40.0)
NSTEMI	5 (5.0)
STEMI	1 (1.0)
Revascularization of ≥1 imaged lesion	79 (79.0)

Values are number (%) or mean ± standard deviation.

BMI body mass index; CABG coronary artery bypass grafting; CCS chronic coronary syndrome; NSTEMI non-ST-segment elevation myocardial infarction; STEMI ST-segment elevation myocardial infarction.

Interobserver variability among expert readers

The interobserver agreement between expert readers is summarized in Table 2. Two expert readers agreed on the presence and absence of lipid plaque in 51.2% and 28.0% of frames, respectively (κ = 0.58, 95% CI 0.54-0.61) and on calcified plaque in 41.6% and 53.5% of frames, respectively (κ = 0.90, 95% CI 0.86-0.94). Across frames without any calcified plaque according to both expert readings, the kappa value for lipid plaques was 0.76 (95% CI 0.70-0.81). The kappa values for the presence of absence of a side branch, plaque rupture, thrombus and microvessel were 0.88 (95% CI 0.84-0.92), 0.66 (95% CI 0.63-0.70), 0.55 (95% CI 0.51-0.59), and 0.63 (95% CI 0.59-0.67), respectively.

The scatterplots and Bland-Altman plots comparing the two expert readings for lipid and calcified plaque quantification are reported in Supplemental Figures 1-2. The ICC for the minimum FCT and lipid arc were 0.55 (95% CI 0.51-0.59) and 0.64 (95% CI 0.61-0.67), respectively. Based on these measurements, interobserver agreement was fair for TCFA (κ = 0.30, 95% CI 0.26-0.33) and moderate for lipid-rich plaque (κ = 0.54, 95% CI 0.50-0.57). The ICC for the minimum calcium depth, maximum calcium thickness and calcium arc were 0.93 (95% CI 0.92-0.93), 0.80 (95% CI 0.78-0.82), and 0.94 (95% CI 0.93-0.95), respectively

Table 2. Interobserver agreement and AI performance for feature identification.

	Interobserver*	Model prediction versus final reference standard							
	Kappa	Prevalence	Kappa	Accuracy, %	Sensitivity, %	Specificity, %	PPV, %	NPV, %	P-value†
Lipid plaque	0.58 (0.54-0.61)	1393 (54.4%)	0.68 (0.64-0.72)	83.9 (82.4-85.3)	77.1 (74.8-79.3)	92.0 (90.3-93.5)	92.0 (90.3-93.5)	77.1 (74.8-79.3)	<0.001
TCFA	0.30 (0.26-0.33)	51 (2.0%)	0.27 (0.23-0.30)	98.0 (97.3-98.5)	19.6 (9.8-33.1)	99.6 (99.2-99.8)	47.6 (25.7-70.2)	98.4 (97.8-98.8)	0.71
Lipid-rich plaque	0.54 (0.50-0.57)	893 (34.9%)	0.72 (0.68-0.76)	87.9 (86.5-89.1)	73.7 (70.7-76.5)	95.4 (94.3-96.4)	89.6 (87.2-91.8)	87.1 (85.5-88.6)	<0.001
Calcified plaque	0.90 (0.86-0.94)	1145 (44.7%)	0.88 (0.84-0.92)	93.9 (93.0-94.8)	91.4 (89.7-93.0)	96.0 (94.8-96.9)	94.8 (93.4-96.1)	93.3 (91.9-94.5)	0.022
Side branch	0.88 (0.84-0.92)	511 (20.0%)	0.78 (0.75-0.82)	93.3 (92.2-94.2)	79.6 (75.9-83.1)	96.7 (95.8-97.4)	85.7 (82.2-88.7)	95.0 (94.0-95.9)	<0.001
Plaque rupture	0.66 (0.63-0.70)	21 (0.8%)	0.33 (0.29-0.36)	98.0 (97.3-98.5)	61.9 (38.4-81.9)	98.3 (97.7-98.7)	22.8 (12.7-35.8)	99.7 (99.4-99.9)	0.006
Thrombus	0.55 (0.51-0.59)	42 (1.6%)	0.40 (0.36-0.43)	96.3 (95.5-97.0)	78.6 (63.2-89.7)	96.6 (95.8-97.3)	27.7 (19.9-36.7)	99.6 (99.3-99.8)	0.09
Microvessel	0.63 (0.59-0.67)	167 (6.5%)	0.63 (0.59-0.66)	94.5 (93.6-95.4)	79.6 (72.7-85.5)	95.6 (94.7-96.4)	55.6 (49.1-62.1)	98.5 (98.0-99.0)	0.93

Performance metrics are reported as value (95% confidence interval). Prevalence is reported as number of frames (percentage).

NPV negative predictive value; PPV positive predictive value; TCFA thin-cap fibroatheroma.

** Evaluated between two independent expert readings.*

† Comparison of kappa values.

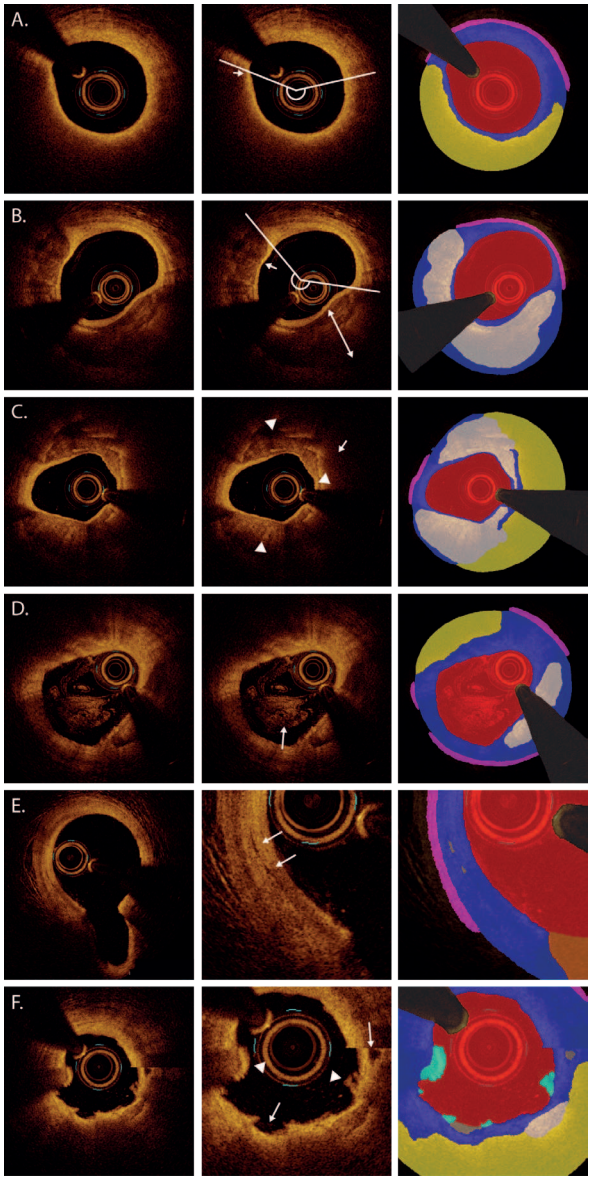


Figure 2. Manual and automated OCT image analysis.

Cross-sectional OCT images (left column), with expert OCT image interpretation (middle column) and automated OCT image analysis (right column). A) Lipid plaque with a manually measured lipid arc of 214° and a minimum fibrous cap thickness of 60 µm (arrow), and an AI-derived lipid arc of 190° and a minimum fibrous cap thickness of 63 µm. B) Calcified plaque with a manually measured calcium arc of 200°, a minimum calcium depth of 40 µm (arrow) and a maximum calcium thickness of 1258 µm (double arrow), and an AI-derived calcium arc of 208°, a minimum calcium depth of 40 µm and a maximum calcium thickness of 1200 µm. C) Combined calcified (arrowheads) and lipid plaque (arrow). D) Blood artefacts (arrow) not interfering with manual or automated OCT image analysis. E)

Correctly identified microvessels (arrows). F) Simultaneous presence of small plaque ruptures (arrows) and thrombus (arrowheads).

Dark grey denotes guidewire artefact, red denotes lumen, blue denotes intima, pink denotes media, white denotes calcium, yellow denotes lipid, orange denotes side branch, taupe denotes plaque rupture, cyan denotes thrombus, and light grey denotes microvessel.

Automated OCT image analysis

Figure 2 and Supplemental Videos 1-2 provide examples comparing the AI-based predictions to the final expert consensus in the external test set. Contingency tables for frame-wise identification are reported in Figure 3. According to the final reading based on predefined criteria, lipid plaque was prevalent in 1393 (54.4%) frames, including TCFA in 51 (2.0%) frames and lipid-rich plaque in 893 (34.9%) frames, calcified plaque in 1145 (44.7%) frames, side branch in 511 (20.0%) frames, plaque rupture in 21 (0.8%) frames, thrombus in 42 (1.6%) frames, and microvessel in 167 (6.5%) frames. Using the final consensus as the reference standard, the algorithm demonstrated almost perfect agreement for the identification of calcified plaque ($\kappa = 0.88$, 95% CI 0.84-0.92), substantial to almost perfect agreement for side branch ($\kappa = 0.78$, 95% CI 0.75-0.82), substantial agreement for lipid plaque ($\kappa = 0.68$, 95% CI 0.64-0.72) and lipid-rich plaque ($\kappa = 0.72$, 95% CI 0.68-0.76), moderate to substantial agreement for microvessel ($\kappa = 0.63$, 95% CI 0.59-0.66), fair to moderate agreement for thrombus ($\kappa = 0.40$, 95% CI 0.36-0.43), and fair agreement for TCFA ($\kappa = 0.27$, 95% CI 0.23-0.30) and plaque rupture ($\kappa = 0.33$, 95% CI 0.29-0.36) (Table 2). Among frames without manually identified calcium by experts, the kappa value for lipid plaque identification between expert readers and the AI algorithm was 0.77 (95% CI 0.72-0.83).

A. Lipid plaque

	Reference +	Reference -	Total
AI +	1074	93	1167
AI -	319	1074	1393
Total	1393	1167	2560

B. Thin-cap fibroatheroma

	Reference +	Reference -	Total
AI +	10	11	21
AI -	41	2498	2539
Total	51	2509	2560

C. Lipid-rich plaque

	Reference +	Reference -	Total
AI +	658	76	734
AI -	235	1591	1826
Total	893	1667	2560

D. Calcified plaque

	Reference +	Reference -	Total
AI +	1047	57	1104
AI -	98	1358	1456
Total	1145	1415	2560

E. Side branch

	Reference +	Reference -	Total
AI +	407	68	475
AI -	104	1981	2085
Total	511	2049	2560

F. Plaque rupture

	Reference +	Reference -	Total
AI +	13	44	57
AI -	8	2495	2503
Total	21	2539	2560

G. Thrombus

	Reference +	Reference -	Total
AI +	33	86	119
AI -	9	2432	2441
Total	42	2518	2560

H. Microvessel

	Reference +	Reference -	Total
AI +	133	106	239
AI -	34	2287	2321
Total	167	2393	2560

Figure 3. Contingency tables.

Contingency tables for the frame-wise evaluation of the presence of lipid plaque (A), thin-cap fibroatheroma (B), lipid-rich plaque (C), calcified plaque (D), side branch (E), plaque rupture (F), thrombus (G) and microvessel (H) as evaluated through expert OCT image analysis (reference) and artificial intelligence-based automated image analysis.

AI artificial intelligence.

The ICC between the final consensus among experts and the algorithm was 0.59 (95 % CI 0.55-0.63) for minimum FCT and 0.79 (95% CI 0.76-0.81) for lipid arc (Figure 4). The ICC for minimum calcium depth, maximum calcium thickness and calcium arc were 0.91 (95% CI 0.90-0.92), 0.79 (95% CI 0.77-0.82), and 0.93 (95% CI 0.92-0.94) (Figure 5).

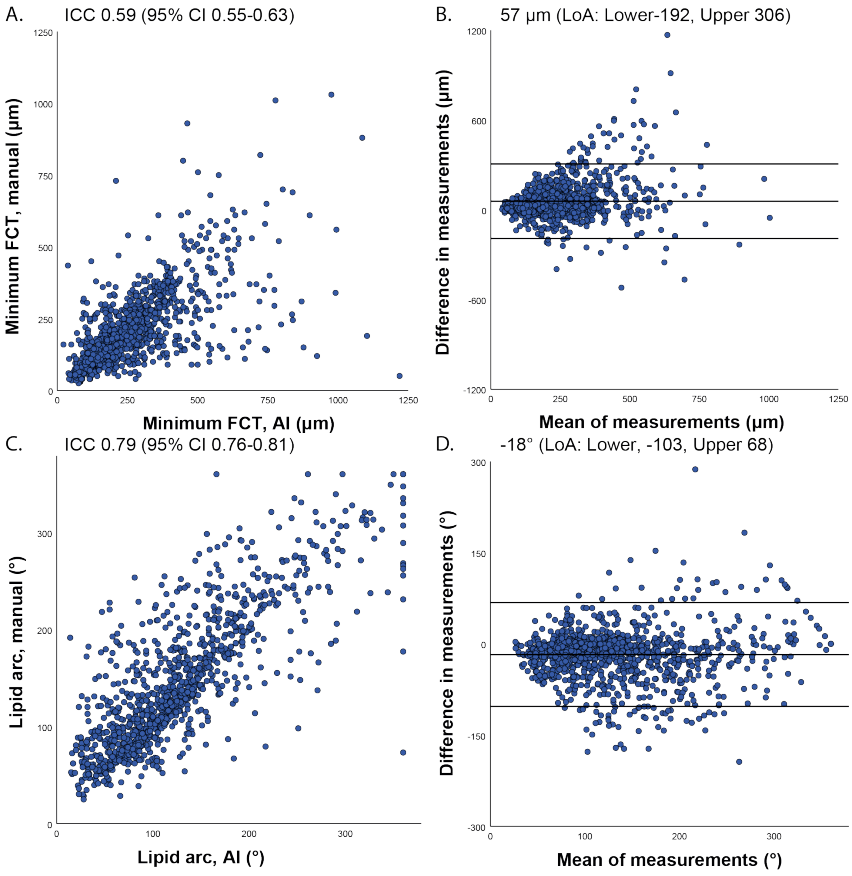


Figure 4. Lipid plaque quantification.

Scatterplots and Bland-Altman plots for the comparison of artificial intelligence-based and expert lipid plaque quantification in terms of the minimum FCT (A-B) and the lipid arc (C-D). Differences are calculated as the artificial intelligence-obtained value minus the final reference standard value, and are reported as mean difference with upper and lower limits of agreement (defined as ±1.96 x standard deviation).

CI confidence interval; FCT fibrous cap thickness; ICC intraclass correlation coefficient; LoA limits of agreement.

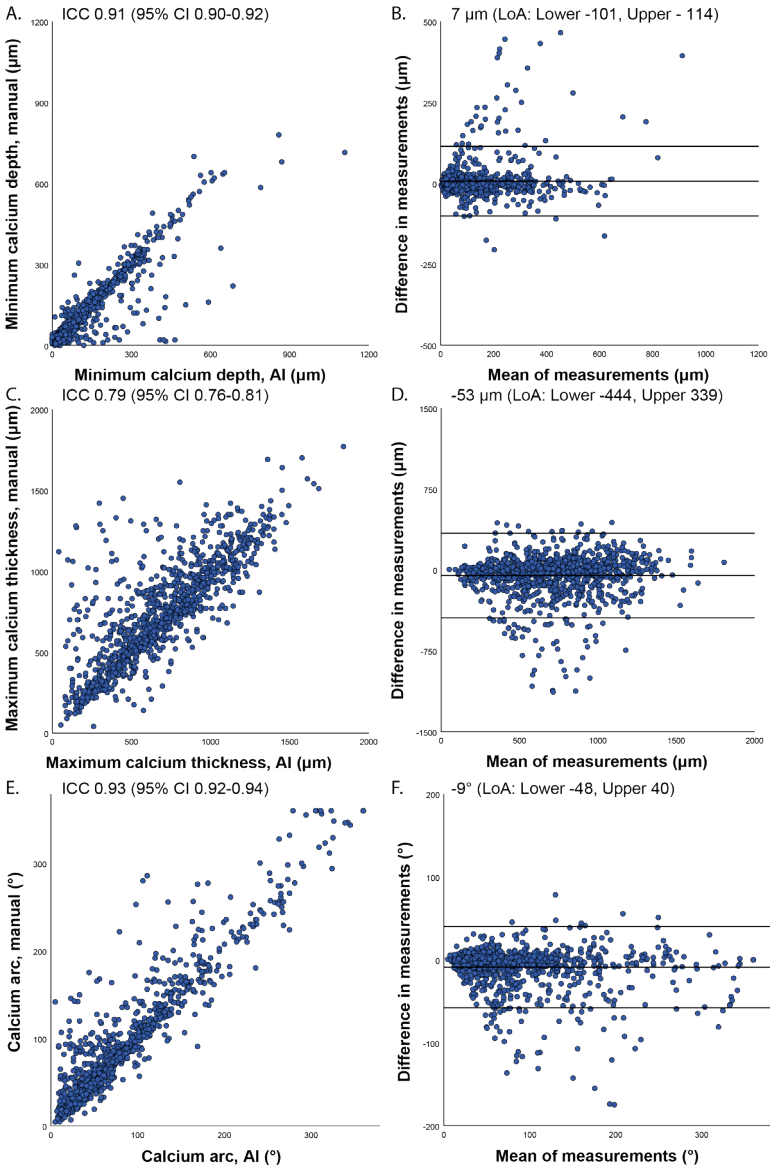


Figure 5. Calcified plaque quantification.

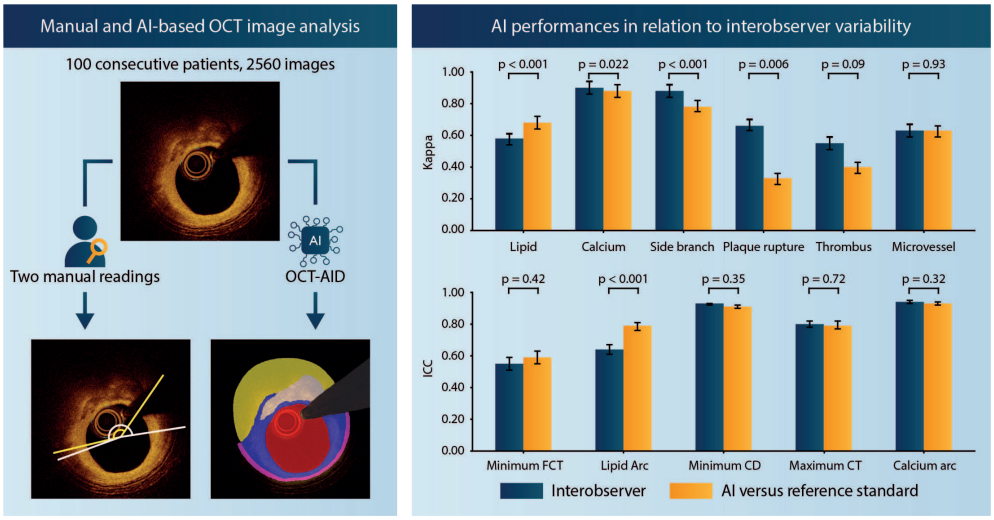
Scatterplots and Bland-Altman plots for the comparison of d artificial intelligence-based and manual calcified plaque quantification in terms of the minimum calcium depth (A-B), maximum calcium thickness (C-D) and calcium arc (E-F). Differences are calculated as the artificial intelligence-obtained value minus the final reference standard value, and are reported as mean difference with upper and lower limits of agreement (defined as ±1.96 x standard deviation).

CI confidence interval; ICC intraclass correlation coefficient; LoA limits of agreement.

Compared with the interobserver agreement between expert readers, the algorithm performance against the final reference standard was significantly higher for lipid plaque identification (p<0.001), lipid-rich plaque identification (p<0.001) and lipid arc quantification (p<0.001), and significantly lower for calcified plaque (p=0.022), side branch (p<0.001), and plaque rupture identification (p<0.006) (Central Illustration and Table 2).

Supplemental Table 1 provides the performance of the AI algorithm against final expert consensus in frames with concordance or discordance between the two expert readers. The kappa values for lipid plaque, lipid-rich plaque, calcified plaque and side branch were higher in frames with concordance than in those with discordance between expert readers.

Results in the internal test set are reported in Supplemental Table 2.



Central Illustration.

AI artificial intelligence; CD calcium depth; CT calcium thickness; FCT fibrous cap thickness; ICC intraclass correlation coefficient; OCT optical coherence tomography.

Inference time

Inference was run on a server with 64 GB of RAM and an NVIDIA A100 with 40GB of memory. The mean inference time was 0.34 ± 0.01 s/frame, including 0.04 ± 0.002 s/frame for pre-processing, 0.07 ± 0.01 s/frame for post-processing.

DISCUSSION

This study evaluated the performance of a recently developed AI algorithm for comprehensive full-vessel segmentation of intracoronary OCT images in an external, real-world cohort of consecutive patients undergoing clinically indicated OCT. We report several key findings. First, agreement among OCT expert readers on the calcified plaques and their measurements was high, whereas interobserver variability was substantial for lipid plaques and high-risk plaque features such as TCFA and microvessels. Second, agreement between AI-based automated OCT image analysis and expert consensus was largely comparable to interobserver variability among expert readers, supporting the feasibility of automated analysis in clinical practice. However, automated evaluation of low-prevalence classes was challenging within the proposed multiclass network.

To our knowledge, this is the largest external validation study of any multiclass algorithm for OCT to date, comprising 2560 frames from 100 consecutive patients who underwent clinically-indicated OCT. Considering this consecutiveness, the studied population closely resembles real-world practice, which contrasts previous external validation datasets comprising selective study populations.[7] In this study, we evaluated the interobserver variability among expert readers and the performance of AI-based automated OCT image interpretation using experts' consensus as the reference standard. Interobserver agreement among expert readers was excellent for identification and quantification of calcified lesions. The AI algorithm also demonstrated an excellent performance in identification and quantification of calcified plaque, with a performance almost comparable to the interobserver agreement among expert readers. These results support the potential of AI-based streamlined decision-making in clinical practice for the decision for advanced calcium modification. In addition, while manual calcified plaque quantification is limited to longitudinal and circumferential measurements, the semantic segmentation AI algorithm allows volumetric evaluation of calcifications, which may have additional clinical implications.

In contrast, interobserver variability among expert readers was high for the evaluation of lipid plaques, particularly for TCFA and in combined lipidic and calcific plaque. These findings emphasize the inherent challenges and variability in evaluating non-calcified plaque in OCT, even among expert readers, and underscore the potential role of automated methodologies to improve standardization in image interpretation. Notably, our study demonstrated that the agreement between the AI algorithm and the experts' final consensus was higher than interobserver agreement among expert readers in both identification and quantification of lipidic plaque, supporting a promising role of the AI algorithm. Interestingly, the agreement between the algorithm and the experts' final consensus for TCFA was only fair, yet comparable to interobserver agreement. However, TCFA was only present in 2.0% of frames, limiting robustness of statistical analyses. Additionally, evaluating TCFA in a binary fashion using strict definitions remains cumbersome and may have limited clinical implications as the difference between a TCFA positive reading and a TCFA negative reading can be as small as one pixel (≈10 µm) and considering that the risk associated with fibrous cap thinning is unlikely to be binary. Nevertheless, and arguably more importantly, we recently demonstrated that TCFA identified using OCT-AID was associated with adverse clinical outcome, providing evidence for the validity of AI-based TCFA identification.[11] Future

three-dimensional evaluation of the fibrous cap thickness, enabled through the comprehensiveness of AI-based image analyses, may improve risk stratification.[12]

The study also indicates some remaining challenges for the AI algorithm, particularly for the evaluation of side branches, thrombus and plaque rupture. While expert readers were allowed to scroll through the complete pullback, the algorithm was restricted to a pseudo-3D input of 7 consecutive frames which may have contributed to the lower performance for the identification of side branches. In this regard, increasing the longitudinal extent of the model's input by concatenating additional consecutive frames could potentially result in better performance. Alternatively, employing different feature aggregation strategies, such as 3D convolutions or attenuation mechanisms to better capture spatial relationships along the pullback, may lead to further improvements. For thrombus and plaque rupture, the limited performance of the AI algorithm was predominantly related to false positive predictions, consistent with our initial validation results.[8] Semantic multiclass segmentation algorithms may be suboptimal for automated identification of these low-prevalence features, as obtaining large quantities of pixel-wise annotated frames with plaque rupture and thrombus remains challenging. Therefore, frame-wise classification or object detection algorithms may be preferential in that regard.[13] Nonetheless, the inclusion of these classes allowed us to include frames with thrombus or plaque rupture in training and testing, enhancing the generalizability.

These results complement previous validation studies for this algorithm in which its value was demonstrated for the evaluation of plaque burden and for prognostication through the automated identification of TCFA.[11,14] Importantly, while the internal training and validation set particularly comprised OCT images of non-flow limiting, deferred lesions, the majority of lesions included in the present study required revascularization. Flow limiting or obstructive lesions are characterized by a more advanced plaque phenotype, including more extensive calcification and combined plaque,[15] which are more difficult to characterize. Furthermore, while the algorithm was developed almost exclusively with data from patients with recent myocardial infarction predominantly from Europe, the current validation set predominantly comprised patients with stable or unstable angina from the United States of America. In addition, the model evaluated in this study provides segmentation predictions in 0.34 seconds per frame, equivalent to a mean time of only 128 seconds to frame-wise analyze a pullback with 375 frames, and a reduction of 60% compared to our previous iteration.[8] The promising performance in this external dataset, despite inclusion of more advanced lesions, combined with high efficiency supports generalizability of the algorithm for frame-wise image evaluation. This study represents an important intermediate validation step towards prospective, multicenter clinical evaluation of the models accuracy for guidance of lesion-level decision making ang its ability to streamline procedural efficiency.

Our study has limitations. First, the external testing data originated from a single center with large experience in clinical OCT, potentially limiting generalizability to other centers. For instance, image artifacts may be present in different extent, depending on center-specific expertise and image acquisition practices. Second, despite being the largest external validation study for any AI algorithm for automated OCT image segmentation to date, the number of evaluated patients remained modest due to the laborious nature of manual OCT image interpretation. Consequently, expert analysis was limited

to frame-wise classification and quantification rather than segmentation, precluding an evaluation of the within-frame overlap between reference standard and AI prediction. Third, frames with substantial artifacts precluding the establishment of a reference standard were excluded. However, these frames were predominantly located at the outer edges of the pullback rather than within the targeted lesion, reflecting clinical care where blood clearance outside of the lesion is not necessarily required and pursued. Additionally, frames with artifacts not limiting manual image analysis were not excluded from analysis. Fourth, the reference standard was obtained through manual OCT image interpretation with related uncertainty.[5,6] In that regard, OCT images with co-registered histopathology would be the preferred reference standard when available. However, such datasets are scarce and not publicly available. Finally, this was a retrospective study, and real-time evaluation of this AI-based algorithm in a clinical setting is warranted. For future time-sensitive applications, further optimization is warranted, particularly for pre- and post-processing, which are currently performed on the CPU and could benefit from GPU acceleration.

CONCLUSION

AI allows fully automated evaluation of OCT images with performances largely in line with interobserver variability in a real-world dataset of consecutive patients, supporting generalizability of the proposed methodology for frame-wise OCT image evaluation.

REFERENCES

1. Vrints C, Andreotti F, Koskinas KC, Rossello X, Adamo M, Ainslie J et al. 2024 ESC Guidelines for the management of chronic coronary syndromes. Eur Heart J 2024;45:3415-3537.
2. Rao SV, O'Donoghue ML, Ruel M, Rab T, Tamis-Holland JE, Alexander JH et al. 2025 ACC/AHA/ACEP/NAEMSP/SCAI Guideline for the Management of Patients With Acute Coronary Syndromes: A Report of the American College of Cardiology/American Heart Association Joint Committee on Clinical Practice Guidelines. Circulation 2025;151:e771-e862.
3. Volleberg R, Rroku A, Mol JQ, Hermanides RS, van Leeuwen M, Berta B et al. FFR-Negative Nonculprit High-Risk Plaques and Clinical Outcomes in High-Risk Populations: An Individual Patient-Data Pooled Analysis From COMBINE (OCT-FFR) and PECTUS-obs. Circ Cardiovasc Interv 2025;18:e014667.
4. Koskinas KC, Nakamura M, Raber L, Colleran R, Kadota K, Capodanno D et al. Current use of intracoronary imaging in interventional practice - Results of a European Association of Percutaneous Cardiovascular Interventions (EAPCI) and Japanese Association of Cardiovascular Interventions and Therapeutics (CVIT) Clinical Practice Survey. EuroIntervention 2018;14:e475-e484.
5. Gruslova AB, Singh S, Hoyt T, Vela D, Vengrenyuk Y, Buja LM et al. Accuracy of OCT Core Labs in Identifying Vulnerable Plaque. JACC Cardiovasc Imaging 2024;17:448-450.
6. Kini AS, Vengrenyuk Y, Yoshimura T, Matsumura M, Pena J, Baber U et al. Fibrous Cap Thickness by Optical Coherence Tomography In Vivo. J Am Coll Cardiol 2017;69:644-657.
7. van der Waerden RGA, Volleberg R, Luttikholt TJ, Cancian P, van der Zande JL, Stone GW et al. Artificial intelligence for the analysis of intracoronary optical coherence tomography images: a systematic review. Eur Heart J Digit Health 2025;6:270-284.
8. Volleberg R, van der Waerden RGA, Luttikholt TJ, van der Zande JL, Cancian P, Gu X et al. Comprehensive full-vessel segmentation and volumetric plaque quantification for intracoronary optical coherence tomography using deep learning. Eur Heart J Digit Health 2025;6:404-416.
9. Araki M, Park SJ, Dauerman HL, Uemura S, Kim JS, Di Mario C et al. Optical coherence tomography in coronary atherosclerosis assessment and intervention. Nat Rev Cardiol 2022;19:684-703.
10. Isensee F, Wald T, Ulrich C, Baumgartner M, Roy S, Maier-Hein K et al. nnU-Net Revisited: A Call for Rigorous Validation in 3D Medical Image Segmentation. Cham: Springer Nature Switzerland, 2024:488-498.
11. Volleberg R, Luttikholt TJ, van der Waerden RGA, Cancian P, van der Zande JL, Gu X et al. Artificial intelligence-based identification of thin-cap fibroatheromas and clinical outcomes: the PECTUS-AI study. Eur Heart J 2025;46:5032-5041.
12. Luttikholt TJ, Thannhauser J, van Royen N. Detection of large areas of thin-cap fibroatheroma in a recurrent STEMI patient using a novel artificial intelligence algorithm: moving from 2D to 3D. Eur Heart J 2025.
13. Park S, Araki M, Nakajima A, Lee H, Fuster V, Ye JC et al. Enhanced Diagnosis of Plaque Erosion by Deep Learning in Patients With Acute Coronary Syndromes. JACC Cardiovasc Interv 2022;15:2020-2031.
14. Volleberg R, Shin D, Saitta S, Shlofmitz RA, Shlofmitz E, Jeremias A et al. Deep Learning-Derived Plaque Burden for Intracoronary Optical Coherence Tomography: An Intravascular Ultrasound-Based Validation Study. JACC Cardiovasc Interv 2025;18:2432-2434.
15. Driessen RS, Stuijfzand WJ, Raijmakers PG, Danad I, Min JK, Leipsic JA et al. Effect of Plaque Burden and Morphology on Myocardial Blood Flow and Fractional Flow Reserve. J Am Coll Cardiol 2018;71:499-509.

SUPPLEMENTAL MATERIAL

Supplemental Method 1. Model parameters.

Hyperparameter	Value
Image coordinates	Cartesian
Input image size	704 x 704 x 7 in greyscale
Output image size	704 x 704 x 1
Batch size	5
Initial learning rate	0.01
Learning rate scheduler	Polynomial learning rate decay
Optimizer	Stochastic gradient descent
Epochs	1000
Loss function	Equally weighted Dice and cross-entropy loss
Weight decay coefficient	0.00003
Number of learnable parameters	126M

Supplemental Table 1. AI performance in concordant and discordant cases.

	Frames with interobserver agreement		Frames without interobserver agreement		
	Number	Kappa*	Number	Kappa*	P-value
Lipid plaque	2027 (79.2%)	0.72 (0.68-0.76)	533 (20.8%)	0.19 (0.10-0.27)	<0.001
TCFA	2428 (94.8%)	0.33 (0.29-0.36)	132 (5.2%)	0.11 (0.0-0.25)	0.15
Lipid-rich plaque	1964 (76.7%)	0.80 (0.75-0.84)	596 (23.3%)	0.33 (0.25-0.41)	<0.001
Calcified plaque	2435 (95.1%)	0.91 (0.87-0.95)	125 (4.9%)	0.35 (0.20-0.51)	<0.001
Side branch	2465 (96.3%)	0.81 (0.77-0.85)	95 (3.7%)	0.33 (0.09-0.50)	<0.001
Plaque rupture	2549 (99.6%)	0.22 (0.19-0.25)	11 (0.4%)	-0.17 (-0.60-0.25)	0.58
Thrombus	2533 (98.9%)	0.23 (0.20-0.26)	27 (1.1%)	0.32 (0.04-0.60)	0.68
Microvessel	2454 (95.9%)	0.59 (0.55-0.62)	106 (4.1%)	0.47 (0.29-0.66)	0.21

TCFA thin-cap fibroatheroma.

** Agreement between artificial intelligence-based assessment with final expert consensus..*

Supplemental Table 2. Internal test set.

Class	Prevalence	Dice*	True Positive Dice†	Kappa‡	ICC‡
Guidewire	218 (100%)	0.94 ± 0.05 0.95 (0.93-0.97)	0.94 ± 0.05 0.95 (0.93-0.97)	-	-
Lumen	218 (100%)	0.99 ± 0.01 0.99 (0.99-1.00)	0.99 ± 0.01 0.99 (0.99-1.00)	-	-
Side branch	46 (21.1%)	0.64 ± 0.38 0.82 (0.26-0.93)	0.82 ± 0.19 0.90 (0.77-0.93)	0.79 (0.66-0.92)	-
Intima	218 (100%)	0.90 ± 0.06 0.91 (0.87-0.94)	0.90 ± 0.06 0.91 (0.87-0.94)	-	-
Media	206 (94.5%)	0.79 ± 0.21 0.86 (0.77-0.90)	0.82 ± 0.14 0.86 (0.79-0.90)	-	-
Lipid plaque	102 (46.8%)	0.64 ± 0.31 0.77 (0.58-0.85)	0.76 ± 0.16 0.79 (0.70-0.86)	0.84 (0.70-0.97)	-
Arc	-	0.75 ± 0.35 0.92 (0.73-0.98)	0.89 ± 0.15 0.95 (0.84-0.98)	-	0.73 (0.62-0.82)
Minimum FCT	-	-	-	-	0.72 (0.61-0.81)
Calcified plaque	53 (24.3%)	0.57 ± 0.39 0.76 (0.00-0.90)	0.79 ± 0.18 0.85 (0.72-0.92)	0.79 (0.65-0.92)	-
Arc	-	0.63 ± 0.41 0.86 (0.04-0.95)	0.87 ± 0.14 0.92 (0.84-0.96)	-	0.86 (0.75-0.92)
Minimum depth	-	-	-	-	0.79 (0.65-0.88)
Maximum thickness	-	-	-	-	0.75 (0.59-0.86)
Plaque rupture	6 (2.8%)	0.10 ± 0.22 0.00 (0.00-0.02)	0.30 ± 0.31 0.33 (0.01-0.58)	0.45 (0.36-0.57)	-
Thrombus	21 (9.6%)	0.65 ± 0.36 0.86 (0.38-0.90)	0.78 ± 0.22 0.88 (0.77-0.91)	0.89 (0.76-1.00)	-
Microvessel	12 (5.5%)	0.38 ± 0.41 0.22 (0.00-0.85)	0.75 ± 0.17 0.84 (0.59-0.87)	0.68 (0.56-0.81)	-

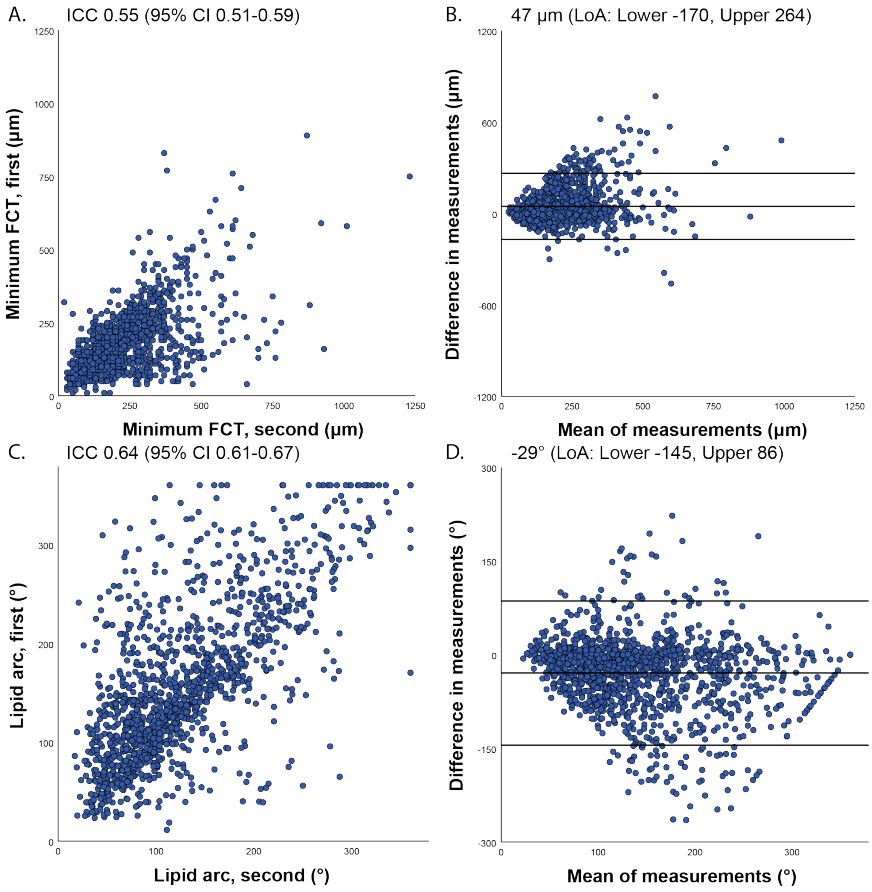
Numbers are value (percentage), value ± standard deviation or value (95% confidence interval).

FCT fibrous cap thickness; ICC intraclass correlation coefficient..

** The Dice score is calculated per class in each frame as two times the number of pixels with overlap between the reference standard and the artificial intelligence-based predictions of that particular class, divided by the sum of the number of pixels of that particular class from the reference standard and the prediction. False positive and false negative frames result in a Dice score of 0, while predictions perfectly aligning with the reference standard result in a Dice score of 1. True negative frames are excluded.*

† Dice score calculated among true positive frames, excluding false positive, false negative and true negative frames..

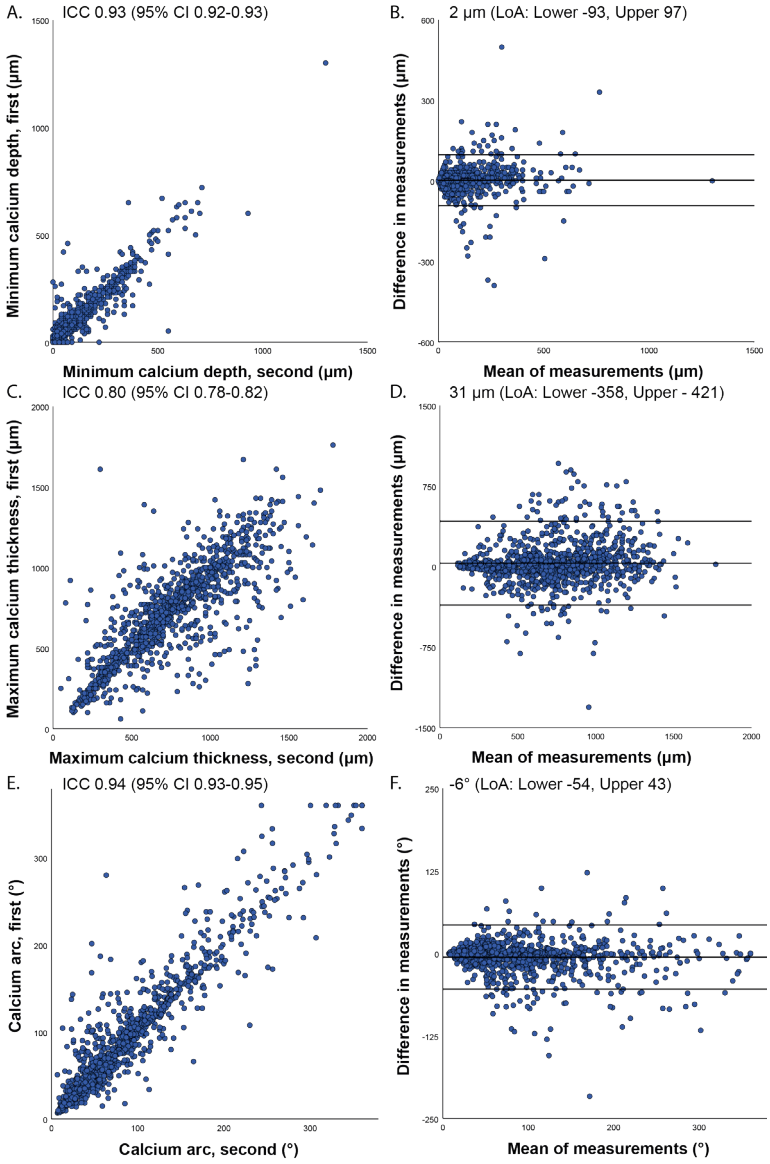
‡ Agreement between artificial intelligence-based assessment with final expert consensus.



Supplemental Figure 1. Interobserver variability for lipid plaque quantification.

Scatterplots and Bland-Altman plots for the evaluation of interobserver variability for lipid plaque quantification in terms of the minimum FCT (A-B) and the lipid arc (C-D). Differences between the two readings are reported as mean difference with upper and lower limits of agreement (defined as ±1.96 x standard deviation).

CI confidence interval; FCT fibrous cap thickness; ICC intraclass correlation coefficient; LoA limits of agreement.



Supplemental Figure 2. Interobserver variability for calcified plaque quantification.

Scatterplots and Bland-Altman plots for the evaluation of interobserver variability for calcified plaque quantification in terms of the minimum calcium depth (A-B), maximum calcium thickness (C-D) and calcium arc (E-F). Differences between the two readings are reported as mean difference with upper and lower limits of agreement (defined as ±1.96 x standard deviation).

CI confidence interval; ICC intraclass correlation coefficient; LoA limits of agreement.



CHAPTER 16

Deep learning-derived plaque burden for intracoronary optical coherence tomography: an intravascular ultrasound-based validation study

Rick Volleberg | Doosup Shin | Simone Saitta | Richard Shlofmitz | Evan Shlofmitz | Allen Jeremias | Ruben van der Waerden | Jos Thannhauser | Niels van Royen* | Ziad Ali*

JACC Cardiovascular Interventions
2025 Oct13;18(19):2432-2434

** joined senior authorship*

Both optical coherence tomography (OCT) and intravascular ultrasound (IVUS) allow the identification of high-risk plaque features.[1,2] Although OCT allows the detection of thin-cap fibroatheroma (TCFA), its limited penetration depth generally precludes the evaluation of plaque burden (PB), which is assessed using IVUS. The ability to simultaneously evaluate TCFA and PB could enhance the identification of high-risk plaques. We aimed to validate a recently developed artificial intelligence (AI) algorithm conducting full-vessel segmentation of OCT images[3] to assess PB, using IVUS as the reference standard.

Twenty patients who underwent both pre-intervention OCT (Dragonfly Opstar, Abbott Laboratories) and high-definition IVUS (OptiCross, Boston Scientific) of the same target vessel were analyzed by the core laboratory (OPCI). The study was conducted in accordance with the Declaration of Helsinki and was approved by the Institutional Review Board of St. Francis Hospital & Heart Center. The requirement to obtain informed consent was waived because of minimal risk.

Cross-sectional OCT and IVUS images were coregistered at 1-mm intervals throughout the complete imaged segment (including the angiographically targeted lesion [50-90% stenosis] and diseased and non-diseased adjacent sections) using anatomical landmarks, excluding 39 frames (4.3%) with insufficient image quality (Figure 1A). IVUS images were analyzed to measure the external elastic membrane (EEM) and luminal areas (square millimeters). Plaque area was calculated as the difference between the EEM and luminal areas, and PB (percentage) was defined as (plaque area/EEM area) × 100. Coregistered OCT images were analyzed using a validated AI algorithm for fully automated vessel segmentation (OCT-AID).[3] In regions without EEM visibility, this algorithm estimates the EEM border on the basis of intima and/or plaque boundaries, incorporating spatial information from 3 consecutive frames on each side of the frame of interest. Cubic spline interpolation was applied to reconstruct the lumen and EEM contours across regions affected by guidewire artifacts or side branches.

The correlation between IVUS-derived and OCT-derived measures was evaluated using Pearson's correlation coefficient (r). Bias and limits of agreement were evaluated using Bland-Altman analysis. Agreement between OCT-derived PB and IVUS-derived PB ≥70%[2] was evaluated using the area under the receiver operating characteristic curve. Metrics are reported as value (95% CI). A subgroup analysis was performed according to the predominant plaque type in each frame (fibrous, lipid, or calcified). A P value <0.05 was considered to indicate statistical significance.

Among 20 patients (mean age 63 ± 9 years), 862 coregistered frames were included in the final analysis. There were significant correlations between OCT and IVUS for EEM area (r = 0.91; 95% CI: 0.89-0.92), plaque area (r = 0.87; 95% CI: 0.86-0.89), and luminal area (r = 0.92; 95% CI: 0.91-0.93) (P < 0.001 for all). Overall, OCT-derived PB demonstrated a very strong correlation with IVUS-derived PB (r = 0.90; 95% CI: 0.89-0.91; P < 0.001), with a mean difference of 3.5° ± 6.5° (Figure 1B). The correlation in PB was consistent among predominantly fibrous (n = 162; r = 0.81; 95% CI: 0.74-0.85; P < 0.001), lipidic (n = 360; r = 0.88; 95% CI: 0.85-0.90; P < 0.001), and calcified (n = 226; r = 0.81; 95% CI: 0.76-0.85; P < 0.001) plaques (Figure 1C). The area under the curve for IVUS-derived PB ≥70% was 0.95 (95% CI: 0.93-0.97; P < 0.001), with an optimal OCT-derived PB cutoff of 67.2%.

This is the largest study to date evaluating the correspondence between OCT-derived PB and IVUS-derived PB, demonstrating that PB assessment through fully automated AI-based evaluation of OCT

images is feasible and strongly correlates with IVUS-derived PB. Our results complement those of previous smaller scale studies using EEM enhancement or AI algorithms.[4,5] Whether OCT-derived PB is related to adverse clinical outcome remains to be elucidated, although the strong correlation with IVUS-derived measurements suggests that insights from prior IVUS studies may be applicable. Furthermore, the incremental prognostic value of simultaneous identification of high PB and TCFA, beyond each individual marker alone, remains to be established.

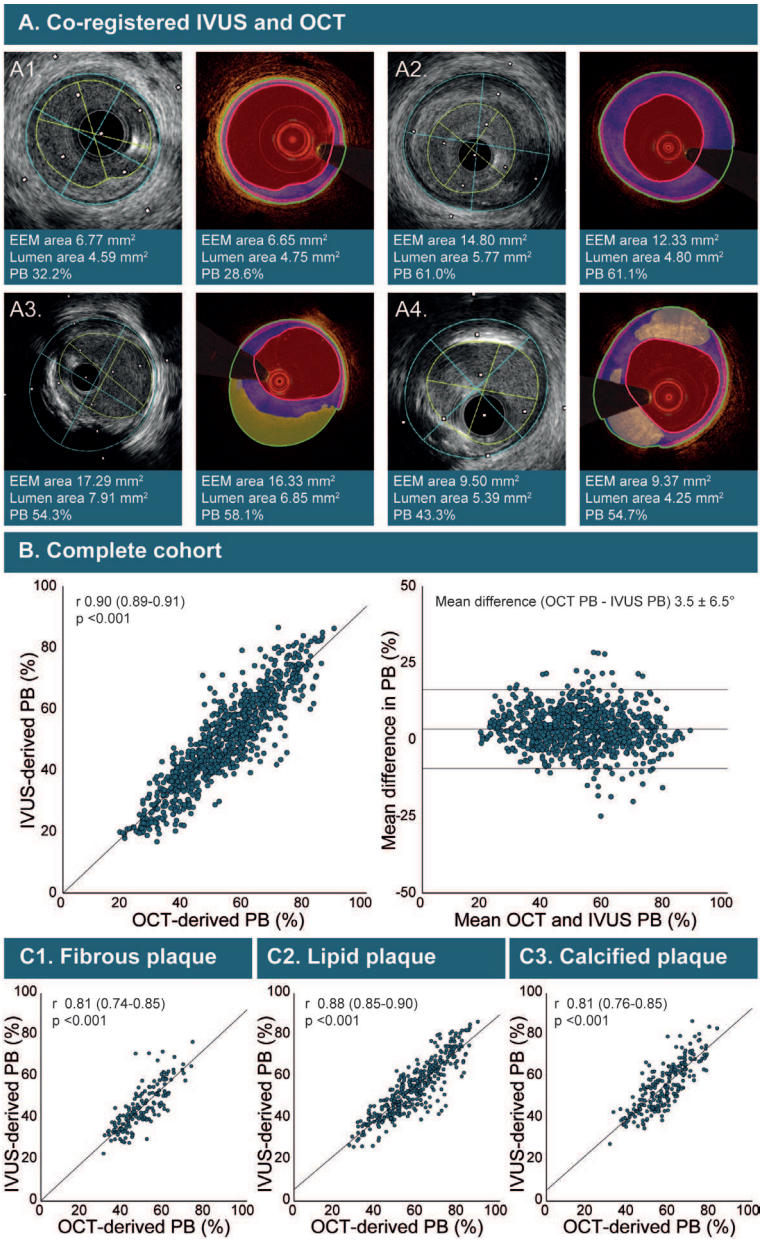


Figure 1. Comparison of OCT-derived and IVUS-derived plaque burden.

A) Coregistered intravascular ultrasound (IVUS) (left) and optical coherence tomography (OCT) (right) images with no (A1), fibrous (A2), lipidic (A3), or calcified (A4) plaque. The inner lines represent the luminal contour and the outer lines the external elastic membrane (EEM) contour. (B,C) Scatterplots and Bland-Altman plots comparing OCT-derived with IVUS-derived plaque burden (PB) in the complete cohort (B) and according to predominant plaque type (C).

REFERENCES

1. Volleberg R, Rroku A, Mol JQ, Hermanides RS, van Leeuwen M, Berta B et al. FFR-Negative Nonculprit High-Risk Plaques and Clinical Outcomes in High-Risk Populations: An Individual Patient-Data Pooled Analysis From COMBINE (OCT-FFR) and PECTUS-obs. Circ Cardiovasc Interv 2025;18:e014667.
2. Erlinge D, Maehara A, Ben-Yehuda O, Botker HE, Maeng M, Kjoller-Hansen L et al. Identification of vulnerable plaques and patients by intracoronary near-infrared spectroscopy and ultrasound (PROSPECT II): a prospective natural history study. Lancet 2021;397:985-995.
3. Volleberg R, van der Waerden RGA, Luttikholt TJ, van der Zande JL, Cancian P, Gu X et al. Comprehensive full-vessel segmentation and volumetric plaque quantification for intracoronary optical coherence tomography using deep learning. Eur Heart J Digit Health 2025;6:404-416.
4. Gerbaud E, Weisz G, Tanaka A, Luu R, Osman H, Baldwin G et al. Plaque burden can be assessed using intravascular optical coherence tomography and a dedicated automated processing algorithm: a comparison study with intravascular ultrasound. Eur Heart J Cardiovasc Imaging 2020;21:640-652.
5. Huang J, Tu S, Masuda S, Ninomiya K, Dijkstra J, Chu M et al. Plaque burden estimated from optical coherence tomography with deep learning: In vivo validation using co-registered intravascular ultrasound. Catheter Cardiovasc Interv 2023;101:287-296.



CHAPTER 17

Artificial intelligence-based identification of thin-cap fibroatheromas and clinical outcomes: the PECTUS-AI study

Rick Volleberg* | Thijs Luttikholt* | Ruben van der Waerden | Pierandrea Cancian | Joske van der Zande | Xiaojin Gu | Jan-Quinten Mol | Tomasz Roleder | Mathias Prokop | Clara Sánchez | Bram van Ginneken | Ivana Išgum | Simone Saitta | Jos Thannhauser† | Niels van Royen†

European Heart Journal
2025 Dec 8;46(46):5032-5041

** joined first authorship*
† joined senior authorship

ABSTRACT

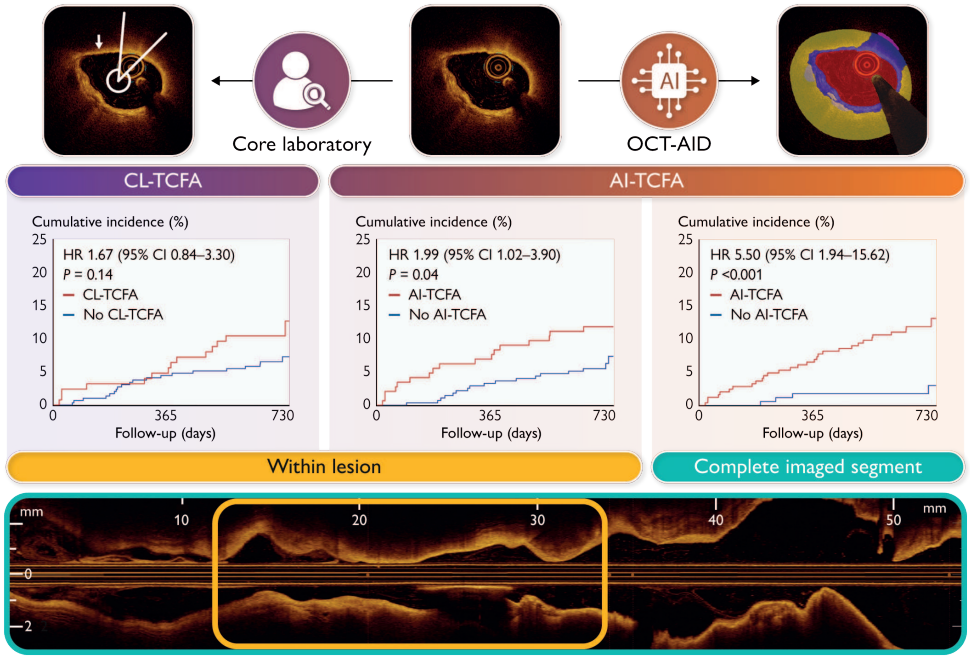
Background and aims Coronary thin-cap fibroatheromas (TCFA) are associated with adverse outcome, but identification of TCFA requires expertise and is highly time-demanding. This study evaluated the utility of artificial intelligence (AI) for TCFA identification in relation to clinical outcome.

Methods The PECTUS-AI study is a secondary analysis from the prospective observational PECTUS-obs study, in which 438 patients with myocardial infarction underwent optical coherence tomography (OCT) of all fractional flow reserve-negative non-culprit lesions (i.e. target lesions). OCT images were analyzed for the presence of TCFA by an independent core laboratory (CL-TCFA) and OCT-AID, a recently developed and validated AI segmentation algorithm (AI-TCFA). The primary outcome was defined as the composite of death from any cause, non-fatal myocardial infarction or unplanned revascularisation at 2 years (±30 days), excluding periprocedural and stent-related events.

Results Among 414 patients, AI-TCFA and CL-TCFA were identified in 143 (34.5%) and 124 (30.0%) patients, respectively. AI-TCFA within the target lesion was significantly associated with the primary outcome [hazard ratio (HR) 1.99, 95% confidence interval (CI) 1.02–3.90, P = .04], while the HR for CL-TCFA was non-significant (1.67, 95% CI: .84–3.30, P = .14). When evaluating the complete pullback, AI-TCFA showed an even stronger association with the primary outcome (HR 5.50, 95% CI: 1.94–15.62, P < .001; negative predictive value 97.6%, 95% CI: 94.0%–99.3%).

Conclusions AI-based OCT image analysis allows standardized identification of patients at increased risk of adverse cardiovascular outcome, offering an alternative to manual image analysis. Furthermore, AI-assisted evaluation of complete imaged segments results in better prognostic discriminatory value than evaluation of the target lesion only.

GRAPHICAL ABSTRACT



Artificial intelligence-based versus core laboratory-based TCFA identification

AI-TCFA, artificial intelligence-identified thin-cap fibroatheroma; CI, confidence interval; CL-TCFA, core laboratory-identified thin-cap fibroatheroma; HR, hazard ratio; TCFA, thin-cap fibroatheroma

Volleberg R, *et al. European Heart Journal.*

Structured Graphical Abstract. Artificial intelligence-based versus core laboratory-based TCFA identification.

Key question: Can artificial intelligence (AI) identify patients at increased risk of adverse cardiovascular outcomes after myocardial infarction through the automated identification of thin-cap fibroatheromas (TCFA) on optical coherence tomography (OCT) images of non-flow limiting lesions?

Key finding: The presence of AI-identified TCFA in non-flow limiting lesions and vessels was associated with adverse cardiovascular outcomes, with a hazard ratio greater than based on core laboratory-based OCT analyses.

Take home message: AI-based image analysis of the complete OCT pullback allows identification of patients at increased risk of adverse cardiovascular outcomes, with a higher predictive value compared to core laboratory-based analyses.

AI-TCFA artificial intelligence-identified thin-cap fibroatheroma; CI confidence interval; CL-TCFA core laboratory-identified thin-cap fibroatheroma; HR hazard ratio; TCFA thin-cap fibroatheroma.

INTRODUCTION

Intracoronary optical coherence tomography (OCT) allows most detailed *in vivo* evaluation of coronary atherosclerosis, including the identification of high-risk plaques. Such plaques are characterized by a large lipid content and a small overlying fibrous cap, which is referred to as a thin-cap fibroatheroma (TCFA).[1] Multiple prospective observational studies demonstrated that OCT-identified high-risk plaques, when evaluated by experienced core laboratories, are associated with adverse patient-level and lesion-level events, and that they may be a driving force behind coronary events originating from non-flow limiting lesions.[2-5] However, all these studies were based on offline OCT image analyses by core laboratories, which may reduce the generalizability of the findings to the daily clinical practice where OCT images will be evaluated by operating physicians, who may not have the same experience as core laboratory personnel. Furthermore, high-risk plaque identification is subject to substantial interobserver variability, even among highly experienced core laboratories.[6,7] Finally, frame-by-frame evaluation of a complete OCT pullback is highly time-demanding, posing a challenge for real-time on-site evaluation. However, immediate on-site image interpretation is essential when pre-emptive treatment of TCFA is to be pursued.[8] Therefore, automated image interpretation methods that can accurately identify TCFA with an association with adverse clinical outcomes are warranted.

We previously developed and validated OCT-AID, a comprehensive artificial intelligence (AI) model for automated full-vessel segmentation of OCT images.[9] This AI model is able to accurately quantify plaques, including the fibrous cap thickness, in a standardized manner. However, it remains to be demonstrated whether this algorithm can be used for prognostication.

Therefore, we aimed to evaluate whether our previously proposed AI algorithm can identify TCFA when compared with core lab analyses, and whether AI-detected TCFA is associated with adverse clinical outcome in patients with myocardial infarction and non-culprit plaques.

METHODS AND ANALYSIS

Study design

The PECTUS-AI study is a pre-planned secondary analysis from the prospective, multicenter, observational PECTUS-obs study (NCT03857971), of which the design and primary results were reported previously.[4,10] In brief, this study evaluated the association between core lab-identified high-risk plaques in intermediate, non-flow limiting, deferred, non-culprit lesions (i.e. target lesions) and clinical outcome in 438 patients with myocardial infarction. In- and exclusion criteria are listed in Supplementary data online, Method S1. Included patients underwent OCT imaging of all eligible target lesions meeting the criteria of a visually estimated stenosis grade 30%-90% with a fractional flow reserve (FFR) > 0.80. Patients subsequently underwent structured clinical follow-up at 1 and 2 years (±30 days) after inclusion through telephone contact. The study was approved by the institutional review boards and/or medical ethics

committee of each participating centre and was conducted in accordance with the 1964 Declaration of Helsinki and its later amendments. Signed informed consent was obtained from all participants.

OCT imaging acquisition and core laboratory evaluation

OCT images were acquired using the Dragonfly Optis imaging catheter (Abbott Vascular, Illinois, CA, USA). An independent OCT core laboratory performed blinded OCT image interpretation with the use of the angiogram as reference for localisation of the target lesion(s) on each OCT pullback. OCT image analyses were conducted in accordance with contemporary consensus documents,[11,12] as described in detail elsewhere.[4] Core laboratory-identified TCFA (CL-TCFA) was defined as a lipid plaque with a lipid arc ≥90° and a minimum fibrous cap thickness <65 µm at the frame-level. Patients with at least one CL-TCFA were considered CL-TCFA-positive irrespective of the number of included lesions per patient.

AI-based OCT image analysis

AI-based OCT image evaluation was performed on the region(s) that were previously identified by the OCT core laboratory as the target lesion(s) and on the complete imaged segment using two previously developed algorithms.[9,13]

AI-based plaque segmentation. We built on our previously developed OCT-AID algorithm for multiclass segmentation of OCT pullbacks.[9] OCT-AID performs pixelwise labelling of each OCT frame, distinguishing among ten classes: background, guidewire artefact, lumen, intima, media, lipid, calcium, side branch, plaque rupture and thrombus. This study introduces an updated version based on nnU-Net version 2[14] which integrates a residual encoder U-Net within the previously described self-configuring framework. Details on the algorithm are described in Supplementary data online, Method S2.

The total dataset consisted of 475 pullbacks, of which 207 (43.6%) had manually defined pixelwise reference annotations in a selected set of frames (n = 3026) as described previously. [9] The remaining 268 (56.4%) pullbacks had no reference annotations. We performed stratified 10-fold cross-validation on the frames with reference annotations, ensuring data separation across folds on a patient level. Dataset stratification across folds also maintained a balanced class distribution, with an absolute difference ≤5.0% per class. For each fold, an OCT-AID model instance was trained on 90% of this dataset and evaluated on the left out 10% (see Supplementary data online, Method S3). Model predictions were used to evaluate algorithm performance on a frame-level and pixel-level (see Supplementary data online, Method S4).

The pullbacks without reference annotations were divided into 10 subsets of approximately equal size. Each of these 10 subsets was segmented by a trained OCT-AID model instance selected to ensure separation between the training and test data on the patient level and thereby preventing data leakage.

AI-based artefact detection and frame/lesion exclusion. A previously developed deep learning-based algorithm was used for the identification of A-lines containing severe attenuation artefacts caused by blood or gas bubbles, which impair image interpretation.[13] Frames were excluded from further analyses if >25% of A-lines were affected by severe artefacts. Subsequently, lesions that retained

<50% of their frames were excluded from further analyses. The same was done for pullbacks for the pullback-level analyses.

AI-based TCFA identification. After exclusion of frames affected by artefacts, the automatically segmented frames were included in the final analysis and were used for quantification of lipid plaques, including the calculation of the lipid arc and minimum fibrous cap thickness as described before.[9] The latter was calculated as the shortest distance between segmented lumen an lipid pixels measured from the centroid of the lumen, ignoring directly neighbouring pixels. An AI-identified TCFA (AI-TCFA) was defined as a lipid plaque with a lipid arc ≥90° and a minimum fibrous cap thickness <65 µm in at least 3 out of 10 consecutive frames. Patients with at least one AI-TCFA were considered AI-TCFA-positive, irrespective of the number of included lesions per patient.

Clinical outcome

The primary outcome was defined as the composite of death from any cause, non-fatal myocardial infarction or unplanned revascularisation at 2-year follow-up (±30 days). Periprocedural and stent failure-related events and myocardial infarction not clearly attributable to a specific coronary segment were not considered for the current analysis. Secondary outcomes included the individual components of the primary outcome. All potential events were evaluated by a central, independent event adjudication committee consisting of two members who were blinded to the OCT images and OCT image evaluation results. Events were adjudicated with the use of health records obtained from participating centres, general practitioners and/or other treating physicians, and by comparing index and event angiograms.

Statistical analysis

Categorical variables are summarized as absolute values (percentages) and compared using the Chi-squared test or Fisher's exact test. Normally distributed continuous variables are presented as means ± standard deviation and analyzed using the Student's independent samples t-test. Non-normally distributed variables are provided as median (interquartile range [IQR]) and evaluated using the Mann–Whitney U test. The correspondence between AI-TCFA and CL-TCFA is presented using 2 × 2 contingency tables and was evaluated using Cohen's Kappa. Values are reported with 95% confidence intervals (CI). Clinical outcomes were evaluated on a patient level according to the presence or absence of AI-TCFA or CL-TCFA in any target lesion, irrespective of the number of included lesions per patient. This analysis is based on the rationale that the potential risk associated with the presence of high-risk plaques is not restricted to the identified TCFA site. Instead, it is considered a marker of patient-level vulnerability. Second, we evaluated the presence of AI-TCFA within the complete imaged segment. Time-to-event data for the primary outcome is presented using Kaplan-Meier curves and was evaluated using the log-rank test. The hazard ratio (HR) for the clinical outcomes associated with the presence of at least one TCFA was estimated using univariable Cox proportional hazard models. The discriminatory value of AI-TCFA (within the target lesion and within the complete imaged segment) and CL-TCFA (within the target lesion) was also evaluated using the C-statistic, which was compared using the DeLong test.

A two-sided P-value <.05 was considered statistically significant. All analyses were performed using IBM SPSS Statistics software version 29.0 (IBM Corp., Armonk, NY, USA) and R version 4.4.1 (R Foundation for Statistical Computing, Vienna, Austria)

RESULTS

Study population

A total of 414 patients (with 488 lesions) were eligible for the present analysis (Figure 1). Baseline clinical and procedural characteristics are summarized in Table 1. The mean age was 63 ± 10 years, and 335 (80.9%) patients were male. Diabetes and hypertension were present in 14.5% and 52.9% of patients, respectively. The proportions of patients who had presented with ST-segment elevation (51.4%) and with non-ST-segment elevation (48.6%) were comparable.

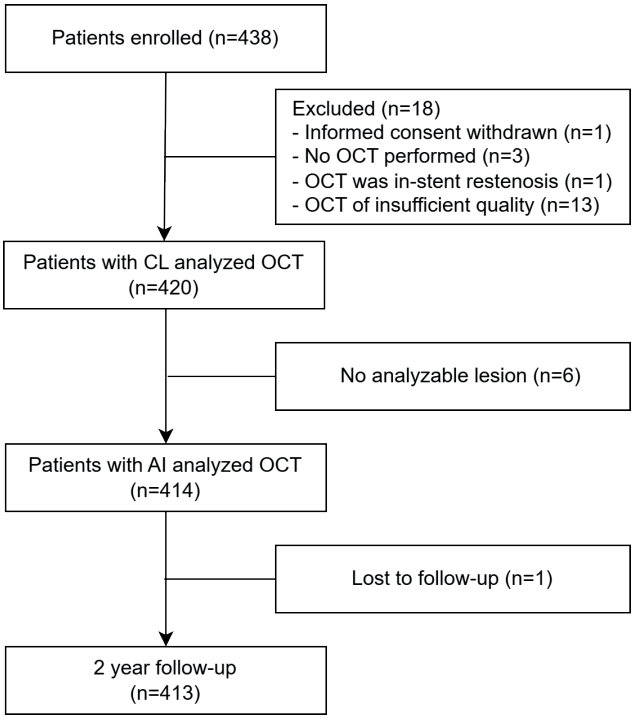


Figure 1. Study flowchart.
AI artificial intelligence; CL core laboratory; OCT optical coherence tomography.

Target lesions were most frequently located in the left anterior descending artery (37.9%) and the left circumflex artery (33.6%), and had a mean FFR of 0.89 ± 0.05 (Table 2). Based on core laboratory quantitative OCT analyses, the mean lesion length was 18.8 ± 8.8 mm. The mean minimum lumen diameter and mean minimum lumen area were 1.51 ± 0.44 mm and 2.70 ± 1.53 mm^2, respectively.

Table 1. Baseline characteristics.

Characteristic	n	Total (n=414)
Age, years		63 ± 10
Male sex		335 (80.9%)
BMI, kg/m^2	408	27.8 ± 4.6
Smoking status	411	
Current		122 (29.7%)
Previous		125 30.4%)
Never		164 (39.9%)
Hypertension		219 (52.9%)
Type 1 or 2 diabetes		60 14.5%)
Hypercholesterolemia	413	152 (36.7%)
Family history of premature atherosclerosis	410	123 (30.5%)
Previous MI		63 (15.2%)
Previous PCI		62 (15.0%)
Previous CVA		8 (1.9%)
History of carotid artery disease		13 (3.1%)
History of PAD		17 (4.1%)
Index presentation		
STEMI		213 (51.4%)
NSTEMI		201 (48.6%)
GRACE score	411	117 ± 33
Cholesterol level, mmol/L		
Total	349	4.98 ± 1.36
LDL	329	3.01 ± 1.20
Triglyceride level, mmol/L	345	1.60 (1.06-2.20)
eGFR, $mL/min/1.73m^2$	410	79.8 ± 19.1
CRP, mg/L	325	2.80 (1.00-5.00)
Leukocyte count, $x10^9/L$	408	9.76 ± 3.23
Lipid-lowering therapy at presentation		108 (26.1%)

Table 1. Continued

Infarct-related artery	
LM	5 (1.2%)
LAD	166 (40.1%)
Cx	105 (25.4%)
RCA	155 (37.4%)
Number of target lesions	1.18 ± 0.42
Target vessel distribution	
LM	4 (1.0%)
LAD	173 (41.8%)
Cx	151 (36.5%)
RCA	121 (19.2%)

BMI body mass index; CRP c-reactive protein; CVA cerebrovascular accident; Cx circumflex artery; eGFR estimated glomerular filtration rate; FFR fractional flow reserve; LAD left anterior descending artery; LDL low-density lipoprotein; LM left main stem; MI myocardial infarction; NSTEMI non-ST-segment elevation myocardial infarction; PAD peripheral artery disease; PCI percutaneous coronary intervention; RCA right coronary artery; STEMI ST-segment elevation myocardial infarction.

Table 2. Lesion-level characteristics.

Characteristic	Total (n=488)
Lesion distribution	
LM	4 (0.8%)
LAD	185 (37.9%)
Cx	164 (33.6%)
RCA	135 (27.7%)
Fractional flow reserve	0.89 ± 0.05
Quantitative OCT analyses	
Lesion length, mm	18.8 ± 8.8
Minimum lumen diameter, mm	1.51 ± 0.44
Minimum lumen area, mm^2	2.70 ± 1.53
Percentage area stenosis	62.3 ± 16.0

Cx circumflex artery; LAD left anterior descending artery; LM left main stem; OCT optical coherence tomography; RCA right coronary artery.

Automated artefact detection

The median percentage of excluded number of frames per lesion based on artefact detection was 0% (IQR 0–0%, 90th percentile 3.2%). Consequently, the median number of analyzable frames per lesion was 195 (IQR 136–264) compared with 201 (IQR 137–268) frames before artefact identification. A total of 6 patients had more than 50% non-analyzable frames and were excluded from further analysis.

AI-based TCFA identification vs. core laboratory reference in target lesions

AI-TCFA was present in 150 (30.7%) target lesions, while CL-TCFA was present in 134 (27.5%) target lesions. Fair to moderate agreement was observed between AI-TCFA and CL-TCFA (κ = 0.38, 95% CI: .28–.47) on a lesion-level. Overall, the core laboratory and the AI algorithm agreed on the presence and absence of TCFA in 79 (16.2%) and 283 (58.0%) lesions, respectively (Figure 2A). For lesions that qualified as CL-TCFA but not as AI-TCFA (n = 55), the median AI-identified minimum fibrous cap thickness on CL-TCFA-containing frames was 81 µm (IQR 71–104 µm). For lesions that qualified as AI-TCFA but not as CL-TCFA (n = 71), the median CL-identified minimum fibrous cap thickness within the lesion was 105 µm (IQR 78–138 µm) among 55 lesions with CL-identified lipid. The remaining 16 lesions are presented in Supplementary data online, Figure S1.

On a patient-level, 143 (34.5%) patients had at least one AI-TCFA in any target lesion, while 271 (65.5%) had no AI-TCFA. CL-TCFA was present in 124 (30.0%) patients and absent in 290 (70.0%) patients. The patient-wise agreement for TCFA identification was fair to moderate (κ = 0.40, 95% CI: .30–.49) (Figure 2B).

A. Lesion-level

	CL-TCFA +	CL-TCFA -	Total
AI-TCFA +	79	71	150
AI-TCFA -	55	283	338
Total	134	354	488

B. Patient-level

	CL-TCFA +	CL-TCFA -	Total
AI-TCFA +	79	64	143
AI-TCFA -	45	226	271
Total	124	290	414

Figure 2. Correspondence between AI-TCFA and CL-TCFA.

Contingency tables for the correspondence between AI-TCFA and CL-TCFA on a lesion level (A) and patient level (B).

AI-TCFA artificial intelligence-identified thin-cap fibroatheroma; CL-TCFA core laboratory-identified thin-cap fibroatheroma.

TCFA in target lesions and clinical outcome

One patient was lost to follow-up between the first and second years of follow-up. The clinical outcome at 2-year follow-up is summarized in Table 3. At 2-year follow-up, the primary outcome had occurred in 34 (8.2%) patients. Compared with those identified as not having AI-TCFA, those with AI-TCFA had a 1.99 (95% CI: 1.02–3.90, 11.9% vs. 6.3%, P = .04) higher rate of experiencing the primary outcome (Figure 3A). Compared with those identified as not having CL-TCFA, those with CL-TCFA had a 1.67 (95% CI: .84–3.30, 11.3% vs. 6.9%, P = .14) higher rate of experiencing the primary outcome (Figure 3B). The C-statistic for AI-based evaluation was not significantly different from core laboratory-based analysis (0.58, 95% CI: .50–.67 vs. 0.56, 95% CI: .47–.65, P = .65).

Table 3. Clinical outcome at two-year follow-up according to the presence or absence of TCFA.

Within lesion analyses (N = 414)				
	AI-TCFA (n=143)	**No AI-TCFA (n=271)**	**P-value**	**Univariable HR (95% CI)[a]**
Primary endpoint	17 (11.9%)	17 (6.3%)	.04	1.99 (1.02-3.90)
Death	6 (4.2%)	8 (3.0%)	.49	1.46 (.51-4.19)
Non-fata MI	2 (1.4%)	5 (1.8%)	.76	0.77 (.15-3.98)
Unplanned revascularization	12 (8.4%)	9 (3.3%)	.02	2.65 (1.12-6.28)
	CL-TCFA (n=124)	**No CL-TCFA (n=290)**	**P-value**	**Univariable HR (95% CI)[b]**
Primary endpoint	14 (11.3%)	20 (6.9%)	.14	1.67 (.84-3.30)
Death	5 (4.0%)	9 (3.1%)	.62	1.32 (.44-3.93)
Non-fata MI	4 (3.2%)	3 (1.0%)	.12	3.10 (.69-13.87)
Unplanned revascularization	9 (7.3%)	12 (4.1%)	.19	1.77 (.75-4.21)
Within imaged segment analyses (N = 411)				
	AI-TCFA (n=243)	**No AI-TCFA (n=168)**	**P-value**	**Univariable HR (95% CI)[a]**
Primary endpoint	30 (12.3%)	4 (2.4%)	<.001	5.50 (1.94-15.62)
Death	13 (5.3%)	1 (0.6%)	.009	9.34 (1.22-71.39)
Non-fata MI	6 (2.5%)	1 (0.6%)	.14	4.30 (.52-35.69)
Unplanned revascularization	18 (7.4%)	3 (1.8%)	.01	4.35 (1.28-14.78)

AI-TCFA artificial intelligence-identified thin-cap fibroatheroma; CI confidence interval; CL-TCFA core laboratory-identified thin-cap fibroatheroma; HR hazard ratio; MI myocardial infarction.

[a] Patient-level comparison of AI-TCFA positive vs. AI-TCFA negative cases.

[b] Patient-level comparison of CL-TCFA positive vs. CL-TCFA negative cases.

TCFA across the complete imaged segment and clinical outcome

At least one complete imaged segment was analyzable for >50% in 411 patients, of whom 243 (59.1%) had AI-TCFA. Those with AI-TCFA within the complete imaged segment had a 5.50 (95% CI: 1.94–15.62, P < .001) higher rate of experiencing the primary outcome than those without any AI-TCFA (Figure 3C, Table 3). While non-fatal myocardial infarction occurred numerically more frequently in patients with vs. without AI-TCFA (2.5% vs. 0.6%, P = .14), a statistically higher incidence of death (5.3% vs. 0.6%, P = .009) and of unplanned revascularization (7.4% vs. 1.8%, P = .01) were observed in patients with AI-TCFA.

AI-based evaluation of the complete imaged segment had superior discriminatory ability compared with core laboratory-based evaluation of the target lesion only (C-statistics 0.66, 95% CI: .60–.72 vs. 0.56, 95% CI: .47–.65, P = .03). A numerical difference in C-statistic was observed in favour of AI-based evaluation of the complete imaged segment compared with AI-based evaluation of the target lesion only; however, without reaching statistical significance (0.66, 95% CI: .60–.72 vs. 0.58, 95% CI: .50–.67, P = .08).

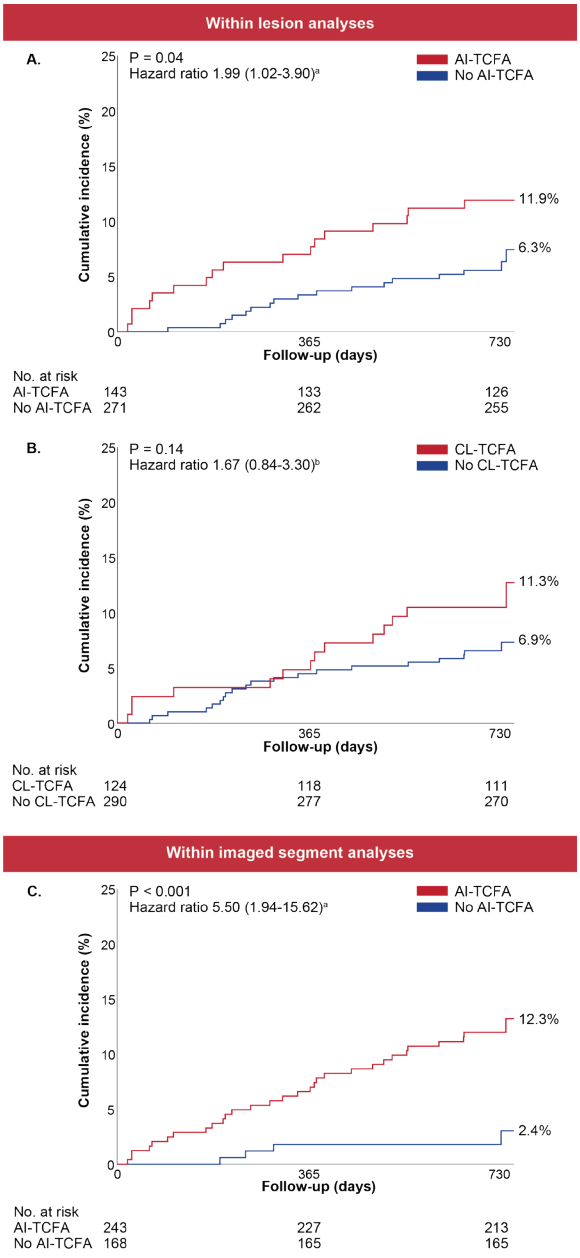


Figure 3. Survival curves for the primary outcome according to the presence or absence of TCFA.

Survival curves for the primary composite outcome according to the presence of AI-TCFA in the target lesion (A), CL-TCFA in the target lesion (B) and AI-TCFA in the complete imaged segment (C).

AI-TCFA artificial intelligence-identified thin-cap fibroatheroma; CL-TCFA core laboratory-identified thin-cap fibroatheroma.

[a] *Patient-level comparison of AI-TCFA positive vs. AI-TCFA negative cases.*

[b] *Patient-level*

DISCUSSION

This study evaluated the value of OCT-AID for prognostication of patients after myocardial infarction through the identification of TCFA. The main findings were: (i) AI-based TCFA identification using OCT was feasible, requiring exclusion of only a very small percentage of frames; (ii) the agreement between AI-TCFA and CL-TCFA was fair to moderate on both a patient level and lesion level; (iii) AI-TCFA showed a significant association with adverse cardiovascular events; (iv) incremental prognostic discriminatory value of AI was achieved by evaluating a complete OCT pullback compared with evaluation of the target lesion only. These results indicate the potential of AI for prognostication in a robust, standardized and comprehensive manner, offering an alternative to manual, non-standardized, on-site image assessment, and potentially facilitating *ad hoc* interventions (Structured Graphical Abstract).

To overcome the interobserver variability in high-risk plaque identification, which is a laborious task, automated methodologies are warranted. Such methodologies would ideally allow standardisation of OCT image interpretation with accuracies comparable to dedicated core laboratories, and most importantly with an association with clinical outcome. We previously demonstrated that our deep learning-based algorithm can provide accurate full-vessel segmentation and plaque quantification.[9] In the present study, we only found a fair to moderate correspondence between AI-TCFA and CL-TCFA, which is, however, in line with previous studies demonstrating important interobserver variability for TCFA identification.[6,7] Furthermore, the median AI-determined minimum fibrous cap thickness on CL-TCFA-containing frames was close to the 65 µm cut-off value used to define TCFA.

Despite this limited agreement, AI-TCFA was significantly associated with the patient-level primary outcome, with discriminatory value at least comparable to core laboratory-based analyses when evaluated within the target lesion and superior discriminatory value when used to evaluate the complete imaged segment. These results are indicative of the potential of AI for prognostication. First, OCT-AID allows rapid and comprehensive evaluation of each analyzable frame, while manual image analyses are generally limited to screening of the lesion, with at best measurements in a single frame or limited number of frames. Second, the proposed methodology allows reproducible image evaluation and can thereby help bridge the gap between findings from standardized research settings and daily clinical practice. Additionally, it overcomes the limitation of manual interobserver variability. For example, the randomized PREVENT trial demonstrated that preventive treatment of high-risk plaques may be beneficial; however, the discrepancies between manual on-site image evaluation and *post hoc* core laboratory-based analyses accentuated the challenges in high-risk plaque detection.[8] Therefore, the proposed algorithm has the potential to enable standardized, periprocedural assessment of OCT images, potentially facilitating *ad hoc* interventions for high-risk plaques. Future validation studies are required to support the findings of our study and enhance the validity of our AI-based approach. In that regard, a validation study comparing the algorithm to histology as the reference standard and a web-based reader study are currently ongoing. Ultimately, prospective clinical evaluation is warranted to evaluate the feasibility and value of an AI-based high-risk plaque identification in clinical care.

A small number of studies have previously applied AI for the same purpose. Niioka et al. evaluated a frame-wise classification algorithm for the presence of TCFA and found a significant association with AI-identified TCFA and both patient-level and lesion-level events.[15] However, classification algorithms generally have lower explainability compared with semantic segmentation models such as OCT-AID of which the predictions can be compared with the corresponding pixels. Hong et al. defined the lipid-to-cap ratio as new measurement to identify high-risk plaques using another semantic segmentation model. Patients with an lipid-to-cap ratio >0.33 were at an almost 20-fold increased risk of patient-level non-culprit lesion events.[16] Finally, Biccirè et al. obtained a lipid-spread out plot using deep learning alike those normally obtained using near-infrared spectroscopy. When evaluated in the CLIMA dataset,[2] the lipid core burden index within 4 mm was associated with a 2.5-fold increased risk of the primary CLIMA endpoint, which was below the HRs obtained using core laboratory analyses.[17] However, core laboratory analyses were performed with different plaque characteristics, limiting direct comparison between AI and core laboratory findings. In contrast, our direct comparison between core lab and AI findings demonstrates, for the first time, that AI can be at least comparable to core laboratory-based evaluation for prognostication through high-risk plaque identification.

Intriguingly, AI-TCFA was found outside of the target lesion in ~35% of patients without AI-TCFA in the target lesion, and an even stronger association was observed with AI-TCFA with adverse outcome when evaluating the complete imaged segment. These results indicate that plaque vulnerability is not limited to visually identifiable non-culprit lesions but that it affects the whole epicardial coronary vasculature. Remarkably, AI identified all but one patient who died during the first 2 years of follow-up, and <2% of patients without AI-TCFA required revascularisation during follow-up. This very high negative predictive value (97.6%) could be of great clinical value for prognostication after myocardial infarction. These findings again emphasize the potential value of AI, especially considering that comprehensive, manual image evaluation of a complete imaged segment is practically impossible on-site.

Importantly, AI-TCFA in the present study was defined according to standard criteria based on single-point measurements. To reduce the risk of false positive TCFA diagnoses due to single measurements, we applied a threshold of three frames meeting the TCFA criteria before a lesion would qualify as TCFA. Such threshold mimics human interpretation, as it is unlikely that human observers would classify a lesion as TCFA-positive if only one frame would meet the defined criteria while the others do not. Whether more comprehensive plaque analyses enabled through the application of AI and that may be impossible to perform manually,[18] provide superior predictive value remains speculative.

Limitations

This study was conducted on the data from a single prospective observational study, which may limit the generalizability of the findings. Furthermore, the PECTUS-obs study was not specifically designed to test superiority of AI-based OCT analysis compared with core laboratory-based analysis. Future validation studies are therefore warranted. Furthermore, the AI-based OCT analyses were performed offline. Therefore, it remains to be prospectively investigated how the proposed algorithm would perform and would be perceived when adopted directly on-site after OCT image acquisition. This is of

particular importance when focal treatment of high-risk plaques would be performed. Additionally, core laboratory analyses were only available for the target lesion, precluding comparison between AI and core laboratory analyses in the complete imaged segment. Finally, PECTUS-obs was designed to address the high-risk patient hypothesis, and was not powered to demonstrate differences in lesion-level events. Likewise, the study was not powered to evaluate differences in individual components of the composite outcome. The final 5-year follow-up results may provide additional insights in that regard.

CONCLUSIONS

AI-based OCT image analysis allows standardized identification of patients at increased risk of adverse cardiovascular outcome, offering an alternative to manual image analysis. Furthermore, AI-assisted evaluation of complete imaged segments provides more prognostic impact than evaluation of the target lesion only.

REFERENCES

1. Burke AP, Farb A, Malcom GT, Liang YH, Smialek J, Virmani R. Coronary risk factors and plaque morphology in men with coronary disease who died suddenly. N Engl J Med 1997;336:1276-82.
2. Prati F, Romagnoli E, Gatto L, La Manna A, Burzotta F, Ozaki Y et al. Relationship between coronary plaque morphology of the left anterior descending artery and 12 months clinical outcome: the CLIMA study. Eur Heart J 2020;41:383-391.
3. Kedhi E, Berta B, Roleder T, Hermanides RS, Fabris E, AJJ IJ et al. Thin-cap fibroatheroma predicts clinical events in diabetic patients with normal fractional flow reserve: the COMBINE OCT-FFR trial. Eur Heart J 2021;42:4671-4679.
4. Mol JQ, Volleberg R, Belkacemi A, Hermanides RS, Meuwissen M, Protopopov AV et al. Fractional Flow Reserve-Negative High-Risk Plaques and Clinical Outcomes After Myocardial Infarction. JAMA Cardiol 2023;8:1013-1021.
5. Volleberg R, Rroku A, Mol JQ, Hermanides RS, van Leeuwen M, Berta B et al. FFR-Negative Nonculprit High-Risk Plaques and Clinical Outcomes in High-Risk Populations: An Individual Patient-Data Pooled Analysis From COMBINE (OCT-FFR) and PECTUS-obs. Circ Cardiovasc Interv 2025;18:e014667.
6. Gruslova AB, Singh S, Hoyt T, Vela D, Vengrenyuk Y, Buja LM et al. Accuracy of OCT Core Labs in Identifying Vulnerable Plaque. JACC Cardiovasc Imaging 2024;17:448-450.
7. Kini AS, Vengrenyuk Y, Yoshimura T, Matsumura M, Pena J, Baber U et al. Fibrous Cap Thickness by Optical Coherence Tomography In Vivo. J Am Coll Cardiol 2017;69:644-657.
8. Park SJ, Ahn JM, Kang DY, Yun SC, Ahn YK, Kim WJ et al. Preventive percutaneous coronary intervention versus optimal medical therapy alone for the treatment of vulnerable atherosclerotic coronary plaques (PREVENT): a multicentre, open-label, randomised controlled trial. Lancet 2024;403:1753-1765.
9. Volleberg R, van der Waerden RGA, Luttikholt TJ, van der Zande JL, Cancian P, Gu X et al. Comprehensive full-vessel segmentation and volumetric plaque quantification for intracoronary optical coherence tomography using deep learning. Eur Heart J Digit Health 2025;6:404-416.
10. Mol JQ, Belkacemi A, Volleberg RH, Meuwissen M, Protopopov AV, Laanmets P et al. Identification of anatomic risk factors for acute coronary events by optical coherence tomography in patients with myocardial infarction and residual nonflow limiting lesions: rationale and design of the PECTUS-obs study. BMJ Open 2021;11:e048994.
11. Tearney GJ, Regar E, Akasaka T, Adriaenssens T, Barlis P, Bezerra HG et al. Consensus standards for acquisition, measurement, and reporting of intravascular optical coherence tomography studies: a report from the International Working Group for Intravascular Optical Coherence Tomography Standardization and Validation. J Am Coll Cardiol 2012;59:1058-72.
12. Araki M, Park SJ, Dauerman HL, Uemura S, Kim JS, Di Mario C et al. Optical coherence tomography in coronary atherosclerosis assessment and intervention. Nat Rev Cardiol 2022;19:684-703.
13. Cancian P, Saitta S, Gu X, van Herten RLM, Luttikholt TJ, Thannhauser J et al. Attenuation artifact detection and severity classification in coronary OCT using mixed image representations. SPIE Medical Imaging, Image Processing 2025.
14. Isensee F, Wald T, Ulrich C, Baumgartner M, Roy S, Maier-Hein K et al. nnU-Net Revisited: A Call for Rigorous Validation in 3D Medical Image Segmentation. Cham: Springer Nature Switzerland, 2024:488-498.
15. Niioka H, Kume T, Kubo T, Soeda T, Watanabe M, Yamada R et al. Automated diagnosis of optical coherence tomography imaging on plaque vulnerability and its relation to clinical outcomes in coronary artery disease. Sci Rep 2022;12:14067.
16. Hong H, Jia H, Zeng M, Gutierrez-Chico JL, Wang Y, Zeng X et al. Risk Stratification in Acute Coronary Syndrome by Comprehensive Morphofunctional Assessment With Optical Coherence Tomography. JACC Asia 2022;2:460-472.

17. Biccirè FG, Budassi S, Ozaki Y, Boi A, Romagnoli E, Di Pietro R et al. Optical coherence tomography-derived lipid core burden index and clinical outcomes: results from the CLIMA registry. Eur Heart J Cardiovasc Imaging 2023;24:437-445.

18. Luttikholt TJ, Thannhauser J, van Royen N. Detection of large areas of thin-cap fibroatheroma in a recurrent STEMI patient using a novel artificial intelligence algorithm: moving from 2D to 3D. Eur Heart J 2025.

SUPPLEMENTAL MATERIAL

Supplemental material related to this article can be found in the online version:
https://academic.oup.com/eurheartj/article/46/46/5032/8244402





CHAPTER 18

General discussion

GENERAL DISCUSSION

This thesis aimed to evaluate the value of optical coherence tomography (OCT) for procedural guidance and high-risk plaque imaging, and to provide a framework for automated image analysis. By combining these objectives, this work sought to explore the full potential of OCT.

Procedural guidance

In recent years, a multitude of randomized trials have demonstrated the benefit of intracoronary imaging as a supplement to conventional angiography for guidance of revascularization.[1] OCT appears particularly useful for guidance of stent implantation and optimization once the indication for revascularization has been established. Little evidence supports the use of OCT for establishing the revascularization indication,[2,3] which is also reflected in **Chapter 3**, where the fractional flow reserve (FFR) appeared to have influenced this decision making more profoundly. Importantly, the optimal threshold for defining ischemia remains unknown and likely dependents on the evaluated coronary artery and the amount of myocardium subtended. As such, anatomical cut-offs may be unsuitable. The recent development of OCT-derived computational flow indices may overcome this limitation and expand the usability of OCT for establishing revascularization indications.[4] However, dedicated randomized data on the clinical efficacy and safety of such indices are urgently needed, also considering the inferiority of an angiography-derived flow index compared with pressure-wire derived fractional flow reserve in the FAVOR III Europe trial.[5] Finally, recognition of imaging artefacts is fundamental for appropriate use of OCT for guidance of revascularization. In **Chapters 4** and **5**, two frequently underappreciated artefacts are illustrated.

High-risk plaque or patient hypothesis

A major advantage of OCT compared to angiography alone is its ability to study plaque morphology. This can be particularly helpful for prognostication through the detection of so-called high-risk plaques.

High-risk plaque

Two important hypotheses exist for the identification of lesions at increased risk of cardiovascular events. First, the stenosis hypothesis states that the lesions at risk are characterized by a large degree of stenosis that impairs coronary blood flow.[6] In daily practice, we predominantly focus our decision making on this hypothesis. Nevertheless, recurrent events remain common despite FFR-guided deferral of revascularization, especially after myocardial infarction and in diabetic patients. [7-9]

The high-risk plaque hypothesis emphasizes that lesion morphology, rather than stenosis severity alone, is crucial for identifying lesions at risk.[6] Multiple post-mortem and *in vivo* studies have provided valuable insights into what characterizes a high-risk plaque, and what prognostic implications they bear.[10-13] However, prior *in vivo* studies did not specifically investigate the high-risk plaque hypothesis outside the stenosis hypothesis (i.e. in confirmed absence of flow limitations), or combined parameters of both

hypotheses. For example, in the landmark PROSPECT study, high-risk plaques were characterized by a minimum lumen area ≤4.00 mm^2, a plaque burden ≥70% and a thin-cap fibroatheroma (TCFA) as identified using intravascular ultrasound (IVUS).[11] The minimum lumen area and, to a lesser degree, the plaque burden could be considered markers of the stenosis hypothesis and they provide little information on plaque morphology. The hazard ratio for TCFA was substantially lower (3.35, 95% confidence interval 1.77-6.36) compared to the overall hazard ratio of approximately 11 for the complete high-risk plaque criterium.[11] Besides, TCFA was identified using virtual histology-IVUS, which is no longer available following concerns regarding its validity. Likewise in the PROSPECT-II study, using near-infrared spectroscopy-IVUS, the hazard ratio for the minimum lumen area ≤4.00 mm^2 and plaque burden ≥70% were higher than for the plaque morphology marker of a high lipid core burden index within 4 mm.[12] Furthermore, ischemia was not routinely excluded in these studies.

Therefore, we conducted the PECTUS-obs study, a prospective natural-history study on the association between FFR-negative non-culprit lesions and clinical outcome in 438 patients with myocardial infarction (**Chapter 6**). In this study, lesions were considered high-risk if they met at least two out of three predefined plaque morphology criteria: 1) a lipid arc ≥90°, 2) a minimum fibrous cap thickness <65 µm and/or 3) presence of either plaque rupture or thrombus. The rationale behind these criteria was that the first two criteria reflect the hallmarks of TCFA, which has been used in the majority of studies on high-risk plaques. The adoption of either plaque rupture or thrombus is relatively uncommon, but is supported by literature. First, subclinical plaque rupture in the presence of a well-functioning healing capacity contributes to rapid, stepwise lesion progression[14] and can consequently induce ischemia requiring revascularization.[14-16] Second, culprit plaque rupture has been associated with signs of panvulnerability, including more non-culprit TCFA and plaque rupture,[17] and multiple NC plaque ruptures are more common among patients with acute coronary syndrome compared to patients with chronic coronary syndrome.[18] These observations indicate likeliness of future repeat ruptures in these patients. Thrombus was also included as marker of vulnerability as its presence can obscure a potential underlying plaque rupture, which may otherwise have led to an underestimation of high-risk plaques.

Our observations in **Chapter 10**, in which we pooled the 2-year follow-up data from PECTUS-obs with the long-term data from the similarly designed prospective COMBINE (OCT-FFR) study comprising 390 patients with diabetes and FFR-negative deferred lesions,[19,20] provide unique evidence on the complementary nature of the high-risk plaque hypothesis on top of the stenosis hypothesis. Indeed, presence of a high-risk plaque according to the PECTUS-obs criteria was associated with a 2.6 to 3.8-fold increased risk of lesion-level events once more, including an increased risk of target-vessel related myocardial infarction.

High-risk patient

Although the high-risk plaque hypothesis originally referred to identification of individual high-risk lesions that cause lesion-related events, the hypothesis has been extrapolated to the whole coronary

epicardial vasculature ("the high-risk patient"). The main rationale behind this extrapolation is that atherosclerosis is a systemic disease. Therefore, a single focal high-risk plaque could be regarded as a marker of panvulnerability across the vasculature rather than a focal problem restricted to that specific location. Indeed, multiple high-risk lesions are frequently observed within a patient.[21] The findings in this thesis support this extrapolated hypothesis. In **Chapters 6**, **9** and **10**, OCT-identified high-risk plaques were associated with a twofold increased risk of the patient-level composite of mortality, non-fatal myocardial infarction and unplanned revascularization. **Chapter 7** emphasizes that these results sustain across the spectrum of myocardial infarction. Additionally, this chapter provides reassurance regarding one of the major concerns for PECTUS-obs, namely that in the proportion of patients that presented with non-ST-segment elevation myocardial infarction, OCT may have been performed on misidentified culprit lesions. In this prespecified subgroup analysis, we did not observe a higher prevalence of non-culprit plaque rupture and/or thrombus in these patients, signs that may indicate 'missed' culprit lesions. **Chapter 8** provides preliminary evidence on potential sex-related differences in non-culprit plaque morphology. Interestingly, female patients had a higher prevalence of high-risk plaques but that did not translate into a higher number of events. It could be postulated that other processes more profoundly affect prognosis in female patients, such as those involved in endothelial denudation and consequent plaque erosion.[22] However, the relative low number of patients in this subgroup analysis precluded any firm conclusions.

Pre-emptive treatment of high-risk plaques

The totality of evidence originating from previous studies and this thesis provides robust evidence that high-risk plaques are associated with adverse prognosis, both on a lesion and patient level. As a result, we are now challenged with the subsequent question: can we reduce the risk of recurrent cardiovascular events in these patients by pre-emptive treatment of such plaques. Two important treatment strategies should be distinguished in that regard.

Systemic therapy

First, systemic therapy through intensive lipid lowering therapy or anti-inflammatory therapy has been proposed. Multiple blinded randomized trials with (high-intensity) statin therapy, ezetimibe, proprotein convertase subtilisin/kexin type 9-inhibitors, or combination strategies consistently demonstrated the potential of intensive lipid lowering therapy for plaque stabilization.[23] For example, the PACMAN-AMI trial, comprising 300 patients randomized to alirocumab versus placebo on top of high-intensity statin therapy, demonstrated that intensified lipid lowering therapy with alirocumab (as also confirmed by lower levels of low density lipoprotein cholesterol during follow-up) led to a larger decrease in plaque atheroma volume and maximum lipid core burden index within 4 mm, and a larger increase in the minimum fibrous cap thickness.[24] Interestingly, in an unpowered secondary analysis, patients demonstrating triple regression were at lower risk for recurrent events during the first year of follow-up compared to patients without triple regression.[25] Anti-inflammatory therapy may also help stabilize plaques, considering the importance of inflammation in the development and progression of atherosclerotic disease.[26] The

randomized COLOCT trial demonstrated that low-dose colchicine led to a larger increase in fibrous cap thickness compared to placebo with a slightly greater reduction in macrophage accumulation in the intervention group. However, no difference was observed in the prevalence of TCFA, which was low in general.[27]

The observations in this thesis support ongoing trials on systemic therapy, as our research indicates that the increased risk associated with high-risk plaques is not restricted to the target-lesion only. Instead, this thesis underscores the systemic nature of atherosclerosis and plaque vulnerability, and therefore supports the high-risk patient hypothesis more strongly than high-risk plaque hypothesis. Largescale trials on systemic treatment of high-risk plaque harboring patients, powered for clinical endpoints, are now warranted.

Focal treatment

Second, it has been postulated that focal treatment of high-risk plaques could potentially result in sealing of high-risk plaques, thereby preventing devastating clinical manifestations resulting from plaque destabilization. At first, this strategy was tested using bioresorbable vascular scaffolds in the PROSPECT-ABSORB and PECTUS trials.[28,29] The rationale was that plaques could be stabilized with these devices, while the foreign material would dissolve overtime, thereby preventing long-term stent-related problems. Unfortunately, the history of bioresorbable scaffolds turned out differently, with an excess in stent thrombosis in patients treated with bioresorbable scaffolds. Nevertheless, the PROSPECT-ABSORB trial demonstrated that the median neointima cap at 25 months was 210 µm, thereby providing preliminary evidence that plaques can be stabilized through neointima formation.[28] With newer generation bioresorbable scaffolds, we may see a revival in this treatment approach. Similarly targeting a leave-nothing-behind rationale, drug-eluting balloons or cryoballoons have been tested for focal treatment of high-risk plaques. However, available evidence is restricted to data from non-randomized proof-of-concept studies.[30] As such, the only data from a randomized clinical trial, powered to demonstrate differences in clinical outcome, are largely obtained with non-resorbable drug-eluting stents.

The PREVENT trial compared preventive percutaneous coronary intervention (PCI) on top of optimal medical therapy compared to optimal medical therapy only for high-risk plaques. After 2 years, the occurrence of cardiac death, target vessel-related myocardial infarction, target vessel-related unplanned revascularization or hospitalization for unstable or progressive angina was significantly lower in patients undergoing preventive PCI (0.4% versus 3.4%).[31] These results provide the first evidence that preventive focal treatment of high-risk plaques may improve patient outcomes with a number needed to treat of 33.3. However, these findings must be interpreted cautiously in view of several important limitations. First, although all components of the primary endpoint occurred numerically less frequently in the intervention arm, the results were predominantly driven by a higher incidence of ischemia driven revascularization and recurrent hospitalization for unstable or progressive angina

in the control arm. This is an important consideration in view of the non-blinded design of the study. Second, the studied population was relatively low-risk with less than 4% of patients being included after myocardial infarction. This may explain the low event rate compared to those observed in the higher-risk populations presented in this thesis. Finally, and arguably most importantly, over 95% of included lesions were characterized by a minimum lumen area <4.00 mm^2 and a plaque burden >70%. As discussed before, these could at least partially be regarded as markers of the stenosis hypothesis rather than the plaque hypothesis. In contrast, OCT-identified TCFA encompassed only 1% of included lesions. Besides, the low absolute risk reduction questions the value and cost-effectiveness of this strategy, unless patient selection is improved.

Several ongoing trials will provide additional data on the effectiveness of preventive focal treatment of high-risk plaques. However, it remains questionable whether these trials will provide us a definitive answer. For example, the INTERCLIMA and COMBINE-INTERVENE trials, that compare OCT-guidance versus FFR-guidance, both incorporate a lesion severity marker in the OCT arm. In the INTERCLIMA trial, PCI is indicated in presence of a minimum fibrous cap thickness <75 um in combination with at least two out of three criteria: 1) minimum lumen area <3.5 mm^2, a lipid arc >180° and/or macrophage accumulation. However, at operator's discretion, PCI is also allowed with a minimum lumen area <2.0 mm^2 and/or a FFR ≤0.80. In the experimental-arm of the COMBINE-INTERVENE trial, PCI is indicated in presence of OCT-identified TCFA, plaque rupture and/or plaque erosion in combination with an area stenosis of at least 70% or a minimum lumen area <2.5 mm^2, but also if the FFR is ≤0.75. These design choices may dilute the analyses and thereby reduce the statistical power to demonstrate the true benefit of focal treatment of high-risk plaque. In contrast, the VULNERABLE trial is randomizing patients with vulnerable plaques to preventive PCI on top of optimal medical therapy versus optimal medical therapy as stand-alone therapy. Patients with myocardial infarction and FFR-negative non-culprit lesions are eligible, in line with the patient population described in this thesis. However, this study is relatively modestly sized, with 600 participants, and the primary endpoint includes target-lesion revascularization which can become cumbersome when interpreting this non-blinded trial.

Another interesting approach is the use of OCT to directly evaluate both the stenosis hypothesis (e.g. through measurement of the minimum lumen area or through computational flow indices) and plaque hypothesis. Such a strategy would omit the need for concurrent use of pressure wires and imaging catheters, and simultaneously allows stent guidance. As noted, COMBINE-INTERVENE and INTERCLIMA will actually test this strategy rather than treatment of high-risk plaques only as both studies compare OCT-guidance to FFR-guidance. Additionally, the FLAVOUR (using IVUS) and FORZA (using OCT) demonstrated equipoise between intracoronary imaging guidance and FFR-guided revascularization, albeit at cost of increased rate of revascularization following intracoronary imaging guidance.[2,3,32,33] Both studies combined anatomical and morphological features for guidance of revascularization. While in FLAVOUR a plaque burden >70% was used as morphological marker, plaque rupture was adopted in FORZA.[2,3,32,33] The inclusion of plaque rupture in their criteria is reinforced by the observations in **Chapters**

7 and 9, in which we demonstrated the prognostic implications of non-culprit plaque rupture. However, other markers of vulnerability such as TCFA were not used to advocate treatment in the FORZA trial.

In conclusion, a growing body of evidence supports the notion that high-risk plaque identification can be used for prognostication. Awaiting additional evidence from randomized trials, strict adherence to guideline recommendations for intensive lipid lowering therapy could be considered in patients harboring high-risk plaques. However, routine preventive focal treatment seems too early in the present state, particularly in view of the limited data on efficacy and remaining challenges of this approach.

Limiting factors for clinical usability of the high-risk plaque hypothesis

Several factors should be acknowledged that limit the translation of the high-risk plaque or patient hypotheses to daily clinical practice.

First, the high-risk plaque hypothesis in its presently studied form only focusses on the rupture-prone plaque. While plaque rupture remains the most prevalent underlying mechanism of type-1 myocardial infarction, its contribution is diminishing in response to contemporary, intensive lipid-lowering therapy regimens. In contrast, the number of cases attributable to plaque erosion is increasing, of which the precursors remain largely unknown and are vastly understudied.[22]

Second, high-risk plaques are found in only approximately one in three patients and lesions, which is a critical consideration in view of the invasive nature of OCT and related costs. In **Chapter 11**, we evaluated whether high-risk plaques could be predicted *a priori* using clinical risk factors. Unfortunately, clinical risk scores had no discriminative value for the prediction of high-risk plaques. These results correspond with another study that found a significant association between clinical risk factors and high-risk plaques in culprit lesions but not in nonculprit lesions.[34] Therefore, additional efforts are required to predict the presence of high-risk plaques. The value of conventional energy-integrating detector computed tomography as first line screening modality has been shown to be limited as the association between computed tomography-identified and invasive imaging-identified high-risk plaques is modest.[35,36] We are actively investigating whether state-of-the-art photon-counting detector computed tomography has superior discriminatory value. Alternatively, circulating inflammatory markers and/or lipid particles could be studied for the prediction of high-risk plaque presence.

Third, the positive predictive value for patient-level and especially lesion-level events remains limited. This is particularly important when pursuing preventive focal treatment of high-risk plaques. For example, in a recent meta-analysis, the positive predictive value at a lesion-level was only 1% (interquartile range 1-2%).[13] This means that, theoretically, 100 patients would need to be preventively treated to potentially prevent a single event if no stent-related issues would occur. The lesion-level positive predictive value of the PECTUS-obs criteria in **Chapter 10** was 10.8%. Therefore, efforts should be made to improve both patient and lesion selection. Regarding the latter, the concurrent presence of multiple high-risk plaque

features results in incremental risk of cardiovascular events. In the aforementioned meta-analyses, the lesion-level positive predictive value increased to 14% (interquartile range 8-20%) in the presence of at least two high-risk plaque features.[13] Within this thesis we demonstrate similar results in **Chapter 10**. In the copresence of all three high-risk plaque criteria from PECTUS-obs, the lesion-level positive predictive value of target lesion failure attributable to the target lesion was 13.3%, compared to 9.5% in the presence of two criteria and 4.4% in the presence of a single feature. Likewise, the positive predictive value may also improve by integrating hemodynamic forces in the equation.[6] As a result, designing trials that incorporate multiple high-risk plaque criteria seems beneficial. However, it remains unclear what the optimal threshold would be to prevent both over- and undertreatment of high-risk plaques. Next generation imaging catheters such as micro-OCT or hybrid catheters (e.g. OCT-near infrared spectroscopy or OCT-IVUS) may also be more informative than single technology approaches.[37,38] Regarding patient selection, greater absolute benefit can be expected when targeting high-risk populations such as patients with myocardial infarction or diabetes. In **Chapter 11**, we demonstrate that patients with both a high-risk clinical profile and a high-risk plaque were indeed at the highest risk for recurrent events, making them most amenable to intervention with the lowest number needed to treat. However, we found a consistent hazard associated with the presence of a high-risk plaque across clinical risk profiles. Therefore, the findings do not support restrictive screening in lower risk patients for prognostication. Ultimately, the optimal strategy for screening remains to be investigated. We postulate that a stepwise approach may help identify patients at the highest risk. As discussed before, intensive medical therapy can help stabilize high-risk plaques. However, high-risk plaques remain in a subset of patients despite intensive treatment.[25] Consequently, an interesting strategy would be to target focal treatment of high-risk plaques only in those patients who still have high-risk plaques despite intensive lipid lowering therapy.

Finally, substantial interobserver variability has been reported for identification of high-risk plaques. For example, *post-hoc* core lab imaging analyses from the PREVENT trial revealed that 10% of included lesions did not meet the criteria of a high-risk plaque, while site operators had identified all these lesions as high-risk.[31] How many lesions were falsely excluded by site operators remains unknown. Remarkably, this disparity in image interpretation was observed even though high-risk plaques in PREVENT were predominantly characterized by relatively easily identifiable features such as area-based measures. In this view, the expected disparity for more qualitative and challenging markers such as TCFA might even be larger. Indeed, prior OCT-based studies specifically investigating this issue demonstrated high variability, even among very experienced readers.[39,40] These observations should be interpreted as an urgent call for automated image analysis algorithms.

Convenient automated image analysis using artificial intelligence

Artificial intelligence can contribute to reliable and standardized OCT image interpretation. Safe adoption of artificial intelligence in daily clinical care, however, requires adherence to high standards for development and validation. In **Chapter 12**, we provide a multidisciplinary view on the development of artificial intelligence particularly for the identification of high-risk coronary plaques, addressing fundamentals including bias, reliability, fairness, and generalizability. Unfortunately, the majority of proposed algorithms for OCT do not adhere to the recommended quality standards, as outlined in the systematic review in **Chapter 13**. In particular, external validation was performed in only one in eight studies. Additionally, the transparency with which study characteristics and performances are reported is remarkably low. This concerning caveat limits comparison of algorithms, which may lead to unnecessary use of resources and unjustified trust in certain algorithms. Although it may not solve the complete problem, an easy step towards improving transparency is adherence to artificial intelligence-specific reporting guidelines[41], as well as implementation of artificial intelligence-specific quality assessment tools.[42]

In **Chapter 14**, we provide the first results of our deep learning-based multiclass semantic segmentation model. We evaluated its performance on both internal and external datasets for various purposes. For example, we demonstrate its performance on a pixel-level and frame-level for the identification, localization and quantification of various plaque-related and non-plaque related features. Importantly, we presented our results in a transparent manner so that future algorithms can be compared to our current results. Additionally, compared to previous multiclass segmentation models, challenging frames were not excluded during training and testing, such as those containing artefacts and destabilized plaques. This aspect greatly improves the generalizability of our method. In **Chapter 15**, the large-scale external validation results are presented, comprising 100 patients and 2560 analyzed OCT images. The need for such an algorithm is again stressed in this study by the substantial interobserver variability, particularly for lipidic plaque assessment. The results indicate high generalizability of our methodology to a real-world dataset of consecutive patients. Specifically, the performance for the identification and quantification of calcific plaques was very high and close to interobserver variability among expert reads. Most intriguingly, the performance for the evaluation of lipidic plaques, which are inherently more challenging to evaluate, was surpassing expert interobserver variability.

Using this algorithm, this thesis provides evidence that may induce a shift in high-risk plaque evaluation. While OCT, IVUS and near-infrared spectroscopy provide distinct, and likely complementary, information on plaque morphology, concomitant use of all three imaging modalities is restricted by financial and time constraints. In **Chapters 16** and **17**, we demonstrated that all this information can now be obtained within a single OCT pullback using AI. Specifically, **Chapter 16** demonstrates the feasibility of estimating plaque burden from OCT, a variable long believed to be unanalyzable with OCT due to the light-absorbing nature of lipidic and heavily calcific plaque. **Chapter 17** demonstrates the potential of automated identification of TCFA, with a discriminatory capability for prognostication at least comparable to core

laboratory-based image analyses. Furthermore, by leveraging the comprehensiveness and speed of AI, we were able to evaluate all information available within OCT pullbacks for improved prognostication. Overall, these chapters demonstrate how AI can overcome inherent limitations of OCT and how AI can be used to leverage more information for improved prognostication. These chapters question the future need for IVUS and near-infrared spectroscopy as a tool for high-risk plaque imaging. However, future studies are needed to externally validate these findings.

Although the work described in these chapters provide a solid foundation, it is not yet the final product of our research group. Instead, we will continue to develop and improve algorithms for intracoronary OCT in the newly founded artifical intelligence lab (CARA lab), a collaboration between the Amsterdam UMC and Radboudumc. Ongoing projects focus on optimization of the processing time, new modules for the identification of destabilized plaques, artifact identification and correction, modules targeting stents, and the incorporation of uncertainty and explainability measures. Finally, user-friendly interfaces are required for streamlined processing in the catheterization laboratory. In the coming years, researchers within the CARA lab will devote their efforts to achieving these goals.

Down the line, we hypothesize that artificial intelligence-assisted OCT-guidance of revascularization may improve patient outcome by providing a comprehensive overview of the preprocedural coronary status, predictions regarding procedural successfulness and evaluation of post-procedural results. However, the clinical benefit of such strategy has yet to be established, as is the case for the majority of artificial intelligence models proposed, and sometimes even already adopted, throughout medicine.[43,44] A final interesting approach is the direct use of AI for prognostication in an end-to-end manner. Can artificial intelligence help identify plaque features associated with adverse outcome that we have not yet thought of, or even any that are not discernible by the human eye?

Conclusions

In **Chapter 2**, we hypothesized that OCT could serve a future all-in-one function for guidance of coronary revascularization. Although this may be considered premature at the current state, a growing body of evidence has been accumulated during the writing of this thesis that supports the use of OCT for various indications. This thesis contributes by extending the available evidence on OCT-based identification of high-risk plaques, particularly demonstrating that the high-risk plaque and patient hypotheses are complementary to the stenosis hypothesis. Additionally, this thesis provides an evaluation of the current status of artificial intelligence models for OCT including its strengths and weaknesses and provides a framework for successful model development, so that in the future high-quality algorithms can aid clinicians with comprehensive and trustworthy automated image analysis. Our results demonstrate the feasibility of such an approach, and the potential to revolutionize high-risk plaque imaging. In conclusion, although additional evidence is needed before OCT can be endorsed as an all-in-one tool for guidance of coronary revascularization, this thesis provides new evidence supporting that hypothesis.

REFERENCES

1. Stone GW, Christiansen EH, Ali ZA, Andreasen LN, Maehara A, Ahmad Y et al. Intravascular imaging-guided coronary drug-eluting stent implantation: an updated network meta-analysis. Lancet 2024;403:824-837.
2. Burzotta F, Leone AM, Aurigemma C, Zambrano A, Zimbardo G, Arioti M et al. Fractional Flow Reserve or Optical Coherence Tomography to Guide Management of Angiographically Intermediate Coronary Stenosis: A Single-Center Trial. JACC Cardiovasc Interv 2020;13:49-58.
3. Burzotta F, Zito A, Aurigemma C, Romagnoli E, Bianchini F, Bianchini E et al. Fractional flow reserve or optical coherence tomography for angiographically intermediate coronary stenoses: 5-year outcomes in the FORZA trial. Eur Heart J 2024;45:2785-2788.
4. Jeremias A, Maehara A, Matsumura M, Shlofmitz RA, Maksoud A, Akasaka T et al. Optical Coherence Tomography-Based Functional Stenosis Assessment: FUSION-A Prospective Multicenter Trial. Circ Cardiovasc Interv 2024;17:e013702.
5. Andersen BK, Sejr-Hansen M, Maillard L, Campo G, Råmunddal T, Stähli BE et al. Quantitative flow ratio versus fractional flow reserve for coronary revascularisation guidance (FAVOR III Europe): a multicentre, randomised, non-inferiority trial. Lancet 2024;404:1835-1846.
6. Stone PH, Libby P, Boden WE. Fundamental Pathobiology of Coronary Atherosclerosis and Clinical Implications for Chronic Ischemic Heart Disease Management-The Plaque Hypothesis: A Narrative Review. JAMA Cardiol 2023;8:192-201.
7. Cerrato E, Mejia-Renteria H, Dehbi HM, Ahn JM, Cook C, Dupouy P et al. Revascularization Deferral of Nonculprit Stenoses on the Basis of Fractional Flow Reserve: 1-Year Outcomes of 8,579 Patients. JACC Cardiovasc Interv 2020;13:1894-1903.
8. Kennedy MW, Hermanides RS, Kaplan E, Hemradj V, Fabris E, Koopmans PC et al. Fractional Flow Reserve-Guided Deferred Versus Complete Revascularization in Patients With Diabetes Mellitus. Am J Cardiol 2016;118:1293-1299.
9. Ekmejian A, Sritharan H, Selvakumar D, Venkateshka V, Allahwala U, Ward M et al. Outcomes of deferred revascularisation following negative fractional flow reserve in diabetic and non-diabetic patients: a meta-analysis. Cardiovasc Diabetol 2023;22:22.
10. Burke AP, Farb A, Malcom GT, Liang YH, Smialek J, Virmani R. Coronary risk factors and plaque morphology in men with coronary disease who died suddenly. N Engl J Med 1997;336:1276-82.
11. Stone GW, Maehara A, Lansky AJ, de Bruyne B, Cristea E, Mintz GS et al. A prospective natural-history study of coronary atherosclerosis. N Engl J Med 2011;364:226-35.
12. Erlinge D, Maehara A, Ben-Yehuda O, Botker HE, Maeng M, Kjoller-Hansen L et al. Identification of vulnerable plaques and patients by intracoronary near-infrared spectroscopy and ultrasound (PROSPECT II): a prospective natural history study. Lancet 2021;397:985-995.
13. Gallone G, Bellettini M, Gatti M, Tore D, Bruno F, Scudeler L et al. Coronary Plaque Characteristics Associated With Major Adverse Cardiovascular Events in Atherosclerotic Patients and Lesions: A Systematic Review and Meta-Analysis. JACC Cardiovasc Imaging 2023;16:1584-1604.
14. Araki M, Yonetsu T, Kurihara O, Nakajima A, Lee H, Soeda T et al. Predictors of Rapid Plaque Progression: An Optical Coherence Tomography Study. JACC Cardiovasc Imaging 2021;14:1628-1638.
15. Vergallo R, Crea F. Atherosclerotic Plaque Healing. N Engl J Med 2020;383:846-857.
16. Kurihara O, Russo M, Kim HO, Araki M, Shinohara H, Lee H et al. Clinical significance of healed plaque detected by optical coherence tomography: a 2-year follow-up study. J Thromb Thrombolysis 2020;50:895-902.

17. Vergallo R, Ren X, Yonetsu T, Kato K, Uemura S, Yu B et al. Pancoronary plaque vulnerability in patients with acute coronary syndrome and ruptured culprit plaque: a 3-vessel optical coherence tomography study. Am Heart J 2014;167:59-67.
18. Vergallo R, Uemura S, Soeda T, Minami Y, Cho JM, Ong DS et al. Prevalence and Predictors of Multiple Coronary Plaque Ruptures: In Vivo 3-Vessel Optical Coherence Tomography Imaging Study. Arterioscler Thromb Vasc Biol 2016;36:2229-2238.
19. Kennedy MW, Fabris E, Ijsselmuiden AJ, Nef H, Reith S, Escaned J et al. Combined optical coherence tomography morphologic and fractional flow reserve hemodynamic assessment of non- culprit lesions to better predict adverse event outcomes in diabetes mellitus patients: COMBINE (OCT-FFR) prospective study. Rationale and design. Cardiovasc Diabetol 2016;15:144.
20. Kedhi E, Berta B, Roleder T, Hermanides RS, Fabris E, AJJ IJ et al. Thin-cap fibroatheroma predicts clinical events in diabetic patients with normal fractional flow reserve: the COMBINE OCT-FFR trial. Eur Heart J 2021;42:4671-4679.
21. Kubo T, Imanishi T, Kashiwagi M, Ikejima H, Tsujioka H, Kuroi A et al. Multiple coronary lesion instability in patients with acute myocardial infarction as determined by optical coherence tomography. Am J Cardiol 2010;105:318-22.
22. Meteva D, Pedicino D, Abdelwahed YS, Kränkel N, Anwari E, Leistner DM et al. Acute coronary syndrome with plaque erosion: clinical characteristics, mechanisms, and unmet needs. Eur Heart J 2025.
23. Kim H, Ahn JM, Kang DY, Lee J, Choi Y, Park SJ et al. Management of Coronary Vulnerable Plaque With Medical Therapy or Local Preventive Percutaneous Coronary Intervention. JACC Asia 2024;4:425-443.
24. Raber L, Ueki Y, Otsuka T, Losdat S, Haner JD, Lonborg J et al. Effect of Alirocumab Added to High-Intensity Statin Therapy on Coronary Atherosclerosis in Patients With Acute Myocardial Infarction: The PACMAN-AMI Randomized Clinical Trial. JAMA 2022;327:1771-1781.
25. Biccire FG, Haner J, Losdat S, Ueki Y, Shibutani H, Otsuka T et al. Concomitant Coronary Atheroma Regression and Stabilization in Response to Lipid-Lowering Therapy. J Am Coll Cardiol 2023;82:1737-1747.
26. Libby P. The changing landscape of atherosclerosis. Nature 2021;592:524-533.
27. Yu M, Yang Y, Dong SL, Zhao C, Yang F, Yuan YF et al. Effect of Colchicine on Coronary Plaque Stability in Acute Coronary Syndrome as Assessed by Optical Coherence Tomography: The COLOCT Randomized Clinical Trial. Circulation 2024;150:981-993.
28. Stone GW, Maehara A, Ali ZA, Held C, Matsumura M, Kjoller-Hansen L et al. Percutaneous Coronary Intervention for Vulnerable Coronary Atherosclerotic Plaque. J Am Coll Cardiol 2020;76:2289-2301.
29. Mol JQ, Bom MJ, Damman P, Knaapen P, van Royen N. Pre-Emptive OCT-Guided Angioplasty of Vulnerable Intermediate Coronary Lesions: Results from the Prematurely Halted PECTUS-Trial. J Interv Cardiol 2020;2020:8821525.
30. van Veelen A, Kucuk IT, Garcia-Garcia HM, Fuentes FH, Kahsay Y, Delewi R et al. Paclitaxel-coated balloons for vulnerable lipid-rich plaques. EuroIntervention 2024;20:e826-e830.
31. Park SJ, Ahn JM, Kang DY, Yun SC, Ahn YK, Kim WJ et al. Preventive percutaneous coronary intervention versus optimal medical therapy alone for the treatment of vulnerable atherosclerotic coronary plaques (PREVENT): a multicentre, open-label, randomised controlled trial. Lancet 2024;403:1753-1765.
32. Koo BK, Hu X, Kang J, Zhang J, Jiang J, Hahn JY et al. Fractional Flow Reserve or Intravascular Ultrasonography to Guide PCI. N Engl J Med 2022;387:779-789.
33. Lee JM, Kim H, Hong D, Hwang D, Zhang J, Hu X et al. Clinical Outcomes of Deferred Lesions by IVUS Versus FFR-Guided Treatment Decision. Circ Cardiovasc Interv 2023;16:e013308.
34. Covani M, Niccoli G, Fujimoto D, Scalamera R, Vergallo R, Porto I et al. Plaque Vulnerability and Cardiovascular Risk Factor Burden in Acute Coronary Syndrome: An Optical Coherence Tomography Analysis. J Am Coll Cardiol 2025;86:77-89.

35. Kinoshita D, Suzuki K, Usui E, Hada M, Yuki H, Niida T et al. High-Risk Plaques on Coronary Computed Tomography Angiography: Correlation With Optical Coherence Tomography. JACC Cardiovasc Imaging 2024;17:382-391.

36. Ramasamy A, Parasa R, Sokooti H, Zhang X, Tanboga IH, Kitslaar P et al. Computed tomography versus near-infrared spectroscopy for the assessment of coronary atherosclerosis. EuroIntervention 2024;20:e1465-e1475.

37. Nishimiya K, Tearney G. Micro Optical Coherence Tomography for Coronary Imaging. Front Cardiovasc Med 2021;8:613400.

38. Tufaro V, Jaffer FA, Serruys PW, Onuma Y, van der Steen AFW, Stone GW et al. Emerging Hybrid Intracoronary Imaging Technologies and Their Applications in Clinical Practice and Research. JACC Cardiovasc Interv 2024;17:1963-1979.

39. Kini AS, Vengrenyuk Y, Yoshimura T, Matsumura M, Pena J, Baber U et al. Fibrous Cap Thickness by Optical Coherence Tomography In Vivo. J Am Coll Cardiol 2017;69:644-657.

40. Gruslova AB, Singh S, Hoyt T, Vela D, Vengrenyuk Y, Buja LM et al. Accuracy of OCT Core Labs in Identifying Vulnerable Plaque. JACC Cardiovasc Imaging 2024;17:448-450.

41. Tejani AS, Klontzas ME, Gatti AA, Mongan JT, Moy L, Park SH et al. Checklist for Artificial Intelligence in Medical Imaging (CLAIM): 2024 Update. Radiol Artif Intell 2024;6:e240300.

42. Sounderajah V, Ashrafian H, Rose S, Shah NH, Ghassemi M, Golub R et al. A quality assessment tool for artificial intelligence-centered diagnostic test accuracy studies: QUADAS-AI. Nat Med 2021;27:1663-1665.

43. Chouffani El Fassi S, Abdullah A, Fang Y, Natarajan S, Masroor AB, Kayali N et al. Not all AI health tools with regulatory authorization are clinically validated. Nat Med 2024;30:2718-2720.

44. Han R, Acosta JN, Shakeri Z, Ioannidis JPA, Topol EJ, Rajpurkar P. Randomised controlled trials evaluating artificial intelligence in clinical practice: a scoping review. Lancet Digit Health 2024;6:e367-e373.



CHAPTER 19

Summary
Nederlandse samenvatting

SUMMARY

Intracoronary optical coherence tomography (OCT) is a valuable imaging modality within interventional cardiology, with a potential that extends beyond contemporary guidelines endorsed indications. However, these theoretical benefits lack a robust scientific base. Additionally, the large amount of data obtained with OCT form a barrier for widespread adoption.

This thesis aimed to evaluate the value of OCT for (1) procedural guidance and (2) high-risk plaque imaging, and (3) to provide a framework for automated image analysis, enhancing the applicability of OCT and contribute towards widespread, convenient application.

Part I – Procedural guidance

In **Chapter 2**, we reviewed the literature on the use of OCT at the start of the writing of this thesis. We discussed its value for evaluation of stenosis severity, for culprit lesion evaluation, for high-risk plaque evaluation, for the identification of lesions that require advanced preparation prior to stent placement, for guidance of stent platform selection and placement, and for stent optimization. We hypothesized that OCT, considering its versatility, could potentially serve as a future all-in-one-tool for guidance of percutaneous coronary intervention (PCI).

In **Chapter 3**, we demonstrated that OCT and physiological lesion evaluation using the fractional flow reserve (FFR) provide distinct yet complementary information beyond conventional coronary angiography. While FFR informed revascularization decision making, OCT informed PCI strategy. We hypothesized that novel integrated computational flow indices derived from OCT will allow simultaneous lesion assessment and precise device selection, omitting the need for concomitant use of OCT and FFR.

Chapters 4 and **5** outlined two image artefacts that are frequently underappreciated, but that may have consequences when not adequately recognized. First, we described an artefact that results in a dissection-like appearance, which may prompt operators to erroneously implant a stent. Second, we illustrated how repeat imaging can occur, which can result in misleading lesion length assessment and selection of overly long stents.

Part II – High-risk plaque identification

In the second part of this thesis, we focused on the value of OCT for prognostication through the identification of high-risk plaques, plaques that may cause future cardiovascular events.

The primary results of the prospective, observational PECTUS-obs study are presented in **Chapter 6**. In this study comprising 438 patients with recent myocardial infarction, we demonstrated that the presence of OCT-identified high-risk plaques in FFR-negative, deferred, non-culprit lesions was associated with the primary patient-level endpoint of major adverse cardiovascular events (composite of all-cause mortality,

non-fatal myocardial infarction or unplanned revascularization) at two-year follow-up (hazard ratio [HR] 1.93, 95% confidence interval [CI] 1.08-3.47, p=0.02). High-risk plaques were defined as the presence of at least two out of three predefined criteria: (1) a lipid arc ≥90°, (2) a minimum fibrous cap thickness <65 µm, and (3) presence of plaque rupture or thrombus. Presence of an OCT-identified high-risk plaque remained independently associated with the primary clinical outcome after adjusting for conventional clinical risk factors, highlighting its independent value for prognostication after myocardial infarction.

In a subgroup analysis from PECTUS-obs in **Chapter 7**, we evaluated differences between patients with non-ST-segment elevation and ST-segment elevation myocardial infarction. We observed a comparable prevalence of high-risk plaques, and the presence of at least one high-risk plaque was equally associated with the primary clinical outcome. While non-culprit plaque rupture was associated with adverse outcome in both groups, we highlighted potential differences in the high-risk plaque features that imply high risk between groups in an exploratory analysis.

In **Chapter 8**, we demonstrated that female patients in PECTUS-obs demonstrated more high-risk plaque features than male patients, also after correcting for the more adverse clinical risk profile of female patients. However, this did not translate into a higher risk of adverse events among female patients. Although the sample size precluded definitive conclusions, this study may be considered a call for research on sex-specific high-risk plaque features, potentially focusing on plaque erosion precursors among female patients.

The long-term outcome results of the PECTUS-obs study are described in **Chapter 9**. Follow-up was complete in 99% of patients. At a median follow-up of 5.0 years, presence of at least one high-risk plaques remained significantly associated with the primary endpoint excluding non-cardiac mortality, all periprocedural and stent-related events, and all events that could not be clearly attributed to a specific coronary segment based on the evaluated baseline and event angiograms. Among different high-risk plaque features, plaque rupture demonstrated the strongest prognostic association.

In **Chapter 10**, we provided an individual patient-data pooled analysis of PECTUS-obs and the similarly designed prospective, observational COMBINE (OCT-FFR) study comprising patients with diabetes. Among 810 patients, the presence of a high-risk plaque was associated with an increased risk of patient-level major adverse cardiovascular events (HR 2.13, 95% CI 1.45-3.12. p<0.001) and lesion-level target lesion failure (composite of cardiac death, target-vessel related myocardial infarction or target-lesion unplanned revascularization, HR 2.62, 95% CI 1.56-4.14, p<0.001). Copresence of multiple high-risk plaque features led to an incremental risk. This study again highlights the value of high-risk plaque imaging on top of physiological lesion evaluation. Compared to the previous studies that were focused on patient-level risk, this study also demonstrated increased lesion-level risk.

In a subsequent study on this dataset in **Chapter 11**, we demonstrated that clinical risk factors cannot predict the presence of a high-risk plaque. Furthermore, we demonstrated that high-risk plaques were comparably associated with adverse patient-level and lesion-level outcome across different clinical risk profiles. However, by combining clinical risk factors and high-risk plaque imaging, we were able to identify patients at the highest risk of adverse outcome. We propose that this subgroup may benefit most from preventive therapies.

Part III – Artificial intelligence-based image interpretation

Finally, in the third part, we shift our focus to automated analysis of OCT images using artificial intelligence (AI), focusing on methodology validity, full-vessel segmentation and automated identification of high-risk plaques.

Chapter 12 provides a multidisciplinary framework for the development of AI for high-risk plaque imaging. We reviewed existing evidence on the application of AI for high-risk plaque imaging. Additionally, we provided consensus recommendations for future algorithm development, focusing on requirements for trustworthiness such as robustness and fairness.

In **Chapter 13**, we systematically reviewed 91 articles on AI for OCT. We reported an increasing number of articles on this topic in recent years, with a shift from machine learning to deep learning. While the performance of proposed algorithms was high for the evaluation of the coronary lumen and stent struts, the performance of more intricate tasks such as plaque characterization was lower. Furthermore, we reported a lack of transparency in reporting and substantial risk of bias in the majority of reviewed studies. This review invites readers of AI research to remain critical and evaluate performances in view of the methodology. Additionally, we called for better adherence to reporting guidelines.

In **Chapter 14**, we introduced a new multiclass segmentation algorithm for OCT named OCT-AID, which we evaluated in an internal and external data set. We demonstrated a promising performance across a variety of frames, including those affected by artefacts or with destabilized plaque, which contrasts earlier studies on other algorithms.

A larger-scaled external validation study, comprising 100 consecutive patients from St. Francis Hospital & Heart Center, is presented in **Chapter 15**. In this study, the performance of OCT-AID for the identification and quantification of calcific plaque was excellent and close to interobserver variability. Its performance for the evaluation of lipid plaque, which is inherently more challenging, was superior to interobserver variability. We reported that its performance for low-prevalence classes was limited. This was the largest study to date on any multiclass AI algorithm, and the only one to use a consecutive, unselected cohort of patients, demonstrating the generalizability of our algorithm.

In **Chapter 16**, we evaluated whether OCT-AID could derive plaque burden from OCT, a variable long-believed not to be analyzable with OCT considering its limited penetration depth. Using intravascular ultrasound as the reference standard, we reported an excellent correlation between OCT-derived and intravascular ultrasound-derived plaque burden (r=0.90, 95% CI 0.89-0.91, p<0.001), with consistent correlations across various predominant plaque types. As such, this chapter demonstrates that AI can help overcome inherent limitations of imaging modalities, and illustrates that we can now, for the first time, evaluate thin-cap fibroatheroma (TCFA) and plaque burden simultaneously.

Chapter 17 details the results of the PECTUS-AI study, in which we employed OCT-AID for automated identification of TCFA in PECTUS-obs. AI-identified TCFA within the target lesion was associated with adverse clinical outcome, with a discriminatory value at least comparable with core laboratory-based TCFA identification. When evaluating the complete imaged segment – a task not feasible to perform manually –, the discriminatory value of AI-identified TCFA was significantly higher than based on core laboratory-based analysis of the target lesion only, particularly due to an increase in the negative predictive value. This study demonstrates that AI-based high-risk plaque identification is a reasonable alternative to manual image analysis, and allows easier translation from research findings obtained with highly-experienced core laboratory readers to daily clinical care.

NEDERLANDSE SAMENVATTING

Intracoronaire optische coherentietomografie (OCT) is een waardevolle beeldvormingstechniek binnen de interventiecardiologie met een potentiaal dat verder rijkt dan de toepassingen zoals aanbevolen in de huidige richtlijnen. Echter is er voor deze theoretische meerwaarde nog weinig bewijs. Daarnaast wordt er met OCT een grote hoeveelheid data verkregen, wat als een barrière kan worden gezien voor brede toepassing.

Dit proefschrift richtte zich op de waarde van OCT voor (1) procedurele ondersteuning tijdens percutane coronaire interventie (PCI) en (2) voor het afbeelden van hoog-risico aderverkalking, en (3) op het automatisch analyseren van OCT beelden middels artificiële intelligentie (AI).

Deel I – Procedurele begeleiding

In **Hoofdstuk 2** hebben we de literatuur over het gebruik van OCT die beschikbaar was bij de start van dit promotieonderzoek samengevat. We bespraken de waarde ervan voor de evaluatie van de ernst van een coronaire vernauwing, voor het identificeren van de culprit laesie, voor de evaluatie van hoog-risico aderverkalking, voor het identificeren van laesies die geavanceerde voorbereiding vereisen voorafgaand aan stentplaatsing, voor begeleiding bij de keuze van het type stent en de plaatsing daarvan, en voor stentoptimalisatie. We stelden dat OCT, gezien zijn veelzijdigheid, mogelijk zou kunnen dienen als een toekomstig alles-in-één instrument voor begeleiding van PCI.

In **Hoofdstuk 3** toonden we aan dat OCT en fysiologische laesiebeoordeling met behulp van de fractionele flow reserve (FFR) unieke en complementaire maar complementaire informatie bieden bovenop conventionele coronaire angiografie. Terwijl FFR met name gebruikt wordt om te bepalen of revascularisatie noodzakelijk is, informeert OCT de operateur over de PCI-strategie. Onze hypothese is dat met nieuwe geïntegreerde computationele flow-indices afgeleid van OCT gelijktijdig de ernst van een vernauwing kan worden beoordeeld en nauwkeurig een stent kan worden gekozen, geplaatst en geoptimaliseerd, waardoor het gelijktijdig gebruik van OCT en FFR overbodig wordt.

Hoofdstukken 4 en **5** beschreven twee beeldvormingsartefacten die vaak niet worden onderkend, maar die mogelijke gevolgen hebben. Ten eerste beschreven we een artefact dat leidt tot een dissectie-achtig beeld, wat ertoe kan leiden dat de operateur ten onrechte een stent plaatst. Ten tweede illustreerden we hoe herhaalde beeldvorming van hetzelfde coronaire segment kan optreden, wat kan leiden tot een misleidende beoordeling van de laesielengte en de selectie van een te lange stent.

Deel II – Identificatie van hoog-risico aderverkalking

In het tweede deel van dit proefschrift richtten we ons op de waarde van OCT om de prognose te bepalen middels het beoordelen van hoog-risico aderverkalking. Hierbij keken we naar aderverkalking

waarvan wordt aangenomen dat het in de toekomst tot nieuwe cardiovasculaire gebeurtenissen kan leiden.

De primaire resultaten van de prospectieve, observationele PECTUS-obs study werden gepresenteerd in **Hoofdstuk 6**. In deze studie, waarin 438 patiënten met een recent myocardinfarct werden geïncludeerd, toonden we aan dat de aanwezigheid van door OCT geïdentificeerde hoog-risico aderverkalking in FFR-negatieve, niet-behandelde, non-culprit laesies geassocieerd was met het primaire eindpunt van majeure cardiovasculaire gebeurtenissen (een samengesteld eindpunt van sterfte door alle oorzaken, niet-fatale myocardinfarcten of ongeplande revascularisaties) na twee jaar follow-up (hazard ratio [HR] 1,93, 95% betrouwbaarheidsinterval [BI] 1,08-3,47, p=0.02). Hoog-risico aderverkalking was gedefinieerd als de aanwezigheid van ten minste twee van drie vooraf bepaalde criteria: (1) een lipide hoek ≥90°, (2) een minimale fibreuze kapdikte <65 µm, en (3) aanwezigheid van een plaque ruptuur of stolsel. De aanwezigheid van door OCT geïdentificeerde hoog-risico aderverkalking bleef onafhankelijk geassocieerd met het primaire klinische eindpunt na correctie voor standaard klinische risicofactoren, wat de onafhankelijke waarden van OCT ter beoordeling van de prognose na een myocardinfarct onderstreept.

In een subgroupanalyse van PECTUS-obs, beschreven in **Hoofdstuk 7**, evalueerden we verschillen tussen patiënten met een non-ST-segment elevatie en een ST-segment elevatie myocardinfarct. We observeerden een vergelijkbare prevalentie van hoog-risico aderverkalking in beide groepen. De aanwezigheid van ten minste één laesie met hoog-risico aderverkalking was in beide groepen geassocieerd met het primaire klinische eindpunt. Hoewel non-culprit plaque rupturen in beide groepen geassocieerd waren met een ongunstige uitkomst, lieten we in een verkennende analyse mogelijke verschillen zien tussen de groepen in de kenmerken van hoog-risico aderverkalking die risico impliceren.

In **Hoofdstuk 8** toonden we aan dat vrouwelijke patiënten in PECTUS-obs meer kenmerken van hoog-risico aderverkalking vertoonden dan mannelijke patiënten, ook na correctie voor het ongunstigere klinische risicoprofiel van vrouwen. Dit vertaalde zich echter niet in een hoger risico op ongunstige uitkomsten bij vrouwelijke patiënten. Hoewel een definitieve conclusie niet getrokken kon worden met het oog op het beperkte aantal patiënten in deze studie, kan deze studie worden beschouwd als een oproep tot onderzoek naar sekse-specifieke kenmerken van hoog-risico aderverkalking, waarbij bij vrouwen mogelijk een focus moet komen te liggen op voorlopers van plaque erosie.

De lange termijnresultaten van het PECTUS-obs onderzoek staan beschreven in **Hoofdstuk 9**. Follow-up was compleet in 99% van de patiënten, met een mediane follow-up van 5.0 jaar. De aanwezigheid van ten minste één hoog-risico plaque bleef significant geassocieerd met het primaire eindpunt exclusief non-cardiovasculaire sterfte, alle periprocedurele en stent-gerelateerde events, en alle events die niet evident te linken waren aan een specifiek coronair segment met behulp van het baseline en het event

angiogram. Plaque ruptuur toonde de sterkste prognostische associatie van alle geteste hoog-risico plaque kenmerken.

In **Hoofdstuk 10** presenteerden we een samengestelde analyse van individuele patiënten data van PECTUS-obs en de vergelijkbaar opgezette prospectieve, observationele COMBINE (OCT-FFR) studie bij patiënten met diabetes. Onder 810 patiënten was de aanwezigheid van hoog-risico aderverkalking geassocieerd met een verhoogd risico op slechtere uitkomsten op patiënten niveau (HR 2,13, 95% BI 1,45-3,12, p<0,001) en op laesie niveau (HR 2,62, 95% BI 1,56-4,14, p<0,001). Gelijktijdige aanwezigheid van meerdere hoog-risico aderverkalking kenmerken vergrootte het risico op slechtere uitkomsten. Deze studie benadrukte opnieuw de waarde van het beoordelen van hoog-risico aderverkalking bovenop fysiologie laesiebeoordeling. In tegenstelling tot de eerdere studies gericht op patiëntniveau risico, toonde deze studie ook een verhoogd risico aan op laesieniveau.

In een opvolgende studie binnen dezelfde dataset, beschreven in **Hoofdstuk 11**, toonden we aan dat klinische risicofactoren de aanwezigheid van hoog-risico aderverkalking niet kunnen voorspellen. Daarnaast toonden we aan dat hoog-risico aderverkalking een verhoogd risico impliceerde, ongeacht het klinische risicoprofiel van patiënten. Echter, door klinische risicofactoren te combineren met beeldvorming ter identificatie van hoog-risico aderverkalking konden we een patiëntengroep identificeren met het hoogste risico op ongunstige uitkomsten. We stelden voor dat deze subgroep mogelijk het meeste baat zal hebben van preventieve behandeling van hoog-risico aderverkalking.

Deel III – Automatische beeldanalyse middels artificiële intelligentie

Tot slot verlegden we in het derde deel van dit proefschrift de focus naar geautomatiseerde analyse van OCT beelden met behulp van AI, met aandacht voor methodologische validiteit, segmentatie van de volledige kransslagader en automatische identificatie van hoog-risico aderverkalking.

Hoofdstuk 12 beschrijft een multidisciplinair raamwerk voor de ontwikkeling van AI voor automatische beoordeling van hoog-risico aderverkalking. We bespraken bestaand bewijs voor de toepassing van AI op dit gebied en formuleerden consensusaanbevelingen voor toekomstige algoritmeontwikkeling, met een nadruk op vereisten die de betrouwbaarheid vergroten, zoals robuustheid en eerlijkheid.

In **Hoofdstuk 13** voerden we een systematische review uit van 91 artikelen over AI voor OCT. We rapporteerden een toename van publicaties in recente jaren, waarbij er een verschuiving zichtbaar was van machine learning naar deep learning. Hoewel de prestaties van voorgestelde algoritmes hoog waren voor de automatische evaluatie van het coronaire lumen en stents, waren de prestaties voor complexere taken zoals karakteriseren van aderverkalking lager. Daarnaast rapporteerden we een gebrek aan transparantie in rapportage van de onderzoeksmethodologie en -resultaten en we observeerden een substantieel risico op bias in de meerderheid van de beoordeelde studies. Deze review nodigt lezers

van AI onderzoeken uit om kritisch te blijven en prestaties te beoordelingen in het licht van de gebruikte methodologie. Tevens riepen we op tot betere naleving van rapportagerichtlijnen.

In **Hoofdstuk 14** introduceerden we een nieuw multiclass segmentatie-algoritme voor OCT, genaamd OCT-AID. We evalueerden dit algoritme in een interne en externe dataset. We lieten een veelbelovende eerste prestatie zien, beoordeeld over een breed scala aan beelden, inclusief die met artefacten of reeds gedestabiliseerde laesies, wat contrasteert met eerdere studies over andere algoritmes.

Een grootschalige externe validatiestudie, bestaande uit 100 opeenvolgende patiënten van het St. Francis Hospital & Heart Center, staat beschreven in **Hoofdstuk 15**. In deze studie was de prestatie van OCT-AID voor de identificatie en kwantificatie van gecalcificeerde laesies uitstekend en grotendeels vergelijkbaar met de interobserver variabiliteit. De prestatie voor de evaluatie van lipide laesies, die lastiger te beoordelen zijn, was zelfs beter dan de interobserver variabiliteit. Daarentegen was de presentatie voor plaque onderdelen met een lage prevalentie beperkt. Al met al was dit de grootste studie tot nu toe over een multiclass AI-algoritme, en de enige die een opeenvolgende, niet-geselecteerde patiënten cohort gebruikte, waarmee de generaliseerbaarheid van ons algoritme werd ondersteund.

In **Hoofdstuk 16** evalueerden we of OCT-AID plaque burden kon afleiden vanuit OCT beelden, een variabele waarvan lang werd aangenomen dat dit niet met OCT beoordeeld kon worden vanwege de beperkte penetratiediepte van OCT. Met intravasculaire echografie als referentiestandaard rapporteerden we een uitstekende correlatie tussen OCT-afgeleide en echografie-afgeleide plaque burden (r=0,90, 95% BI 0,89-0,91, p<0,001), met consistente correlaties over verschillende plaque types. Dit hoofdstuk toont aan dat AI kan helpen om inherente beperkingen van beeldvormingstechnieken te overwinnen, en het toont aan dat hiermee nu voor het eerst gelijktijdig dunne kap fibroatheromen (TCFA) en plaque burden beoordeeld kan worden.

Hoofdstuk 17 beschrijft de resultaten van de PECTUS-AI studie, waarin we OCT-AID gebruikten voor automatische identificatie van TCFA binnen de PECTUS-obs dataset. AI-geïdentificeerde TCFA binnen de laesie was geassocieerd met een ongunstige klinische uitkomst, met een discriminerende waarde die minstens vergelijkbaar was met TCFA-identificatie door een core laboratorium. Bij evaluatie van het volledige in beeld gebrachte segment – een taak die handmatig niet uitvoerbaar is – was de discriminerende waarde van AI-geïdentificeerde TCFA significant hoger dan dit gebaseerd op analyse van enkel de laesie door het core laboratorium, met name door een toename in de negatief voorspellende waarden. Deze studie toont aan dat AI-gebaseerde identificatie van hoog-risico plaques een redelijk alternatief is voor handmatige OCT analyses en stelt ons in staat om onderzoeksbevindingen met ervaren core laboratorium-analisten eenvoudiger te vertalen naar de dagelijkse klinische praktijk.



APPENDIX

Research data management
PhD portfolio
Dankwoord
Curriculum vitae
List of publications

RESEARCH DATA MANAGEMENT

Ethics and privacy

This thesis is based on the results of research involving human participants (or existing data from published papers), which were conducted in accordance with relevant national and international legislation and regulations, guidelines, codes of conduct and Radboudumc policy. The recognized Medical Ethics Review Committees 'METC Oost-Nederland' (file number: NL67426.091.18) and 'institutional Review Board at St. Francis Hospital & Heart Center' have given approval to conduct these studies. The institutional ethical review committee CMO Radboudumc, Nijmegen, the Netherlands has also given approval to conduct these studies (CMO Radboudumc dossier number: 2018-4763).

According to Dutch legislation, data collection from electronic patient files was performed with personnel with a treatment relationship with the patient and by the researchers upon consent by the study participant. The privacy of the participants in these studies was warranted by the use of pseudonymization. The pseudonymization key was stored on a secured network drive that was only accessible to members of the project who needed access to it because of their role within the project. The pseudonymization key was stored separately from the research data.

Informed consent was obtained from participants to collect and process their data for this research project. Consent was also obtain for sharing the (pseudonymized) data after research.

Data collection and storage

Data for chapters 6-11, 14 and 17 was collected through electronic Case Report Forms (eCRF) of a prospective data collection in Castor EDC. Data for chapter 3 were reused from a previous prospective data collection. Data for chapters 14-17 were obtained through automated image analysis, the results of which were stored in csv format. All data were converged to SPSS or R. Data were stored and analyzed at the respective department servers of the Radboudumc or St. Francis Hospital & Heart Center and respective eCRF, and are only accessible by project members working at the respective departments. Paper (hardcopy) data for chapters 6-11, 14 and 17 are stored in cabinets on the department. All data will be archived for 15 years after termination of the respective studies. No new data were generated for chapters 2, 4-5 and 12-13.

Data sharing

The datasets from chapters 6-11 are published in Data Sharing Collections in the Radboud Data Repository under doi 10.34973/teed-7114. Datasets from chapters 14 and 17 are published in Data Sharing Collections in the Radboud Data Repository under doi 10.34973/esd0-n164. The datasets were published with restricted access. Requests for access will be checked by prof. dr. Niels van Royen, the principal investigator. Data will be shared upon reasonable request and against the conditions for sharing the data as described in the signed informed consent. The data used for chapter 3 are not owned by the Radboudumc. The data are archived by Abbott Vascular. Questions about the data can be addressed to jana.buccola@abbott.com. The data used for chapters 15-16 are not owned by the Radboudumc. The data are archived by St. Francis Hospital & Heart Center. Questions about the data can be addressed to ziad.ali@dcvi.org.

PHD PORTFOLIO

Department: Cardiology
PhD period: 01/01/2021 – 31/12/2025
PhD Supervisor(s): Prof. dr. Niels van Royen and prof. dr. Mathias Prokop

Training activities	Hours
Courses	
- Introduction day Radboudumc (2021)	7.00
- RIMLS - Introduction course "In the lead of my PhD" (2021)	15.00
- PubMed workshop (2021)	2.80
- Radboudumc - eBROK course (2021)	26.00
- Meet the Expert: Rebuttal (2021)	2.00
- RU - Statistics for PhD's by using SPSS (2022)	60.00
- AI for health (2023)	147.00
- The Physiology Course 16the edition: A New Wave (2024)	20.00
- Radboudumc - Scientific integrity (2024)	20.00
Seminars	
- Quarterly cardiology grand round (2022)	14.00
- Monthly journal club (2022)	21.00
- Research Integrity Round (2023)	1.50
- Research Integrity Round (2024)	1.50
Conferences	
- EuroPCR 2021 (2021) – oral presentation	31.00
- RIMLS PhD Retreat (2021)	14.00
- DCVA and NLHI - 6th Translational Cardiovascular Research Meeting (2022)	12.00
- 2nd Quantitative Cardiovascular Imaging Meeting (2022)	8.00
- PhD Retreat (2023) – poster presentation	21.00
- EuroPCR 2023 (2023) – oral presentation	43.00
- ESC 2023 (2023) – oral and poster presentation	50.00
- Imperial Vulnerable Plaque and Patient Meeting 2023 (2023)	24.00
- EuroPCR 2024 (2024) – 4 oral presentations	48.00
- DRES meetigng 2024 (2024) – oral presentation	16.00
- iPCI Meeting 2024 (2024)	18.00
- DCVA and NLHI - 8th Translational Cardiovascular Research Meeting (2024) – oral presentation	19.00
- ESC 2024 (2024) – poster presentation	39.00
- Imperial Vulnerable Plaque and Patient Meeting 2024 (2024)	28.00
- EuroPCR 2025 (2025) – oral presentation	43.00
- OPCI 2025 (2025)	16.00
- Imperial Vulnerable Plaque and Patient Meeting 2025 (2025)	27.00
- ESC 2025 (2025) – oral presentation	39.00
Other	
- Organization regional cardiology grand rounds (2023-2024)	96.00
- Reviewer for scientific journal (30x) (2022-2025)	30.00

Teaching activities	
Lecturing	
- Lectures on ECG interpretation (2023-2024)	40.00
- Lectures on coronary artery disease, heart failure and cardiovascular drugs (2023-2024)	28.00
Supervision	
- Bachelor students research proposal (2021)	37.00
- Bachelor student internship (2021)	19.00
- Master student internship (2022)	46.00
Total	**1129.80**

DANKWOORD

Dit promotietraject was allereerst niet mogelijk en ten tweede niet zo leuk geweest zonder de hulp van velen. Graag wil ik in dit dankwoord stilstaan bij de vele mensen die hieraan hebben bijgedragen.

Prof. dr. N. van Royen, beste **Niels**, vanaf het begin af aan heb je mij een hoop vrijheid en vertrouwen geboden. Er was altijd de mogelijkheid om even binnen te lopen voor vragen en voor vele uren telefonisch overleg in de auto naar huis. Ik ben jou ontzettend dankbaar voor alle mogelijkheden die je mij hebt geboden om mijzelf te ontwikkelen en het maximale uit mijn tijd als promovendus te halen, waaronder leerzame cursussen, mijn tijd in New York en de vele mooie congressen. Ik zal nooit vergeten hoe je mij onder jouw vleugels hebt genomen. Deze ervaringen neem ik de rest van mijn leven met mij mee.

Prof. dr. M. Prokop, beste **Mathias**, het was altijd plezierig om van jouw expertise gebruik te mogen maken. Vooral in de beginfase van de modelontwikkeling, toen we het CARA lab nog niet gestart waren, waren jouw aansturing van onschatbare waarde.

Beste **leden van de manuscriptcommissie**, bedankt voor jullie tijd en moeite om mijn proefschrift te beoordelen. Ik kijk ernaar uit om dit proefschrift samen met jullie te mogen bediscussiëren.

Mijn paranimfen, ik ben trots jullie aan mijn zijde te hebben tijdens mijn verdediging. **Mick,** wat ben ik blij dat onze paden vroeg bij elkaar zijn gekomen en nog steeds samen verder lopen. In vele fantastische herinneringen kom je voor: van wekelijks samen lunchen tijdens onze basisschooltijd tot geweldige vakanties en tripjes. Niet alleen tijdens leuke momenten, maar ook in moeilijke tijden ben je er altijd voor mij geweest. Ik waardeer je enorm, ik ben trots op hoe je je de laatste jaren hebt ontwikkeld, en ik ben blij jou als vriend te hebben. **Ruben**, hoe bijzonder om samen als vrienden aan hetzelfde project te mogen werken. Bedankt voor hoe je bent, als persoon, als vriend, voor je steun in moeilijke tijden, de vele gezellige avonden in Goesting, de koffietjes bij Knisper en de kilometers op de hardloopschoenen. Ik hoop dat wij dit nog in lengte der jaren zullen voortzetten.

Jan-Quinten, JQ, zonder jou was dit proefschrift dit proefschrift niet geweest. Je was de machinist op de trein waar ik op mocht stappen. Met momenten een boemeltrein, met momenten een sneltrein. Uiteindelijk heeft het ons beide naar een hele mooie bestemming gebracht. Ik ben je ontzettend dankbaar voor onze samenwerking, voor alles wat ik van je heb geleerd, je kritische blik, en onze wekelijkse diepgang momentjes. Maar minstens net zo voor de gezellige etentjes, borrels en bootje varen. Ik had het niet beter kunnen treffen. Hopelijk weten we elkaar in de toekomst nog net zo gemakkelijk te vinden: via Utrecht, en dan kom je er vanzelf (mits je bij het juiste adres aanbelt).

Grote dank aan alle **coauteurs**, alle betrokken **research medewerkers** en **patiënten** die hebben bijgedragen aan de totstandkoming van de hoofdstukken in dit proefschrift.

Prof. dr. M. Schreuder, beste **Michiel**, bedankt voor de aansturing en in het bijzonder voor de tips om vroegtijdig te beginnen met het proefschrift tot een geheel te maken.

Dear **Laura Rodwell** and **Aysun Cetinyurek-Yavuz**, thank you for your time and energy to guide me through the statistical analyses.

Dr. P. Damman, beste **Peter**, vanaf het begin voelde ik met jou een goede klik. Bedankt voor de persoonlijke begeleiding, de vele koffietjes, de samenwerking, het samen verrichten van OCT-geleide procedures, en het delen van fotografie-ervaringen. Op naar nog vele jaren fijne samenwerking. Groetjes Frank.

Dr. M. Brouwer, **dr. S. Westra**, **dr. F. Gommans** en **drs. S.P.G. van Vugt**, beste **Marc**, **Sjoerd**, **Frank** en **Stijn**, bij jullie is mijn avontuur begonnen. Marc, als wij elkaar niet na een van jouw colleges hadden gesproken en je mij niet had uitgenodigd om naar de cardiologie te komen, dan zou mijn pad er wellicht compleet anders uit hebben gezien. Bedankt allen voor jullie begeleiding bij mijn eerste stappen binnen de wetenschap, mijn eerste internationale congres en de vele gesprekken met een kopje koffie of diner. Frank en Stijn, excuses nog voor de deurbewegingen.

Beste **collega's van de afdeling cardiologie van het Radboudumc**, beste **cardiologen**, bedankt voor jullie vertrouwen en fijne samenwerking. In het bijzonder wil ik de **interventiecardiologen** bedanken voor hun bijdrage aan onze studies, en **dr. A. van Dijk** en **dr. R. Evertz** voor de vele onderwijsmomenten. Ik kijk er naar uit om over een aantal jaren bij jullie terug te keren als AIOS. Beste **assistenten**, ook jullie bedankt voor de fijne samenwerking in de kliniek en de gezamenlijke borrels. En als laatste alle **medewerkers van de researchafdeling**, bedankt voor jullie ondersteuning.

Members of the CARA lab, dear **prof. I. Išgum**, **prof. B. van Ginneken**, **prof. C.I Sánchez** and **prof. T. Blanke**, dear **Ivana**, **Bram**, **Clarisa** and **Tobias**, thank you for all the discussions and valuable feedback throughout. **Dr. S. Saitta**, dear **Simone**, thank you for the fruitful and enjoyable collaboration. Your different insight has been very helpful and I look forward extending our collaboration. **Dr. J. Thannhauser**, dear **Jos**, we already knew each other for a while before we started working together. I cherish the memories of our trip to Boston with cloudy cocktails, spoiled hotdogs, inside jokes and in-flight poker games. The PhD candidates of the CARA lab, **Ruben**, **Thijs**, **Pierandrea**, **Joske**, **Xiaojin** and **Leah**, thank you for all your hard work, and for dealing with my (annoying) questions or requests. This thesis marks just the beginning, I am more than confident that all your efforts will result in many great algorithms and manuscripts. Good luck to you all!

Dr. K. Nishimiya, dear **Kensuke**, thank you for all the OCT analyses and other collaborations together with Peter. I wish you all the best in Vietnam.

During my PhD, I had the honor of gaining experience at St. Francis Hospital and Heart Center (Roslyn, NY), the world-leading center in intracoronary imaging. **Prof. Z.A. Ali**, dear **Ziad**, thank you very much for hosting my research fellowship, your guidance throughout, and all research opportunities you offered and continue to offer. I won't forget your motivating energy and I will always keep your 'if you snooze, you lose' mentality in mind. **Dr. D. Shin**, dear **Doosup**, you are truly a remarkable talent, a publication machine, a very humble person and a great friend. Thank you for all your help, the discussions, and Korean BBQ we shared. **Dr. R. Shlofmitz**, dear **Rich**, I couldn't have been happier to have walked into your lab. Seeing you at work, and having had the opportunity to work with and learn from the most experienced operator in the world was unforgettable. Your personal attention and guidance made me feel more than welcome. You will always be my personal godfather of interventional cardiology. **Dr. E. Shlofmitz** and **dr. A. Jeremias**, dear **Evan** and **Allen**, and all **other interventional cardiologists**, thank you for being so welcoming, your enthusiasm, for taking the time to explain your procedures and letting me participate. **Craig** and **Susan** thank you for showing me your daily practice as imaging experts, for the discussions on difficult cases and allowing me to actively participate in the daily caseload of imaging-guided cases. You always downplayed your impact, but the knowledge that I obtained through you will be invaluable for my future career, thank you. Finally, **Fernando** and **Liz**, thank you for your support. Looking forward seeing you all again!
Ik wil ook graag mijn grote dank uitspreken naar het **Netherlands Heart Institute** en **Stichting de Drie Lichten** voor het mede mogelijk maken van deze onvergetelijke ervaring.

Een groot deel van dit dankwoord wil ik wijden aan mijn collega promovendi van het Radboudumc. Jullie hebben allen op jullie eigen manier een unieke bijdrage geleverd aan mijn tijd als promovendus, waarvoor ik jullie enorm dankbaar ben. **Yvonne** en **Lara**, ik heb zo veel respect voor jullie doorzettingsvermogen. Jullie hebben alle recht om meer dan trots te zijn op waar jullie nu zijn. **Jacqueline**, je was altijd overal goedlachs aanwezig en droeg een belangrijk steentje bij aan de gezelligheid. Helaas hebben wij te kort samen mogen werken. **Dominique**, niemand leek alles zo goed op orde te hebben als jij, voor jezelf maar ook zeker voor de hele promovendigroep. Jouw secretariële ondersteuning van mijn compagnon was goud waard. Bovenal ben ik jou dankbaar voor alle gezelligheid en jouw oprechte interesse. **Joris**, de koning van het mapjes maken, ergens verscholen tussen stapels troponine kits. Vol verwondering heb ik geleerd over jouw niet-alledaagse interesses en hobby's. **Amber**, altijd goedlachs, soms wat onhandig maar bovenal vol overgave, wat heb ik geweldige herinneringen aan veel van deze momenten. **Casper**, ouwe berggeit, je gaat heerlijk jouw eigen weg en keert gelukkig meestal ook weer zonder kleerscheuren terug. Bedankt voor de mentale ondersteuning als we beiden urenlang cirkels aan het intekenen waren, en voor het aanwijzen van dieren in de tuinen van het Radboudumc. Team FITTER, **Frans** en **Jan**, wat heb ik genoten van jullie onderlinge dynamiek: van ongekende oneliners tot het manoeuvreren in de lichtgrijze zone. Geniet van jullie NIRS-analyse pensioen! **Eva**, **Denise** en

Bahram, ik ben vol bewondering hoe jullie het ieder congres weer voor elkaar spelen om legio abstracts te mogen presenteren op mooie podia, maar ook hoe jullie altijd bij ieders praatje aanwezig proberen te zijn (fit of niet). **Tijn** en **Caïa**, eindeloze bronnen van energie, bedankt voor jullie enorme bijdrage aan de extra curriculaire activiteiten bij alle congressen waar we samen heen hebben mogen gaan. Met jullie erbij hoef je je nooit zorgen te maken dat je tot in de late uurtjes op een goede (of foute) plek eindigt. **Bibi**, je nam mij onder jouw hoede tijdens mijn tijd als senior-co. Hoewel een familiegesprek schijnbaar nog te hoog gegrepen was voor mij, heb ik veel van jou mogen leren. Bedankt ook dat ik Jos zo nu en dan mocht lenen voor overleg in de avonduren. **Max**, als broekies zaten wij samen op de gang bij de cardiologie tijdens onze onderzoeksstage. Niets was zo motiverend om jouw hardloopactiviteiten voorbij te zien komen, waarvoor meer dan petje af. Binnenkort maar eens samen een rondje hobbelen? **Alexander**, samen hebben wij vele mooie congressen mogen bezoeken en hotelkamers gedeeld. Bedankt voor het eindeloos willen luisteren naar mijn praatjes en voor de steun als ik op een onmogelijk moment werd opgepiept op congressen. **Job**, je bent echt een allemansvriend, en ik begrijp goed waarom. Heerlijk gewoon, heerlijk Tilburgs, en oprecht geïnteresseerd. Ik ben blij jou als vriend te mogen hebben en ik geniet iedere keer weer van de borrels en dinertjes samen met Nieky. **Nieky**, wandelende Michelin gids van het extreem lage tot het hoge segment. Zonder zelf moeite te hoeven doen kon ik dankzij jou genieten van de lekkerste noedels, birria en bagels. Op naar nog vele mooie jaren vriendschap en hopelijk ook samenwerkingen als zelfstandige onderzoekers! **Roos**, ik geniet van jouw oprechtheid wat jou zeker ver gaat brengen. Vol trots heb ik gekeken hoe je de ene na de andere prijs binnen het gehaald. En niet vergeten: a peertje a day keeps the doctor away. **Peter David**, wat heb jij mij verrast. Ik heb genoten van jouw humor, hoe je altijd weer verrassend uit de hoek komt, en hoe we samen stuntelend de skipistes zijn afgegaan. **Joske**, **Thijs** en **Leah**, jullie kunnen niet meer verschillend zijn, maar juist dat zorgde voor een unieke mix van kwaliteiten. Joske, bedankt voor het delen van alle juice en het bediscussiëren van reality-tv. Thijs en Leah, bedankt voor al jullie hulp en de intensieve samenwerking binnen alle high-risk plaque projecten. **Geert**, aan de top soms een vurig temperament, in het midden een hele hardwerkende en goede onderzoeker, en in de basis vooral een hele goede gast. Hoewel we vaak een compleet andere weg gingen, heb ik veel plezier gehad met jou op PCR. **Carolien** en **Vince**, vol bewondering kijk ik naar jullie onderzoeken, wat voor mij echt het schoolvoorbeeld van onderzoek doen is. Naast jullie onuitputtelijke vermogen om powerpoint presentaties te maken, zijn jullie altijd op alle borrels te vinden. Tot de volgende! **Madelon**, inmiddels mede-Venraynaar. Ik vind het mooi hoe je jouw weg gaat op onbekende plekken en je snel thuis voelt. Veel plezier Down Under! **Mark**, wat was het fijn om een medestander te hebben als het ging om het levenslied en Tino Martin in het bijzonder. Ik ben nog steeds jaloers op die borrel met privé-optreden in Nijmegen. **Behruz,** bedankt voor jouw samenwerking op het gebied van MINOCA. Ik hoop dat we dit nog verder uit gaan diepen de komende jaren! **Catharina**, **Eveline**, **Fleur**, **Lente** en **Luc**, met jullie heb ik helaas minder samen kunnen werken. Geniet van jullie tijd als promovendi en heel veel succes!

Abel, **Bas**, **Maarten**, **Nigel**, **Olivier**, en **Sem**, bedankt voor jullie vriendschap. De tussentijdse ontspanning en de flauwekul zijn erg belangrijk geweest tijdens mijn promotietraject en daarbuiten. Ik

hoop nog vele dagen en avonden samen door te brengen, of het nou is tijdens een borrelavond, een vriendenweekend, de vastelaovend, of een avond in de tuin. Weet dat ik jullie ontzettend waardeer en veel geluk haal uit tijd doorbrengen met jullie.

Mama, **ome Hans** en **Gerry**, **Anouk** en **Ruud**, we hebben het niet altijd even makkelijk gehad, maar samen zijn we een heel eind gekomen. Ik ben trots op hoe iedereen, op een eigen manier, hieraan heeft bijgedragen. Anouk, weet dat ik ontzettend trots op je ben, op wat je hebt weten te bereiken door altijd hard te blijven werken.

Het laatste jaar van mijn promotietraject was een aaneenschakeling van hoogtepunten, waarbij ik als kerst op de taart jou nog leerde kennen, **Susan**. Ik ben je ongelofelijk dankbaar voor jouw liefde, empathie en enthousiasme. Met jou erbij ziet de dag er altijd net wat zonniger uit. Dat we nog vele mooie herinneringen samen mogen gaan maken. Ik hou van jou!

CURRICULUM VITAE

Rick Volleberg werd op 15 juli 1996 geboren in Venray, alwaar hij opgroeide. In 2014 behaalde hij zijn gymnasiumdiploma aan het Raayland College te Venray. Hierna studeerde hij geneeskunde aan de Radboud Universiteit te Nijmegen. Eind 2020 rondde hij deze studie *cum laude* af.

Vanaf de bachelor fase van de studie is hij betrokken geweest bij diverse onderzoeksprojecten binnen de afdeling cardiologie van het Radboudumc te Nijmegen gericht op hypertrofische cardiomyopathie, onder begeleiding van dr. F. Gommans, en atriumfibrilleren, onder begeleiding van drs. S. van Vugt, drs. S. Westra en dr. M. Brouwer. Na zijn afsluitende seniorcoschap bij deze afdeling, is hij gestart met zijn promotietraject onder leiding van prof. dr. N. van Royen en prof. dr. M. Prokop gericht op intracoronaire optical coherence tomography en kunstmatige intelligentie. In 2021 werd dit promotietraject tijdelijk onderbroken om klinische ervaring op te doen als arts-assistent. In 2024 en 2025 bracht hij acht maanden door aan het toonaangevende St. Francis Hospital & Heart Center (Roslyn, NY, Verenigde Staten) voor verdere verdieping in de wetenschap en in invasieve en non-invasieve coronaire beeldvorming.

Tijdens zijn promotietraject heeft hij meerdere onderzoeken uit dit proefschrift gepresenteerd op nationale en internationale congressen. Hiervoor ontving hij de 'Personalized Vascular Care Award' (EuroPCR 2023) en prijs voor 'Beste startende onderzoeker' (DRES meeting 2024), en behoorde hij tot de 'top three finalists of EuroPCR got talent' (EuroPCR 2024). Daarnaast was hij actief betrokken bij de organisatie van de regionale nascholingsavonden cardiologie, gaf hij onderwijs aan (gespecialiseerde) verpleegkundigen, en is hij guest-contributor van de EAPCI/PCR Journal Club.

Buiten zijn werkzaamheden draagt hij de *Venrodse vastelaovestredisie* een warm hart toe, en haalt hij veel plezier uit zich afwisselend verdiepen in verschillende hobby's, waaronder hardlopen, schilderkunst, koffie, koken en fotografie.

In januari 2026 startte hij met de opleiding tot cardioloog aan het Radboudumc, waarvoor hij momenteel de vooropleiding volgt in het Canisius Wilhelmina Ziekenhuis te Nijmegen.

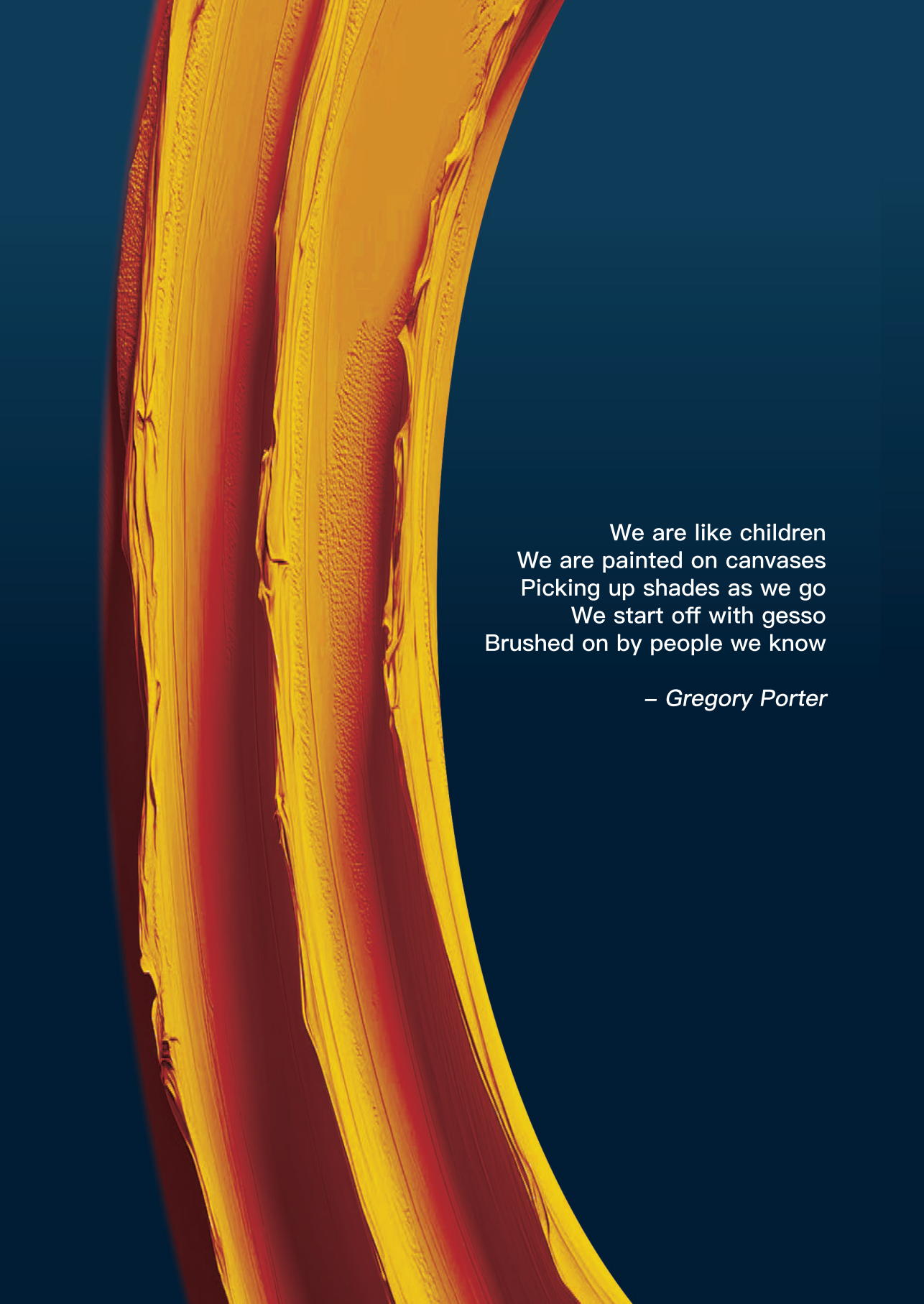
LIST OF PUBLICATIONS

1. Mol JQ, Belkacemi A, **Volleberg R**, Meuwissen M, Protopopov AV, Laanmets P, Krestyaninov OV, Dennert R, Oemrawsingh RM, van Kuijk JP, Arkenbout K, van der Heijden DJ, Rasoul S, Lipsic E, Teerenstra S, Camaro C, Damman P, van Leeuwen MA, van Geuns RJM, van Royen N. Identification of anatomic risk factors for acute coronary events by optical coherence tomography in patients with myocardial infarction and residual nonflow limiting lesions: rationale and design of the PECTUS-obs study. BMJ Open 2021;11:e048994.
2. van Vugt SPG, Westra SW, **Volleberg RHJA**, Hannink G, Nakamura R, de Asmundis C, Chierchia GB, Navarese EP, Brouwer MA. Meta-analysis of controlled studies on minimally interrupted vs. continuous use of non-vitamin K antagonist oral anticoagulants in catheter ablation for atrial fibrillation. Europace 2021;23:1961-1969.
3. **Volleberg R**, van den Oord S, Van Geuns RJM. Hangover after Side Branch Stenting: The Discomfort Comes Afterwards. Interv Cardiol 2022;17:e08.
4. **Volleberg R**, Mol JQ, van der Heijden DJ, Meuwissen M, van Leeuwen MAH, Escaned J, Holm N, Adriaenssens T, van Geuns RJM, Tu S, Crea F, Stone GW, van Royen N. Optical coherence tomography and coronary revascularization: from indication to procedural optimization. Trends Cardiovasc Med 2023;33:92-106.
5. Vázquez Mézquita AJ, Biavati F, Falk V, Alkadhi H, Hajhosseiny R, Maurovich-Horvat P, Manka R, Kozerke S, Stuber M, Derlin T, Channon KM, Išgum I, Coenen A, Foellmer B, Dey D, **Volleberg RHJA**, Meinel FG, Dweck MR, Piek JJ, van de Hoef T, Landmesser U, Guagliumi G, Giannopoulos AA, Botnar RM, Khamis R, Williams MC, Newby DE, Dewey M. Clinical quantitative coronary artery stenosis and coronary atherosclerosis imaging: a Consensus Statement from the Quantitative Cardiovascular Imaging Study Group. Nat Rev Cardiol 2023;20:696-714.
6. Mol JQ, **Volleberg RHJA**, Belkacemi A, Hermanides RS, Meuwissen M, Protopopov AV, Laanmets P, Krestyaninov OV, Dennert R, Oemrawsingh RM, van Kuijk JP, Arkenbout K, van der Heijden DJ, Rasoul S, Lipsic E, Rodwell L, Camaro C, Damman P, Roleder T, Kedhi E, van Leeuwen MAH, van Geuns RJM, van Royen N. Fractional Flow Reserve-Negative High-Risk Plaques and Clinical Outcomes After Myocardial Infarction. JAMA Cardiol 2023;8:1013-1021.
7. Follmer B, Williams MC, Dey D, Arbab-Zadeh A, Maurovich-Horvat P, **Volleberg RHJA**, Rueckert D, Schnabel JA, Newby DE, Dweck MR, Guagliumi G, Falk V, Vázquez Mézquita AJ, Biavati F, Isgum I, Dewey M. Roadmap on the use of artificial intelligence for imaging of vulnerable atherosclerotic plaque in coronary arteries. Nat Rev Cardiol 2024;21:51-64.
8. Los J, Mensink FB, Mohammadnia N, Opstal TSJ, Damman P, **Volleberg RHJA**, Peeters DAM, van Royen N, Garcia-Garcia HM, Cornel JH, El Messaoudi S, van Geuns RJM. Invasive coronary imaging of inflammation to further characterize high-risk lesions: what options do we have? Front Cardiovasc Med 2024;11:1352025.
9. **Volleberg R**, Damman P, van Royen N. Dissection-like appearance of focal catheter-induced vasospasm in intracoronary optical coherence tomography. Eur Heart J 2024;45:2793.

10. **Volleberg RHJA**, Mol JQ, Belkacemi A, Hermanides RS, Meuwissen M, Protopopov AV, Laanmets P, Krestyaninov OV, Dennert R, Oemrawsingh RM, van Kuijk JP, Arkenbout K, van der Heijden DJ, Rasoul S, Lipsic E, Rodwell L, Camaro C, Damman P, Roleder T, Kedhi E, van Leeuwen MAH, van Geuns RJM, van Royen N. Sex differences in plaque characteristics of fractional flow reserve-negative non-culprit lesions after myocardial infarction. Atherosclerosis 2024;397:118568.
11. **Volleberg RHJA**, Mol JQ, Belkacemi A, Hermanides RS, Meuwissen M, Protopopov AV, Laanmets P, Krestyaninov OV, Lacle CF, Oemrawsingh RM, van Kuijk JP, Arkenbout K, van der Heijden DJ, Rasoul S, Lipsic E, Rodwell L, Camaro C, Damman P, Roleder T, Kedhi E, van Leeuwen MAH, van Geuns RM, van Royen N. High-risk plaques in non-culprit lesions and clinical outcome after NSTEMI vs. STEMI. Eur Heart J Cardiovasc Imaging 2025;26:197-206.
12. **Volleberg RHJA**, Rroku A, Mol JQ, Hermanides RS, van Leeuwen M, Berta B, Meuwissen M, Alfonso F, Wojakowski W, Belkacemi A, Roleder T, Kedhi E, van Royen N. FFR-Negative Nonculprit High-Risk Plaques and Clinical Outcomes in High-Risk Populations: An Individual Patient-Data Pooled Analysis From COMBINE (OCT-FFR) and PECTUS-obs. Circ Cardiovasc Interv 2025;18:e014667.
13. **Volleberg R**, Cancian P, van Royen N. Optical Coherence Tomography in Motion: Potential Cause for Artifacts. JACC Cardiovasc Interv 2025;18:680-681.
14. van der Waerden RGA, **Volleberg RHJA**, Luttikholt TJ, Cancian P, van der Zande JL, Stone GW, Holm NR, Kedhi E, Escaned J, Pellegrini D, Guagliumi G, Mehta SR, Pinilla-Echeverri N, Moreno R, Raber L, Roleder T, van Ginneken B, Sanchez CI, Isgum I, van Royen N, Thannhauser J. Artificial intelligence for the analysis of intracoronary optical coherence tomography images: a systematic review. Eur Heart J Digit Health 2025;6:270-284.
15. Kaldas M, Weber J, Parikh R, Pipitone K, Chau K, Shin D, **Volleberg R**, Ali Z, Khalique OK. Coronary Calcium Scoring Using True and Virtual Non-Contrast Reconstructions on Photon-Counting CT with Differing Slice Increment: Impact on Calcium Severity Classifications. J Clin Med 2025;14.
16. **Volleberg RHJA**, van der Waerden RGA, Luttikholt TJ, van der Zande JL, Cancian P, Gu X, Mol JQ, Quax S, Prokop M, Sanchez CI, van Ginneken B, Isgum I, Thannhauser J, Saitta S, Nishimiya K, Roleder T, van Royen N. Comprehensive full-vessel segmentation and volumetric plaque quantification for intracoronary optical coherence tomography using deep learning. Eur Heart J Digit Health 2025;6:404-416.
17. Dakroub AH, Shin D, Singh M, Malik S, **Volleberg RHJA**, Weber J, Ciftcikal Y, Fazal A, Sakai K, Sato T, Maehara A, Matsumura M, Moses JW, Mintz GS, Khalique OK, Sosa F, Shlofmitz E, Jeremias A, Shlofmitz RA, Ali ZA. Procedural and Clinical Outcomes After Orbital Atherectomy Versus Intravascular Lithotripsy in Patients With Calcified Nodules. Circ Cardiovasc Interv 2025;18:e015254.
18. Jeremias A, **Volleberg RHJA**, Ali ZA. FLAVOUR: Just a Difference in Taste? J Am Coll Cardiol 2025;86:607-609.
19. **Volleberg R**, Luttikholt TJ, van der Waerden RGA, Cancian P, van der Zande JL, Gu X, Mol JQ, Roleder T, Prokop M, Sanchez CI, van Ginneken B, Isgum I, Saitta S, Thannhauser J, van Royen N. Artificial intelligence-based identification of thin-cap fibroatheromas and clinical outcomes: the PECTUS-AI study. Eur Heart J 2025;46:5032-5041.

20. **Volleberg RHJA**, Shin D, Saitta S, Shlofmitz RA, Shlofmitz E, Jeremias A, van der Waerden RGA, Thannhauser J, van Royen N, Ali ZA. Deep Learning-Derived Plaque Burden for Intracoronary Optical Coherence Tomography: An Intravascular Ultrasound-Based Validation Study. JACC Cardiovasc Interv 2025;18:2432-2434.
21. Shin D, **Volleberg RHJA**, Parikh R, Yang Koo CC, Malik S, Cannata M, Caron E, Ciftcikal Y, Sakai K, Cao JJ, Chen L, Sosa F, Weber J, Khan JM, Cohen DJ, Moses JW, van Royen N, Collet C, Shlofmitz RA, Shlofmitz E, Jeremias A, Khalique OK, Ali ZA. Photon-counting detector computed tomography for the assessment of coronary stents and in-stent restenosis. EuroIntervention 2025;21:e1137-e1146.
22. **Volleberg RHJA**, Rroku A, Mol JQ, Hermanides RS, van Leeuwen M, Berta B, Meuwissen M, Alfonso F, Wojakowski W, Belkacemi A, De Luca G, Rodwell L, Roleder T, Kedhi E, van Royen N. Impact of clinical risk characteristics on the prognostic value of high-risk plaques. EuroIntervention 2025;21:e1147-e1158.
23. Parikh R, Shin D, Sakai K, Singh M, Caron E, Cannata M, Ciftcikal Y, Weber J, **Volleberg R**, Pipitone K, Cao JJ, Chen L, Sosa F, Patel KK, Duggan M, Khan JM, Cohen DJ, Moses JW, Shlofmitz RA, Collet C, Shlofmitz E, Jeremias A, Ali ZA, Khalique OK. Photon-counting detector computed tomography for evaluation of coronary artery disease in older adults. J Cardiovasc Comput Tomogr 2025;19:658-664.
24. Shin D, **Volleberg RHJA**, Parikh R, Koo CCY, Sosa F, Shlofmitz E, Shlofmitz RA, Jeremias A, Khalique OK, Ali ZA. Characterization of In-Stent Restenosis Using Photon-Counting Detector Computed Tomography. JACC Cardiovasc Imaging 2025;18:1265-1269.
25. **Volleberg R**, Shin D, Shlofmitz RA, Maksoud A, Chehab B, Phalakornkule K, Buccola J, Teraphongphom NT, Gopinath A, Netravali A, Ali ZA, Jeremias A. Combining Optical Coherence Tomography and Fractional Flow Reserve for Decision Making in Percutaneous Coronary Intervention: Insights From the FUSION Study. J Soc Cardiovasc Angiogr Interv 2025;4:104001.
26. Griffioen AM, Meijers TA, Roolvink V, van der Heijden DJ, **Volleberg R**, van Wely M, van Royen N, van Geuns RJ, van Leeuwen M. Use of physioLogy to evaluaTe procedural Result After percutaneous coronary intervention of Chronic Total Occlusion (ULTRA-CTO): protocol for a prospective, single-arm, multicentre, exploratory study. BMJ Open 2025;15:e108995.
27. Malik S, Shin D, Caron E, **Volleberg R**, Sakai K, Collet C, Shlofmitz E, Jeremias A, Ali ZA, Khalique OK. Validation of Coronary Stent Measurements Using Photon-Counting Detector Computed Tomography: A Comparison With Optical Coherence Tomography. JACC Cardiovasc Imaging 2026;19:126-129.
28. Ali ZA, **Volleberg R**, Shin D, Chong L, Calistro C, Ansari A, Sosa F, Shlofmitz RA, Shlofmitz E, Moses JW, Jeremias A. Intravascular Imaging in Chronic Total Occlusion Percutaneous Coronary Intervention. Interv Cardiol Clin 2026;15:111-120.
29. **Volleberg R**, Shin D, Jeremias A, Sosa F, Shlofmitz E, Ali ZA. Lipid Base Confers Calcified Nodule Deformability: A Marble on Jelly. JACC Cardiovasc Interv 2026;19:134-136.
30. **Volleberg R**, Shin D, Calistro C, Ansari A, Chong L, Sosa F, Shlofmitz RA, Shlofmitz E, Jeremias A, Ali ZA. Stent Failure in Contemporary Practice. Interv Cardiol Clin 2026;15:299-305.

31. van der Zande JL, Alvarez-Florez L, **Volleberg R**, Brás C, Karkalousos D, Nijveldt R, van Royen N, Leiner T, Khalili N, Litjens G, Thannhauser J, Išgum I. Deep Learning for Cardiac Image Analysis: Unveiling Advances in Deep Learning Architectures. JACC Cardiovasc Imaging 2026.
32. **Volleberg R**, Mol JQ, Versteeg GAA, van der Zande J, Belkacemi A, Hermanides RS, Meuwissen M, Protopopov AV, Laanmets P, Krestyaninov OV, Laclé CF, Oemrawsingh RM, van Kuijk JP, Arkenbout K, van der Heijden DJ, Rasoul S, Lipsic E, Camaro C, Damman P, Roleder T, Kedhi E, van Leeuwen MAH, van Geuns RM, van Royen N. Long-Term Clinical Outcomes of High-Risk Plaques with Negative fractional flow reserve: the PECTUS-obs study. EuroIntervention 2026.
33. Nishimiya K, Yosofi B, Dimitriu-Leen AC, **Volleberg R**, Focks JJ, van Helden G, Jansen TPJ, Camaro C, Cate TCT, van Wely M, van Nunen LX, Thannhauser J, Elias-Smale S, van Geuns RJ, van Royen N, Nijveldt R, Damman P. Feasibility and Yield of a Diagnostic Protocol for Myocardial Infarction With Nonobstructive Coronary Arteries. Am J Cardiol 2026.



We are like children
We are painted on canvases
Picking up shades as we go
We start off with gesso
Brushed on by people we know

– Gregory Porter

